Breaking the cell cycle to treat cancer *p. 865*

Watching metal atoms order and organize *pp. 909 & 916*

Enhancer dynamics in blood development *p. 943*

Science

$10
22 AUGUST 2014
sciencemag.org
AAAS

Fostering reef recovery

Young corals and fishes colonize healthy habitats *pp. 879 & 892*

CONTENTS

875 & 933

A nucleus controls its own destruction

22 AUGUST 2014 • VOLUME 345 • ISSUE 6199

NEWS

IN BRIEF

856 Roundup of the week's news

IN DEPTH

859 STUDY EXPOSES CHINESE CENSORS' DEEPEST FEARS
The power of the masses proves most unnerving *By M. Hvistendahl*
▸ RESEARCH ARTICLE P. 891

860 IS ATLANTIC HOLDING EARTH'S MISSING HEAT?
New leads in the hunt to explain the global warming hiatus *By E. Kintisch*
▸ RESEARCH ARTICLE P. 897

861 A ONE-TWO PUNCH AGAINST POLIO
Injected vaccine promises a boost for eradication *By L. Roberts*
▸ REPORT P. 922

862 WHEELS WHEN YOU NEED THEM
Can special algorithms help keep shared bicycles rolling? *By C. Wald*

864 WOLVES COOPERATE BUT DOGS SUBMIT, STUDY SUGGESTS
Dependence may have driven initial dog domestication *By V. Morell*

FEATURE

865 THE CANCER DRUG THAT ALMOST WASN'T
A neglected compound that blocks cell division stirs excitement *By K. Garber*

INSIGHTS

PERSPECTIVES

868 IMPRINT OF AN ANCIENT CONFLAGRATION
Evidence is found for the massive stars that populated the early universe
By V. Bromm
▸ REPORT P. 912

870 CARBON CYCLING IN THE ARCTIC
Sunlight drives the emission of carbon from arctic waters *By L. Tranvik*
▸ REPORT P. 925

878 & 929

871 A PHOTON STEERS A PHOTON WITH AN ATOM
Nonlinear optics with single quanta of light and matter becomes reality
By G. Rempe
▸ REPORT P. 903

872 GLACIER RETREAT CROSSES A LINE
Mountain glacier loss since the 1970s has mostly been caused by human influences on climate change *By S. Marshall*
▸ REPORT P. 919

873 BOOSTING GDP GROWTH BY ACCOUNTING FOR THE ENVIRONMENT
Including air pollution and greenhouse gas damages increases estimated U.S. growth *By N. Z. Muller*

875 MAKING PHLOEM—A NEAR-DEATH EXPERIENCE
How to get rid of the phloem cell nucleus to make a root-to-shoot tip transport system *By N. Geldner*
▸ REPORT P. 933

876 RIBOSWITCH REGULATES RNA
Nutrient metabolism in bacteria is controlled by a circuit in which RNA is regulated by RNA
By J. Chen and S. Gottesman
▸ REPORTS PP. 937 & 940

878 SENSING NECTAR'S SWEETNESS
A taste receptor evolves to sense sugar in adapting to the diet of some birds
By P. Jiang and G. K. Beauchamp
▸ REPORT P. 929

879 HOW DO CORAL REEFS RECOVER?
Experiments on juvenile coral and fish behavior may have implications for reef restoration efforts *By J. F. Bruno*
▸ RESEARCH ARTICLE P. 892

881 JOEP LANGE (1954–2014)
A leader in developing therapy for AIDS is tragically killed *By J. Goudsmit*

BOOKS *ET AL.*

882 MORALITY FOR HUMANS
By M. Johnson, reviewed by L. Beldo

883 THE ENTREPRENEURIAL STATE
By M. Mazzucato, reviewed by D. Consoli

LETTERS

884 FAUNA IN DECLINE: PLIGHT OF THE PANGOLIN
By Y. Liu and Q. Weng

884 FAUNA IN DECLINE: FIRST DO NO HARM
By A. Ricciardi and D. Simberloff

885 FAUNA IN DECLINE: GLOBAL ASSESSMENTS
By H. Mooney and H. Tallis

885 AILING ACADEMIA NEEDS CULTURE CHANGE
By V. Callier and N. L. Vanderford

885 LET MINORITY-SERVING INSTITUTIONS LEAD
By F. Jackson et al.

DEPARTMENTS

855 EDITORIAL
A swan in the making
By Timothy Gardner

974 WORKING LIFE
Playing a new tune
By Jim Austin

882

Science Staff 854
New Products 954
Science Careers 955

PHOTO: (MIDDLE) LUKE SEITZ/WWW.LUKESEITZART.COM

Published by AAAS

CONTENTS

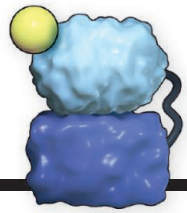

876, 937, & 940

Riboswitch-based regulation

22 AUGUST 2014 • VOLUME 345 • ISSUE 6199

RESEARCH

IN BRIEF

886 From *Science* and other journals

REVIEW

889 STEM CELL THERAPY
Use of differentiated pluripotent stem cells in replacement therapy for treating disease *I. J. Fox* et al.
REVIEW SUMMARY; FOR FULL TEXT: dx.doi.org/10.1126/science.1247391

RESEARCH ARTICLES

891 POLITICAL SCIENCE
Reverse-engineering censorship in China: Randomized experimentation and participant observation *G. King* et al.
RESEARCH ARTICLE SUMMARY; FOR FULL TEXT: dx.doi.org/10.1126/science.1251722
▸ NEWS STORY P. 859; PODCAST

892 REEF ECOLOGY
Chemically mediated behavior of recruiting corals and fishes: A tipping point that may limit reef recovery *D. L. Dixson* et al.
▸ PERSPECTIVE P. 879

897 CLIMATE
Varying planetary heat sink led to global-warming slowdown and acceleration *X. Chen and K.-K. Tung*
▸ NEWS STORY P. 860

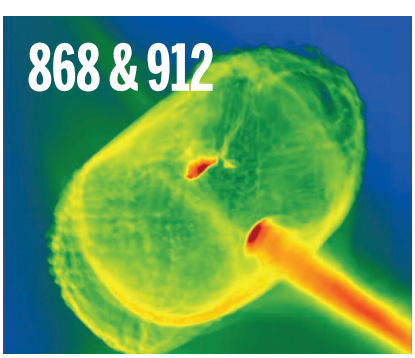

REPORTS

903 QUANTUM OPTICS
All-optical routing of single photons by a one-atom switch controlled by a single photon *I. Shomroni* et al.
▸ PERSPECTIVE P. 871

906 HELIUM SUPERFLUIDITY
Shapes and vorticities of superfluid helium nanodroplets *L. F. Gomez* et al.

909 NANOPARTICLE IMAGING
Electron microscopy of gold nanoparticles at atomic resolution *M. Azubel* et al.

912 MASSIVE STARS
A chemical signature of first-generation very massive stars *W. Aoki* et al.
▸ PERSPECTIVE P. 868

916 NANOPARTICLE GROWTH
Facet development during platinum nanocube growth *H.-G. Liao* et al.

919 GLACIERS
Attribution of global glacier mass loss to anthropogenic and natural causes *B. Marzeion* et al.
▸ PERSPECTIVE P. 872

922 POLIO ERADICATION
Efficacy of inactivated poliovirus vaccine in India *H. Jafari* et al.
▸ NEWS STORY P. 861

925 CARBON CYCLE
Sunlight controls water column processing of carbon in arctic fresh waters *R. M. Cory* et al.
▸ PERSPECTIVE P. 870

929 SENSORY BIOLOGY
Evolution of sweet taste perception in hummingbirds by transformation of the ancestral umami receptor *M. W. Baldwin* et al.
▸ PERSPECTIVE P. 878

933 PLANT DEVELOPMENT
Arabidopsis NAC45/86 direct sieve element morphogenesis culminating in enucleation *K. M. Furuta* et al.
▸ PERSPECTIVE P. 875

RIBOSWITCHES

937 A riboswitch-containing sRNA controls gene expression by sequestration of a response regulator *S. DebRoy* et al.

940 Sequestration of a two-component response regulator by a riboswitch-regulated noncoding RNA *J. R. Mellin* et al.
▸ PERSPECTIVE P. 876

943 IMMUNOGENETICS
Chromatin state dynamics during blood formation *D. Lara-Astiaso* et al.

950 PLANT GENETICS
Early allopolyploid evolution in the post-Neolithic *Brassica napus* oilseed genome *B. Chalhoub* et al.

ON THE COVER

Tropical corals and reef fishes (like the fish *Priacanthus* sp. and the coral *Turbinaria mesenterina* shown here) are in global decline. Recovery in degraded reefs may be limited because dispersing juveniles from these groups are attracted to chemical cues produced by organisms in healthy reefs and are repelled by cues from seaweeds in degraded areas. See pages 879 and 892. *Photo: Tim Laman/ National Geographic Creative*

PHOTO: (RIGHT) GEORGE KLING

SCIENCE (ISSN 0036-8075) is published weekly on Friday, except the last week in December, by the American Association for the Advancement of Science, 1200 New York Avenue, NW, Washington, DC 20005. Periodicals mail postage (publication No. 484460) paid at Washington, DC, and additional mailing offices. Copyright © 2014 by the American Association for the Advancement of Science. The title SCIENCE is a registered trademark of the AAAS. Domestic individual membership and subscription (51 issues): $153 ($74 allocated to subscription). Domestic institutional subscription (51 issues): $1282; Foreign postage extra: Mexico, Caribbean (surface mail) $55; other countries (air assist delivery) $85. First class, airmail, student, and emeritus rates on request. Canadian rates with GST available upon request, GST #1254 88122. Publications Mail Agreement Number 1069624. **Printed in the U.S.A.**
Change of address: Allow 4 weeks, giving old and new addresses and 8-digit account number. **Postmaster:** Send change of address to AAAS, P.O. Box 96178, Washington, DC 20090–6178. **Single-copy sales:** $10.00 current issue, $15.00 back issue prepaid includes surface postage; bulk rates on request. **Authorization to photocopy** material for internal or personal use under circumstances not falling within the fair use provisions of the Copyright Act is granted by AAAS to libraries and other users registered with the Copyright Clearance Center (CCC) Transactional Reporting Service, provided that $30.00 per article is paid directly to CCC, 222 Rosewood Drive, Danvers, MA 01923. The identification code for *Science* is 0036-8075. *Science* is indexed in the *Reader's Guide to Periodical Literature* and in several specialized indexes.

Published by AAAS

Science
AAAS
1200 New York Avenue, NW, Washington, DC 20005
Bateman House, 82-88 Hills Road, Cambridge, UK CB2 1LQ

Editor-in-Chief Marcia McNutt
Executive Editor Monica M. Bradford **News Editor** Tim Appenzeller
Managing Editor, Research Journals Katrina L. Kelner
Deputy Editors Barbara R. Jasny, Andrew M. Sugden(UK), Valda J. Vinson, Jake S. Yeston

Research and Insights

SR. EDITORS Caroline Ash(UK), Gilbert J. Chin, Lisa D. Chong, Maria Cruz(UK), Julia Fahrenkamp-Uppenbrink(UK), Pamela J. Hines, Stella M. Hurtley(UK), Paula A. Kiberstis, Marc S. Lavine(Canada), Kristen L. Mueller, Ian S. Osborne(UK), Beverly A. Purnell, L. Bryan Ray, Guy Riddihough, H. Jesse Smith, Peter Stern(UK), Phillip D. Szuromi, Brad Wible, Nicholas S. Wigginton, Laura M. Zahn **ASSOCIATE EDITORS** Brent Grocholski, Melissa R. McCartney, Margaret M. Moerchen, Jelena Stajic, Sacha Vignieri **BOOK REVIEW EDITOR** Sherman J. Suter **ASSOCIATE LETTERS EDITOR** Jennifer Sills **EDITORIAL MANAGER** Cara Tate **SR. COPY EDITORS** Jeffrey E. Cook, Chris Filiatreau, Cynthia Howe, Harry Jach, Lauren Kmec, Barbara P. Ordway, Trista Wagoner **SR. EDITORIAL COORDINATORS** Carolyn Kyle, Beverly Shields **EDITORIAL COORDINATORS** Ramatoulaye Diop, Joi S. Granger, Lisa Johnson, Anita Wynn **PUBLICATIONS ASSISTANTS** Aneera Dobbins, Jeffrey Hearn, Dona Mathieu, Le-Toya Mayne Flood, Shannon McMahon, Scott Miller, Jerry Richardson, Rachel Roberts(UK), Alice Whaley(UK), Brian White **ADMINISTRATIVE SUPPORT** Janet Clements(UK), Joan Cuthbert(UK), Maryrose Madrid, John Wood(UK)

News

NEWS MANAGING EDITOR John Travis **INTERNATIONAL EDITOR** Richard Stone **DEPUTY NEWS EDITORS** Daniel Clery(UK), Robert Coontz, Elizabeth Culotta, David Grimm, David Malakoff, Leslie Roberts **CONTRIBUING EDITORS** Martin Enserink(Europe), Mara Hvistendahl (Asia) **SR. CORRESPONDENTS** Jeffrey Mervis, Elizabeth Pennisi **NEWS WRITERS** Adrian Cho, Jon Cohen, Jennifer Couzin-Frankel, Carolyn Gramling, Eric Hand, Jocelyn Kaiser, Kelly Servick, Robert F. Service, Erik Stokstad, Emily Underwood **CONTRIBUTING INTERNS** Hassan DuRant, XochitI Rojas-Rocha, Nadia Whitehead **CORRESPONDENTS** Pallava Bagla(South Asia), Michael Balter(Paris), John Bohannon, Ann Gibbons, Sam Kean, Richard A. Kerr, Eli Kintisch, Kai Kupferschmidt(Berlin), Andrew Lawler, Christina Larson(Beijing), Mitch Leslie, Charles C. Mann, Eliot Marshall, Virginia Morell, Dennis Normile(Tokyo), Heather Pringle, Tania Rabesandratana(Brussels), Gretchen Vogel(Berlin), Lizzie Wade(Mexico City) **CAREERS** Jim Austin(Editor), Donisha Adams **COPY EDITORS** Kara Estelle, Nora Kelly, Jennifer Levin **ADMINISTRATIVE SUPPORT** Scherraine Mack

Executive Publisher Alan I. Leshner
Publisher Beth Rosner **Chief Digital Media Officer** Rob Covey

BUSINESS OPERATIONS AND ADMINISTRATION DIRECTOR Deborah Rivera-Wienhold **BUSINESS SYSTEMS AND FINANCIAL ANALYSIS DIRECTOR** Randy Yi **MANAGER OF FULFILLMENT SYSTEMS** Neal Hawkins **SYSTEMS ANALYST** Nicole Mehmedovich **ASSISTANT DIRECTOR, BUSINESS OPERATIONS** Eric Knott **MANAGER, BUSINESS OPERATIONS** Jessica Tierney **BUSINESS ANALYSTS** Cory Lipman, Cooper Tilton, Celeste Troxler **FINANCIAL ANALYST** Jeremy Clay **RIGHTS AND PERMISSIONS ASSISTANT DIRECTOR** Emilie David **PERMISSIONS ASSOCIATE** Elizabeth Sandler **RIGHTS, CONTRACTS, AND LICENSING ASSOCIATE** Lili Kiser

MARKETING DIRECTOR Ian King **MARKETING MANAGER** Julianne Wielga **MARKETING ASSOCIATE** Elizabeth Sattler **SR. MARKETING EXECUTIVE** Jennifer Reeves **SR. ART ASSOCIATE, PROJECT MANAGER** Tzeitel Sorrosa **ART ASSOCIATE** Seil Lee **ASSISTANT COMMERCIAL EDITOR** Selby Frame **MARKETING PROJECT MANAGER** Angelissa McArthur **SR. WRITER** Bill Zimmer **PROGRAM DIRECTOR, AAAS MEMBER CENTRAL** Peggy Mihelich **FULFILLMENT SYSTEMS AND OPERATIONS** membership@aaas.org **MANAGER, MEMBER SERVICES** Pat Butler **SPECIALISTS** LaToya Casteel, Javia Flemmings, Latasha Russell **MANAGER, DATA ENTRY** Mickie Napoleoni **DATA ENTRY SPECIALISTS** JJ Regan, Jaimee Wise, Fiona Giblin

DIRECTOR, SITE LICENSING Tom Ryan **DIRECTOR, CORPORATE RELATIONS** Eileen Bernadette Moran **SR. PUBLISHER RELATIONS SPECIALIST** Kiki Forsythe **PUBLISHER RELATIONS MANAGER** Catherine Holland **PUBLISHER RELATIONS, EASTERN REGION** Keith Layson **PUBLISHER RELATIONS, WESTERN REGION** Ryan Rexroth **MANAGER, SITE LICENSE OPERATIONS** Iquo Edim **FULFILLMENT ANALYST** Lana Guz **ASSOCIATE DIRECTOR, MARKETING** Christina Schlecht **MARKETING ASSOCIATES** Thomas Landreth, Minah Kim

DIRECTOR OF WEB TECHNOLOGIES Ahmed Khadr **SR. DEVELOPER** Chris Coleman **DEVELOPER** Dan Berger **SR. PROJECT MANAGER** Trista Smith **SYSTEMS ENGINEER** Luke Johnson **PRODUCT MANAGER** Walter Jones

CREATIVE DIRECTOR, MULTIMEDIA Martyn Green **DIRECTOR OF ANALYTICS** Enrique Gonzales **SR. WEB PRODUCER** Sarah Crespi **WEB PRODUCER** Alison Crawford **VIDEO PRODUCER** Nguyen Nguyen **SOCIAL MEDIA PRODUCER** Meghna Sachdev

DIRECTOR OF OPERATIONS PRINT AND ONLINE Lizabeth Harman **PRINT PRODUCTION DIRECTOR** Wendy K. Shank **PREFLIGHT MANAGER** Marcus Spiegler **ASSISTANT MANAGER ONLINE** Lisa Stanford **ASSISTANT MANAGER PRINT** Rebecca Doshi **SR SPECIALISTS** Steve Forrester, Jason Hillman, Antoinette Hodal, Tara Kelly, Anthony Rosen **SPECIALISTS** Jacob Hedrick, Nichele Johnston, Lori Murphy, Kimberley Oster

DESIGN DIRECTOR Beth Rakouskas **ASSOCIATE ART DIRECTOR** Laura Creveling **SR. ILLUSTRATORS** Chris Bickel, Katharine Sutliff **ILLUSTRATOR** Valerie Altounian **SR. ART ASSOCIATES** Holly Bishop, Preston Huey **ART ASSOCIATES** Kay Engman, Garvin Grullón, Chrystal Smith **SR. PHOTO EDITOR** William Douthitt **PHOTO EDITOR** Leslie Blizard

DIRECTOR, GLOBAL COLLABORATION, CUSTOM PUBLICATIONS, ADVERTISING Bill Moran **EDITOR, CUSTOM PUBLISHING** Sean Sanders: 202-326-6430 **ASSISTANT EDITOR, CUSTOM PUBLISHING** Tianna Hicklin: 202-326-6463 **ADVERTISING MARKETING MANAGER** Justin Sawyers: 202-326-7061 science_advertising@aaas.org **ADVERTISING MARKETING ASSOCIATE** Javia Flemmings **ADVERTISING SUPPORT MANAGER** Karen Foote: 202-326-6740 **ADVERTISING PRODUCTION OPERATIONS MANAGER** Deborah Tompkins **SR. PRODUCTION SPECIALIST/GRAPHIC DESIGNER** Amy Hardcastle **PRODUCTION SPECIALIST** Yuse Lajiminmuhip **SR. TRAFFIC ASSOCIATE** Christine Hall **SALES COORDINATOR** Shirley Young **ASSOCIATE DIRECTOR, COLLABORATION, CUSTOM PUBLICATIONS/CHINA/TAIWAN/KOREA/SINGAPORE** Ruolei Wu: +86-186 0822 9345, rwu@aaas.org **COLLABORATION/CUSTOM PUBLICATIONS/JAPAN** Adarsh Sandhu + 81532-81-5142 asandhu@aaas.org **EAST COAST/E. CANADA** Laurie Faraday: 508-747-9395, FAX 617-507-8189 **WEST COAST/W. CANADA** Lynne Stickrod: 415-931-9782, FAX 415-520-6940 **MIDWEST** Jeffrey Dembksi: 847-498-4520 x3005, Steven Loerch: 847-498-4520 x3006 **UK EUROPE/ASIA** Roger Goncalves: TEL/FAX +41 43 243 1358 **JAPAN** Katsuyoshi Fukamizu(Tokyo): +81-3-3219-5777 kfukamizu@aaas.org **CHINA/TAIWAN** Ruolei Wu: +186-0082-9345

WORLDWIDE ASSOCIATE DIRECTOR OF SCIENCE CAREERS Tracy Holmes: +44 (0) 1223 326525, FAX +44 (0) 1223 326532 tholmes@science-int. co.uk **CLASSIFIED** advertise@sciencecareers.org **U.S. SALES** Tina Burks: 202-326-6577, Nancy Toema: 202-326-6578 **SALES ADMINISTRATOR** Marci Gallun **EUROPE/ROW SALES** Axel Gesatzki, Sarah Lelarge **SALES ASSISTANT** Kelly Grace **JAPAN** Hiroyuki Mashiki(Kyoto): +81-75-823-1109 hmashiki@aaas.org **CHINA/TAIWAN** Ruolei Wu: +86-186 0082 9345 rwu@aaas.org **MARKETING MANAGER** Allison Pritchard **MARKETING ASSOCIATE** Aimee Aponte

AAAS BOARD OF DIRECTORS RETIRING PRESIDENT, CHAIR Phillip A. Sharp **PRESIDENT** Gerald R. Fink **PRESIDENT-ELECT** Geraldine (Geri) Richmond **TREASURER** David Evans Shaw **CHIEF EXECUTIVE OFFICER** Alan I. Leshner **BOARD** Bonnie L. Bassler, May R. Berenbaum, Carlos J. Bustamante, Claire M. Fraser, Laura H. Greene, Elizabeth Loftus, Raymond Orbach, Inder M. Verma

SUBSCRIPTION SERVICES For change of address, missing issues, new orders and renewals, and payment questions: 866-434-AAAS (2227) or 202-326-6417, FAX 202-842-1065. Mailing addresses: AAAS, P.O. Box 96178, Washington, DC 20090-6178 or AAAS Member Services, 1200 New York Avenue, NW, Washington, DC 20005

INSTITUTIONAL SITE LICENSES 202-326-6755 **REPRINTS:** Author Inquiries 800-635-7181 **COMMERCIAL INQUIRIES** 803-359-4578 **PERMISSIONS** 202-326-6765, permissions@aaas.org **AAAS Member Services** 202-326-6417 or http://membercentral.aaas.org/discounts

Science serves as a forum for discussion of important issues related to the advancement of science by publishing material on which a consensus has been reached as well as including the presentation of minority of conflicting points of view. Accordingly, all articles published in *Science*—including editorials, news and comment, and books reviews—are signed and reflect the individual views of the authors and not official points of view adopted by AAAS or the institutions with which the authors are affiliated.

INFORMATION FOR AUTHORS See pages 680 and 681 of the 7 February 2014 issue or access www.sciencemag.org/about/authors

SENIOR EDITORIAL BOARD
A. Paul Alivisatos, *Lawrence Berkeley Nat'l. Laboratory,* **Ernst Fehr,** *U. of Zürich*
Susan M. Rosenberg, *Baylor College of Medicine,* **Michael S. Turner,** *U. of Chicago*

BOARD OF REVIEWING EDITORS (Statistics board members indicated with **(S)**)
Adriano Aguzzi, *U. Hospital Zürich*
Takuzo Aida, *U. of Tokyo*
Leslie Aiello, *Wenner-Gren Foundation*
Judith Allen, *U. of Edinburgh*
Sonia Altizer, *U. of Georgia*
Virginia Armbrust, *U. of Washington*
Sebastian Amigorena, *Institut Curie*
Kathryn Anderson, *Memorial Sloan-Kettering Cancer Center*
Peter Andolfatto, *Princeton U.*
Meinrat O. Andreae, *Max-Planck Inst. Mainz*
Paola Arlotta, *Harvard U.*
Johan Auwerx, *EPFL*
David Awschalom, *U. of Chicago*
Jordi Bascompte, *Estación Biológica de Doñana CSIC*
Facundo Batista, *London Research Inst.*
Ray H. Baughman, *U. of Texas, Dallas*
David Baum, *U. of Wisconsin*
Mark Bear, *Massachusetts Inst. of Technology*
Kamran Behnia, *ESPCI-ParisTech*
Yasmine Belkaid, *NIAID, NIH*
Philip Benfey, *Duke U.*
Stephen J. Benkovic, *Penn State U.*
Gabriele Bergers, *U. of California, San Francisco*
Christophe Bernard, *Aix-Marseille U.*
Bradley Bernstein, *Massachusettes General Hospital.*
Peer Bork, *EMBL*
Bernard Bourdon, *Ecole Normale Supérieure de Lyon*
Chris Bowler, *École Normale Supérieure*
Ian Boyd, *U. of St. Andrews*
Emily Brodsky, *U. of California, Santa Cruz*
Ron Brookmeyer, *U. of California Los Angeles* **(S)**
Christian Büchel, *U. Hamburg-Eppendorf*
Joseph A. Burns, *Cornell U.*
William P. Butz, *Population Reference Bureau*
Gyorgy Buzsaki, *New York U. School of Medicine*
Blanche Capel, *Duke U.*
Mats Carlsson, *U. of Oslo*
David Clapham, *Children's Hospital Boston*
David Clary, *U. of Oxford*
Joel Cohen, *Rockefeller U., Columbia U.*
Jonathan D. Cohen, *Princeton U.*
James Collins, *Boston U.*
Robert Cook-Deegan, *Duke U.*
Alan Cowman, *Walter & Eliza Hall Inst.*
Robert H. Crabtree, *Yale U.*
Janet Currie, *Princeton U.*
Jeff L. Dangl, *U. of North Carolina*
Tom Daniel, *U. of Washington*
Frans de Waal, *Emory U.*
Stanislas Dehaene, *Collège de France*
Robert Desimone, *MIT*
Claude Desplan, *New York U.*
Ap Dijksterhuis, *Radboud U. of Nijmegen*
Dennis Discher, *U. of Pennsylvania*
Gerald W. Dorn II, *Washington U. School of Medicine*
Jennifer A. Doudna, *U. of California, Berkeley*
Bruce Dunn, *U. of California, Los Angeles*
Christopher Dye, *WHO*
Todd Ehlers, *U. of Tuebingen*
David Ehrhardt, *Carnegie Inst. of Washington*
Tim Elston, *U. of North Carolina at Chapel Hill*
Gerhard Ertl, *Fritz-Haber-Institut, Berlin*
Barry Everitt, *U. of Cambridge*
Ernst Fehr, *U. of Zurich*
Anne C. Ferguson-Smith, *U. of Cambridge*
Michael Feuer, *The George Washington U.*
Peter Fratzl, *Max-Planck Inst.*
Elaine Fuchs, *Rockefeller U.*
Daniel Geschwind, *UCLA*
Andrew Gewirth, *U. of Illinois*
Karl-Heinz Glassmeier, *TU Braunschweig*
Julia R. Greer, *Caltech*
Elizabeth Grove, *U. of Chicago*
Kip Guy, *St. Jude's Children's Research Hospital*
Taekjip Ha, *U. of Illinois at Urbana-Champaign*
Christian Haass, *Ludwig Maximilians U.*
Steven Hahn, *Fred Hutchinson Cancer Research Center*
Michael Hasselmo, *Boston U.*
Martin Heimann, *Max-Planck Inst. Jena*
Yka Helariutta, *U. of Finland*
James A. Hendler, *Rensselaer Polytechnic Inst.*
Janet G. Hering, *Swiss Fed. Inst. of Aquatic Science & Technology*
Michael E. Himmel, *National Renewable Energy Lab.*
Kai-Uwe Hinrichs, *U. of Bremen*
Kei Hirose, *Tokyo Inst. of Technology*
David Hodell, *U. of Cambridge*
David Holden, *Imperial College*
Lora Hooper, *UT Southwestern Medical Ctr. at Dallas*
Thomas Hudson, *Ontario Inst. for Cancer Research*
Raymond Huey, *U. of Washington*
Steven Jacobsen, *U. of California, Los Angeles*
Kai Johnsson, *EPFL Lausanne*
Peter Jonas, *Inst. of Science & Technology (IST) Austria*
Matt Kaeberlein, *U. of Washington*
William Kaelin Jr., *Dana-Farber Cancer Inst.*
Daniel Kahne, *Harvard U.*
Daniel Kammen, *U. of California, Berkeley*
Masashi Kawasaki, *U. of Tokyo*
Joel Kingsolver, *U. of North Carolina at Chapel Hill*
Robert Kingston, *Harvard Medical School*
Alexander Kolodkin, *Johns Hopkins U.*
Roberto Kolter, *Harvard Medical School*
Alberto R. Kornblihtt, *U. of Buenos Aires*
Leonid Kruglyak, *UCLA*
Thomas Langer, *U. of Cologne*
Mitchell A. Lazar, *U. of Pennsylvania*
David Lazer, *Harvard U.*
Thomas Lecuit, *IBDM*
Virginia Lee, *U. of Pennsylvania*
Stanley Lemon, *U. of North Carolina at Chapel Hill*
Ottoline Leyser, *Cambridge U.*
Marcia C. Linn, *U. of California, Berkeley*
Jianguo Liu, *Michigan State U.*
Luis Liz-Marzan, *CIC biomaGUNE*
Jonathan Losos, *Harvard U.*
Ke Lu, *Chinese Acad. of Sciences*
Christian Lüscher, *U. of Geneva*
Laura Machesky, *CRUK Beatson Inst. for Cancer Research*
Anne Magurran, *U. of St. Andrews*
Oscar Marin, *CSIC & U. Miguel Hernández*
Charles Marshall, *U. of California, Berkeley*
C. Robertson McClung, *Dartmouth College*
Graham Medley, *U. of Warwick*
Yasushi Miyashita, *U. of Tokyo*
Richard Morris, *U. of Edinburgh*
Alison Motsinger-Reif, *NC State U.* **(S)**
Sean Munro, *MRC Lab. of Molecular Biology*
Thomas Murray, *The Hastings Center*
James Nelson, *Stanford U. School of Med.*
Karen Nelson, *J. Craig Venter Institute*
Daniel Neumark, *U. of California, Berkeley*
Timothy W. Nilsen, *Case Western Reserve U.*
Pär Nordlund, *Karolinska Inst.*
Helga Nowotny, *European Research Advisory Board*
Ben Olken, *MIT*
Luke O'Neill, *Trinity College, Dublin*
Joe Orenstein, *U. of California Berkeley & Lawrence Berkeley National Lab*
Harry Orr, *U. of Minnesota*
Andrew Oswald, *U. of Warwick*
Steve Palumbi, *Stanford U.*
Jane Parker, *Max-Planck Inst. of Plant Breeding Research*
Giovanni Parmigiani, *Dana-Farber Cancer Inst.* **(S)**
Donald R. Paul, *U. of Texas, Austin*
John H. J. Petrini, *Memorial Sloan-Kettering Cancer Center*
Joshua Plotkin, *U. of Pennsylvania*
Philippe Poulin, *CNRS*
David Randall, *Colorado State U.*
Colin Renfrew, *U. of Cambridge*
Trevor Robbins, *U. of Cambridge*
Jim Roberts, *Fred Hutchinson Cancer Research Ctr.*
Barbara A. Romanowicz, *U. of California,Berkeley*
Jens Rostrup-Nielsen, *Haldor Topsoe*
Mike Ryan, *U. of Texas, Austin*
Mitinori Saitou, *Kyoto U.*
Shimon Sakaguchi, *Kyoto U.*
Miquel Salmeron, *Lawrence Berkeley National Lab*
Jürgen Sandkühler, *Medical U. of Vienna*
Alexander Schier, *Harvard U.*
Randy Seeley, *U. of Cincinnati*
Vladimir Shalaev, *Purdue U.*
Robert Siliciano, *Johns Hopkins School of Medicine*
Joseph Silk, *Institut d'Astrophysique de Paris*
Denis Simon, *Arizona State U.*
Alison Smith, *John Innes Centre*
Richard Smith, *U. of North Carolina* **(S)**
John Speakman, *U. of Aberdeen*
Allan C. Spradling, *Carnegie Institution of Washington*
Jonathan Sprent, *Garvan Inst. of Medical Research*
Eric Steig, *U. of Washington*
Paula Stephan, *Georgia State U. and National Bureau of Economic Research*
Molly Stevens, *Imperial College London*
V. S. Subrahmanian, *U. of Maryland*
Ira Tabas, *Columbia U.*
Sarah Teichmann, *Cambridge U.*
John Thomas, *North Carolina State U.*
Christopher Tyler-Smith, *The Wellcome Trust Sanger Inst.*
Herbert Virgin, *Washington U.*
Bert Vogelstein, *Johns Hopkins U.*
Cynthia Volkert, *U. of Göttingen*
Douglas Wallace, *Dalhousie U.*
David Wallach, *Weizmann Inst. of Science*
Ian Walmsley, *U. of Oxford*
David A. Wardle, *Swedish U. of Agric. Sciences*
David Waxman, *Fudan U.*
Jonathan Weissman, *U. of California, San Francisco*
Chris Wikle, *U. of Missouri* **(S)**
Ian A. Wilson, *The Scripps Res. Inst.* **(S)**
Timothy D. Wilson, *U. of Virginia*
Rosemary Wyse, *Johns Hopkins U.*
Jan Zaanen, *Leiden U.*
Kenneth Zaret, *U. of Pennsylvania School of Medicine*
Jonathan Zehr, *U. of California, Santa Cruz*
Len Zon, *Children's Hospital Boston*
Maria Zuber, *MIT*

BOOK REVIEW BOARD
David Bloom, *Harvard U.,* **Samuel Bowring,** *MIT,* **Angela Creager,** *Princeton U.,* **Richard Shweder,** *U. of Chicago,* **Ed Wasserman,** *DuPont*

Published by AAAS

EDITORIAL

A swan in the making

Reproducibility is the ugly duckling of science. It provokes distress, denial, and passionate calls for action. With $1.5 trillion spent globally each year on R&D,* the idea that 80% of it is irreproducible† can cause downright dread. It threatens the foundations and credibility of the scientific enterprise. But look past the surface, and reproducibility may well be a swan in the making.

In my previous role in industrial microbe and process engineering, I saw quality practices double the productivity of R&D and deliver microbes from half-liter fermentations to 200,000-liter manufacturing with absolute performance reproducibility. That kind of outcome is electrifying.

Achieving such reproducibility in every lab may offer one of the greatest opportunities in decades to advance the practice of science. The path to transformation already exists; we need only look into the "unsexy" world of manufacturing to learn.

After World War II, the teachings of engineer W. Edwards Deming on quality helped revolutionize a Japanese manufacturing industry then known for cheap, unreliable products. By the 1980s, the quality of Japanese products was shaking the foundations of American electronics and car companies. Today, such uncompromising quality is ubiquitous and expected.

This kind of quality didn't "just happen." When I was an intern at a General Motors subsidiary in the 1980s, the halls were rife with complaints that it was impossible to meet new and stricter specifications. Discussions today in the halls of science are not so different. Researchers complain about the seemingly impossible task of tracking all the variables needed to ensure reproducibility; they question whether the obsession with reproducibility is overkill; and they fear that the methods of quality improvement will snuff out the flexibility needed to innovate.

Such reactions are actually quite correct. Today's methods of manufacturing quality are too cumbersome and too restrictive for the dynamic and evolutionary nature of scientific thinking.

It's time to fix that.

Behavioral economics has shown that removing even trivial hurdles can vastly improve the adoption of beneficial practices. In one randomized study, people were 29% more likely to attend college when their student aid forms were automatically populated.‡ Similarly, the digital capabilities in your pocket can lower the barriers to quality by automating most of its complexity. For example, my own company is building tools to automate data acquisition via mobile devices, break down lab procedures into modular steps that are evolvable and reusable like lines of software code, and automatically analyze data trends within and across experiments to catch errors and their root causes. Other companies are also contributing to a fast-growing ecosystem of related tools.

"Achieving reproducible research...will take a collective movement to change the incentives, culture, and tool sets of science."

Achieving reproducible research—research we can trust and build on efficiently, like high-quality parts in a supply chain—will take a collective movement to change the incentives, culture, and tool sets of science. The good news is that movement has begun. Publishers, funders, foundations, universities, regulators, and companies are raising visibility, developing standards, and creating tools and incentives that make reproducible research more accessible and more rewarding.

It is often said that the first step in solving a problem is recognizing that you have one. Step one...check. The scientific community is aware and taking action. The ugly duckling is becoming a swan.

– Timothy Gardner

Timothy Gardner is chief executive officer of Riffyn, Inc., in Oakland, CA, and an advisor to the European Union Scientific Committees. E-mail: tg@riffyn.com

*M. Grueber, T. Studt, *R&D Magazine* (December 2012). †F. Prinz *et al.*, *Nat. Rev. Drug Discovery* **10**, 712 (2011). ‡E. P. Bettinger *et al.*, *The Role of Simplification and Information in College Decisions* (National Bureau of Economic Research, Cambridge, MA, 2009).

10.1126/science.1259740

PHOTOS: (RIGHT) WENDY GARDNER; (INSET) ANDREAS KRONE/ISTOCKPHOTO.COM

Downloaded from www.sciencemag.org on August 24, 2014

Published by AAAS

NEWS

> “Um … no. That’s a prank.”
>
> **Google software engineer** in response to an anonymous e-mail tip on 12 August, claiming that Google was secretly planning to create an online platform that would allow scientists to publish their research for free and keep data and papers open access forever.

IN BRIEF

Glowing plasma in a polywell fusion reactor.

U.S. to fund unconventional fusion

ARPA-E, the U.S. government agency for funding innovative energy technologies, is preparing to launch a program to support alternative approaches to fusion energy that might steal a march on existing mainstream projects. The new funding stream, called Accelerating Low-cost Plasma Heating and Assembly, will target the largely untested middle ground between the two main standard approaches to fusion energy: tokamaks, which confine ionized gases called plasmas at low densities for long periods of time, and laser fusion, which squeezes plasmas to extremely high density for billionths of a second. The Department of Energy previously funded other moderate-density approaches through a program called High Energy Density Plasma (HEDP). But the ballooning cost of the U.S. contribution to the international ITER fusion reactor project in France put a squeeze on such experiments, and HEDP was zeroed out of the budget last October. ARPA-E gave researchers advance notice of the funding program on 11 August; a formal announcement could come within weeks. http://scim.ag/fusionUS

AROUND THE WORLD

WHO eyes Ebola survivors’ serum

GENEVA, SWITZERLAND | Desperate to treat Ebola patients in West Africa, the World Health Organization (WHO) is considering using blood from people who have recovered from the infection. Convalescent serum was first tried on an Ebola patient in 1976, after the first documented outbreak, and was used in eight patients in 1995. A U.S. health care worker in Liberia was treated with serum late last month. The approach is appealing because it wouldn’t require regulatory approval, and there are many survivors who could supply blood. But researchers debate whether the treatment has really caused improvement. WHO has no official plans to administer the serum to ill people but says it will assess whether the approach is “safe and feasible.” http://scim.ag/WHOserum

Velvet worm ancestor revealed

CAMBRIDGE, U.K. | *Hallucigenia sparsa*, an extinct 3.5-centimeter-long worm discovered nearly 40 years ago as a fossil in the Burgess Shale in the Canadian Rockies, has never quite fit into the evolutionary tree. Scientists have confused the ocean dweller’s defensive dorsal spines with its legs and its tail with its head. This week, however, a study online in *Nature* identifies the 505-million-year-old creature as an ancestor of modern velvet worms, based on its spiny claws. Velvet worms use their spiny claws to navigate uneven terrain, as *Hallucigenia* might have on the sea floor.

Fossil of *Hallucigenia sparsa* in the Burgess Shale.

PHOTOS: (TOP TO BOTTOM) EMC2; M. R. SMITH/SMITHSONIAN INSTITUTION

Downloaded from www.sciencemag.org on August 24, 2014

Published by AAAS

Baby Amazonian turtles chirp to one another as they hatch.

The talkative turtles of the Amazon River

Once per dry season in Brazil, based on some unseen cue, female giant South American river turtles decide that it's time to leave the Amazon River to lay their eggs. Clambering ashore in single file, with impressive coordination they spread out across the beach to dig their sandy nests. The apparent secret to the threatened species' teamwork: good communication. After analyzing 220 hours of audio recordings of turtles in the wild, researchers found six different types of vocalization correlated with specific behaviors, such as gathering together, or waiting for hatchlings to enter the Amazon. Baby turtles also seem to talk to each other while hatching, possibly coordinating their first migration to the river, the research team reports in the latest issue of the quarterly journal *Herpetologica*. The study provides the first evidence that turtles use vocalizations to synchronize activities and rear young, the group says. **http://scim.ag/turtlestalk**

Museum IDs skeleton in closet

PHILADELPHIA, PENNSYLVANIA | An unmarked skeleton lurking for decades in storage at the University of Pennsylvania (Penn) Museum of Archaeology and Anthropology has been identified. The 6500-year-old skeleton, of a man probably in his 50s who lived in the ancient Mesopotamian city-state of Ur, was obtained during excavations led by British archaeologist Leonard Woolley from 1922 to 1934 in southern Iraq. Penn Museum archaeologists looking over Woolley's notes discovered to their surprise that he had saved two skeletons for the museum; his description of one of the skeletons exactly matched that of their mystery body. The museum now plans to digitally recreate the skeleton for a virtual display. Meanwhile, the second skeleton is still waiting to be found. **http://scim.ag/Pennskeleton**

A 6500-year-old skeleton from the ancient city-state of Ur.

PHOTOS: (TOP TO BOTTOM) PROVIDED BY R. C. VOGT/INPA; MATT ROURKE/AP PHOTO

BY THE NUMBERS

581

Metric tons of precursor chemical for sarin gas removed from Syria and destroyed, according to the Organisation for the Prohibition of Chemical Weapons.

40%

Fraction of Americans who will develop type 2 diabetes at some point during their adult lives, according to a study in *The Lancet Diabetes & Endocrinology*.

58

Millions of dollars spent by the National Institutes of Health in research funds for papers retracted due to scientific misconduct between 1992 and 2012—less than 1% of the agency's spending during that period, according to an analysis in *eLife*.

DARPA chikungunya challenge

ARLINGTON, VIRGINIA | The U.S. Department of Defense has launched its first health-related challenge, focusing on a mosquito-borne virus of increasing concern in the Western hemisphere. The Defense Advanced Research Projects Agency last week announced a $150,000 prize for the team whose model can best predict where and how chikungunya virus might spread in the Americas and the Caribbean over the next 6 months. Although rarely fatal, chikungunya causes fever, joint pain, headache, and rash, and no vaccine is available. The first locally acquired U.S. cases were reported last month in Florida. A better forecasting method might also be applicable to other infectious diseases. **http://scim.ag/_chik**

Published by AAAS

Portrait of astronomer Brahe by an unknown painter, circa 1620s.

A Brahe in your boudoir

The landed gentry once kept prized scientific prints under lock and key in their private libraries. But the new print-on-demand service by the United Kingdom's Royal Society provides a visual feast of scientific history to anyone with a credit card. Accessorize your kitchen with a 1-meter-tall reproduction of an 1807 illustration of a turkey's gizzard by noted naturalist William Clift. Decorate your office with microscopic views of silk and taffeta drawn in 1665 by scientific pioneer Robert Hooke. Adorn your bedroom with a portrait of Danish astronomer Tycho Brahe that includes his prosthetic nose. (He lost his in a duel.) From landmark botanical studies to paintings of famous scientific buildings, some 2500 images from the society's library and archives are available for order at prints.royalsociety.org.

A DIY digital supercollider

GENEVA, SWITZERLAND | Hunt the Higgs boson with *Particle Clicker*, a nerdily addictive game in which you manage a fictitious supercollider, gaining "data," "reputation," and "funding" points through furious clicking and measured choices. Researching certain particles provides rewards and physics lessons. ("The J/ψ meson consists of a c and an anti-c quark.") Meanwhile, you can also invest in postdocs ("here only to serve your needs"), an accelerator upgrade ("[T]hree times more data"), or beer ("Students will produce +2 data"). The game won a hackathon this month at CERN. "We wanted to make the content so that the people who live and work here at CERN get the jokes," says Gábor Bíró, one of five current or former summer students who built the game.

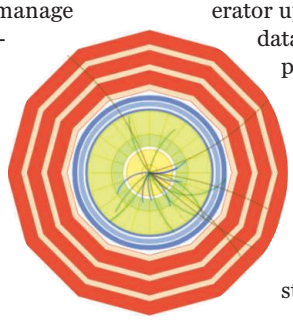

For particle-smashing fun, click here.

Indian students flock to U.S.

WASHINGTON, D.C. | For the second straight year, the number of Indian students applying to graduate programs at U.S. universities has skyrocketed, and the number of Chinese applicants has stagnated. Applications from Indian students to the 285 schools responding to a survey by the Council of Graduate Schools (CGS) soared by 33% this year, after a jump of 22% in 2013, while 1% fewer Chinese students applied, compounding a 3% drop in 2013. Offers of admission to Chinese students were flat for the first time in 8 years. "We started seeing these trends last year," says CGS's Jeff Allum. "Now we are more and more convinced it's real and not just a blip." http://scim.ag/india-ap

NEWSMAKERS

Three Q's

Those who bemoan a scientifically illiterate public are misdiagnosing society's problem, says German psychologist **Gerd Gigerenzer** of the Max Planck Institute for Human Development in Berlin in his new book *Risk Savvy: How to Make Good Decisions*. Gigerenzer talked with *Science* about why he says understanding risk is "the lifeblood of a democracy."

Q: What is "risk literacy"?
A: Understanding scientific topics is one element, but also how to evaluate decisions amid uncertainty.

Q: What's required for risk literacy, and why does it matter?
A: You need both statistical reasoning and intuition. When I asked decision-makers in a number of major companies, I found that 50% of all decisions were gut decisions. But managers will not dare admit that. Instead, a manager will hire a consulting firm that provides a 200-page document and present the gut decision as fact-based. Billions are wasted in this way.

Q: What can scientists do?
A: Health researchers could use their results to train doctors to understand risk. Just as doctors need to understand what a positive screening test means, I have trained judges to understand uncertainty in DNA test results. But both medical schools and law schools don't teach that [well].

CREDITS: (TOP LEFT TO RIGHT) © THE ROYAL SOCIETY; © MAX PLANCK INSTITUTE FOR HUMAN DEVELOPMENT/DIETMAR GUST; (BOTTOM) *PARTICLE CLICKER*/CERN

Published by AAAS

IN DEPTH

POLITICAL SCIENCE

Study exposes Chinese censors' deepest fears

The power of the masses proves most unnerving

By **Mara Hvistendahl**, *in Shanghai, China*

Police corral a man in Shanghai in February 2011 in response to Internet exhortations for a "Jasmine Revolution."

PHOTO: CARLOS BARRIA/REUTERS/CORBIS

Behind China's vaunted system of Internet censorship are throngs of specialized police officers, fake commentators, and ever-changing technologies. But China watchers have puzzled over the system's modus operandi. Some posts are swiftly culled, whereas others on seemingly more sensitive topics are left untouched. In the most revealing study yet of Chinese censorship, on page 891 researchers at Harvard University describe how they peered behind the curtain to find out what China's censors—and presumably the government officials operating behind the scenes—fear most: discussion of mass protests and other forms of collective action.

The unprecedented participatory experiment on China's blogs, microblogs, and forums "probes much deeper than earlier studies," says Noah Smith, a computer scientist at Carnegie Mellon University in Pittsburgh, Pennsylvania, who was not involved with the paper. The study also flouts the conventional wisdom that the censorship apparatus is designed to squelch criticism of the Communist Party or its leaders.

China's Internet censorship is thought to be the most pervasive in the world. Online forums employ in-house censors whom users playfully dub "big mamas," while so-called "50-cent party members" post pro-government comments on social media sites. (The moniker stems from the fee they supposedly receive for each post.) And according to state media, a veritable army of 2 million government employees monitors microblogs and drafts reports on blog posts for leaders.

Those soldiers are not always marching to the same tune. Lists of censored keywords—terms that automatically get a post deleted or flagged for review—vary from location to location and from one website to the next. Complicating the task for researchers, social media in China is highly decentralized. Whereas Twitter, Facebook, and a few others dominate in the United States, in China users split their attention among hundreds of websites, some of which are tied to local areas and don't allow outsiders to post. "The logistics of studying that are complicated," says political scientist Gary King of the Institute for Quantitative Social Science at Harvard University.

When King and Ph.D. students Jennifer Pan and Margaret Roberts began examining censorship in China in 2011, many scholars assumed that calling for policy changes, criticizing government leaders, and raising sensitive topics like the Tiananmen Square crackdown in 1989 were verboten. To test that assumption, the trio downloaded millions of social media posts from more than 1300 sites between January and July 2011, then selected roughly 127,000 of them to examine in more detail. Hoping that an analysis of which posts were deleted and which were allowed to stand might offer a "bird's-eye view of [a] very heterogeneous process," King says, they watched in real time as posts were taken down. Censorship in China, King says, is "like an elephant tiptoeing around. It leaves big footprints."

In most cases, censors reacted swiftly, deleting messages within a day of posting. They also seemed to follow a surprising logic. The researchers found that posts on topics they themselves classified as highly sensitive were only slightly more likely than average to be deleted—24% of posts, versus 13% overall. That was "completely unexpected," King says. They next looked at bursts of posts following significant events. During events with potential for collective action, the vast majority of posts were censored—regardless of whether they supported or criticized the state.

That study, published in *American Political Science Review* in May 2013, was blind to posts that never went online in the first place because they were snagged in an automated censorship filter. To truly understand what is censored in China, King and colleagues realized, they would need to write their own posts. And that meant creating the first randomized experimental study on censorship in China.

Over three 1- to 2-week periods last year, the researchers oversaw assistants in China and the United States who opened 200 user accounts at 100 sites and then authored 1200 unique posts. Some commented on events

Downloaded from www.sciencemag.org on August 24, 2014

Published by AAAS

involving collective action, such as volatile demonstrations over government land grabs in Fujian province. Others responded to events involving no collective action, like a corruption investigation of a provincial vice governor. For each event, the assistants authored both pro- and antigovernment posts.

Within the same period, the researchers found, posts advocating collective action were between 20% and 40% more likely to be censored than were posts not advocating it. Posts critical of the government, on the other hand, were not significantly more likely to be censored than supportive posts—even when they called out leaders by name. "Criticisms of the state are quite useful for the government in identifying public sentiment, whereas the spread of collective action is potentially very damaging," Roberts explains. China's so-called Jasmine Revolution, in which protesters inspired by the Arab Spring in early 2011 called for democracy, is a case in point. Many sites promptly blocked words like "jasmine" and "Egypt."

To trawl for insights into how the censorship machine works, the researchers set up a bulletin board system—a popular type of community forum in China—and asked for advice about "how to stay out of trouble with the Chinese government," King says. Staff at the software platform they used cheerfully answered questions posed online and by phone. (The trio "didn't advertise that we were Harvard researchers," King says, and no one asked their identities.) One piece of advice was to muscle up on staff who can watch for troublesome posts: Even when a site uses automated review, King says, most posts are still vetted by a pair of eyeballs.

The Harvard team didn't demystify the process entirely. Yu Xie, a sociologist at the University of Michigan, Ann Arbor, says that although the study is methodologically sound, it overemphasizes the importance of coherent central government motives. Political outcomes in China, he notes, often rest on local officials, who are evaluated on how well they maintain stability. Such officials have a "personal interest in suppressing content that could lead to social movements," Xie says.

One factor that complicates any study of censorship in China is a rapidly shifting social media landscape. Local governments now frequently insert themselves into conversations as well as control them. And the study omitted WeChat, a burgeoning social network set up by Chinese Internet giant Tencent that combines features from Facebook and the mobile application WhatsApp. Earlier this year, the app started censoring keywords and in some cases deleting entire accounts. That, King says, may be fodder for future studies. ■

CLIMATE CHANGE

Is Atlantic holding Earth's missing heat?

New leads in the hunt to explain the global warming hiatus

By **Eli Kintisch**

Armchair detectives might call it the case of Earth's missing heat: Why have average global surface air temperatures remained essentially steady since 2000, even as greenhouse gases have continued to accumulate in the atmosphere? The suspects include changes in atmospheric water vapor, a strong greenhouse gas, or the noxious sunshade of haze emanating from factories. Others believe the culprit is the mighty Pacific Ocean, which has been sending vast slugs of cold bottom water to the surface.

But two fresh investigations finger a new suspect: the Atlantic Ocean. One study, on page 897 of this issue of *Science*, presents sea temperature data implying that most of the missing heat has been stored deep in the Atlantic. The other, published online on 3 August in *Nature Climate Change*, suggests a warming Atlantic is abetting the Pacific by driving wind patterns that help that ocean cool the atmosphere. Together, the papers "raise the tantalizing possibility" that the Atlantic is playing a major role in the warming hiatus, says climate dynamicist Shang-Ping Xie of the University of California, San Diego, who was not involved in the studies.

Some climate specialists remain skeptical. In a third recent paper, published online in *Nature Climate Change* on 17 August, other researchers argue that the Pacific remains the kingpin. "It's the Pacific driving the Atlantic, not the other way around," says one of the authors, climate dynamicist Kevin Trenberth of the National Center for Atmospheric Research in Boulder, Colorado.

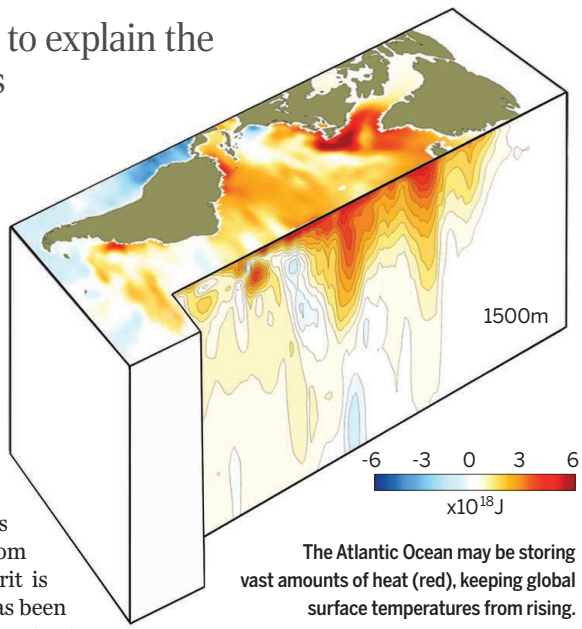

The Atlantic Ocean may be storing vast amounts of heat (red), keeping global surface temperatures from rising.

CREDIT: XIANYAO CHEN/KA-KIT TUNG

Warming takes a pause

After a rapid rise, global mean temperatures have stabilized.

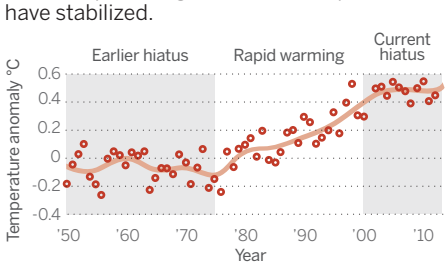

Source: Xianyao Chen/Ka-Kit Tung

The new *Science* study, from oceanographer Xianyao Chen of the Ocean University of China in Qingdao and atmospheric scientist Ka-Kit Tung of the University of Washington, Seattle, draws on tens of millions of ocean temperature and salinity measurements taken globally by buoys, floats, and ships since 1970. The data, which cover 24 depths from the sea surface down to 1500 meters, enabled the researchers to calculate how the heat content of ocean water (a measure of stored energy) has changed over time. They found that, during the hiatus, the Atlantic has been absorbing heat that would have otherwise warmed the surface. Over the last 14 years, they write, water below 300 meters in the North and South Atlantic oceans has stored more energy than the rest of the global oceans combined. "We found the missing heat," Chen concludes.

A key heat storage mechanism, they say, is the "conveyor belt" current that moves salty tropical water to the North Atlantic, where it sinks, carrying heat with it. Chen and Tung think that, because of a

Published by AAAS

natural cycle, the conveyor sped up during the 1990s and slowed around 2006. Atlantic heat storage has meanwhile "gone straight up" by 30 zettajoules (sextillion joules) since 1999, while global air temperatures remained relatively flat, Tung says. In contrast, their data show little heat being stored in the deep Pacific. "We were surprised—especially by the difference between the two oceans," Chen says.

One reason some scientists remain convinced the Pacific is behind the hiatus is a measured speedup in trade winds that drive a massive upwelling of cold water in the eastern Pacific. But there, too, the Atlantic may be responsible, modeling experiments suggest. In the 3 August *Nature Climate Change* study, scientists fed measurements of the Atlantic's warming surface temperatures into a global climate simulation. The result was a "seesaw" in which air rose over the Atlantic and fell toward the Pacific, fueling the Pacific trade winds, says climate dynamicist Axel Timmermann of University of Hawaii, Manoa, a co-author. The resulting increase in Pacific upwelling could be responsible for a global cooling effect of between 0.1° and 0.2°C, researchers have estimated, enough to explain a healthy chunk of the hiatus.

The evidence for the central role of the seesaw mechanism isn't conclusive, some climate researchers say. And in the 17 August *Nature Climate Change* study, a team led by Trenberth suggests that natural variability in the Pacific explains more than half of the hiatus. Based on data and climate simulations, they argue that a pattern known as the Pacific Decadal Oscillation, which shifts every 20 to 30 years, is driving the increased upwelling as well as other climate trends, including the rapid warming of the Arctic and recent cold winters in Europe.

A consensus about what has put global warming on pause may be years away, but climate scientist Judith Curry of the Georgia Institute of Technology in Atlanta applauds how the debate is forcing scientists to grapple with a long-standing challenge: reconciling human-caused warming with the random wiggles in the global climate system. The hunt for the missing heat also helps scientists respond to global warming misinformation, says climate scientist Michael McPhaden of the National Oceanic and Atmospheric Administration in Seattle. "Climate change denialists have made hay with [the hiatus] in an attempt to discredit the science and confuse the public," he writes in an e-mail.

The recent papers confirm that Earth's warming has continued during the hiatus, McPhaden notes, at least in the ocean depths, if not in the air. ■

A child in Ivory Coast gets the Salk vaccine.

PHOTO: UNICEF/OLIVIER ASSELIN

PUBLIC HEALTH

A one-two punch against polio

The once-sidelined injected vaccine could boost eradication

By **Leslie Roberts**

In 1988, the world set out to eradicate polio with two drops of a sugary vaccine. Compared with the injected vaccine used in wealthy countries, the live oral polio vaccine (OPV) developed by physician Albert Sabin in the 1950s was cheap—pennies as opposed to dollars a dose—and easy to use, which made it well-suited for massive immunization campaigns in poor countries where polio persisted. OPV has another benefit as well: It not only prevents paralytic disease, as does the injectable vaccine, but also blocks infection and transmission of the virus—key to wiping it out. But in the dirty, crowded corners of the world where the poliovirus hangs on, as many as 10 separate doses of OPV might be needed to confer immunity. Those areas are often tumultuous and conflict-ridden—think of northern Nigeria and the tribal areas of Pakistan—making it difficult to stage repeated vaccination campaigns.

Now, two new studies suggest that the injectable polio vaccine, sidelined long ago in the eradication effort, may offer a way out of the impasse. Published today on page 922 and online in *The Lancet* on 11 July, they show that in kids who have already received multiple doses of OPV, adding a shot of Jonas Salk's inactivated polio vaccine (IPV) can be more effective at stopping polio transmission than another dose of OPV.

Together with an early test of this combination vaccine strategy last year in a refugee camp in Kenya, the new findings could give IPV an expanded role in the Global Polio Eradication Initiative (GPEI). "This is the evidence the program has been waiting for," says Nicholas Grassly, an epidemiologist at Imperial College London and a co-author on both studies. John Modlin, deputy director of the polio program at the Bill & Melinda Gates Foundation, which funded the *Lancet* study, adds that the results suggest IPV "can play a major role in completing the goal of eradication."

Since 1988, billions of doses of OPV have been delivered in door-to-door campaigns, to remarkable effect: Global polio cases have dropped more than 99%. Wealthy countries, meanwhile, turned away from OPV because it contains live but weakened virus, which has the potential to revert to its disease-causing form. In those countries IPV, which contains only killed virus, became the vaccine of choice.

Because of the risk of outbreaks sparked by the vaccine, the use of OPV must be stopped as eradication nears. In anticipation, the World Health Organization (WHO) has called on all countries to introduce at least one dose of IPV into routine immunization by the end of 2015. But the new studies may persuade many public health experts that IPV should be brought into the polio-fighting armamentarium even before the war is won.

Downloaded from www.sciencemag.org on August 24, 2014

Published by AAAS

The two trials were conducted in India, where the battle against polio has been perhaps the most intense—the *Science* study in Moradabad in the northern state of Uttar Pradesh in 2011, and the *Lancet* in Vellore in the southern state of Tamil Nadu in 2013.

India reported its last case of polio in January 2011, but when the Moradabad study began, that victory was by no means secure. Indeed, Moradabad was the "polio heartland" at the time, says Hamid Jafari, who directs polio research and operations at WHO in Geneva, Switzerland, and who led the *Science* study. The virus thrived in the heat and the open sewers, and the huge burden of diarrhea interfered with the vaccine. In this holdout, where kids were bombarded with OPV from birth and still poliovirus circulated, OPV clearly needed some help. Jafari and his colleagues wondered if IPV might provide it.

To find out, the collaborators recruited almost 1000 kids in three age groups—6- to 11-month-olds, 5-year-olds, and 10-year-olds—who had all received multiple doses of OPV. At the start of the study, children were given either a dose of IPV or OPV, or, for controls, no vaccine. Four weeks later, each child was given a "challenge" dose of OPV, as a proxy for infection with the wild type virus.

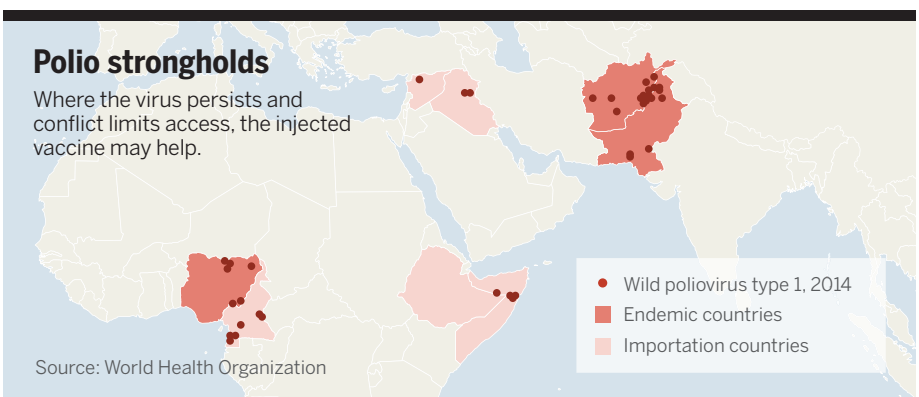

To gauge how well the two vaccines blocked transmission, the researchers looked at viral shedding in the children's stool, a measure of so-called gut immunity, several days after the challenge. The team found the greatest reduction in viral shedding in the children who had received IPV—up to 75% in the oldest age group. In other words, IPV did a better job at boosting gut immunity than another dose of OPV did.

The Moradabad study "showed very elegantly and persuasively that giving a dose of IPV to a child receiving the full dose of OPV does an excellent job at boosting intestinal immunity," says Stephen Cochi of the U.S. Centers for Disease Control and Prevention (CDC) in Atlanta. The *Lancet* study, led by Jacob John of Christian Medical College in Vellore and his colleagues, showed strikingly similar results in 500 kids there in 2013.

When news of the encouraging findings began circulating through the polio community last year, health officials were grappling with a polio outbreak in the Horn of Africa. It had erupted in May 2013 near Mogadishu, Somalia's capital, and Kenya's Dadaab refugee camp, and spread fast across the war-torn region.

Over the next few months, GPEI tried every new tactic that seemed to have helped in other outbreaks: vaccinating older kids and sometimes adults, instead of just children under age 5; setting up vaccination posts along major transit routes; and, where access was compromised, sending in volunteers to deliver vaccine in short, quick bursts. Then in December GPEI and the Kenyan Ministry of Health decided to try the combination strategy, despite the challenges of administering shots and the fear that people would not accept them. Vaccinators in Dadaab targeted 126,000 kids with a one-two punch of IPV and OPV drops, as CDC epidemiologist Concepcion Estivariz and colleagues described in the 21 March issue of the *Morbidity and Mortality Weekly Report*.

No one is asserting that one campaign turned the tide in Dadaab, and immunological data are lacking. What's remarkable, experts say, is that, a few glitches aside, the program was able to pull it off, and coverage reached about 95%. Nigeria isn't waiting for more data. The country just wrapped up its first IPV-OPV campaign in the northern states of Borno and Yobe. Plans are afoot to try it in Pakistan in the Federally Administered Tribal Areas.

But as the December Dadaab pilot showed, the cost and logistics of IPV are still daunting, so these campaigns should be saved for the toughest spots—"small geographic areas where transmission is occurring and access to kids is tough," Modlin says. As Estivariz puts it, that's when you "go in and give them everything you've got." ■

MATHEMATICS

Wheels when you need them

Can special algorithms help keep shared bicycles rolling?

By **Chelsea Wald**, *in Vienna*

Grigorij Kuklin pulls his van over as far as he can while cars stream past. It's nearly rush hour in Vienna, and intermittent July rainstorms are worsening the traffic. A driver for Citybike Wien, Vienna's bike-sharing system, Kuklin is helping test a new algorithm to route vans like his, which pick up bikes from stations that are full and take them to ones that are empty.

Kuklin is keen to see whether mathematics can really make his job more efficient. But the instructions that appear on his smart phone are telling him to stop and pick up bikes where it's not safe. "I'm not going to do that," he says as he jumps back into the van and pulls into traffic.

Perhaps it was the right call. But computer scientist Günther Raidl of the Vienna University of Technology, who is developing the algorithm, is hopeful that his work will ultimately help drivers like Kuklin better address what bike-sharing operators call the "rebalancing" problem. Raidl is one of many scientists drawn to a challenge that is both mathematically complex and practically important. "There may be 20 to 30 researchers that are devoting significant parts of their research agendas to rebalancing," says computer scientist David Shmoys of Cornell University.

For most, it's still a theoretical exercise, but a few have also seen their work applied. Shmoys collaborates with NYC Bike Share, the company that operates New York City's system; his algorithms now provide "the overarching vision for how we like our system to look," says Michael Pellegrino, director of operations for NYC Bike Share. Cornell is also running tests in Chicago, Illinois.

Some 600 cities in 52 countries have introduced bike-sharing systems, according to the Earth Policy Institute in Washington, D.C.; Vienna, which was among the early adopters in 2003, now has 1500 bikes. (The largest system, in Wuhan, China, has 90,000.) Nearly all of them share the same problem: Riders tend to take some routes—downhill, for example—and not others. As a result, the bikes tend to collect in a few places.

Published by AAAS

A bicycle station in New York City has almost filled up.

PHOTO: TIM CLAYTON/CORBIS

For users, an unbalanced system is a drag: You either can't get a bike, or there's no room to drop one off. For operators, it's a costly headache. Unbalanced systems can cause riders to abandon their bikes, which increases the risk of theft. In Vienna, two to three vans haul 20 bikes at a time from full stations to empty ones. In New York City's 6000-bicycle system, introduced last year, managing rebalancing "is a good part of my day-to-day," Pellegrino says.

Oliver O'Brien of University College London, who runs the online Bike Share Map, says that in most systems, drivers or dispatchers "squint at a map" of the system to rebalance it. "They'll say 'OK, these ones are full, these ones are empty,' " and then route a truck between them, he says. That often doesn't work well enough; unbalanced stations are among the top user complaints in many cities. Mathematicians believe there has to be a more efficient way.

Raidl's approach, which he developed with colleagues at the Austrian Institute of Technology, resembles the "pickup and delivery vehicle routing" algorithms that package delivery services use to route their trucks most efficiently. His algorithm—which gives updated suggestions throughout the day—also takes into account a forecast of demand based mainly on season, day of the week, and weather. The problem is too complex to allow an exact solution; instead, Raidl came up with ways to approximate one.

The algorithm works well on paper, but this summer's trials showed that its suggestions don't always suit drivers in the thick of things. It can also irk drivers by suggesting they pick up fewer than the 20 bikes the van can carry, which "seems inefficient," even though it may not be, Kuklin says.

New York also has a fleet of trucks to do the rebalancing. The system that Cornell developed works differently than Raidl's: It doesn't give drivers specific instructions, but produces an online map showing the stations that are farthest off from the predicted need. Dispatchers use the map, in combination with precomputed truck routes, to guide the drivers, especially overnight when there's time to prepare for the next day. New York drivers, too, balk when instructed not to fill their trucks to capacity, says Ph.D. student Eoin O'Mahony, who works with Shmoys; luckily, he adds, "we've seen from data that moving nothing but truckloads of bikes gets you close" to the same solution anyway, so the map now prescribes only full loads.

Because traffic seriously hinders the trucks during rush hour, New York has also introduced ricksha-like trailers, powered by human pedaling, which carry up to three bicycles at a time. (In rush hour, a single trailer can move more bikes per hour than a truck, O'Mahony says.) He and Shmoys came up with an algorithm for routing the trailers as well. The researchers first figured out which stations normally ran empty and which full; then they paired nearby stations—one normally empty and one normally full. Bike trailers can now shuttle between those two stations.

A London-based company called Stage Intelligence envisions an alternative to such top-down planning. Computer scientist Lin Li modeled autonomous rebalancing trucks, which self-organize like a bee colony, he says. The trucks flit from station to station like bees to flowers, attracted by signals that the stations feed into the model, announcing whether they are short of bikes or have too many.

No operator is ready to give rebalancing over to an algorithm entirely, because it can never know everything. A big sporting event or a transit failure can drastically change demand or traffic conditions; media attention or political pressure could force an operator to give a certain station priority. That's why in New York, human dispatchers are ultimately in charge, Pellegrino says.

And sometimes, the riders themselves do part of the rebalancing. Some cities are giving users rewards—such as a small refund or extra riding time—if they ride against the flow, Shmoys says. "That's another means for letting rebalancing be done in an automatic kind of way." ■

Chelsea Wald is a science writer in Vienna.

Published by AAAS

ANIMAL BEHAVIOR

Wolves cooperate but dogs submit, study suggests

Breeding for dependence, not cooperation, may have driven initial dog domestication

By **Virginia Morell**

For dog lovers, comparative psychologists Friederike Range and Zsófia Virányi have an unsettling conclusion. Many researchers think that as humans domesticated wolves, they selected for a cooperative nature, resulting in animals keen to pitch in on tasks with humans. But when the two scientists at the Messerli Research Institute at the University of Veterinary Medicine Vienna studied lab-raised dog and wolf packs, they found that wolves were the tolerant, cooperative ones. The dogs, in contrast, formed strict, linear dominance hierarchies that demand obedience from subordinates, Range explained last week at the Animal Behavior Society meeting at Princeton University. As wolves became dogs, she thinks, they were bred for the ability to follow orders and to be dependent on human masters.

Range and Virányi developed their new portrayal of dogs and wolves by giving a series of tests to socialized packs of mixed-breed dogs and wolves, four packs of each species, containing anywhere from two to six animals each. The scientists raised all the animals from about 10 days old at the Wolf Science Center in Game Park Ernstbrunn, Austria, living with them 24 hours a day until they were introduced to pack life, so that they were accustomed to humans.

Range and her colleagues tested the dogs' and wolves' tolerance for their fellow pack members with a mealtime challenge. The researchers paired a high-ranking dog with a low-ranking pack buddy and set out a bowl of food, then gave the same challenge to a pair of wolves. In every matchup, "the higher ranking dog monopolized the food," Range told the meeting. "But in the wolf tests, both high- and low-ranking animals had access" and were able to chow down at the same time. At times, the more dominant wolves were "mildly aggressive toward their subordinates, but a lower ranking dog won't even try" when paired with a top dog, Range said. "They don't dare to challenge."

Wolves also beat the hounds on tests that assessed whether the canids were able to follow the gaze of their fellows to find food. "They are very cooperative with each other, and when they have a disagreement or must make a group decision, they have a lot of communication or 'talk' first," Range said. The same was not true for the center's dog packs; for even the smallest transgression, a higher ranked dog "may react aggressively" toward one that is subordinate.

Range and Virányi suspect that the relationship between dogs and humans is hierarchical, with humans as top dogs, rather than cooperative, as in wolf packs. The notion of "dog-human cooperation" needs to be reconsidered, Range said, as well as "the hypotheses that domestication enhanced dogs' cooperative abilities." Instead, our ancestors bred dogs for obedience and dependency. "It's not about having a common goal," Range said. "It's about being with us, but without conflict. We tell them something, and they obey."

"It's wonderful work," says James Serpell, an ethologist at the University of Pennsylvania. "But it's not what the dog training community wants to hear; you can't say the word 'dominance' around them. Does dominance exist as a phenomenon in dogs? The answer is clearly 'yes,' " Serpell says, although he notes that there are breed differences. Other researchers, for example, have shown that when in packs, poodles and Labrador retrievers are more aggressive than are malamutes and German shepherds.

Monique Udell, an animal behaviorist at Oregon State University, Corvallis, says her own study of dog and wolf behavior, also presented at the meeting, supports Range's contention that dogs are waiting for orders. To find out if dogs are "independent problem solvers," she presented 20 adult dogs (10 pets and 10 from shelters) with sealed containers of summer sausage. Each animal was allotted 2 minutes to open it. Ten captive wolves were given the same test. Not one of the adult dogs succeeded; most did not even try. Meanwhile, eight of the 10 wolves opened the container in less than 2 minutes. So did dog puppies, indicating that dogs are no less capable of the task than wolves, but "as the dog grows and becomes more dependent on its human owner that [independent] behavior is inhibited," Udell said.

Underscoring the point, she found that adult pooches could open the container after all—when their human owner told them to do so. Because dogs "suppress their independence, it's difficult to know what their normal problem-solving abilities are," she told the meeting.

It may be that we have to give Fido a command to find out. ■

Wolves dine together, but dogs have a strict hierarchy and expect to be told what to do.

PHOTOS: (LEFT TO RIGHT) FRIEDERIKE RANGE/WOLF SCIENCE CENTER; PETER KAUT/WOLF SCIENCE CENTER

Downloaded from www.sciencemag.org on August 24, 2014

Published by AAAS

A dividing breast cancer cell.

PHOTO: STEVE GSCHMEISSNER/SCIENCE SOURCE

The cancer drug that almost wasn't

After years in drug development limbo, a compound that interrupts cell division has revitalized a troubled area of cancer research

By **Ken Garber**

Progress in cancer treatment can be frustratingly incremental. A new therapy often does no more than stall the disease by a few extra weeks. At a cancer meeting in San Diego, California, in April, however, University of California, Los Angeles (UCLA), oncologist Richard Finn reported that adding a drug called palbociclib to standard therapy doubled the time that women with metastatic breast cancer experienced no new tumor growth, from a median of 10 months to 20. "No study, despite efforts, has shown this dramatic improvement in progression-free survival, with the addition of a novel agent," Finn told the audience.

The results won't dispel all doubts about the drug—or the new treatment strategy it represents. The phase II trial Finn discussed enrolled just 165 women, and it is too early to know whether those taking the drug combination live significantly longer than women on standard therapy. But palbociclib, which is under development by pharmaceutical giant Pfizer, has captivated the cancer field nonetheless. "The … buzz is that these are extremely impressive data that are really way beyond what anybody had expected," says Frank McCormick, a veteran cancer researcher at UC San Francisco, who played an early role in the drug's discovery.

Palbociclib has traveled a long and tortuous road. The product of a project started in 1995 by researchers at Parke-Davis, a now-vanished drug company, the compound blocks key enzymes driving the cell cycle, the ordered set of processes by which a cell divides. Mounting scientific evidence suggested its potential in breast cancer. Yet Pfizer, where the compound was ultimately synthesized by the Parke-Davis

Downloaded from www.sciencemag.org on August 24, 2014

Published by AAAS

team after Pfizer acquired their company, later shelved the then-unique drug for much of the decade. In the end, it took a handful of dedicated outside researchers to demonstrate its worth. Palbociclib "has reinvigorated the whole cell cycle area," says Dennis Slamon, another UCLA oncologist involved in the breast cancer trial.

"Right now this looks like one of the bigger stories in the field for a long time," adds Clifford Hudis, an oncologist at the Memorial Sloan Kettering Cancer Center in New York City and immediate past president of the American Society of Clinical Oncology (ASCO). He is excited not just by the potential of palbociclib to benefit women with metastatic disease, but also by plans to test it in early-stage breast cancer, where it might help cure patients. "That's a no-brainer."

Clinical trials of palbociclib are under way in at least six other tumor types. And in June at ASCO's annual meeting, very similar drugs, from Novartis and Eli Lilly, showed excellent early results, often shrinking tumors or stabilizing them for long periods in people with melanoma and lung cancer. "The implications of this [drug] class will be wide," predicts Thehang Luu, an oncologist at the City of Hope cancer center in Duarte, California. "We're not even touching the surface yet."

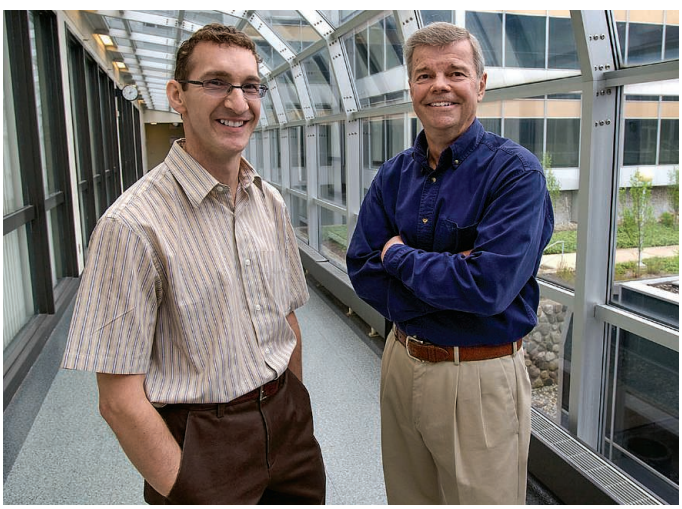

Biochemist Dave Fry (*right*) and chemist Peter Toogood led the Parke-Davis effort that identified the promising cancer drug palbociclib.

THE SPECIAL APPEAL OF palbociclib and its competitors lies in the nature of the cell cycle. Targeted cancer therapies such as Herceptin and Tarceva interrupt one strand of a weblike network of growth signals within the cell, but it's hard for a single drug to overcome multiple, redundant signaling pathways and feedback loops. But the cell cycle is not a web; it's a one-way street. So blocking any component should, in theory, stop the frenetic cell division of cancer cold.

Dividing human cells cycle through four distinct phases, known as G1, S, G2, and M (for mitosis). Experiments in the 1970s and 1980s in three different organisms revealed this cycle's key molecular components and earned Leland Hartwell, Tim Hunt, and Paul Nurse the 2001 Nobel Prize in physiology or medicine (*Science*, 19 October 2001, p. 502). Proteins called cyclins and cyclin-dependent kinases (CDKs) lock together and drive each step of the cycle. By 1995, there was strong circumstantial evidence that cyclin D and either CDK4 or CDK6—the complex that triggers human cells to move from G1 to S (see graphic, p. 867)—often drives uncontrolled cell division and tumor growth.

"Even back then it was pretty clear [that] different components of this pathway are mutated, or altered in some way or another, in the majority of cancers," says UC San Francisco's McCormick. That made the CDK4/6 system an obvious target for inhibitory compounds. In 1995, Parke-Davis, the pharmaceutical research arm of health care company Warner-Lambert, approached McCormick, the founder of Onyx Pharmaceuticals, to collaborate. Work began that year at the Parke-Davis labs in Ann Arbor, Michigan. Investigators used lab-made versions of CDK4 and other cell cycle proteins, supplied by Onyx, to guide discovery of compounds that specifically inhibit CDK4.

Because the many CDK family members are almost identical, "creating a truly selective CDK4 inhibitor was very difficult," says former Parke-Davis biochemist Dave Fry, who co-chaired the project with chemist Peter Toogood. "A lot of pharmaceutical companies failed at it, and just accepted broad-spectrum CDK inhibitors as their lead compounds." But after 6 years of work, the pair finally succeeded with the help of some clever screens that could quickly weed out nonspecific "dirty" compounds.

Their synthesis in 2001 of palbociclib, known internally as PD-0332991, was timely. By then, many dirty CDK inhibitors from other companies were already in clinical trials, but they worked poorly, if at all. Because they hit multiple CDK targets, these compounds caused too much collateral damage to normal cells. "They had a lot of toxicity," Slamon notes. That made it hard to give these drugs at the doses necessary to shut down the cell cycle in tumors. It soon also became clear that the cell cycle had some built-in redundancies of its own, leaving many to wonder if taking out a single component would really stop a tumor in its tracks. Eventually, most efforts to fight cancer by targeting the cell cycle ground to a halt. "Everything sort of got hung up, and I think people lost enthusiasm," Slamon says.

PD-0332991 fell off the radar screen. Pfizer, which had acquired Warner-Lambert/Parke-Davis in 2000 mainly for the cholesterol drug Lipitor, did not consider the compound especially promising, Fry says, and moved it forward haltingly at best. "We had one of the most novel compounds ever produced," Fry says, with a mixture of pride and frustration. "The only compound in its class."

A major merger helped bury the PD-0332991 program. In 2003, Pfizer acquired Swedish-American drug giant Pharmacia, which flooded Pfizer's pipeline with multiple cancer drugs, all competing for limited clinical development resources. Organizational disarray followed, says cancer biologist Dick Leopold, who led cancer drug discovery at the Ann Arbor labs from 1989 to 2003. "Certainly there were some politics going on," he says. "Also just some logistics with new management and reprioritization again and again." In 2003, Pfizer shut down cancer research in Ann Arbor, which left PD-0332991 without scientists and managers who could demand it be given a chance, Toogood says. "All compounds in this business need an advocate."

Pfizer finally launched a phase I human trial in 2004 to establish a safe dose for PD-0332991. Typically, drug developers start phase II trials about a year later, but Pfizer did not follow up. In a statement, the company notes that the drug failed to show much antitumor effect in the phase I trial. But Fry and Toogood say the trial was inadequate. Patient selection was "essentially solid tumor, all comers, looking for a signal," Toogood says. "That's a tough way to get really exciting data on a compound as targeted as this is." Fry says that Pfizer could have tracked biomarkers in patients' tumors showing whether palbociclib was having its desired effect. And, he says, it could have monitored alterations in the CDK4 system that could later be used to predict who would benefit from the drug. Pfizer has stated that the biological knowledge to predict responses back then was lacking and says, "We have moved rapidly and responsibly, utilizing emerging evidence, to advance

PHOTO: MARK BIALEK

Published by AAAS

Putting the brakes on cancer cell division

Cell division proceeds when two cell cycle proteins, CDK4 and cyclin D, form a complex that inhibits Rb (left). CDK4 inhibitors block this process, freeing Rb to slam the cell cycle to a stop.

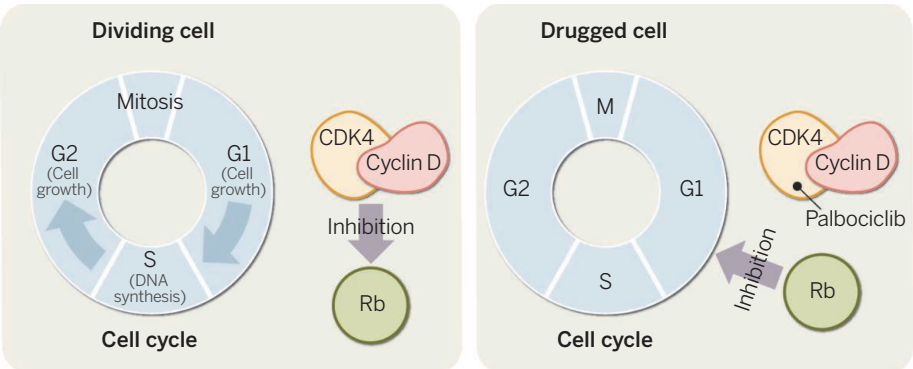

ILLUSTRATION: KAY ENGMAN/*SCIENCE*

the clinical development of palbociclib."

But a phase II trial of the drug did not start until 2009, 5 years after the phase I study. By then, strong genetic evidence already existed that certain breast tumors are completely dependent on CDK4. Piotr Sicinski, a geneticist at the Dana-Farber Cancer Institute in Boston, reported in 2001 in *Nature* that mice lacking cyclin D1 (CDK4's partner) cannot develop breast cancer driven by the *Ras* or *Her2* oncogenes. "Unfortunately this study went unnoticed to the pharmaceutical industry," says Mariano Barbacid, a cancer researcher at the Spanish National Cancer Research Center in Madrid.

Then, in January 2006, Sicinski reported in *Cancer Cell* that mice needed CDK4 as well as cyclin D to develop breast tumors. In an accompanying editorial, Barbacid and a colleague acknowledged that human tumors are more genetically complex than Sicinski's mouse models, but wrote that "these considerations should not be an excuse to further delay testing in patients suffering from … breast tumors the effectiveness of selective Cdk4/6 inhibitors." But the only such drug, Pfizer's, remained on the shelf.

IN THE END, PD-0332991 WAS resurrected by investigators outside the company. In late 2004, Selina Chen-Kiang, a molecular biologist at Weill Cornell Medical College, obtained PD-0332991 from Pfizer as a research tool for studying the cell cycle in normal immune cells. Convinced of the drug's potential in blood cancers, she persuaded Pfizer to sponsor a 17-patient phase I clinical trial in mantle cell lymphoma that began in 2007. In that trial, about one-fifth of patients had significant tumor shrinkage—decent but not spectacular results. Still, Toogood says, "her advocacy was important in helping ensure that the program continued."

In May 2007, Slamon, whose earlier research had led to the breast cancer drug Herceptin, applied PD-0332991 to a large panel of breast cancer cell lines. Slamon expected the cell cycle inhibitor to work best in aggressive "triple-negative" tumor cells, which proliferate rapidly, but to his surprise estrogen receptor (ER)–positive lines were most sensitive. More than 60% of all breast cancers are ER-positive.

Slamon and UCLA's Finn then tested PD-0332991 in combination with letrozole, a standard antiestrogen, in a dozen women with ER-positive metastatic breast cancer. Three of the women had at least 30% tumor shrinkage. "That encouraged us even more," says Slamon, who says that one woman is still taking the combination treatment more than 4 years later.

At this point, Pfizer got excited, too. It sponsored the randomized phase II trial, which involved UCLA and other medical centers internationally and started in December 2009. While awaiting proof that the drug improves overall survival, Pfizer announced this week it has asked the Food and Drug Administration to approve the drug for ER-positive metastatic breast cancer, based just on the phase II results—the agency has designated it a "breakthrough therapy," earning it priority for evaluation. Yet both Sloan Kettering's Hudis and Martine Piccart, a breast cancer researcher at the Jules Bordet Institute in Brussels, say that results from a larger, phase III trial are necessary to really know palbociclib's worth. Two phase III breast cancer trials have completed patient enrollment, and others are under way.

On the basic research side, scientists are still seeking to explain an unexpected bonus: palbociclib's ability to shrink tumors. In theory, a cell cycle inhibitor should only stop a tumor from growing. And that, indeed, is what happens in cancer cell lines. But, back in 2001, at the Ann Arbor labs, the drug completely eradicated human colon tumors transplanted into mice. "That was a very exciting result," Toogood recalls.

In the clinic, one lymphoma patient taking just palbociclib early on had a complete remission, and dozens of breast cancer patients have seen their tumors shrink. Lilly's CDK4/6 inhibitor, given alone, has also shrunk both breast and lung tumors. "The phenomenon is real," Slamon says. "And we're left to explain it."

Mouse studies suggest one possibility. Eliminating the genes encoding CDK4 in a rodent—a process that palbociclib roughly mimics—can put its cells into senescence, a permanent inability to divide. Such senescent cells may ultimately be cleared by the immune system, leading to tumor shrinkage. In addition, Chen-Kiang has data from human tumor tissue showing that the prolonged cell cycle arrest by palbociclib makes the tumor cells highly vulnerable to other cancer drugs. And, in a few animal models of leukemia and lymphoma, the drug causes tumor cells to commit suicide.

Cancer cells are notorious for their ability to develop drug resistance. But investigators suspect resistance to palbociclib and other CDK4/6 inhibitors may be slow to arise; initial studies of people taking the drugs have so far shown no evidence that their tumors acquire mutations in the genes for the CDKs. CDK4 and CDK6 "are extremely stable drug targets," Chen-Kiang says. Still, some studies of cells dosed with palbociclib suggest that resistance can develop indirectly, if the cells lower amounts of a negative protein regulator of the cell cycle, for example.

Pfizer leads the race for the first approved CDK4/6 inhibitor, but its sluggish development gave competitors time to catch up. Novartis and Lilly already have their compounds in phase III trials in breast cancer, and Lilly will soon start a phase III trial of its drug in lung cancer. Both companies apparently identified their compounds only about 5 years ago, almost a decade after Fry and Toogood found palbociclib.

But thanks to their drug, the cell cycle is again a hot field for cancer research. The ultimate payoff on palbociclib or its competitors remains anyone's guess. "If we don't really know why they work so well, quite frankly, it's quite difficult to predict the impact overall," McCormick says. "I would guess it's just the beginning of a whole new era of developing this approach to targeting cancer. But how far it'll go, I really couldn't say." ■

Ken Garber is a writer in Ann Arbor, Michigan.

Published by AAAS

RNA regulation of RNA *p. 876*

A sweet repurposed receptor *p. 878*

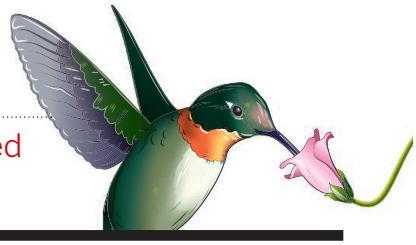

PERSPECTIVES

ASTRONOMY

Imprint of an ancient conflagration

Evidence is found for the massive stars that populated the early universe

By **Volker Bromm**

One of the key events in cosmic history was the onset of star formation in the hitherto dark and featureless universe. Once the first stars, also called population III stars, appeared, they began to transform the simple initial state of the primordial universe into one of ever-increasing complexity, endowing it with growing bubbles of high-energy radiation and heavy chemical elements (*1*). The nature of this transition crucially depends on the mass of the first stars. Massive stars are efficient sources for both ionizing photons and heavy chemical elements, or "metals," comprising all species heavier than the hydrogen and helium made in the Big Bang. Theoretical models have predicted that the first stars were predominantly very massive, possibly a few hundred solar masses (*2*, *3*). This prediction, however, has proven to be out of reach for direct empirical testing. There are a number of indirect constraints, such as the apparent absence of any low-mass population III survivors in the Milky Way, but all of them admit alternative explanations. On page 912 of this issue, Aoki *et al.* (*4*) present evidence that the first stars indeed were able to reach very high masses, in accordance with theory (*5*).

Aoki *et al.* scrutinize the chemical abundance pattern in the outer layer of a metal-poor, second-generation star that had formed out of material enriched by a preceding population III supernova, thus preserving the peculiar signature of this ancient explosion. Indeed, the peculiar pattern is highly suggestive of an unusual kind of violent stellar demise, termed a "pair-instability supernova" (PISN).

Department of Astronomy, University of Texas, Austin, TX 78712, USA. E-mail: vbromm@astro.as.utexas.edu

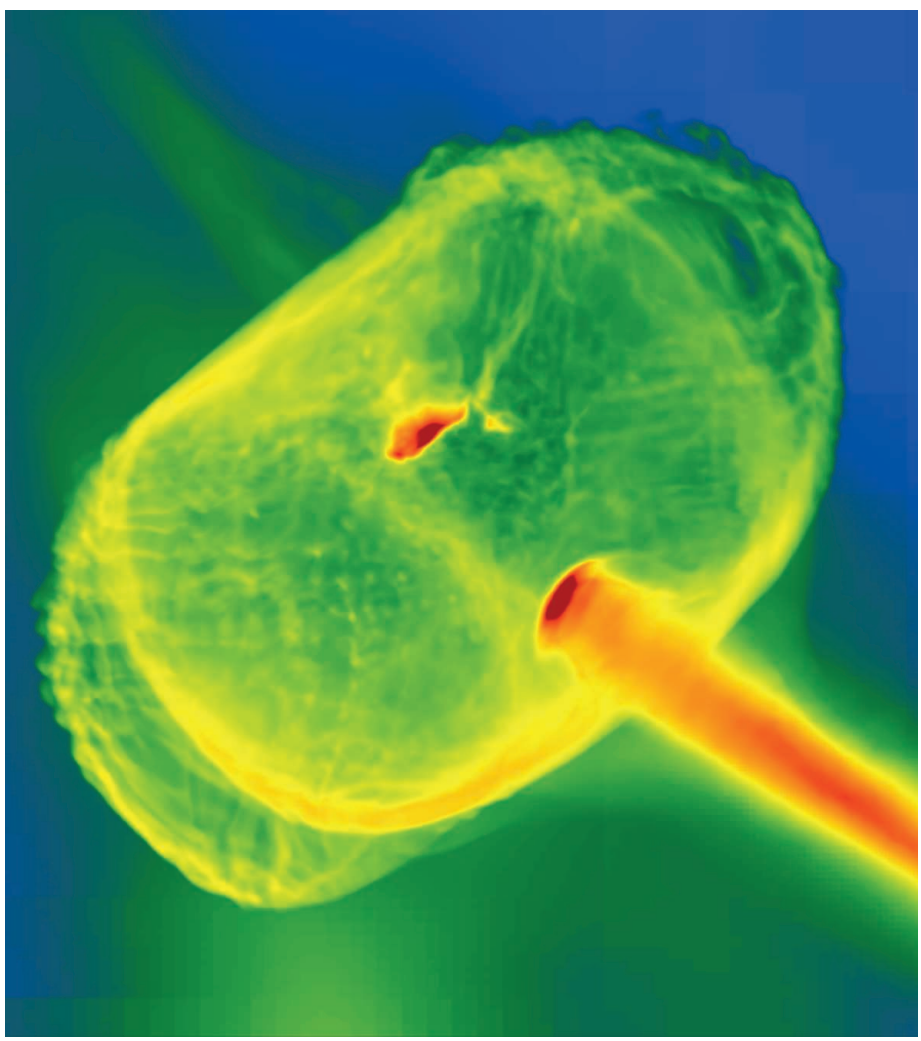

Cosmological impact of the first supernova explosions. This supercomputer frame shows how supernova feedback disrupts the gas inside the dark matter halo, hosting a small group of primordial stars (not shown), about 200 million years after the Big Bang. The frame is 3000 light years across; the color scheme depicts the density of hydrogen gas, such that dark red denotes highest density and blue lowest. The explosions, with energies similar to that of a PISN, greatly damage the host system by blowing out the gas into the surrounding intergalactic medium. The high-density filamentary structure, reaching from upper left to lower right, traces the underlying distribution of the dark matter, which is organized into a network of such intersecting filaments—the so-called cosmic web.

IMAGE: JEREMY RITTER, UNIVERSITY OF TEXAS, AUSTIN; TEXAS ADVANCED COMPUTING CENTER

Published by AAAS

Theory had predicted the existence of the PISN mechanism nearly four decades ago, positing that sufficiently massive stars, in excess of 100 solar masses or so, would encounter a catastrophic instability at the end of their short life (*6*). Photons, which provide the bulk of the pressure that counteracts the crushing gravity in such massive stars, eventually become so energetic as to allow their conversion into electron-positron pairs. These particles, however, contribute little to the outward pressure, such that the force of gravity suddenly becomes unbalanced, causing the runaway collapse of the star. The resulting compression leads to a jump in internal temperature, which in turn triggers the near-simultaneous burning of all remaining nuclear fuel in the star. This sets off a colossal thermonuclear explosion. A PISN is 10 to 100 times as energetic as both a standard (white dwarf–related) supernova explosion and the usual death encountered by a massive star. Because a PISN requires a very massive progenitor star, the case was made that this might be the typical endpoint of population III (*2*, *3*). For decades the PISN mechanism remained confined to the realm of theoretical speculation.

"The … result is a prime example of 'stellar archaeology,' the endeavor to constrain the properties of the first stars with local fossils that have survived from the end of the cosmic dark ages …"

This situation has changed in the past few years, with the emergence of tantalizing hints for PISN-like events. First, there is the case of supernova SN2007bi, a superluminous explosion in a nearby dwarf galaxy (*7*), with prolonged bright emission that points to the presence of a large amount of radioactive nickel—exactly what is predicted for PISN nucleosynthesis (*8*, *9*). Then there are two examples of such superluminous explosions found in archival galaxy survey data much earlier in cosmic history, reaching back to the first 2 billion years of cosmic history (*10*). These events serve as existence proof that the PISN class of explosions may provide us with ideal signposts of the very high redshift universe, probing its formative first billion years after the Big Bang. A PISN is luminous enough to allow the upcoming James Webb Space Telescope (JWST), planned for launch in 2018, to detect individual population III stars at the moment of their violent death (*11*).

The new Aoki *et al.* result is a prime example of "stellar archaeology," the endeavor to constrain the properties of the first stars with local fossils that have survived from the end of the cosmic dark ages, thus preserving clues from these ancient times (*12*). More specifically, those fossils are metal-poor (so-called population II) stars, with masses less than our Sun, such that their lifetimes are on the order of the age of the universe. Despite its great power, stellar archaeology can typically only provide indirect hints about the nature of the first stars, because any chemical fingerprint is often consistent with multiple interpretations as to how many, and what kind of, supernova explosions have contributed. It has therefore been a long-standing goal to identify clean cases, where only one supernova—or, at most, a very small number of them—has produced the bulk of the metals locked up in the stellar fossil. The star identified by Aoki *et al.* may just be such a "Rosetta stone" of cosmic chemical evolution. Its peculiar, PISN-generated, abundance pattern would have been wiped out if multiple supernovae had contributed. Recently, an analogous maximally primitive (and therefore maximally simple) galaxy, comprising a few hundred population II stars, has been identified: the Segue 1 ultrafaint dwarf galaxy in our local group (*13*). In each case, the great reward of finding such Rosetta-stone systems is that direct constraints on the nature of the first stars can be obtained.

Increasingly large surveys of old, metal-poor stars in the halo of our galaxy, such as the Hamburg/ESO survey and, more recently, the stellar extension (SEGUE) of the Sloan Digital Sky Survey (SDSS), have provided a wealth of abundance data, allowing us to constrain the mass scale and possibly the rotation state of the first stars (*12*). There is a peculiar class of stellar fossils, extremely poor in almost all chemical elements with the prominent exception of the lightest ones, such as carbon and oxygen (*14*). This pattern has been related to element production in population III stars that were massive enough, having perhaps 40 to 60 solar masses, to form black holes in their cores (*9*). The black hole would permanently lock up most heavy elements; only the lighter ones, synthesized in the outer layers, could escape. A second, majority class of abundances in metal-poor stars points to the more standard core-collapse enrichment, implying progenitor masses of a few tens of solar masses.

Indeed, this evidence has sometimes been taken to imply that the first stars were massive but not very massive, such that PISN enrichment never took place. As Aoki *et al.* now show, such conclusions may have been premature. With hindsight, the culprit may have been a subtle observational selection effect, related to the very large amount of metals locally inserted into the cosmic gas by even a single PISN (*15*). Any second-generation star would then sample material that is already quite enriched, above the usual thresholds used by traditional stellar archaeology to select candidates for follow-up observations with high-resolution spectroscopy. Basically, the selection bias may arise by focusing on stars with the lowest total metal content as the most direct probes of population III stars, thus excluding any PISN-enriched candidates by design.

The totality of existing theoretical and observational evidence suggests that the first stars typically died as conventional core-collapse supernovae (*1*). It is of great importance that population III stars can reach the very high masses required to trigger a PISN. Such energetic supernovae can greatly influence the early universe (see the figure), with a spatial reach well beyond the dark matter halo hosting the first stars. Another reason is that the upper mass limit reached by the first stars offers key insight into their detailed formation physics. A fundamental problem here is whether the process of primordial gas accretion onto the growing protostar can be shut off by its increasingly energetic radiation, pushing outward. If the observations of Aoki *et al.* are correct, such radiative feedback was unable to completely suppress growth, at least in select cases.

We are entering an exciting period in the immediate run-up to the JWST launch, where we may increasingly be afforded intriguing previews, such as the Aoki *et al.* result, beyond the current horizon of observational cosmology. Over the coming decade, we may finally be able to complete cosmology's enduring quest to probe the entire history of cosmic star formation, including its elusive initial stages. ■

REFERENCES AND NOTES

1. V. Bromm, *Rep. Prog. Phys.* **76**, 112901 (2013).
2. T. Abel, G. L. Bryan, M. L. Norman, *Science* **295**, 93 (2002).
3. V. Bromm *et al.*, *Astrophys. J.* **564**, 23 (2002).
4. W. Aoki *et al.*, *Science* **345**, 912 (2014).
5. S. Hirano *et al.*, *Astrophys. J.* **781**, 60 (2014).
6. Z. Barkat *et al.*, *Phys. Rev. Lett.* **18**, 379 (1967).
7. A. Gal-Yam *et al.*, *Nature* **462**, 624 (2009).
8. A. Heger, S. E. Woosley, *Astrophys. J.* **567**, 532 (2002).
9. K. Nomoto, C. Kobayashi, N. Tominaga, *Annu. Rev. Astron. Astrophys.* **51**, 457 (2013).
10. J. Cooke *et al.*, *Nature* **491**, 228 (2012).
11. D. J. Whalen *et al.*, *Astrophys. J.* **762**, L6 (2013).
12. T. C. Beers, N. Christlieb, *Annu. Rev. Astron. Astrophys.* **43**, 531 (2005).
13. A. Frebel, J. D. Simon, E. N. Kirby, *Astrophys. J.* **786**, 74 (2014).
14. S. C. Keller *et al.*, *Nature* **506**, 463 (2014).
15. T. Karlsson *et al.*, *Rev. Mod. Phys.* **85**, 809 (2013).

ACKNOWLEDGMENTS

Supported by NSF grant AST-1009928 and resources of the Texas Advanced Computing Center.

10.1126/science.1255524

Published by AAAS

BIOGEOCHEMISTRY

Carbon cycling in the Arctic

Sunlight drives the emission of carbon from arctic waters

By **Lars Tranvik**

The arctic landmass is covered by numerous shallow ponds, lakes, and streams (see the photo). On page 925 of this issue, Cory *et al.* (*1*) show that sunlight drives the production of substantial amounts of carbon dioxide in these waters through photochemical oxidation of organic matter. The results have important implications for the carbon cycle in the Arctic and how it responds to, and possibly even magnifies, climate change.

Inland waters—lakes, rivers, and streams, as well as reservoirs created by humans—cover only a few percent of Earth's continents and were long considered to be merely a pipe that transports carbon from land to sea (*2*). But recently, scientists have shown that these waters are responsible for transforming and transporting substantial amounts of carbon (*3*): Sediments in inland waters store carbon, whereas the waters themselves emit carbon dioxide (*4*) and methane (*5*) to the atmosphere. Each year, inland waters emit an estimated 1 gigaton of carbon as carbon dioxide to the atmosphere (*6*). For comparison, the global net flux of carbon dioxide into the oceans is about 2 gigatons of carbon per year.

Much of the organic carbon in lakes comes from soils and wetlands. This dissolved organic carbon (DOC) is a mixture of colloidal and dissolved substances, which carry the brownish color often seen in lake water. Bacteria slowly degrade DOC to form carbon dioxide, most of which is emitted to the atmosphere. Photochemical processes driven by ultraviolet and visible sunlight also contribute to DOC degradation, creating carbon dioxide, as well as substances that are easier for bacteria to metabolize than the original DOC (*7*). This phenomenon has been widely studied in the laboratory and in lakes, but information about its wider importance is only beginning to emerge (*8*).

Cory *et al.* performed a large set of experiments in ponds, lakes, streams, and rivers across the 8000-km^2 Kuparuk Basin at the North Slope of Alaska. They incubated samples under different light conditions to tease apart how much sunlight and bacteria contribute to the production of carbon dioxide in these waters. The authors take into account several factors, including the importance of different wavelengths in the sunlight, changes in light with water depth, and the amount of incoming solar radiation. They conclude that sunlight is a dominant driver of carbon processing in the water column. The results, scaled up to represent all inland waters of the Kuparuk basin, suggest that photochemical processes cause 70 to 95% of all degradation of DOC to carbon dioxide ("mineralization") in these waters.

Previous studies at lower latitudes have pointed to a less dominant role of sunlight in driving DOC processing. Koehler *et al.* recently concluded that direct photochemical mineralization is responsible for about 10% of the emissions of carbon dioxide from all lakes on Earth (*8*). Sequential photochemical-bacterial mineralization may account for a similar amount (*9*), giving a global contribution of photochemical mineralization of about 20%. In contrast, Cory *et al.* (*1*) suggest that photochemical mineralization in arctic waters drives up to 40% of the carbon dioxide emissions.

The authors propose several possible reasons for the larger relative share of mineralization attributed to sunlight in the Arctic. The most plausible may be the predominance of very shallow waters (see the photo). In shallow waters, sunlight penetrates most of the water column, leaving only a small dark zone where sunlight-independent microbial degradation dominates the decay of the organic matter.

It remains unclear whether the high relative importance of photochemical mineralization is specific to the Arctic. If the findings of Cory *et al.* also apply outside of the Arctic, the global estimate that photochemical mineralization causes about 10 to 20% of lake carbon dioxide emissions (*8*) may be too low.

Thawing of permafrost soils may contribute large amounts of DOC, with a great potential to be mineralized by the Sun. On the other hand, the increasing DOC will also stimulate microbial mineralization. Higher concentrations of colored DOC may change the light climate in lakes and ponds in favor of bacterial mineralization, resulting in a more modest future importance of photochemical mineralization relative to other processes than reported by Cory *et al.* Regardless of the relative roles of microbes and sunlight as the arctic warms up, their study points to an important mechanism that controls how much carbon is evaded to the atmosphere and how much is carried to the Arctic Ocean. ■

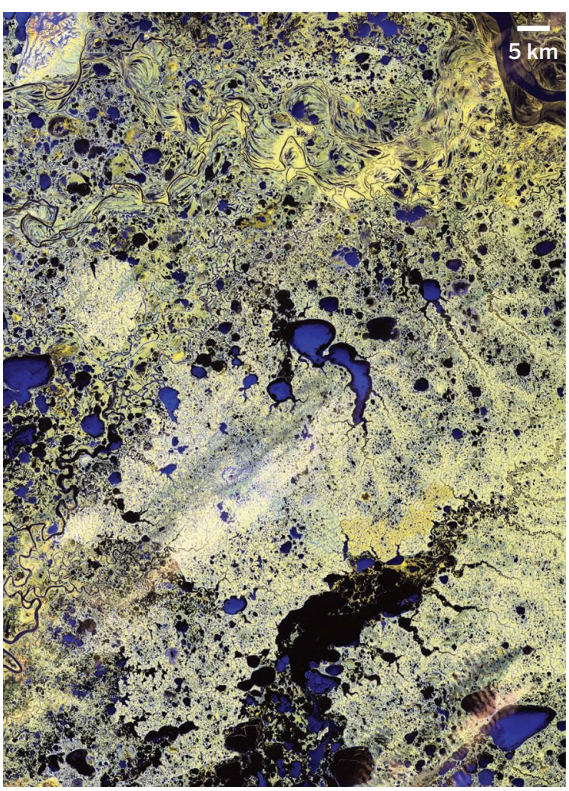

The power of sunlight. Cory *et al.* (*1*) evaluate the role of sunlight in carbon dioxide production in arctic inland waters in the Kuparuk Basin, Alaska. The authors consider both direct and indirect (bacteria-mediated) pathways and find a surprisingly strong role of sunlight.

PHOTO: U.S. GEOLOGICAL SURVEY

Limnology, Department of Ecology and Genetics, Uppsala University, Norbyvägen 18D, 75236, Uppsala, Sweden. E-mail: lars.tranvik@ebc.uu.se

REFERENCES

1. R. M. Cory *et al.*, *Science* **345**, 925 (2014).
2. Intergovernmental Panel on Climate Change (IPCC), *Climate Change 2007: The Physical Science Basis. Contribution of Working Group I to the Fourth Assessment Report of the Intergovernmental Panel on Climate Change*, S. Solomon *et al.*, Eds. (Cambridge Univ. Press, Cambridge/New York, 2007).
3. J. J. Cole *et al.*, *Ecosystems (N. Y.)* **10**, 172 (2007).
4. P. A. Raymond *et al.*, *Nature* **503**, 355 (2013).
5. D. Bastviken, L. J. Tranvik, J. A. Downing, P. M. Crill, A. Enrich-Prast, *Science* **331**, 50 (2011).
6. IPCC, *Climate Change 2013: The Physical Science Basis, in Contribution of Working Group I to the Fifth Assessment Report of the Intergovernmental Panel on Climate Change*, P. F. Stocker *et al.*, Eds. (Cambridge Univ. Press, Cambridge/New York, 2013).
7. R. G. Wetzel, P. G. Hatcher, T. S. Bianchi, *Limnol. Oceanogr.* **40**, 1369 (1995).
8. B. Koehler, T. Landelius, G. A. Weyhenmeyer, N. Machida, L. J. Tranvik, *Global Biogeochem. Cycles* 10.1002/2014GB004850 (2014).
9. W. L. Miller, M. A. Moran, *Limnol. Oceanogr.* **42**, 1317 (1997).

10.1126/science.1258235

Published by AAAS

QUANTUM OPTICS

A photon steers a photon with an atom

Nonlinear optics with single quanta of light and matter becomes reality

By **Gerhard Rempe**

Light beams cross each other unperturbed, at least in vacuum. To induce an interaction, optically nonlinear media are needed, but the polarizability of these materials is usually so small that long propagation lengths and high-intensity laser beams are required. However, that situation has changed, as reported on page 903 of this issue by Shomroni *et al.* (*1*), who performed an experiment in which just a single atom induces an interaction between two light pulses containing only a few photons.

Single photons are enabling tools for high-speed and low-power optical switches and transistors in future integrated photonic circuits (*2*). They are also ideal information carriers in long-distance secure quantum communication links and quantum networks such as a quantum Internet (*3*). Coherent single-photon sources and detectors exist as prototypes (*4*), but the small energy contained in a single photon makes it nontrivial to realize the optical nonlinearities that are required for the anticipated photonic circuits, located between sources and detectors.

Large photon-photon nonlinearities can be implemented by mapping the photons onto atoms and exploiting large atom-atom interactions (*5*). This idea has very recently been implemented in the form of single-photon switches and even single-photon transistors (*6*, *7*). However, the presence of many atoms was a source of decoherence that reduced the retrieval efficiency for the gate photon and the transmission of the target photons. A more coherent scheme is provided by cavity quantum electrodynamics with only a single atom as nonlinear medium. A single atom can be highly nonlinear, given that the absorption of a single photon is sufficient to take the atom from the ground to the excited state, which then changes the atom's optical properties from absorption to emission. Such an effect can lead to an optical nonlinearity per photon that is many orders of magnitude greater than in atomic ensembles, where the effect of a single photon typically has less dramatic consequences on the whole medium (*8*).

Max Planck Institute of Quantum Optics, 85748 Garching, Germany. E-mail: gerhard.rempe@mpq.mpg.de

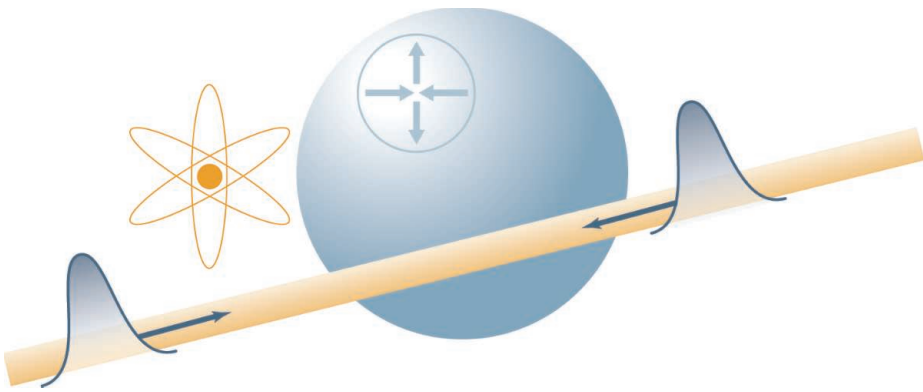

A micro-optical router. One atom close to a glass microsphere is triggered by a control photon (propagating through the fiber from the right) to transmit or reflect a subsequent target photon (approaching from the left).

The challenge, however, is to implement a scheme that makes a single atom interact strongly with a single photon. This goal can be achieved by placing the atom in a good optical resonator, where the photon is stored for sufficiently long times that the atom has enough time for absorption and emission processes to occur. The resonator must also be small in order to compress the photon energy to a small region and thus to make the intensity large. The good-resonator condition is difficult to meet, whereas the small-resonator condition is perfectly compatible with the requirement of chip integration.

Such a cavity quantum electrodynamics system has now been used to steer a target photon by means of a control photon. Both photons are propagating in an optical fiber toward a glass microsphere that acts as an ultralow-loss whispering-gallery light resonator (see the figure). Evanescent fields can escape the fiber and enter the sphere. Single laser-cooled rubidium atoms near the microsphere are the nonlinear medium and are coupled to circulating resonator photons via evanescent surface fields. Instead of two atomic levels, three levels are used, two of them being long-lived ground states. In this scheme, the control photon does not excite the atom but transfers it from one ground state to the other. An advantage is that photon absorption is accompanied by photon emission so that the control photon is automatically retrieved. Most important is that the transition induced by the control photon changes the coupling strength of the atom to the subsequent target photon. This change allows for the routing effect.

The experiment opens up new possibilities but needs to be advanced in several different directions. For example, it has been performed with highly attenuated laser pulses at the single-photon level, but these are not true single photons. Furthermore, for quantum applications, the functionality needs to be demonstrated for photonic quantum bits, which could be encoded in the photon polarization or the photon arrival time. Moreover, the reported overall efficiency is very low; because the atom was not held at rest, its stay in the vicinity of the microsphere was too short, and its arrival time was random. Nonetheless, in combination with other recent achievements in single-atom cavity quantum electrodynamics—such as the nondestructive detection of a single flying photon (*9*), the realization of a nanophotonic quantum phase switch (*10*), and the implementation of a quantum gate between a single atom and a single photon (*11*)—the new photon-routing experiment is an important milestone toward the implementation of an optical quantum technology with individual particles of light and matter. ■

REFERENCES

1. I. Shomroni *et al.*, *Science* **345**, 903 (2014).
2. D. A. B. Miller, *Nat. Photonics* **4**, 3 (2010).
3. H. J. Kimble, *Nature* **453**, 1023 (2008).
4. S. Ritter *et al.*, *Nature* **484**, 195 (2012).
5. D. Jaksch, J. I. Cirac, P. Zoller, R. Côté, M. D. Lukin, *Phys. Rev. Lett.* **85**, 2208 (2000).
6. H. Gorniaczyk, C. Tresp, J. Schmidt, H. Fedder, S. Hofferberth, *Phys. Rev. Lett.* **113**, 053601 (2014).
7. D. Tiarks, S. Baur, K. Schneider, S. Dürr, G. Rempe, *Phys. Rev. Lett.* **113**, 053602 (2014).
8. A. Ourjoumtsev *et al.*, *Nature* **474**, 623 (2011).
9. A. Reiserer, S. Ritter, G. Rempe, *Science* **342**, 1349 (2013).
10. T. G. Tiecke *et al.*, *Nature* **508**, 241 (2014).
11. A. Reiserer, N. Kalb, G. Rempe, S. Ritter, *Nature* **508**, 237 (2014).

10.1126/science.1258142

ILLUSTRATION: C. SMITH/*SCIENCE*

Published by AAAS

CLIMATE CHANGE

Glacier retreat crosses a line

Mountain glacier loss since the 1970s has mostly been caused by human influences on climate change

By **Shawn Marshall**

Retreating glaciers, bleached coral reefs, stranded polar bears, parched East African earth, receding tropical shorelines: These are the symbols of climate change in our young century. But how much responsibility do humans bear for these changes? In the case of glaciers, their worldwide retreat began in the 19th century, well before human effects on global climate are believed to have been significant. How much glacier retreat can be attributed to human influences on climate? On page 919 of this issue, Marzeion *et al.* (*1*) use climate models to assess the natural and anthropogenic (caused by humans) contributions to historical glacier mass loss.

Rapid retreat. Mountain glaciers around the world have receded since the 1850s. Marzeion *et al.* show that since the late 1970s, most of this retreat can be attributed to human influences on global climate. The image shows Columbia Glacier in the Canadian Rocky Mountains, photographed in 2010. The abrupt edges of today's vegetation define the late-19th century extent of the glacier.

Their analysis builds on earlier work (*2*) that fed into the 2013 IPCC report (*3*). The authors use an ensemble of global climate models (GCMs) to simulate glacier mass balance, that is, snow accumulation minus snow and ice melt. To do so they must first interpolate from the GCMs, which represent Earth's surface at a resolution of hundreds of kilometers, to the detailed topography and high elevations of mountain glaciers. With these interpolated climate fields, the authors then simulate glacier mass balance for the global suite of almost 200,000 glaciers.

Marzeion *et al.* simulate glacier mass balance from 1851 to 2010 for two scenarios. The first scenario combines natural and human influences on climate, whereas the second is a control run with only natural forcing. The results indicate that most glacier mass loss between 1850 and 1980 and about 75% of the total glacier retreat since 1850 can be attributed to natural climate forcing. However, in the late 1970s, glaciers appear to have crossed an invisible line into a state of decline that can be deemed unnatural. Over the past three decades, the human fingerprint on glacier mass balance emerges clearly, accounting for about 70% of glacier mass loss from 1991 to 2010. Glacier mass loss from 2001 to 2010 exceeded that of any other decade studied.

The results are subject to many uncertainties; it is a giant leap from GCM climate fields to mountain snowpacks and glacier melt processes. The mass losses that Marzeion *et al.* simulate are consistent with available glacier mass balance observations from the past several decades (*3*, *4*). In contrast, reconstructed glacier mass loss in (*1*) for 1851 to 1950, before worldwide mass balance observations, exceeds earlier estimates that were based on observations of glacier length changes (*5*, *6*). The magnitude of sea-level rise due to glacier attrition from 1851 to 2010 in (*1*) is also high relative to other reconstructions (*5*–*9*). Both naturally and anthropogenically forced glacier mass loss estimates may therefore be on the high side in the study of Marzeion *et al.*

The numbers will gradually come into better focus with improved resolution of mountain regions in climate models, application of more detailed models of snow and ice melt (*9*), and observational innovations (*8*). The main conclusions of Marzeion *et al.* with respect to attribution are unlikely to change, however; if there is a tendency to too much melting in the simulations, modeled glacier mass losses will be equally oversensitive to both natural and anthropogenic warming.

More subtle is the question of how time lags play into the attribution of natural versus anthropogenic forcing in (*1*). Glaciers are superb measuring sticks of climate, because they ignore the fluctuations of day-to-day weather. The geometry of mountain glaciers reflects the integrated meteorological conditions over decades to centuries. Glacier motion transfers mass slowly downhill; it can take decades for the glacier terminus to respond to a shift in climate. It is thus difficult to determine the contributions of natural and anthropogenic forcing based on glacier length or area records.

Marzeion *et al.* overcome this problem by examining mass balance records, which reflect annual snowfall and snow/ice melt. Mass balance is tightly linked to annual climatology, without a lag, although there are gradual mass balance feedbacks associated with glacier geometric adjustments. It is therefore unsurprising that glacier mass loss increased and anthropogenic forcing rose above the noise in the late 1970s, as did global mean temperatures (*10*).

The transition from natural to anthropogenic forcing of glacier mass loss could also be inferred from the relative stabilization of glaciers in the 1960s and early 1970s, which preceded the recent reinvigorated retreat. It remains to be seen how glaciers will weather the world that awaits them in this century of intensified anthropogenic forcing. Based on Marzeion *et al.*'s results, the past three decades provide a good indication of what is to come. Retreating glaciers will continue to be symbols of climate change. ■

Department of Geography, University of Calgary, Calgary, Alberta, T2N 1N4, Canada. E-mail: shawn.marshall@ucalgary.ca

REFERENCES

1. B. Marzeion *et al.*, *Science* **345**, 919 (2014).
2. B. Marzeion *et al.*, *Cryosphere* **6**, 1295 (2012).
3. D. G. Vaughan *et al.*, in *Climate Change 2013: The Physical Science Basis, Fifth Assessment Report of the Intergovernmental Panel on Climate Change*, T. F. Stocker *et al.*, Eds. (Cambridge Univ. Press, Cambridge, 2013), chap. 4.
4. J. G. Cogley, *Ann. Glaciol.* **50**, 96 (2009).
5. J. Oerlemans *et al.*, *The Cryosphere* **1**, 77 (2007).
6. P. W. Leclercq *et al.*, *Surv. Geophys.* **32**, 519 (2011).
7. V. Radić, R. Hock, *Nat. Geosci.* **4**, 91 (2011).
8. A. S. Gardner *et al.*, *Science* **340**, 852 (2013).
9. S. H. Mernild *et al.*, *J. Clim.* **27**, 6051 (2014).
10. K. E. Trenberth, J. T. Fasullo, *Earth's Future* **1**, 19 (2013).

10.1126/science.1258584

CREDIT: REPRODUCED WITH PERMISSION FROM R. W. SANDFORD

Published by AAAS

ECONOMICS

Boosting GDP growth by accounting for the environment

Including air pollution and greenhouse gas damages increases estimated U.S. growth

By **Nicholas Z. Muller**[1,2]

Governments around the world use national income accounting to measure economic performance. However, it is widely recognized that indices that focus exclusively on market production, such as gross domestic product (GDP), are incomplete. National accounts could be extended to include many nonmarket services. This paper presents an analysis of how adjusting GDP to reflect the effects of air pollution would affect economic growth rates in the United States. Inclusion of monetized measures of environmental quality is a potentially important step in moving toward a measure that captures social welfare more accurately than GDP.

POLICY

Environmental accounts include the capacity of natural systems to act as a source of inputs to production or as a sink for anthropogenic residuals. Advances in modeling and empirical environmental accounting (*1*–*6*) bolster the case made by the U.S. National Research Council (NRC) (*7*) for extending the U.S. National Income and Product Accounts (NIPAs) to include air pollution. The focus on air quality also has a conceptual basis in that it is a near-market extension; air pollution emissions stem from, and are attributable to, market production. From the perspective of prioritizing areas to augment NIPAs, it makes sense to include air pollution because of (i) high-quality data, (ii) potentially large effects on the NIPAs, and (iii) effects that are directly linkable to activities in markets.

This paper tabulates gross external damages (GED), a "price-times-quantity" measure of air pollution effects, over multiple years in the United States (*3*). The analysis also estimates damages due to carbon dioxide (CO_2) emissions. The paper then computes environmentally adjusted value added (EVA), which is GDP less GED (*4*, *5*).

In contrast with most previous empirical environmental accounting papers, this analysis focuses on how inclusion of GED affects real growth rates. After all, the primary value of the market NIPAs resides in reporting changes over time. As further motivation, the NRC panel concluded that the result of an improvement in air quality "might be a substantial increase in the estimate of growth of comprehensive consumption over this period" (*7*). The paper tests this proposition over a period in which aggregate air pollution emissions decreased substantially.

INTEGRATED ASSESSMENT. GED are computed using AP2, a new version of an existing integrated assessment model (*3*, *4*). [See a full description in the supplementary materials (SM)]. AP2 connects emissions of five common air pollutants (nitrogen oxides, sulfur dioxide, fine particulate matter, ammonia, and volatile organic compounds) to estimates of ambient concentrations, exposures, physical effects, and monetary damage. Data years 1999, 2002, 2005, and 2008 correspond to available emissions data from the U.S. Environmental Protection Agency (EPA) National Emissions Inventory.

An air quality model links emissions to annual average concentrations by county. Exposures are tabulated by tracking predicted concentrations and populations of sensitive receptors at the county level (e.g., human populations and crops). Physical effects (reduced crop yields or increased mortality rates, for example) are estimated using concentration-response functions from peer-reviewed publications. Valuation uses reported market prices (for crops) or standard nonmarket techniques (e.g., the Value of a Statistical Life approach for human mortality risks).

The AP2 model computes marginal (dollar per ton) damages, which are used as "prices" in the GED calculations. The marginal damage algorithm (see SM) is repeated for all five pollutants, for 10,000 pollution sources, and for four data years. To compute GED, marginal damages are matched to, and multiplied by, emissions data by source, pollutant, and year. CO_2 emissions data are provided by U.S. Department of Energy (*8*) and valued using a \$32/ton CO_2 social cost of carbon (*9*). Total CO_2 damage is computed by multiplying reported emissions times this per-unit cost.

REDUCE POLLUTION, INCREASE GROWTH. Between 1999 and 2008, the air pollution intensity of U.S. economic output (GED/GDP) fell by one-half: from 6.4% to 3.2% (Table 1, top). Including CO_2 damage, this ratio dropped from 8.4% to 4.8%. Including damages from CO_2 emissions increases the GED by 31% to 53%. The spread between EVA and GDP, the GED, narrows appreciably from 1999 to 2008.

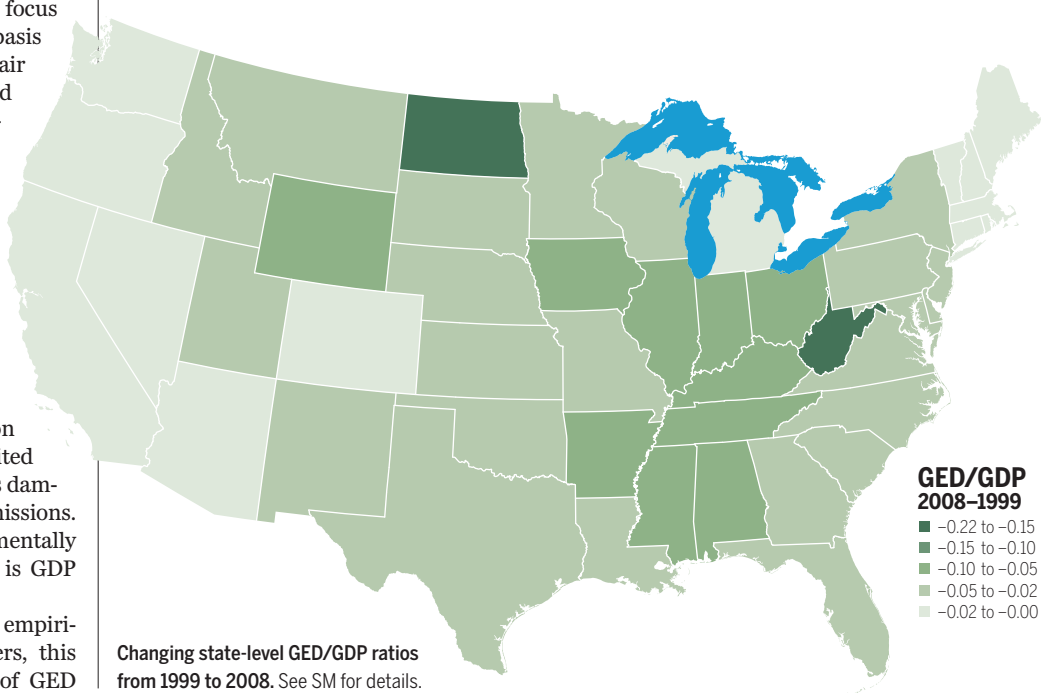

Changing state-level GED/GDP ratios from 1999 to 2008. See SM for details.

Downloaded from www.sciencemag.org on August 24, 2014

Published by AAAS

Relative to GDP, accounting for air pollution damage in the EVA increases the ex post estimated rate of economic growth in the U.S. economy because GED dropped so sharply over this time period (see the table, at the bottom). The difference between EVA and GDP growth was greatest from 1999 to 2002 (+0.58%). For growth between the 2002–2005 and 2005–2008 periods, EVA expanded by about +0.3% faster than GDP.

Including damages from CO_2 has a small effect on the EVA growth rate. CO_2 damages were essentially flat from 1999 to 2008. Growth in air pollution damages is consistently negative. Combining the two yields GED that contract by between 5% and 1.5% annually. CO_2 reduces the rate of change in GED, which lowers the EVA growth rate. However, the lower EVA value in the base period (due to including CO_2 damage) increases EVA growth (see SM).

The figure maps the change in GED/GDP ratio by state from 1999 to 2008. There was a dramatic reduction in GED/GDP between 1999 and 2008 (over 0.15 in both North Dakota and West Virginia).

Aggregate levels and annual rates of growth

Levels	1999	2002	2005	2008
GED	589 [768]	478 [661]	443 [632]	351 [535]
EVA	8,575 [8,395]	9,399 [9,216]	10,276 [10,086]	10,750 [10,566]
GDP	9,164	9,877	10,718	11,101
GED/GDP	0.064 [0.084]	0.048 [0.067]	0.041 [0.059]	0.032 [0.048]
Growth	**1999**	**2002**	**2005**	**2008**
GED	*	−6.75 [−4.91]	−2.53 [−1.49]	−7.46 [−5.39]
EVA	*	3.11 [3.16]	3.02 [3.05]	1.52 [1.56]
GDP	*	2.53	2.76	1.18

Aggregate levels and annual rates of growth. GED, EVA, and GDP. All "Levels" are expressed in real year-2000 US$, in billions. Values in brackets include damages from CO_2 produced from energy production and consumption. All "Growth" is expressed in annualized rates of change from the previous period (%); GDP is from (*13*). GED and EVA are from the author's calculations (see SM).

AUGMENTING GDP. Including air pollution and CO_2 damages in the NIPAs increases real rates of growth relative to conventional market indices between 1999 and 2008. The conceptual basis for inclusion of these damages is as a cost of production (*10*). Firms pay fees for solid waste disposal because property rights are well defined over land areas used as permanent repositories. Such fees are an accepted part of doing business and are encompassed by the NIPAs. Absent property rights on the atmosphere (either real or implied by regulation), firms face no costs, or inefficiently low costs, for disposal of air emissions. The augmented accounting system deducts these costs from GDP (*4*, *5*, *10*).

One concern with this approach is that these costs of disposal, the GED, are already in the NIPAs. Although expenditures on abatement technology are in the NIPAs, the present study values remaining emissions after abatement. Further, research has shown that the vast majority of the GED are composed of premature mortality risks (*1*–*3*) that lie beyond the accounting boundary established in the NIPA (*11*). For other pollutants with effects within the market boundary, considerations of double counting may be more relevant.

In the state accounts, GED are attributed to the region of emission. This implies that, although EVA growth in the emitting region increases if GED drops, the real beneficiaries may not be within the same region, and the only way in which EVA growth of this sort would actually manifest in the emitting region is if the polluter faces the costs of waste disposal. The GED are external costs, and if there is no means by which polluters realize these costs, whether they increase or decrease only matters to the exposed population. The argument says nothing about how costs would enter the polluter's balance sheet—for example, through corrective taxation or pollution allowances. Also unaddressed is whether these costs, once paid by polluters, are redistributed to victims or what an optimal level of GED would be.

Four important caveats are worth noting. First, the GED estimates embody considerable uncertainty in inputs to each stage of the integrated assessment model (*12*) and in the social cost of carbon (*9*). Second, the relationship between GED, GDP, and EVA in this paper is specific to the application. Expanding the NIPA to include air pollution and CO_2 damage in other countries (or in the United States in an earlier decade) may result in augmented growth rates lower than GDP.

Third, EVA is intended as an augmentation of GDP rather than a replacement. A complete augmentation would need to include home production, leisure time, and other areas in the environmental context. Fourth, although air pollution and greenhouse gas emissions are substantial contributors to aggregate environmental damages, the analysis does not include solid waste, water pollution, or incremental emissions of toxins such as mercury because of data and modeling limitations. Also omitted are measures of net natural resource consumption. These other dimensions are likely to be important in international contexts and developing economies and could change the orientation between EVA and GDP growth. ■

[1]Department of Economics and Environmental Studies Program, Middlebury College, Middlebury, VT 05753 USA. [2]Faculty Research Fellow, National Bureau of Economic Research, Cambridge, MA 02138 USA. nmuller@middlebury.edu

REFERENCES

1. United States Environmental Protection Agency, *The Benefits and Costs of the Clean Air Act: 1990–2010*. EPA Report to Congress. EPA 410-R-99-001 (Office of Air and Radiation, Office of Policy, Washington, DC, 1999).
2. H. S. Banzhaf, D. Burtraw, K. Palmer, *Resour. Energy Econ.* **26**, 317 (2004).
3. N. Z. Muller, R. O. Mendelsohn, W. D. Nordhaus, *Am. Econ. Rev.* **101**, 1649 (2011).
4. N. Z. Muller, "Towards the Measurement of Net Economic Welfare: Air Pollution Damage in the United States National Accounts - 2002, 2005, 2008," forthcoming in *Measuring Economic Sustainability and Progress*, D. W. Jorgensen, J. S. Landefeld, P. Schreyer, Eds. NBER Book Series in Income and Wealth (2014). Available at www.nber.org/chapters/c12839
5. P. Bartelmus, *Ecol. Econ.* **68**, 1850 (2008).
6. National Academy of Sciences, National Research Council, *Hidden Costs of Energy: Unpriced Consequences of Energy Production and Use* (National Academies Press, Washington, DC, 2010).
7. National Academy of Sciences, National Research Council, *Nature's Numbers: Expanding the U.S. National Economic Accounts to Include the Environment*. W. D. Nordhaus, E. C. Kokkelenberg, Eds. (National Academy Press, Washington, D.C., 1999).
8. United States Department of Energy, Energy Information Administration, December, 2013 Monthly Energy Review: Table 12.1 Carbon Dioxide Emissions from Energy Consumption by Source (2013); www.eia.gov/totalenergy/data/monthly/index.cfm
9. United States Office of Management and Budget, Technical Support Document: Technical Update of the Social Cost of Carbon for Regulatory Impact Analysis – Under Executive Order 12866 (2013); www.whitehouse.gov/sites/default/files/omb/inforeg/social_cost_of_carbon_for_ria_2013_update.pdf
10. K. G. Abraham, C. Mackie, in *A New Architecture for the U.S. National Accounts: NBER Studies in Income and Wealth, Vol. 66*, D. W. Jorgensen, J. S. Landefeld, W. D. Nordhaus, Eds. (University of Chicago Press, Chicago, IL, 2006).
11. W. D. Nordhaus, in *A New Architecture for the U.S. National Accounts: NBER Studies in Income and Wealth, Vol. 66*, D. W. Jorgensen, J. S. Landefeld, W. D. Nordhaus, Eds. (University of Chicago Press, Chicago, IL, 2006).
12. N. Z. Muller, *B.E. Press J. Econ. Analy. Pol.* **11**(1), Contribution, Article 32 (2011).
13. United States Bureau of Economic Analysis, (2013); www.bea.gov/iTable/index_nipa.cfm

SUPPLEMENTARY MATERIALS

www.sciencemag.org/content/345/6199/873/suppl/DC1

10.1126/science.1253506

Published by AAAS

BOTANY

Making phloem—a near-death experience

How to get rid of the phloem cell nucleus to make a root-to-shoot tip transport system

By **Niko Geldner**

Differentiation in complex multicellular organisms generates a plethora of different cell types that often display drastically altered physiology, morphology, and size in comparison to the common stem cells from which they are all derived. An extreme example of differentiation is apoptosis, a programmed, active cellular suicide as the final stage of differentiation. Yet, even more fascinating are cells whose differentiation program pushes them to the edge of death but then maintains them there in a delicate balance. On page 933 of this issue Furuta *et al.* (*1*) begin to unravel the pathway of just such a cell type in plants that has lost its nuclei and depends on neighboring (nucleated) cells for survival.

Plants have solved the challenge of long-distance transport of signals and nutrients in a remarkable way. Instead of generating specialized extracellular spaces, lined by cells, as in the case of blood vessels, plants have come up with a way to generate a transport route within the transport cells themselves. This is achieved by the generation of a syncytium that stretches from the roots to the youngest leaflets. These interconnected "phloem sieve elements" fortify their cell walls, get rid of their nucleus and most of their organelles, and generate a highly fluid cytosol that allows for flow rates of up to 110 μm/s (see the figure) (*2*). Remaining organelles become attached just beneath the plasma membrane. In the absence of a nucleus, sieve elements depend on "companion cells," which are intimately connected to the sieve element by numerous plasmodesmata, elaborate cytoplasmic tunnels that connect plant cells (*3*). Thus, phloem sieve element cells undergo a differentiation program that impairs their ability to maintain cellular metabolism but remain alive thanks to life support provided by their neighbors, whose extensions they effectively become.

Phloem differentiation challenges our basic concepts of cells as functional units and our definition of what constitutes a living cell. Physiology and ontogeny of phloem cells have been extensively studied in the literature (*4*–*6*), but we have remained surprisingly ignorant about the molecules that drive phloem differentiation. Seedling roots of *Arabidopsis thaliana* combine an unequaled molecular toolbox with the possibility to image the innermost root cell layers thanks to their being very thin and rather transparent.

Furuta *et al.* use these two features to identify the molecular players that drive enucleation in phloem sieve elements. The first specific determinant of phloem identity was the myeloblastosis (MYB) family transcription factor ALTERED PHLOEM DEVELOPMENT (APL) (*7*). Comparing phloem-specific expression profiles between wild-type and MYB-mutant plants, Furuta *et al.* identified two NAC [NAM (no apical meristem), ATAF, CUC (cup-shaped cotyledon)] family transcription factors as potential downstream targets of APL. Upon generation of NAC double-mutant plants, some aspects of phloem differentiation, notably nuclear breakdown and cytosolic dilution, are strongly affected, whereas many other differentiation events, such as sieve plate formation or cell wall thickening proceed normally. The authors then compare potential downstream targets in another round of cell-type–specific expression profiling, comparing NAC45/86 double mutants, a NAC45 overexpressing plant, and wild-type plants. Among the differentially expressed genes was a family of nucleases (NEN1-4). Specific expression in developing phloem sieve element cells before enucleation was confirmed by live imaging of reporter lines. A knock-out of one of the nucleases, NEN4, displays a distinct defect in the breakdown of nuclear content. With this

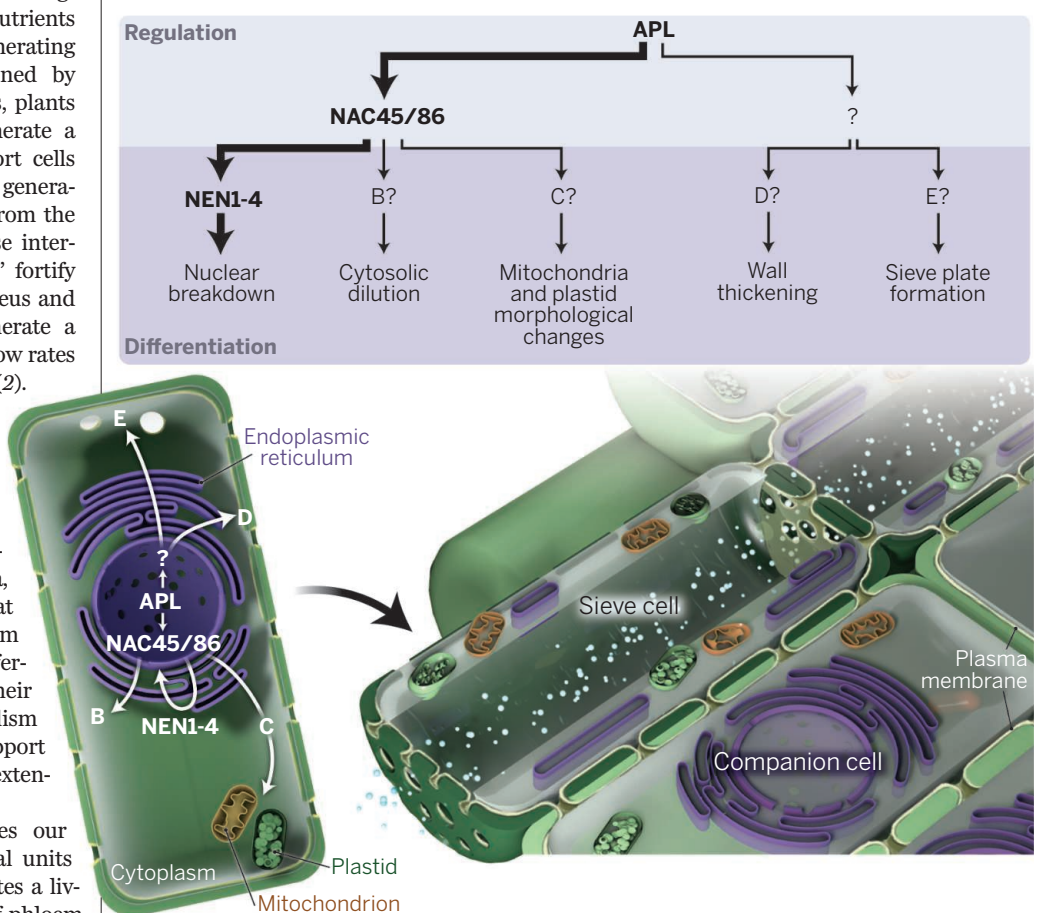

Barely living. Differentiation of a phloem sieve element. The schematic (**top**) highlights known and unknown branches of the phloem specification and differentiation pathway. B, C, D, and E indicate as-yet-unidentified genes that drive different aspects of phloem sieve element differentiation. The illustration (**bottom**) indicates the location at which these gene products are acting during differentiation and the final form of the phloem and companion cell.

ILLUSTRATION: V. ALTOUNIAN/*SCIENCE*

University of Lausanne, DBMV, Biophore, UNIL-Sorge, 1015 Lausanne, Switzerland. E-mail: niko.geldner@unil.ch

Published by AAAS

study, Furuta *et al.* connect the activity of a transcription factor involved in early phloem specification events to the expression of specific enzymes that actually execute phloem differentiation. Such a "rooting" of the transcription factor cascade will help to better define and understand the functional architecture of the transcriptional regulatory networks leading to phloem differentiation. In the future, it will be intriguing to understand through which factors APL drives other sieve element differentiation processes that are not dependent on NAC45/86. The first demonstration of an enzyme family that is clearly associated with a distinct differentiation feature of sieve elements—the breakdown of nuclear material—raises the question of what other players there might be and whether this differentiation process is better viewed as a case of an arrested programmed cell death (PCD) or whether it should be seen as a distinct process that merely resembles PCD. The progress made in defining the molecular and cell biological events of PCD in *Arabidopsis* (*8*) will certainly help in deciding in how far sieve element differentiation resembles PCD observed in other cells. The timing and formation of plasmodesmatal connection to the companion cells, how long enucleated sieve elements can survive without a companion cell, and who initiates and controls the establishment of plasmodesmata—the differentiating sieve element cell or the future companion cell—are open questions.

Finally, it will be important to understand how other factors regulating phloem differentiation, such as BREVIS-RADIX (BRX), BARELY ANY MERISTEM 3 (BAM3), or OCTOPUS (OPS) are interconnected with APL and NAC45/86. In contrast to APL, genes like BRX are not absolutely required for phloem differentiation but rather seem to be involved in determining the rate and timing of differentiation, possibly in response to hormonal/environmental signals (*9*).

With the NEN nucleases uncovered by Furuta *et al.*, we are starting to appreciate how phloem sieve elements enter this extremely derived state in which they act as little segments of a vast cellular transport highway that sustains the life of higher plants. ■

REFERENCES

1. K. M. Furuta *et al.*, *Science* **345**, 933 (2014).
2. R. D. Sjolund, *Plant Cell* **9**, 1137 (1997).
3. T. M. Burch-Smith, P. C. Zambryski, *Annu. Rev. Plant Biol.* **63**, 239 (2012).
4. B. K. Ham, W. J. Lucas, *J. Exp. Bot.* **65**, 1799 (2014).
5. H. Wu, X. F. Zheng, *Acta Bot. Sin.* **45**, 322 (2003).
6. K. Esau, *Anatomy of Seed Plants* (Wiley, New York, ed. 2, 1977).
7. M. Bonke *et al.*, *Nature* **426**, 181 (2003).
8. M. Fendrych *et al.*, *Curr. Biol.* **24**, 931 (2014).
9. A. Rodriguez-Villalon *et al.*, *Proc. Natl. Acad. Sci. USA*, PNAS Early Edition, 10.1073/pnas.1407337111 (2014).

10.1126/science.1258711

RNA

Riboswitch regulates RNA

Nutrient metabolism in bacteria is controlled by a circuit in which RNA is regulated by RNA

By **Jiandong Chen** *and* **Susan Gottesman**

Bacteria are expert at adapting to various ecological niches, including the human gut, amid multiple other competing organisms. Their success in these many environments means that they have perfected the ability to use what is available, to not waste resources making RNA and protein for unnecessary processes, and to sense and respond when conditions and requirements change. It has become increasingly clear that RNA-based regulation plays an important part in empowering bacteria to respond to environmental changes. On pages 937 and 940 of this issue, DebRoy *et al.* (*1*) and Mellin *et al.* (*2*), respectively, report a new example of adaptation in which type of RNA-based regulation is controlled by another, allowing the integrated sensing of two different nutrients. The finding points to an unexpected role for riboswitches, RNA binding proteins, and noncoding RNAs in controlling gene expression by joining forces.

DebRoy *et al.* and Mellin *et al.* investigated the regulated utilization of ethanolamine as a carbon and nitrogen source in the pathogens *Enterococcus faecalis* and *Listeria monocytogenes*. The genes necessary for ethanolamine catabolism are clustered together in the bacterial genome, with most of them under the control of a single promoter. This unit, called the *eut* operon, is present in a wide spectrum of bacterial species, and in all studied cases, the metabolic genes are well expressed only when two nutrients are present—the substrate ethanolamine and vitamin B_{12}, an essential cofactor for enzymes in the catabolic pathway. In the pathogen *Salmonella enterica*, this response is mediated by the transcriptional activator EutR. EutR is activated upon binding to both ethanolamine and vitamin B_{12} (*3*). Now, DebRoy *et al.* and Mellin *et al.* have uncovered a more sophisticated RNA-based circuitry for controlling ethanolamine metabolism in response to both nutrient signals.

Ethanolamine is directly sensed by EutW, a histidine kinase. EutW, in turn, phosphorylates and thereby activates EutV, an RNA binding protein (*4*). EutV binds to RNA hairpin motifs and act as an "antiterminator"—that is, the dimer blocks the formation of RNA hairpins that terminate further transcription of the *eut* operons. Therefore, when EutV is active and available, ethanolamine metabolism genes are expressed. The surprise arises from how this system uses a riboswitch to integrate a vitamin B_{12} signal into this control system—it regulates the availability of active EutV.

A riboswitch is a metabolite-sensing RNA element predominantly present in the 5′ untranslated region of mRNA. Ligand binding to the aptamer domain of a riboswitch causes structural changes downstream in the RNA, usually resulting in inhibition of translation initiation or premature transcription termination (*5*). Riboswitches that recognize vitamin B_{12} and lead to the down-regulation of vitamin B_{12} synthesis genes were among the first to be studied (*5*, *6*). For these, vitamin B_{12} acts as an OFF switch—when vitamin B_{12} is abundant, more vitamin B_{12} synthesis is not needed. DebRoy *et al.* and Mellin *et al.* report a vitamin B_{12}-binding riboswitch (see the first figure) that regulates transcription termination in the same manner as a classical vitamin B_{12} switch. However, the RNA made in the absence of vitamin B_{12} has a unique role. Instead of encoding a protein, the transcript produced in the absence of vitamin B_{12} is a noncoding RNA that sequesters the activated EutV protein. This prevents EutV from stimulating the synthesis of ethanolamine metabolic genes (see the second figure). Thus, this vitamin B_{12} riboswitch

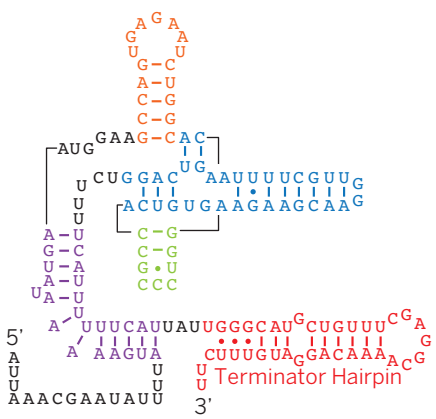

The secondary structure of the vitamin B_{12} riboswitch.

CREDIT: WADE C. WINKLER/UNIVERSITY OF MARYLAND, COLLEGE PARK

Laboratory of Molecular Biology, National Cancer Institute, Bethesda, MD 20892, USA. E-mail: gottesms@helix.nih.gov

Published by AAAS

study, Furuta *et al.* connect the activity of a transcription factor involved in early phloem specification events to the expression of specific enzymes that actually execute phloem differentiation. Such a "rooting" of the transcription factor cascade will help to better define and understand the functional architecture of the transcriptional regulatory networks leading to phloem differentiation. In the future, it will be intriguing to understand through which factors APL drives other sieve element differentiation processes that are not dependent on NAC45/86. The first demonstration of an enzyme family that is clearly associated with a distinct differentiation feature of sieve elements—the breakdown of nuclear material—raises the question of what other players there might be and whether this differentiation process is better viewed as a case of an arrested programmed cell death (PCD) or whether it should be seen as a distinct process that merely resembles PCD. The progress made in defining the molecular and cell biological events of PCD in *Arabidopsis* (*8*) will certainly help in deciding in how far sieve element differentiation resembles PCD observed in other cells. The timing and formation of plasmodesmatal connection to the companion cells, how long enucleated sieve elements can survive without a companion cell, and who initiates and controls the establishment of plasmodesmata—the differentiating sieve element cell or the future companion cell—are open questions.

Finally, it will be important to understand how other factors regulating phloem differentiation, such as BREVIS-RADIX (BRX), BARELY ANY MERISTEM 3 (BAM3), or OCTOPUS (OPS) are interconnected with APL and NAC45/86. In contrast to APL, genes like BRX are not absolutely required for phloem differentiation but rather seem to be involved in determining the rate and timing of differentiation, possibly in response to hormonal/environmental signals (*9*).

With the NEN nucleases uncovered by Furuta *et al.*, we are starting to appreciate how phloem sieve elements enter this extremely derived state in which they act as little segments of a vast cellular transport highway that sustains the life of higher plants. ■

REFERENCES

1. K. M. Furuta *et al.*, *Science* **345**, 933 (2014).
2. R. D. Sjolund, *Plant Cell* **9**, 1137 (1997).
3. T. M. Burch-Smith, P. C. Zambryski, *Annu. Rev. Plant Biol.* **63**, 239 (2012).
4. B. K. Ham, W. J. Lucas, *J. Exp. Bot.* **65**, 1799 (2014).
5. H. Wu, X. F. Zheng, *Acta Bot. Sin.* **45**, 322 (2003).
6. K. Esau, *Anatomy of Seed Plants* (Wiley, New York, ed. 2, 1977).
7. M. Bonke *et al.*, *Nature* **426**, 181 (2003).
8. M. Fendrych *et al.*, *Curr. Biol.* **24**, 931 (2014).
9. A. Rodriguez-Villalon *et al.*, *Proc. Natl. Acad. Sci. USA*, PNAS Early Edition, 10.1073/pnas.1407337111 (2014).

10.1126/science.1258711

RNA

Riboswitch regulates RNA

Nutrient metabolism in bacteria is controlled by a circuit in which RNA is regulated by RNA

By **Jiandong Chen** *and* **Susan Gottesman**

Bacteria are expert at adapting to various ecological niches, including the human gut, amid multiple other competing organisms. Their success in these many environments means that they have perfected the ability to use what is available, to not waste resources making RNA and protein for unnecessary processes, and to sense and respond when conditions and requirements change. It has become increasingly clear that RNA-based regulation plays an important part in empowering bacteria to respond to environmental changes. On pages 937 and 940 of this issue, DebRoy *et al.* (*1*) and Mellin *et al.* (*2*), respectively, report a new example of adaptation in which type of RNA-based regulation is controlled by another, allowing the integrated sensing of two different nutrients. The finding points to an unexpected role for riboswitches, RNA binding proteins, and noncoding RNAs in controlling gene expression by joining forces.

DebRoy *et al.* and Mellin *et al.* investigated the regulated utilization of ethanolamine as a carbon and nitrogen source in the pathogens *Enterococcus faecalis* and *Listeria monocytogenes*. The genes necessary for ethanolamine catabolism are clustered together in the bacterial genome, with most of them under the control of a single promoter. This unit, called the *eut* operon, is present in a wide spectrum of bacterial species, and in all studied cases, the metabolic genes are well expressed only when two nutrients are present—the substrate ethanolamine and vitamin B_{12}, an essential cofactor for enzymes in the catabolic pathway. In the pathogen *Salmonella enterica*, this response is mediated by the transcriptional activator EutR. EutR is activated upon binding to both ethanolamine and vitamin B_{12} (*3*). Now, DebRoy *et al.* and Mellin *et al.* have uncovered a more sophisticated RNA-based circuitry for controlling ethanolamine metabolism in response to both nutrient signals.

Ethanolamine is directly sensed by EutW, a histidine kinase. EutW, in turn, phosphorylates and thereby activates EutV, an RNA binding protein (*4*). EutV binds to RNA hairpin motifs and act as an "antiterminator"—that is, the dimer blocks the formation of RNA hairpins that terminate further transcription of the *eut* operons. Therefore, when EutV is active and available, ethanolamine metabolism genes are expressed. The surprise arises from how this system uses a riboswitch to integrate a vitamin B_{12} signal into this control system—it regulates the availability of active EutV.

A riboswitch is a metabolite-sensing RNA element predominantly present in the 5′ untranslated region of mRNA. Ligand binding to the aptamer domain of a riboswitch causes structural changes downstream in the RNA, usually resulting in inhibition of translation initiation or premature transcription termination (*5*). Riboswitches that recognize vitamin B_{12} and lead to the down-regulation of vitamin B_{12} synthesis genes were among the first to be studied (*5*, *6*). For these, vitamin B_{12} acts as an OFF switch—when vitamin B_{12} is abundant, more vitamin B_{12} synthesis is not needed. DebRoy *et al.* and Mellin *et al.* report a vitamin B_{12}-binding riboswitch (see the first figure) that regulates transcription termination in the same manner as a classical vitamin B_{12} switch. However, the RNA made in the absence of vitamin B_{12} has a unique role. Instead of encoding a protein, the transcript produced in the absence of vitamin B_{12} is a noncoding RNA that sequesters the activated EutV protein. This prevents EutV from stimulating the synthesis of ethanolamine metabolic genes (see the second figure). Thus, this vitamin B_{12} riboswitch

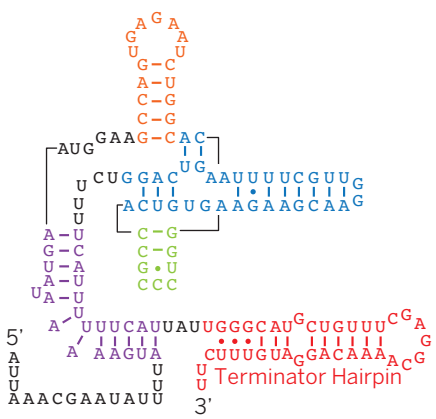

The secondary structure of the vitamin B_{12} riboswitch.

CREDIT: WADE C. WINKLER/UNIVERSITY OF MARYLAND, COLLEGE PARK

Laboratory of Molecular Biology, National Cancer Institute, Bethesda, MD 20892, USA. E-mail: gottesms@helix.nih.gov

Published by AAAS

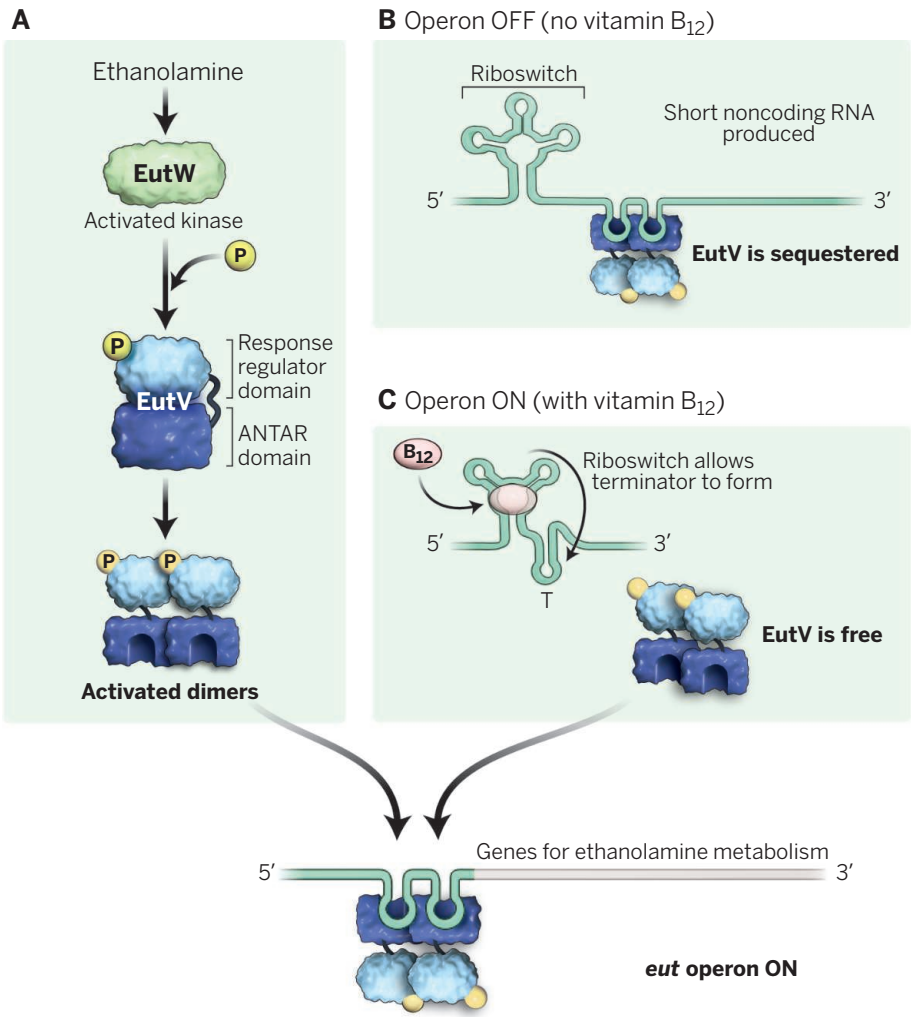

Riboswitch-based regulation. The *eut* operon contains genes involved in ethanolamine metabolism in bacteria. (**A**) EutV is phosphorylated and activated by EutW in response to ethanolamine. Active EutV forms a dimer that binds to adjacent RNA hairpins in the target transcript. Binding at these sites leads to antitermination; thus, transcription of the operon is turned ON, but this can only happen in the presence of vitamin B_{12}. (**B**) In the absence of vitamin B_{12}, a noncoding RNA is generated that sequesters EutV; thus, transcription of the operon is turned OFF. (**C**) In the presence of vitamin B_{12}, the riboswitch blocks transcription of the noncoding RNA through a structural change that produces a terminating hairpin RNA (T). Active EutV protein is then free to bind to the target transcript and promote expression of ethanolamine metabolic genes.

acts as an ON switch for the catabolism of a nutrient by blocking the formation of a negatively acting RNA.

The finding of DebRoy *et al.* and Mellin *et al.* extends the ways by which bacteria exploit riboswitches to modulate RNA structure and function in response to specific ligands. Loh *et al.* found that two *S*-adenosylmethionine riboswitches control expression of the virulence regulator PrfA by acting as noncoding RNAs (*7*). Another *Listeria* vitamin B_{12} riboswitch controls the metabolism of the nutrient propanediol (a carbon source). Vitamin B_{12} is a cofactor of enzymes for this catabolic process as well. Here, the vitamin B_{12} riboswitch controls transcript length—and therefore the activity—of the antisense RNA AspocR. AspocR is a negative regulator of the propanediol-activated transcription factor PocR. In the absence of vitamin B_{12}, the long isoform antisense RNA inhibits PocR expression; binding of vitamin B_{12} to the riboswitch leads to early transcription termination of the antisense RNA, allowing PocR expression and activation of propanediol catabolism (*8*). Thus, for both ethanolamine and propanediol, the vitamin B_{12} riboswitch ensures expression of the metabolic genes only when both the substrate and vitamin B_{12} are present. It seems likely that in addition to downstream protein-coding genes, many other regulatory RNAs will be found downstream of riboswitches.

EutV is a member of the AmiR and NasR transcriptional antiterminator regulator domain (ANTAR) family of RNA binding proteins. It has an N-terminal response regulator domain that is separated by a coiled-coil structure from the RNA-binding ANTAR domain, the most common architecture for this family of proteins (*9*). When activated, ANTAR proteins dimerize and bind to two short RNA stem-loops in the target transcript (*9*). Few ANTAR proteins have been studied, and although they all control antitermination, each is regulated differently. The ANTAR protein AmiR is controlled by an inhibitor protein, AmiC, that itself is regulated by a ligand. ANTAR protein NasR is controlled by direct binding of a small molecule to the regulatory domain (*9*). One would expect activation of the ANTAR proteins to be fully reversible; certainly, most response regulatory domains can be rapidly dephosphorylated when the inducing signal is absent, although this has not been studied for EutV.

DebRoy *et al.* and Mellin *et al.* demonstrate an additional level of negative control: the sequestration of ANTAR proteins by an RNA that mimics the ANTAR binding site of the target RNA. This theme of controlling RNA binding proteins by regulatory RNAs that titrate their availability has been well studied for the RNA translational regulatory proteins of the bacterial CsrA family (*10*, *11*). For regulation to work effectively, the titrating RNA must be abundant and/or have a higher affinity than the target RNAs for the regulatory protein, yet must also have some way of being removed when no longer needed. Instability of the titrating RNA would be sufficient, but a cascade of titrators is another possibility: antisense RNAs, for example, which bind to and remove the primary titrating RNAs.

The world of RNA regulators is intricately interlinked, with no clear boundaries separating trans-acting regulatory RNAs, cis-acting sites for RNA binding proteins, and riboswitches. Every combination is possible and will probably be found, and each of the many regulatory RNA binding proteins is probably subject to multiple levels of regulation by, not surprisingly, RNAs. ■

REFERENCES AND NOTES

1. S. DebRoy *et al.*, *Science* **345**, 937 (2014).
2. J. R. Mellin *et al.*, *Science* **345**, 940 (2014).
3. D. A. Garsin, *Nat. Rev. Microbiol.* **8**, 290 (2010). .
4. K. A. Baker, M. Perego, *J. Bacteriol.* **193**, 2575 (2011).
5. A. Serganov, E. Nudler, *Cell* **152**, 17 (2013).
6. A. Nahvi *et al.*, *Chem. Biol.* **9**, 1043 (2002).
7. E. Loh *et al.*, *Cell* **139**, 770 (2009).
8. J. R. Mellin *et al.*, *Proc. Natl. Acad. Sci. U.S.A.* **110**, 13132 (2013).
9. A. Ramesh *et al.*, *PLOS Genet.* **8**, e1002666 (2012).
10. M. G. Jørgensen *et al.*, *Genes Dev.* **27**, 1132 (2013).
11. T. Romeo *et al.*, *Environ. Microbiol.* **15**, 313 (2013).

ACKNOWLEDGMENTS

Supported by the Intramural Research Program of the National Cancer Institute, Center for Cancer Research. We thank G. Storz, K. Ramamurthi, M. M. Gottesman, and S. Gottesman lab members for comments.

10.1126/science.1258494

ILLUSTRATION: V. ALTOUNIAN/SCIENCE

Published by AAAS

EVOLUTION

Sensing nectar's sweetness

A taste receptor evolves to sense sugar in adapting to the diet of some birds

By **Peihua Jiang** *and* **Gary K. Beauchamp**

In a brief comment on the sense of taste, Charles Darwin noted that "Real taste [in] the mouth, in my theory must be acquired by certain foods being habitual—[and] hence become hereditary" (*1*). This view, that taste perception and diet form a coordinated evolutionarily guided system, has received renewed support from recent behavioral, physiological, and molecular studies of comparative taste. On page 929 of this issue, Baldwin *et al.* (*2*) describe a striking example of this coordination in sweet nectar–eating hummingbirds—the repurposing of an amino acid taste receptor to respond to sugars and other sweeteners, permitting these birds to occupy a whole new avian niche.

In vertebrates, taste responses to sugars and some other sweeteners and to some amino acids are mediated by G protein–coupled receptor heterodimers—the T1R2-T1R3 sweet taste receptor and the T1R1-T1R3 umami or amino acid taste receptor (*3*). Functions of these taste receptors are often closely related to a species' feeding ecology. For instance, it has long been believed that sweet taste serves to identify and motivate consumption of plant-based small-molecule carbohydrates. This presumption received strong support from findings that loss of the sweet taste receptor gene *Tas1r2*, which encodes the T1R2 receptor component, occurred independently in many obligate carnivores from the order Carnivora (*4*). These animals do not consume sugars such as sucrose, glucose, or fructose, all of which taste sweet to humans and are highly preferred by many omnivorous and herbivorous species. Such animals thus appear to be insensitive ("blind") to the taste of sugar.

Species of birds, like mammals, also differ dramatically in their typical diets, ranging from completely plant-based to completely animal-based. Yet, it appears that all birds have lost the *Tas1r2* taste receptor gene and thus might all be expected to also be sweet taste blind (*5*). For example, the domestic chicken has an omnivorous diet but is indifferent to sugar sweeteners. But if this is so, there is a puzzle: How can one explain the appetitive behavior of bird species such as hummingbirds that typically consume foods that consist primarily of sweet sugars? When tested behaviorally, hummingbirds do indeed demonstrate a "sweet tooth." What then is the hummingbird's sweet receptor?

Baldwin *et al.* provided the answer by using a variety of experimental approaches. The authors identified *Tas1r1* and *Tas1r3* from whole-genome sequences available for 10 bird species, including the hummingbird. However, they failed to detect *Tas1r2* in any of these bird genomes. By comparison, the *Tas1r2* gene is present in non-avian reptiles, which belong to the sister group to birds. This suggests that the loss of *Tas1r2* most likely occurred sometime shortly after birds and non-avian reptiles diverged.

To determine whether the T1R1-T1R3 amino acid taste receptor might have taken over responsiveness to sweet sugars, Baldwin *et al.* expressed the chicken, swift (a close relative of hummingbirds), and hummingbird T1R1-T1R3 receptors in a cell-based assay system and evaluated responses of each toward amino acids and sugars. Remarkably, the hummingbird T1R1–T1R3 amino acid receptor responded to sweet-tasting sugars, sugar alcohols, and sucralose (an artificial sweetener derived from sucrose), as well as to high concentrations of amino acids. In marked contrast, the only stimuli that chicken and swift responded to were two of the three amino acids tested. Baldwin *et al.* propose that the hummingbird T1R1-T1R3 receptor acquired a new function to recognize carbohydrates in the past 42 to 72 million years after the hummingbird-swift divergence. Using a series of chimeras made between the hummingbird and chicken T1R3 receptors, Baldwin *et al.* found that a number of residues in the hummingbird T1R3 subunit are critical for the acquired sensitivity of the receptor

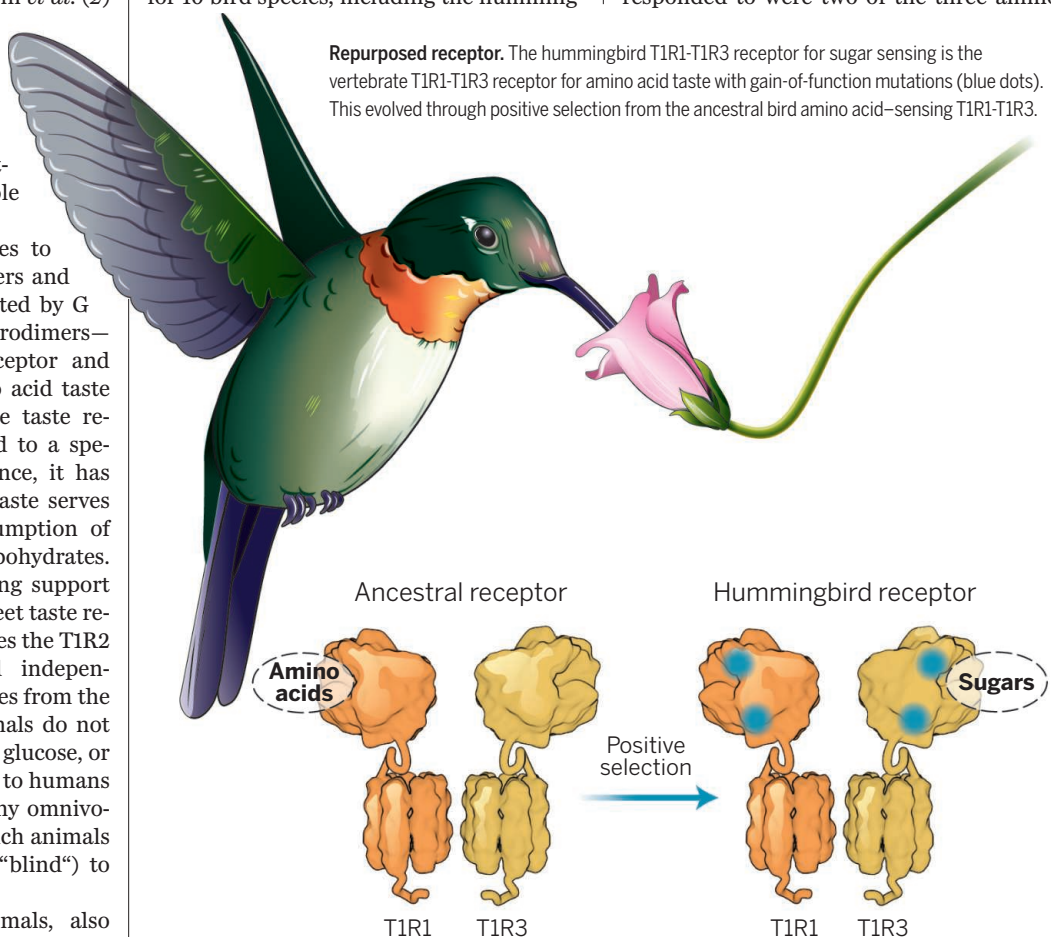

Repurposed receptor. The hummingbird T1R1-T1R3 receptor for sugar sensing is the vertebrate T1R1-T1R3 receptor for amino acid taste with gain-of-function mutations (blue dots). This evolved through positive selection from the ancestral bird amino acid–sensing T1R1-T1R3.

ILLUSTRATION: V. ALTOUNIAN/*SCIENCE*

Monell Chemical Senses Center, Philadelphia, PA 19104, USA. E-mail: pjiang@monell.org; beauchamp@monell.org

Published by AAAS

toward sugars (see the figure). Importantly, some of these residues are apparently under positive selection.

In behavioral taste testing with both captive and wild hummingbirds, Baldwin *et al.* observed a general agreement between these results and the results of in vitro receptor assays. One exception occurred for the sweet-tasting (to humans), nonnutritive sweetener, sucralose. Although sucralose was a potent agonist for the hummingbird T1R1-T1R3 receptor, hummingbirds behaviorally exhibited no avidity for it and seemed to reject sucralose-sucrose mixtures. The latter indicates that sucralose may actually have negative, perhaps bitter, taste properties. Another, alternative possibility to explain the absence of agreement between behavior and in vitro assays is that a T1R-independent mechanism such as sugar transporters and metabolic sensors located on taste receptor cells (*6*) may also contribute to the sweet taste perception of hummingbirds. The possibility of using new techniques (*7*) to genetically ablate the hummingbird T1R1-T1R3 taste receptor to test for sweet taste perception, presuming such animals are viable, would be fascinating.

Much of the recent work designed to match taste receptor function and feeding ecology has focused on sweet taste. For amino acid or umami taste, the correlations between diets and T1R1 function have received less attention. However, in giant pandas, the *T1R1* gene is mutated and nonfunctional (a "pseudogene"), and this could be related to the animal's unique monophagous herbivorous diet (*8*). For sea lions, dolphins, and whales, mammals that migrated back to the sea from land 25 to 55 million years ago, all T1Rs are no longer functional (*4*, *9*). It remains a puzzle as to what aspects of the return to sea life underlies their independent loss of sweet, amino acid, and even bitter (detected by the T2R family of receptors) taste perception. How bitter, salty, and sour taste perception relate to species variation in diet is even less well understood but is likely to also vary in interesting and illuminating ways. ■

REFERENCES

1. P. H. Barrett, P. J. Gautrey, S. Herbert, D. Kohn, S. Smith, *Charles Darwin's Notebooks, 1836–1844: Geology, Transmutation of Species, Metaphysical Enquiries* [British Museum (Natural History) and Cornell Univ. Press, London/Ithaca, NY, 1987).
2. M. W. Baldwin *et al.*, *Science* **345**, 929 (2014).
3. E. R. Liman, Y. V. Zhang, C. Montell, *Neuron* **81**, 984 (2014).
4. P. Jiang *et al.*, *Proc. Natl. Acad. Sci. U.S.A.* **109**, 4956 (2012).
5. H. Zhao *et al.*, *Mol. Biol. Evol.* **27**, 2642 (2010).
6. K. K. Yee, S. K. Sukumaran, R. Kotha, T. A. Gilbertson, R. F. Margolskee, *Proc. Natl. Acad. Sci. U.S.A.* **108**, 5431 (2011).
7. P. D. Hsu, E. S. Lander, F. Zhang, *Cell* **157**, 1262 (2014).
8. R. Li *et al.*, *Nature* **463**, 311 (2010).
9. P. Feng, J. Zheng, S. J. Rossiter, D. Wang, H. Zhao, *Genome Biol. Evol.* **6**, 1254 (2014).

10.1126/science.1259175

ECOLOGY

How do coral reefs recover?

Experiments on juvenile coral and fish behavior may have implications for reef restoration efforts

By **John F. Bruno**

A key challenge for ecologists is to understand why ecosystems are being degraded and how to restore their natural structure and function. On page 892 of this issue, Dixson *et al.* (*1*) use an impressive series of experiments to determine whether chemical signals in seawater from corals and seaweeds affect the behavior and settlement choices of juvenile corals and fish. The results reveal the surprising ability of dispersing reef larvae to detect habitat quality under well-controlled conditions. However, differences with previous research suggest that we are a long way from understanding where this ability fits into the complex settlement process and what it means for reef restoration and recovery.

Larvae from neighboring or distant reefs can replenish populations wiped out by natural disturbances or overharvesting. Working in Fiji, Dixson *et al.* used water from healthy (coral-dominated) and degraded (seaweed-dominated) reefs to examine the potential role of chemical cues in the recovery of coral and fish populations. Their findings suggest that odors from degraded reefs are repulsive, whereas those from healthy reefs are an attractant. In one experiment, coral larvae were placed in a Y-shaped tank, from which they could swim toward waters with different odors. By a large margin, they swam toward the smells of their own kind.

The study elaborates on a chemically based explanation for a frequently observed pattern: high concentrations of juvenile corals on seaweed-free sea floor (*2*). Other factors affecting coral larval settlement and survival include light, current velocity, predators, competition, disease, sound, and physical abrasion and shading by large, fleshy seaweeds that can kill small corals (*3*). Multifactorial experiments and field manipulations of the putative odor signals will be needed to determine the relative importance of odor relative to other mechanisms.

Dixson *et al.* also report a more surprising finding: The water source and odors can affect the choices made by juvenile fishes arriving from distant reefs. In one experiment, several reef fish species were deterred by the presence of brown seaweed often prevalent on disturbed reefs. If fish larvae behave similarly in nature, then overfished, seaweed-dominated reefs could be difficult to restore even when fishing is regulated, because fish would choose to settle in coral-dominated areas.

Dixon *et al.*'s results suggest that degraded reefs might have trouble recovering because fewer fish larvae will choose to settle there. Reconciling these findings with the broader marine ecological literature will be challenging, however. Recent evidence indicates that fisheries restrictions

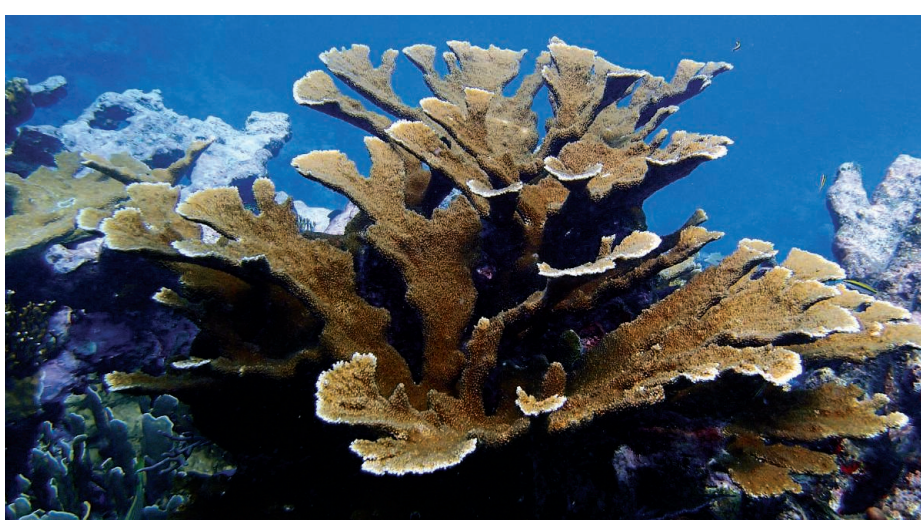

PHOTO: JOHN BRUNO

Reef recovery. Most elkhorn corals (*Acropora palmata*) in the Mesoamerican Barrier Reef were killed off by disease, storms, and ocean warming. Some are now recovering, as shown by this coral colony near Akumal, Mexico.

Published by AAAS

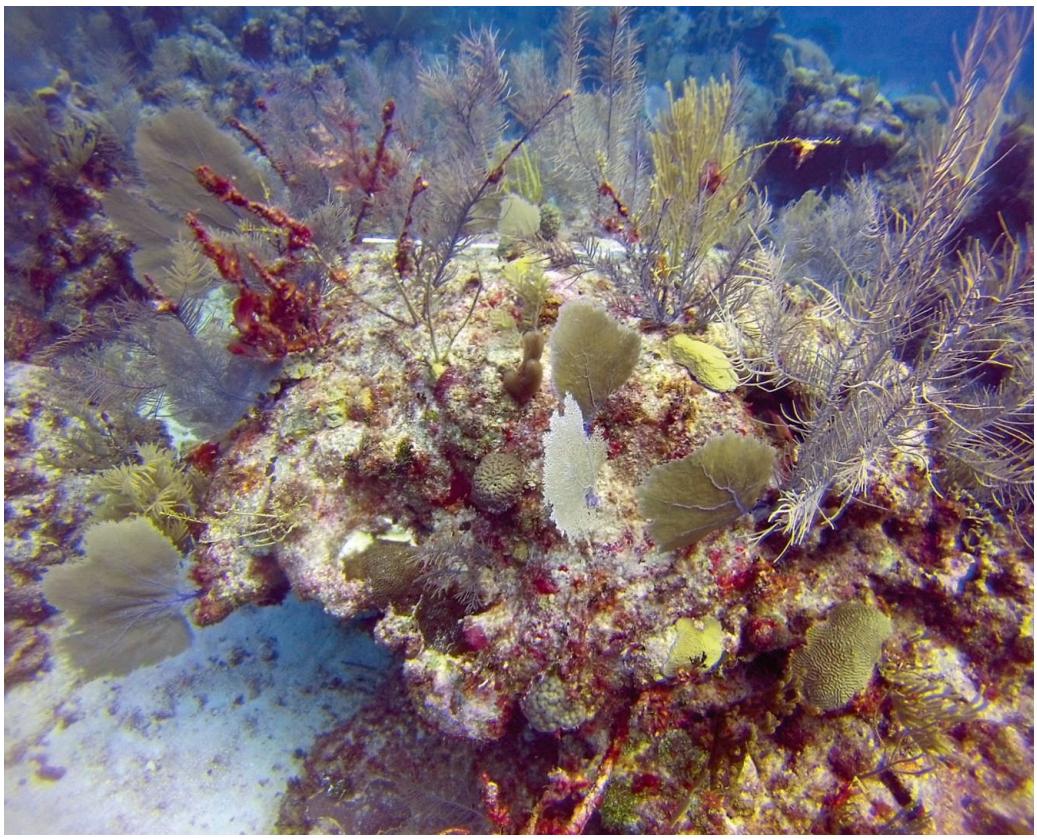

Dead and overgrown. A dead colony of *Orbicella sp.* near Akumal, Mexico, is overgrown by invertebrates such as sponges, gorgonians, and weedy corals. The *Orbicella* colony is over 1 m tall and 2 m wide and was centuries old when it was killed by yellow band disease in the early 2000s. Note the absence of seaweed on the colony surface due to intense grazing by urchins and fish.

can restore coral reef fish (*4*, *5*), regardless of the abundance of corals and seaweed. Adam *et al*. have reported that increases in seaweed boosted parrotfish populations on the reefs of Mo'orea in French Polynesia (*6*), providing a positive feedback that could return a reef to coral dominance. Furthermore, as seawater warms due to climate change, herbivorous coral reef fishes are invading temperate ecosystems despite the absence of corals and the dominance of large algae (*7*). Many tropical fishes first recruit into mangroves, seagrass beds, and other plant-dominated habitats before migrating onto the reef as they mature (*8*); the response of juvenile fishes to seaweed or coral odors may not be relevant in those cases. Finally, Edmunds and Carpenter (*9*) found that small, algae-free surfaces are quickly colonized by juvenile corals even on reefs with few fish and large amounts of seaweed. These previous studies suggest that the dynamics controlling reef colonization are complex and not easily described by any single set of results.

In the regions studied by Dixson *et al*., seaweed heavily dominated the degraded sites (49 to 91% coverage of the sea floor) and was essentially absent on the healthy reefs (1 to 2%). Although such conditions exist in nature, average seaweed cover on reefs is just 15 to 25% on Caribbean reefs and typically lower across much of the Indo-Pacific; in 2006, just 10% of Caribbean reefs and 1% of Indo-Pacific reefs had seaweed coverage of more than 50% (*10*). It remains to be shown whether the odor signal can also be detected under the less extreme conditions found on most reefs.

I am writing this article in Akumal, Mexico, while working on the restoration of reefs off the Yucatán Peninsula. Most massive boulder corals and branching corals of the 1000-km-long Mesoamerican Barrier Reef have been killed by disease, storms, and ocean warming since the 1980s. The reefs are degraded by any measure, yet there are signs of hope. Abundant herbivorous fishes and sea urchins consume seaweed, resulting in minimal seaweed coverage. Elkhorn coral (*Acropora palmata*, a formerly dominant species listed as threatened under the U.S. Endangered Species Act) is recovering (see the first figure), possibly enabled by the seaweed-free space.

Understanding of the dynamics of reef recovery is in a state of flux. Contrary to a common assumption, reefs in regions with high fish and coral diversity do not recover more quickly (*11*). In some locations, there appears to be a shift toward dominance by other invertebrate animals and weedy coral species rather than seaweeds (see the second figure). Coral reef scientists also once believed that reefs overgrown by seaweed would be permanently locked in to an alternative stable state, but that now appears unlikely. Once herbivores are restored, seaweed quickly disappears and coral populations usually return, although this process can take decades (*12*, *13*).

Yet, sometimes reefs fail to recover, for reasons that are often unclear. Why are the largely unprotected reefs in Mexico showing signs of recovery, whereas some in fully protected marine reserves just to the south in Belize are not? A better understanding of the factors that drive reef recovery may come from multifactor experiments, recognition of the complexity and variability of the natural world (*14*), and far more openness to unexpected discoveries, such as the possible role of odors from seaweeds in controlling reef recovery highlighted by Dixson *et al*. Results from one reef might not apply to another, and conservation strategies might be most successful if they combine global recommendations from academics with first-hand knowledge of local conditions. ■

Department of Biology, The University of North Carolina at Chapel Hill, Chapel Hill, NC 27517, USA. E-mail: jbruno@unc.edu

REFERENCES

1. D. L. Dixson, D. Abrego, M. E. Hay, *Science* **345**, 892 (2014).
2. L. J. McCook, J. Jompa, G. Diaz-Pulido, *Coral Reefs* **19**, 400 (2001).
3. G. F. River, P. J. Edmunds, *J. Exp. Mar. Biol. Ecol.* **261**, 159 (2001).
4. P. J. Mumby *et al*., *Proc. Natl. Acad. Sci. U.S.A.* **104**, 8362 (2007).
5. K. L. Kramer, K. L. J. Heck Jr., *Mar. Ecol. Prog. Ser.* **349**, 111 (2007).
6. T. C. Adam *et al*., *PLOS ONE* **6**, e23717 (2011).
7. A. Vergés *et al*., *Proc. Biol. Sci.* **281**, 20140846 (2014).
8. I. Nagelkerken, C. H. Faunce, *Estuar. Coast. Shelf Sci.* **75**, 417 (2007).
9. P. J. Edmunds, R. C. Carpenter, *Proc. Natl. Acad. Sci. U.S.A.* **98**, 5067 (2001).
10. J. F. Bruno, H. Sweatman, W. F. Precht, E. R. Selig, V. G. W. Schutte, *Ecology* **90**, 1478 (2009).
11. S. Y. Zhang *et al*., *Peer J* **2**, e308 (2014).
12. J. A. Idjadi *et al*., *Coral Reefs* **25**, 209 (2006).
13. G. Diaz-Pulido *et al*., *PLOS ONE* **4**, e5239 (2009).
14. J. F. Bruno, W. F. Precht, P. S. Vroom, R. B. Aronson, *Mar. Pollut. Bull.* **80**, 24 (2014).

10.1126/science.1258556

PHOTO: JOHN BRUNO

Published by AAAS

RETROSPECTIVE

Joep Lange (1954–2014)

A leader in developing therapy for AIDS is tragically killed

By **Jaap Goudsmit**

Joep Lange and his partner Jacqueline van Tongeren were among the AIDS experts killed on 17 July 2014 in the downing of the Malaysia Airways plane over eastern Ukraine. They were all on their way to the International AIDS conference in Melbourne, Australia. AIDS was the cause to which Joep dedicated most of his professional life—with inimitable passion, tenacity, and energy. He was my friend for 30 years.

Joep was a Dutch physician, born in 1954 in Nieuwenhagen, Netherlands. He received his medical degree in 1981 from the University of Amsterdam. I met Joep in 1984 on medical rounds at the university's Academic Medical Center where he was a resident internist and I was the attending virologist. The AIDS epidemic was in its early days then, and Joep was interested in the clinical evolution of HIV infection and how to fight it. In January 1986, the *British Medical Journal* published his paper describing the mysterious disappearance of antibodies to specific viral proteins from the blood of HIV-infected individuals who were progressing to AIDS. Joep then unraveled that mystery and published his findings that same year.

The rest is history. Joep showed that elevated amounts of the HIV protein p24 in the blood of HIV-infected individuals predicted immune deficiency and progression to AIDS, and that long-term survivors had reduced p24 antigen in their blood. This insight supported the early use of antiretroviral drugs to reduce the amount of HIV antigen and postpone the onset of AIDS. The antigen test was later replaced by the more accurate and sensitive HIV viral load test.

There was much comradery in our retrovirology lab at the Academic Medical Center in the 1980s. Joep was the thesis advisor for all but one of the MD-Ph.D. students. Four became professors at leading academic institutions. Joep stayed on at the lab until 1995, turning his attention to exploring technologies to benefit AIDS patients. His clinical vision led to a series of pivotal clinical trials of antiretroviral drugs. The most important of these was the INCAS trial (short for Italy, Netherlands, Canada, and Australia Study), published in 1998. It was a close collaboration between Joep and his new comrades-in-arms, the researchers Julio Montaner, David Cooper, Stefano Vella, and Mark Wainberg. The trial showed that three drugs (nevirapine, didanosine, and zidovudine) reduced the HIV viral load better than two, resulted in less drug resistance, and halted the progression to AIDS. From then on, Joep concentrated on getting triple-drug therapy to all in need, particularly people in the developing world.

Joep's efforts extended well beyond the lab. He served as president of the International Aids Society from 2002 to 2004 and was chief of clinical research and drug development at the World Health Organization's AIDS program from 1992 to 1995. He also established the Amsterdam Institute for Global Health and Development with the aim of bringing together disciplines, health care delivery, research, and education in search of sustainable solutions to major health problems.

PHOTO: MAAIKE DANZ

Department of Internal Medicine, Academic Medical Center, University of Amsterdam, Amsterdam, Netherlands. E-mail: jaap@jaapgoudsmit.nl

My wife Fransje van der Waals had her own special ties with Joep. She was his physician as well as a collaborator on programs to improve the lives of people infected with HIV. In 2003, they jointly launched Health[e] Foundation to give health care workers in the developing world access to the latest information about HIV and other diseases. By then, Joep had co-founded PharmAccess and other organizations with the aim of wiping out AIDS.

Over the past 10 years, Joep increasingly focused on the fight against poverty and for health care access. He was deeply dedicated to eradicating the global inequality in access to life-saving medicines. Lately, he envisioned a new frontier for himself: the rising tide of noncommunicable diseases in sub-Saharan Africa.

Joep and I connected right away not only in our research interests but through a profound love of literature. We started a project to list the 100 books we loved most, with the rule that adding one book meant having to remove another. It took us 5 years to compose the list. He had a comprehensive knowledge of all the Russian classics and was fascinated by the absurd and surreal, eastern European writers and Europe between the two world wars. Joep kept this book list alive for 30 years, often giving me books in the hope that the list would be amended. He carried his favorites around with him and loved giving them to friends. His increasing appetite for *The New York Review of Books* may have hinted at wanting to become a nonfiction writer himself when earlier this year he gave me the book *New Ways to Kill Your Mother: Writers and Their Families* by Colm Tóibín. It was his final gift to me.

As a passionate person, Joep could be caring and difficult at the same time. He could shout at his loved ones and write offensive e-mails to his best friends. Joep was also enigmatic in his ability to be both meticulous and careless. His research was impeccably executed and reported, and he was fastidious about the wording of manuscripts. Yet, he lost the raw data for part of his thesis in an Amsterdam tram and left the entire manuscript in "an even more improbable place," from where it was rescued by his mother-in-law.

Joep will be remembered for many things. He was a scientist, clinician, activist, father, opera lover, bird watcher, debater, intellectual, and marathon runner. The only consolation we have is this: The AIDS fighter Joep Lange died in action on the frontline, with his Jacqueline by his side. ■

10.1126/science.1259453

Published by AAAS

BOOKS *et al.*

PHILOSOPHY

Morality for skeptics?

By **Les Beldo**

Morality for Humans
Ethical Understanding from the Perspective of Cognitive Science
Mark Johnson
University of Chicago Press, 2014. 273 pp.

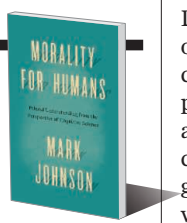

Over the past 25 years, a growing number of cognitive scientists have taken it as their mission to find an empirical basis within brain science for the distinctive character of moral judgments. Investigators such as Marc Hauser, Steven Pinker, and Jonathan Haidt have posited the existence of an innate, domain-specific moral faculty in humans, be it a "universal moral grammar," a "moral instinct," or an "intuitive ethics."

In *Morality for Humans*, Mark Johnson introduces an approach he calls "moral naturalism." It is committed to the idea that moral knowledge does not exist on some separate plane but rather in the everyday habits, practices, institutions, and "bio-regulation" of lived organisms. Johnson is skeptical, however, of claims about the existence of a moral module in the human brain. He notes that "there are simply far too many complexly interacting multifunctional systems … in our intuitive moral judgments for there to be anything remotely resembling a distinct moral faculty." Although he never uses the term, Johnson argues that moral problem-solving relies entirely on cognitive processes like logic, empathy, or narration. He sees the idea of an innate moral faculty as just another attempt to prove the existence of immutable moral laws, not in divine will or in pure reason but in a strong normative reading of cognitive science and evolutionary biology.

Johnson's second major contribution in the book is his attempt to rediscover a place for rational deliberation in cognitive moral psychology. Generally speaking, scholars in this emerging field have been hostile to the idea that rational deliberation plays much of a role in moral reasoning. They tend to posit two parallel "tracks" of moral judgment: a fast, emotional, moral appraisal that happens almost immediately and a more deliberate, reflective, and principled form of moral reasoning that serves mostly to justify and rationalize emotions after the fact. Johnson's solution is to suggest a third approach, an imaginative process of moral deliberation in which individuals engage in a kind of moral problem-solving. This is accomplished, Johnson suggests, by imagining different alternatives and considering the feeling each outcome engenders. Moral problem-solving works as a kind of "simulation" in which an individual tests out emotional responses to the imagined outcomes of various solutions to specific moral problems.

Rational deliberation plays no role, however, in Johnson's account of where moral knowledge comes from, which is one of the chief preoccupations of the book. Instead, Johnson locates the source of values in our social and biological needs, cultural representations, and personal experiences. Here, Johnson has no qualms about violating the so-called naturalistic fallacy, which suggests that normative statements about how things ought to be cannot be derived from factual statements about what is. He moves freely between descriptions of human needs and human tendencies, on the one hand, and the normative suggestion that we ought to fulfill those needs and support those tendencies. Dismissing the naturalistic fallacy is easy if one thinks of it as an esoteric philosophical concept. But the term refers to a real logical problem of which Johnson is in fact acutely aware: "the fact that we have come to value certain states of affairs," he writes, "is no guarantee that we *should* value them in the way we do." This has been a particular weakness of studies that would make normative claims based on findings in cognitive neuroscience. How can descriptions of how our brains work tell us anything about what we ought to do in particular situations? It is a problem Johnson never resolves.

An important stylistic weakness of the book is Johnson's penchant for bundling disparate ideas under the heading of a "folk theory," which he subsequently debunks. In dispelling the "myth of a uniquely moral kind of judgment," for instance, Johnson rejects the idea that experiences come differentiated into distinct kinds that correlate with certain kinds of judgment. However, morality can exist as a domain of social judgment with its own standards and values without there being such a thing as distinct moral problems.

Morality is typically distinguished from other domains of social judgment by its unconditionality. A moral judgment refers to something that is considered right or wrong in and of itself. Johnson rejects the idea that moral judgments are unconditional, saying instead that the "trumping force" of morality owes to the fact that "certain things tend to matter more for us because they are thought to be necessary for the well-being of ourselves and others." Individual well-being and societal cohesion are practical ends, however, and concerns about achieving them are matters of prudent conduct and prudent governance. This, along with Johnson's repeated insistence that moral problem-solving is no different in kind from any other form of problem-solving, leads one to wonder why he bothers to retain the concept of "morality" at all. Johnson suggests that values exist only in relation to some predefined or agreed-upon set of goods, feelings, or human needs, but that still creates fertile ground for hypothetical imperatives that are binding upon anyone who accepts the most basic premises of society. Why is this not enough? Is the stigma of moral relativism so frightening? What's so bad about prudence?

PHOTO: GETTY IMAGES/ISTOCKPHOTO

The reviewer is at the Department of Comparative Human Development, University of Chicago, Chicago, IL 60637, USA. E-mail: lesbeldo@gmail.com

10.1126/science.1256368

Downloaded from www.sciencemag.org on August 24, 2014

Published by AAAS

Innovation: myths and prospects

By **Davide Consoli**

The Leviathan is a recurrent metaphor for portraying governments as clumsy and pervasive entities that hinder the initiative of business enterprise. *The Entrepreneurial State* by Mariana Mazzucato begs to differ and exposes the ideological foundations and perils of a rhetoric that, it is claimed, conveniently neglects instances in which the State has had a key role in shaping visionary undertakings and implementing strategic plans. At a time when innovation is expected to solve current economic woes, this book is a welcome opportunity to take stock of what can be expected from the main characters.

The central argument of *The Entrepreneurial State* is that most of the radical technologies that define our contemporary lifestyle owe their genesis to audacious risk-taking on the part of the State. The Internet is a paradigmatic case. Through mission-oriented funding and a variety of policy instruments, the U.S. government sparked development of a technological infrastructure whose magnitude and influence stretches well beyond what was foreseeable in the 1950s. Who could have anticipated that sending a man to the moon would pave the way to markets for miniature vacuum cleaners and plasma-screen televisions?

As a heterodox group of economists has long argued, the mainstream economics view of innovation either as random or deterministic misses the point altogether (*1, 2*). Technology brings about opportunities and challenges whose extent can neither be imagined beforehand nor predicted. Indeed, innovation is not invention alone, in that it involves the orchestration of different forms of knowledge, not just from science and technology but also from entrepreneurial know-how and the institution of markets. However, fundamental uncertainty implies that the information to guide investments in innovation is often incomplete, which reduces the scope for futures contracts and calls for different forms of coordination beyond the archetypal market system. As Mazzucato convincingly argues, governments have the capacity to brave this uncertainty and to pursue opportunities where few business firms would dare. By this account, the State is more akin to Prometheus, who gave fire to humanity despite the risk of enraging the gods. And for those who are sensitive to government spending, the author has proposals for redressing the risk-reward balance in favor of taxpayers.

The main claims of this book are supported by meticulous accounts of how particular innovations came about and how, on more than one occasion, the State did not just fix markets, it created them. *The Entrepreneurial State* is at its best in its central part thanks to a skillful combination of the history of technology, empirical evidence, and policy analysis. The chapter that most will find familiar recounts how Apple's "hunger and foolishness" owes a lot to the technological complex that became possible through the vision of the U.S. government. Even more engaging is the analysis of how governments (United States, China, Brazil, as well as some in Europe) around the world strive to stimulate investments in green technology. There, the State is portrayed as enabling transformation of the existing energy infrastructure.

CREDIT: MUSEUMSLANDSCHAFT HESSEN KASSEL UTE BRUNZEL/BRIDGEMANART.COM

Contrary to popular belief, there is more to this story than increasing research and development, encouraging small firms, and hoping for venture capital. It is also different from the case of communication technologies, which is a story about trajectory creation. Mazzucato argues that the "green revolution" can be as wide-ranging and disruptive as the revolution in information and communication technology if governments will actively support the buildup of innovation ecosystems, where public and private investments coexist in a symbiotic fashion.

On the whole, the book contains a critical reading of data and arguments that run counter to established views while never falling short of offering constructive solutions. One thing I would have liked to see more of is an articulation of how governments might deal with disruptive changes in the demand for skills. If the impending transition to low-carbon societies plays out in a similar way to the digital transition, substantial imbalances may soon emerge in labor markets, income distribution, and educational policy—all traditionally understood to be within the remit of governments.

The question that looms large throughout these chapters and in the debate that followed its publication is this: if the State-Prometheus has been capable of creating a grand vision and of pursuing it, why is this no longer happening? Has society given up on grand visions, or has the Leviathan rhetoric managed to suppress that desire? *The Entrepreneurial State* is surely not the last word on these themes, nor is it meant to be: rather than a static summary of the state of the art, this book seems to have been written with the intention of providing a platform and letting its content evolve as the debate continues. After reading it, most will come away with a deeper appreciation of the triumphs and frustrations involved in innovation and, perhaps, with a slight unease at the erosion of collective expectations.

The Entrepreneurial State
Debunking Public vs. Private Sector Myths
Mariana Mazzucato
Anthem Press, 2013. 265 pp.

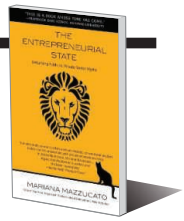

The reviewer is at INGENIO (Instituto de Gestión de la Innovación y del Conocimiento, Consejo Superior de Investigaciones Científicas–Universitat Politècnica de València), Ciudad Politecnica de la Innovacion, Edificio 8E–Camino de Vera, s/n, 46022 Valencia, Spain. E-mail: davide.consoli@ingenio.upv.es

REFERENCES

1. N. Rosenberg, *Perspectives on Technology* (*Cambridge Univ. Press*, Cambridge, 1976).
2. R. R. Nelson, S. G. Winter, *An Evolutionary Theory of Economic Change* (Belknap, Cambridge, MA, 1982).

10.1126/science.1257029

Published by AAAS

Downloaded from www.sciencemag.org on August 24, 2014

LETTERS

Edited by **Jennifer Sills**

Fauna in decline: Plight of the pangolin

IN THEIR REVIEW "Defaunation in the Anthropocene" (special section on Vanishing Fauna, 25 July, p. 401), R. Dirzo *et al.* discuss the human impacts on species decline and extinction. The pangolin is a good example of these anthropogenic effects. On 12 May, about 4 tons of smuggled frozen pangolins were seized in Zhuhai, China, making the country's largest smuggling case of a national protected animal in the past several years (*1*). The pangolin turns out to be "the most traded" wild animal, due to the large demand for its scale and flesh (*2*).

According to the *Chinese Medicinal Pharmacopoeia*, roasted pangolin scale can be used for detoxification, draining pus, attenuating palsy, and stimulating lactation (*3*). Since the 1990s, the price of pangolin scale has been continuously climbing, rising from £8.50 to £360 per kilogram (*4*). In even greater demand is the pangolin meat, despite the risk of infection associated with eating it. The excessive consumption has been catastrophic for the species, as the pangolin typically produces only one offspring per year.

In China, pangolins are facing the risk of extinction due to human consumption, which will have devastating effects on pangolins in other areas of the world. Similar to its cracking down on the smuggling of ivory and rhinoceros horn, the Chinese government should strengthen enforcement against illegal pangolin transactions and ban the wild animal markets. Further publicity and education are also called for to put an end to the chase for "wildlife delicacies." Finally, developing herbal alternatives to pangolin scales would benefit the population. These actions may be crucial to prevent the extinction of the pangolin in China.

Yuning Liu and Qiang Weng*

College of Biological Sciences and Biotechnology, Beijing Forestry University, Beijing, 100083, China.

*Corresponding author.
E-mail: qiangweng@bjfu.edu.cn

REFERENCES

1. "Zhuhai border seized about four tons of smuggled frozen pangolins," *Xinhua Net* (13 May 2013); http://news.xinhuanet.com/local/2014-05/13/c_1110670956.htm [in Chinese].
2. "The most traded wild mammal—the Pangolin—is being eaten to extinction," *IUCN Net* (22 July 2013); www.iucn.org/news_homepage/news_by_date/?13434/The-most-traded-wild-mammal---the-Pangolin---is-being-eaten-to-extinction.
3. S. Z. Li, B. C. G. Mu, *Compendium of Materia Medica* (People's Medical Publishing House, Beijing, 1982).
4. Z.-M. Zhou, Y. Zhou, C. Newman, D. W. Macdonald, *Front. Ecol. Environ.* **12**, 97 (2014).

Fauna in decline: First do no harm

IN THEIR REVIEW "Reversing defaunation: Restoring species in a changing world" (special section on Vanishing Fauna, 25 July, p. 406), P. J. Seddon *et al.* warn that loss of animal species can disrupt ecological communities, cause cascading effects, and alter ecosystem functions. Introduced nonnative animals can have similar consequences.

Confiscated pangolin scales.

Burgeoning evidence implicates nonnative species as driving biodiversity loss (*1*–*3*) and a host of other ecological disruptions (*4*). Whereas some can have positive effects on ecosystem services, others have disproportionately large negative effects. Risk assessment of these outcomes is undermined by context-dependence and time lags (*4*, *5*). An introduced species that has negligible effects in some areas, or whose population is threatened in its native range, can have strong impacts when translocated elsewhere (*6*, *7*). Such species may appear innocuous for decades—well beyond the attention span of monitoring programs—before suddenly becoming problematic (*8*). Moreover, their impacts may be subtle, but nonetheless great, and remain unrecognized until damage is incurred and containment is impossible (*9*). Even carefully planned introductions for conservation purposes can have devastating consequences (*10*, *11*).

These considerations are largely ignored by Seddon *et al.* in their discussion of assisted colonization and ecological replacements—deliberate introductions of species beyond their native range. Although Seddon *et al.* reassuringly cite new approaches (quantitative risk analysis, active adaptive management, and structured decision-making) for managing what could go wrong, none of the cited references offer reliable methods for predicting impacts of nonnative animal releases. Despite making considerable progress in understanding impact (*5*), invasion science has not developed a predictive capacity sufficient to engage in frequent introductions without harming biodiversity and ecosystems (*7*). Thus, risks of unintended effects cannot be evaluated and weighed against expected benefits.

At best, assisted colonization is analogous to other human interventions (such as geoengineering) that are prone to unpredictable consequences and do not address root causes of the problems they are supposed to mitigate (*7*, *12*). Ironically, in an earlier article on using nonnative species for conservation purposes, Seddon *et al.* (*13*) rightly conclude that "the concern is not the failure to establish the intended ecological interactions, but rather the risk of creating new and unwanted interactions." Perhaps what is needed is a Hippocratic oath ("Do no harm") applicable to conservation biologists.

Anthony Ricciardi*[1] *and* ***Daniel Simberloff*[2]**

[1]Redpath Museum, McGill University, Montreal, QC H3A 2K6, Canada. [2]Department of Ecology and Evolutionary Biology, University of Tennessee, Knoxville, TN 37996, USA.

*Corresponding author.
E-mail: tony.ricciardi@mcgill.ca

REFERENCES

1. M. Clavero, E. García-Berthou, *Trends. Ecol. Evol.* **20**, 110 (2005).
2. M. Clavero *et al.*, *Biol. Conserv.* **142**, 2043 (2009).
3. R. E. Gozlan, *Nature* **435**, 1046 (2005).
4. D. Simberloff *et al.*, *Trends Ecol. Evol.* **28**, 58 (2013).
5. A. Ricciardi *et al.*, *Ecol. Monogr.* **83**, 263 (2013).
6. C. E. Turner *et al.*, *Wetlands Ecol. Mgmt.* **5**, 165 (1998).
7. A. Ricciardi, D. Simberloff, *Trends Ecol. Evol.* **24**, 248 (2009).
8. G. Rilov *et al.*, *Biol. Inv.* **6**, 347 (2004).
9. K. Douda *et al.*, *Div. Distrib.* **19**, 933 (2013).
10. C. W. Benkman, A. M. Siepelski, T. L. Parchman, *Mol. Ecol.* **17**, 395 (2008).
11. C. N. Spencer *et al.*, *BioScience* **41**, 14 (1991).
12. H. D. Matthews, S. E. Turner, *Environ. Res. Lett.* **4**, 045105 (2009).
13. P. J. Seddon *et al.*, *Conserv. Biol.* **25**, 212 (2011).

PHOTO: ALEX HOFFORD/EPA/NEWSCOM

Downloaded from www.sciencemag.org on August 24, 2014

Published by AAAS

Fauna in decline: Global assessments

THE POLICY FORUM "Wildlife decline and social conflict" (J. S. Brashares *et al.*, 25 July, p. 376) points to the need for a formalized, international, multidisciplinary program with government involvement that can address the detrimental environmental and social consequences of wildlife depletion. They suggest creating a working group from the Millennium Ecosystem Assessment (MA) as a platform. This program is now closed and has been replaced by an even stronger body intended to support this kind of work, the Intergovernmental Platform on Biodiversity and Ecosystem Services (IPBES). Established in 2012, IPBES has been approved by 119 nations and has many characteristics of the IPCC. IPBES has an explicit objective to "strengthen the science-policy interface for biodiversity and ecosystem services..." (*1*). It is conducting issue-specific assessments as well as regional and global assessments. It could serve as a suitable platform for a detailed global assessment of the natural and social consequences of wildlife decline, as called for by Brashares *et al.*

We believe that such an assessment is needed, with explicit focus on the social drivers of illegal harvest and social instability. Brashares *et al.* suggest that clear and enforced local resource tenure is what is needed to reduce wildlife conflict. However, this is not always a silver bullet. For example, both land and resource tenure are clear and strictly enforced in Kenya, with a shoot-to-kill policy on rhino and elephant poachers. Lands harboring rhinos have secure tenure on both the land and resources, and they go through a rigorous process to be established as rhino reserves. Even those reserves surrounded by lands that also have secure tenure continually fall prey to serious poaching events. Tenure and enforcement clearly are not enough there, and an assessment would yield much more rigorous and useful information on what the key social drivers are and how they can best be addressed.

Harold Mooney[1]* and Heather Tallis[2]

[1]Department of Biology, Stanford University, Stanford, CA 94305, USA. [2]The Nature Conservancy, Santa Cruz, CA 95060, USA.

*Corresponding author. E-mail: haroldmooney@gmail.com

REFERENCE

1. IPBES, "Functions, operating principles, and institutional arrangements of the Intergovernmental Science-Policy Platform on Biodiversity and Ecosystem Services" (IPBES, Panama City, Panama, 2012).

Ailing academia needs culture change

IN HER WORKING LIFE column "The stressed-out postdoc" (1 August, p. 594), C. Arnold describes the pressure felt by many postdocs, in part because there are not enough jobs available in academia. The problems they face are a symptom of a bigger issue: The research enterprise has become unsustainable in its current form. Research funding levels/mechanisms, the peer-review process, and the methods of training Ph.D.'s are flawed, and these issues are crippling the pipeline of future, successful academic researchers (*1*). We believe that the value system in academia perpetuates these issues and thus prevents positive change.

Universities and individual faculty are addicted to grant funding and to the cheap labor provided by Ph.D. trainees, to the point that funding and access to scores of underpaid and underappreciated graduate students and postdoctoral fellows have become entitlements. University rankings and faculty promotions are tied to funding and publications, which are highly political and not necessarily an accurate reflection of scientific excellence.

Overall, there is little incentive for senior academics and higher-level university administrators to systematically admit—much less address—the flaws in the system. Fixing the flaws must start with creating the incentives to change the academic culture and values that have led to the current unsustainable system. Substantial changes to funding policies are the best way to create better incentives, and funding bodies such as the National Institutes of Health (NIH) and the National Science Foundation (NSF) must lead these efforts. Agencies should find ways to help depoliticize funding decisions; perhaps the grant-review process could be more similar to the peer-review process at some academic journals, which increase transparency and value external perspectives. Research funding should support staff scientists, whereas training grants or fellowships should support Ph.D. trainees and postdocs, thus eliminating the incentive to admit too many students into graduate programs just for their cheap labor potential. Tying Ph.D. trainee career outcomes to funding decisions would further incentivize good mentoring and career development opportunities. Finally, NIH and NSF could do more to support career development bridges to nonacademic careers through, for example, providing funding for internships in industry and other nonacademic sectors and for coursework that will build key transferable skills.

Money talks, and in this case, changing funding policies and practices is the only way to drive the culture change required to save the research enterprise from systemic failure.

Viviane Callier[1] and Nathan L. Vanderford[2]*

[1]The Ronin Institute, Montclair, NJ 07043, USA. [2]Markey Cancer Center and Graduate Center for Toxicology, University of Kentucky, Lexington, KY 40536, USA.

*Corresponding author. E-mail: nathan.vanderford@uky.edu

REFERENCE

1. B. Alberts *et al.*, *Proc. Natl. Acad. Sci. U.S.A.* **111**, 5773 (2014).

Let minority-serving institutions lead

THE PERVASIVE AND insidious institutional racism detailed in the Features News story about Richard Tapia ("Minority voice," J. Mervis, 6 June, p. 1076) is consistent with what many ethnic minority faculty have experienced at predominantly white institutions. Where Tapia falters is in not attributing as also racist, in addition to elitist, his statements that "Pedigree is alive and well.... So if minority students earn their degrees at minority-serving institutions, they won't get hired by Stanford."

Minority-serving institutions continue to do the lion's share in producing minority STEM Ph.D.'s. These scientists are well qualified and on par with those graduating from the top-tier schools. The only impediment to their being recognized as such and hired by elite, predominantly white institutions is the intransigent racism that still haunts the academy. In spite of highly capable mentors like Tapia, majority institutions will not be able to fill the growing need for minority STEM Ph.D.'s without substantial input from minority-serving institutions that have been successfully producing scholars of color for more than 100 years. Rather than dismissing the accomplishments of these institutions, it makes sense to support their track record and learn from their expertise.

Fatimah Jackson,[1]* Clarence M. Lee,[1] Sherese Taylor[2]

[1]Department of Biology, Howard University, Washington, DC 20059, USA. [2]Cobb Research Laboratory, Howard University, Washington, DC 20059, USA.

*Corresponding author. E-mail: fatimah.jackson@howard.edu

Published by AAAS

LETTERS

Edited by **Jennifer Sills**

Fauna in decline: Plight of the pangolin

IN THEIR REVIEW "Defaunation in the Anthropocene" (special section on Vanishing Fauna, 25 July, p. 401), R. Dirzo *et al.* discuss the human impacts on species decline and extinction. The pangolin is a good example of these anthropogenic effects. On 12 May, about 4 tons of smuggled frozen pangolins were seized in Zhuhai, China, making the country's largest smuggling case of a national protected animal in the past several years (*1*). The pangolin turns out to be "the most traded" wild animal, due to the large demand for its scale and flesh (*2*).

According to the *Chinese Medicinal Pharmacopoeia*, roasted pangolin scale can be used for detoxification, draining pus, attenuating palsy, and stimulating lactation (*3*). Since the 1990s, the price of pangolin scale has been continuously climbing, rising from £8.50 to £360 per kilogram (*4*). In even greater demand is the pangolin meat, despite the risk of infection associated with eating it. The excessive consumption has been catastrophic for the species, as the pangolin typically produces only one offspring per year.

In China, pangolins are facing the risk of extinction due to human consumption, which will have devastating effects on pangolins in other areas of the world. Similar to its cracking down on the smuggling of ivory and rhinoceros horn, the Chinese government should strengthen enforcement against illegal pangolin transactions and ban the wild animal markets. Further publicity and education are also called for to put an end to the chase for "wildlife delicacies." Finally, developing herbal alternatives to pangolin scales would benefit the population. These actions may be crucial to prevent the extinction of the pangolin in China.

Yuning Liu and Qiang Weng*

College of Biological Sciences and Biotechnology, Beijing Forestry University, Beijing, 100083, China.

*Corresponding author.
E-mail: qiangweng@bjfu.edu.cn

REFERENCES

1. "Zhuhai border seized about four tons of smuggled frozen pangolins," *Xinhua Net* (13 May 2013); http://news.xinhuanet.com/local/2014-05/13/c_1110670956.htm [in Chinese].
2. "The most traded wild mammal—the Pangolin—is being eaten to extinction," *IUCN Net* (22 July 2013); www.iucn.org/news_homepage/news_by_date/?13434/The-most-traded-wild-mammal---the-Pangolin---is-being-eaten-to-extinction.
3. S. Z. Li, B. C. G. Mu, *Compendium of Materia Medica* (People's Medical Publishing House, Beijing, 1982).
4. Z.-M. Zhou, Y. Zhou, C. Newman, D. W. Macdonald, *Front. Ecol. Environ.* **12**, 97 (2014).

Fauna in decline: First do no harm

IN THEIR REVIEW "Reversing defaunation: Restoring species in a changing world" (special section on Vanishing Fauna, 25 July, p. 406), P. J. Seddon *et al.* warn that loss of animal species can disrupt ecological communities, cause cascading effects, and alter ecosystem functions. Introduced nonnative animals can have similar consequences.

Confiscated pangolin scales.

Burgeoning evidence implicates nonnative species as driving biodiversity loss (*1*–*3*) and a host of other ecological disruptions (*4*). Whereas some can have positive effects on ecosystem services, others have disproportionately large negative effects. Risk assessment of these outcomes is undermined by context-dependence and time lags (*4*, *5*). An introduced species that has negligible effects in some areas, or whose population is threatened in its native range, can have strong impacts when translocated elsewhere (*6*, *7*). Such species may appear innocuous for decades—well beyond the attention span of monitoring programs—before suddenly becoming problematic (*8*). Moreover, their impacts may be subtle, but nonetheless great, and remain unrecognized until damage is incurred and containment is impossible (*9*). Even carefully planned introductions for conservation purposes can have devastating consequences (*10*, *11*).

These considerations are largely ignored by Seddon *et al.* in their discussion of assisted colonization and ecological replacements—deliberate introductions of species beyond their native range. Although Seddon *et al.* reassuringly cite new approaches (quantitative risk analysis, active adaptive management, and structured decision-making) for managing what could go wrong, none of the cited references offer reliable methods for predicting impacts of nonnative animal releases. Despite making considerable progress in understanding impact (*5*), invasion science has not developed a predictive capacity sufficient to engage in frequent introductions without harming biodiversity and ecosystems (*7*). Thus, risks of unintended effects cannot be evaluated and weighed against expected benefits.

At best, assisted colonization is analogous to other human interventions (such as geoengineering) that are prone to unpredictable consequences and do not address root causes of the problems they are supposed to mitigate (*7*, *12*). Ironically, in an earlier article on using nonnative species for conservation purposes, Seddon *et al.* (*13*) rightly conclude that "the concern is not the failure to establish the intended ecological interactions, but rather the risk of creating new and unwanted interactions." Perhaps what is needed is a Hippocratic oath ("Do no harm") applicable to conservation biologists.

Anthony Ricciardi*[1] *and* ***Daniel Simberloff*[2]**

[1]Redpath Museum, McGill University, Montreal, QC H3A 2K6, Canada. [2]Department of Ecology and Evolutionary Biology, University of Tennessee, Knoxville, TN 37996, USA.

*Corresponding author.
E-mail: tony.ricciardi@mcgill.ca

REFERENCES

1. M. Clavero, E. García-Berthou, *Trends. Ecol. Evol.* **20**, 110 (2005).
2. M. Clavero *et al.*, *Biol. Conserv.* **142**, 2043 (2009).
3. R. E. Gozlan, *Nature* **435**, 1046 (2005).
4. D. Simberloff *et al.*, *Trends Ecol. Evol.* **28**, 58 (2013).
5. A. Ricciardi *et al.*, *Ecol. Monogr.* **83**, 263 (2013).
6. C. E. Turner *et al.*, *Wetlands Ecol. Mgmt.* **5**, 165 (1998).
7. A. Ricciardi, D. Simberloff, *Trends Ecol. Evol.* **24**, 248 (2009).
8. G. Rilov *et al.*, *Biol. Inv.* **6**, 347 (2004).
9. K. Douda *et al.*, *Div. Distrib.* **19**, 933 (2013).
10. C. W. Benkman, A. M. Siepelski, T. L. Parchman, *Mol. Ecol.* **17**, 395 (2008).
11. C. N. Spencer *et al.*, *BioScience* **41**, 14 (1991).
12. H. D. Matthews, S. E. Turner, *Environ. Res. Lett.* **4**, 045105 (2009).
13. P. J. Seddon *et al.*, *Conserv. Biol.* **25**, 212 (2011).

PHOTO: ALEX HOFFORD/EPA/NEWSCOM

Downloaded from www.sciencemag.org on August 24, 2014

Published by AAAS

Fauna in decline: Global assessments

THE POLICY FORUM "Wildlife decline and social conflict" (J. S. Brashares *et al.*, 25 July, p. 376) points to the need for a formalized, international, multidisciplinary program with government involvement that can address the detrimental environmental and social consequences of wildlife depletion. They suggest creating a working group from the Millennium Ecosystem Assessment (MA) as a platform. This program is now closed and has been replaced by an even stronger body intended to support this kind of work, the Intergovernmental Platform on Biodiversity and Ecosystem Services (IPBES). Established in 2012, IPBES has been approved by 119 nations and has many characteristics of the IPCC. IPBES has an explicit objective to "strengthen the science-policy interface for biodiversity and ecosystem services..." (*1*). It is conducting issue-specific assessments as well as regional and global assessments. It could serve as a suitable platform for a detailed global assessment of the natural and social consequences of wildlife decline, as called for by Brashares *et al.*

We believe that such an assessment is needed, with explicit focus on the social drivers of illegal harvest and social instability. Brashares *et al.* suggest that clear and enforced local resource tenure is what is needed to reduce wildlife conflict. However, this is not always a silver bullet. For example, both land and resource tenure are clear and strictly enforced in Kenya, with a shoot-to-kill policy on rhino and elephant poachers. Lands harboring rhinos have secure tenure on both the land and resources, and they go through a rigorous process to be established as rhino reserves. Even those reserves surrounded by lands that also have secure tenure continually fall prey to serious poaching events. Tenure and enforcement clearly are not enough there, and an assessment would yield much more rigorous and useful information on what the key social drivers are and how they can best be addressed.

Harold Mooney[1]* and Heather Tallis[2]

[1]Department of Biology, Stanford University, Stanford, CA 94305, USA. [2]The Nature Conservancy, Santa Cruz, CA 95060, USA.

*Corresponding author. E-mail: haroldmooney@gmail.com

REFERENCE

1. IPBES, "Functions, operating principles, and institutional arrangements of the Intergovernmental Science-Policy Platform on Biodiversity and Ecosystem Services" (IPBES, Panama City, Panama, 2012).

Ailing academia needs culture change

IN HER WORKING LIFE column "The stressed-out postdoc" (1 August, p. 594), C. Arnold describes the pressure felt by many postdocs, in part because there are not enough jobs available in academia. The problems they face are a symptom of a bigger issue: The research enterprise has become unsustainable in its current form. Research funding levels/mechanisms, the peer-review process, and the methods of training Ph.D.'s are flawed, and these issues are crippling the pipeline of future, successful academic researchers (*1*). We believe that the value system in academia perpetuates these issues and thus prevents positive change.

Universities and individual faculty are addicted to grant funding and to the cheap labor provided by Ph.D. trainees, to the point that funding and access to scores of underpaid and underappreciated graduate students and postdoctoral fellows have become entitlements. University rankings and faculty promotions are tied to funding and publications, which are highly political and not necessarily an accurate reflection of scientific excellence.

Overall, there is little incentive for senior academics and higher-level university administrators to systematically admit—much less address—the flaws in the system. Fixing the flaws must start with creating the incentives to change the academic culture and values that have led to the current unsustainable system. Substantial changes to funding policies are the best way to create better incentives, and funding bodies such as the National Institutes of Health (NIH) and the National Science Foundation (NSF) must lead these efforts. Agencies should find ways to help depoliticize funding decisions; perhaps the grant-review process could be more similar to the peer-review process at some academic journals, which increase transparency and value external perspectives. Research funding should support staff scientists, whereas training grants or fellowships should support Ph.D. trainees and postdocs, thus eliminating the incentive to admit too many students into graduate programs just for their cheap labor potential. Tying Ph.D. trainee career outcomes to funding decisions would further incentivize good mentoring and career development opportunities. Finally, NIH and NSF could do more to support career development bridges to nonacademic careers through, for example, providing funding for internships in industry and other nonacademic sectors and for coursework that will build key transferable skills.

Money talks, and in this case, changing funding policies and practices is the only way to drive the culture change required to save the research enterprise from systemic failure.

Viviane Callier[1] and Nathan L. Vanderford[2]*

[1]The Ronin Institute, Montclair, NJ 07043, USA. [2]Markey Cancer Center and Graduate Center for Toxicology, University of Kentucky, Lexington, KY 40536, USA.

*Corresponding author. E-mail: nathan.vanderford@uky.edu

REFERENCE

1. B. Alberts *et al.*, *Proc. Natl. Acad. Sci. U.S.A.* **111**, 5773 (2014).

Let minority-serving institutions lead

THE PERVASIVE AND insidious institutional racism detailed in the Features News story about Richard Tapia ("Minority voice," J. Mervis, 6 June, p. 1076) is consistent with what many ethnic minority faculty have experienced at predominantly white institutions. Where Tapia falters is in not attributing as also racist, in addition to elitist, his statements that "Pedigree is alive and well.... So if minority students earn their degrees at minority-serving institutions, they won't get hired by Stanford."

Minority-serving institutions continue to do the lion's share in producing minority STEM Ph.D.'s. These scientists are well qualified and on par with those graduating from the top-tier schools. The only impediment to their being recognized as such and hired by elite, predominantly white institutions is the intransigent racism that still haunts the academy. In spite of highly capable mentors like Tapia, majority institutions will not be able to fill the growing need for minority STEM Ph.D.'s without substantial input from minority-serving institutions that have been successfully producing scholars of color for more than 100 years. Rather than dismissing the accomplishments of these institutions, it makes sense to support their track record and learn from their expertise.

Fatimah Jackson,[1]* Clarence M. Lee,[1] Sherese Taylor[2]

[1]Department of Biology, Howard University, Washington, DC 20059, USA. [2]Cobb Research Laboratory, Howard University, Washington, DC 20059, USA.

*Corresponding author. E-mail: fatimah.jackson@howard.edu

Published by AAAS

RESEARCH

The caged heart in a cluster of gold atoms
Azubel et al., *p. 909*

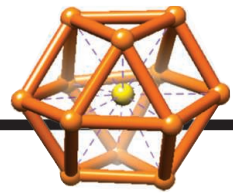

IN *SCIENCE* JOURNALS

Edited by **Melissa McCartney** *and* **Margaret Moerchen**

MASSIVE STARS

How huge early stars enriched the universe

How big did the first generation of stars get? Knowing their size is critical to understanding how they enriched the chemistry of the universe through supernova explosions. According to numerical simulations, some of the earliest stars were more than 100 times the Sun's mass. However, no traces of these live-fast, die-young stars had been detected in any low-mass stars still extant from that era. Aoki *et al*. now show spectra of one such metal-poor star that may have recorded the activity of a very massive predecessor (see the Perspective by Bromm). This observational evidence will spur further supernova models, as none predicts this specific chemical signature. — MMM

Science, this issue p. 912; see also p. 868

REEF ECOLOGY

Corals and reef fish choose nice homes

Young animals tend to disperse into new habitats. Can we use populations in protected areas to colonize nearby recovering or overused habitats? It seems that for corals and reef fish, the answer may be no. Dixson *et al.* show that dispersing juvenile corals and reef fish were overwhelmingly attracted to healthy reefs but were repelled by seaweeds that colonize degraded reefs (see the Perspective by Bruno). Thus, even species that appear passive in their choice of habitat may have stronger preferences than we thought. — SNV

Science, this issue p. 892; see also p. 879

QUANTUM OPTICS

Routing one photon with a few others

Single particles of light, photons, are ideal carriers of quantum information because they can travel far and fast and don't interact much with each other. However, this behavior has hampered attempts to control the propagation of single photons using all-optical setups. Shomroni *et al.* coupled a trapped atom to an optic fiber. That allowed them to control the polarization and propagation direction of a single photon in the fiber by controlling the atom's state (see the Perspective by Rempe). Because a faint pulse containing between 1.5 and 3 photons can switch the atom's state, the scheme provides a route to develop all-optical quantum networks. — ISO

Science, this issue p. 903; see also p. 871

SENSORY BIOLOGY

The makings of a powerful sweet tooth

The main attraction of nectar, a hummingbird favorite, is the sweet taste of sugar. Oddly, though, birds lack the main vertebrate receptor for sweet taste, TIR2. Baldwin *et al.* show that a related receptor, TIR1-T1R3, which generally controls savory taste in vertebrates, adapts in hummingbirds to detect sweet (see the Perspective by Jiang and Beauchamp). This repurposing probably allowed hummingbirds to specialize in nectar feeding and may have assisted the evolution of the many and varied hummingbird species seen today. — SNV

Science, this issue p. 929; see also p. 878

BONE BIOLOGY

An inhibitor breaks RANK

Osteoclasts are cells that break down bone; however, excessive bone loss leads to conditions such as osteoporosis. When three proteins called RANKL bind to three receptors called RANK on the osteoclasts' surfaces, the osteoclasts go to work. Warren *et al.* linked three mutant versions of RANKL protein together to generate an inhibitor of RANK (see the Perspective by Ou-Yang and Siegel). Two of the proteins bound more strongly to RANK, and the third protein could not bind to RANK. This engineered RANKL variant bound to RANK without activating the receptor, preventing osteoclasts from breaking down bone in mice. — JFF

Sci. Signal. **7**, ra80 and pe20 (2014).

Downloaded from www.sciencemag.org on August 24, 2014

CREDITS: (X-RAY) NASA/CXC/SAO/F. SEWARD *ET AL.*, (OPTICAL) NOAO/CTIO/MCELS, DSS

Published by AAAS

POLIO ERADICATION

Two vaccines together are better than one alone

Polio is proving difficult to eradicate. Making the choice between administering a live attenuated vaccine orally (Sabin) or an inactivated vaccine (Salk) by injection has been highly controversial. Patients prefer the Sabin vaccine, but it requires many doses to offer immunity. Jafari *et al.* tested the two vaccines together in northern India. The injected vaccine significantly reduced virus shedding and boosted intestinal mucosal immunity in children already given the oral vaccine. Thus, using both vaccines could help speed the eventual global demise of polio. — CA

Science, this issue p. 922

CLIMATE

Deep-sea warming slows down global warming

Global warming seems to have paused over the past 15 years while the deep ocean takes the heat instead. The thermal capacity of the oceans far exceeds that of the atmosphere, so the oceans can store up to 90% of the heat buildup caused by increased concentrations of greenhouse gases such as carbon dioxide. Chen and Tung used observational data to trace the pathways of recent ocean heating. They conclude that the deep Atlantic and Southern Oceans, but not the Pacific, have absorbed the excess heat that would otherwise have fueled continued warming. — HJS

Science, this issue p. 897

Oceans stow recent heat excesses

PHOTOS: (TOP TO BOTTOM) TUFTS UNIVERSITY; GETTY IMAGES/ISTOCKPHOTO

TUBERCULOSIS

How immune cells fight TB and show it

Mycobacterium tuberculosis causes an infection that can sometimes kill, but it proceeds to disease in only about 10% of individuals. Now, Montoya *et al*. provide a clue to how most people keep this bacterium in check. They show that when people fight tuberculosis, their immune cells secrete the cytokine interleukin-32, which may work through an antimicrobial pathway that uses vitamin D. The researchers analyzed five different clinical data sets and found that interleukin-32 may indicate latent tuberculosis. Interleukin-32 therefore may both contribute directly to the host response to tuberculosis and reflect protection against the disease. — ACC

Sci. Transl. Med. **6**, 250ra114 (2014).

IMMUNOGENETICS

Opening and closing blood enhancers

As cells develop and differentiate into different types, the shape and accessibility of their DNA can change. Lara-Astiaso *et al.* studied this phenomenon in blood. They developed a technique that examines a relatively small number of cells to identify the changes that affect DNA during blood development. They found that the DNA of noncoding regions, called enhancers, is set in an open position when cells are undifferentiated and able to take on a variety of roles and gradually closes as cells mature into their final forms. — LMZ

Science, this issue p. 943

IN OTHER JOURNALS

Edited by **Kristen Mueller** *and* **Jesse Smith**

NEUROSCIENCE

Tissue mimics brain's cortical layers

They may look like Play-Doh, but these colorful spongy rings are alive and may one day even learn. Tang-Schomer *et al.* engineered the rings to mimic the structure and function of the six layers of human cortical brain tissue. The researchers coaxed the neurons to grow around a matrix of silk proteins immersed in collagen gel. The cells cling to the structure as they branch out and connect, forming 3D networks resembling real neural circuits, the authors say. The team hopes to keep the neuronal sponge alive for 6 months, longer than any previous model, to study how its neural networks respond to insults such as disease or traumatic injury, and perhaps to see if its activity is altered by experience, a form of learning. — EU

Brainlike tissue is a practical test bed

Proc. Natl. Acad. Sci. U.S.A. 10.1073/pnas.1324214111.(2014).

CANCER TREATMENT

How to boost cancer immunotherapy

Why does our immune system protect us so well against infection but not against cancer? In part, this is because cancer cells use clever ways to escape immune responses designed to destroy them. A therapeutic strategy called "immune checkpoint blockade" thwarts these escape tactics and renders cancer cells vulnerable to immune attack. Although remarkably effective, only a subset of patients respond to it. Seeking possible explanations for this limited response, Kim *et al.* identified a specific immune cell population that interferes with the therapy in mouse tumor models. When the authors coadministered drugs that reduced the levels of these cells (called myeloid-derived suppressor cells), the efficacy of immune checkpoint blockade therapy greatly improved. — PAK

Proc. Natl. Acad. Sci. U.S.A. 10.1073/pnas.1410626111 (2014).

EDUCATION

Students produce assessment materials

If teaching someone else is the best way to learn, what will students gain from writing their own test questions? Every week, as part of an introductory undergraduate physics class, Bates *et al.* required students to contribute one original test question, answer five others, and critique an additional three. The researchers used Bloom's taxonomy criteria for cognitive

Published by AAAS

ALSO IN *SCIENCE* JOURNALS

Edited by **Melissa McCartney** *and* **Margaret Moerchen**

GLACIERS

Putting the heat on Mother Nature

Humans are now the biggest cause of glacier melting. Until recently, that was not true. Glaciers take a long time—decades to centuries—to respond to the environmental changes that control their sizes. They have been retreating gradually from the peak levels they reached in the middle of the 19th century, at the end of a 500-year-long cold period called the Little Ice Age. Marzeion *et al.* show that that has recently changed though, as climate warming has continued: Over the past 20 or so years, the anthropogenic contribution to glacial mass loss has increased markedly (see the Perspective by Marshall). — HJS

Science, this issue p. 919; see also p. 872

STEM CELL THERAPY

Challenges for stem cell–based therapies

Patient-derived pluripotent stem cells (PSCs) hold promise in the treatment of injury and disease. An ever-increasing number of specific cell types can be generated from PSCs, but technical challenges remain in applying these cells in the clinic. Fox *et al.* review the challenges in attaining this goal. These include gene modification, cell rejection, and delivery and localization issues involved in transplantation of cells for the treatment of diabetes and disorders of the blood, liver, heart, and brain. — BAP

Science, this issue p. 889

POLITICAL SCIENCE

Censorship of social media in China

Figuring out how many and which social media comments are censored by governments is difficult because those comments, by definition, cannot be read. King *et al.* have posted comments to social media sites in China and then waited to see which of these never appeared, which appeared and were then removed, and which appeared and survived. About 40% of their submissions were reviewed by an army of censors, and more than half of these never appeared. By varying the content of posts across topics, they conclude that any mention of collective action is selectively suppressed. — GJC

Science, this issue p. 891

PLANT DEVELOPMENT

Removing the nucleus in sieve elements

Although a cell's nucleus performs critical command and control functions, some cell types, such as enucleated red blood cells, seem to do without. Sieve element cells in plants similarly carry out their function of transporting nutrients and signals from one end of the plant to the other without the guidance of a nucleus. Furuta *et al.* watched how the nucleus self-destructs during the development of sieve element cells (see the Perspective by Geldner). The process is regulated under the control of transcription factors, even as the entire nuclear edifice crumbles into nothingness. – PJH

Science, this issue p. 933; see also p. 875

RIBOSWITCHES

A dual-action RNA switch for expression

Riboswitches are short segments of RNA that bind small molecules and switch between two different conformations, thereby regulating gene expression (see the Perspective by Chen and Gottesman). DebRoy *et al*. and Mellin *et al.* find a new class of riboswitches—in two different species of bacteria—that are both part of and regulate the production of a noncoding RNA. Each riboswitch ensures that a particular metabolic pathway is only activated in the presence of an essential small-molecule cofactor. In the absence of the cofactor, the full-length noncoding RNA is made and binds a regulator protein, preventing the regulator protein from inappropriately activating the metabolic pathway. — GR

Science, this issue p. 937 and p. 940; see also p. 876

NANOPARTICLE GROWTH

Watching platinum nanocube growth

Size and shape drive the properties of metal nanoparticles. Understanding the factors that affect their growth is central to making use of the particles in a range of applications. Liao *et al.* tracked the growth of platinum nanoparticle shapes at high resolution using state-of-the-art liquid cells for in situ monitoring inside an electron microscope. The authors tracked changes in the growth rates at different

Published by AAAS

crystal facets caused by differences in the mobility of the capping ligand. — MSL

Science, this issue p. 916

NANOPARTICLE IMAGING

Detailed structure of a gold nanoparticle

Adding only a few atoms or changing the capping ligand can dramatically change the structure of individual metal nanoparticles. Azubel *et al.* used aberration-corrected transmission electron microscopy to derive a three-dimensional reconstruction of water-soluble gold nanoparticles. Small-angle x-ray scattering and other techniques have also corroborated this model. They used this to determine the atomic structure, which compared favorably with density functional theory calculations, without assuming any a priori structural knowledge or the use of model fitting. — MSL

Science, this issue p. 909

HELIUM SUPERFLUIDITY

X-raying superfluid helium droplets

When physicists rotate the superfluid ^{4}He, it develops a regular array of tiny whirlpools, called vortices. The same phenomenon should occur in helium droplets half a micrometer in size, but studying individual droplets is tricky. Gomez *et al.* used x-ray diffraction to deduce the shape of individual rotating droplets and image the resulting vortex patterns, which confirmed the superfluidity of the droplets. They found that superfluid droplets can host a surprising number of vortices and can rotate faster than normal droplets without disintegrating. — JS

Science, this issue p. 906

PLANT GENETICS

The genomic origins of rape oilseed

Many domesticated plants arose through the meeting of multiple genomes through hybridization and genome doubling, known as polyploidy. Chalhoub *et al.* sequenced the polyploid genome of *Brassica napus*, which originated from a recent combination of two distinct genomes approximately 7500 years ago and gave rise to the crops of rape oilseed (canola), kale, and rutabaga. *B. napus* has undergone multiple events affecting differently sized genetic regions where a gene from one progenitor species has been converted to the copy from a second progenitor species. Some of these gene conversion events appear to have been selected by humans as part of the process of domestication and crop improvement. — LMZ

Science, this issue p. 950

CARBON CYCLE

Illuminating the pathway to destruction

Arctic lakes are an important source of atmospheric CO_2 and therefore play a role in climate change. It is thus vital to know how the rapid Arctic warming will affect them. Cory *et al.* now show that light is the biggest culprit in the breakdown of carbon from thawing permafrost soils (see the Perspective by Tranvik). This carbon then moves out into Arctic lakes and streams. Contrary to previous expectations, these photochemical processes cause much more destruction of the organic molecules in fresh water than bacterial respiration does. — HJS

Science, this issue p. 925; see also p. 870

Published by AAAS

level and quality of explanation—a standard scale—to rate the questions. Seventy-five percent of questions produced by first-year students were of high quality, with a large portion of the questions constituting true problems, as opposed to simple multiple choice questions. Overall, involving students in the summative assessment strategy for their own course increased both engagement and learning. — MM

Phys. Rev. ST Phys. Educ. Res. 10.1103/PhysRevSTPER.10.020105 (2014).

ENVIRONMENTAL SCIENCE

How much methane from landfills?

Landfill sites emit substantial amounts of the greenhouse gas methane, but how much of the methane in the atmosphere comes from such sites?

Methane emission varies daily at landfills

Scientists have measured widely varying fluxes, so estimates have been highly uncertain. Xu *et al.* measured methane emissions from a landfill site in Lincoln, Nebraska, from June to December 2010. They found that emissions varied widely from one day to the next, depending on the air pressure: The higher the air pressure, the lower the emissions. They conclude that measurements must be taken for at least 10 days to obtain a good estimate of annual methane emissions from landfill sites. This conclusion also could apply to other environmental sources of methane, such as wetlands and peatlands. — JFU

Global Biogeochem. Cy. 10.1002/2013GB004571 (2014).

STEM CELL NUMBER

Counting human intestinal stem cells

The cells that line the intestine, called intestinal epithelial cells, turn over, meaning that old ones die and new ones take their place. Stem cells located at the base of fingerlike structures called intestinal crypts support this high rate of turnover. Baker *et al.* investigated how this process works using human cells. The authors traced the lineage of cells in human intestinal crypts by counting naturally occurring mitochondrial DNA mutations. They identified five to six stem cells per crypt, which itself divides about once every 30 to 40 years. People who had a mutation in the APC gene, common in colon cancer, had more stem cells, and their crypts divided at a faster rate. — BAP

Cell Rep. 10.1016/j.celrep.2014.07.019 (2014).

MYCOBACTERIA

Bacteria scrimp and save themselves

Proteasomes are large protein complexes that degrade cellular proteins. Although widely conserved in mammals, only some bacteria species have machinery resembling the mammalian system (called Pup in bacteria). But why? In *Mycobacterium tuberculosis*, Pup contributes to virulence. Elharar *et al.* now report that in order to survive starvation, non-virulent mycobacteria need Pup too. If nitrogen supplies are low (nitrogen is key for mycobacteria growth), the Pup machinery will chew up some of the bacterium's own proteins to recycle amino acids. This diverts amino acids into maintaining basic metabolism until, hopefully, living conditions improve. — CA

EMBO J. 10.15252/embj.201387076 (2014).

Frequency matters in bat calls

ANIMAL COMMUNICATION

Bat calls shaped by sexual selection

Animals use a variety of signals to communicate, especially during mating. Bats, however, face an unusual problem. Using visual signals is challenging because they are nocturnal; and because they use calls to locate food, food demands constrain how these calls can evolve. Peuchmaille *et al.* now report that sexual selection shapes the calls of Meheley's horseshoe bats. They found that the frequency of males' calls indicated their size and that females preferred the higher-frequency calls emitted by larger males. Furthermore, these larger males sired more offspring. Higher-frequency calls may make these bats less efficient at tracking food, which suggests that the calls evolved in response to countervailing constraints. — SNV

PLOS One 10.1371/journal.pone.0103452 (2014).

ASTROPHYSICS

Giants in the outer halo of the Milky Way

Most stars in the Milky Way reside in the familiar spiral disk structure and probably formed in place. Stars in the galaxy's much larger and far sparser spherical halo, on the other hand, are unlikely to have formed where the gas density is so low. Too few halo stars are known, however, for scientists to model their origins. Bochanski *et al.* examined the motion and brightness of some candidate stars, and identified two that are the most distant members of our galaxy yet found, more than 30 times farther from the galactic center than the Sun. These observations should help tell whether these stars were captured from dwarf galaxies or ejected from the Milky Way disk. — MMM

Astrophys. J. Lett. 10.1088/2041-8205/790/1/L5 (2014).

PHOTOS: (TOP TO BOTTOM) © FRANZ CHRISTOPH ROBILLER/IMAGEBROKER/CORBIS; GETTY IMAGES/FUSE

Published by AAAS

REVIEW SUMMARY

STEM CELL THERAPY

Use of differentiated pluripotent stem cells in replacement therapy for treating disease

Ira J. Fox,* George Q. Daley, Steven A. Goldman, Johnny Huard, Timothy J. Kamp, Massimo Trucco

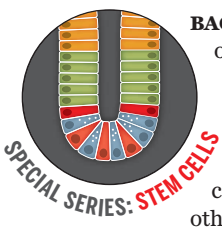

BACKGROUND: Decades of laboratory and clinical investigation have led to successful therapies using hematopoietic stem cells (HSCs), but few other cell therapies have transitioned from experimental to standard clinical care. Providing patients with autologous rather than allogeneic HSCs reduces morbidity and mortality, and in some circumstances broader use could expand the range of conditions amenable to HSC transplantation. The availability of a homogeneous supply of mature blood cells would also be advantageous. An unlimited supply of pluripotent stem cells (PSCs) directed to various cell fates holds great promise as source material for cell transplantation and minimally invasive therapies to treat a variety of disorders. In this Review, we discuss past experience and challenges ahead and examine the extent to which hematopoietic stem cell transplantation and cell therapy for diabetes, liver disease, muscular dystrophies, neurodegenerative disorders, and heart disease would be affected by the availability of precisely differentiated PSCs.

ON OUR WEB SITE

Read the full article at http://dx.doi.org/10.1126/science.1247391

ADVANCES: Although it is not yet possible to differentiate PSCs to cells with characteristics identical to those in the many organs that need replacement, it is likely a matter of time before these "engineering" problems can be overcome. Experience with cell therapies, both in the laboratory and the clinic, however, indicate that many challenges remain for treatment of diseases other than those involving the hematopoietic system. There are issues of immunity, separate from controlling graft rejection, and identifying the optimal cell type for treatment in the case of muscular dystrophies and heart disease. Optimization is also needed for the transplant site, as in diabetes, or when dealing with disruption of the extracellular matrix in treating degenerative diseases, such as chronic liver and heart disease. Finally, when the pathologic process is diffuse and migration of transplanted cells is limited, as is the case with Alzheimer's disease, amyotrophic lateral sclerosis, and the muscular dystrophies, identifying the best means and location for cell delivery will require further study.

OUTLOOK: Considering the pace of progress in generating transplantable cells with a mature phenotype, and the availability of PSC-derived lineages in sufficient mass to treat some patients already, the challenges to scaling up production and eliminating cells with tumor-forming potential are probably within reach. However, generation of enough cells to treat an individual patient requires time for expansion, differentiation, selection, and testing to exclude contamination by tumorigenic precursors. Current methods are far too long and costly to address the treatment of acute organ injury or decompensated function. Immune rejection of engrafted cells, however, is likely to be overcome through transplantation of autologous cells from patient-derived PSCs. Availability of PSC-derived cell populations will have a dramatic effect on blood cell transfusion and the use of hematopoietic stem cell transplantation, and it will likely facilitate treatment of diabetes, some forms of liver disease and neurologic disorders, retinal diseases, and possibly heart disease. Close collaboration between scientists and clinicians—including surgeons and interventional radiologists—and between academia and industry will be critical to overcoming challenges and to bringing new therapies to patients in need. ■

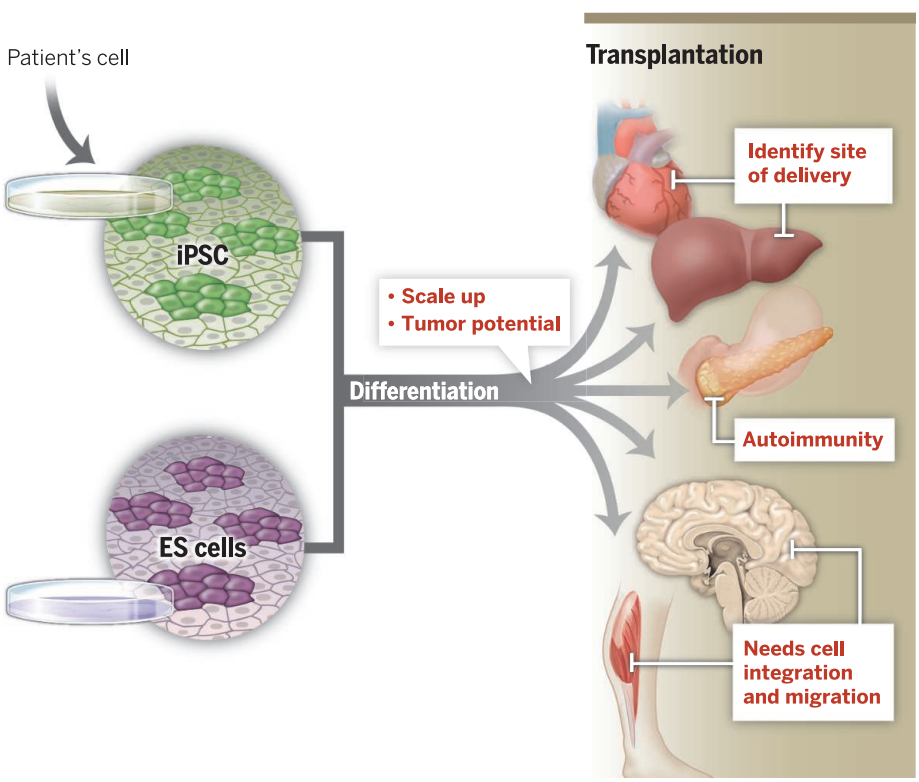

Unlimited populations of differentiated PSCs should facilitate blood therapies and hematopoietic stem cell transplantation, as well as the treatment of heart, pancreas, liver, muscle, and neurologic disorders. However, successful cell transplantation will require optimizing the best cell type and site for engraftment, overcoming limitations to cell migration and tissue integration, and possibly needing to control immunologic reactivity (challenges indicated in red). iPSC, induced PSC; ES cells, embryonic stem cells.

The list of author affiliations is available in the full article online.
*Corresponding author. E-mail: foxi@upmc.edu
Cite this article as I. J. Fox *et al.*, *Science* 345, 1247391 (2014); DOI: 10.1126/science.1247391

ILLUSTRATION: K.SUTLIFF/*SCIENCE*

Published by AAAS

REVIEW

STEM CELL THERAPY

Use of differentiated pluripotent stem cells in replacement therapy for treating disease

Ira J. Fox,[1]* George Q. Daley,[2,3,4] Steven A. Goldman,[5,6] Johnny Huard,[7] Timothy J. Kamp,[8] Massimo Trucco[9]

Pluripotent stem cells (PSCs) directed to various cell fates holds promise as source material for treating numerous disorders. The availability of precisely differentiated PSC-derived cells will dramatically affect blood component and hematopoietic stem cell therapies and should facilitate treatment of diabetes, some forms of liver disease and neurologic disorders, retinal diseases, and possibly heart disease. Although an unlimited supply of specific cell types is needed, other barriers must be overcome. This review of the state of cell therapies highlights important challenges. Successful cell transplantation will require optimizing the best cell type and site for engraftment, overcoming limitations to cell migration and tissue integration, and occasionally needing to control immunologic reactivity, as well as a number of other challenges. Collaboration among scientists, clinicians, and industry is critical for generating new stem cell–based therapies.

Induced pluripotent stem cells (PSCs) are generated by reprogramming somatic cells to a pluripotent state by transient expression of pluripotency factors. These cells can self-renew indefinitely and are able to differentiate into any cell lineage (*1*, *2*). The ability to generate PSCs from individual patients and differentiate them into an unlimited supply of tissue and organ-specific cells capable of circumventing immunologic rejection after transplantation could facilitate development of cell-based therapies for the treatment of a variety of debilitating disorders and dramatically change the practice of medicine.

Before these cells can be used in the clinic, a variety of barriers must be overcome. For many diseases, it is not yet possible to differentiate PSCs to cells with characteristics identical to those in the organs that need replacement. There are also challenges like scaling up production, eliminating cells with tumor-forming potential, and decreasing the time needed for expansion, differentiation, selection, and testing. Furthermore, treatment of a genetic mutation using autologous cells will often require genetic manipulation, which might result in changes that could increase cancer risk.

Some form of immune suppression may also be required to control cell loss after transplantation, whether due to rejection, an immune response to a genetically corrected protein, or recurrence of autoimmunity, with destruction of the transplant, as might be the case for diabetes. The standard signs of rejection used in solid organ transplantation are not likely to be useful because the sensitivity of functional changes has been shown, after islet transplantation, to be inadequate to diagnose rejection before damage to the engrafted cells is irreversible (*3*). Of course, it might be possible to engineer PSC-derived grafts, with the usual caveats concerning activating oncogenes, so that they would be immunologically inert and identifiable by an array of imaging strategies.

Although decades of laboratory and clinical investigation have led to successful therapies using hematopoietic cells, few other cell therapies have transitioned from experimental to standard clinical care. Here, we discuss the present state of cell therapy in the context of having available differentiated PSC-derived cells. The "gold standard," blood and hematopoietic stem cell (HSC) transplantation, is highlighted first, followed by an examination of cell therapy for diabetes, liver disease, neurologic and retinal disorders, muscular dystrophies, and heart disease.

[1]Department of Surgery, Children's Hospital of Pittsburgh and McGowan Institute for Regenerative Medicine, University of Pittsburgh, Pittsburgh, PA, USA. [2]Boston Children's Hospital and Dana Farber Cancer Institute, Boston, MA, USA. [3]Department of Biological Chemistry and Molecular Pharmacology, Harvard Medical School Broad Institute, Cambridge, MA, USA. [4]Howard Hughes Medical Institute, Chevy Chase, MD, USA. [5]Center for Translational Neuromedicine, The University of Rochester Medical Center, Rochester, NY, USA. [6]Center for Basic and Translational Neuroscience, University of Copenhagen, Denmark. [7]Stem Cell Research Center, Department of Orthopaedic Surgery, University of Pittsburgh, School of Medicine, Pittsburgh, PA, USA. [8]Stem Cell and Regenerative Medicine Center, Cellular and Molecular Arrhythmia Research Program, Department of Medicine, School of Medicine and Public Health, University of Wisconsin, Madison, WI, USA. [9]Division of Immunogenetics, Children's Hospital of Pittsburgh, University of Pittsburgh, Pittsburgh, PA, USA.
*Corresponding author. E-mail: foxi@upmc.edu

Hematopoietic cell-based therapies

Many of the principles of cell transplantation derive from our long experience with transfusion of blood products. Infused red blood cells (RBCs), platelets, and HSCs are the most widely employed cellular therapies in use today. The relative ease of HSC transplantation (HSCT) derives in large part from the intrinsic potential of HSCs to home to and integrate into native niches, give rise to differentiated progeny, and thereafter to egress into the circulation. Thus, HSCT avoids the challenges of restoring integrity and function of more anatomically complex organs like the lung, heart, liver, and brain.

Despite the successes of HSCT, isolated HSCs cannot be expanded to the degree needed, although there has been limited success with cord blood. Furthermore, allogeneic HSCT is associated with considerable treatment-related morbidity and mortality. Thus, transplantation with autologous HSCs for the same indications would eliminate the major morbidities of immune mismatch and could potentially expand the range of conditions, including cancers, amenable to HSCT. One of the most promising applications of somatic cell reprogramming is the production of customized pluripotent stem cells followed by gene correction (*4*), differentiation into HSCs, and autotransplant with intention to cure any one of dozens of inherited genetic disorders of the blood-forming system. Such a proof of principle has been achieved for treating murine models of severe combined immune deficiency and sickle cell anemia (*4*, *5*). HSCs have been derived from murine embryonic stem cells that manifest the cardinal features of clonal self-renewal and multilineage lymphoid-myeloid engraftment in primary and secondary irradiated hosts (*6*, *7*). The derivation of HSCs from human PSCs has proven elusive, although several examples of low-level engraftment have been reported (*8*–*10*). Although true HSCs are not yet available, methods exist to produce RBCs (*11*, *12*) and platelets (*13*) in vitro that are suitable for transfusion. To eliminate the costly and sometimes unreliable system of volunteer blood supply, as well as the risk of transmission of infectious agents, a reliable method for generating an inexhaustible, uniform supply of pathogen-free blood products has tremendous appeal. Ultimately, advances in in vitro cell manufacture should soon be able to reduce costs and enable an off-the-shelf supply.

Diabetes

One of several approaches to resolving the long-term complications associated with diabetes has been beta cell replacement by allogeneic whole-pancreas or isolated pancreatic islet transplantation, using immune suppression in an attempt to control rejection and recurrent autoimmune destruction of the transplanted tissue. Cadaver pancreas transplantation has been

shown to reduce the complications associated with type 1 diabetes. However, it is a complex surgical procedure associated with morbidity and measureable mortality (*14*). An important lesson from this experience, however, is that conventional immune suppression is able to inhibit recurrent destruction of insulin-producing cells while controlling allograft rejection.

After years of laboratory and clinical investigation, islet transplantation has become a realistic alternative therapy, which, over the past several decades has become increasingly more successful (*15*–*17*). Experience with autologous islet transplantation after total or near-total pancreatic resection for severe chronic pancreatitis and allogeneic islet transplantation for type 1 diabetes have both been instructive (*18*). The preferred site for implantation is the liver, and engraftment is accomplished by minimally invasive transcutaneous catheter infusion through the liver into the portal vein. This approach is associated with a small but measureable risk of hemorrhage and partial portal vein thrombosis. More important, an immediate blood-mediated inflammatory response and pathologic activation of the coagulation system results in a large loss of the infused islets as soon as they come into direct contact with blood (*19*). As the yield of islets from a chronically injured pancreas is already reduced, this constitutes a limiting factor in trying to reach an islet mass sufficient for insulin independence after autologous islet transplantation. It is also a serious issue after islet allotransplantation, where success often requires multiple infusions from different donors and transplantation of a much greater islet mass to achieve insulin independence. Although it is not completely understood why so many more islets are required for initial success in allo- than for autotransplants, this barrier to successful insulin replacement by cell therapy should be resolvable with an inexhaustible supply of donor beta cells.

Failure to achieve long-term insulin independence is more problematic. Five-year insulin independence rates after islet allotransplantation in selected centers are approaching 50% (*17*, *20*). These improved outcomes have resulted from the transplantation of a larger islet mass and more effective control of rejection and autoimmunity, with late graft loss being attributed to toxicity to beta cells arising from medications that suppress immunity and an inability to diagnose or treat recurrent disease or rejection. Advances in donor cell imaging by genetic engineering of PSCs and the development of new strategies for controlling the immune response should resolve some of these issues.

However, experience with islet autotransplantation indicates a more serious problem for long-term function of engrafted islet cells, independent of the need to control rejection or recurrent autoimmune destruction (*21*). Although short-term insulin independence has been accomplished, almost all patients are back on insulin therapy after 5 years. This loss of graft function may be attributable to chronic stimulation of an initially marginal intrahepatic beta cell mass that produces metabolic deterioration and loss of beta cells (*18*). Transplantation of a larger mass of islets may alleviate this problem and result in indefinite graft function. However, the site of engraftment in the liver may also be responsible for poor long-term survival. Islets ectopically engrafted in the liver are known to produce a number of pathologic histologic abnormalities, including extensive amyloid deposition within the islets (*22*). Thus, it remains unclear whether whole islets can remain functionally intact in the liver over time.

The use of PSC-derived beta cells could resolve many of the above issues. Beta cells that have been dissociated and isolated from intact islets successfully engraft within the liver lobule. This is in contrast to how intact islets engraft, which is by partially remaining within the portal circulation (Fig. 1) and requiring neovascularization. Isolated cells may not be as susceptible to forming amyloid deposits, and transplantation of a large mass of individual beta cells might avoid metabolic exhaustion and apoptosis. Dissociated cells do not, however, engraft when infused as individual beta cells but require reaggregation (*23*). In addition, individual beta cells function less well when isolated. It has been reported that more insulin by a factor of 30 is released from beta cells within intact islets as compared with that released from purified single beta cells, and reaggregated beta cells and beta cells aggregated with alpha cells respond better to glucose challenge by a factor of 4 than do single beta cells alone (*24*). Thus, to treat type 1 diabetes, it may be necessary to transplant PSC-derived beta cells as aggregates or possibly to transplant them with PSC-derived non–beta cells.

Whether PSC–derived surrogate beta cells will have the same capacity to engraft in the liver-like primary beta cells is not known. Because they are small, they might pass through the liver into the lungs, as has been described after hepatocyte transplantation. Other sites of transplantation, like the gastric submucosal space, might offer some advantages over the portal vein (Fig. 2).

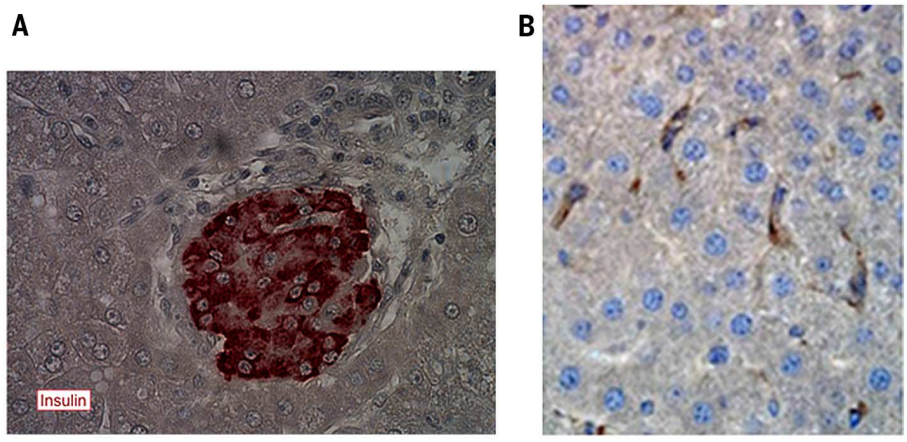

Fig. 1. Comparison of intrahepatic engraftment of intact islets versus isolated beta cells after intraportal transplantation. (**A**) Transplanted islet (in brown) within the blood vessel of the liver after intraportal transplantation [From (*28*), with permission]. (**B**) Induced PSC-derived beta cells (in brown) engraft as cells scattered throughout the liver parenchyma [From (*150*), with permission].

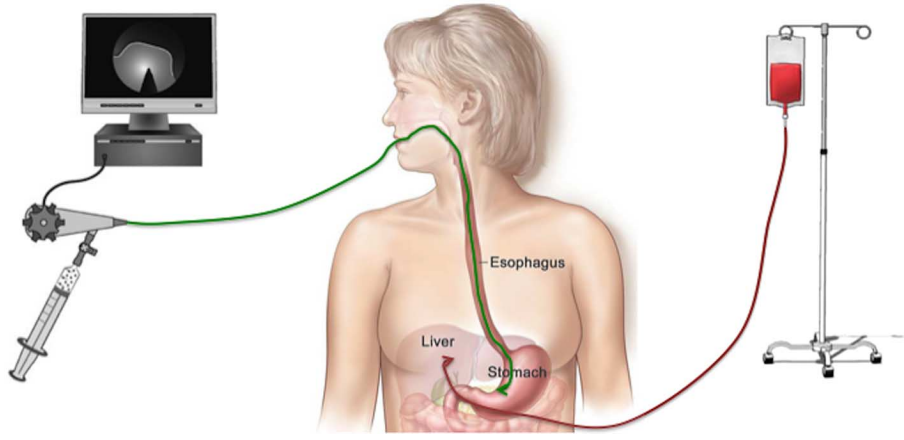

Fig. 2. Transplantation of insulin-producing cells. Illustration of traditional portal-vein infusion of insulin-producing cells for engraftment in the liver versus endoscopic placement of transplanted cells in the gastric submucosal space.

Surrogate beta cells could be implanted in the gastic submucosal space endoscopically, where they would be accessible for biopsy to monitor the graft status (*25*).

Without concomitant use of immune suppression, autoimmunity will mediate destruction of grafts composed of even autologous cells (*26*). Whether autoimmunity can be suppressed in a way that is less detrimental to the insulin-producing cells than conventional drug-based allogeneic protection is as yet unknown. Strategies for potentially controlling this process by inducing tolerance are in development (*27*). To modulate immunologically mediated problems, transgenes might help confer long-term function and reduce early loss of the graft in diabetic recipients. Candidates for this approach are like the ones targeting the tissue factor and coagulation cascade, or exerting anti-inflammatory activity, that have already been tested in cloned pigs (*28*). An alternative approach is to encapsulate the PSC-derived insulin-producing surrogates, providing a protective barrier from immune rejection and autoimmunity while allowing free exchange of nutrients, waste, and, most important, insulin and glucose. Unfortunately, thus far these approaches have shown mixed results, at least after transplantation of intact islets in diabetic patients with low levels of circulating C-peptide, and rarely achieve full and lasting insulin independence (*29*). A variation on this encapsulation and transplant strategy, using PSC-derived beta cells, will soon be tested in clinical trials for the treatment of type 1 diabetes (*30*).

Liver Disease

Hepatocyte transplantation holds great promise as a therapy for individuals with life-threatening liver diseases, where organ transplantation is often the only available treatment option. Patients with both acute liver failure and liver-based inborn errors of metabolism, leading to life-threatening extrahepatic complications, are ideal candidates for cell therapy. Numerous studies in rodents have shown that hepatocyte transplantation can reverse acute fulminant hepatic failure (*31*) and correct liver-based metabolic deficiencies (*32*–*37*). Because the native architecture of the liver is intact in these diseases, the transplant procedure involves simple injection of hepatocytes through the portal vein into the liver, where the cells integrate into the host liver and are indistinguishable from the native liver cells (*38*, *39*). Infusion of hepatocytes is a minimally invasive procedure, so it can be performed on severely ill patients with relatively low risk. Because the native liver is not removed, the transplanted hepatocytes only need to improve liver function enough to stabilize a patient with acute liver failure until their own liver is able to regenerate or to replace the enzyme deficiency that is missing in liver-based metabolic disorders, a goal similar to that of gene therapy.

Clinical trials of hepatocyte transplantation have only demonstrated the long-term safety of the procedure (*40*–*46*). Transplanted hepatocytes have not restored liver function enough to circumvent the need for organ replacement in patients with liver failure, and transplantation has only resulted in partial correction of metabolic disorders (*47*). Efficacy has been limited by relatively poor initial and long-term engraftment and an inability to monitor graft function in real time, which makes diagnosing and treating rejection nearly impossible. In acute liver failure, the severity of liver dysfunction requires that the transplanted hepatocytes function immediately, and the lack of a clinically relevant disease model means that the number of cells that need to engraft to reverse hepatic failure is essentially unknown (*48*, *49*). Although animal models of metabolic liver disease recapitulate the human processes better, achieving an adequate level of engraftment is still a problem because the number of donor cells that can be safely transplanted into the liver at any one time is small, usually less than 1% of the liver mass (*50*). Transplantation of a larger number of cells can lead to severe portal hypertension and translocation of cells into the systemic circulation with embolization to the lungs. Liver-directed radiation has been proposed as a way to facilitate repopulation of the native liver by transplanted hepatocytes, whose viability is relatively short once isolated (*51*). Preparative radiation inhibits host hepatocyte proliferation and induces postmitotic hepatocyte death, allowing donor hepatocytes to preferentially proliferate and repopulate the irradiated host liver. This strategy has been employed to completely correct a rodent model of Crigler-Najjar syndrome (*52*).

An immediately available, inexhaustible supply of functioning donor hepatocytes would allow early intervention in patients with hepatic failure and would allow hepatocytes to be infused over a longer period of time. It is possible that daily large-scale portal-vein PSC-derived hepatocyte infusions could provide the hepatocyte mass necessary to normalize the encephalopathy, coagulation defects, and other life-threatening consequences of hepatic failure and completely correct liver-based enzyme deficiencies. In addition, unrestricted availability of donor hepatocytes could allow treatment of patients with less severe, but debilitating, liver-based metabolic disorders, which are not now considered candidates for organ transplantation, such as phenylketonuria and partial urea cycle disorders. Whether acute hepatic failure is associated with changes in the local microenvironment that might interfere with engraftment and function of transplanted hepatocytes is not yet known and will need to be addressed with further clinical experience.

Although PSC-derived hepatocytes may help advance cell therapies for acute liver failure and metabolic liver diseases, the vast majority of patients who are in need of life-saving intervention are patients with end-stage cirrhosis and chronic hepatic failure. After infusion through the portal vein, hepatocytes have a difficult time entering the hepatic cords through the pathologically expanded extracellular matrix (Fig. 3) present in advanced cirrhosis (*53*). As a result, transplantation by this route generates severe portal hypertension and may produce portal thrombosis. Animal studies suggest that transplantation by direct injection into an extrahepatic site, such as the spleen, can circumvent this engraftment difficulty, improve liver function, and prolong survival in end-stage cirrhosis (*43*, *54*, *55*). Even then, however, transplanted hepatocytes

Fig. 3. Cirrhosis and chronic liver failure. Normal control liver (behind) and liver with advanced cirrhosis (in front), highlighting the structural differences that make liver failure from cirrhosis difficult to treat by intrahepatic cell therapy [Images courtesy of R. Markin, University of Nebraska Medical Center].

provide function for only a period of months. Because it is not clear that transplanted cells can function for any sustained period of time in the abnormal environment produced by hepatic failure and portal hypertension, the same fate may await hepatocytes transplanted into other extra-anatomic locations, such as the lymph node (*56*), although diversion of the portal circulation may be able to enhance survival (*55*, *57*). For a variety of reasons, anecdotal reports of hepatocyte transplantation in humans with end-stage cirrhosis has not produced any measurable level of success (*58*). Treatment of chronic liver failure might benefit from transplantation of a large mass of hepatocytes into a decellularized human or animal liver scaffold (*59*). When repopulated with donor hepatocytes and nonparenchymal cells, the biohybrid graft might then be vascularized through the portal circulation as an engineered internal auxiliary liver graft. Because this strategy would leave the native cirrhotic liver in place, it would still leave unresolved the management of coexisting portal hypertension and the risk of developing hepatocellular carcinoma in the native liver.

Neurologic and retinal diseases

The brain is arguably the most difficult of organs in which to employ stem cell–based therapeutics; the myriad connections of its neurons and their complex interdependency with macroglia, including astrocytes, oligodendrocytes, and glial progenitor cells, defy precise structural reconstitution. Neurodegenerative disorders, in particular, include diseases of both single and multiple phenotypes, the heterogeneity of which can dictate how amenable each might be to cell-based therapeutics. Some prototypic degenerative dementias, such as Alzheimer's disease and Lewy body disease, involve a multitude of neuronal phenotypes—and in some cases glial as well, in multisystem atrophy. These multiphenotypic disorders span anatomic and functional domains and may exhibit both contiguous and transsynaptic patterns of spread. For these reasons, they remain poor targets for neuronal replacement strategies, at least for the near future.

However, many diseases of the brain involve single cell types, and these conditions lend themselves to phenotype-specific cell replacement, whether by transplantation or by the induction of endogenous neural stem or progenitor cells (*60*) (Fig. 4). Degenerative disorders in which the loss of single phenotypes predominate, especially those in which a single region is differentially affected—such as Parkinson's disease (PD), in which nigrostriatal neurons are lost before other neurons, and Huntington's disease (HD), in which medium spiny neuronal loss and striatal atrophy become apparent long before the onset of cortical neuronal loss—have proven more amenable to phenotype-specific cell replacement (*61*, *62*). Memory disorders, which can involve loss of the basal forebrain cholinergic neurons projecting to the hippocampus, have responded to PSC-derived cholinergic neuronal replacement in rodents (*63*). Yet the memory loss of early Alzheimer's and frontotemporal dementia typically heralds

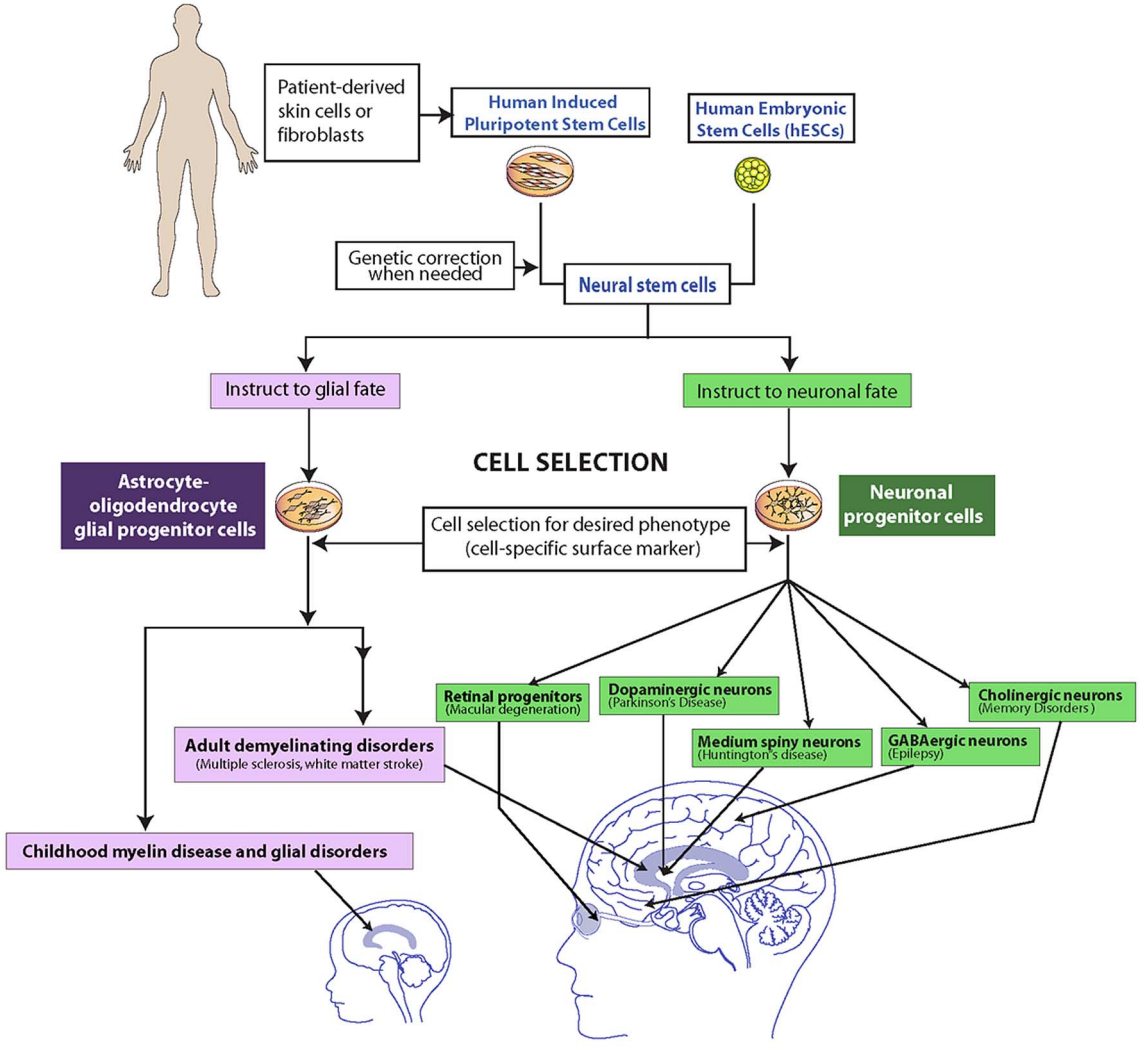

Fig. 4. PSC-derived glial and neural cells. Schematic representation of how PSC-derived glial and neural cells populations might be employed to treat a vast array of neurologic and retinal diseases.

deterioration across all cognitive modalities; thus, isolated replacement of cholinergic neurons is likely to prove effective in only very selected cases of memory loss, which remain difficult to identify at the onset. Nonetheless, for each of these subcortical neuronal phenotypes, animal studies have proven sufficiently promising to justify both the production of cells appropriate for clinical transplantation and the design of clinical trials by which to evaluate their safety and efficacy.

Clinical trials of cell transplantation have already been performed in PD and HD (*61*, *62*). These trials used fetal tissue dissected from the regions of interest, so that the specific cell types needed comprised but a fraction of the cells delivered. Perhaps as a result, these early trials yielded largely disappointing results with considerable variability in outcome and frequent untoward side effects, the most prominent being refractory dyskinesias after fetal mesencephalic tissue grafts in PD. Nonetheless, some transplanted PD patients did experience durable benefit, providing at least a proof of principle in favor of dopaminergic neuronal transplantation. The generation of midbrain dopaminergic neurons (*64*, *65*) and medium spiny neurons (*66*, *67*) from human PSCs (*64*–*67*) thus permit a leap forward in the availability of well-defined engraftable neurons of relative phenotypic homogeneity. This advance should enable a new generation of therapeutic trials less compromised by donor variability and compositional heterogeneity.

Some disorders affect single neuronal types but are so dispersed throughout the central nervous system (CNS) as to present problems of delivery. Several primary epilepsies may derive from deficits in γ-aminobutyric acid (GABAergic) interneuron numbers and function. A number of groups have asked whether transplantation of healthy, migration-competent interneurons into epileptic cortex may provide benefit to patients with medication-refractory epilepsy. The production of GABAergic interneurons from PSCs (*68*) has permitted assessment of this promising approach to epileptic therapy. That said, GABAergic neurons comprise a plethora of functionally distinct phenotypes, thus rendering the effects of their transplantation on host neural circuits unpredictable.

Phenotype-specific disorders of the eye may prove more straightforward targets for cell therapy. Loss of the retinal pigment epithelium (RPE) in age-related macular degeneration has been a particular target of interest in that efficient protocols for generating RPE cells from PSCs have been developed (*69*, *70*). PSC-derived RPEs are now in trials for macular degeneration. As more efficient protocols are developed for producing specific retinal phenotypes from PSCs, a broad variety of both intrinsic retinal disorders and optic neuropathies may prove appropriate targets for cell replacement.

Other disorders of single phenotype are not attractive as targets for cell-based therapy because of their multicentric pathology, the nonmigratory nature of potential replacement cells, or both. The motor neuronopathies, such as amyotrophic lateral sclerosis (ALS) and spinal muscular atrophy, are examples. Spinal motor neurons may be generated from PSCs (*71*–*73*), and yet their clinical utility has been limited by the multisegmental nature of motor neuron loss in these diseases and by our current inability to direct long-distance axonal regrowth and target reinnervation. Cell-based treatment approaches for ALS have thus shifted away from neuronal replacement toward the delivery of astrocytes, with the goal of correcting underlying glial metabolic deficiencies that may contribute to disease progression in ALS (*74*). If successful, such studies may herald the use of PSC-derived glia for ALS and related disorders, in which neurons may be the paracrine victims of glial dysfunction.

Diseases of glia may prove especially accessible targets for cell-based therapy. The myelin diseases, which involve the loss or dysfunction of oligodendrocytes, are among the most prevalent and disabling conditions in neurology and may be particularly appropriate targets for replacement (*75*). They include multiple sclerosis and white matter stroke, the cerebral palsies, and the hereditary pediatric leukodystrophies. As a result, oligodendrocyte progenitor cells (OPCs), which can give rise to myelinogenic oligodendrocytes, have become of great interest as potential therapeutic agents (*76*–*78*). Recently, transplantation of OPCs derived from human PSCs rescued otherwise lethally hypomyelinated shiverer mice (*79*). As such, one might expect that efforts under way using tissue-derived cells to treat myelin disorders, such as childhood Pelizaeus-Merzbacher disease (*80*) and adult progressive multiple sclerosis, may be supplanted by PSC-derived OPCs.

Because OPCs produce astrocytes as well as oligodendrocytes and are highly migratory, they might prove useful in rectifying the demyelination-associated enzymatic deficiencies of the lysosomal storage disorders, such as Krabbe disease, metachromatic leukodystrophy, and Tay-Sachs disease, as well as the astrocytic pathology of vanishing white matter disease (*81*). In particular, transcription activator-like effector nuclease (TALEN) and clustered regularly interspaced short pallendromic repeats (CRISPR)/Cas gene editing technologies (*82*) may allow correction of mutations in PSCs, thus allowing autologous and allogeneic therapy to be assessed across the entire range of hereditary leukodystrophies.

Their promise notwithstanding, introducing PSC-derived cells into the postnatal and mature CNS has its own set of risks, which include immune rejection, the induction of neuroepithelial neoplasms and teratomas (*65*, *80*, *83*), heterotopic neuronal differentiation and epileptogenesis, and the mass effect that may accompany exuberant cell expansion. Neural stem cells have been reported to have escaped to the ventricular system and subarachnoid space, adventitious growths that may present a risk of hydrocephalus, syringomyelia, or surface venous compression, as well as disruption of cerebrospinal fluid flow and waste clearance. The list goes on and serves to highlight the degree to which we must always be concerned that any cell therapeutic not result in unintended consequences.

Muscular Dystrophies

Duchenne muscular dystrophy (DMD) is a devastating, heritable X-linked muscle disease characterized by progressive muscle weakness due to the lack of dystrophin expression at the sarcolemma of muscle fibers (*84*–*87*). Although various approaches have been investigated for delivering dystrophin to dystrophic muscle, there is still no effective treatment that alleviates progression of the disease. Satellite cells play a key role in development of skeletal muscle during embryogenesis and in regeneration of muscle fibers during postnatal life. Upon isolation and culturing, satellite cells re-enter the cell cycle as myoblasts and eventually fuse to form myotubes in vitro (*88*). Transplantation of normal myoblasts into dystrophin-deficient muscle can create a reservoir of normal myoblasts capable of fusing with one another and with dystrophic muscle fibers, restoring dystrophin to the muscle (*89*–*97*).

Myoblast transplantation in animal models and DMD patients can transiently deliver dystrophin and improve the strength of injected dystrophic muscle, but this approach is hindered by poor cell survival and limited migration of injected cells from the original injection site (*89*–*97*). Researchers have used preparative irradiation or injection of myonecrotic agents into the transplantation site to improve efficiency (*89*–*98*), and although these approaches have led to an improvement in restoration of dystrophin in *mdx* mice, success remains limited.

Many scientists consider satellite cells to be the only myogenic cells responsible for muscle growth, regeneration, and repair; however, reports suggest that other cell populations may be able to support muscle regeneration, making them a potential alternative source of cells (*99*–*103*). Cells from bone marrow (*101*, *103*), blood vessels (*100*, *104*–*106*), the neuronal compartment (*99*, *102*), and connective tissue can differentiate toward a myogenic lineage, suggesting that transplantation of these nonsatellite cell populations could be effective in improving muscle regeneration (*107*). Animal studies have shown that many have a very limited capacity to enhance muscle regeneration after transplantation; however, mesoangioblasts, pericytes, and muscle-derived stem cells (MDSCs) survive postimplantation (Fig. 5) and repair skeletal muscle after injury and disease (*96*, *100*, *104*–*106*, *108*). As a result, their human counterparts have been isolated and are undergoing clinical trials for the treatment of stress urinary incontinence (*108*, *109*).

Most cell therapies for treating DMD employ an intramuscular route of administration; however, systemic delivery would be a far superior method because it is the heart, intercostal muscles, and diaphragm that are involved in the early death of DMD patients and are almost impossible to reach by intramuscular injection. Systemic delivery of stem cells can achieve widespread delivery and leads to dystrophin expression in various muscle groups, although with varying

levels of success (*110*). This technology is still under development and is technically challenging, especially when using small-animal models (*110*, *111*).

Although most cell transplant studies for DMD have focused on the use of postnatal stem cells, the progeny of PSCs may eventually be useful for muscle regeneration and repair. A number of stem cell lineages can be easily generated in vitro, but differentiation into skeletal muscle has proven to be difficult (*112*–*116*). PSCs transfected with myogenic regulatory factors, in particular Pax3 and Pax7, undergo partial myogenic differentiation and participate in skeletal muscle regeneration (*117*, *118*), whereas MyoD and Myf5 have also been used to produce myoblasts from normal and dystrophic human PSCs (*119*). Intramuscular transplantation of human skeletal myogenic progenitors derived from PSCs results in durable engraftment, contributing to the satellite cell pool (*120*). Furthermore, PSCs derived from patients with muscular dystrophies, differentiated into satellite and mesoangioblast-like cells, have been genetically corrected and, after reintroduction into dystrophic mice, ameliorate their dystrophic phenotype (*121*, *122*). Although PSCs have the potential to create an inexhaustible source of therapeutic cells for muscle repair, the availability of large numbers of muscle progenitor cells has not been a major limitation. Poor cell survival and the limited ability of the cells to migrate from their initial site of injection remain the two major hurdles to muscle cell–based therapies, even using PSC-derived cell populations.

Finally, despite the lack of dystrophin at birth, the initiation of acute, severe muscle weakness does not occur in DMD patients until they have reached the age of 4 to 8 years, which coincides with gradual exhaustion of their muscle progenitor cells (MPCs). Impairment in the myogenic potential of the MPCs isolated from DMD muscle in various animal models has been described (*123*–*125*), and recent studies indicate that sparing of the extraocular muscles in DMD patients may be related to the existence of a subpopulation of MPCs that that do not become exhausted with age, indicating that muscle weakness in DMD patients is related to MPC exhaustion during disease progression (*126*). These findings, taken together, suggest that a relationship likely exists between the rapid progression of muscular dystrophy and stem cell exhaustion, and the development of cell therapeutic approaches to delay the exhaustion of MPCs may represent an important alternative avenue to explore for delaying the onset of pathologies associated with muscular dystrophies.

Heart Disease

Heart disease is the most common cause of death worldwide. Because the disease can result in the replacement of contractile cardiomyocytes (CMs) with scar tissue, cellular and regenerative therapies hold great promise. A wide variety of cell types have been investigated for their ability to repair the heart. These include skeletal myoblasts, bone marrow–derived cells, cardiac stem cells, and mesenchymal stem cells (*127*). Most effort has focused on treating ischemic heart disease by infusing cells intravascularly (intravenous, intracoronary, or retrograde coronary sinus), by intramyocardial injection (transendocardial catheter–based injection or epicardial injection), or by scaffold or patch-based epicardial delivery to the myocardium (*127*).

When skeletal myoblasts are transplanted by direct epicardial injection into the heart, they form stable skeletal muscle grafts that do not couple to the native cardiac muscle (*128*), and clinical experience in the setting of coronary artery bypass surgery has not demonstrated significant benefit (*129*). Initial studies in a post–myocardial infarction (MI) mouse model showed that injection of bone marrow–derived c-kit$^+$ and lineage negative (lin$^-$) cells dramatically regenerated myocardium and improved cardiac function (*130*). Subsequent studies, however, failed to demonstrate myocardial regeneration using this approach (*131*, *132*). Nevertheless, clinical trials evaluating the ability of bone marrow mononuclear cells (BMNCs) to repair the myocardium were initiated, and phase 1 trials of intracoronary BMNC delivery via the reperfused infarct-related artery hinted at efficacy. Larger phase 2 trials, however, have produced mixed results, ranging from no effect to a modest improvement in ejection fraction (*133*). In small phase 1 trials, mesenchymal stem cells, autologous cardiac stem cells, and cardiosphere-derived cells have similarly shown possible benefit with respect to left ventricular structure and function in patients post-MI with ischemic cardiomyopathy (*133*).

Cell survival and engraftment have been major limitations with adult stem cell sources, and the vast majority of transplanted cells are lost within days in most investigations (*134*). Thus, robust myocardial regeneration has not been observed, and the beneficial effects on cardiac function and structure have been attributed to other mechanisms, largely acting by paracrine signaling to preserve the border zone around the infarction, reduce apoptosis, blunt adverse remodeling, potentially stimulate endogenous stem cells, modulate inflammation, and promote angiogenesis.

PSCs can differentiate into a range of cell types relevant for cardiac repair, including CMs

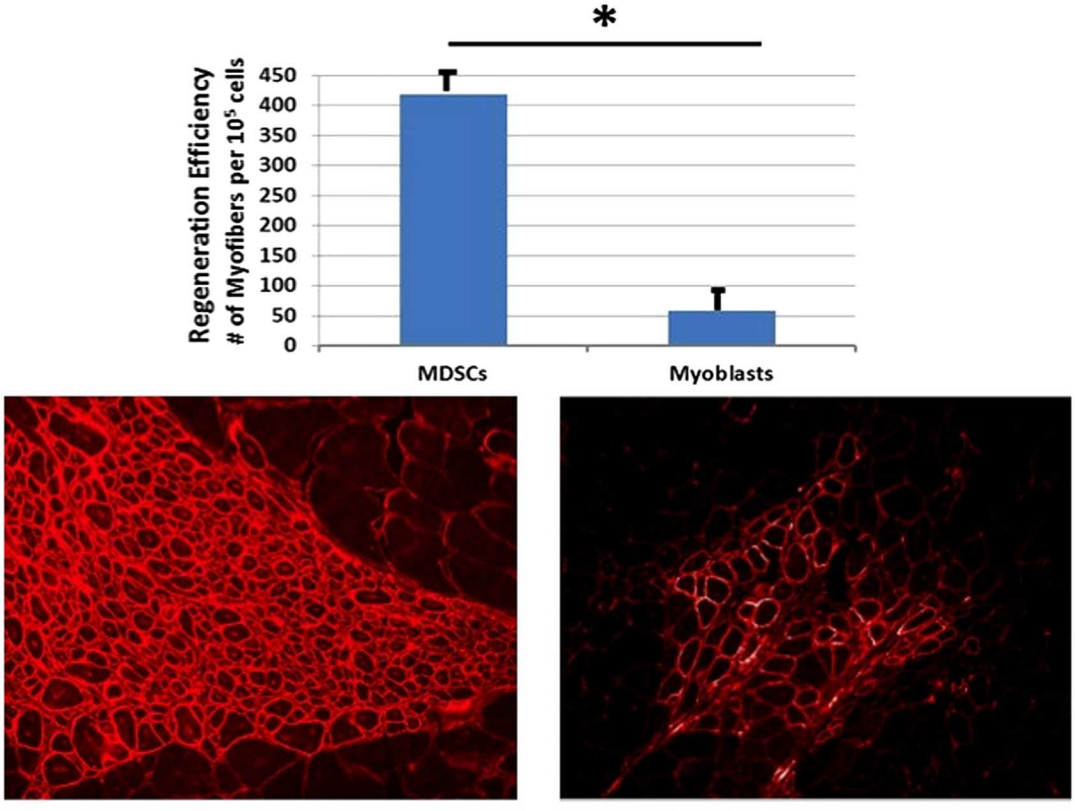

Fig. 5. Importance of cell type for restoration of dystrophin-expressing myofibers. Engraftment efficiency for muscle-derived stem cells (**left**) and myoblasts (**right**) after transplant.

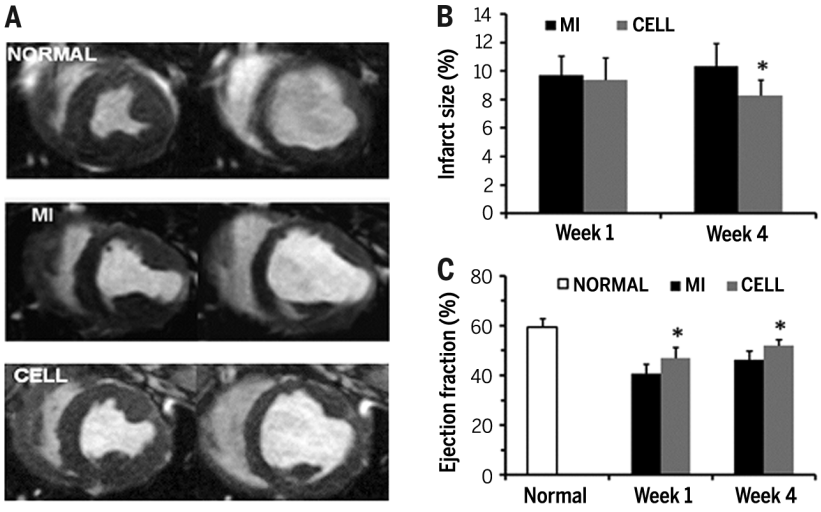

Fig. 6. Fibrin patch–based delivery of human PSC–derived ECs and SMCs. (**A**) Cardiac magnetic resonance image (MRI) from normal, MI, and cell-treatment groups at end systole (left) and end diastole (right). (**B**) After infarction, the cell treatment produced significantly smaller infarct size (delayed-enhancement MRI) and (**C**) improved ejection fraction compared with MI alone. *$P < 0.05$ versus MI alone. Modified from (*147*), with permission.

(*135*), cardiac progenitors (*136*, *137*), endothelial cells (ECs) (*138*), and smooth muscle cells (SMCs) (*138*), which have been tested in small-animal models. Protocols for efficient generation of CMs from human PSCs have been developed (*139*), and purification of CMs has been accomplished using cell surface markers or glucose-free culture conditions optimized for survival of CMs (*140*, *141*). However, PSC-derived CMs are, in general, a mixture of nodal-like, atrial-like and ventricular-like cells (*142*) that have limited proliferative capacity and have a relatively immature phenotype based on electrophysiological characteristics, contractile performance, and metabolic profile. Despite these limitations, mouse PSC–derived CMs are capable of integration into the mouse myocardium, but this is an extremely rare event (*113*). Survival of transplanted PSC-derived CMs has been a limitation, but by modulating multiple cellular processes a prosurvival cocktail was developed, which enabled the survival of human PSC-derived CMs as islands in athymic rat hearts post-MI, improving cardiac function (*143*). Transplanted mouse PSC–derived cardiac progenitors improve the function of infarcted mouse hearts (*144*), and, in guinea pigs, where the heart exhibits an intrinsic heart rate closer to that in man, human PSC–derived CMs engraft and functionally couple to host CMs to improve left ventricular function and reduce ventricular arrhythmias (*145*).

Preclinical studies are beginning to test PSC cell therapy in large-animal models of heart disease. Epicardial delivery of cell sheets composed of PSC-derived CMs in post-MI pig hearts has shown encouraging results (*146*), and epicardial application of human PSC–derived ECs and SMCs, incorporated into a fibrin-based patch, post-MI, to the hearts of immune-suppressed pigs has reduced infarction size and improved left ventricular function (Fig. 6) (*147*). In addition, direct intramyocardial injection of human PSC–derived CMs in immune-suppressed nonhuman primate hearts post-MI has produced large areas of engraftment and electrical coupling, but no clear improvement in cardiac function has been observed (*148*). However, a transient increase in ventricular arrhythmias has occurred, raising a potential safety concern. Transplantation of human PSC–derived cardiac progenitors has been associated with multilineage regeneration in the immunosuppressed rhesus monkey heart post-MI (*149*). Thus, large-animal studies are beginning to define which cell preparations and delivery strategies hold promise.

Overall, clinical studies using adult cell sources have not yet demonstrated robust clinical benefits. Animal studies using PSC-derived cardiac cells, however, have shown promising results, with some evidence of improvement in left ventricular function and structure. Strategies that combine cells with bioengineered patches or decellularized cardiac matrices are now also being explored, especially for use in congenital heart disease. At this time, however, the mechanisms by which different cell populations and delivery strategies affect the various cardiac disease states remain poorly understood, and the optimal cell populations to use and the best delivery strategies for clinical translation have not yet been defined. Further research is required.

Conclusions

As discussed above, the generation of an unlimited supply of specific cell types is crucial for cell and regenerative therapies, because they offer great hope for the treatment of a wide spectrum of diseases. However, numerous challenges remain. Recurrent autoimmunity will probably require immune suppression for some diseases, and it is still unclear which specific cell type will be useful for the treatment of disorders such as DMD and heart disease. Optimization will also be needed for the transplant site, as in diabetes, or when dealing with disruption of the extracellular matrix in treating degenerative diseases, as in chronic liver and heart disease. Finally, when the pathologic process is diffuse and migration of transplanted cells is limited, as is the case with Alzheimer's disease, ALS, and the muscular dystrophies, identifying the best means and location for cell delivery will require further study in many cases. Using autologous cells and genetic engineering should help control rejection and autoimmunity and improve monitoring of short- and long-term engraftment. Despite existing challenges, the availability of an unlimited supply of clinically useful PSC-derived cell populations will facilitate studies into the biology of those cells and will likely assist in the treatment of diabetes, acute hepatic failure, metabolic liver diseases, retinal diseases, PD, HD, and possibly heart disease. Close collaboration between scientists and clinicians, and between academia and industry, will be critical to overcoming remaining challenges to bringing novel therapies to patients in need.

REFERENCES AND NOTES

1. K. Takahashi *et al.*, Induction of pluripotent stem cells from adult human fibroblasts by defined factors. *Cell* **131**, 861–872 (2007). doi: 10.1016/j.cell.2007.11.019; pmid: 18035408
2. J. A. Thomson *et al.*, Embryonic stem cell lines derived from human blastocysts. *Science* **282**, 1145–1147 (1998). doi: 10.1126/science.282.5391.1145; pmid: 9804556
3. S. Lacotte, T. Berney, A. J. Shapiro, C. Toso, Immune monitoring of pancreatic islet graft: Towards a better understanding, detection and treatment of harmful events. *Expert Opin. Biol. Ther.* **11**, 55–66 (2011). doi: 10.1517/14712598.2011.536530; pmid: 21073277
4. J. Hanna *et al.*, Treatment of sickle cell anemia mouse model with iPS cells generated from autologous skin. *Science* **318**, 1920–1923 (2007). doi: 10.1126/science.1152092; pmid: 18063756
5. W. M. Rideout 3rd, K. Hochedlinger, M. Kyba, G. Q. Daley, R. Jaenisch, Correction of a genetic defect by nuclear transplantation and combined cell and gene therapy. *Cell* **109**, 17–27 (2002). doi: 10.1016/S0092-8674(02)00681-5; pmid: 11955443
6. M. Kyba, R. C. Perlingeiro, G. Q. Daley, HoxB4 confers definitive lymphoid-myeloid engraftment potential on embryonic stem cell and yolk sac hematopoietic progenitors. *Cell* **109**, 29–37 (2002). doi: 10.1016/S0092-8674(02)00680-3; pmid: 11955444
7. S. L. McKinney-Freeman *et al.*, Surface antigen phenotypes of hematopoietic stem cells from embryos and murine embryonic stem cells. *Blood* **114**, 268–278 (2009). doi: 10.1182/blood-2008-12-193888; pmid: 19420357
8. M. H. Ledran *et al.*, Efficient hematopoietic differentiation of human embryonic stem cells on stromal cells derived from hematopoietic niches. *Cell Stem Cell* **3**, 85–98 (2008). doi: 10.1016/j.stem.2008.06.001; pmid: 18593561
9. X. Tian, P. S. Woll, J. K. Morris, J. L. Linehan, D. S. Kaufman, Hematopoietic engraftment of human embryonic stem cell-derived cells is regulated by recipient innate immunity. *Stem Cells* **24**, 1370–1380 (2006). doi: 10.1634/stemcells.2005-0340; pmid: 16456127
10. L. Wang, P. Menendez, C. Cerdan, M. Bhatia, Hematopoietic development from human embryonic stem cell lines. *Exp. Hematol.* **33**, 987–996 (2005). doi: 10.1016/j.exphem.2005.06.002; pmid: 16140146
11. C. Mazurier, L. Douay, H. Lapillonne, Red blood cells from induced pluripotent stem cells: Hurdles and developments. *Curr. Opin. Hematol.* **18**, 249–253 (2011). doi: 10.1097/MOH.0b013e3283476129; pmid: 21519239
12. G. F. Rousseau, M. C. Giarratana, L. Douay, Large-scale production of red blood cells from stem cells: What are the technical challenges ahead? *Biotechnol. J.* **9**, 28–38 (2014). doi: 10.1002/biot.201200368; pmid: 24408610
13. S. Nakamura *et al.*, Expandable megakaryocyte cell lines enable clinically applicable generation of platelets from

human induced pluripotent stem cells. *Cell Stem Cell* **14**, 535–548 (2014). doi: 10.1016/j.stem.2014.01.011; pmid: 24529595
14. R. Bottino, M. Trucco, A. N. Balamurugan, T. E. Starzl, Pancreas and islet cell transplantation. *Best Pract. Res. Clin. Gastroenterol.* **16**, 457–474 (2002). doi: 10.1053/bega.2002.0318; pmid: 12079269
15. C. B. Kemp, M. J. Knight, D. W. Scharp, P. E. Lacy, W. F. Ballinger, Transplantation of isolated pancreatic islets into the portal vein of diabetic rats. *Nature* **244**, 447 (1973). doi: 10.1038/244447a0; pmid: 4200461
16. C. Ricordi, P. E. Lacy, E. H. Finke, B. J. Olack, D. W. Scharp, Automated method for isolation of human pancreatic islets. *Diabetes* **37**, 413–420 (1988). doi: 10.2337/diab.37.4.413; pmid: 3288530
17. E. A. Ryan *et al*., Five-year follow-up after clinical islet transplantation. *Diabetes* **54**, 2060–2069 (2005). doi: 10.2337/diabetes.54.7.2060; pmid: 15983207
18. R. Alejandro *et al*., Natural history of intrahepatic canine islet cell autografts. *J. Clin. Invest.* **78**, 1339–1348 (1986). doi: 10.1172/JCI112720; pmid: 3095376
19. B. Nilsson, K. N. Ekdahl, O. Korsgren, Control of instant blood-mediated inflammatory reaction to improve islets of Langerhans engraftment. *Curr. Opin. Organ Transplant.* **16**, 620–626 (2011). doi: 10.1097/MOT.0b013e32834c2393; pmid: 21971510
20. F. B. Barton *et al*., Improvement in outcomes of clinical islet transplantation: 1999-2010. *Diabetes Care* **35**, 1436–1445 (2012). doi: 10.2337/dc12-0063; pmid: 22723582
21. D. E. Sutherland *et al*., Total pancreatectomy and islet autotransplantation for chronic pancreatitis. *J. Am. Coll. Surg.* **214**, 409–424, discussion 424–426 (2012). doi: 10.1016/j.jamcollsurg.2011.12.040; pmid: 22397977
22. G. T. Westermark, P. Westermark, C. Berne, O. Korsgren; Nordic Network for Clinical Islet Transplantation, Widespread amyloid deposition in transplanted human pancreatic islets. *N. Engl. J. Med.* **359**, 977–979 (2008). doi: 10.1056/NEJMc0802893; pmid: 18753660
23. M. E. De Paepe, B. Keymeulen, D. Pipeleers, G. Klöppel, Proliferation and hypertrophy of liver cells surrounding islet grafts in diabetic recipient rats. *Hepatology* **21**, 1144–1153 (1995). doi: 10.1002/hep.1840210438; pmid: 7705790
24. D. G. Pipeleers *et al*., Transplantation of purified islet cells in diabetic rats. I. Standardization of islet cell grafts. *Diabetes* **40**, 908–919 (1991). doi: 10.2337/diab.40.7.908; pmid: 2060727
25. G. J. Echeverri *et al*., Endoscopic gastric submucosal transplantation of islets (ENDO-STI): Technique and initial results in diabetic pigs. *Am. J. Transplant.* **9**, 2485–2496 (2009). doi: 10.1111/j.1600-6143.2009.02815.x; pmid: 19775318
26. Worcester Human Islet Transplantation Group, Autoimmunity after islet-cell allotransplantation. *N. Engl. J. Med.* **355**, 1397–1399 (2006). doi: 10.1056/NEJMc061530; pmid: 17005967
27. R. J. Creusot, N. Giannoukakis, M. Trucco, M. J. Clare-Salzler, C. G. Fathman, It's time to bring dendritic cell therapy to type 1 diabetes. *Diabetes* **63**, 20–30 (2014). doi: 10.2337/db13-0886; pmid: 24357690
28. D. J. van der Windt *et al*., Long-term controlled normoglycemia in diabetic non-human primates after transplantation with hCD46 transgenic porcine islets. *Am. J. Transplant.* **9**, 2716–2726 (2009). doi: 10.1111/j.1600-6143.2009.02850.x; pmid: 19845582
29. S. W. Liao *et al*., Maintaining functional islets through encapsulation in an injectable saccharide-peptide hydrogel. *Biomaterials* **34**, 3984–3991 (2013). doi: 10.1016/j.biomaterials.2013.02.007; pmid: 23465491
30. T. C. Schulz *et al*., A scalable system for production of functional pancreatic progenitors from human embryonic stem cells. *PLOS ONE* **7**, e37004 (2012). doi: 10.1371/journal.pone.0037004; pmid: 22623968
31. A. A. Demetriou *et al*., Transplantation of microcarrier-attached hepatocytes into 90% partially hepatectomized rats. *Hepatology* **8**, 1006–1009 (1988). doi: 10.1002/hep.1840080505; pmid: 3047034
32. J. M. De Vree *et al*., Correction of liver disease by hepatocyte transplantation in a mouse model of progressive familial intrahepatic cholestasis. *Gastroenterology* **119**, 1720–1730 (2000). doi: 10.1053/gast.2000.20222; pmid: 11113093
33. C. G. Groth, B. Arborgh, C. Björkén, B. Sundberg, G. Lundgren, Correction of hyperbilirubinemia in the glucuronyltransferase-deficient rat by intraportal hepatocyte transplantation. *Transplant. Proc.* **9**, 313–316 (1977). pmid: 405772
34. A. J. Matas *et al*., Hepatocellular transplantation for metabolic deficiencies: Decrease of plasms bilirubin in Gunn rats. *Science* **192**, 892–894 (1976). doi: 10.1126/science.818706; pmid: 818706
35. H. E. Rugstad, S. H. Robinson, C. Yannoni, A. H. Tashjian Jr., Transfer of bilirubin uridine diphosphate-glucuronyltransferase to enzyme-deficient rats. *Science* **170**, 553–555 (1970). doi: 10.1126/science.170.3957.553; pmid: 4319199
36. J. C. Wiederkehr, G. T. Kondos, R. Pollak, Hepatocyte transplantation for the low-density lipoprotein receptor-deficient state. A study in the Watanabe rabbit. *Transplantation* **50**, 466–471 (1990). doi: 10.1097/00007890-199009000-00021; pmid: 2144923
37. Y. Yoshida, Y. Tokusashi, G. H. Lee, K. Ogawa, Intrahepatic transplantation of normal hepatocytes prevents Wilson's disease in Long-Evans cinnamon rats. *Gastroenterology* **111**, 1654–1660 (1996). doi: 10.1016/S0016-5085(96)70029-X; pmid: 8942746
38. S. Gupta *et al*., Entry and integration of transplanted hepatocytes in rat liver plates occur by disruption of hepatic sinusoidal endothelium. *Hepatology* **29**, 509–519 (1999). doi: 10.1002/hep.510290213; pmid: 9918929
39. K. P. Ponder *et al*., Mouse hepatocytes migrate to liver parenchyma and function indefinitely after intrasplenic transplantation. *Proc. Natl. Acad. Sci. U.S.A.* **88**, 1217–1221 (1991). doi: 10.1073/pnas.88.4.1217; pmid: 1899924
40. A. Dhawan, J. Puppi, R. D. Hughes, R. R. Mitry, Human hepatocyte transplantation: Current experience and future challenges. *Nat. Rev. Gastroenterol. Hepatol.* **7**, 288–298 (2010). doi: 10.1038/nrgastro.2010.44; pmid: 20368738
41. C. M. Habibullah, I. H. Syed, A. Qamar, Z. Taher-Uz, Human fetal hepatocyte transplantation in patients with fulminant hepatic failure. *Transplantation* **58**, 951–952 (1994). doi: 10.1097/00007890-199410270-00016; pmid: 7940741
42. S. P. Horslen *et al*., Isolated hepatocyte transplantation in an infant with a severe urea cycle disorder. *Pediatrics* **111**, 1262–1267 (2003). doi: 10.1542/peds.111.6.1262; pmid: 12777539
43. M. Mito *et al*., Morphology and function of isolated hepatocytes transplanted into rat spleen. *Transplantation* **28**, 499–505 (1979). doi: 10.1097/00007890-197912000-00013; pmid: 516133
44. M. Mito, M. Kusano, Y. Kawaura, Hepatocyte transplantation in man. *Transplant. Proc.* **24**, 3052–3053 (1992). pmid: 1466053
45. M. Muraca *et al*., Hepatocyte transplantation as a treatment for glycogen storage disease type 1a. *Lancet* **359**, 317–318 (2002). doi: 10.1016/S0140-6736(02)07529-3; pmid: 11830200
46. E. M. Sokal *et al*., Hepatocyte transplantation in a 4-year-old girl with peroxisomal biogenesis disease: Technique, safety, and metabolic follow-up. *Transplantation* **76**, 735–738 (2003). doi: 10.1097/01.TP.0000077420.81365.53; pmid: 12973120
47. I. J. Fox *et al*., Treatment of the Crigler-Najjar syndrome type I with hepatocyte transplantation. *N. Engl. J. Med.* **338**, 1422–1427 (1998). doi: 10.1056/NEJM199805143382004; pmid: 9580649
48. P. N. Newsome, J. N. Plevris, L. J. Nelson, P. C. Hayes, Animal models of fulminant hepatic failure: A critical evaluation. *Liver Transpl.* **6**, 21–31 (2000).pmid: 10648574
49. J. Terblanche, R. Hickman, Animal models of fulminant hepatic failure. *Dig. Dis. Sci.* **36**, 770–774 (1991). doi: 10.1007/BF01311235; pmid: 2032519
50. B. M. Bilir *et al*., Hepatocyte transplantation in acute liver failure. *Liver Transpl.* **6**, 32–40 (2000). doi: 10.1002/lt.500060113; pmid: 10648575
51. H. Zhou *et al*., Repopulation of individual liver lobes by transplanted hepatocytes using regiospecific hepatic irradiation cures jaundice in the Gunn rat model of Crigler-Najjar Syndrome type I. *Hepatology* **50**, 303A (2009).
52. C. Guha *et al*., Normal hepatocytes correct serum bilirubin after repopulation of Gunn rat liver subjected to irradiation/partial resection. *Hepatology* **36**, 354–362 (2002). doi: 10.1053/jhep.2002.34516; pmid: 12143043
53. S. Gagandeep *et al*., Transplanted hepatocytes engraft, survive, and proliferate in the liver of rats with carbon tetrachloride-induced cirrhosis. *J. Pathol.* **191**, 78–85 (2000). doi: 10.1002/(SICI)1096-9896(200005)191:1<78::AID-PATH587>3.0.CO;2-P; pmid: 10767723
54. N. Kobayashi *et al*., Hepatocyte transplantation in rats with decompensated cirrhosis. *Hepatology* **31**, 851–857 (2000). doi: 10.1053/he.2000.5636; pmid: 10733539
55. J. Ribeiro *et al*., Intrasplenic hepatocellular transplantation corrects hepatic encephalopathy in portacaval-shunted rats. *Hepatology* **15**, 12–18 (1992). doi: 10.1002/hep.1840150104; pmid: 1727787
56. T. Hoppo, J. Komori, R. Manohar, D. B. Stolz, E. Lagasse, Rescue of lethal hepatic failure by hepatized lymph nodes in mice. *Gastroenterology* **140**, 656–666.e2 (2011). doi: 10.1053/j.gastro.2010.11.006; pmid: 21070777
57. I. K. Schumacher *et al*., Transplantation of conditionally immortalized hepatocytes to treat hepatic encephalopathy. *Hepatology* **24**, 337–343 (1996). doi: 10.1002/hep.510240209; pmid: 8690402
58. K. A. Soltys *et al*., Barriers to the successful treatment of liver disease by hepatocyte transplantation. *J. Hepatol.* **53**, 769–774 (2010). doi: 10.1016/j.jhep.2010.05.010; pmid: 20667616
59. B. E. Uygun *et al*., Organ reengineering through development of a transplantable recellularized liver graft using decellularized liver matrix. *Nat. Med.* **16**, 814–820 (2010). doi: 10.1038/nm.2170; pmid: 20543851
60. A. Benraiss *et al*., Sustained mobilization of endogenous neural progenitors delays disease progression in a transgenic model of Huntington's disease. *Cell Stem Cell* **12**, 787–799 (2013). doi: 10.1016/j.stem.2013.04.014; pmid: 23746982
61. A. Benraiss, S. A. Goldman, Cellular therapy and induced neuronal replacement for Huntington's disease. *Neurotherapeutics* **8**, 577–590 (2011). doi: 10.1007/s13311-011-0075-8; pmid: 21971961
62. O. Lindvall, Dopaminergic neurons for Parkinson's therapy. *Nat. Biotechnol.* **30**, 56–58 (2012). doi: 10.1038/nbt.2077; pmid: 22231097
63. Y. Liu *et al*., Medial ganglionic eminence-like cells derived from human embryonic stem cells correct learning and memory deficits. *Nat. Biotechnol.* **31**, 440–447 (2013). doi: 10.1038/nbt.2565; pmid: 23604284
64. S. Kriks *et al*., Dopamine neurons derived from human ES cells efficiently engraft in animal models of Parkinson's disease. *Nature* **480**, 547–551 (2011).pmid: 22056989
65. N. S. Roy *et al*., Functional engraftment of human ES cell-derived dopaminergic neurons enriched by coculture with telomerase-immortalized midbrain astrocytes. *Nat. Med.* **12**, 1259–1268 (2006). doi: 10.1038/nm1495; pmid: 17057709
66. A. D. Carri *et al*., Developmentally coordinated extrinsic signals drive human pluripotent stem cell differentiation toward authentic DARPP-32+ medium-sized spiny neurons. *Development* **140**, 301–312 (2013). doi: 10.1242/dev.084608; pmid: 23250204
67. The HD iPSC Consortium, Induced pluripotent stem cells from patients with Huntington's disease show CAG-repeat-expansion-associated phenotypes. *Cell Stem Cell* **11**, 264–278 (2012). doi: 10.1016/j.stem.2012.04.027; pmid: 22748968
68. C. R. Nicholas *et al*., Functional maturation of hPSC-derived forebrain interneurons requires an extended timeline and mimics human neural development. *Cell Stem Cell* **12**, 573–586 (2013). doi: 10.1016/j.stem.2013.04.005; pmid: 23642366
69. D. E. Buchholz *et al*., Rapid and efficient directed differentiation of human pluripotent stem cells into retinal pigmented epithelium. *Stem Cells Transl. Med.* **2**, 384–393 (2013). doi: 10.5966/sctm.2012-0163; pmid: 23599499
70. J. H. Stern, S. Temple, Stem cells for retinal replacement therapy. *Neurotherapeutics* **8**, 736–743 (2011). doi: 10.1007/s13311-011-0077-6; pmid: 21948217
71. N. Singh Roy *et al*., Enhancer-specified GFP-based FACS purification of human spinal motor neurons from embryonic stem cells. *Exp. Neurol.* **196**, 224–234 (2005). doi: 10.1016/j.expneurol.2005.06.021; pmid: 16198339
72. S. Karumbayaram *et al*., Directed differentiation of human-induced pluripotent stem cells generates active motor neurons. *Stem Cells* **27**, 806–811 (2009). doi: 10.1002/stem.31; pmid: 19350680
73. X. J. Li *et al*., Specification of motoneurons from human embryonic stem cells. *Nat. Biotechnol.* **23**, 215–221 (2005). doi: 10.1038/nbt1063; pmid: 15685164
74. A. C. Lepore *et al*., Human glial-restricted progenitor transplantation into cervical spinal cord of the SOD1 mouse model of ALS. *PLOS ONE* **6**, e25968 (2011). doi: 10.1371/journal.pone.0025968; pmid: 21998733
75. S. A. Goldman, M. Nedergaard, M. S. Windrem, Glial progenitor cell-based treatment and modeling of neurological disease. *Science* **338**, 491–495 (2012). doi: 10.1126/science.1218071; pmid: 23112326
76. D. R. Archer, P. A. Cuddon, D. Lipsitz, I. D. Duncan, Myelination of the canine central nervous system by glial cell transplantation: A model for repair of human myelin disease. *Nat. Med.* **3**, 54–59 (1997). doi: 10.1038/nm0197-54; pmid: 8986741
77. M. S. Windrem *et al*., Fetal and adult human oligodendrocyte progenitor cell isolates myelinate the congenitally dysmyelinated

brain. *Nat. Med.* **10**, 93–97 (2004). doi: 10.1038/nm974; pmid: 14702638
78. M. S. Windrem *et al*., Neonatal chimerization with human glial progenitor cells can both remyelinate and rescue the otherwise lethally hypomyelinated shiverer mouse. *Cell Stem Cell* **2**, 553–565 (2008). doi: 10.1016/j.stem.2008.03.020; pmid: 18522848
79. S. Wang *et al*., Human iPSC-derived oligodendrocyte progenitor cells can myelinate and rescue a mouse model of congenital hypomyelination. *Cell Stem Cell* **12**, 252–264 (2013). doi: 10.1016/j.stem.2012.12.002; pmid: 23395447
80. N. Gupta *et al*., Neural stem cell engraftment and myelination in the human brain. *Sci. Transl. Med.* **4**, 155ra137 (2012). doi: 10.1126/scitranslmed.3004373; pmid: 23052294
81. S. A. Goldman, Progenitor cell-based treatment of the pediatric myelin disorders. *Arch. Neurol.* **68**, 848–856 (2011). doi: 10.1001/archneurol.2011.46; pmid: 21403006
82. M. Li, K. Suzuki, N. Y. Kim, G. H. Liu, J. C. Izpisua Belmonte, A cut above the rest: Targeted genome editing technologies in human pluripotent stem cells. *J. Biol. Chem.* **289**, 4594–4599 (2014). doi: 10.1074/jbc.R113.488247; pmid: 24362028
83. M. H. Tuszynski *et al*., Neural stem cell dissemination after grafting to CNS injury sites. *Cell* **156**, 388–389 (2014). doi: 10.1016/j.cell.2014.01.016; pmid: 24485445
84. E. P. Hoffman, R. H. Brown Jr., L. M. Kunkel, Dystrophin: The protein product of the Duchenne muscular dystrophy locus. *Cell* **51**, 919–928 (1987). doi: 10.1016/0092-8674(87)90579-4; pmid: 3319190
85. S. C. Watkins, E. P. Hoffman, H. S. Slayter, L. M. Kunkel, Immunoelectron microscopic localization of dystrophin in myofibres. *Nature* **333**, 863–866 (1988). doi: 10.1038/333863a0; pmid: 3290684
86. K. Arahata *et al*., Immunostaining of skeletal and cardiac muscle surface membrane with antibody against Duchenne muscular dystrophy peptide. *Nature* **333**, 861–863 (1988). doi: 10.1038/333861a0; pmid: 3290683
87. E. E. Zubrzycka-Gaarn *et al*., The Duchenne muscular dystrophy gene product is localized in sarcolemma of human skeletal muscle. *Nature* **333**, 466–469 (1988). doi: 10.1038/333466a0; pmid: 3287171
88. R. Bischoff, Proliferation of muscle satellite cells on intact myofibers in culture. *Dev. Biol.* **115**, 129–139 (1986). doi: 10.1016/0012-1606(86)90234-4; pmid: 3516758
89. J. R. Beauchamp, J. E. Morgan, C. N. Pagel, T. A. Partridge, Dynamics of myoblast transplantation reveal a discrete minority of precursors with stem cell-like properties as the myogenic source. *J. Cell Biol.* **144**, 1113–1122 (1999). doi: 10.1083/jcb.144.6.1113; pmid: 10087257
90. Y. Fan, M. Maley, M. Beilharz, M. Grounds, Rapid death of injected myoblasts in myoblast transfer therapy. *Muscle Nerve* **19**, 853–860 (1996). doi: 10.1002/(SICI)1097-4598(199607)19:7<853::AID-MUS7>3.0.CO;2-8; pmid: 8965839
91. E. Gussoni *et al*., Normal dystrophin transcripts detected in Duchenne muscular dystrophy patients after myoblast transplantation. *Nature* **356**, 435–438 (1992). doi: 10.1038/356435a0; pmid: 1557125
92. J. Huard *et al*., Human myoblast transplantation: Preliminary results of 4 cases. *Muscle Nerve* **15**, 550–560 (1992). doi: 10.1002/mus.880150504; pmid: 1584246
93. G. Karpati *et al*., Dystrophin is expressed in mdx skeletal muscle fibers after normal myoblast implantation. *Am. J. Pathol.* **135**, 27–32 (1989). pmid: 2672825
94. J. R. Mendell *et al*., Myoblast transfer in the treatment of Duchenne's muscular dystrophy. *N. Engl. J. Med.* **333**, 832–838 (1995). doi: 10.1056/NEJM199509283331303; pmid: 7651473
95. J. E. Morgan, E. P. Hoffman, T. A. Partridge, Normal myogenic cells from newborn mice restore normal histology to degenerating muscles of the mdx mouse. *J. Cell Biol.* **111**, 2437–2449 (1990). doi: 10.1083/jcb.111.6.2437; pmid: 2277066
96. Z. Qu *et al*., Development of approaches to improve cell survival in myoblast transfer therapy. *J. Cell Biol.* **142**, 1257–1267 (1998). doi: 10.1083/jcb.142.5.1257; pmid: 9732286
97. J. T. Vilquin, E. Wagner, I. Kinoshita, R. Roy, J. P. Tremblay, Successful histocompatible myoblast transplantation in dystrophin-deficient mdx mouse despite the production of antibodies against dystrophin. *J. Cell Biol.* **131**, 975–988 (1995). doi: 10.1083/jcb.131.4.975; pmid: 7490298
98. Y. Torrente, E. El Fahime, N. J. Caron, N. Bresolin, J. P. Tremblay, Intramuscular migration of myoblasts transplanted after muscle pretreatment with metalloproteinases. *Cell Transplant.* **9**, 539–549 (2000). pmid: 11038070
99. D. L. Clarke *et al*., Generalized potential of adult neural stem cells. *Science* **288**, 1660–1663 (2000). doi: 10.1126/science.288.5471.1660; pmid: 10834848
100. L. De Angelis *et al*., Skeletal myogenic progenitors originating from embryonic dorsal aorta coexpress endothelial and myogenic markers and contribute to postnatal muscle growth and regeneration. *J. Cell Biol.* **147**, 869–878 (1999). doi: 10.1083/jcb.147.4.869; pmid: 10562287
101. G. Ferrari *et al*., Muscle regeneration by bone marrow–derived myogenic progenitors. *Science* **279**, 1528–1530 (1998). doi: 10.1126/science.279.5356.1528; pmid: 9488650
102. R. Galli *et al*., Skeletal myogenic potential of human and mouse neural stem cells. *Nat. Neurosci.* **3**, 986–991 (2000). doi: 10.1038/79924; pmid: 11017170
103. M. F. Pittenger *et al*., Multilineage potential of adult human mesenchymal stem cells. *Science* **284**, 143–147 (1999). doi: 10.1126/science.284.5411.143; pmid: 10102814
104. M. Crisan *et al*., A perivascular origin for mesenchymal stem cells in multiple human organs. *Cell Stem Cell* **3**, 301–313 (2008). doi: 10.1016/j.stem.2008.07.003; pmid: 18786417
105. A. Dellavalle *et al*., Pericytes of human skeletal muscle are myogenic precursors distinct from satellite cells. *Nat. Cell Biol.* **9**, 255–267 (2007). doi: 10.1038/ncb1542; pmid: 17293855
106. B. Zheng *et al*., Prospective identification of myogenic endothelial cells in human skeletal muscle. *Nat. Biotechnol.* **25**, 1025–1034 (2007). doi: 10.1038/nbt1334; pmid: 17767154
107. H. M. Blau, T. R. Brazelton, J. M. Weimann, The evolving concept of a stem cell: Entity or function? *Cell* **105**, 829–841 (2001). doi: 10.1016/S0092-8674(01)00409-3; pmid: 11439179
108. B. Péault *et al*., Stem and progenitor cells in skeletal muscle development, maintenance, and therapy. *Mol. Ther.* **15**, 867–877 (2007). doi: 10.1038/mt.sj.6300145; pmid: 17387336
109. L. K. Carr *et al*., 1-year follow-up of autologous muscle-derived stem cell injection pilot study to treat stress urinary incontinence. *Int. Urogynecol. J. Pelvic Floor Dysfunct.* **19**, 881–883 (2008). doi: 10.1007/s00192-007-0553-z; pmid: 18204978
110. M. Sampaolesi *et al*., Mesoangioblast stem cells ameliorate muscle function in dystrophic dogs. *Nature* **444**, 574–579 (2006). doi: 10.1038/nature05282; pmid: 17108972
111. E. Bachrach *et al*., Systemic delivery of human microdystrophin to regenerating mouse dystrophic muscle by muscle progenitor cells. *Proc. Natl. Acad. Sci. U.S.A.* **101**, 3581–3586 (2004). doi: 10.1073/pnas.0400373101; pmid: 14993597
112. M. Kennedy *et al*., A common precursor for primitive erythropoiesis and definitive haematopoiesis. *Nature* **386**, 488–493 (1997). doi: 10.1038/386488a0; pmid: 9087406
113. M. G. Klug, M. H. Soonpaa, G. Y. Koh, L. J. Field, Genetically selected cardiomyocytes from differentiating embronic stem cells form stable intracardiac grafts. *J. Clin. Invest.* **98**, 216–224 (1996). doi: 10.1172/JCI118769; pmid: 8690796
114. M. Müller *et al*., Selection of ventricular-like cardiomyocytes from ES cells in vitro. *FASEB J.* **14**, 2540–2548 (2000). doi: 10.1096/fj.00-0002com; pmid: 11099473
115. F. Rinaldi, R. C. Perlingeiro, Stem cells for skeletal muscle regeneration: Therapeutic potential and roadblocks. *Transl. Res.* **163**, 409–417 (2014). doi: 10.1016/j.trsl.2013.11.006; pmid: 24299739
116. D. Vittet *et al*., Embryonic stem cells differentiate in vitro to endothelial cells through successive maturation steps. *Blood* **88**, 3424–3431 (1996). pmid: 8896407
117. T. Barberi *et al*., Derivation of engraftable skeletal myoblasts from human embryonic stem cells. *Nat. Med.* **13**, 642–648 (2007). doi: 10.1038/nm1533; pmid: 17417652
118. J. Rohwedel *et al*., Muscle cell differentiation of embryonic stem cells reflects myogenesis in vivo: Developmentally regulated expression of myogenic determination genes and functional expression of ionic currents. *Dev. Biol.* **164**, 87–101 (1994). doi: 10.1006/dbio.1994.1182; pmid: 8026639
119. S. Goudenege *et al*., Myoblasts derived from normal hESCs and dystrophic hiPSCs efficiently fuse with existing muscle fibers following transplantation. *Mol. Ther.* **20**, 2153–2167 (2012). doi: 10.1038/mt.2012.188; pmid: 22990676
120. R. Darabi *et al*., Human ES- and iPS-derived myogenic progenitors restore DYSTROPHIN and improve contractility upon transplantation in dystrophic mice. *Cell Stem Cell* **10**, 610–619 (2012). doi: 10.1016/j.stem.2012.02.015; pmid: 22560081
121. A. Filareto *et al*., An ex vivo gene therapy approach to treat muscular dystrophy using inducible pluripotent stem cells. *Nat. Commun.* **4**, 1549 (2013). doi: 10.1038/ncomms2550; pmid: 23462992
122. F. S. Tedesco *et al*., Transplantation of genetically corrected human iPSC-derived progenitors in mice with limb-girdle muscular dystrophy. *Sci. Transl. Med.* **4**, 140ra89 (2012). doi: 10.1126/scitranslmed.3003541; pmid: 22745439
123. G. Jasmin, C. Tautu, M. Vanasse, P. Brochu, R. Simoneau, Impaired muscle differentiation in explant cultures of Duchenne muscular dystrophy. *Lab. Invest.* **50**, 197–207 (1984). pmid: 6694359
124. S. Liechti-Gallati, H. Moser, H. P. Siegrist, U. Wiesmann, N. N. Herschkowitz, Abnormal growth kinetics and 5′-nucleotidase activities in cultured skin fibroblasts from patients with Duchenne muscular dystrophy. *Pediatr. Res.* **15**, 1411–1414 (1981). doi: 10.1203/00006450-198111000-00004; pmid: 6272184
125. A. Sacco *et al*., Short telomeres and stem cell exhaustion model Duchenne muscular dystrophy in mdx/mTR mice. *Cell* **143**, 1059–1071 (2010). doi: 10.1016/j.cell.2010.11.039; pmid: 21145579
126. K. M. Kallestad *et al*., Sparing of extraocular muscle in aging and muscular dystrophies: A myogenic precursor cell hypothesis. *Exp. Cell Res.* **317**, 873–885 (2011). doi: 10.1016/j.yexcr.2011.01.018; pmid: 21277300
127. S. K. Sanganalmath, R. Bolli, Cell therapy for heart failure: A comprehensive overview of experimental and clinical studies, current challenges, and future directions. *Circ. Res.* **113**, 810–834 (2013). doi: 10.1161/CIRCRESAHA.113.300219; pmid: 23989721
128. B. Leobon *et al*., Myoblasts transplanted into rat infarcted myocardium are functionally isolated from their host. *Proc. Natl. Acad. Sci. U.S.A.* **100**, 7808–7811 (2003). doi: 10.1073/pnas.1232447100; pmid: 12805561
129. P. Menasché *et al*., The Myoblast Autologous Grafting in Ischemic Cardiomyopathy (MAGIC) trial: First randomized placebo-controlled study of myoblast transplantation. *Circulation* **117**, 1189–1200 (2008). doi: 10.1161/CIRCULATIONAHA.107.734103; pmid: 18285565
130. D. Orlic *et al*., Bone marrow cells regenerate infarcted myocardium. *Nature* **410**, 701–705 (2001). doi: 10.1038/35070587; pmid: 11287958
131. L. B. Balsam *et al*., Haematopoietic stem cells adopt mature haematopoietic fates in ischaemic myocardium. *Nature* **428**, 668–673 (2004). doi: 10.1038/nature02460 pmid: 15034594
132. C. E. Murry *et al*., Haematopoietic stem cells do not transdifferentiate into cardiac myocytes in myocardial infarcts. *Nature* **428**, 664–668 (2004). doi: 10.1038/nature02446; pmid: 15034593
133. S. A. Fisher *et al*., Stem cell therapy for chronic ischaemic heart disease and congestive heart failure. *Cochrane Database Syst. Rev.* **4**, CD007888 (2014). pmid: 24777540
134. P. K. Nguyen, F. Lan, Y. Wang, J. C. Wu, Imaging: Guiding the clinical translation of cardiac stem cell therapy. *Circ. Res.* **109**, 962–979 (2011). doi: 10.1161/CIRCRESAHA.111.242909; pmid: 21960727
135. O. Caspi *et al*., Transplantation of human embryonic stem cell-derived cardiomyocytes improves myocardial performance in infarcted rat hearts. *J. Am. Coll. Cardiol.* **50**, 1884–1893 (2007). doi: 10.1016/j.jacc.2007.07.054; pmid: 17980256
136. A. Moretti *et al*., Multipotent embryonic isl1+ progenitor cells lead to cardiac, smooth muscle, and endothelial cell diversification. *Cell* **127**, 1151–1165 (2006). doi: 10.1016/j.cell.2006.10.029; pmid: 17123592
137. L. Yang *et al*., Human cardiovascular progenitor cells develop from a KDR+ embryonic-stem-cell-derived population. *Nature* **453**, 524–528 (2008). doi: 10.1038/nature06894; pmid: 18432194
138. L. S. Ferreira *et al*., Vascular progenitor cells isolated from human embryonic stem cells give rise to endothelial and smooth muscle like cells and form vascular networks in vivo. *Circ. Res.* **101**, 286–294 (2007). doi: 10.1161/CIRCRESAHA.107.150201; pmid: 17569886
139. C. L. Mummery *et al*., Differentiation of human embryonic stem cells and induced pluripotent stem cells to cardiomyocytes: A methods overview. *Circ. Res.* **111**, 344–358 (2012). doi: 10.1161/CIRCRESAHA.110.227512; pmid: 22821908
140. N. C. Dubois *et al*., SIRPA is a specific cell-surface marker for isolating cardiomyocytes derived from human pluripotent stem cells. *Nat. Biotechnol.* **29**, 1011–1018 (2011). doi: 10.1038/nbt.2005; pmid: 22020386
141. S. Tohyama *et al*., Distinct metabolic flow enables large-scale purification of mouse and human pluripotent

stem cell-derived cardiomyocytes. *Cell Stem Cell* **12**, 127–137 (2013). doi: 10.1016/j.stem.2012.09.013; pmid: 23168164
142. J. Q. He, Y. Ma, Y. Lee, J. A. Thomson, T. J. Kamp, Human embryonic stem cells develop into multiple types of cardiac myocytes: Action potential characterization. *Circ. Res.* **93**, 32–39 (2003). doi: 10.1161/01.RES.0000080317.92718.99; pmid: 12791707
143. M. A. Laflamme *et al*., Cardiomyocytes derived from human embryonic stem cells in pro-survival factors enhance function of infarcted rat hearts. *Nat. Biotechnol.* **25**, 1015–1024 (2007). doi: 10.1038/nbt1327; pmid: 17721512
144. N. Christoforou *et al*., Implantation of mouse embryonic stem cell-derived cardiac progenitor cells preserves function of infarcted murine hearts. *PLOS ONE* **5**, e11536 (2010). doi: 10.1371/journal.pone.0011536; pmid: 20634944
145. Y. Shiba *et al*., Human ES-cell-derived cardiomyocytes electrically couple and suppress arrhythmias in injured hearts. *Nature* **489**, 322–325 (2012). doi: 10.1038/nature11317; pmid: 22864415
146. M. Kawamura *et al*., Feasibility, safety, and therapeutic efficacy of human induced pluripotent stem cell-derived cardiomyocyte sheets in a porcine ischemic cardiomyopathy model. *Circulation* **126** (suppl. 1), S29–S37 (2012). doi: 10.1161/CIRCULATIONAHA.111.084343; pmid: 22965990
147. Q. Xiong *et al*., Functional consequences of human induced pluripotent stem cell therapy: Myocardial ATP turnover rate in the in vivo swine heart with postinfarction remodeling. *Circulation* **127**, 997–1008 (2013). doi: 10.1161/CIRCULATIONAHA.112.000641; pmid: 23371930
148. J. J. H. Chong *et al*., Human embryonic-stem-cell-derived cardiomyocytes regenerate non-human primate hearts. *Nature* **510**, 273–277 (2014). doi: 10.1038/nature13233; pmid: 24776797
149. G. Blin *et al*., A purified population of multipotent cardiovascular progenitors derived from primate pluripotent stem cells engrafts in postmyocardial infarcted nonhuman primates. *J. Clin. Invest.* **120**, 1125–1139 (2010). doi: 10.1172/JCI40120; pmid: 20335662
150. Z. Alipio *et al*., Reversal of hyperglycemia in diabetic mouse models using induced-pluripotent stem (iPS)-derived pancreatic beta-like cells. *Proc. Natl. Acad. Sci. U.S.A.* **107**, 13426–13431 (2010). doi: 10.1073/pnas.1007884107; pmid: 20616080

ACKNOWLEDGMENTS

We thank E. Tafaleng, N. Giannoukakis, and J. H. Cummins for providing figures and for text editing. This work was supported in part by NIH R01DK48794, P01DK096990, and R01DK099320 (I.J.F.); National Institute of Neurological Disorders and Stroke, National Institute of Mental Health, the Mathers Charitable Foundation, the National Multiple Sclerosis Society, the Adelson Medical Research Foundation, Child Health and Development Institute, and the New York Stem Cell Research Program (S.A.G.); NIH 1P01AG043376 (J.H.); U01HL099773 (T.J.K.); and DOD W81XWH-10-1-1055 (M.T.). I.J.F. is a member of the Scientific Advisory Board of Regenerative Medicine Solutions, Inc.; G.Q.D. is a member of the Senior Advisory Board of MPM Capital, Inc.; S.A.G. is a consultant for Biogen Idec; T.J.K. is a founding shareholder in Cellular Dynamics International; and J.H. is a consultant for Cook Myosite. S.A.G. is an inventor on patents owned by the University of Rochester and Cornell University concerning the use of tissue- and iPSC-derived glial progenitor cells.

10.1126/science.1247391

RESEARCH ARTICLE SUMMARY

POLITICAL SCIENCE

Reverse-engineering censorship in China: Randomized experimentation and participant observation

Gary King,[1]* Jennifer Pan,[2] Margaret E. Roberts[2]

INTRODUCTION: Censorship has a long history in China, extending from the efforts of Emperor Qin to burn Confucian texts in the third century B.C.E. to the control of traditional broadcast media under Communist Party rule. However, with the rise of the Internet and new media platforms, more than 1.3 billion people can now broadcast their individual views, making information far more diffuse and considerably harder to control. In response, the government has built a massive social media censorship organization, the result of which constitutes the largest selective suppression of human communication in the recorded history of any country. We show that this large system, designed to suppress information, paradoxically leaves large footprints and so reveals a great deal about itself and the intentions of the government.

RATIONALE: Chinese censorship of individual social media posts occurs at two levels: (i) Many tens of thousands of censors, working inside Chinese social media firms and government at several levels, read individual social media posts and decide which ones to take down. (ii) They also read social media submissions that are prevented from being posted by automated keyword filters, and decide which ones to publish.

To study the first level, we devised an observational study to download published Chinese social media posts before the government could censor them, and to revisit each from a worldwide network of computers to see which was censored. To study the second level, we conducted the first large-scale experimental study of censorship by creating accounts on numerous social media sites throughout China, submitting texts with different randomly assigned content to each, and detecting from a worldwide network of computers which ones were censored.

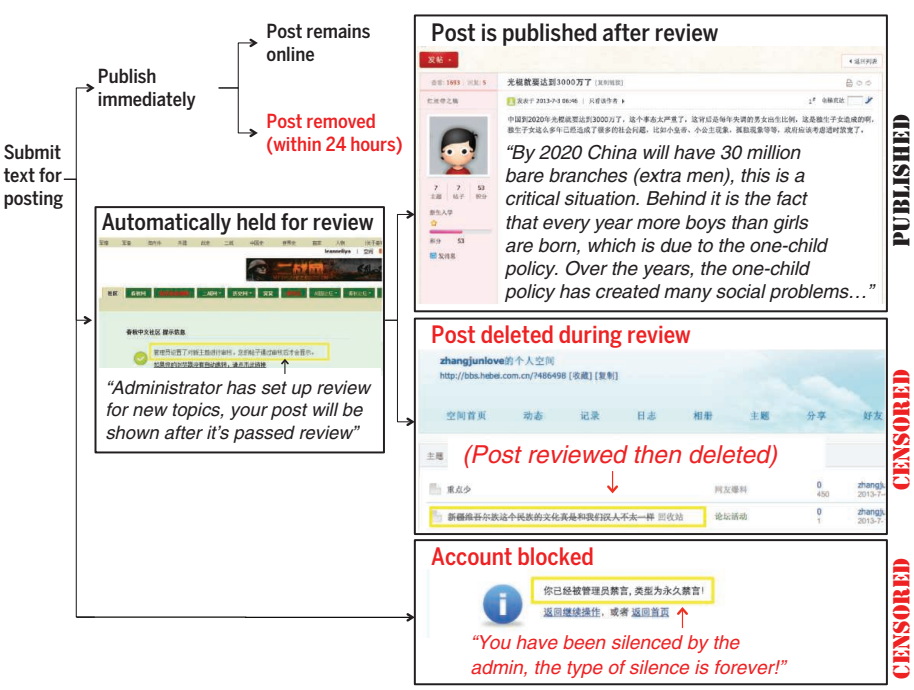

The Chinese censorship decision tree. The pictures shown are examples of real (and typical) websites, along with our translations.

To find out the details of how the system works, we supplemented the typical current approach (conducting uncertain and potentially unsafe confidential interviews with insiders) with a participant observation study, in which we set up our own social media site in China. While also attempting not to alter the system we were studying, we purchased a URL, rented server space, contracted with Chinese firms to acquire the same software as used by existing social media sites, and—with direct access to their software, documentation, and even customer service help desk support—reverse-engineered how it all works.

RESULTS: Criticisms of the state, its leaders, and their policies are routinely published, whereas posts with collective action potential are much more likely to be censored—regardless of whether they are for or against the state (two concepts not previously distinguished in the literature). Chinese people can write the most vitriolic blog posts about even the top Chinese leaders without fear of censorship, but if they write in support of or opposition to an ongoing protest—or even about a rally in favor of a popular policy or leader—they will be censored.

ON OUR WEB SITE

Read the full article at http://dx.doi.org/10.1126/science.1251722

We clarify the internal mechanisms of the Chinese censorship apparatus and show how changes in censorship behavior reveal government intent by presaging their action on the ground. That is, it appears that criticism on the web, which was thought to be censored, is used by Chinese leaders to determine which officials are not doing their job of mollifying the people and need to be replaced.

CONCLUSION: Censorship in China is used to muzzle those outside government who attempt to spur the creation of crowds for any reason—in opposition to, in support of, or unrelated to the government. The government allows the Chinese people to say whatever they like about the state, its leaders, or their policies, because talk about any subject unconnected to collective action is not censored. The value that Chinese leaders find in allowing and then measuring criticism by hundreds of millions of Chinese people creates actionable information for them and, as a result, also for academic scholars and public policy analysts. ■

[1]Department of Political Science, University of California, San Diego, La Jolla, CA 92093, USA. [2]Department of Government, Harvard University, Cambridge, MA 02138, USA. *Corresponding author. E-mail: king@harvard.edu

Cite this article as G. King *et al.*, *Science* 345, 1251722 (2014). DOI: 10.1126/science.1251722

Published by AAAS

RESEARCH ARTICLE

POLITICAL SCIENCE

Reverse-engineering censorship in China: Randomized experimentation and participant observation

Gary King,[1]* Jennifer Pan,[1] Margaret E. Roberts[2]

Existing research on the extensive Chinese censorship organization uses observational methods with well-known limitations. We conducted the first large-scale experimental study of censorship by creating accounts on numerous social media sites, randomly submitting different texts, and observing from a worldwide network of computers which texts were censored and which were not. We also supplemented interviews with confidential sources by creating our own social media site, contracting with Chinese firms to install the same censoring technologies as existing sites, and—with their software, documentation, and even customer support—reverse-engineering how it all works. Our results offer rigorous support for the recent hypothesis that criticisms of the state, its leaders, and their policies are published, whereas posts about real-world events with collective action potential are censored.

The Chinese government has implemented "the most elaborate system for Internet content control in the world" (*1*), marshaling hundreds of thousands of people to strategically slow the flow of certain types of information among the Chinese people. Yet the sheer size and influence of this organization make it possible to infer via passive observation a great deal about its purpose and procedures, as well as the intentions of the Chinese government. To get around the well-known inferential limitations inherent in observational work, our experiment depended on large-scale random experimentation and participant observation.

We begin with the theoretical context. The largest previous study of the purpose of Chinese censorship (*2*) distinguished between the "state critique" and "collective action potential" theories of censorship and found that, with few exceptions, the first was wrong and the second was right: Criticisms of the government in social media (even vitriolic ones) are not censored, whereas any attempt to physically move people in ways not sanctioned by the government is censored. Even posts that praise the government are censored if they pertain to real-world collective action events (*2*).

In both theories, regime stability is the assumed ultimate goal (*3*–*6*). Scholars had previously thought that the censors pruned the Internet of government criticism and biased the remaining news in favor of the government, thinking that others would be less moved to action on the ground as a result (*7*–*9*). However, even if biasing news positively would in fact reduce the potential for collective action, this state critique theory of censorship misses the value to the central Party organization of the information content provided by open criticism in social media (*10*–*13*). After all, much of the job of leaders in an autocratic system is to keep the people sufficiently mollified that they will not take action that may affect their hold on power. In line with the literature on responsive authoritarianism, the knowledge that a local leader or government bureaucrat is engendering severe criticism—perhaps because of corruption or incompetence—is valuable information (*14*, *15*). That leader can then be replaced with someone more effective at maintaining stability, and the system can then be seen as responsive. This responsiveness would seem likely to have a considerably larger effect on reducing the probability of collective action than merely biasing the news in predictable ways.

The collective action potential hypothesis holds that the Chinese censorship organization first detects a volume burst of social media posts within a specific topic area, and then identifies the real-world event that gives rise to the volume burst (*2*). If the event is classified as having collective action potential, then all posts within the burst are censored, regardless of whether they are critical or supportive of the state and its leaders. Unlike the uncertain process involved in coherently classifying individual posts as to their collective action potential, this procedure is easily implemented with extremely high levels of intercoder reliability. No evidence exists as to whether any such rules were invented and directed by a person or committee in the Chinese government, or whether they merely represent an emergent pattern of this large-scale activity.

Although the largest existing study analyzed more than 11 million social media posts from almost 1400 websites across China (*2*), it and other quantitative studies of censorship (*16*, *17*) were solely observational, with some conclusions necessarily depending on untestable assumptions. For example, the data for these studies were controlled by an earlier stage in which many social media websites use automated review (based on techniques such as keyword matching) to immediately move large numbers of prospective posts into a temporary limbo to receive extra scrutiny before possible publishing (for a guide, see Fig. 1). Whereas the ex post content-filtering decision is conducted largely by hand and takes as long as 24 hours, the ex ante decision of whether posts are slotted for review is automated, instantaneous, and thus cannot be detected by observational methods. This also means that the automated review process could induce selection bias in existing studies of censorship, which could only observe those submissions that were not stopped from publication by automated review. And, of course, observational research generally also risks endogeneity bias, confounding bias, and other problems.

To avoid these potential biases and to study how automated review works, we conducted a large-scale experimental study in which random assignment, controlled by the investigators, substituted for statistical assumptions. We created accounts on numerous social media sites across China; wrote a large number of unique social media posts; randomized the assignment of different types of posts to accounts; and, to evade detection, observed from a network of computers all over the world which types were published or censored. Throughout, we attempted to avoid disturbing the flow of normal discourse by producing social media content on topics similar to those in real social media posts (including the content of those censored, which our methods could access). Although very-small-scale nonrandomized efforts to post on Chinese websites and observe censorship have been informative (*18*), randomized experiments have not before been used in the study of Chinese censorship.

In addition to our randomized experiment, from which we drew causal inferences, we also sought to produce more reliable descriptive knowledge of how the censorship process works. This is important information in its own right; the process is intensely studied and contested in the academic and policy communities. Until now, such information has mostly come from highly confidential interviews with censors or their agents at social media sites or in government. This information is necessarily partial, incomplete, potentially unsafe for research subjects, and otherwise difficult to gather. Participant observation provided us with a new source of information absent from previous studies of censorship. From inside China, we created our own social media website, purchased a URL, rented server space, contracted with one of the most popular software platforms in China used to create these sites, submitted, automatically

[1]Institute for Quantitative Social Science, Harvard University, Cambridge, MA 02138, USA. [2]Department of Political Science, University of California, San Diego, La Jolla, CA 92093, USA.
*Corresponding author. E-mail: king@harvard.edu

reviewed, posted, and censored our own submissions. The website we created was available only to our research team, so as to avoid affecting the object of our study or otherwise interfering with existing Chinese social media discourse. However, we had complete access to the software, documentation, help forums, and extensive consultation with support staff; we were even able to get their recommendations on how to conduct censorship on our own site in compliance with government standards. The "interviews" we conducted in this way were unusually informative because the job of our sources was in fact to answer the questions we posed.

Overall, this work offers three intended contributions. First, by analyzing large numbers of posts at numerous social media sites, we are able to resolve some disagreements in the policy and academic literatures on the subject, such as explanations for the presence of conflicting keyword lists and the absence of a coherent or unified interpretation for the operation of these lists at individual sites. Consistent with this disagreement, we show that the large number of local social media sites in China have considerable flexibility, and choose diverse technical and software options, in implementing censorship. Second, we show that the automated review process affects large numbers of posts on fully two-thirds of Chinese social media sites, but is a largely ineffective step in implementing the government's censorship goals. This is surprising but consistent with the known poor performance of most keyword-based approaches to text classification. Finally, despite automated review's large presence, high potential for generating selection bias in observational studies, and overall ineffectiveness due to keyword matching, we find that the government is still able accomplish its objectives—as summarized by the collective action potential hypothesis—by using very large numbers of human coders to produce post hoc corrections to automated review and to censorship in general.

Our research offers clear support for the collective action potential hypothesis and then offers some important extensions. We find—consistent with the implications of this theory, but untested in prior research—that there is no censorship of posts about collective action events outside mainland China, collective action events occurring solely online, social media posts containing critiques of top leaders, and posts about highly sensitive topics (such as Tibet and Xinjiang) that do not occur during collective action events.

Research designs

We now describe the challenges involved in large-scale experimentation, participant observation,

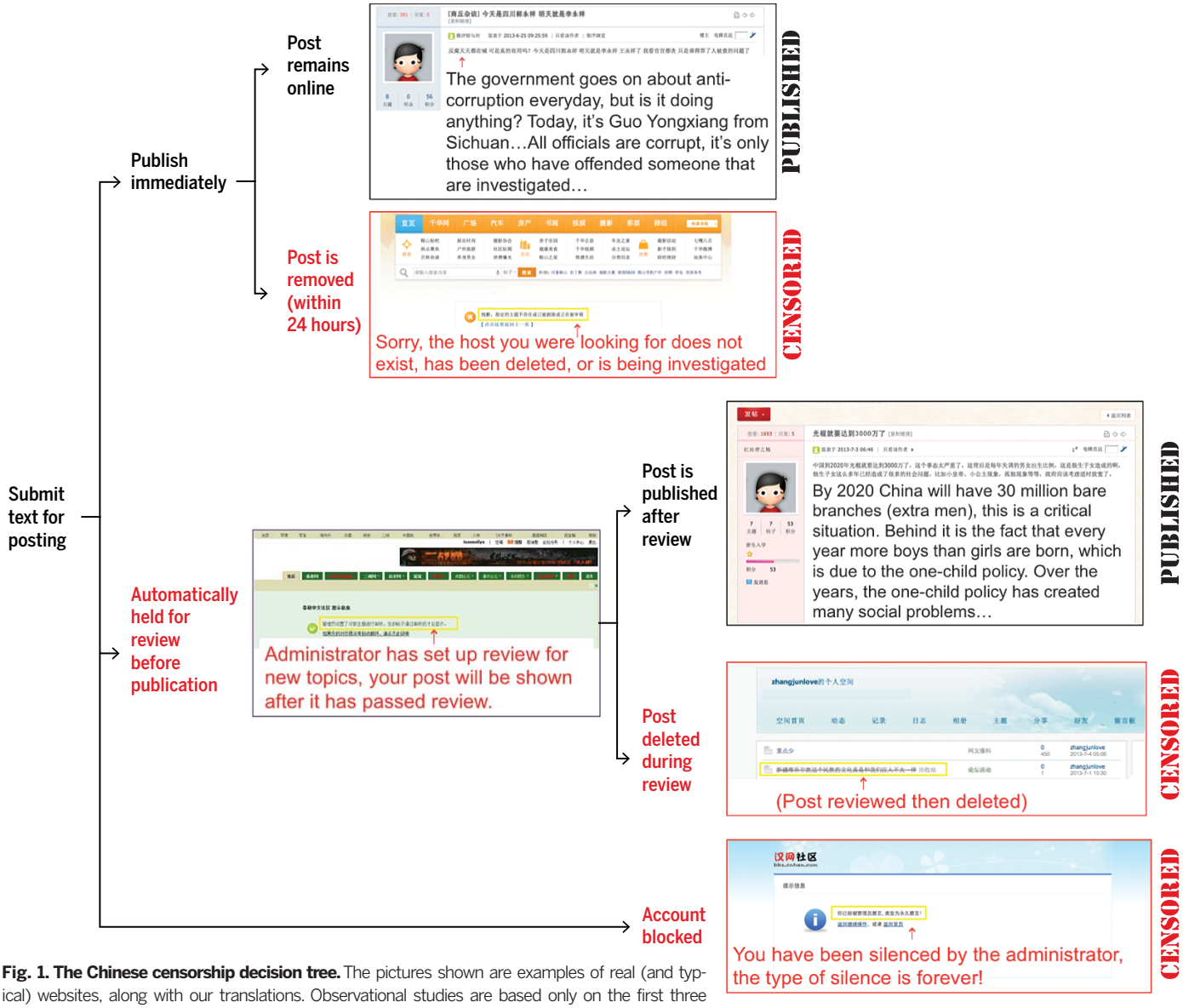

Fig. 1. The Chinese censorship decision tree. The pictures shown are examples of real (and typical) websites, along with our translations. Observational studies are based only on the first three paths through this decision tree; our experimental study includes all five. Full screen shots are in (*19*).

and data collection in a system designed to prevent the free flow of information, especially about the censors [see (*19*) for additional details]. These include avoiding detection, implementing the experiment in many geographically distant places, keeping a large research team safe, and ensuring that we did not disturb or alter the system we were studying. The human subjects aspects of our experimental protocol were preapproved by our university's institutional review board (IRB). For obvious reasons, we are unable to reveal certain details of how we implemented this design, but we do give complete information on the statistical and scientific logic behind our choices (*20*).

We begin with the outcome variable we are studying and then describe our experimental protocols.

Participant observation

Aspects of the process by which censors in the Chinese government and social media companies implement censorship directives have been gleaned over the years in interviews with sources who have first-hand knowledge, including the censors themselves. We have also conducted many such interviews, and each one produces some information, but it is necessarily a partial picture, highly uncertain, and potentially unsafe for the sources and researchers.

Thus, we looked for a way to learn more by changing the incentives of our sources. We did this by creating our own Chinese social media site from inside China, using all the infrastructure, procedures, and rules that existing sites must follow. We purchased a URL, contracted with a company that provides hosting services, and arranged with another company to acquire the software necessary to establish a community discussion forum [a bulletin board system (BBS)]. We downloaded the software and installed it ourselves. This infrastructure gave us complete access to the software and its documentation so that we could fully understand and make use of its functionality. Support employees at these firms were happy to help show us how to censor in such a way as to maintain our website in accordance with their view of government requirements. Thus, instead of trying to convince people to spare some of their time for researchers, we were able to have conversations with employees whose job was to answer questions like those we posed; fortunately, they seemed quite good at this. We then studied and customized the software, submitted posts ourselves, and used the software's mechanisms to censor some of them. We took every step we could (short of letting individuals in China post on the site) to avoid causing any interference to actual social media discourse.

The biggest surprise we found relative to the literature was the huge variety of technical methods by which automated review and human censorship can be conducted. Table 1 summarizes some of these options.

When we installed the software, we found that, by default, it included no automated review or blocking. But webmasters can easily change the option of automatically reviewing specific types of users (those who are moderators, super users, users who have been banned from posting, or those who have been banned from visiting the site), Internet protocol (IP) addresses, new threads, or every response—all of which can be tailored for each of as many forums as desired on each website. Functionality also exists to bulk-delete posts, which can be implemented by date range, user name, user IP, content containing certain keywords, or length of post. On the back end, the webmaster also has flexible search tools to examine content, search by user name, post titles, or post content. What the user sees can also be limited: The search function can be disabled for users, and webmasters have the option of allowing users to see whether posts of theirs are being automatically reviewed (and, if so, which ones).

We found employees of the software application company to be forthcoming when we asked for recommendations as to which technologies have been most useful to their other clients in following government information management guidelines. On the basis of their recommendations as well as user guides, detailed analyses from probing the system, and additional personal interviews (with sources granted anonymity), we deduce that most social media websites that conduct automatic review do so via a version of keyword matching, probably using hand-curated sets of keywords (we reverse-engineer the specific keywords below) (*21*).

We summarize our understanding of the censorship process in Fig. 1. The process begins when one writes and submits a blog or microblog post at a social media website (left). This post is either published immediately (top left node) or held for review before publication (middle left node in red). If the post is published immediately, it may be manually read by a censor within about 24 hours and, depending on the decision, either remains online indefinitely (top box) or is removed from the Internet (second box). As can be seen from the screen shots of actual websites in Fig. 1 [full examples in (*19*)], the decisions of the censors, and the fact that they are making these decisions, are unambiguous.

The censors then read each post in review (usually within a day or two) and either publish the post (third box of Fig. 1) or delete it before publication (fourth box). We are able to identify review when it occurs because typically the user receives a message after post submission that the text has been slotted for review. In the absence of a warning message, the user can tell when a post is put into review because no public URL is associated with the post, and the user's account page will show the status of the post as "under review." Finally, on the basis of the current and previous posts, a submitted post can be censored and the account blocked so that no additional posts may be made (last box of Fig. 1). In this last case, when a user submits a text for

Table 1. Options for content filtering on forum platform.

Automated review options	
Content-based review can be based on:	• Moderator-supplied keywords • Plug-ins for reviewing posts with minimal influence on the user • Plug-ins advertising better keyword-blocking technology • Review specific to post type (e.g., comment or main post) • Review specific to forum topic
User-based review can be based on:	• User IP • Payments by user • Points won by user (e.g., for number of posts, comments) • Previous user posts • Last login
Time-period review and censorship allows:	• Periods of time when all posts are audited • Prevention of posting during certain hours of the day
Workflow for reviewed posts:	• Different censors for different types of postings (e.g., spam versus political content) • Batch deletion of posts • Review interface with search functionality
Account blocking options	• Blocking for specific types of posts (e.g., comment or main post) • Blocking for specific forums • Blocking based on points • Blocking based on user IP • Blocking posting and/or reading

posting, an error message notifying the user of account blocking is encountered. A key point is that the massive data set in (2) corresponds only to the first three boxes, whereas in our experiment we are able to study all five paths down the decision tree.

Experimental protocol

We designed our experimental protocol to make causal inferences without certain modeling assumptions. We first selected 100 social media sites, including 97 of the top blogging sites in the country, representing 87% of blog posts now on the web. We included the top three microblogging (i.e., Twitter-like) sites: Sina Weibo (weibo.com), Tencent Weibo (t.qq.com), and Sohu Weibo (t.sohu.com). The first two of these microblogging sites each have more than 500 million registered users and 50 to 100 million daily active users (22). Together, the 100 sites are geographically spread all over China; 20 are run by the government, 25 are state-owned enterprises, and 55 are private firms. Some cater to national audiences, whereas some only allow posting within a local area. Creating accounts on some of these sites requires the user to be in the country at a specific geographic locale, to have a local e-mail address, or to provide another method of communication for identification. We devised procedures to create two accounts at each of these 100 social media sites.

We kept our design close to aspects of (2). The theory in that paper was not that every social media post with the potential to generate collective action is censored; after all, almost any issue could in principle be used as a hook to generate protest activity. Instead, the theory is that pro- or anti-government posts concerning a collective action event are censored. Collective action events are those "which (a) involve protest or organized crowd formation outside the Internet; (b) relate to individuals who have organized or incited collective action on the ground in the past; or (c) relate to nationalism or nationalist sentiment that have incited protest or collective action in the past" [(2), p. 6].

We conducted three rounds of experiments (18 to 28 April, 24 to 29 June, and 30 June to 4 July 2013) during which social media posts would need to be written in real time about current issues. This presented a logistical challenge. At the beginning of each round, we scoured the news and selected ongoing collective action events and non–collective action events about which there was a volume burst in social media discussion. We chose a ratio of one collective action event to two non–collective action events, because collective action events are more scarce and so that we could average over different non–collective action events. We included non–collective action events only if they were widely discussed topics pertaining to actions taken by the Chinese government, officials, or the Chinese Communist Party (CCP) that were unrelated to events with collective action potential. We also attempted where possible to select events that mentioned specific officials' names and addressed what has been described as especially "sensitive" topics. (We also included several edge cases, described below.) Details of all events appear in (19), but here are the four collective action events we found when our study was conducted, all of which meet the definition but some of which are more incendiary than others:

1. Qui Cuo, a 20-year-old mother, self-immolated to protest China's repressive policies over Tibet. Her funeral drew protesters.

2. Protesters in Panxu, a village in Xiamen Fujian, took to the streets because they claimed officials did not adequately compensate them for requisitioning their collectively owned farmland to build a golf course. Village representatives went to local authorities to demand compensation but were instead detained. Thousands of villagers went to the town hall to demand the release of the village representatives, police moved in to arrest the villagers, and the villagers retaliated by smashing police cars and taking the local Party secretary into custody.

3. On the second anniversary of the 2011 arrest of artist-dissident Ai Weiwei, he released a music album that talked about his imprisonment. Ai Weiwei was arrested in 2011 on charges of tax evasion, but more likely the true reason was either that he called upon his followers to mimic the Arab Spring or that he organized volunteers to collect the names of children who died in the Sichuan earthquake. The release of the album by Ai Weiwei is chosen as an example of collective action under part (b) of the definition, where posts about individuals who have organized or incited collective action on the ground in the past are censored.

4. An altercation between protesting Uyghurs (a minority ethnic group) and local police in Lekeqin township of Shanshan county in Turpan, Xinjiang, led to the deaths of 24 people, including 16 Uyghurs. Police and many official news reports of the event termed it an act of Uyghur terrorism, but rumors circulated in social media that the protest was precipitated by forced housing demolition.

For each event, we had a group of native Chinese speakers write some posts supportive and others critical of the government. These posts were based on social media posts that had already appeared online, including posts that were censored as well as those that remained online. [We used the technology of (2) to obtain access to the censored posts.] In other words, we obtained posts that were immediately published after submission, including those that remained online and those that were removed (top two boxes of Fig. 1). We provided our writers with background on the event, the definition of what we meant by pro- and anti-government for each topic (19), and examples of real posts from Chinese social media similar to those we needed written. So that we could minimize any experimenter effect, we checked each text ourselves by hand and attempted throughout to ensure that the posts we submitted were similar in language, sentiment, and content to those already found in (or written and censored in) Chinese social media.

From a statistical point of view, we ensured balance by blocking (23) on (that is, randomly sampling only within each cell of the cross-classification of) three variables: First, our posts included the same keywords in both the treatment and control conditions. Second, we controlled for individual writing style by blocking on author in our experimental design. That is, posts in each set of four experimental conditions (defined by our two variables: pro- or anti-government, and with or without collective action potential) were written by the same set of research assistants. Finally, we constrained all posts to be between 100 and 200 characters in length. In addition, we also ensured that no two posts submitted were exactly identical to each other or to any we found in social media. All posts were submitted between 8 a.m. and 8 p.m. China time, either from the United States or from the appropriate place within China, depending on what was feasible because of the technology used at each social media site (24).

We were interested in testing the causal effect of both pro- versus anti-government content and collective action versus non–collective action content, leading by cross-classification to four logical treatment categories. To make the most efficient use of each individual account, we submitted two posts to each. But it makes little sense for one account (representing a single person) to write both pro- and anti-government posts regarding the same event. Thus, we submitted posts about two different events to each account; some of these posts were pro-government collective action and anti-government non–collective action, and others were anti-government collective action and pro-government non–collective action. In this way, every account contributed to the causal effect estimate of each hypothesis. We also ensured our ability to make causal inferences without extra modeling assumptions by randomizing (i) the choice between these two pairs, (ii) the order within each pair, and (iii) the specific collective action and policy events we wrote about in each submission. Missingness could occur when websites were down, if an account we created expired, or if an account had been blocked because of prior posts. Largely because of the design, any missingness is almost exactly independent of our two treatment variables; empirically that proved to be the case.

Each of the 100 different social media websites in our study offers a different way of expressing oneself online. When possible, we submitted posts on the home page we created for each account. For discussion forums, we started a new thread with the content of the post in the most popular subforum. On sites where users are not permitted to create new threads, we submitted posts as a reply to an existing thread relevant to the topic. In all cases, we wrote our posts so as not to stand out from the stream of existing information; we followed all social media, website, and cultural norms. In total, we wrote 1200 posts by hand, every one unique, and none referring to each other (25).

After submitting a post, we observed whether it was caught by the process of automated review; if in automated review, whether and when it was eventually published; and if not caught by the automated review process, whether it was eventually censored after the fact or remained on the web. When a post appeared on the web, we recorded the URL and verified censorship from computers inside and outside of China. We recorded the outcome in terms of censorship, which corresponds to the branches of the decision tree in Fig. 1.

Throughout, our goal was that anyone looking at our submissions would have no idea that this was part of an academic research project, and that the posts were typical of what anyone might otherwise find online and would not in any way disrupt or change the social media ecosystem we were studying. We also needed to ensure that our checking of published posts for censorship was not obtrusive. So far as we are aware, no one outside of our research team and confidants were aware of this experiment before now, and no one on the web indicated any suspicion about or undue attention toward any of our posts.

Results

We find that in aggregate, automated review affects a remarkably large portion of the social media landscape in China. In total, 66 of the 100 sites in our sample (automatically) review at least some social media submissions, and 40% of all of our individual social media submissions from our 100 sites (and 52% of submissions from sites that review at least sometimes) are put into review. Of those submissions that go into review, 63% never appear on the web.

These figures indicate that automated review affects a large component of intended speech in China and so deserves systematic attention from researchers. This is especially so because of conflicting conclusions and lack of a unified interpretation in the academic and policy literatures about which keywords provoke action by the government, how automated review works, and what impact this process ultimately has on the content of speech that is blocked and that which can be consumed by the Chinese people (*26*, *27*). We offer a possible resolution to these issues here.

Censorship

Using our broader sample, unaffected by selection during the automated review process, and with our experimental randomization, we began by testing the collective action potential hypothesis. On the basis of a difference in means between the treatment and control groups, the black dots in the left panel of Fig. 2 summarize the point estimate for the causal effects on censorship of submitting posts about four separate collective action events. The vertical lines are 95% confidence intervals (as with all our figures). The effects are substantial, ranging from about 20 to 40 percentage point differences (denoted on the vertical axis) solely due to writing about an ongoing collective action event as compared to an ongoing non–collective action event.

We also examined some of the other decision paths in Fig. 1. To do this, we estimated the "causal mediation effect" (*28*, *29*) of submitting posts about collective action events (versus non–collective action events) on censorship, and found that almost none of this effect is mediated through automated review: The overall effect is a trivial 0.003 probability, with a 95% confidence interval of (−0.007, 0.016) (*19*). The (non)effect for each of the four collective action events we studied is displayed in the right panel of Fig. 2, and each is similarly approximately zero, with a small confidence interval. Review, which appears to be fully automated, is thus applied in a manner independent of other relevant variables, and, like most keyword-only methods of automated text analysis, it does not work well when applied to large numbers of documents. From this result, it even appears that the censors largely ignore it, or at least do not get much information from it (see below).

In parallel to the large causal effect for collective action, Fig. 3 reports tests of the state critique hypothesis for each of our four collective action events and eight (non–collective action) policy events. The black dots summarize point estimates of the causal effect of submitting posts in favor of the government versus opposed to the government about each event. As can be seen, the dots are all very close to the horizontal dashed line, drawn at zero effect, with six dots above and six below, and all but one of the confidence intervals crossing the zero line. Note especially that there is no hint of more censorship of anti-government posts when they involve topics that might be viewed as more sensitive or which specifically mention the names of Chinese leaders [see (*19*) for contextual details]. This finding runs counter to anecdotal evidence that rumors and names of leaders unrelated to collective action lead to censorship.

Automated review

The overall results in favor of the collective action potential hypothesis and against the state critique hypothesis thus appear unambiguous. The automated review process has a nearly undetectable effect on evidence about that hypothesis, because the human censors correct errors after the keyword-matching techniques are applied in automated review (although even incorrect keyword filtering slows down communications on many subjects). We now go back up the decision tree of Fig. 1 to study the automated review process more directly.

We first noticed that not all websites have automated review turned on, and that the method of censorship varies enormously by website [this is also true for account blocking (*19*)]. This

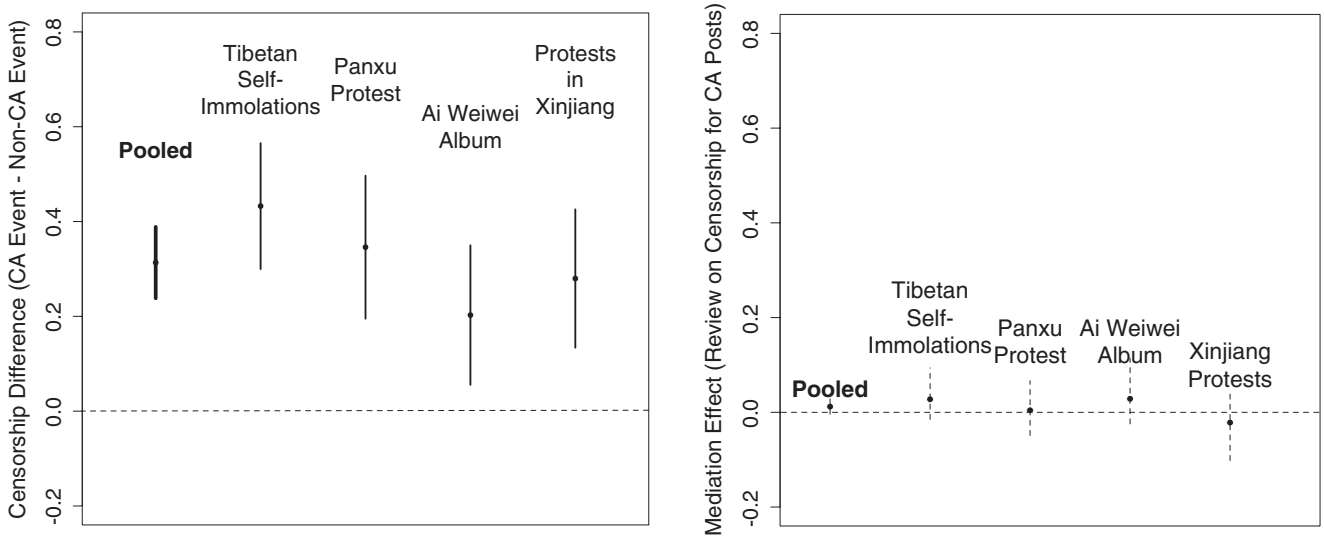

Fig. 2. The causal effect on censorship of posts with collective action potential (left panel) and the mediation effect of review (right panel). Collective action events are more highly censored than non–collective action events within the same time period. However, censorship of collective action events is not mediated through automated review.

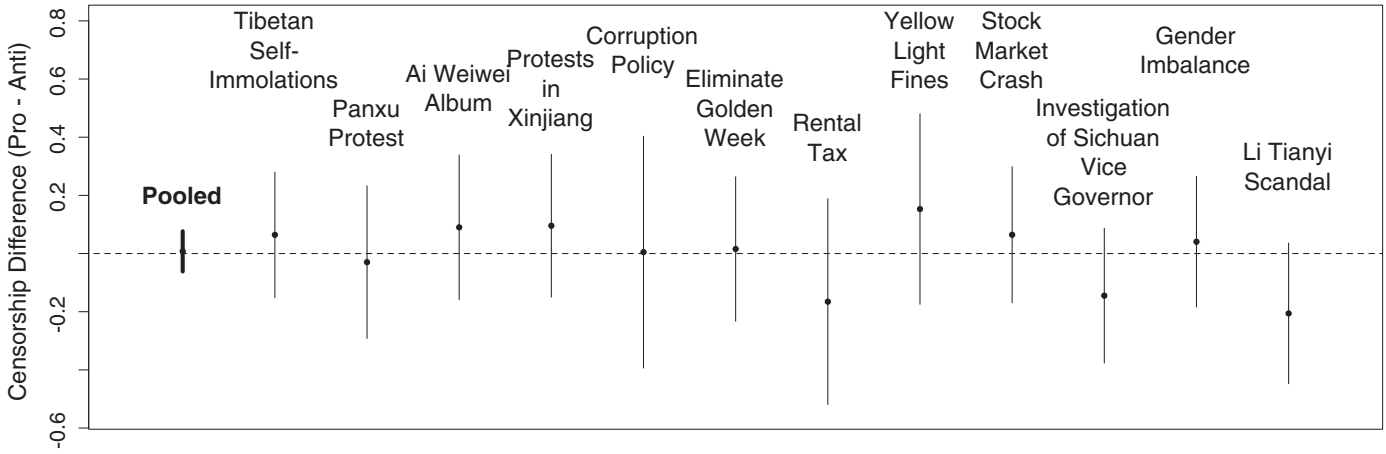

Fig. 3. The causal effect on censorship of posts for or against the government. Posts that support the government are not more or less likely to be censored than posts that oppose the government, within the same topic.

is consistent with what we learned from creating our own social media site, where the software platform not only allows the option of whether to review, but also offers a large variety of choices of the criteria by which to review. Indeed, there exists considerable diversity in the technologies used by different social media sites for automated review (*17*). It is this diversity in technology across sites, then, that appears to account for why different researchers typically find different patterns when looking at different sites or at specific issues. This also accounts for why researchers have been unable to offer unified interpretations of their observations that are consistent with reasonable assumptions about the goals of the Chinese leadership. Only by looking at the whole process does the simplicity of the Chinese government's goals become clear.

Why would the government, in the course of providing top-down authoritarian control, allow for a free choice from a large number of censorship methods? To answer this question, we collected detailed information about all software platforms and plug-ins available for purchase or license by social media sites to control information. From this study, we conclude that the government is (perhaps intentionally) promoting innovation and competition in the technologies of censorship. Such decentralization of policy implementation as a technique to promote innovation is common in China (*30*–*33*).

On the basis of interviews with those involved in the process, we also found a great deal of uncertainty over the exact censorship requirements and the precise rules under which the government would interfere with the operation of social media sites, especially for smaller sites with limited government connections. This uncertainty is in part a result of encouraging innovation, but it may also in some situations be a means of control as well; it is easier to keep people away from a fuzzy line than from a clearly drawn one.

Our systematic empirical study began by investigating which social media websites use any automated review process. Figure 4 presents a density estimate (a continuous version of a histogram) of the distribution of the proportion of posts reviewed for three types of sites, depending on ownership. As can be seen, it is government sites that have the highest probability of a post being put into review, followed by the state-owned enterprises, followed last by privately owned sites (which tend to have the largest user bases).

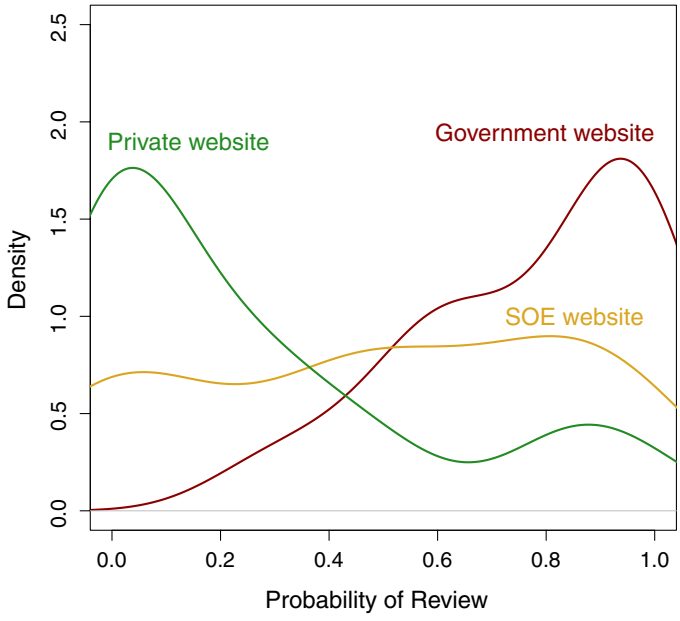

Fig. 4. Histogram (density estimate) of the proportion of posts reviewed by site. The graph shows that government-controlled social media sites catch many more posts by automated review than do privately owned sites; social media sites controlled by state-owned enterprises (SOEs) are in the middle.

Why would government sites be more likely to delay publication until after automated review, whereas private sites publish first and make censorship decisions later? So far as we can tell from qualitative evidence, the reason is that the penalty for letting offending posts through differs between government and private sites. A government worker who fails to stem collective action could lose his or her job immediately; in contrast, a worker in a private site who makes the same mistake cannot usually be directly fired by the government. Indeed, government workers have a historical legacy of giving priority to following orders and not making mistakes, even if it is considerably more inefficient to do so (*34*). Private social media sites, on the other hand, have incentives to publish as much as they can, so as to attract more users. A private site can, of course, be taken down entirely, but that kind of "nuclear option" is used less often than more generalized pressure on the leadership of these private sites.

What are these largely government sites reviewing? In a manner directly parallel to Figs. 2 and 3 for the ultimate variable of censorship, we analyzed the effects on automated review of collective action and pro- and anti-government posts. Figure 5 gives results for the effect of collective action on review; they include four positive estimated effects, but two are small and three have zero inside their confidence intervals. If the goal of the censors is to capture collective action events, the automated algorithm is performing marginally at best, although this is quite

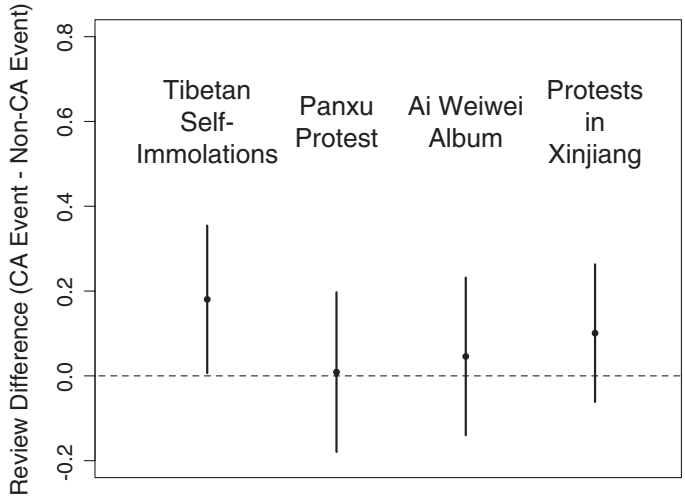

Fig. 5. Causal effect on review of collective action potential events. Collective action events are overall slightly more likely to be reviewed than non–collective action events.

common for keyword algorithms, which tend to work well for specific examples for which they can be designed but often have low rates of sensitivity and specificity when used for large numbers of documents.

Also interesting is the causal effect of pro- versus anti-government posts in Fig. 6. These are all small, and most of the confidence intervals cross zero. If there exists a nonzero relationship here, it is that submissions in favor of the government are reviewed more often than those against the government. Indeed, 9 of 12 point estimates are above zero, and two even have their entire confidence interval above zero. This presents a mystery: Government social media sites are slightly more likely to delay publication of submissions that favor the government, its leaders, or their policies. Private sites do not use automated review much at all. Why is this? We found that the answer again is the highly inexact keyword algorithms used to conduct the automated review.

To understand this better, we reverse-engineered the Chinese keyword algorithms in order to discover the keywords that distinguish submissions reviewed from those not reviewed. Because the number of unique words written overwhelms the number of published posts, we could not find these keywords uniquely. However, we could identify words highly associated with review using a "term frequency, inverse document frequency" algorithm (*35*, *36*). That is, we took the frequency of each word within the review posts and divided this number by the number of nonreviewed documents in which that same word appeared. Thus, for every word we obtained a measure of its frequency in review posts, relative to posts that were not reviewed. Words with high values on these measures are likely to be used within the automated review process.

Table 2 gives the top keywords (and key phrases) that we estimate were used to select posts we wrote into automated review. We can see that the words associated with review could plausibly detect collective action and relate to the government and its actions, but are also just as likely to appear in pro-government posts as in anti-government posts. For example, more pro- than anti-government posts are reviewed in the Corruption Policy topic in Fig. 6. This appears to be because the reviewed pro-government posts used the word corruption (腐败) more frequently than did anti-government posts. However, corruption was used in the context of praising how the new policy would strengthen anti-corruption (反腐败) efforts. Not only is automated review conducted by only a subset of websites and largely ineffective at detecting posts related to collective action events, it also can backfire by delaying the publication of pro-government material.

It turned out that we could provide an independent test of the veracity of these keywords. In the context of setting up our own website, we unearthed a list of keywords for review that a software provider offered to its clients running social media websites. The list is dated April 2013, and all of the keywords we found related to events taking place prior to April 2013 were on this list; the exceptions were from events that occurred after April 2013.

It thus appears that the workers in government-controlled websites are so risk-averse that they have marshaled a highly error-prone methodology to try to protect themselves. They apparently know not to take this automated review methodology very seriously; whether it is used or not, the manual process of reading individual posts must still be used widely, as our results show that automated review does not affect the causal effect of collective action events on censorship decisions.

Edge cases

We now attempt to define the outer boundaries of the theory of collective action potential by examining cases close to but outside the theory (where no effect is anticipated), as well as one extreme case inside the theory: criticism of the top leaders.

Internet-only and external-only collective action

The first case is an event in which collective action took place, but only on the Internet. At the end of May 2013, the principal of Hainan Wanning City No. 2 Elementary School was being investigated for taking six elementary school girls to a hotel. Ye Haiyan, a women's rights advocate, went to the elementary school and protested with a sign in her hand that read "Principal: Get a hotel room with me, let the elementary students go! Contact telephone: 12338 (Ye Haiyan)." Ye's protest went viral and her sign became an online meme, where individuals would take and share photos of themselves, holding a sign saying the same thing with their own phone numbers or often with China's 911 equivalent (110) as the contact phone number (*37*).

The second event occurred on 1 July 2013, which was the 16th anniversary of the handover of sovereignty of Hong Kong from Britain to China. Every year on this day, thousands take to the streets of Hong Kong in protest, but typically with little or no such protest on the mainland. In 2013, between 30,000 people (according to the police) and 430,000 people (according to the organizers) took to the streets to call for true democracy and Chief Executive C. Y. Leung's resignation (*38*).

Neither of these "edge case" examples meet the definition of collective action events given above, but they are obviously close. We ran our experimental design for these events too (Fig. 7, left panel). In both cases, the overall causal effect is near zero, with confidence intervals that overlap zero. There is a hint of a possibly positive effect only for posts reviewed about Hong Kong protests, but in the context of the natural variability of Figs. 2 and 3, this effect is not obviously different from zero.

Corruption and wrongdoing among senior leaders

Next, we consider the effects of writing about corruption and wrongdoing among senior leaders in the government, Party, and military on censorship. Nothing in the theory of collective action potential supports this effect, but because corruption so directly implicates leaders who could control censoring, considerable suspicion exists in the literature that posts about corruption are censored (*16*, *18*, *26*). We can even point to the odd result that posts supporting the government's efforts to deal with corruption are more censored than posts opposed to the government's efforts to deal with corruption (see Fig. 6).

We selected three corruption-related topics for the analysis. The first relates to a new corruption policy that imposes criminal charges against bribes exceeding 10,000 Chinese yuan. The second topic relates to the investigation of Guo Yongxiang, a member of the Sichuan Province Central Committee and a Vice Governor of Sichuan, for serious breaches in discipline. The final topic relates to the naming of Li Tianyi, the son of the well-known People's Liberation Army performer Li Shuangjiang, for participating in a gang rape. The Li Tianyi case led to speculations of corruption that Li's father's ties to the People's Liberation Army would allow Li to avoid punishment commensurate with his crimes. The results for an analysis of the three corruption events

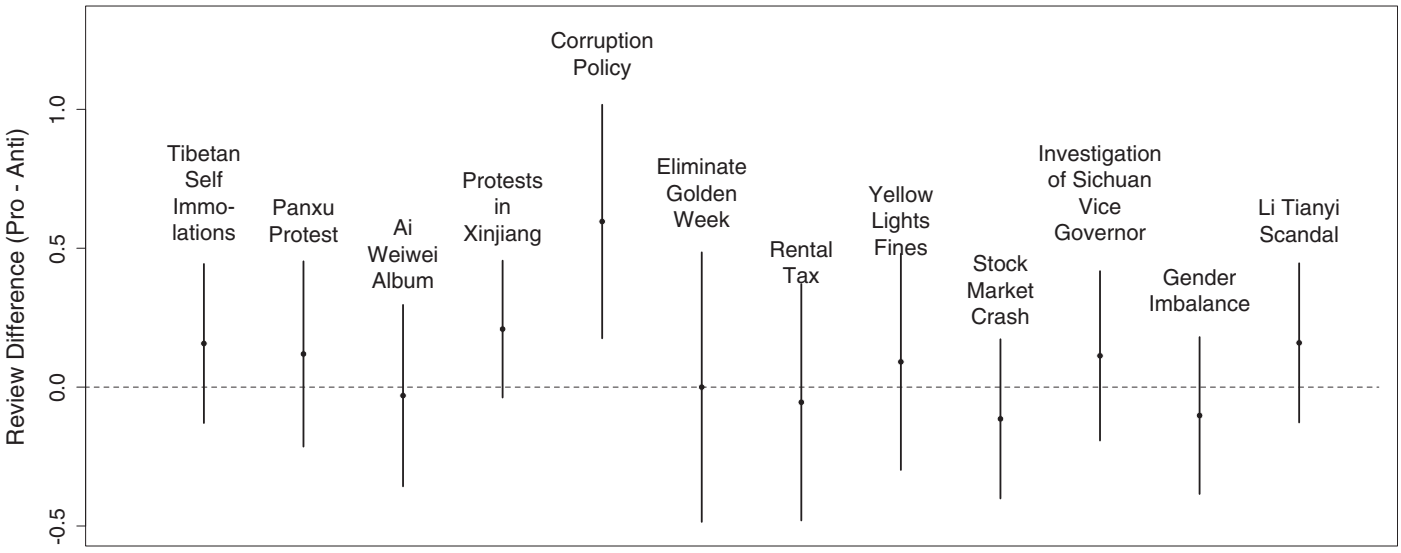

Fig. 6. Causal effect on review of posts for or against the government. Automated review picks up slightly more posts that are for the government as compared to posts that are against the government.

Table 2. Top keywords distinguishing posts held versus not held for review. Words within this list match keyword lists provided by the software provider.

Chinese	English
群众	masses
政府	government
事件	incident
恐怖	terror
新疆	Xinjiang
中国	China
上街	go on the streets
李天一	Li Tianyi
法律	law
达赖	Dalai Lama
游行	demonstration
香港	Hong Kong
行贿	to bribe
腐败	corruption

(Fig. 7, right panel) clearly show no effect, thus again supporting the theory of collective action potential. Similarly supportive is the fact that posts in these topics name specific Chinese government and CCP leaders, both at central and local levels of government (*19*).

Top leaders and highly sensitive issues

Finally, we used observational methods to study the question of the censorship of discussions about top Chinese leaders, arguments for deep political reform, and discussion of highly sensitive or salient issues.

To study more directly whether Chinese censors allow direct criticism of top leaders, we began by finding a social media volume burst about Chinese President Xi Jinping that (i) by our specific definitions does not have collective action potential, (ii) includes posts that cover meaningful and important topics, and (iii) is about a topic that could generate highly critical posts about the leader. We found the following volume burst that met these conditions.

On 28 December 2013, President Xi Jinping visited a Feng Qing Steamed Bun Shop in Beijing (Feng Qing is a chain restaurant) and ate steamed buns "just like the rest of us." He waited in line, he paid 21 CNY for steamed pork and onion buns along with a side of stir-fried liver, and he brought his own tray to a table. Xi's visit unleashed a storm of traditional media coverage and a large volume burst on social media. Although Xi's visit to the bun shop sounds like an innocuous event, online discussions related the visit to important and high-profile issues such as Xi's China Dream, corruption of government officials, rising real estate prices, and the plight of China's elderly and impoverished, as well as propaganda, censorship, the absence of elections, and multiparty competition. However, this event is not connected to any ongoing collective action events.

During this volume burst, we collected 82,280 social media posts related to this event before any posts were censored, and then checked each one from a network of computers around the world that were eventually censored. Finally, we applied the Hopkins-King algorithm (*39*) (using a training set of 592 hand-coded posts) to determine the proportion of censored posts that were critical versus supportive, and applied the Bayesian algorithm derived in (*2*) to invert this. We found, consistent with the collective action potential hypothesis, that posts critical of President Xi were censored just about as much as those that were supportive. Among posts that were critical of Xi and his actions, 18% were censored (95% confidence interval, 13 to 22%). Among the posts supportive of Xi, 14% were censored (95% confidence interval, 8 to 22%). [The proportion of posts censored among posts that simply described the event was 21% (95% confidence interval, 18 to 24%).]

The supplementary materials (*19*) include the text of examples of uncensored posts that are highly critical of President Xi and that use this event to discuss important issues. These posts involve many vivid personal attacks on Xi and his policies. In our experience, these posts are not surprising or unusual.

Next, we looked for uncensored discussion of deep political reform. In August 2013, three commentaries were published in *People's Daily* condemning constitutionalism, describing constitutionalism as incompatible with socialism and doomed to fail in China. These commentaries sparked a social media volume burst with intensive online discussions about whether China should adopt American-style constitutionalism and multiparty competition. In the days after these commentaries, we collected a random sample of 9850 blog posts related to political reform. Although this sample includes posts that toe the party line and criticize constitutionalism, there are also many uncensored posts advocating for the adoption of multiparty competition, describing reform as the only way to empower the Chinese people and to rein in corruption. We include several examples in (*19*).

Finally, we sought and identified social media volume bursts related to three highly salient and politically sensitive issues about real-world events that did not have collective action potential. These are discussions related to Tibet, Uyghurs, and Ai Weiwei.

First is the case of a volume burst in Tibet: In early August 2013, a post by a woman who claimed to have spurned her true love in order to marry a man who lived within view of Lhasa's Potala Palace went viral. As expected, censorship of posts in this burst was low at 12%.

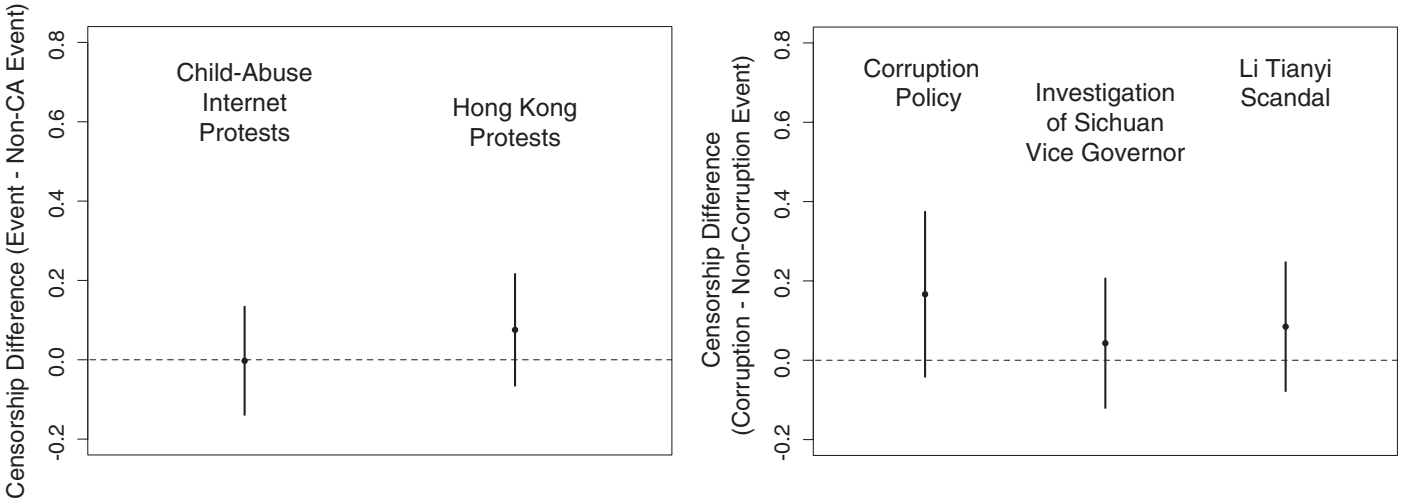

Fig. 7. Testing edge cases for the causal effect of collective action potential (left panel) and of posts about corruption (right panel).

Second is a volume burst related to Xinjiang and Uyghurs, which occurred in March 2013 when a post poking fun at a government entity with an exceptionally long, 54-character name (新疆维吾尔自治区乌鲁木齐国家高新技术产业开发区社会管理综合治理委员会学校及周边治安综合治理工作领导小组办公室) went viral. The government entity is located in Xinjiang, and the name can be roughly translated as the "Public Security and Management Office of the Working Small Group of the Holistic Social Management Committee's School and Surrounding Areas of Xinjiang Uyghur Autonomous Region Urumqi's Chinese High Tech Development Zone." This post was the butt of jokes and satire related to Chinese government bureaucracy but was completely unrelated to any ongoing collective action event. As expected, censorship of this volume burst was low, only 10%.

Finally, we identified a volume burst related to artists—including Ai Weiwei along with Matisse, Picasso, Andy Warhol, and others—and their cats. Censorship of this burst was also low, at 6%. Our definition of collective action potential includes real-world events related to those who have catalyzed or organized collective action in the past. This volume burst relates to Ai Weiwei but falls outside the definition because the burst is not related to a real-world event, nor is it solely related to Ai Weiwei.

Concluding Remarks

We offer the first large-scale randomized experimental analysis of censorship in China, along with participant observation of how censorship is conducted. We use these designs to conduct a rigorous test of the theory of collective action potential, and to further uncover and resolve academic conflicts about crucial aspects of the Chinese censorship program. With them, we are able to subject to empirical estimation what had previously been left to statistical assumption. We are also able to study the large program whereby enormous numbers of social media submissions are put into limbo before being considered for possible publication or censorship. Whereas censorship is a "publish first, censor later" process, automated review involves a "review first, maybe publish later" process.

Our flexible research designs also enabled us to study edge cases, just beyond the reigning theory of collective action potential, so that we can define the boundaries of where it applies. This includes the effects of highly salient and sensitive topics about events without collective action potential; posts about corruption; posts that name Chinese leaders specifically; and collective action events that are solely on the Internet or about collective action on the ground outside the Chinese mainland—none of which are predicted by the theory of collective action potential to be censored more than others, and which our data clearly show are not censored more than other non–collective action topics. We also show that academic controversies over confusing interpretations of which keywords are being censored in automated review are resolved once we realize that the Chinese government is surprisingly flexible concerning what methods and technology each social media site can use, even while imposing uniformity of results by requiring post hoc censoring by human coders.

Future researchers should consider comparing these results on censorship in social media with censorship in traditional media and other ways the Chinese government impedes the free flow of information.

REFERENCES AND NOTES

1. Freedom House, "Freedom of the press, 2012"; www.freedomhouse.org.
2. G. King, J. Pan, M. E. Roberts, How censorship in China allows government criticism but silences collective expression. *Am. Pol. Sci. Rev.* **107**, 326–343 (2013). doi: 10.1017/S0003055413000014
3. S. L. Shirk, *China: Fragile Superpower: How China's Internal Politics Could Derail Its Peaceful Rise* (Oxford Univ. Press, New York, 2007).
4. S. L. Shirk, *Changing Media, Changing China* (Oxford Univ. Press, New York, 2011).
5. M. K. Whyte, *Myth of the Social Volcano: Perceptions of Inequality and Distributive Injustice in Contemporary China* (Stanford Univ. Press, Stanford, CA, 2010).
6. L. Zhang, A. Nathan, P. Link, O. Schell, *The Tiananmen Papers* (Public Affairs, New York, 2002).
7. A. Esarey, Q. Xiao, Political expression in the Chinese blogosphere: Below the radar. *Asian Surv.* **48**, 752–772 (2008). doi: 10.1525/AS.2008.48.5.752
8. R. MacKinnon, *Consent of the Networked: The Worldwide Struggle For Internet Freedom* (Basic Books, New York, 2012).
9. P. Marolt, Grassroots agency in a civil sphere? Rethinking internet control in China. In *Online Society in China: Creating, Celebrating, and Instrumentalising the Online Carnival*, D. Herold, P. Marolt, Eds. (Routledge, New York, 2011), pp. 53–68.
10. M. Dimitrov, The resilient authoritarians. *Curr. Hist.* **107**, 24–29 (2008).
11. P. L. Lorentzen, Regularizing rioting: Permitting public protest in an authoritarian regime. *Q. J. Pol. Sci.* **8**, 127–158 (2013). doi: 10.1561/100.00012051
12. P. L. Lorentzen, China's strategic censorship. *Am. J. Pol. Sci.* **58**, 402–414 (2014). doi: 10.1111/ajps.12065
13. X. Chen, *Social Protest and Contentious Authoritarianism in China* (Cambridge Univ. Press, New York, 2012).
14. E. Malesky, P. Schuler, Nodding or needling: Analyzing delegate responsiveness in an authoritarian parliament. *Am. Pol. Sci. Rev.* **104**, 482–502 (2010). doi: 10.1017/S0003055410000250
15. G. Distelhorst, Y. Hou, Ingroup bias in official behavior: A national field experiment in China. *Q. J. Pol. Sci.* **9**, 203–230 (2014). doi: 10.1561/100.00013110
16. D. Bamman, B. O'Connor, N. Smith, Censorship and deletion practices in Chinese social media. *First Monday* **17** (no. 3) (March 2012). doi: 10.5210/fm.v17i3.3943
17. T. Zhu, D. Phipps, A. Pridgen, J. Crandall, D. Wallach, The velocity of censorship: High-fidelity detection of microblog post deletions. In *22nd USENIX Security Symposium* (Washington, DC, 14 to 16 August 2013); www.usenix.org/conference/usenixsecurity13/technical-sessions/paper/zhu.
18. R. MacKinnon, China's censorship 2.0: How companies censor bloggers. *First Monday* **14** (no. 2) (February 2009). doi: 10.5210/fm.v14i2.2378
19. See supplementary materials on *Science* Online.
20. We also added our own ethics rules, not required by the IRB, which dictate that we avoid, wherever possible, influencing or disturbing the system we are studying (*19*). The similarity to the Prime Directive in *Star Trek* notwithstanding, this seems like the appropriate stance for scientists attempting to understand the world, as distinct from advocates trying to change it, and in any event is more likely to yield reliable inferences.
21. In the process of setting up the site, they recommended that we hire two or three censors for every 50,000 users. That enables us to back out an estimate of the total number of censors hired within firms at between 50,000 and 75,000, not

counting censors within government, 50 Cent Party members, or the Internet police.
22. See (*40*, *41*) for numbers of registered users, which are substantial even if we account for automated sites created by marketing firms (*42*).
23. K. Imai, G. King, E. Stuart, Misunderstandings between experimentalists and observationalists about causal inference. *J. R. Stat. Soc. Ser. A* **171**, 481–502 (2008). doi: 10.1111/j.1467-985X.2007.00527.x
24. All posts were made to mainland China accounts. Some were submitted from outside China, when feasible, and many from within China. Recent work has noted that overseas accounts are subject to less stringent censorship regulations than mainland accounts (*43*). This issue does not affect our work because all accounts created and used were mainland China accounts. Users could control account location when creating the account by specifying a location in China, by entering a local mobile number, or by creating the account from a local IP address. We used all of these methods.
25. For each of our three rounds, we wrote 200 posts on non–collective action events (split equally between pro- and anti-government) and 200 posts on collective action events or edge cases (again split equally between pro- and anti-government). Thus, 600 posts submitted relate to non–collective action events, and 600 relate to collective action events or edge cases. We have in total four collective events and two edge cases, and so 400 posts focused on collective action events and 200 on edge cases.
26. J. Crandall *et al*., Chat program censorship and surveillance in China: Tracking TOM-Skype and Sina UC. *First Monday* **18** (no. 7) (July 2013). doi: 10.5210/fm.v18i7.4628
27. J. Fallows, The connection has been reset. *Atlantic* (March 2008); www.theatlantic.com/magazine/archive/2008/03/-the-connection-has-been-reset/306650.
28. K. Imai, L. Keele, D. Tingley, T. Yamamoto, Unpacking the black box of causality: Learning about causal mechanisms from experimental and observational studies. *Am. Pol. Sci. Rev.* **105**, 765–789 (2011). doi: 10.1017/S0003055411000414
29. J. Pearl, Direct and indirect effects. In *Proceedings of the Seventeenth Conference on Uncertainty in Artificial Intelligence* (Morgan Kaufmann, San Francisco, 2001), pp. 411–420; https://dslpitt.org/uai/papers/01/p411-pearl.pdf.
30. O. Blanchard, A. Shleifer, "Federalism with and without political centralization: China versus Russia" (National Bureau of Economic Research, Cambridge, MA, 2000); www.nber.org/papers/w7616.
31. S. Heilmann, E. Perry, *Mao's Invisible Hand: The Political Foundations of Adaptive Governance in China* (Harvard University Asia Center, Cambridge, MA, 2011).
32. Y. Qian, G. Roland, Federalism and the soft budget constraint. *Am. Econ. Rev.* **88**, 1143–1162 (1998).
33. Y. Qian, B. R. Weingast, Federalism as a commitment to perserving market incentives. *J. Econ. Perspect.* **11**, 83–92 (1997). doi: 10.1257/jep.11.4.83
34. G. Egorov, K. Sonin, Dictators and their viziers: Endogenizing the loyalty-competence trade-off. *J. Eur. Econ. Assoc.* **9**, 903–930 (2011). doi: 10.1111/j.1542-4774.2011.01033.x
35. G. Salton, *Automatic Text Processing: The Transformation, Analysis, and Retrieval of Information by Computer* (Addison-Wesley, Reading, MA, 1988).
36. D. Kelleher, S. Luz, Automatic hypertext keyphrase detection. In *Proceedings of the 19th International Joint Conference on Artificial Intelligence* (Erlbaum, Hillsdale, NJ, 2005), pp. 1608–1609.
37. For examples, see (*44*).
38. For news coverage of the protests, see (*45*–*48*).
39. D. Hopkins, G. King, A method of automated nonparametric content analysis for social science. *Am. J. Pol. Sci.* **54**, 229–247 (2010). doi: 10.1111/j.1540-5907.2009.00428.x
40. K. Hong, China's Twitter-like Sina Weibo service now has over 50 million active users per day. *The Next Web*, 13 August 2013; http://tnw.co/1fdNFPS.
41. S. Millward, Tencent Weibo, the 'other weibo' that nobody cares about, reaches 540 million users. *Tech in Asia*, 22 January 2013. http://bit.ly/1byjSNW.
42. K. W. Fu, M. Chau, Reality check for the Chinese microblog space: A random sampling approach. *PLOS ONE* **8**, e58356 (2013). doi: 10.1371/journal.pone.0058356; pmid: 23520502
43. J. Q. Ng, Weibo keyword un-blocking is not a victory against censorship. *Tea Leaf Nation*, 21 June 2013; http://bit.ly/1kfqNBC.
44. P. Barefoot, "Principal, get a room with me, spare the schoolchildren!" *China Smack*, 31 May 2013; http://j.mp/19yuv7E.
45. Al-Jazeera, Democracy push as Hong Kong marks handover. 1 July 2013; http://j.mp/145Jvpp.
46. S. Lee, K. Wong, Hong Kong protests to underscore Leung's record-low appeal. *Bloomberg BusinessWeek*, 28 June 2013; http://j.mp/13r3v7v.
47. J. Ngo, July 1 protest is Hong Kong's taste of democracy. *South China Morning Post*, 30 June 2013; http://j.mp/15PcwBt.
48. C. Yung, Annual Hong Kong protest to focus ire on leader. *Wall Street Journal*, 28 June 2013; http://j.mp/13FJB3w.
49. G. King, J. Pan, M. E. Roberts, Replication Data for: Reverse Engineering Chinese Censorship: Randomized Experimentation and Participant Observation (2014). doi: 10.7910/DVN/26212

ACKNOWLEDGMENTS

For helpful advice, we thank P. Bol, S. Chestnut, P. Gries, Y. Herrera, H. Huang, I. Johnston, S. Shirk, D. Tingley, and participants in a panel at the American Political Science Association meeting, 31 August 2013, and at the Midwest Political Science Association meeting, 3 April 2014. For expert research assistance over many months, we are tremendously appreciative of the efforts and insights of F. Chen, W. Cheng, A. Jiang, A. Jin, F. Meng, C. Li, H. Liu, J. Sun, H. Waight, A. Xiang, L.-S. Xu, M. Yu, and a large number of others whom we shall leave anonymous. We thank Crimson Hexagon Inc. for help with data. See (*49*) for replication data and information.

SUPPLEMENTARY MATERIALS

www.sciencemag.org/content/345/6199/1251722/suppl/DC1
Materials and Methods
Figs. S1 to S7
References (*50*, *51*)

3 February 2014; accepted 2 July 2014
10.1126/science.1251722

RESEARCH ARTICLES

REEF ECOLOGY

Chemically mediated behavior of recruiting corals and fishes: A tipping point that may limit reef recovery

Danielle L Dixson,[1] David Abrego,[2] Mark E Hay[1]*

Coral reefs are in global decline, converting from dominance by coral to dominance by seaweed. Once seaweeds become abundant, coral recovery is suppressed unless herbivores return to remove seaweeds, and corals then recruit. Variance in the recovery of fishes and corals is not well understood. We show that juveniles of both corals and fishes are repelled by chemical cues from fished, seaweed-dominated reefs but attracted to cues from coral-dominated areas where fishing is prohibited. Chemical cues of specific seaweeds from degraded reefs repulsed recruits, and cues from specific corals that are typical of healthy reefs attracted recruits. Juveniles were present at but behaviorally avoided recruiting to degraded reefs dominated by seaweeds. For recovery, degraded reefs may need to be managed to produce cues that attract, rather than repel, recruiting corals and fishes.

Corals are foundation species, creating the biogenic matrix on which reef structure, function, and biodiversity depend (*1*, *2*). However, corals are in decline. Coral cover has declined by 80% in the Caribbean and 50% throughout the tropical Pacific (*3*, *4*). As corals decline, species-rich and topographically complex reefs transition to flattened, species-poor beds of seaweeds and coral rubble with compromised ecosystem function (*1*, *5*). Once degraded, reefs can recover if the right mix of herbivores recolonizes them to remove seaweeds and facilitate corals (*5*–*9*), but this process sometimes fails because of poorly understood feedback mechanisms that facilitate seaweeds and suppress corals (*10*–*13*).

Adequate coral cover is essential for producing the topographic complexity that supports reef fishes (*2*, *7*, *11*). Loss of corals leads to loss of reef fishes (*2*). Loss of reef fishes leads to coral decline, because intact fish communities aid coral recovery after coral loss to bleaching, predation, or other disturbances (*5*, *7*, *8*). Loss of both fishes and corals is catastrophic for coral reefs, which make up <0.1% of oceanic areas but support 32 of 34 animal phyla (rainforests support 9); are valued at $29 billion/year for fisheries, tourism, and other uses; and provide critical protein to hundreds of millions of humans (*14*).

Reef decline is driven by many factors, including overfishing, climate change, disease, pollution, and predation (*5*, *7*), but stresses affecting adult corals are better understood than are processes preventing juvenile recruitment (*10*–*12*). Some seaweeds chemically reduce the recruitment and survival of corals for centimeters around seaweed perimeters (*15*), possibly selecting for coral larvae that use chemical cues to reject seaweed-dominated reefs. If so, recovery could be suppressed by larval behavior, rather than just post-recruitment mortality. Understanding these chemical cues could be critical to developing effective conservation strategies (*7*, *11*), such as protecting producers of positive cues or managing to remove producers of negative cues.

If coral larvae respond to chemical cues of reef quality, they might avoid degraded reefs, thus promoting the stability of seaweed-dominated reefs and preventing coral recovery. The nervous systems of planula larvae display a high level of histological, cytological, and biochemical complexity (*16*), suggesting that such responses are possible.

We tested the potential role of chemical cues from healthy versus degraded reefs in coral and fish recruitment, using pairs of no-take marine protected areas (MPAs) and adjacent non-MPAs associated with three villages along the coast of Viti Levu, Fiji (fig. S1). Coral cover on hard substrates in the MPAs was 38 to 56% (versus 4 to 16% in non-MPAs), seaweed cover on hard substrates was 1 to 2% (versus 49 to 91% in non-MPAs), and herbivorous fish biomass was 660 to 1615% greater in the MPAs than in fished areas (*9*). Although we used MPAs and non-MPAs, these reefs may represent functioning coral-dominated versus degraded seaweed-dominated reefs, regardless of the factors creating these divergent communities. Our paired MPAs and degraded reefs were adjacent, on the same continuous reef flat; were oriented similarly; and were exposed to the same oceanic waters, storm swell, and presumably other physical conditions (fig. S1). Our non-MPA reefs have higher seaweed and lower coral cover than many nonprotected reefs, but some unprotected reefs in the Caribbean (*5*), Red Sea (*17*), and Indian Ocean (*18*) are similar in seaweed and coral cover, and numerous reefs are trending toward the conditions on our non-MPA reefs (*3*, *4*). Thus, the contrasts of juvenile fish and coral behavior toward the divergent reef states we investigated may be informative about some present and numerous future reefs.

Responses of coral larvae

Coral larvae discriminate among environments, as shown by their behavior in response to different waters (*19*), substrates (*20*), settlement-inducing crustose coralline algae (*21*), or biofilms (*22*). Additionally, some seaweeds chemically suppress the settlement and survival of coral larvae within centimeters of their thalli (*15*). The low survival of coral recruits at sites occupied by certain competitors (*23*) suggests that the avoidance of specific competitors by settling larvae could be adaptive. If so, chemically mediated larval behavior could affect recruitment densities and reef resilience.

To test this possibility, we exposed larvae of corals within the genus *Acropora* to cues from divergent environments. Acroporid corals are major providers of topographic complexity, which is negatively related to algal cover and positively related to fish density, biomass, diversity, and coral recovery after disturbances (*2*).

We obtained larvae from *Acropora millepora*, *A. nasuta*, and *A. tenuis* by holding four fertile colonies of each species in separate pools, collecting gametes, facilitating fertilization, collecting embryos, and raising these to competent planula after 6 to 7 days. We evaluated planula preferences for water collected from the centers of MPA versus non-MPA sites using two-channel Atema flumes (*24*), offering organisms a pairwise choice of each water source flowing at 4.2 mm s^{-1}. A planula was pipetted into the downstream center of the flume, where it swam toward its preferred water source. A 2-min acclimation period was followed by a 3-min testing period in which the planula's position was recorded at 5-s intervals. After 3 min, the planula was removed for 1 min, the water was flushed, the water sources were exchanged from one side to the other, and the test was repeated to ensure that preferences were not biased for one side of the chamber.

All *Acropora* larvae expressed a 558 to 561% preference for MPA over non-MPA water ($P < 0.001$, Fig. 1A); this was consistent across all pairs of MPA versus non-MPA reefs [$P > 0.9$ for among-site contrasts, factorial analysis of variance (ANOVA); table S1]. Thus, their preference was for healthy reefs within MPA sites and was not a location effect. We therefore pooled data for all MPAs versus non-MPAs for subsequent comparisons ($n = 60$ per species, Fig. 1).

To identify the sources of water-borne cues, we hypothesized that larvae might cue to corals and crustose coralline algae (CCA) from healthy reefs

[1]School of Biology, Georgia Institute of Technology, 310 Ferst Drive, Atlanta, GA 30332, USA. [2]Department of Natural Sciences and Public Health, Zayed University, Abu Dhabi, United Arab Emirates.
*Corresponding author. E-mail: mark.hay@biology.gatech.edu

or be repelled by seaweeds from degraded reefs. We tested these hypotheses by holding upright seaweeds (20 g), CCA (50 g), or corals (100 g) in 10 liters of MPA- or non-MPA–sourced water for 1 hour (the variable masses were due to density differences among species) and testing the effects of leached cues on the preferences of *A. tenuis* larvae in flumes. Cues from conspecifics were 389% more attractive than cues from a congeneric (*A. millepora*), but cues from a mix of five corals (*Porites cylindrica, Pocillipora damicornis, Montipora digitata, Merulina scabricula, and A. formosa*) were 570% more attractive than an equal mass of the conspecific alone (Fig. 1A). Adding cues from the CCA *Hydrolithon reinboldii* to MPA water increased larval attraction by 800%; the same magnitude of CCA cue added to non-MPA water increased preference by only 184% and did not fully counter larval avoidance of non-MPA water (Fig. 1A). Chemical cues from the common seaweeds *Padina gymnospora, Sargassum polycystum*, and *Galaxaura filamentosa* decreased larval attraction by 28, 81, and 86%, respectively ($P < 0.001$ for all contrasts, Fig. 1A).

In the above assays, larvae responded to cues dissolved in the water. However, known seaweed allelochemicals are lipophilic molecules on algal surfaces that damage corals after contact (*25*, *26*). Using larvae of *A. tenuis*, we evaluated the possibility that such lipids could deter coral settlement if transferred to benthic surfaces. We brushed settlement tiles with five strokes of either CCA, *Padina*, *Galaxaura*, or *Sargassum* (mimicking contact via wave motion) and compared settlement on these tiles to settlement on control tiles brushed with inert, plastic seaweeds. Paired treatment and control tiles were placed into aquaria ($n = 6$), 10 competent larvae were added to each, and larval settlement was monitored at 2, 6, 12, and 24 hours.

Rubbing tiles with CCA increased settlement by 1600% as compared to control tiles (Fig. 1B), with 70% of all larvae settling within 2 hours and 90% within 24 hours. In contrast, rubbing tiles with *Galaxaura*, which produces allelopathic loliolide derivatives (*25*), resulted in 0% settlement. Rubbing tiles with *Sargassum* produced no differential effect between treatment and control tiles, but at 12 and 24 hours, 62% [±4.0 SE] and 48% [±3.1] of larvae were still swimming and had delayed settling. Rubbing tiles with *Padina* slightly increased settlement on treatment versus control tiles, but at 12 hours, 47% (±3.3) of larvae were still swimming. The presence of cues from *Sargassum*, *Padina*, or *Galaxaura* suppressed settlement in general ($F_{(3, 16)} = 7.58$, $P = 0.002$, repeated measures ANOVA); after 24 hours in aquaria, only 10% (±0.0) of larvae in CCA treatments had not settled, compared to 33% (±4.2) for treatment with *Padina*, 31% (±6.5) for *Galaxaura*, and 48% (±3.1) for *Sargassum* (Fig. 1B and table S2).

To see whether attraction to cues from MPAs, corals, and CCA, and repulsion by cues from non-MPAs and upright seaweeds, occurred in the field, we established 18 2 × 2 m benthic plots in MPA and non-MPA areas at two villages. From 9 of the 18 quadrats at each site, we removed all upright seaweeds at 2- to 4-week intervals and monitored coral recruits to the natural substrate monthly during the week of the new moon through the November–February recruitment pulse. Juvenile corals fluoresce under black light, so surveys were conducted nocturnally using an ultraviolet filter and black light.

We also erected four T-shaped poles holding eight 15 × 15 cm settling tiles 50 cm above the benthos. Two poles adjoined seaweed removal

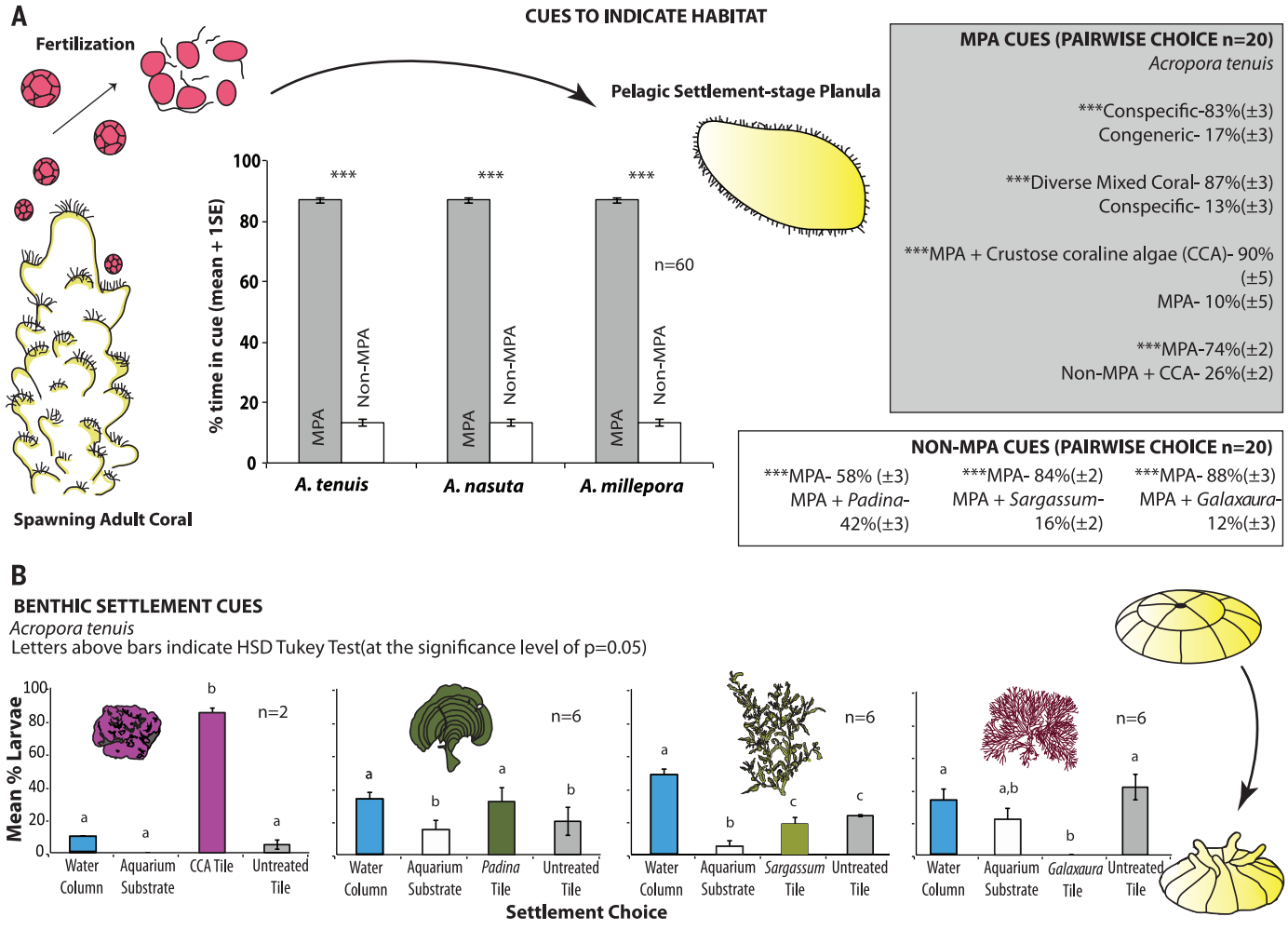

Fig. 1. Influence of chemical cues on coral larvae. (**A**) Larval tracking in a flume and (**B**) larval behavior when offered differently treated substrates. *** indicates $P < 0.001$ via the Kolmogorov-Smirnov test. Letters above bars indicate significant groupings by ANOVA and post-hoc Tukey test at 24 hours.

plots and two adjoined control plots at each location. These tiles evaluated settlement above the benthic boundary layer, where chemical cues from benthic organisms might be reduced. After 6 months, tiles were collected and examined for recruits.

For both the natural benthos and the elevated tiles, there were no effects of village or seaweed removal (table S3). Thus the same patterns occurred in both locations, and larvae were reacting to chemical cues from areas larger than our 4-m^2 removal areas; we therefore pooled results by MPA and non-MPA and ignored location and removal treatment.

Protection status (MPA or non-MPA) had a significant, but opposite, effect on settlement in the field ($P < 0.001$). Corals settled onto the benthos in the MPAs (1.0 ± 0.1/m^2; mean ± 1 SE) but not in the non-MPAs (0 ± 0/m^2; $P < 0.0001$; factorial ANOVA). Settlement onto tiles deployed above the benthos was 4.75 ± 0.4 recruits per tile array (~13/m^2) in the non-MPAs but 0 ± 0 per array in the MPAs ($P < 0.0001$, factorial ANOVA). Thus, larvae occurred in both areas, but in the MPAs they recruited exclusively to the benthos, whereas in the non-MPAs they recruited exclusively to the elevated tiles.

Field recruitment of coral larvae was consistent with laboratory assays. In the non-MPAs where chemical cues from seaweeds would be strong, larvae never settled on the benthos despite occurring there and being competent—as evidenced by their settlement on elevated tiles. In contrast, within the MPA where positive cues from corals and CCA would be abundant, settlement to the benthos was common, and larvae completely avoided the raised tiles. These opposing patterns indicate that larvae make nuanced decisions regarding the relative attractiveness of substrata in differing environmental contexts and act on these complex decisions despite flow and turbulence in the field. These divergent patterns of settlement could be generated by positive cues in MPAs causing larvae to swim down to explore the bottom in search of additional contact cues (such as CCA) and negative cues in non-MPAs causing larvae to avoid swimming down (thus avoiding the benthos in the non-MPAs), but possibly contacting CCA or stimulatory biofilms on the raised tiles and these being sufficient to induce settlement in this otherwise unappealing environment.

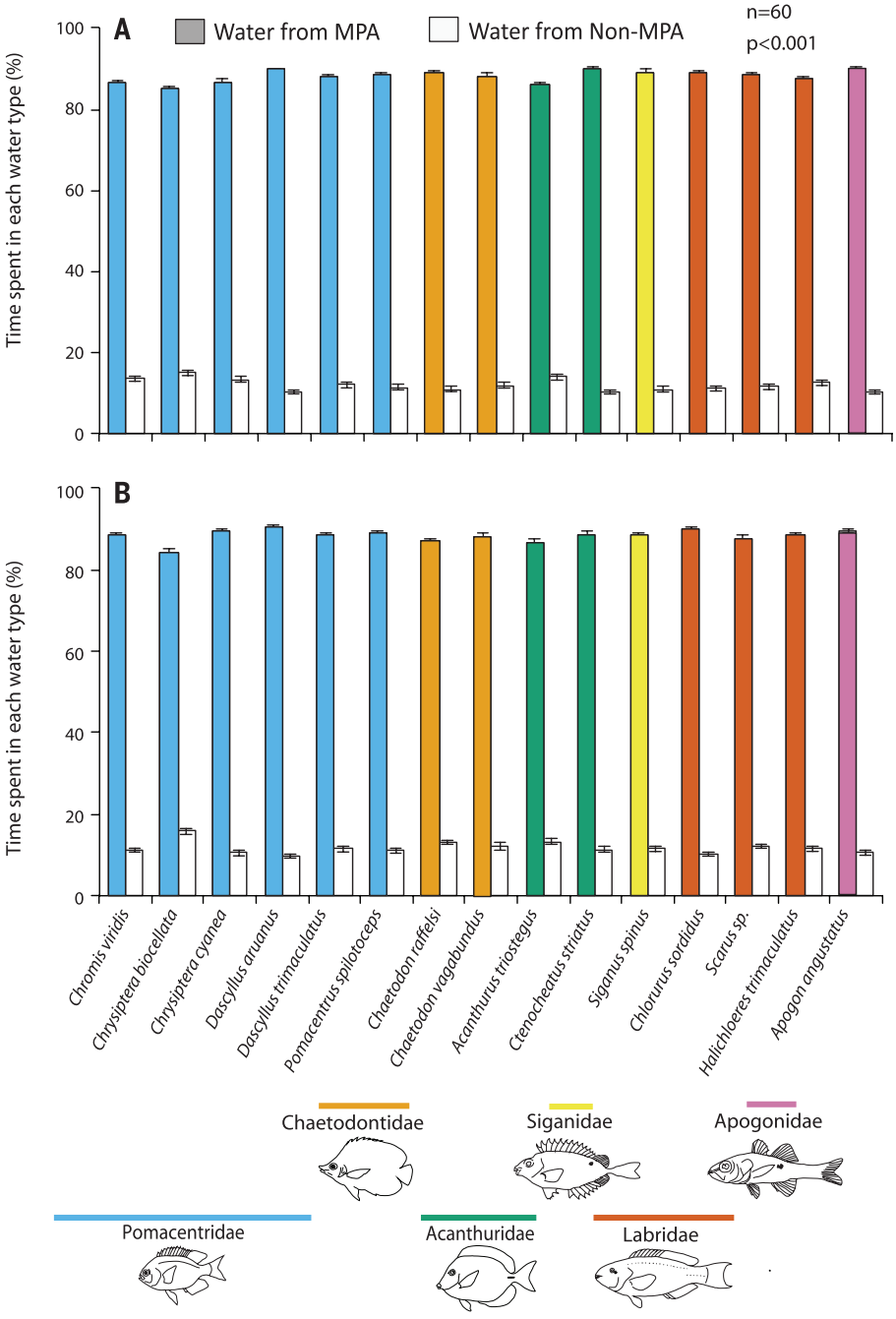

Fig. 2. Attraction of fishes to waters from MPA versus non-MPA areas as a function of fish collection site. (**A**) MPAs, (**B**) Non-MPAs. $n = 60$ independent juvenile fish for each bar. Families are grouped by color below species names. $P < 0.001$ for all contrasts.

Responses of juvenile reef fishes

Given that juvenile fishes respond to chemical cues from predators, conspecifics, their home reef, and reefs differing in community composition or proximity to terrestrial vegetation (*27*–*30*), juveniles might also respond to chemical cues from coral- versus seaweed-dominated reefs. If so, this could compromise healthy reefs as sources for larval export and help explain why seaweed-dominated reefs may fail to recover (*5*, *7*, *10*, *11*).

Using the paired MPAs and non-MPAs described above, we asked (i) whether juvenile fishes were differentially attracted to chemical cues from coral-dominated MPAs versus seaweed-dominated non-MPAs, (ii) whether attraction varied among fish trophic groups, (iii) whether fishes used chemical cues from sessile species to assess habitat desirability, and (iv) whether densities of new recruits in the field were consistent with predictions from juvenile behavior in flumes.

To test juvenile attraction to MPAs versus non-MPAs, we used 20 recently settled juveniles of each of 15 reef fish species (see Fig. 2 for species) from each MPA and adjacent non-MPA at the three villages. We tested recently settled juveniles instead of larvae because we could acquire more species (yields from light traps were taxonomically limited). Attraction to waters from MPAs versus paired non-MPAs was assessed using flumes as described for corals, except that fish observations were for 2 rather than 3 min because their greater mobility produced faster reactions. Assay species represented six families, including six planktivores (Pomacentrids), two coralivore/invertivores (Chaetodonts), five herbivores (Acanthurids, Siganids, and Labrids), and two predators (a Labrid and an Apogonid; see Fig. 2).

Regardless of species, family, or trophic group, each of the 15 species showed a 432 to 844% preference for water from MPAs versus non-MPAs ($P < 0.001$ for all species; Fig. 2). Juveniles collected from MPAs and non-MPAs exhibited equivalent preferences ($P > 0.10$ for all species), indicating no effect of postsettlement experience and suggesting that these preferences are innate. Additionally, responses to MPA versus non-MPA waters from the "home" MPA did not differ from responses when offered this choice of waters from other MPAs ($P > 0.10$ for all species; table S4).

To evaluate habitat cues, common seaweeds or corals were added to 10 liters of water (50 g of coral or 10 g of seaweed) for 1 hour, the organisms were then removed, and flume assays were run using this water versus equivalent water without the cues (as in the coral assays). Cues from the common seaweed *S. polycystum* suppressed attraction to MPA water by 65 to 86% (Fig. 3A, $P < 0.001$ for all species). In contrast, cues of the common coral *Acropora nasuta* enhanced attraction to non-MPA water by 107 to 343% for all 15 fishes (Fig, 3B, $P < 0.001$).

We then assessed variance in response to cues from different corals and seaweeds. We hypothesized that the corals most susceptible to stresses would be reliable indicators of healthy reefs, because they would be among the first lost from stressed reefs, and that seaweeds abundant on stressed reefs would be reliable indicators of reef degradation. We selected *Acropora* corals as appropriate sentinels, because they commonly bleach, are favored by coral predators, and are strongly affected by algal competition (*25*, *31*, *32*). In contrast, *Porites* corals are more resistant to disturbances (*25*, *32*), and *Pocillopora* corals are susceptible to stresses but often recolonize rapidly after disturbances. These latter genera are found on both healthy and degraded reefs, making them poor predictors of reef quality. Consistent with these hypotheses, chemical cues from *A. millepora* or *A. formosa* were preferred by 313 to 1036% over those from *Porites cylindrica* or *Pocillipora damicornis* (Fig. 4, $P < 0.001$ for all species).

Fishes' responses to different seaweeds also varied. Fishes avoided water containing cues from the seaweeds *S. polycystum* or *Turbinaria conoides*, which are abundant on degraded reefs (*6*, *12*, *33*), as compared to water containing cues from *Chlorodesmis fastigiata* or *Hypnea pannosa*, which occur at low abundance on both healthy and degraded reefs (Fig. 4, $P < 0.001$ for all species).

Fishes use visual, auditory, and olfactory cues when selecting settlement sites, but chemical cues should be important because they can extend over long distances, provide directional information, and provide a recent history of the site (*24*, *28*). All 15 fishes distinguished between healthy versus degraded habitats by swimming toward coral and away from seaweed chemical cues (Fig. 3), but this behavior was nuanced (Fig. 4). The stress-sensitive acroporid corals were more attractive than the stress-tolerant *Porites* or the weedy *Pocillopora*, and common seaweeds that

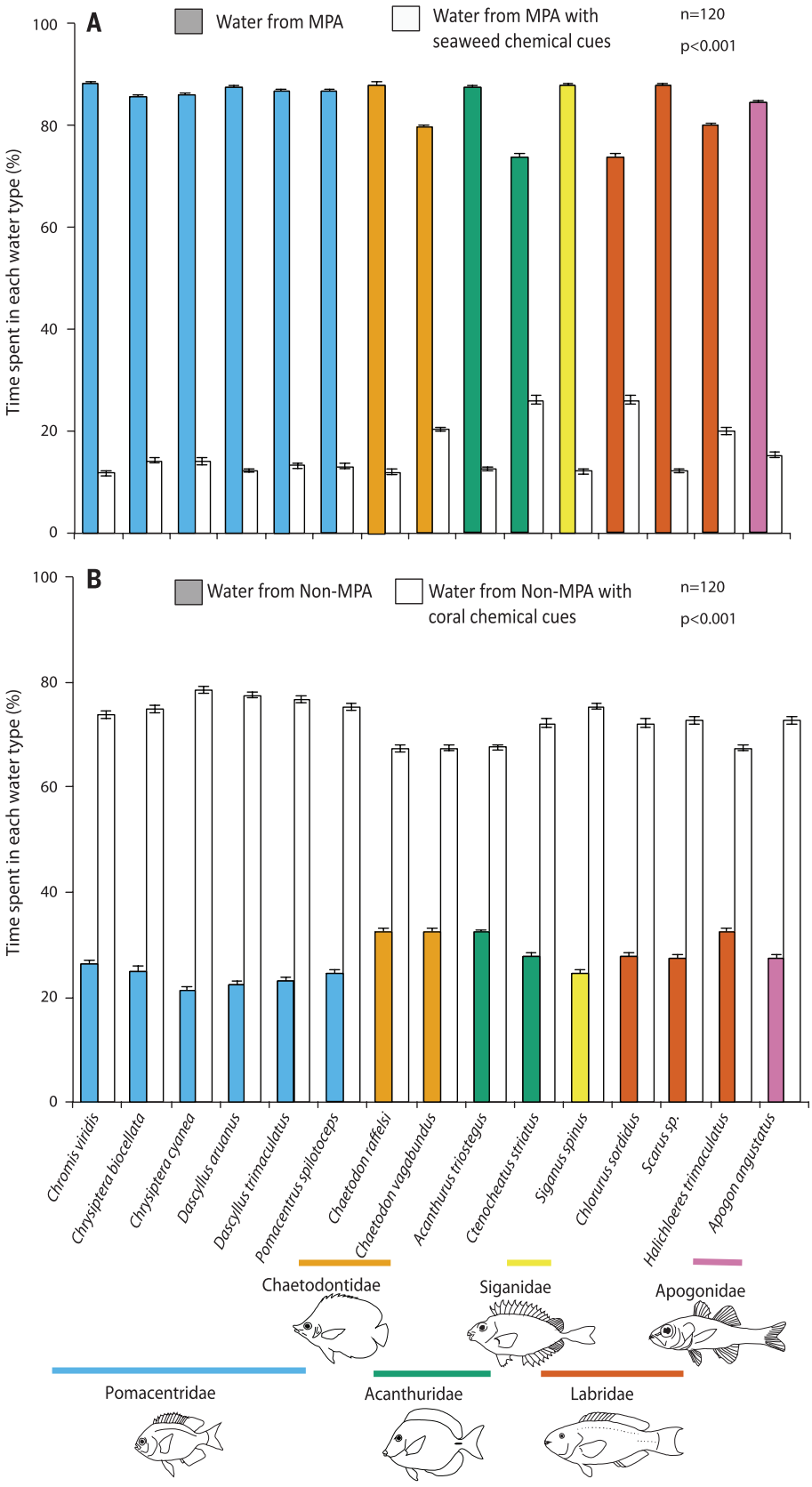

Fig. 3. Effects of seaweed or coral chemical cues on the behavior of recently settled fishes. (**A**) Effects of the seaweed *S. polycystum* and (**B**) the coral *A. nasuta*. $n = 120$ independent juvenile fish for each bar; $P < 0.001$ for all contrasts.

dominate herbivore-impoverished reefs (*Sargassum* and *Turbinaria*) were more deterrent than uncommon seaweeds such as *Chlorodesmis* and *Hypnea* that occupy both healthy and degraded reefs (Fig. 4, $P < 0.001$ for all contrasts). The behavior was not biased by postsettlement experiences. Recently settled juveniles from both MPAs and non-MPAs exhibited an equally strong preference for water from coral-dominated as opposed to seaweed-dominated reefs and for specific corals and seaweeds. These preferences appear innate, could strongly affect settlement choice, and should be included in models of dispersal and connectivity (*34*).

Surveys of recent recruits in each village's MPA and non-MPA during recruitment season documented a 537 to 794% higher density and 80 to 344% greater diversity of recruits on the MPAs versus adjacent fished reefs (Fig. 5). These density differences parallel the degree of preference we found for chemical cues from MPAs in laboratory assays. Additionally, because predators of recruits were 186 to 228% more dense in the MPAs (Fig. 5C), enhanced recruitment in MPAs was not associated with having fewer predators there. However, if predators in non-MPAs were more effective, then postsettlement predation could confound patterns generated by habitat choice. We tested this possibility by building 30 rubble habitats ~30 cm tall by 30 cm in diameter in each of two villages' MPAs and non-MPAs, stocking each with five marked juveniles of the abundant damselfishes *Chromis viridis* and *Dascyllus aruanus* and monitoring survival each morning, noon, and evening for 3 days. Fifteen equivalent structures were stocked and individually enclosed in 1-cm wire mesh in each location to exclude predators, controlling for migration or other losses unrelated to predation. Survival and retention in cage controls was 100% across all sites. Mortality on uncaged structures was ~20% over 3 days in all sites and did not differ between MPAs and non-MPAs ($P = 0.67$ and 0.77 for *C. viridis* and *D. aruanus*, respectively). Thus, if predation on small juveniles is similar to predation on new recruits, then based on our results, postrecruitment predation appears similar between MPAs and non-MPAs, suggesting that differential recruitment may explain the much greater density of juveniles in the MPAs.

Conclusion

MPAs are established to protect contained communities and to provide larvae for export to aid

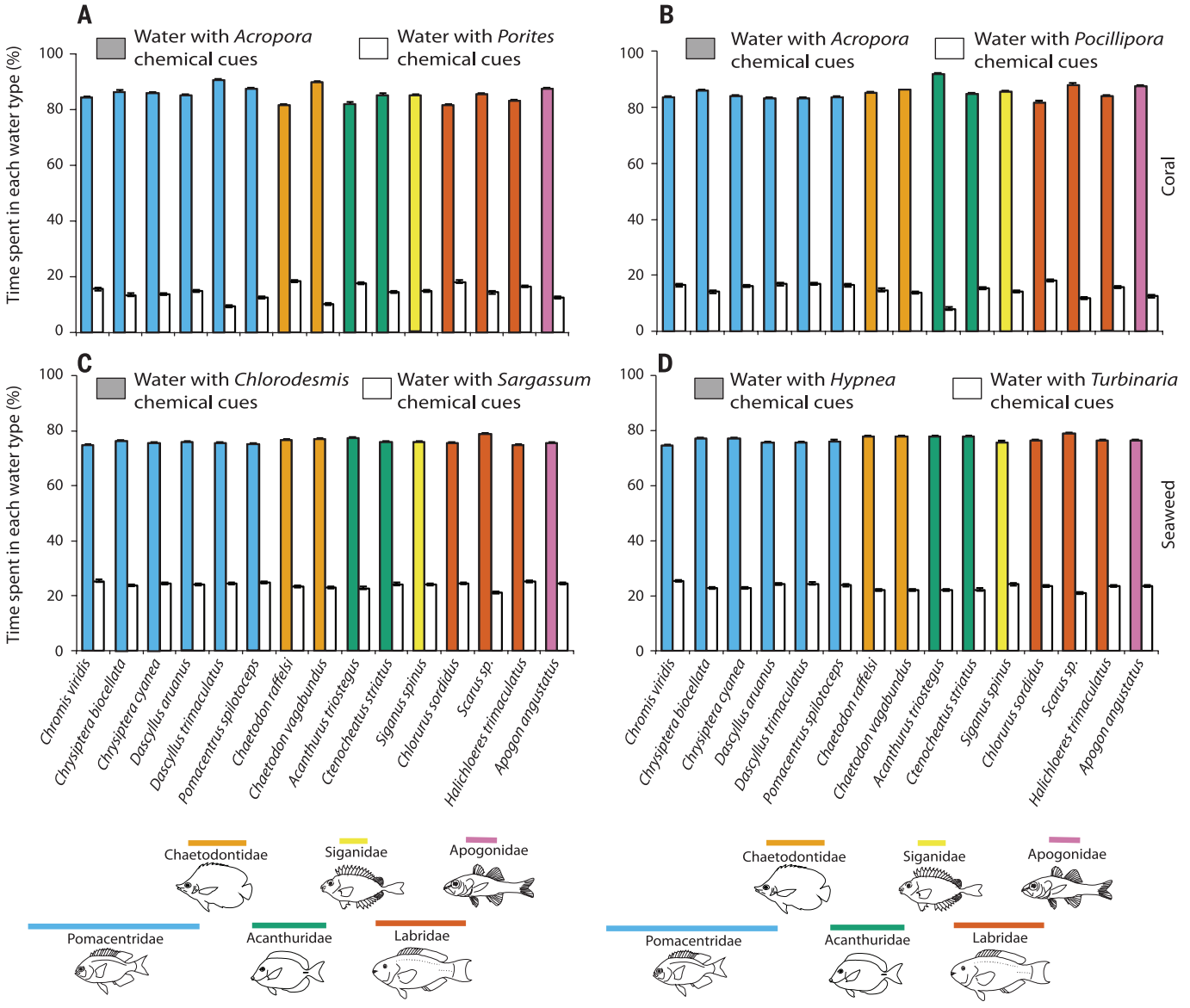

Fig. 4. Effects of chemical cues from different corals or seaweeds on fish behavior. (**A**) *A. millepora* versus *Porites cylindrica*, (**B**) *A. formosa* versus *Pocillipora damicornis*, (**C**) *Chlorodesmis fastigiata* versus *S. polycystum*, or (**D**) *Hypnea pannosa* versus *Turbinaria conoides*. $n = 120$ independent juvenile fish for each bar; $P < 0.001$ for all contrasts.

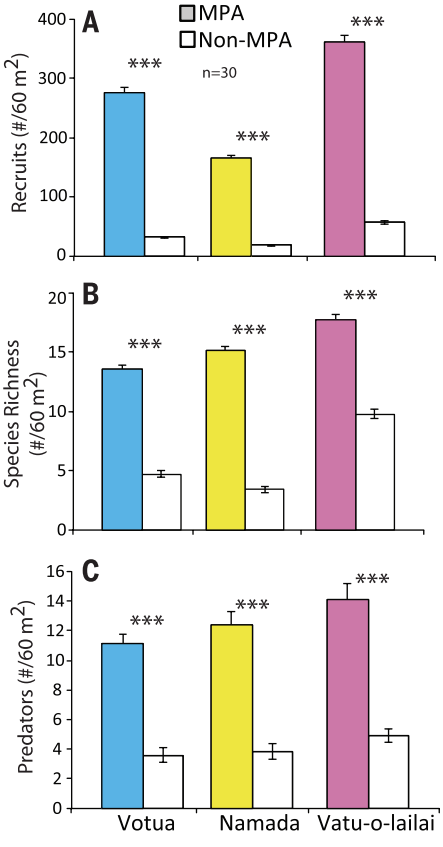

Fig. 5. Density and species richness of fish recruits, and density of predators, in MPAs and non-MPAs. (**A**) Density (±SE) and (**B**) species richness of recruits. (**C**) Density of predators. n = 30 transect per site. $P < 0.001$ for all contrasts.

the recovery of more-degraded habitats (*34*). However, export to degraded reefs will be constrained if recruits avoid chemical cues from degraded reefs. In some locations, export occurs (*35*), but in other areas, there is minimal connectivity, even between protected and exploited populations separated by small distances (*36*). These divergent outcomes could occur if intact reefs export larvae to similar communities but not to degraded, seaweed-dominated communities. The protected and fished areas we studied differ in coral cover, seaweed cover, herbivory rates, and biomass of herbivorous fishes (*9*). Thus, organisms settling only 100 m apart experience dramatically different environments. Our findings suggest that once degradation passes some critical but as yet undetermined threshold, recruit behavior may constrain the value of healthy reefs as larval sources for populations in degraded habitats.

To produce the desired connections between healthy reefs as a source of larvae and degraded reefs as targeted settlement sites where recruitment can promote reef resilience, managers will have to suppress the chemical barrier produced by seaweeds and enhance the chemical "call" of corals and CCA. A promising strategy could be to reduce the harvest of critical species of herbivorous fishes beyond MPA borders. Feeding by specific mixes of these fishes can remove seaweeds, enhance CCA, enhance corals (*6*, *9*, *12*, *33*), and replace chemical cues of degradation with chemical stimulants for recruitment.

REFERENCES AND NOTES

1. L. Alvarez-Filip, N. K. Dulvy, J. A. Gill, I. M. Côté, A. R. Watkinson, *Proc. Biol. Sci.* **276**, 3019–3025 (2009).
2. N. A. J. Graham, K. L. Nash, *Coral Reefs* **32**, 315–326 (2013).
3. T. A. Gardner, I. M. Côté, J. A. Gill, A. Grant, A. R. Watkinson, *Science* **301**, 958–960 (2003).
4. J. F. Bruno, E. R. Selig, *PLOS ONE* **2**, e711 (2007).
5. T. P. Hughes, N. A. J. Graham, J. B. C. Jackson, P. J. Mumby, R. S. Steneck, *Trends Ecol. Evol.* **25**, 633–642 (2010).
6. D. E. Burkepile, M. E. Hay, *Proc. Natl. Acad. Sci. U.S.A.* **105**, 16201–16206 (2008).
7. P. J. Mumby, R. S. Steneck, *Trends Ecol. Evol.* **23**, 555–563 (2008).
8. A. J. Cheal *et al.*, *Coral Reefs* **29**, 1005–1015 (2010).
9. D. B. Rasher, A. S. Hoey, M. E. Hay, *Ecology* **94**, 1347–1358 (2013).
10. S. K. Wilson *et al.*, *Conserv. Biol.* **26**, 995–1004 (2012).
11. M. Nyström *et al.*, *Ecosyst.* **15**, 695–710 (2012).
12. T. P. Hughes *et al.*, *Curr. Biol.* **17**, 360–365 (2007).
13. A. J. Cheal, M. Emslie, M. A. MacNeil, I. Miller, H. Sweatman, *Ecol. Appl.* **23**, 174–188 (2013).
14. H. Cesar, L. Burke, L. Pet-Soede, *The Economics of World Wide Coral Reef Degradation* (Cesar Environmental Economics Consulting, Netherlands, 2003).
15. I. B. Kuffner, V. J. Paul, *Coral Reefs* **23**, 455–458 (2004).
16. H. Watanabe, T. Fujisawa, T. W. Holstein, *Dev. Growth Differ.* **51**, 167–183 (2009).
17. Y. Benayahu, Y. Loya, *Bull. Mar. Sci.* **31**, 514–522 (1981).
18. T. R. McClanahan, R. Arthur, *Ecol. Appl.* **11**, 559–569 (2001).
19. D. F. Gleason, B. S. Danilowicz, C. J. Nolan, *Coral Reefs* **28**, 549–554 (2009).
20. Y. Golbuu, R. H. Richmond, *Mar. Biol.* **152**, 639–644 (2007).
21. L. Harrington, K. Fabricius, G. De'ath, A. Negri, *Ecology* **85**, 3428–3437 (2004).
22. J. Tebben *et al.*, *PLOS ONE* **6**, e19082 (2011).
23. S. N. Arnold, R. S. Steneck, *PLOS ONE* **6**, e28681 (2011).
24. J. Atema, M. J. Kingsford, G. Gerlach, *Mar. Ecol. Prog. Ser.* **241**, 151–160 (2002).
25. D. B. Rasher, E. P. Stout, S. Engel, J. Kubanek, M. E. Hay, *Proc. Natl. Acad. Sci. U.S.A.* **108**, 17726–17731 (2011).
26. T. D. Andras *et al.*, *J. Chem. Ecol.* **38**, 1203–1214 (2012).
27. D. L. Dixson, M. S. Pratchett, P. L. Munday, *Anim. Behav.* **84**, 45–51 (2012).
28. J. M. Leis, U. Siebeck, D. L. Dixson, *Integr. Comp. Biol.* **51**, 826–843 (2011).
29. D. Lecchini, V. P. Waqalevu, E. Parmentier, C. A. Radford, B. Banaigs, *Mar. Ecol. Prog. Ser.* **475**, 303–307 (2013).
30. G. Gerlach, J. Atema, M. J. Kingsford, K. P. Black, V. Miller-Sims, *Proc. Natl. Acad. Sci. U.S.A.* **104**, 858–863 (2007).
31. A. H. Baird, M. S. Pratchett, A. S. Hoey, Y. Herdiana, S. J. Campbell, *Coral Reefs* **32**, 803–812 (2013).
32. M. S. Pratchett, D. McCowan, J. A. Maynard, S. F. Heron, *PLOS ONE* **8**, e70443 (2013).
33. S. M. Lewis, *Ecol. Monogr.* **56**, 183–200 (1986).
34. P. F. Sale *et al.*, *Trends Ecol. Evol.* **20**, 74–80 (2005).
35. H. B. Harrison *et al.*, *Curr. Biol.* **22**, 1023–1028 (2012).
36. S. R. Palumbi, *Annu. Rev. Environ. Resour.* **29**, 31–68 (2004).

ACKNOWLEDGMENTS

Support was provided by NSF grant OCE-0929119, NIH grant U01-TW007401, and the Teasley Endowment. We thank V. Bonito for assistance and the Fijian government and the Korolevu-i-wai district elders for research permissions. Data are tabulated in the supplementary materials.

SUPPLEMENTARY MATERIALS

www.sciencemag.org/content/345/6199/892/suppl/DC1
Materials and Methods
Fig. S1
Tables S1 to S4
References (*37*–*42*)

21 April 2014; accepted 23 June 2014
10.1126/science.1255057

CLIMATE

Varying planetary heat sink led to global-warming slowdown and acceleration

Xianyao Chen[1,2] and Ka-Kit Tung[2]*

A vacillating global heat sink at intermediate ocean depths is associated with different climate regimes of surface warming under anthropogenic forcing: The latter part of the 20th century saw rapid global warming as more heat stayed near the surface. In the 21st century, surface warming slowed as more heat moved into deeper oceans. In situ and reanalyzed data are used to trace the pathways of ocean heat uptake. In addition to the shallow La Niña–like patterns in the Pacific that were the previous focus, we found that the slowdown is mainly caused by heat transported to deeper layers in the Atlantic and the Southern oceans, initiated by a recurrent salinity anomaly in the subpolar North Atlantic. Cooling periods associated with the latter deeper heat-sequestration mechanism historically lasted 20 to 35 years.

Increasing anthropogenic greenhouse-gas emissions perturb Earth's radiative equilibrium, leading to a persistent imbalance at the top of the atmosphere (TOA) despite some longwave radiative adjustment. Energy balance requires that this TOA imbalance for the planet equal the time rate of increase of the total heat content in the atmosphere-ocean system (*1*). Because the heat capacity of the atmosphere and the cryosphere is small, about 90% of the total heat content is in the form of ocean heat content (OHC) (*2*, *3*). Although the magnitude of the TOA

[1]Key Laboratory of Physical Oceanography, Ocean University of China, Qingdao, China. [2]Department of Applied Mathematics, University of Washington, Seattle, WA, USA.
***Corresponding author. E-mail: ktung@uw.edu**

radiative imbalance is uncertain, variously estimated (*1*, *2*, *4*) at 0.5 to 1.0 W m^{-2}, its sign is believed to be positive on multiyear time scales; therefore, this forced total OHC should be increasing monotonically over longer periods even through the current period of slowed warming (*5*, *6*). In fact, that expectation is verified by observation (red curve in Fig. 1A, which is an approximation to the total OHC). What the extent of radiative forcing does not determine, though, is OHC's vertical distribution, which is controlled by the ocean's internal variability, with each ocean basin having its own characteristic time scale. And it is the vertical distribution that is important in determining the sea-surface temperature (SST), given how voluminous the ocean column is.

The current period of global-warming slowdown coincidently occurred during the era of Argo profiling floats (*7*), which were gradually deployed since the end of the 20th century and achieved near-global coverage of the world's oceans by 2005. Before that milestone, other data types, such as the expendable bathythermographs, were available but contained depth bias. After its recent correction (*8*–*10*), the largest remaining uncertainty, related to the infilling of the undersampled areas, especially in the Southern Ocean, was estimated to be less than 0.05×10^{23} J since 1993 by Lyman and Johnson (*11*) for the global mean. Monthly objectively analyzed subsurface temperature and salinity at 24 levels in the upper 1500 m, called the Ishii data (*10*, *12*, *13*), were used in this study (supplementary materials). Data below 2000 m are very sparse, but are probably not needed for our purpose of revealing recent signals from above.

Observed SST and OHC

The global-mean temperature in the first decade of the 21st century has very little trend (*6*, *14*), in contrast to the latter part of the 20th century, which saw rapid global warming (*2*). Figure 1A shows that, in the 21st century, the global-mean SST warming rate has slowed to almost zero for more than a decade—called a slowdown or hiatus—with short-term El Niño–Southern Oscillation (ENSO)–like variation superimposed on it. Thus, two time scales are seen: a

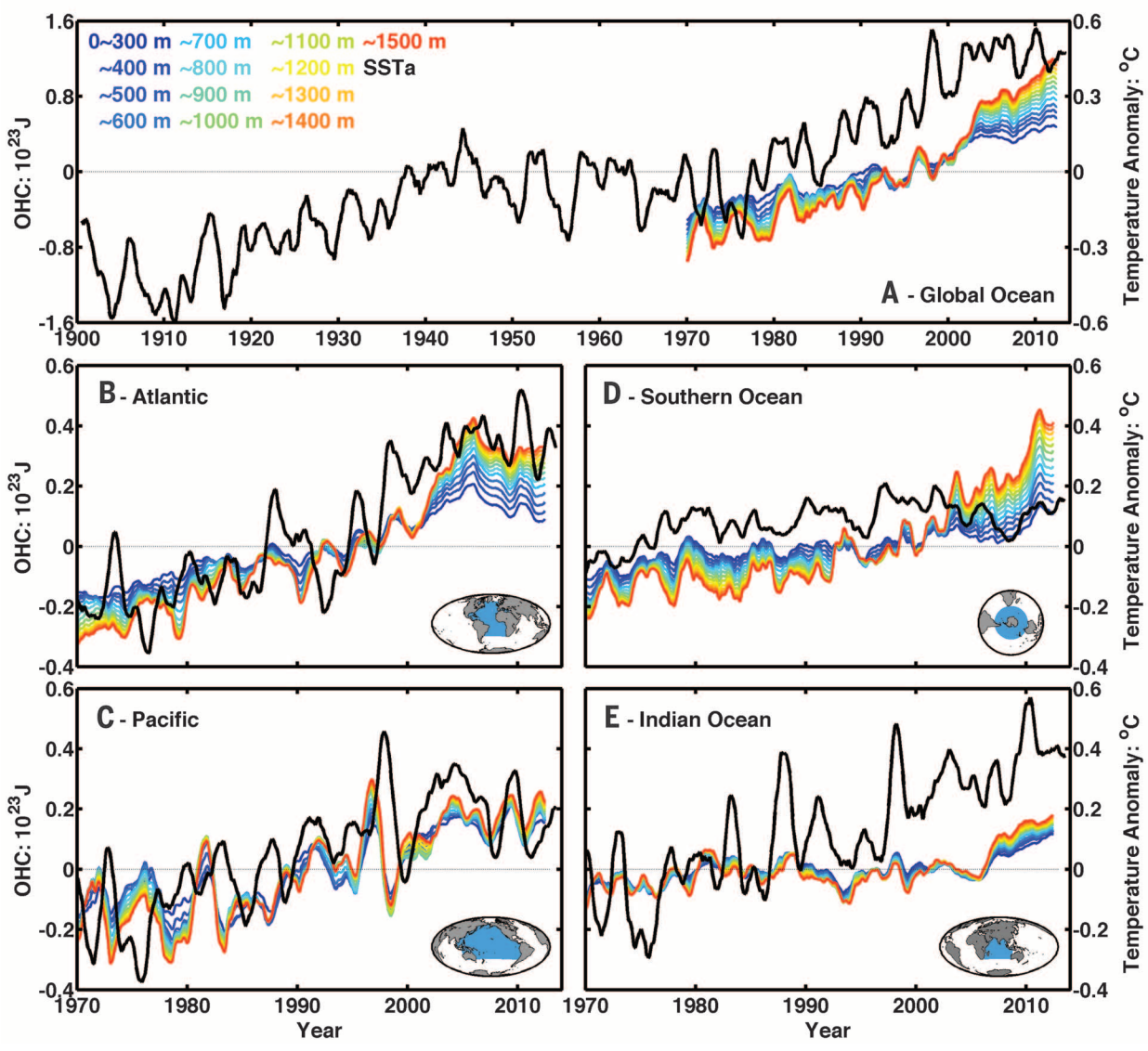

Fig. 1. Integrated OHC. Integrated from the surface to different indicated depths in the global ocean (**A**), the Atlantic (**B**), the Pacific (**C**), the Southern Ocean (**D**), and the Indian Ocean (**E**). Shown is the 12-month running mean deviation from the climatological mean (1970 to 2012) for each layer, so attention should not be focused on the absolute distance between the curves but should be on their relative changes in time. Color lines show the OHC in the left scale, in units of 10^{23} J. The black line shows the mean SST up to 2013. (Insets) The division of the globe into the Pacific, the Atlantic, the Indian Ocean, and the Southern Ocean. Although shown in the figure, data in the earlier decades were not as reliable (see Data and Materials and Methods); the discussion in the text is focused on the better-observed regions and periods.

Fig. 2. In situ data coverage in 5°-by-5° grid as a percentage of full coverage. Shown as background blue color shades at each depth as indicated by the axis on the left. Integrated OHC from the surface to each depth (lines with red to yellow colors) for global (**A**), Atlantic (**B**), and Pacific (**C**) oceans are superimposed, with magnitude scale on the right axis. No climatology is removed; all values refer to difference from their 2000 values.

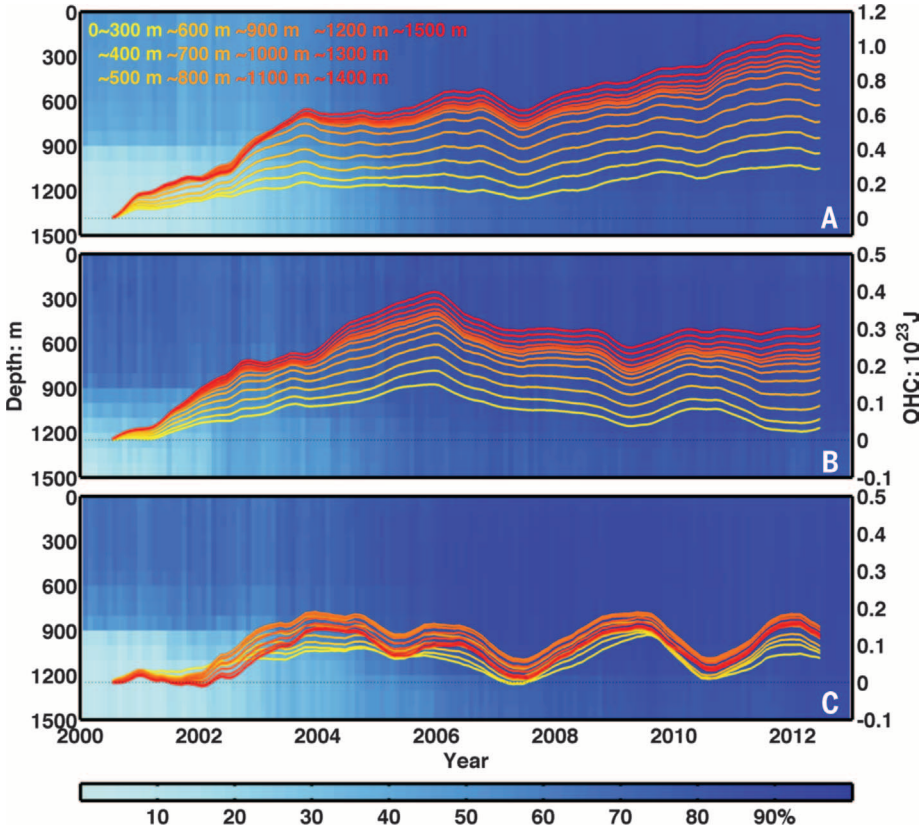

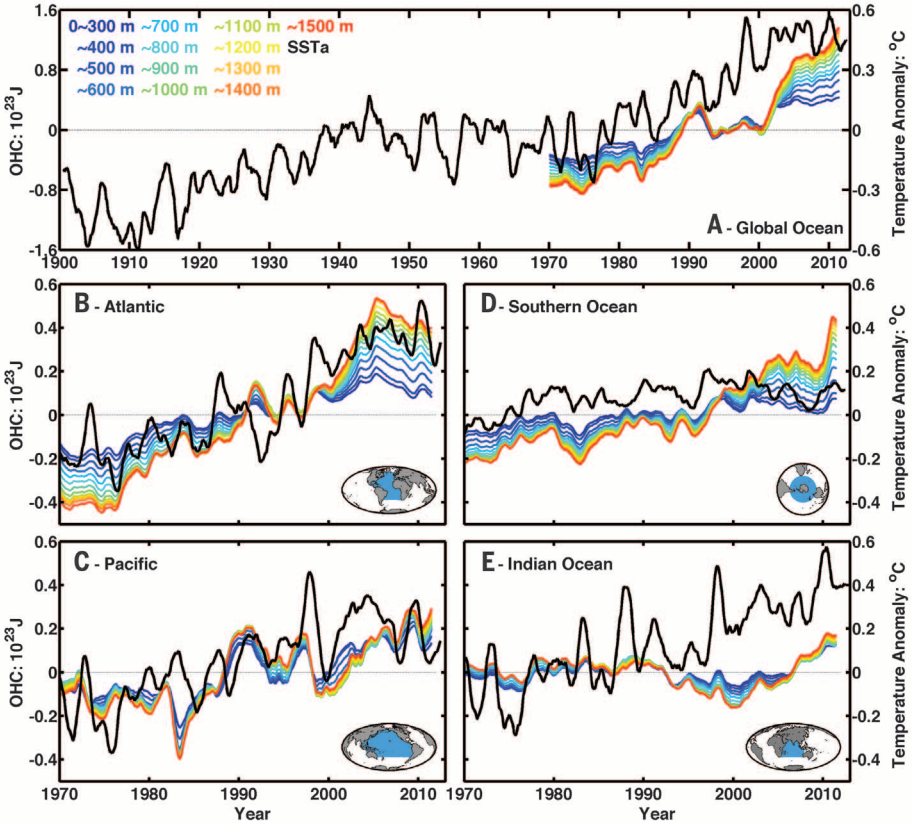

Fig. 3. ORAS4 reanalysis. (**A** to **E**) Same as Fig. 1 except with use of ORAS4 data.

multidecadal nonlinear trend with periods of accelerated warming separated by periods of slowdown and a shorter 2- to 7-year ENSO time scale. We argue that they are caused by different mechanisms.

During the current hiatus, radiative forcing at the TOA by the increasing greenhouse-gas concentration in the atmosphere produces additional warming in deeper and deeper ocean layers. This deepening warming is seen in Fig. 1A, calculated by using the in situ Ishii data (*10*), as an increasing fanning out of the OHC curves (integrated from the surface to different depths) after 1999. Globally, an additional 0.69×10^{23} J has been sequestered since 1999 in the 300- to 1500-m layer by 2012 (Fig. 1A), which, if absent, would have made the upper 300 m warm as fast as the upper 1500 m since 1999. Because the latter has an uninterrupted positive trend, there would have been no slowdown of the warming of the surface or the upper layers. Therefore, the enhanced ocean heat sink is the main cause for the current slowing in surface warming. One can also see from Fig. 1A that there has not been a major reduction in TOA radiative imbalance, as inferred from an absence of a noticeable downward bent in slope in the red curve on multiyear time scales. In the prior two decades, 1980 to 2000, we have the contrasting situation of accelerating surface warming while little additional heat (over the climatological mean) went into the deeper layers. Most of the added heat stayed near the surface, as seen by

the distance between all OHCs integrated from the surface to different depths changing little in time.

Figure 1, B to E, shows that during the 21st century the increased OHC penetration below 300 m occurs mainly in two ocean basins: the Atlantic and the Southern oceans, each accounting for slightly less than half of the global energy storage change since 1999 at those depths. The Pacific shows very little change in the spreading of OHC with depth between the two periods. This recent contrast between the Pacific and the Atlantic is deemed reliable because these are the two basins with adequate data coverage [over 80% on 5°-by-5° grids (Fig. 2)]. A separate analysis of Ocean Reanalysis System 4 (ORAS4) (*15*) data, shown in Fig. 3, verifies the in situ result here (*10*). The reanalysis uses a model to assimilate all forms of observational data and dynamically interpolates across periods of sparse coverage. Although barely noticeable, ORAS4 does have slightly more heat sequestration in the 300 to 700 m in the Pacific since 2001 compared with the Ishii data during the current hiatus period. Nevertheless, neither data set supports the model result of Meehl *et al.* (*5*) that the heat uptake in this layer in the Pacific dominates over other ocean basins during hiatus periods.

The 1997/98 El Niño released a large amount of heat, about 0.42×10^{23} J, from the upper 300 m of the Pacific Ocean to the atmosphere to be radiated as outgoing long-wave radiation. The deeper ocean was not involved, as seen by the OHC curve of the upper 1500 m tracking closely the upper 300-m content in Fig. 1C. Therefore, the time scale was short, and the upper 300 m recovered 3 to 4 years later. The 1982 El Niño also released a large amount of heat from the upper 300 m of the Pacific but did not "trigger" a period of slowdown in global surface warming.

Over the whole globe, the dominant spatial mode of variability in OHC in the upper 300 m [as shown by the first empirical orthogonal function (EOF), which explains the most variance], occurs mainly in the tropical Pacific and has the structure of ENSO variability (Fig. 4, A and B). Figure 4, E and F, shows the time series [called the principal components (PC)] associated with these EOFs. The spatial pattern of the upper 300 m resembles that associated with La Niña in the current period, because the blue PC1 changes to negative around year 2000. The leading pattern is very similar to the La Niña pattern in the SST (fig. S1A), and their PC1s are almost the same (fig. S1I). The prevalence of La Niña, with the associated shallow subduction of heat below the surface in the Pacific, has been proposed as the reason for the current hiatus (*16*). However, our result shows that the change in heat storage under the Pacific is not nearly enough to compensate for the surface hiatus—the entire upper 300 m is itself in a net La Niña phase. Figure 4, C and D, shows that the dominant OHC variability below 300 m occurs mainly in the Atlantic basin and the Antarctic Circumpolar Current (ACC) region. This combined warming pattern in the lower layer became positive toward the end of the 20th century, after two decades with very little heat uptake anomaly below 300 m (see the red PC1). The Atlantic initiated the heat sequestration toward the end of the 20th century below 700 m. Indian Ocean's deeper layers warmed last and with much smaller amplitude. Figure S1 shows these results in finer vertical resolution, whereas fig. S2 reproduces these results by using ORAS4 data.

In the Southern Ocean, the largest warming below 300 m occurs in the ACC region (*17*, *18*), in the Atlantic sector, diminishing in amplitude as the current flows eastward (Fig. 4C), first to the Indian Ocean and then to the Pacific. During the current 14 years, the 300- to 1500-m layer of the North and South Atlantic together contributed

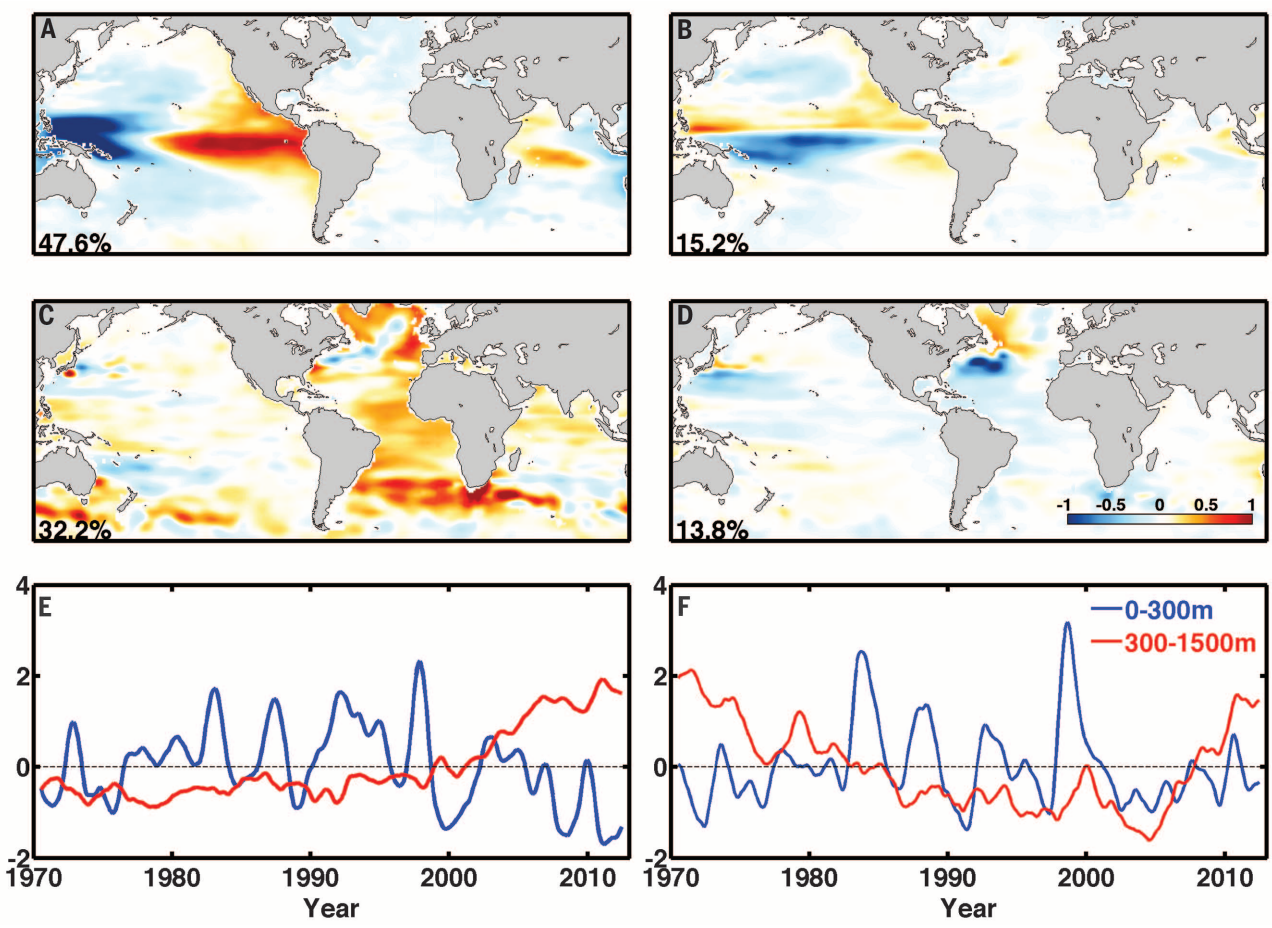

Fig. 4. EOF of the global oceans. The first (left column) and second (right column) EOF modes of the OHC in the layers 0 to 300 m (**A** and **B**) and 300 to 1500 m (**C** and **D**), respectively, in the same unit of 10^{19} J. (**E** and **F**) The PC time series associated with each EOF mode (blue for the upper layer and red for the lower layer). The PCs have been normalized by the standard deviation, which is multiplied to the EOF modes. The percentage of variance explained by each EOF is indicated in each EOF panel. Because the second EOF is small, attention should be focused on the first EOF.

0.16 ± a standard deviation of 0.03 W m^{-2} (per Earth's area) to the global mean of 0.30 ± 0.04 W m^{-2}, slightly more than the rest of the global oceans combined. [The global value for the entire 0 to 1500 m in the Ishii data is 0.49 ± 0.05 W m^{-2}.]

Over a meridional section (Fig. 5, A and B) of OHC across the Atlantic basin, there was a dramatic and broad shift in how heat penetrated all the way to 1500 m in mid- to high-latitude North Atlantic in 1999 to 2012 relative to the prior decades. The detrended version is shown in fig. S3; the spatial pattern in the North Atlantic is consistent with a change of the thermohaline circulation (*19*, *20*). There is a "dipole" meridional pattern near the 200-m depth under a "monopole" SST warming, similar to the pattern generated by regressing the data onto either the Atlantic Meridional Overturning (AMO) index (*21*, *22*) or the detrended tropical North Atlantic SST, known from model "water hosing" experiments to be a manifestation of variations in the Atlantic Meridional Overturning Circulation (AMOC) (*22*). The spatial pattern of this possibly recurring internal variability can be seen in the longer records shown in fig. S4, although poorer, earlier data are needed to see the previous episode.

In contrast to the Atlantic, the OHC change in the Pacific Ocean occurs within a shallow layer (above 300 m) and mainly in the east-west direction (see Fig. 5, C and D, which are the meridional mean of the Pacific Ocean), similar to that during ENSO events. During the current period, a thin layer of colder surface water overlies a very warm pool of water in the tropical western Pacific, driven by an anomalously strong (westward) trade wind (*23*). The warm water was only slightly displaced downward and can quickly slosh up and eastward when the west trade-wind anomaly relaxes, as suggested by England *et al.* (*23*). The Pacific mean is further broken down into the tropical versus the subtropical Pacific in fig. S5. There is some indication of heat subduction by the subtropical cell, as previously proposed (*23*, *24*), but the magnitude is small and does not affect the Pacific mean shown in Fig. 5C.

The salinity mechanism

A mechanism that can account for the speed with which heat penetrates to such great depths is deep convection caused by vertical density differences. Salinity changes at subpolar North Atlantic are known to affect deep-water formation to initiate such an ocean circulation shift (*25*). The salinity there (Fig. 6A) shifted to a positive anomaly that penetrated vertically to 1500 m very rapidly in the 21st century, reaching historically high values since measurements began (*26*). This is in contrast to the negative anomaly during the prior three decades, when surface warming was rapid. Because the ocean data were less sparse in the North Atlantic, we extend the plot back to 1950 and reveal that the salinity anomaly was also positive before 1970, during another episode of surface hiatus. These salinity shifts correspond well in timing to the OHC shifts (Fig. 6B), which are also coincident with surface transitions from global-warming slowdown to rapid warming and then to the current slowdown, with intervals between shifts lasting about three decades. Curry *et al.* (*27*) reported a freshening of the subpolar North Atlantic waters from the 1950s to 1990s and cited global warming as one of the reasons. However, over the longer period reported here, there was very little trend in the salinity, only a vacillating cycle.

There is no accepted single theory, but theoretical explanations of these vacillating regime shifts mostly involve variations of the AMOC (*20*, *25*). Because of excessive evaporation, tropical surface water is more saline. A faster AMOC tends to transport more saline water to the North Atlantic subpolar region, where it loses some heat to the cold atmosphere and sinks. The heat from the transported tropical water tends to melt more ice (*20*), which makes the surface water in the subpolar regions less dense. These two effects oppose each other. Eventually the fresh water from ice melts wins out. The less-dense water then slows the AMOC after a few-years lag (*28*). A slower AMOC then transports less tropical saline water northward, and the opposing phase of the cycle commences. Other versions of the mechanism are also available (*29*, *30*). Because the record for the AMOC strength is short (only since 2004), the above scenario cannot be verified observationally, but it is consistent with the mechanism described by Danabasoglu *et al.* (*31*) as indeed occurring in the Community Climate System Model 4 (CCSM4) (*32*).

Although there is very little trend in the OHC in the subpolar North Atlantic where the salinity-induced vacillation cycle dominates, there is a linear OHC trend equatorward of 45°N and °S in

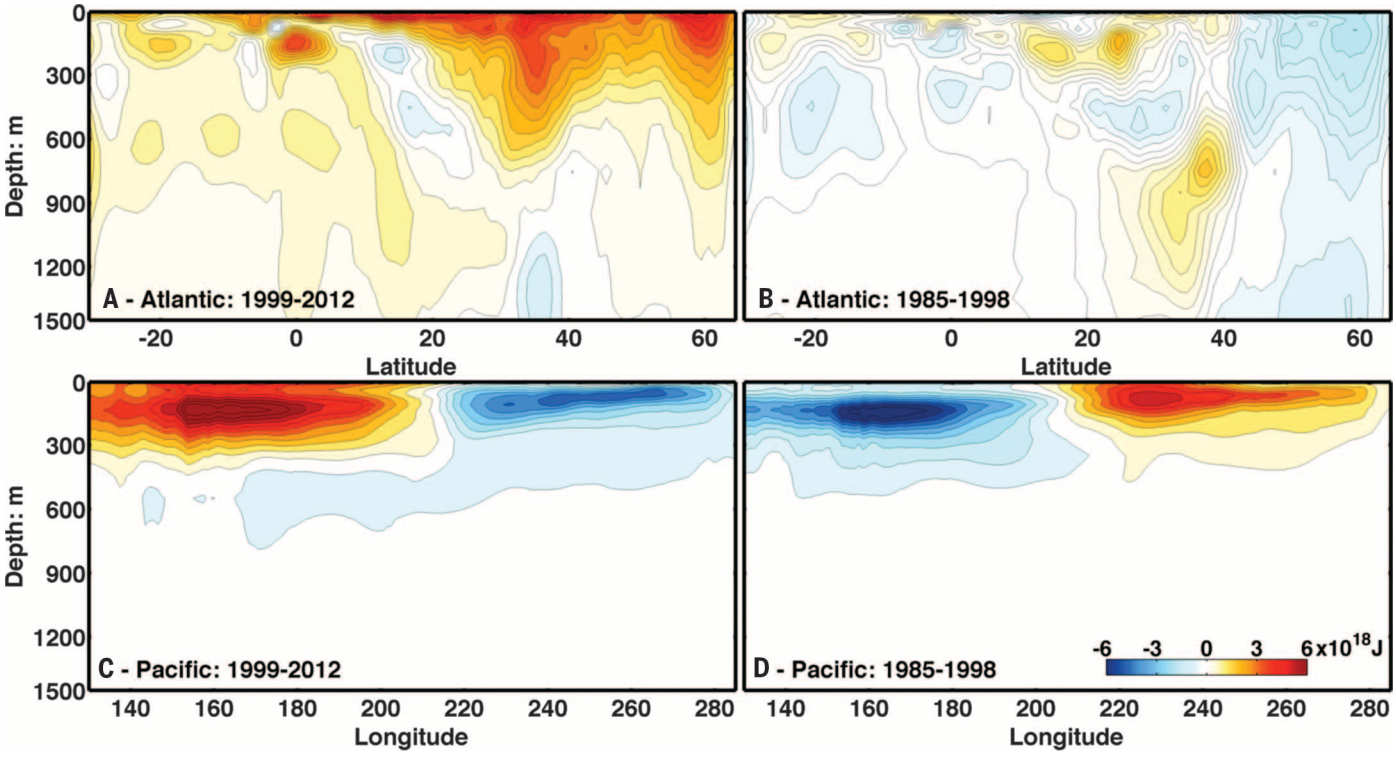

Fig. 5. Contrasting the change in heat content in the Pacific versus the Atlantic. (**A** and **B**) OHC (for each 5-m layer) in the Atlantic basin zonally averaged over the basin as a function of latitude. (**C** and **D**) OHC integrated meridionally (35°S to 65°N) over the Pacific basin as a function of longitude. (A and C) Averaged over the recent 14 years. (B and D) Averaged over the previous 14 years. Not detrended.

the Atlantic basin (including the Southern Ocean) (fig. S6), which is likely anthropogenically forced. This secular increase in OHC is not associated with a corresponding trend in salinity. It reflects mainly the increase in greenhouse heating from above and does not necessarily reflect the speed of the heat transport by the AMOC. In the Pacific, there is again very little heat-uptake trend.

Discussion

Many different explanations for the recent global-warming slowdown have been proposed, but they fall mainly into two categories. The first involves a reduction in TOA radiative forcing: by a decrease in stratospheric water vapor (*33*), an increase in background stratospheric volcanic aerosols (*34*), by 17 small volcano eruptions since 1999 (*35*), increasing coal-burning in China (*36*), the indirect effect of time-varying anthropogenic aerosols (*37*), a low solar minimum (*38*), or a combination of these (*39*). Response to solar cycle changes was found to be small (*40*, *41*). The aerosol cooling should have a signature in subsurface ocean (*42*), and yet it is not seen, perhaps suggesting that the proposed radiative effects may be too small. The second involves ocean heat sequestration: The present work follows the original proposal of Meehl *et al.* (*5*, *24*) regarding global deep-ocean heat sequestration. However, our observational result does not support their Pacific-centric view. The duration of the cooling periods in the CCSM4 model they used is typically 10 years, with one rare 15-year hiatus in 375 years and none over 15 years. The current hiatus already lasted over 15 years using their definition of hiatus as periods with zero trend. Comparing that model with observation, we found that model's Atlantic has too little variability with too high frequency (fig. S7 versus Fig. 6). This artifact appears to be attributable to a new overflow parameterization scheme in CCSM4 in the Denmark Strait and Faroe Bank Channel (*31*).

From another perspective, Wu *et al.* (*43*) showed that the instrumental global-mean surface temperature record since 1850 contains two and a half cycles of a multidecadal variation. Each cycle lasted on average 65 years, consisting of an accelerated warming plus a slowdown period. They showed that the primary location of the multidecadal variability is in the North Atlantic and only secondarily in the Pacific. If this multidecadal variability is indeed related to the variations of the AMOC, then we can infer that the time scale of the latter was also 30 years between regime shifts historically. Tung and Zhou (*41*) showed that these multidecadal cycles exist in the Central England Temperature for the past 353 years, with an average period of 70 years (but could be as short as 40 years), consistent with an earlier study using multiproxy data by Delworth and Mann (*44*). They and Zhang *et al.* (*42*) argued that this oscillation is due to an internal variability and not to anthropogenic aerosol forcing (*37*).

Because the atmosphere and the upper ocean in the equatorial Pacific are intimately coupled, the strong trade winds go hand in hand with the east-west SST gradient generated by the La Niña pattern, known as the Bjerknes feedback. Kosaka and Xie (*16*) proposed that the cold eastern Pacific was key to understanding the current warming hiatus. England *et al.* (*23*) attributed the cold eastern equatorial Pacific to the stronger trade winds for the past 20 years, and the trade wind intensification to the multidecadal negative phase of the Interdecadal Pacific Oscillation (IPO). The IPO, defined using the SST in the Pacific Basin including the ENSO region, describes but does not explain the cold eastern Pacific status.

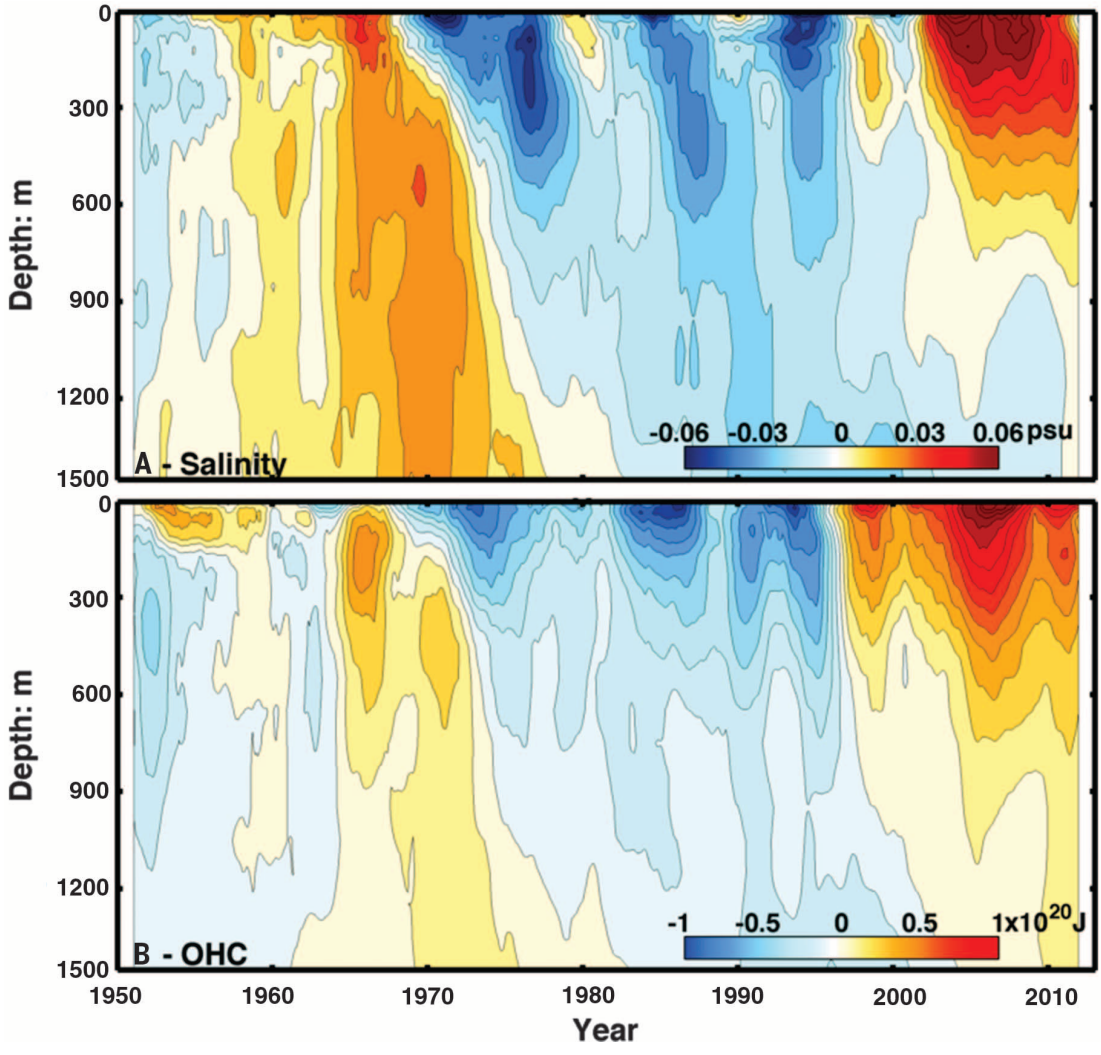

Fig. 6. Climate shifts in salinity and OHC. North Atlantic subpolar (45° to 65°N) mean salinity (A) and 5-m layer OHC (B), 12-month running mean, as a function of years; not detrended, but the climatology for the period 1950 to 2012 was removed.

How could the Pacific SST cool when the heat sink was located in other ocean basins? Why didn't the Atlantic SST simply cool as heat was being subducted in its basin? The Atlantic SST and its upper layers did start to cool (Fig. 1B) after its subpolar salinity peaked and then started to decrease after 2006 (Fig. 6A). Before 2006, our warm salt subduction mechanism does not allow the Atlantic to cool when its subpolar salinity was increasing, because poleward transport of warm salty water and increasing subpolar subduction are parts of the same mechanism of enhanced AMOC upper-ocean transport. During this first part of the hiatus period, the heat deficit must be transferred to other ocean basins, mostly to the Pacific because it is the only other major ocean basin in the Northern Hemisphere, likely through the atmosphere. Zhang and Delworth (*45*) and Zhang *et al.* (*46*) showed by using models that, as the northward heat transport by the AMOC is increased, the atmospheric heat transport decreases in compensation (and vice versa), providing a multidecadal component to the Pacific Decadal Oscillation (PDO). The concept behind the flexible atmospheric heat transport is known as nonlinear baroclinic adjustment (*47*). Thus, almost-"synchronized" hemisphere-wide atmospheric changes are possible (*30*). On climate time scales and from an energy perspective, the amount of radiative energy available to heat the global SST, including the Pacific, is what remains after accounting for the energy sink; it does not matter if the latter is located outside the Pacific.

Conclusion

The fact that the global-mean temperature, along with that of every major ocean basin, has not increased for the past 15 years, as they should in the presence of continuing radiative forcing, requires a planetary sink for the excess heat. Although the tropical Pacific is the source of large interannual fluctuations caused by the exchange of heat in its shallow tropical layer (*3*), the current slowdown is in addition associated with larger decadal changes in the deeper layers of the Atlantic and the Southern oceans. The next El Niño, when it occurs in a year or so, may temporarily interrupt the hiatus, but, because the planetary heat sinks in the Atlantic and the Southern Oceans remain intact, the hiatus should continue on a decadal time scale. When the internal variability that is responsible for the current hiatus switches sign, as it inevitably will, another episode of accelerated global warming should ensue.

REFERENCES AND NOTES

1. K. E. Trenberth, J. T. Fasullo, M. A. Balmaseda, *J. Clim.* **27**, 3129–3144 (2014).
2. Intergovernmental Panel on Climate Change, *Summary for Policymakers, Climate Change 2007: Synthesis Report* (Cambridge Univ. Press, Cambridge, 2007).
3. K. E. Trenberth, J. T. Fasullo, *Earth's Future* **1**, 19–32 (2013).
4. K. E. Trenberth, J. T. Fasullo, *Science* **328**, 316–317 (2010).
5. G. A. Meehl, J. M. Arblaster, J. T. Fasullo, A. Hu, K. E. Trenberth, *Nat. Clim. Change* **1**, 360–364 (2011).
6. D. R. Easterling, M. F. Wehner, *Geophys. Res. Lett.* **36**, L08706 (2009).
7. D. Roemmich *et al.*, *Oceanography* **22**, 46–55 (2009).
8. J. M. Lyman, G. C. Johnson, *J. Clim.* **27**, 1945–1957 (2014).
9. J. M. Lyman *et al.*, *Nature* **465**, 334–337 (2010).
10. M. Ishii, M. Kimoto, *J. Oceanogr.* **65**, 287–299 (2009).
11. J. M. Lyman, G. C. Johnson, *J. Clim.* **21**, 5629–5641 (2008).
12. M. Ishii, A. Shouji, S. Sugimoto, T. Matsuoto, *Int. J. Climatol.* **25**, 865–879 (2005).
13. M. Ishii, M. Kimoto, K. Sakamoto, S. I. Iwasaki, *J. Oceanogr.* **62**, 155–170 (2006).
14. C. A. Katsman, G. J. van Oldenborg, *Geophys. Res. Lett.* **38**, L14610 (2011).
15. M. A. Balmaseda, K. Mogensen, A. T. Weaver, *Q. J. R. Meteorol. Soc.* **139**, 1132–1161 (2013).
16. Y. Kosaka, S.-P. Xie, *Nature* **501**, 403–407 (2013).
17. S. T. Gille, *Science* **295**, 1275–1277 (2002).
18. J. R. Toggweiler, J. Russell, *Nature* **451**, 286–288 (2008).
19. R. Zhang, *Geophys. Res. Lett.* **35**, L20705 (2008).
20. J. Jungclaus, H. Haak, M. Latif, U. Mikolajewicz, *J. Clim.* **18**, 4013–4031 (2005).
21. C. Wang, L. Zhang, *J. Clim.* **26**, 6137–6162 (2013).
22. R. Zhang, *Geophys. Res. Lett.* **34**, L12713 (2007).
23. M. H. England *et al.*, *Nat. Clim. Change* **4**, 222–227 (2014).
24. G. A. Meehl, A. Hu, J. M. Arblaster, J. T. Fasullo, K. E. Trenberth, *J. Clim.* **26**, 7298–7310 (2013).
25. I. V. Polyakov, V. A. Alekseev, U. Bhatt, E. I. Polyakova, X. Zhang, *Clim. Dyn.* **34**, 439–457 (2010).
26. H. Hátún, A. B. Sandø, H. Drange, B. Hansen, H. Valdimarsson, *Science* **309**, 1841–1844 (2005).
27. R. Curry, B. Dickson, I. Yashayaev, *Nature* **426**, 826–829 (2003).
28. M. Dima, G. Lohmann, *J. Clim.* **20**, 2706–2719 (2007).
29. M. G. Wyatt, J. A. Curry, *Clim. Dyn.* **42**, 2763–2782 (2014).
30. M. G. Wyatt, S. Kravtsov, A. A. Tsonis, *Clim. Dyn.* **38**, 929–949 (2012).
31. G. Danabasoglu *et al.*, *J. Clim.* **25**, 5153–5172 (2012).
32. P. R. Gent *et al.*, *J. Clim.* **24**, 4973–4991 (2011).
33. S. Solomon *et al.*, *Science* **327**, 1219–1223 (2010).
34. S. Solomon *et al.*, *Science* **333**, 866–870 (2011).
35. B. D. Santer *et al.*, *Nat. Geosci.* **7**, 185–189 (2014).
36. R. K. Kaufmann, H. Kauppi, M. L. Mann, J. H. Stock, *Proc. Natl. Acad. Sci. U.S.A.* **108**, 11790–11793 (2011).
37. B. B. B. Booth, N. J. Dunstone, P. R. Halloran, T. Andrews, N. Bellouin, *Nature* **484**, 228–232 (2012).
38. J. Hansen, M. Sato, P. Kharecha, K. von Schuckmann, *Atmos. Chem. Phys.* **11**, 13421–13449 (2011).
39. G. A. Schmidt, D. T. Shindell, K. Tsigaridis, *Nat. Geosci.* **7**, 158–160 (2014).
40. J. Zhou, K. K. Tung, *J. Clim.* **23**, 3234–3248 (2010).
41. K. K. Tung, J. Zhou, *Proc. Natl. Acad. Sci. U.S.A.* **110**, 2058–2063 (2013).
42. R. Zhang *et al.*, *J. Atmos. Sci.* **70**, 1135–1144 (2013).
43. Z. Wu, N. E. Huang, J. M. Wallace, B. Smoliak, X. Chen, *Clim. Dyn.* **37**, 759–773 (2011).
44. T. L. Delworth, M. E. Mann, *Clim. Dyn.* **16**, 661–676 (2000).
45. R. Zhang, T. L. Delworth, *Geophys. Res. Lett.* **34**, L23708 (2007).
46. R. Zhang, T. L. Delworth, I. M. Held, *Geophys. Res. Lett.* **34**, L02709 (2007).
47. W. T. Welch, K. K. Tung, *J. Atmos. Sci.* **55**, 1285–1302 (1998).

ACKNOWLEDGMENTS

The research of K.-K.T. is supported by NSF under AGS-1262231. X.C. is supported by Natural Science Foundation of China under 41330960 and 41176029. He thanks First Institute of Oceanography of China for its support during his visit to University of Washington. The authors are grateful to many colleagues and the anonymous reviewers who commented on the manuscript and helped improve it. The data sets used in this study are publicly available in http://rda.ucar.edu/datasets/ds285.3/ and https://climatedataguide.ucar.edu/climate-data/oras4-ecmwf-ocean-reanalysis-and-derived-ocean-heat-content.

SUPPLEMENTARY MATERIALS

www.sciencemag.org/content/345/6199/897/suppl/DC1
Materials and Methods
Data
Figs. S1 to S7
Reference (*48*)

17 April 2014; accepted 11 July 2014
10.1126/science.1254937

REPORTS

QUANTUM OPTICS

All-optical routing of single photons by a one-atom switch controlled by a single photon

Itay Shomroni,* Serge Rosenblum,* Yulia Lovsky, Orel Bechler, Gabriel Guendelman, Barak Dayan†

The prospect of quantum networks, in which quantum information is carried by single photons in photonic circuits, has long been the driving force behind the effort to achieve all-optical routing of single photons. We realized a single-photon–activated switch capable of routing a photon from any of its two inputs to any of its two outputs. Our device is based on a single atom coupled to a fiber-coupled, chip-based microresonator. A single reflected control photon toggles the switch from high reflection (R ~ 65%) to high transmission (T ~ 90%), with an average of ~1.5 control photons per switching event (~3, including linear losses). No additional control fields are required. The control and target photons are both in-fiber and practically identical, making this scheme compatible with scalable architectures for quantum information processing.

Photons are a key player in the growing field of quantum information science. The fact that they do not interact with each other has made them ideal for the communication of quantum information yet has prevented so far the realization of deterministic all-optical quantum gates based on single photons. The difficulty to achieve nonlinear behavior at the level of single photons—namely, photon-photon interactions—is considered a major challenge also in the realization of quantum networks, in which quantum information processing

Department of Chemical Physics, Weizmann Institute of Science, Rehovot 76100, Israel.
*These authors contributed equally to this work. **†Corresponding author. E-mail: barak.dayan@weizmann.ac.il**

would be performed by material quantum nodes interconnected by photonic channels (*1*, *2*).

Accordingly, considerable effort has been invested toward the achievement of photon-photon interactions by the mediation of material systems. This effort was pioneered by the attainment of strong coupling between single atoms and optical microresonators in the context of cavity quantum electrodynamics (*3*, *4*), in which the tight confinement of light in tiny volumes leads to drastic enhancement of the electric field associated with each photon in the cavity mode. Antibunching has been observed both with atoms (*5*, *6*) and quantum dots (*7*), and nonlinear phase shifts of 16° (*8*) and recently even π (*9*, *10*) have also been demonstrated with single atoms.

Most notably, based on a scheme that involves auxiliary control fields (*11*), recent works demonstrated nondestructive measurement of an optical photon (*12*), a single-photon phase switch (*9*), and the realization of a quantum gate between flying photons and a single atom, showing atom-photon, photon-photon, and atom-photon-photon entanglement (*13*), all of which can be directly applied to photonic routing.

Nonlinearities such as electromagnetically induced transparency (*14*) and Rydberg blockade (*15*, *16*) have been harnessed for the demonstration of all-optical interactions at lower and lower powers (*17*–*19*). In particular, all-optical switching—in which a weak gate pulse strongly modifies the attenuation of the system—has been demonstrated with very few photons (*20*) and even just one (*21*) photon in the gate pulse. In order to take the next step toward scalable quantum networks, there is a need for switching schemes that coherently route photons between multiple ports in a way that is compatible with large-scale photonic circuits.

Here, we demonstrate the experimental realization of a robust, simple, and scalable scheme for all-optical coherent routing of single photons by single photons, with no need for any additional control fields. Based on a series of theoretical works (*22*–*28*), this scheme uses the mediation of a single, cavity-enhanced, three-level atom in the regime best described as the fast-cavity limit. The same as in the regime of strong-coupling, the coherent coupling rate g between the atom and the cavity mode is larger than both the incoherent loss of the cavity κ_i and the atomic spontaneous emission rate 2γ. Yet in contrast to strong coupling, here the coupling κ_{ex} between the cavity and its input/output modes (the two directions of propagation in the optical fiber, in our case) is the fastest rate in the system, so that a photon emitted by the atom will exit the cavity by coupling to the fiber before the atom could reabsorb it. Accordingly, the dynamics in this regime are best described by the tools of open quantum systems (*29*) and do not include reversible Rabi oscillations between the atom and the cavity mode, but rather irreversible cavity-enhanced spontaneous emission of the atom into the fiber. The crucial parameter in such a system is the cooperativity, or Purcell enhancement factor, $g^2/\kappa\gamma$ (with $\kappa = \kappa_i + \kappa_{ex}$)—namely, the ratio between the atom's cavity-enhanced spontaneous emission rate into the fiber, to the free-space one, which is proportional to the ratio between the cavity's quality factor Q to its mode volume V. Accordingly, by coupling the atom to high-quality (small κ_i) microresonators with tiny mode volumes, it is therefore possible to reach $g^2/\kappa\gamma > 1$, in which case the atom can be assumed to be interacting primarily with the fiber.

The underlying mechanism in our switching scheme is simple and robust and is in fact similar to the interference mechanism that makes metallic mirrors reflect light. The free charges in the mirror oscillate in response to the incoming field and radiate both forward and backward a field that is opposite in phase to the incoming one. The result is destructive interference in the forward direction, which leaves the incoming light no other choice than to be reflected backward. The same effect occurs with a two-level atom in the one-dimensional atom regime: The atom radiates in both directions, and the destructive interference with the incoming probe in the forward direction leads to reflection of the probe backward. The difference between a single atom and a macroscopic mirror is exhibited by the fact that the reflected light in this case is sub-Poissonian because the atom cannot reflect more than one photon at the same instant.

In order to exploit this mechanism for optical switching, one needs to introduce "memory" into the system—namely, a way to make reflection of a single photon toggle the internal state of the atom. This is performed by using a three-level, Λ-type configuration in which the atom has two transitions, each coupled to only one direction of propagation. Such a configuration is depicted in Fig. 1A, where it is assumed that σ^+ polarization propagates only to the right, and σ^- propagates only to the left.

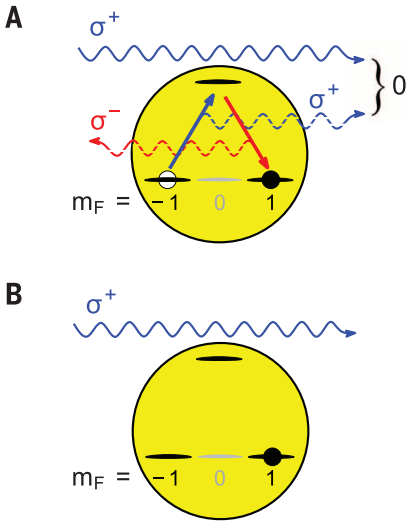

Fig. 1. The two states of the photonic switch. In this three-level atomic Λ-configuration, the σ^+ transition is coupled only to a photonic mode propagating to the right, and the σ^- transition is coupled only to a photonic mode propagating to the left. The atom is irradiated by a σ^+ probe (solid blue wavy arrow). (**A**) For an atom in the $m_F = -1$ ground state, the incoming σ^+ photon will be deterministically reflected as a σ^- photon because of the destructive interference between the probe and the σ^+ emission from the atom (dashed blue wavy arrow), toggling the state of the atom to $m_F = +1$. (**B**) An atom in the $m_F = +1$ ground state does not interact with σ^+ photons, which are accordingly transmitted. The entire scheme is left-right symmetric.

Assuming the initial state of the atom is at $m_F = -1$ and an incoming σ^+ probe, the destructive interference between the probe and the σ^+ field emitted by the atom forces the atom to emit a σ^- photon to the opposite direction, deterministically ending at the $m_F = +1$ state. As a result, any subsequent σ^+ photons will not interact with the atom and will accordingly be transmitted (*27*). Symmetrically, at this stage the system becomes reflective to σ^- photons coming from the right.

This system therefore behaves as a symmetric toggle switch with two inputs, two outputs, and two internal states (Fig. 2A), in which each reflection toggles the internal state. To implement this system as a photonic switch, we use the conventional time-bins protocol and define the first pulse as the control pulse, and the second as the target, which is routed from a certain input to a certain output.

At the heart of our setup is a single ^{87}Rb atom coupled to a chip-based whispering-gallery mode (WGM) silica microsphere resonator (Fig. 2B) (*30*). Light is evanescently coupled to and from the microsphere by a tapered nanofiber, and photons are detected at the outputs by multiple single-photon counting modules (SPCMs). The coupling κ_{ex} between the microsphere and the nanofiber is set by means of careful alignment of their relative position by using a piezo positioning system.

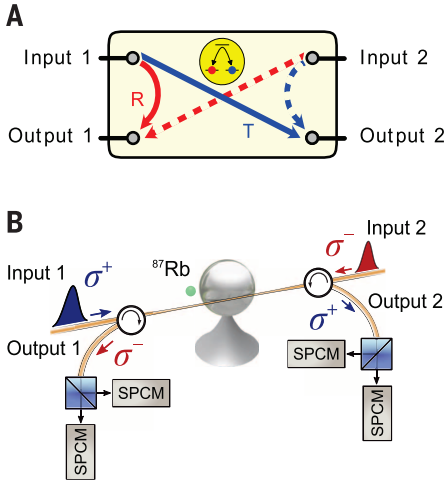

Fig. 2. Schematic of the photonic switch. (**A**) Each input, 1 (solid arrows) or 2 (dashed arrows) may be either transmitted or reflected into one of two outputs, depending on the state of the atom, at $m_F = +1$ (blue) or $m_F = -1$ (red). Each reflection of a single photon toggles the state of the atom. (**B**) The experimental realization of the switch. A single ^{87}Rb atom interacts with a TM WGM resonance of a chip-based silica microsphere resonator. The input-output interface is provided by a tapered optical nanofiber, with the outputs separated from the inputs by optical circulators (*30*). σ^+ modes propagate from left to right, and σ^- modes propagate from right to left. The outputs are delivered to SPCMs.

By working with a transverse-magnetic (TM) mode of the microsphere, we can approximate to a high degree the situation in which σ^+ and σ^- polarizations are coupled to opposite directions. As recently pointed out (*31*), the polarization in the evanescent wave region is very close to σ^+ in one direction, and σ^- in the other, with just ~4% cross-contamination [which naturally leads to some reduction in the efficiency of the switch in this particular realization (*30*)].

The microsphere and the probe were tuned to be resonant with the $F = 1 \rightarrow F' = 0$ transition of the D2 line of ^{87}Rb (Fig. 1). Because atoms in the state $m_F = 0$ barely interact with the TM mode, by choosing this manifold we practically attain the desired Λ-configuration described in Fig. 1, although at the price of decreasing the coherent coupling rate g by a factor of $\sqrt{3}$ compared with the cycling transition ($F = 2 \rightarrow F' = 3$), in which mean $g = 27$ MHz was measured (*30*). To reach the fast cavity limit, we set κ_{ex} to 30 MHz, corresponding to mean $g^2/\kappa\gamma = 2.2$ (*30*).

The rare event of the presence of one atom within the evanescent wave of the TM mode was identified by sending weak (~2.5 photons per pulse) and short [~15 ns full width at half maximum (FWHM)] pulses in the nanofiber in alternating directions and detecting at least three reflected photons within less than 400 ns (*30*). Interleaved between the detection pulses were much weaker (0.24 photons on average in each pulse) and longer (~50 ns FWHM) "target" pulses, whose purpose was to accurately measure the single-photon reflection and transmission properties of the switch. The last detection pulse before each target pulse served as the control, which prepared the atom in a certain initial state. The pulse sequence included control pulses in both directions, preparing the atom half of the times in $m_F = -1$, and half of the times in $m_F = +1$, with the target pulse always polarized σ^+ (*32*).

The measured probabilities for reflection and transmission of the first (and typically the only, if at all) photon in the target pulse are shown in Fig. 3, normalized to the total number of photon detection events (*30*). These are heralded results; namely, they show the statistics of the target pulse conditioned on the detection of one reflected photon in the preceding control pulse.

Specifically, in the cases in which the control pulse was σ^- polarized, detection of a single reflected (σ^+) photon toggled the switch to a state that reflects σ^+ target photons at a probability of 65%. This level is lower than the theoretically expected value of 89% (*30*). We attribute this difference mostly to false events in which the (untrapped) atom was not present in the cavity mode during the entire measurement (*30*).

In cases in which the control pulse was σ^+, detection of a single reflected (σ^-) photon changed the reflection/transmission ratio by a factor of more than 16, leading to ~90% transmission of σ^+ target photons.

To confirm that the toggling of the state is carried out by a single reflection of a control photon, we looked at the normalized probabilities for a second photon detection event in the control pulse. As shown in Fig. 4A, already during the control pulse, after a single reflection the switch becomes highly transmissive, with a probability of only 4.4% to reflect a second photon.

This is a drastic demonstration of single-photon nonlinearity, and as such it is highly nonclassical. Accordingly, the reflected control pulses are antibunched (Fig. 4B), meaning that there is a much larger probability for joint detection of two reflected photons (at different SPCMs) in two unrelated control pulses (from different atom detection events) than within the same control pulse (*30*).

We can therefore conclude that a single reflection of a control photon toggles the state of the atom with high probability. Taking into account the measured probability for such a reflection (~65%), this corresponds to an average of 1.5 control photons per switching event, increasing to ~3 if we include the linear losses in our current realization (which could be practically eliminated by using a higher Q resonance) (*30*).

The potential of this scheme lies in its compatibility with scalable photonic architectures. The device is operated only by the single-photon pulses, which are all in-fiber, identical, and routed to the output ports. This means that a routed target photon can serve as the control photon in the next device, or that the same control photon could activate a few devices. Our demonstration therefore paves the way for the application of this scheme as a versatile, robust, and simple building block for a variety of all-optical photonic devices, from quantum memory (*22*–*24*) through single-photon add/drop filters (*27*), to photonic quantum gates (*24*), all of which being completely passive and compatible with scalable quantum networks.

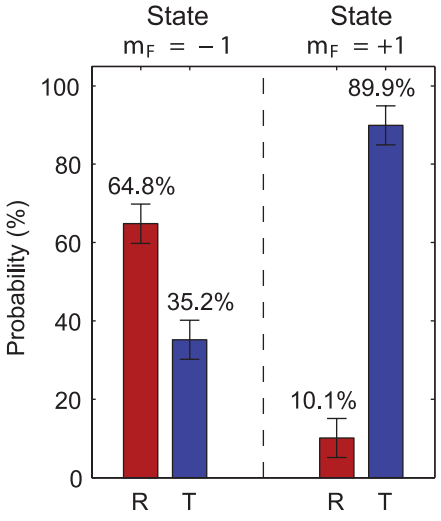

Fig. 3. Single-photon statistics of the photonic switch. In the $m_F = -1$ state, the probability of a σ^+ photon to be reflected is 64.8%, dropping to 10.1% in the $m_F = +1$ state.

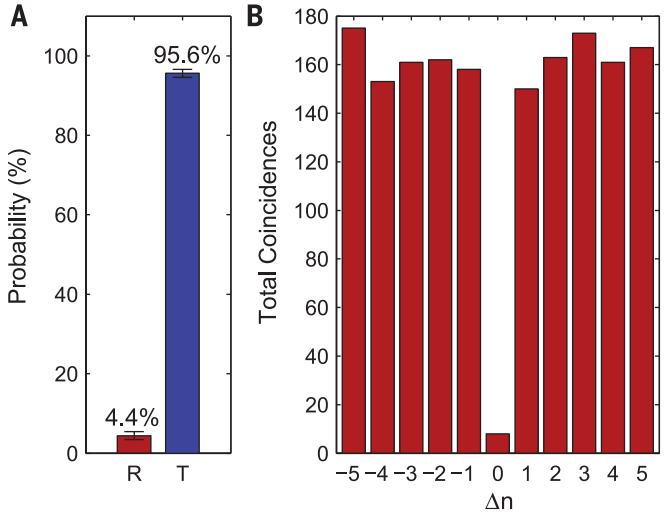

Fig. 4. Single-photon nonlinearity within the control pulse. (**A**) The statistics of the second photon in the control pulse, after the detection of one reflected photon. As shown, the probability of a second reflection drops to 4.4%. (**B**) Antibunching of the reflected control photons, confirming that in most cases only one photon is reflected. For atom-detection events i and j, the total number of coincident detections of two photons in both i and j is shown versus $\Delta n = i - j$. Within the same pulse, the reflection of two photons is accordingly suppressed by a factor of ~20.

REFERENCES AND NOTES

1. J. I. Cirac, P. Zoller, H. J. Kimble, H. Mabuchi, *Phys. Rev. Lett.* **78**, 3221–3224 (1997).
2. H. J. Kimble, *Nature* **453**, 1023–1030 (2008).
3. S. Haroche, J.-M. Raimond, *Exploring the Quantum: Atoms, Cavities, and Photons* (Oxford Univ. Press, New York, 2013).
4. R. J. Thompson, G. Rempe, H. J. Kimble, *Phys. Rev. Lett.* **68**, 1132–1135 (1992).
5. K. M. Birnbaum *et al.*, *Nature* **436**, 87–90 (2005).
6. B. Dayan *et al.*, *Science* **319**, 1062–1065 (2008).
7. D. Press *et al.*, *Phys. Rev. Lett.* **98**, 117402 (2007).
8. Q. A. Turchette, C. J. Hood, W. Lange, H. Mabuchi, H. J. Kimble, *Phys. Rev. Lett.* **75**, 4710–4713 (1995).
9. T. G. Tiecke *et al.*, *Nature* **508**, 241–244 (2014).
10. J. Volz, M. Scheucher, C. Junge, A. Rauschenbeutel, Nonlinear pi phase shift for single fiber-guided photons interacting with a single atom. *arXiv*:1403.1860 (2014).
11. L.-M. Duan, H. J. Kimble, *Phys. Rev. Lett.* **92**, 127902 (2004).
12. A. Reiserer, S. Ritter, G. Rempe, *Science* **342**, 1349–1351 (2013).
13. A. Reiserer, N. Kalb, G. Rempe, S. Ritter, *Nature* **508**, 237–240 (2014).
14. M. Fleischhauer, A. Imamoglu, J. P. Marangos, *Rev. Mod. Phys.* **77**, 633–673 (2005).
15. D. Jaksch *et al.*, *Phys. Rev. Lett.* **85**, 2208–2211 (2000).
16. A. Gaëtan *et al.*, *Nat. Phys.* **5**, 115–118 (2009).
17. A. M. C. Dawes, L. Illing, S. M. Clark, D. J. Gauthier, *Science* **308**, 672–674 (2005).
18. I. Fushman *et al.*, *Science* **320**, 769–772 (2008).
19. T. Peyronel *et al.*, *Nature* **488**, 57–60 (2012).
20. W. Chen *et al.*, *Science* **341**, 768–770 (2013).
21. S. Baur, D. Tiarks, G. Rempe, S. Dürr, *Phys. Rev. Lett.* **112**, 073901 (2014).
22. D. Pinotsi, A. Imamoglu, *Phys. Rev. Lett.* **100**, 093603 (2008).
23. D. E. Chang, A. S. Sørensen, E. A. Demler, M. D. Lukin, *Nat. Phys.* **3**, 807–812 (2007).
24. K. Koshino, S. Ishizaka, Y. Nakamura, *Phys. Rev. A* **82**, 010301 (2010).

25. H. F. Hofmann, K. Kojima, S. Takeuchi, K. Sasaki, . *J. Opt. B* **5**, 218–221 (2003).
26. D. Witthaut, A. S. Sørensen, *New J. Phys.* **12**, 043052 (2010).
27. S. Rosenblum, S. Parkins, B. Dayan, *Phys. Rev. A* **84**, 033854 (2011).
28. J. Gea-Banacloche, W. Wilson, *Phys. Rev. A* **88**, 033832 (2013).
29. H. J. Carmichael, *Phys. Rev. Lett.* **70**, 2273–2276 (1993).
30. Materials and methods are available as supplementary materials on *Science* Online.
31. C. Junge, D. O'Shea, J. Volz, A. Rauschenbeutel, *Phys. Rev. Lett.* **110**, 213604 (2013).
32. We also performed the opposite experiment, in which the control pulses were always σ^-, and the target pulse was half of the times σ^+ and half of the times σ^-. The obtained results were completely consistent with the ones presented here.

ACKNOWLEDGMENTS

Support from the Israeli Science Foundation, the Joseph and Celia Reskin Career Development Chair in Physics, and the Crown Photonics Center is acknowledged. This research was made possible in part by the historic generosity of the Harold Perlman family.

SUPPLEMENTARY MATERIALS

www.sciencemag.org/content/345/6199/903/suppl/DC1
Materials and Methods
Supplementary Text
Figs. S1 to S3
References (*33*, *34*)

11 April 2014; accepted 26 June 2014
Published online 10 July 2014;
10.1126/science.1254699

HELIUM SUPERFLUIDITY

Shapes and vorticities of superfluid helium nanodroplets

Luis F. Gomez,[1]* Ken R. Ferguson,[2] James P. Cryan,[3] Camila Bacellar,[3,4] Rico Mayro P. Tanyag,[1] Curtis Jones,[1] Sebastian Schorb,[2] Denis Anielski,[5,6] Ali Belkacem,[3] Charles Bernando,[7] Rebecca Boll,[5,6,8] John Bozek,[2] Sebastian Carron,[2] Gang Chen,[9]† Tjark Delmas,[10] Lars Englert,[11] Sascha W. Epp,[5,6] Benjamin Erk,[5,6,8] Lutz Foucar,[6,12] Robert Hartmann,[13] Alexander Hexemer,[9] Martin Huth,[13] Justin Kwok,[14] Stephen R. Leone,[3,4,15] Jonathan H. S. Ma,[3,16] Filipe R. N. C. Maia,[17]‡ Erik Malmerberg,[18,19] Stefano Marchesini,[9,20] Daniel M. Neumark,[3,4] Billy Poon,[18] James Prell,[4] Daniel Rolles,[6,8,12] Benedikt Rudek,[5,6]§ Artem Rudenko,[5,6,21] Martin Seifrid,[1] Katrin R. Siefermann,[3]‖ Felix P. Sturm,[3] Michele Swiggers,[2] Joachim Ullrich,[5,6]§ Fabian Weise,[3]¶ Petrus Zwart,[18] Christoph Bostedt,[2,22]# Oliver Gessner,[3]# Andrey F. Vilesov[1,7]#

Helium nanodroplets are considered ideal model systems to explore quantum hydrodynamics in self-contained, isolated superfluids. However, exploring the dynamic properties of individual droplets is experimentally challenging. In this work, we used single-shot femtosecond x-ray coherent diffractive imaging to investigate the rotation of single, isolated superfluid helium-4 droplets containing ~10^8 to 10^{11} atoms. The formation of quantum vortex lattices inside the droplets is confirmed by observing characteristic Bragg patterns from xenon clusters trapped in the vortex cores. The vortex densities are up to five orders of magnitude larger than those observed in bulk liquid helium. The droplets exhibit large centrifugal deformations but retain axially symmetric shapes at angular velocities well beyond the stability range of viscous classical droplets.

The discoveries of superconductors, superfluids, and Bose-Einstein condensates (BECs) (*1*, *2*) reveal that a large number of particles can occupy a single quantum state that extends across macroscopic length scales. A notable example is superfluid ^{4}He (*3*–*6*): It lacks any viscosity below a critical temperature of T_λ = 2.17 K, and its motion is described by a single wave function (*1*, *2*, *5*–*7*). Isolated He nanodroplets were employed to study the onset of superfluidity through the observation of frictionless, quantized rotation of embedded molecules surrounded with varying numbers of ^{4}He atoms (*8*). However, the unambiguous demonstration of a quantum mechanical state of motion of an entire helium nanodroplet remains challenging.

In a finite droplet, any manifestation of liquid flow must involve rotational motion, which, in a superfluid, embodies itself in quantum vortices (*6*, *7*). Indeed, the formation of regular arrays of parallel vortices was detected in a rotating bucket filled with superfluid He (*9*, *10*). However, surprisingly little is known about quantum rotation in superfluid droplets. Calculations predict that vortices may exist in ^{4}He droplets as small as a few nanometers in diameter (*11*–*13*), but experimental studies of this elusive phenomenon remain challenging (*14*). Recently, traces of vortices were detected in He droplets ~1 μm in diameter (*15*). However, these exploratory experiments did not provide detailed hydrodynamic properties of the spinning droplets, such as their shapes or the spatial arrangements of the vortices they contain. In this work, we studied the rotation of single, isolated superfluid He nanodroplets via coherent scattering of x-rays from a free-electron laser (FEL) (*16*–*18*). Figure 1 illustrates the experiment, in which ^{4}He droplets with radii R = 100 to 1000 nm [number of He atoms (N_{He}) = 10^8 to 10^{11}] were produced upon fragmentation of liquid helium expanding into a vacuum (*15*, *19*, *20*) [see section S1 of (*21*)]. After a time of flight of 3.8 ms across a distance of 640 mm from the nozzle, the droplets traversed the focus of the FEL beam [photon energy = 1.5 keV, wavelength λ = 0.827 nm]. Diffraction images were recorded with a pn-junction charge-coupled device detector placed ≈565 mm behind the interaction volume. Each image originates from a single droplet irradiated by a single FEL shot. The low-density core of ^{4}He vortices is ≈0.2 nm in diameter (*7*), which does not provide sufficient contrast for direct detection by x-ray scattering. Therefore, the droplets are doped with Xe atoms ($N_{Xe} \approx 10^{-3} N_{He}$), which cluster along the vortex cores (*10*, *15*) and act as a contrast agent.

Diffraction images of individual neat helium droplets are shown in Fig. 2, A to C. The circular and elliptical diffraction contours in Fig. 2, A and B, are consistent with diffraction from spheroidal droplets with a symmetry half-axis a and two equal perpendicular half-axes b (fig. S2). The aspect ratio AR = (long half-axis)/(short half-axis)

[1]Department of Chemistry, University of Southern California (USC), Los Angeles, CA 90089, USA. [2]Linac Coherent Light Source (LCLS), SLAC National Accelerator Laboratory, 2575 Sand Hill Road, Menlo Park, CA 94025, USA. [3]Ultrafast X-ray Science Laboratory, Chemical Sciences Division, Lawrence Berkeley National Laboratory (LBNL), Berkeley, CA 94720, USA. [4]Department of Chemistry, University of California Berkeley, Berkeley, CA 94720, USA. [5]Max-Planck-Institut für Kernphysik, Saupfercheckweg 1, 69117 Heidelberg, Germany. [6]Max Planck Advanced Study Group at the Center for Free-Electron Laser Science (CFEL), Notkestraße 85, 22607 Hamburg, Germany. [7]Department of Physics and Astronomy, USC, Los Angeles, CA 90089, USA. [8]Deutsches Elektronen-Synchrotron (DESY), Notkestraße 85, 22607 Hamburg, Germany. [9]Advanced Light Source, LBNL, Berkeley, CA 94720, USA. [10]CFEL, DESY, Notkestraße 85, 22607 Hamburg, Germany. [11]Max-Planck-Institut für Extraterrestrische Physik, Giessenbachstraße, 85741 Garching, Germany. [12]Max-Planck-Institut für Medizinische Forschung, Jahnstrasse 29, 69120 Heidelberg, Germany. [13]PNSensor GmbH, Otto-Hahn-Ring 6, 81739 München, Germany. [14]Mork Family Department of Chemical Engineering and Materials Science, USC, Los Angeles, CA 90089, USA. [15]Department of Physics, University of California Berkeley, Berkeley, CA 94720, USA. [16]Department of Physics, The Chinese University of Hong Kong, Hong Kong, China. [17]National Energy Research Scientific Computing Center, LBNL, Berkeley, CA 94720, USA. [18]Physical Biosciences Division, LBNL, Berkeley, CA 94720, USA. [19]Department of Plant and Microbial Biology, University of California Berkeley, Berkeley, CA 94720, USA. [20]Department of Physics, University of California Davis, Davis, CA 95616, USA. [21]James R. Macdonald Laboratory, Department of Physics, Kansas State University, Manhattan, KS 66506, USA. [22]PULSE Institute, Stanford University and SLAC National Accelerator Laboratory, 2575 Sand Hill Road, Menlo Park, CA 94025, USA.
*Present address: New Focus, 3635 Peterson Way, Santa Clara, CA 95054, USA. †Present address: Shanghai Synchrotron Radiation Facility, Shanghai Institute of Applied Physics, Chinese Academy of Sciences, Shanghai 201204, China. ‡Present address: Department of Cell and Molecular Biology, Uppsala University, Husargatan 3, Uppsala 75124, Sweden. §Present address: Physikalisch-Technische Bundesanstalt, Bundesallee 100, D-38116 Braunschweig, Germany. ||Present address: Leibniz Institute of Surface Modification (IOM), Permoserstraße 15, 04318 Leipzig, Germany. ¶Present address: Berliner Glas KGaA Herbert Kubatz GmbH, Waldkraiburger Straße 5, 12347 Berlin, Germany.
#Corresponding author. E-mail: bostedt@slac.stanford.edu (C.B.); ogessner@lbl.gov (O.G.); vilesov@usc.edu (A.F.V.)

≥ 1 of the diffraction contours quantifies the distortion of the droplets from a spherical shape (AR = 1). Each diffraction image reflects the projection of a single droplet's density profile onto the detector plane; the longer axis in the diffraction pattern corresponds to the shorter droplet axis and vice versa. Because the a axis subtends an arbitrary angle with the x-ray beam, only the b axis and an upper boundary $a \leq b/AR$ can be deduced from each image. The pattern in Fig. 2A originates from either a spherical droplet with $R = a = b = 298 \pm 5$ nm or a spheroidal droplet with $b = R$ and its a axis aligned parallel to the x-ray beam. The diffraction pattern in Fig. 2B corresponds to a spheroid with $b = 284 \pm 5$ nm and $a \leq 0.87b = 247 \pm 5$ nm [section S2 of (*21*)].

Approximately ~1% of the diffraction images cannot be described by ellipses and exhibit very high aspect ratios of $1.7 < AR < 2.3$, such as AR = 1.92 in Fig. 2C. Figure 2D shows the outline of the corresponding droplet, which was obtained by inverse Fourier transform (IFT) of Fig. 2C [section S3 of (*21*)]. The droplet is wheel-shaped with two nearly parallel surfaces and half-axes $a = 220 \pm 15$ nm and $b = 422 \pm 10$ nm. The intense diagonal streak in Fig. 2C indicates that the droplet was imaged edge-on within ± 5° [see section S3 of (*21*)]. Thus, values for both a and b can be determined.

Our measurements reveal that, on average, ~40% of He droplets [section S5 of (*21*)] in the beam are not spherical, as was previously assumed (*20*), but are better represented by spheroids or wheel shapes. In general, a droplet may acquire a nonspherical shape due to rotational or vibrational excitation. However, our estimates show that vibrational shape oscillations should decay before the interaction point [section S6 of (*21*)]. Therefore, the elliptical and streaked diffraction patterns are ascribed to oblate rotating droplets. The droplet rotation probably originates from inhomogeneous flow of helium through the nozzle during the expansion (*15*).

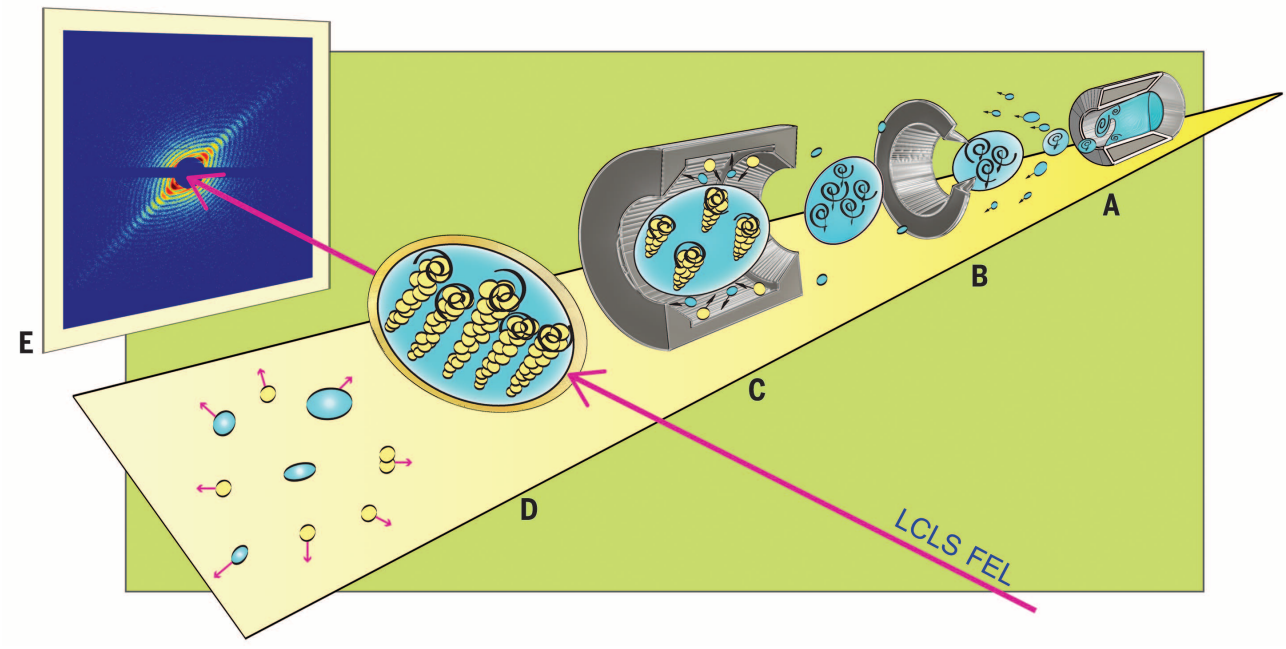

Fig. 1. Experimental setup. (**A**) Rotating droplets are produced by expanding He fluid into a vacuum through a 5-μm nozzle at a temperature of $T_0 \approx 5$ K and a backing pressure $P_0 = 20$ bar. (**B**) Quantum vortices form upon evaporative cooling of rotating droplets to below T_λ. (**C**) Droplets are doped with Xe atoms in a cell filled with Xe gas. (**D** and **E**) X-ray diffraction images of single droplets are recorded using single FEL light pulses.

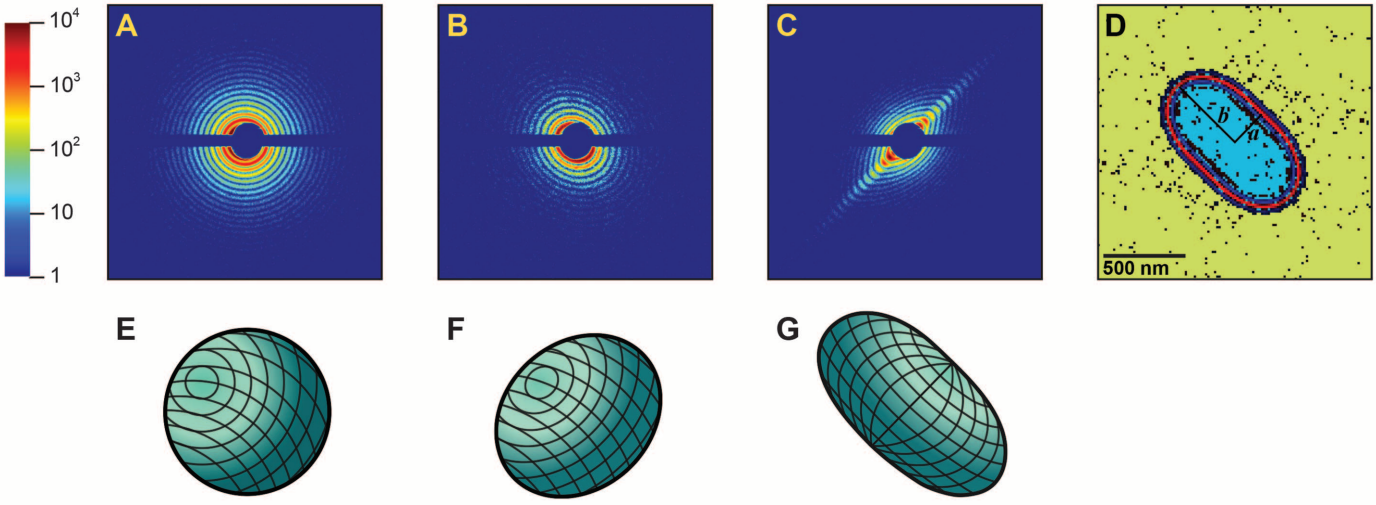

Fig. 2. X-ray diffraction images of neat He droplets. Images in (**A**) to (**C**) represent circular, elliptical, and streaked patterns, respectively, displayed in a logarithmic color scale. (**D**) Image showing a droplet outline reconstructed from the diffraction pattern in (C) by IFT. Note that the droplet itself is not hollow but filled. (**E** to **G**) 3D representations of the droplet shapes in (A) to (C) have been placed below the corresponding images.

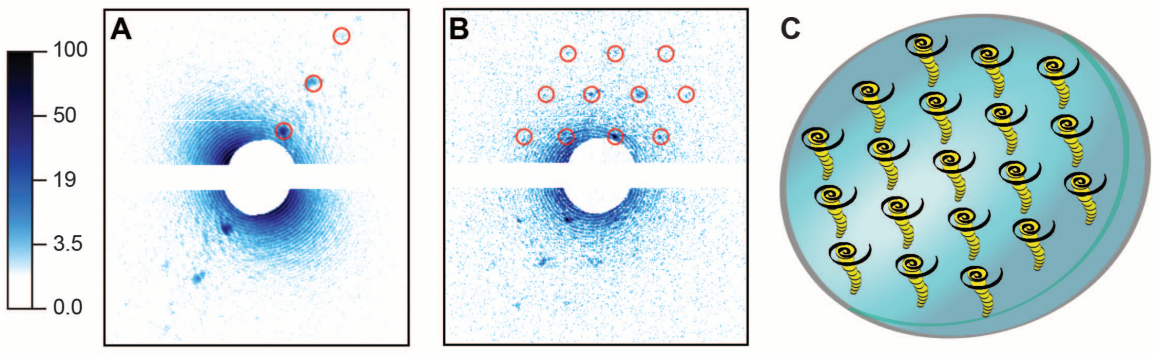

Fig. 3. He droplets doped with Xe atoms. (**A** and **B**) X-ray diffraction images of doped droplets, displayed in a logarithmic intensity scale. (**C**) Droplet and embedded Xe clusters. Images in (A) and (B) correspond to tilted and parallel alignments of the vortex axes with respect to the incident x-ray beam, respectively.

The shapes adopted by the rotating quantum droplets display similarities and pointed differences when compared with their classical counterparts. A classical droplet, rotating as a rigid body, can be described by the reduced angular velocity

$$\Omega = \sqrt{\frac{3\rho V}{32\pi\sigma}}\,\omega \qquad (1)$$

which defines the droplet's aspect ratio (*22*, *23*). Here, ρ is the density, σ is the surface tension, V is the volume of the droplet, and ω is its angular velocity. No droplet is stable beyond the disintegration limit of $\Omega_{MAX} = 0.75$. At small Ω, a droplet has a spheroidal shape. Beyond $\Omega = 0.56$ ($b/a = 1.50$), viscous classical droplets become unstable and begin to exhibit two-lobed shapes, resembling a peanut that rotates around its short axis. Multilobed droplet shapes emerge at even higher Ω (*22*–*24*). In this work, we observe axially symmetric droplets with aspect ratios as high as $b/a = 2.3$, corresponding to $\Omega = 0.71$ [section S4 of (*21*)], which is considerably higher than the shape instability threshold of classical droplets. No evidence for multilobed shapes was detected. Our results confirm the predicted extended range of stability in rotating quantum liquids (*23*) and indicate that superfluid droplets remain axially symmetric up to rotational speeds close to Ω_{MAX}.

The angular velocities (ω) of rotating droplets can be determined from the degree of centrifugal distortion, quantified by the a and b half-axes [section S4 of (*21*)] (*23*). For the image in Fig. 2C, this analysis leads to $\omega = 1.4 \times 10^7\ s^{-1}$. The rotation of a superfluid may manifest as a lattice of uniformly distributed parallel vortices (*1*, *6*, *7*, *9*) with an area density of

$$n_V = \frac{2\omega M}{h} \qquad (2)$$

Here, M is the mass of the ^{4}He atom, h is Planck's constant, and n_V is the number of vortices per unit area in a plane perpendicular to the axis of rotation (*6*, *7*). For the droplet imaged in Fig. 2C, Eq. 2 predicts a vortex density of $n_V = 2.8 \times 10^{14}\ m^{-2}$ and a total number of vortices of $N_V = \pi b^2 n_V = 160$. Evidently, droplets in the beam are characterized by a substantial degree of rotational excitation and thus should contain large numbers of quantum vortices. The existence of these vortices is confirmed by doping the He droplets with Xe atoms.

Figure 3 shows diffraction images of He droplets doped with Xe atoms. In addition to the characteristic ring patterns from the droplets, many images exhibit Bragg spots that either lie on a line crossing the image center (Fig. 3A) or form an equilateral triangular pattern (Fig. 3B). The Bragg spot separations in Fig. 3 correspond to regularly spaced Xe structures with periods of $d \approx 100$ nm, whereas the ring patterns arise from a droplet with $R \approx 1$ μm. These numbers are consistent with the condensation of Xe atoms along the cores of multiple parallel vortices arranged in a lattice within the superfluid droplet (Fig. 3C). According to this model, both linear and triangular Bragg spot arrangements emerge from ordered lattices with different relative angles between the x-ray beam and the vortex lines. The actual shape of the vortices cannot be determined from the Bragg spots, although the vortices in the arrays are expected to have some curvature as they terminate perpendicular to the droplet's surface. Approximately 5% of the doped droplet images exhibit Bragg spots. Considering that the appearance of Bragg spots depends critically on the relative alignment of the vortex structures and the x-ray beam, which is randomly distributed in these experiments, we estimate that ~50% of droplets contain vortex lattices [section S7 of (*21*)].

The identification of quantum vortices provides direct evidence of the superfluidity of He nanodroplets. The appearance of triangular vortex arrangements agrees with previous observations of triangular arrays of quantum vortices in rarified BECs (*25*, *26*). The diameters of the vortex cores in superfluid He, however, are small compared with the droplet sizes and the vortex length scales, which can lead to extended, three-dimensional (3D) vortex arrangements.

The diffraction pattern in Fig. 3B provides a direct measure of the vortex density, $n_V = 4.5 \times 10^{13}\ m^{-2}$, and the droplet radius, $b = 1100$ nm, corresponding to a total number of vortices $N_V = 170$. The angular velocity of the rotating droplet is $\omega = 2.2 \times 10^6\ s^{-1}$ (Eq. 2). The diffraction rings in Fig. 3B are circular within the experimental resolution (~3%). This observation and, in particular, the emergence of the triangular Bragg pattern, indicate that the droplet was imaged almost exactly along the a axis. From the angular velocity and the equatorial radius b, the aspect ratio and reduced angular velocity of the droplet are estimated to be $AR = 1.34$ and $\Omega = 0.50$, respectively [section S4 of (*21*)]. These values fall well within the axisymmetric shape stability limits for rotating droplets. The vortex density in this droplet is about five orders of magnitude larger than previously observed in rotating bucket experiments with bulk superfluid helium (*9*, *10*). These numbers demonstrate that superfluid He droplets provide access to unexplored regimes of rotational excitation in quantum liquids. It is intriguing that, although observation of the wheel shapes in smaller droplets ($b \approx 300$ to 400 nm) indicates the existence of high vortex densities in the range of $n_V \approx 3 \times 10^{14}\ m^{-2}$, no corresponding Bragg patterns were observed in these droplets [section S7 of (*21*)]. This may indicate that vortices at extremely high densities fail to crystallize and instead form a disordered state with little resemblance to a lattice. Another possibility is the existence of nonequilibrium states, which may be related to quantum turbulence. However, estimates [section S6 of (*21*)] show that turbulence, which accompanies establishment (*27*) or breakdown (*28*) of equilibrium quantum rotation, decays before the interaction point. Hydrodynamic instability of the droplet shape at high angular velocities may also disrupt vortex arrays. The possibility for the formation of nonstationary vortex states in superfluid helium has been discussed (*6*) but has never been confirmed experimentally. In addition, BECs at high ω are predicted to undergo a quantum phase transition into a highly correlated nonsuperfluid state devoid of any vortices (*26*). It would therefore be interesting to explore whether similar concepts apply to rotating He droplets at high ω.

REFERENCES AND NOTES

1. L. Pitaevskii, S. Stringari, *Bose-Einstein Condensation*, J. Birman *et al.*, Eds. (vol. 116 of The International Series of Monographs on Physics, Clarendon Press, Oxford, 2003).
2. D. R. Tilley, J. Tilley, *Superfluidity and Superconductivity* (Institute of Physics Publishing, Bristol, UK, 1990).
3. J. F. Allen, A. D. Misener, *Nature* **141**, 75 (1938).

4. P. Kapitza, *Nature* **141**, 74 (1938).
5. L. D. Landau, *J. Phys. (Moscow)* **5**, 185–204 (1941).
6. R. P. Feynman, in *Progress in Low Temperature Physics*, C. J. Gorter, Ed. (North-Holland, Amsterdam, 1955), vol. 1, pp. 1–53.
7. R. J. Donnelly, *Quantized Vortices in Helium II*, A. M. Goldman, P. V. E. McKlintock, M. Springford, Eds. (vol. 3 of Cambridge Studies in Low Temperature Physics, Cambridge Univ. Press, Cambridge, 1991).
8. S. Grebenev, J. P. Toennies, A. F. Vilesov, *Science* **279**, 2083–2086 (1998).
9. E. J. Yarmchuk, M. J. V. Gordon, R. E. Packard, *Phys. Rev. Lett.* **43**, 214–217 (1979).
10. G. P. Bewley, D. P. Lathrop, K. R. Sreenivasan, *Nature* **441**, 588 (2006).
11. G. H. Bauer, R. J. Donnelly, W. F. Vinen, *J. Low Temp. Phys.* **98**, 47–65 (1995).
12. K. K. Lehmann, R. Schmied, *Phys. Rev. B* **68**, 224520 (2003).
13. M. Barranco *et al.*, *J. Low Temp. Phys.* **142**, 1–81 (2006).
14. M. A. Weilert, D. L. Whitaker, H. J. Maris, G. M. Seidel, *J. Low Temp. Phys.* **106**, 101–131 (1997).
15. L. F. Gomez, E. Loginov, A. F. Vilesov, *Phys. Rev. Lett.* **108**, 155302 (2012).
16. L. Strüder *et al.*, *Nucl. Instrum. Methods A* **614**, 483–496 (2010).
17. C. Bostedt *et al.*, *J. Phys. B* **46**, 164003 (2013).
18. T. Gorkhover *et al.*, *Phys. Rev. Lett.* **108**, 245005 (2012).
19. L. F. Gomez, E. Loginov, R. Sliter, A. F. Vilesov, *J. Chem. Phys.* **135**, 154201 (2011).
20. J. P. Toennies, A. F. Vilesov, *Angew. Chem. Int. Ed.* **43**, 2622–2648 (2004).
21. Materials and methods and supporting analysis of the experimental data are available as supplementary materials on *Science* Online.
22. R. A. Brown, L. E. Scriven, *Proc. R. Soc. London Ser. A* **371**, 331–357 (1980).
23. S. Chandrasekhar, *Proc. R. Soc. London Ser. A* **286**, 1–26 (1965).
24. R. J. A. Hill, L. Eaves, *Phys. Rev. Lett.* **101**, 234501 (2008).
25. J. R. Abo-Shaeer, C. Raman, J. M. Vogels, W. Ketterle, *Science* **292**, 476–479 (2001).
26. A. L. Fetter, *Rev. Mod. Phys.* **81**, 647–691 (2009).
27. A. P. Finne *et al.*, *Nature* **424**, 1022–1025 (2003).
28. P. M. Walmsley, A. I. Golov, H. E. Hall, A. A. Levchenko, W. F. Vinen, *Phys. Rev. Lett.* **99**, 265302 (2007).

ACKNOWLEDGMENTS

This work was supported by NSF grant CHE-1112391 (A.F.V.) at USC; the U.S. Department of Energy (DOE), Office of Basic Energy Sciences (OBES), Chemical Sciences, Geosciences and Biosciences Division through contract no. DE-AC02-05CH11231; and the Max Planck Society by funding the development and operation of the CFEL Advanced Study Group (ASG) Multi-Purpose (CAMP) instrument. Portions of this research were carried out at the LCLS, a national user facility operated by Stanford University on behalf of the U.S. DOE OBES under beam-time grant L549: Imaging of quantum vortices in superfluid helium droplets. S.R.L. and J.P. acknowledge support from the Office of the Secretary of Defense, National Security Science and Engineering Faculty Fellowship. C.B. was partially supported through the PULSE Institute at SLAC National Accelerator Laboratory funded by the U.S. DOE OBES under contract no. DE-AC02-76SF00515. J.K. was supported by the USC Undergraduate Research Associates Program. S.M. was supported by the Center for Applied Mathematics for Energy Research Applications (CAMERA). A.R. was supported by the NSF. M. Seifrid was supported by the USC Dornsife College of Letters, Arts and Sciences Student Opportunities for Academic Research and Summer Undergraduate Research Fund fellowships. K.R.S. was supported by the Alexander von Humboldt Foundation.

SUPPLEMENTARY MATERIALS

www.sciencemag.org/content/345/6199/906/suppl/DC1
Materials and Methods
Supplementary Text
Figs. S1 to S6
References (*29*–*39*)

19 February 2014; accepted 20 June 2014
10.1126/science.1252395

NANOPARTICLE IMAGING

Electron microscopy of gold nanoparticles at atomic resolution

Maia Azubel,[1] Jaakko Koivisto,[2] Sami Malola,[3] David Bushnell,[1] Greg L. Hura,[4] Ai Leen Koh,[5] Hironori Tsunoyama,[6]* Tatsuya Tsukuda,[6]† Mika Pettersson,[2] Hannu Häkkinen,[2,3] Roger D. Kornberg[1]‡

Structure determination of gold nanoparticles (AuNPs) is necessary for understanding their physical and chemical properties, but only one AuNP larger than 1 nanometer in diameter [a 102–gold atom NP (Au_{102}NP)] has been solved to atomic resolution. Whereas the Au_{102}NP structure was determined by x-ray crystallography, other large AuNPs have proved refractory to this approach. Here, we report the structure determination of a Au_{68}NP at atomic resolution by aberration-corrected transmission electron microscopy, performed with the use of a minimal electron dose, an approach that should prove applicable to metal NPs in general. The structure of the Au_{68}NP was supported by small-angle x-ray scattering and by comparison of observed infrared absorption spectra with calculations by density functional theory.

Gold nanoparticles (AuNPs) are of both fundamental and practical interest. Particles on the order of 1 nm in diameter exhibit distinctive physical and chemical properties, with potential applications ranging from quantum electronics to biomedicine (*1*–*3*). The x-ray crystal structure of a 102–gold atom NP (Au_{102}NP), 1.5 nm in diameter, showed the cluster of gold atoms surrounded by 44 thiolate ligands (*4*). This atomic structure had threefold importance: (i) It identified the Au_{102}NP as a molecule, with a precise composition and distinct arrangement of atoms; (ii) it led to the idea of the gold cluster as a "super atom," stabilized by the filling of electron shells; and (iii) it revealed a layer of alternating gold and ligand molecules at the interface with solution (*5*). Subsequent x-ray structures of much smaller organosoluble AuNPs have supported the super-atom idea and have shown a similar gold-thiol surface layer [reviewed in (*6*)]. Structure determination of other water-soluble AuNPs, and of larger NPs in general, has so far been unsuccessful. Although water-soluble AuNPs ranging from 1 to 3 nm in diameter have been crystallized, x-ray diffraction has not extended beyond ~5 Å resolution. Here, we demonstrate the structure determination of a AuNP by a combination of a low-dose approach and aberration-corrected transmission electron microscopy (TEM), and we report an atomic structure with both similarities and notable differences from the Au_{102}NP.

Whereas the thiolate ligand of the Au_{102}NP was *p*-mercaptobenzoic acid (*p*-MBA), we have now performed synthesis with 3-MBA, resulting in a different set of uniform, water-soluble particles. The product of synthesis with a thiol:gold ratio of 2:1 formed a single sharp band upon gel electrophoresis, with a mobility greater than that of the Au_{102}NP, indicative of a smaller size, as confirmed by cryogenic TEM (fig. S1). Electrospray ionization time-of-flight mass spectrometry (MS) revealed four peaks corresponding to various charged forms of a compound of ~18 kD with a gold core of ~14 kD (fig. S2). A stable AuNP with a gold core of similar size was previously reported by Whetten *et al.* (*7*). Because the mass difference between three atoms of gold [m = 591 atomic mass units (amu)] and four molecules of 3-MBA (m = 613 amu) could not be resolved, the MS result was consistent with the possible molecular formulas $[Au_{71}(3\text{-MBA})_{27}]^{n-}$, $[Au_{68}(3\text{-MBA})_{31}]^{n-}$, $[Au_{68}(3\text{-MBA})_{32}]^{n-}$, $[Au_{65}(3\text{-MBA})_{35}]^{n-}$, and $[Au_{62}(3\text{-MBA})_{39}]^{n-}$ (where n is 5, 6, 7, or 8). We could distinguish among these possibilities by thermogravimetric analysis (TGA) and x-ray photoelectron spectroscopy (XPS). TGA gave a weight loss of 24.4% (fig. S3), compared with values of 26.2% expected for $Au_{68}(3\text{-MBA})_{31}$ or 26.8% expected for $Au_{68}(3\text{-MBA})_{32}$, both discrepancies within the error of the method (*8*). By contrast, expected TGA weight loss values of 29.6% for $Au_{65}(3\text{-MBA})_{35}$ and 33.0% for $Au_{62}(3\text{-MBA})_{39}$ represent discrepancies three to five times greater. XPS gave signals corresponding to Au, S, C, and O (fig. S4), and the peak intensities corresponding to Au_{4f} and S_{2p} were integrated to establish the ratio between Au and organic material. The difference between the values of 65.5% Au and 34.5% S measured and those of 68.7% Au and 31.3% S expected for $Au_{68}(3\text{-MBA})_{31}$ or 68.0% Au and 32.0% S expected for $Au_{68}(3\text{-MBA})_{32}$ were again within the error of the method (*8*). Values of 72.4% Au and 27.6% S expected for $Au_{71}(3\text{-MBA})_{27}$

[1]Department of Structural Biology, Stanford University School of Medicine, Stanford, CA 94305, USA. [2]Department of Chemistry, Nanoscience Center, University of Jyväskylä, FI-40014 Jyväskylä, Finland. [3]Department of Physics, Nanoscience Center, University of Jyväskylä, FI-40014 Jyväskylä, Finland. [4]Physical Bioscience Division, Lawrence Berkeley National Lab, Berkeley, CA 94720, USA. [5]Stanford Nanocharacterization Laboratory, Stanford University, Stanford, CA 94305, USA. [6]Catalysis Research Center, Hokkaido University, Sapporo, Japan.
*Present address: Department of Chemistry, Faculty of Science and Technology, Keio University, Yokohama 223-8522, Japan.
†Present address: Department of Chemistry, School of Science, The University of Tokyo, Tokyo 113-0033, Japan. **‡Corresponding author. E-mail: kornberg@stanford.edu**

were substantially different. Therefore, of the five molecular formulas consistent with the results from MS, all but two—Au_{68}(3-MBA)$_{31}$ and Au_{68}(3-MBA)$_{32}$—were ruled out by TGA and XPS.

The solubility of the Au_{68}NP and its stability in solution were notable. The Au_{68}NP could be derivatized with proteins and nucleic acids bearing exposed sulfhydryl groups (fig. S5) and is therefore well suited for applications in biological science and biomedicine. The Au_{68}NP could be crystallized, forming hexagonal plates (fig. S6), but x-ray diffraction did not extend beyond 5 Å resolution. Due to the apparent homogeneity of the Au_{68}NP, TEM and single-particle reconstruction (*9*) could be pursued as an alternative for structure determination. Exposure to an electron dose normally used for data collection in materials science (thousands of electrons per square angstrom) visibly perturbed the Au_{68} particles. We therefore turned to low-dose procedures, routinely used for biological TEM, which reduce the exposure to the electron beam by several orders of magnitude by focusing on an area adjacent to the one being imaged and then imaging for the minimal time required to record a signal above the noise, followed by improvement of the signal-to-noise ratio by image averaging. The low-dose strategy was successful (Fig. 1A and fig. S7A): Images of 939 particles acquired in this way and processed with the EMAN2 software package (*10*) (fig. S7) yielded an electron density map with 68 peaks (Fig. 1, B and C). The peaks in the center of the map were of highest intensity, probably because they were most symmetrically arranged and most rigidly fixed. Identification of the peaks with gold atoms is justified by their numbers, the distances between them, and their packing, as well as because their high intensities could be attributed only to heavy atoms. The distances ranged from 2.72 to 3.07 Å (Fig. 1D), in keeping with those for the gold core of the Au_{102}NP, which were from 2.8 to 3.1 Å (*4*). The packing was face-centered cubic (fcc) or truncated fcc-like, similar to that in a recently reported x-ray crystal structure of the organosoluble $Au_{36}(SR)_{24}$ (R, 4-*tert*-butylbenzenethiolate) (*11*). The arrangement of the 68 gold atoms can be described as a 13-atom cuboctahedron with an atom in the center (Fig. 2, A and B), surrounded by 24 atoms extending the fcc-like framework (Fig. 2C) and an additional 31 atoms deviating from fcc packing (Fig. 2D). A Fourier transform of a section of the electron density map (Fig. 1E) showed spots at 2.4 Å, consistent with this arrangement (atoms 2.7 to 3.0 Å apart with fcc packing have lattice planes with spacings of 2.3 to 2.55 Å) and demonstrating the resolution of the analysis.

Support for the electron microscopy (EM) structure came from small-angle x-ray scattering (SAXS), which gave a radius of gyration (R_g) of 7.6 Å, compared with a R_g calculated for the gold cluster of the EM structure of 5.72 Å. The larger measured R_g could be explained by aggregation of gold particles, which occurs in an ionic strength–dependent manner (*12*). The SAXS data could be fit by a mixture of monomers and dimers, with $\chi^2 = 1$ up to a reciprocal space distance (q value) of 0.44 Å^{-1} (fig. S8). At higher q values, a small discrepancy was observed, which may arise partially from the organic surface layer, neglected in the calculation of R_g from the EM structure. The center-to-center distance of the dimer calculated from SAXS was 14 Å, consistent with a model of the surface layer (see below), whereas the diameter of the gold cluster from the EM structure, used in the calculation was 11.5 Å.

Sulfur atoms were introduced into the EM structure, with gold-sulfur distances of ~2.3 Å (Fig. 3A). Aside from 15 gold atoms fully coordinated with gold neighbors (the central atom, the 12 atoms on the vertices of the cuboctahedron, and another 2 atoms), all remaining gold atoms are available for Au-S bond formation. The final model, containing 32 atoms of S for consistency with the model from density functional theory (DFT) described below, can be described as an Au_{15} fcc core decorated with 10 staple motifs (*4*, *6*) and 12 V-shape (or bridge) motifs (*13*) (Fig. 3A).

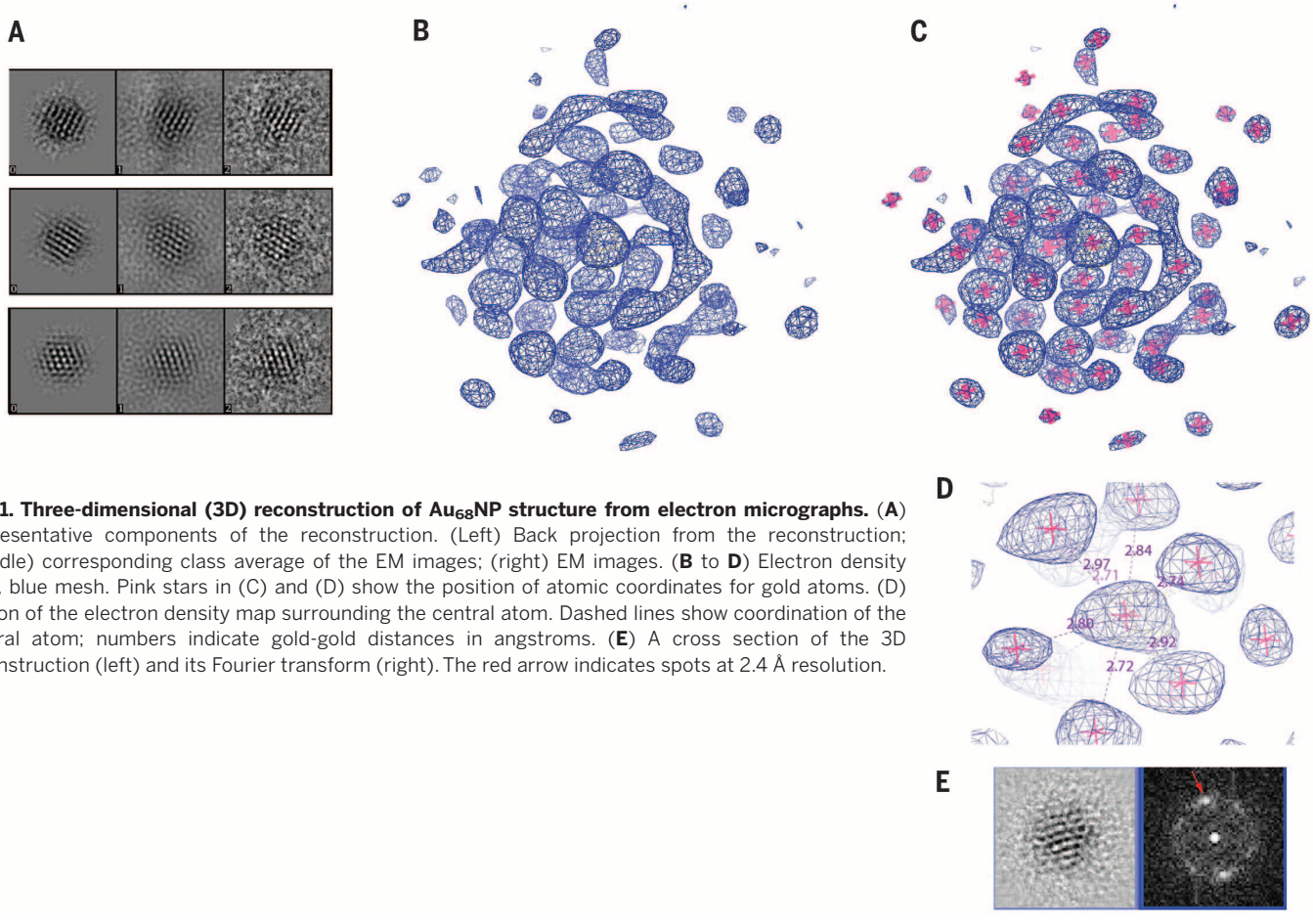

Fig. 1. Three-dimensional (3D) reconstruction of Au_{68}NP structure from electron micrographs. (**A**) Representative components of the reconstruction. (Left) Back projection from the reconstruction; (middle) corresponding class average of the EM images; (right) EM images. (**B** to **D**) Electron density map, blue mesh. Pink stars in (C) and (D) show the position of atomic coordinates for gold atoms. (D) Region of the electron density map surrounding the central atom. Dashed lines show coordination of the central atom; numbers indicate gold-gold distances in angstroms. (**E**) A cross section of the 3D reconstruction (left) and its Fourier transform (right). The red arrow indicates spots at 2.4 Å resolution.

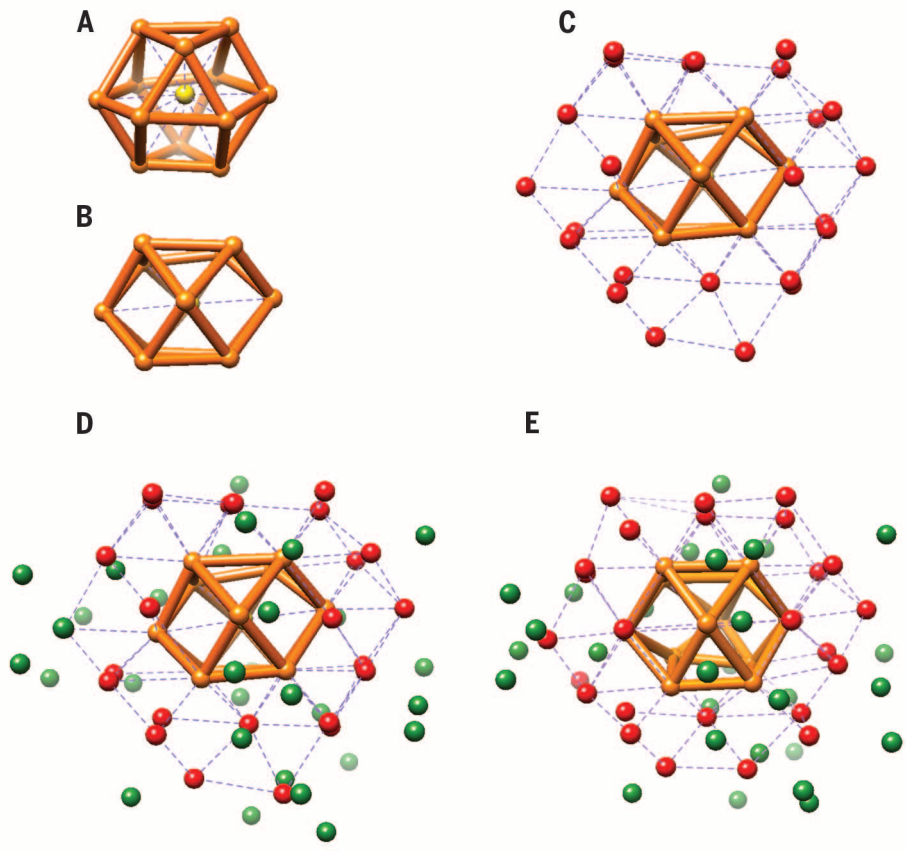

Fig. 2. Arrangement of gold atoms in Au_{68}NP. (**A** to **D**) Coordinates. (A and B) Two orthogonal views of the central 13 atoms: central atom (yellow) caged in a cuboctahedron (orange). (C) Additional 24 atoms (red) extending the fcc-like framework. (D) All 68 atoms. Atoms with lower or no apparent symmetry are in green. (**E**) Au_{68} model from DFT.

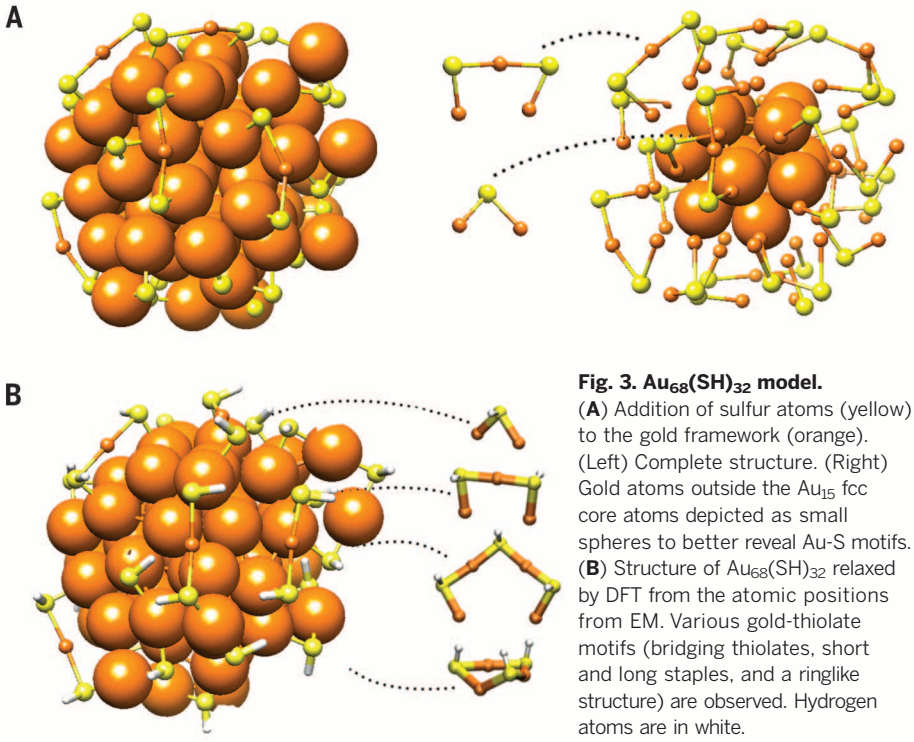

Fig. 3. $Au_{68}(SH)_{32}$ model. (**A**) Addition of sulfur atoms (yellow) to the gold framework (orange). (Left) Complete structure. (Right) Gold atoms outside the Au_{15} fcc core atoms depicted as small spheres to better reveal Au-S motifs. (**B**) Structure of $Au_{68}(SH)_{32}$ relaxed by DFT from the atomic positions from EM. Various gold-thiolate motifs (bridging thiolates, short and long staples, and a ringlike structure) are observed. Hydrogen atoms are in white.

Additional support for the EM structure came from DFT for the hypothetical compound $Au_{68}(SH)_{32}$. When a model of this compound, built from the coordinates of gold atoms in the EM structure, was relaxed to a local energy minimum with DFT, the positions of the gold atoms were largely unaffected (compare Fig. 2, D and E). Most of the gold atoms were shifted by clearly less than 1 Å, with the exception of a few atoms in the surface layer (fig. S9A). The positions of these atoms may be affected by hydrogen bonding between 3-MBA ligands in the surface layer, as observed upon relaxation by DFT of the compound $Au_{68}(SH)_{30}$(3-MBA)$_2$ (fig. S9B). The DFT model displayed gold-sulfur motifs (Fig. 3B) similar to those produced by manual building of sulfur atoms into the EM structure (Fig. 3A).

The electronic structure of the Au_{68}NP was investigated by infrared (IR) and ultraviolet-visible (UV-vis) spectroscopy and linear-response, time-dependent DFT (LR-TDDFT) calculations. The IR-spectrum showed discrete absorption peaks at ~4200 cm^{-1} (0.52 eV) and 5250 cm^{-1} (0.65 eV) and a split transition at 6100 cm^{-1} (0.76 eV) (Fig. 4). A fourth peak at 2500 cm^{-1} (0.31 eV) could not be assigned to any known vibrational mode. This peak persisted even after removing the vibrational contribution of the ligand layer (fig. S10), so we attributed the peak to an electronic transition. The optical gap of the Au_{68}NP is therefore at 2500 cm^{-1} (0.31 eV), which is considerably lower than the gap of 0.45 eV observed for the larger Au_{102}(*p*-MBA)$_{44}$ cluster (*14*). This result is in contrast to the trend toward a smaller optical gap with increasing cluster size, reported for clusters of 25 to 144 gold atoms (*15*–*20*) and expected to approach zero for bulk metal. The optical gap of the Au_{68}NP is presumably lower because of deviation from spherical symmetry, so the cluster wave functions cannot follow a spherical form as they do in the case of Au_{102}NP. The spectrum of the DFT-relaxed $Au_{68}(SH)_{32}$ cluster obtained from the LR-TDDFT calculations (Fig. 4) reproduces the experimental spectral features (positions of absorption lines, not line shapes, which depend on the smoothing function applied in the calculations) with notable accuracy. Intensities are in good agreement for all but the first two transitions. In the UV-vis range, both the measured and computational spectra are rather featureless. This is in contrast to the spectra of the smaller organosoluble $Au_{25}(SCH_2CH_2Ph)_{18}$ and $Au_{38}(SCH_2CH_2Ph)_{24}$ NPs that show notable absorption features in the UV-vis range (*15*–*19*). Additional LR-TDDFT calculations of possible compounds in the range of $Au_{68}(SR)_{31\text{-}34}$ [including $Au_{68}(SR)_{32}$ but with different arrangements of gold atoms] did not satisfactorily reproduce the measured IR data in the optical gap region (fig. S11).

The notable findings of this work are: (i) the synthesis of a water-soluble AuNP, homogeneous in size, stable in solution, and nevertheless reactive toward sulfhydryl compounds, including proteins; (ii) the successful determination of atomic structure by EM, not previously reported; and (iii) the difference between the structure

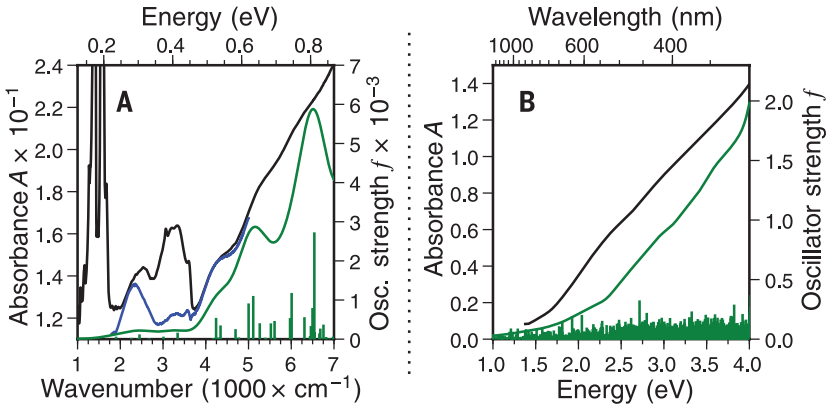

Fig. 4. Measured and computed absorption spectra of the Au_{68}NP. (**A**) IR region. (**B**) UV-vis region. Black curves, experimental data; green curves, LR-TDDFT-computed spectra obtained from the individual optical transitions (green vertical lines) with a Gaussian smoothing function [width 0.09 eV in (A) and 0.25 eV in (B)]. The blue curve in (A) denotes a spectrum from which the vibrational contribution has been subtracted by reference to a spectrum of a larger cluster with the same ligand layer (see fig. S10 for details). Both the computed and experimental data indicate that the lowest electronic transition occurs at 2500 cm^{-1} (0.31 eV).

obtained and the only other structure of a large, water-soluble particle (the Au_{102}NP), solved by x-ray diffraction.

The atomic structure of the Au_{68}NP differs from that of the Au_{102}NP in two important aspects. The symmetry of the Au_{68}NP is lower, and the electronic structure does not indicate a filled electronic shell (*5*). Whereas the Au_{102}NP exhibits global symmetry (based on a truncated decahedral core), with all remaining atoms following fcc packing rules, the Au_{68}NP is based almost entirely on local fcc packing. The low-symmetry Au_{68}NP structure differs from a proposal from theory for a metal core of higher symmetry for an organosoluble particle of similar size, $Au_{67}(SR)_{35}$ (*21*).

Structure determination of water-soluble AuNPs by EM is important because although many can be crystallized, only Au_{102}NP crystals so far diffract to atomic resolution. Aberration-corrected transmission electron microscopes are capable of revealing individual heavy atoms (*22*). Structures of large metal particles imaged under high-dose conditions have been reported: the results of model fitting to EM data (*23*, *24*); actual reconstructions from electron micrographs, in which the exact positions of individual atoms were not fully resolved (*25*); and results for bulklike solid-state systems where atoms are arranged in columns (*26*, *27*). Our implementation of low-dose techniques from biological TEM, combined with the power of the aberration-corrected transmission microscope, has revealed the atomic structure of a AuNP without any prior knowledge, model fitting, or assumptions about packing and should be generally applicable. This finding paves the way for structure determination of many more metal NPs and discovery of the general principles of NP organization.

REFERENCES AND NOTES

1. N. L. Rosi *et al.*, *Science* **312**, 1027–1030 (2006).
2. X. Qian *et al.*, *Nat. Biotechnol.* **26**, 83–90 (2008).
3. M.-C. Daniel, D. Astruc, *Chem. Rev.* **104**, 293–346 (2004).
4. P. D. Jadzinsky, G. Calero, C. J. Ackerson, D. A. Bushnell, R. D. Kornberg, *Science* **318**, 430–433 (2007).
5. M. Walter *et al.*, *Proc. Natl. Acad. Sci. U.S.A.* **105**, 9157–9162 (2008).
6. H. Häkkinen, *Nat. Chem.* **4**, 443–455 (2012).
7. R. L. Whetten *et al.*, *Adv. Mater.* **8**, 428–433 (1996).
8. Y. Levi-Kalisman *et al.*, *J. Am. Chem. Soc.* **133**, 2976–2982 (2011).
9. J. Frank, *Annu. Rev. Biophys. Biomol. Struct.* **31**, 303–319 (2002).
10. G. Tang *et al.*, *J. Struct. Biol.* **157**, 38–46 (2007).
11. C. Zeng *et al.*, *Angew. Chem. Int. Ed.* **51**, 13114–13118 (2012).
12. See supplementary materials on *Science* Online.
13. H. Häkkinen, M. Walter, H. Grönbeck, *J. Phys. Chem. B* **110**, 9927–9931 (2006).
14. E. Hulkko *et al.*, *J. Am. Chem. Soc.* **133**, 3752–3755 (2011).
15. J. Akola, M. Walter, R. L. Whetten, H. Häkkinen, H. Grönbeck, *J. Am. Chem. Soc.* **130**, 3756–3757 (2008).
16. M. W. Heaven, A. Dass, P. S. White, K. M. Holt, R. W. Murray, *J. Am. Chem. Soc.* **130**, 3754–3755 (2008).
17. M. Zhu, C. M. Aikens, F. J. Hollander, G. C. Schatz, R. Jin, *J. Am. Chem. Soc.* **130**, 5883–5885 (2008).
18. O. Lopez-Acevedo, H. Tsunoyama, T. Tsukuda, H. Häkkinen, C. M. Aikens, *J. Am. Chem. Soc.* **132**, 8210–8218 (2010).
19. H. Qian, W. T. Eckenhoff, Y. Zhu, T. Pintauer, R. Jin, *J. Am. Chem. Soc.* **132**, 8280–8281 (2010).
20. J. Koivisto *et al.*, *J. Phys. Chem. Lett.* **5**, 387–392 (2014).
21. P. R. Nimmala, B. Yoon, R. L. Whetten, U. Landman, A. Dass, *J. Phys. Chem. A* **117**, 504–517 (2013).
22. J. A. Scholl, A. L. Koh, J. A. Dionne, *Nature* **483**, 421–427 (2012).
23. D. Bahena *et al.*, *J. Phys. Chem. Lett.* **4**, 975–981 (2013).
24. Z. Y. Li *et al.*, *Nature* **451**, 46–48 (2008).
25. M. C. Scott *et al.*, *Nature* **483**, 444–447 (2012).
26. S. Van Aert, K. J. Batenburg, M. D. Rossell, R. Erni, G. Van Tendeloo, *Nature* **470**, 374–377 (2011).
27. B. Goris *et al.*, *Nat. Mater.* **11**, 930–935 (2012).

ACKNOWLEDGMENTS

The work at Stanford University was supported by the Human Frontier Science Program Organization (M.A.) and NIH grant AI-21144 (R.D.K). The work at the University of Jyväskylä was supported by the Academy of Finland (H.H. and M.P.) and the National Graduate School in Computational Chemistry and Spectroscopy LASKEMO (J.K.). G.L.H was supported by U.S. Department of Energy Biological and Environmental Research grant DE-AC02-05CH11231 under Integrated Diffraction Analysis Technologies. We thank P. Robinson for assistance with EM processing and helpful discussions and E. Hulkko and P. A. Clayborne for help with spectroscopic experiments and preliminary computations, respectively.

SUPPLEMENTARY MATERIALS

www.sciencemag.org/content/345/6199/909/suppl/DC1
Materials and Methods
Figs. S1 to S11
References (*28*–*32*)
Coordinates Files

7 February 2014; accepted 11 July 2014
10.1126/science.1251959

MASSIVE STARS

A chemical signature of first-generation very massive stars

W. Aoki,[1,2]* N. Tominaga,[3,4] T. C. Beers,[5,6] S. Honda,[7] Y. S. Lee[8]

Numerical simulations of structure formation in the early universe predict the formation of some fraction of stars with several hundred solar masses. No clear evidence of supernovae from such very massive stars has, however, yet been found in the chemical compositions of Milky Way stars. We report on an analysis of a very metal-poor star SDSS J001820.5–093939.2, which possesses elemental-abundance ratios that differ significantly from any previously known star. This star exhibits low [α-element Fe] ratios and large contrasts between the abundances of odd and even element pairs, such as scandium/titanium and cobalt/nickel. Such features have been predicted by nucleosynthesis models for supernovae of stars more than 140 times as massive as the Sun, suggesting that the mass distribution of first-generation stars might extend to 100 solar masses or larger.

The mass distribution of the first generations of stars is a key requirement for understanding the history of structure formation and chemical enrichment in the early universe. The formation of stars heavier than 100 solar masses ($M_\odot$) was predicted by early numerical simulations of structure formation (*1*). However, no evidence of supernovae from such very massive stars has yet been found in the chemical compositions of old, low-mass stars in the Milky Way (*2*), implying that the first generations of stars typically had masses no more

than several tens of solar masses (*3*). Recent theoretical studies of star formation from gas clouds containing no heavy elements also predict this mass range, suggesting that very massive stars are rare, if they are present at all, in the early universe (*4*). Very massive stars and their explosions could, however, have a large impact on chemical evolution because of their large chemical yields and explosion energies, even if they are relatively few in number, and searches continue for signatures of nucleosynthesis by the explosions of such very massive stars.

SDSS J001820.5−093939.2 (hereafter SDSS J0018-0939) was identified as a star likely to have a very low abundance of metals, based on medium-resolution spectroscopy obtained during the Sloan Digital Sky Survey (SDSS) as part of the stellar subsurvey Sloan Extension for Galactic Understanding and Exploration (SEGUE) (*5*). We obtained high-resolution spectroscopy with the Subaru Telescope High Dispersion Spectrograph (HDS) (*6*) for candidate very metal-poor stars identified by SDSS/SEGUE, including SDSS J0018-0939 (*7*). This previous study confirmed the low metal abundance ([Fe/H] = −2.5) for this star and reported notably low abundance ratios of the α elements with respect to iron, such as [Mg/Fe]. With the same instrument, we also obtained an additional high-resolution spectrum covering bluer wavelengths on 7 August 2012, in order to measure elemental abundances with higher accuracy based on the large number of spectral lines existing in the blue wavelength range.

SDSS J0018-0939 is a cool main-sequence star with an effective temperature of 4600 K and metallicity of [Fe/H] = −2.5. The absolute visual magnitude (M_v = 8.0) and mass (M = 0.47 $M_\odot$) were estimated from fits to old-stellar-population isochrones (*8*). Based on this star's apparent magnitude (V = 15.8), its distance is estimated to be 300 pc. To demonstrate the veracity of our analysis techniques for cool main-sequence stars, we also obtained a high-resolution spectrum of a bright, cool main-sequence star of similar low metallicity, G39-36 (*9*), with the same instrument, and we performed the same analysis as for SDSS J0018-0939.

We measured the abundances of 13 elements for SDSS J0018-0939, as well as upper limits for five other elements. A standard abundance analysis based on one-dimensional (1D) local thermodynamic equilibrium (LTE) model atmospheres of the ATLAS grid (*10*) is performed for most elements. The carbon abundance is measured from the CH molecular band at around 432 nm, based on application of a spectrum synthesis technique. Al and Si abundances are also determined by spectrum synthesis for the relatively strong absorption lines in the violet region, where the spectral lines are rather crowded. The Si abundance is determined from one strong line that exhibits signs of saturation; hence, it is less certain than those of other elements.

The derived abundance ratios are listed in Table 1. Details of the abundance measurements are provided in the supplementary materials. The comparison star G39-36, with [Fe/H] = −2.0, has abundance ratios that are typically found in stars of such metallicity, indicating that our analysis techniques applied to cool, metal-poor stars on the main sequence are as reliable as those used for the main-sequence turnoff and red giant-branch stars frequently studied in previous works (*2*, *7*, *11*). The star SDSS J0018-0939 has several peculiar elemental-abundance ratios compared to other metal-deficient stars. First, the lighter-element abundance ratios, including C and Mg (with respect to Fe), are comparatively low. A small number of low-metallicity stars with low [Mg/Fe] are known (*12*), but even compared with these objects, the Mg abundance of SDSS J0018-0939 is exceptionally low (Fig. 1, top). Very low carbon abundances are found in some highly evolved red giants and are often interpreted as the result of internal mixing during stellar evolution (*13*). This cannot be the case for SDSS J0018-0930, because it is an unevolved object on the

Table 1. Chemical abundances of SDSS J0018-0939 and the comparison star G39-36. Abundance ratios are given with respect to hydrogen [$\log \varepsilon = \log(N_X/N_H) + 12$], for element X, and the ratio with respect to Fe normalized to the solar value {$[X/Fe] = \log(N_X/N_{Fe}) - \log (N_X/N_{Fe})_\odot$}. [Fe/H] values are presented for Fe (Fe I) in the columns of [X/Fe]. The list of spectral lines used in the analysis is given in the supplementary materials. Random errors in the abundance measurements are estimated to be $\sigma N^{-1/2}$, where σ is the standard deviation of derived abundances from individual lines, and N is the number of lines used in the analysis. When only a few lines are available, the standard deviation of Fe I is adopted and divided by $N^{1/2}$ for the species in the estimates. The errors due to the uncertainty of the atmospheric parameters (δT_{eff} = 100 K; $\delta \log g$ = 0.3 dex; and δv_t = 0.3 km s^{-1}, where T_{eff} is the effective temperature, g is the surface gravity in cgs units, and v_t is the micro-turbulent velocity) are also estimated and added in quadrature to the random errors. The errors for [X/Fe] are also estimated from the changes of the log ε values of element X and Fe for one-sigma changes of the assumed atmospheric parameters. The errors on the upper limits for log ε and [X/Fe] for five species are estimated from the above uncertainties on the atmospheric parameters. The errors are included in the upper limits given in the columns of log ε and [X/Fe]. The measurement of the Si abundance is based on a single strong absorption line, for which the error is estimated from comparisons with synthetic spectra, calculated by changing Si abundances, with the observed feature, and is less certain than the errors estimated for other species. The abundance ratios [Na/Mg], [Sc/Ti], and [Co/Ni] are presented in the bottom three lines of the table.

	SDSS J0018-0939				G39-36			
	log ε	$\sigma_{\log\varepsilon}$	[X/Fe]	$\sigma_{[X/Fe]}$	log ε	$\sigma_{\log\varepsilon}$	[X/Fe]	$\sigma_{[X/Fe]}$
Fe (Fe I)	5.04	0.10	−2.46	0.10	5.41	0.08	−2.09	0.08
Fe (Fe II)	4.80	0.18	−0.24	0.21	5.07	0.16	−0.34	0.20
C	5.10	0.14	−0.84	0.10	6.20	0.11	−0.11	0.13
N	<6.5	0.20	<+1.0	0.22	–	–	–	–
Na	2.77	0.20	−1.08	0.14	4.20	0.16	−0.03	0.13
Mg	4.62	0.14	−0.52	0.10	5.62	0.09	+0.11	0.09
Al	3.30	0.29	−0.69	0.27	–	–	–	–
Si	4.6	0.3	−0.4	0.3	–	–	–	–
Ca	3.61	0.09	−0.26	0.04	4.54	0.11	+0.29	0.06
Sc	<−0.2	0.12	<−0.89	0.14	1.05	0.11	−0.01	0.11
Ti (Ti I)	2.58	0.16	+0.10	0.08	3.45	0.16	+0.59	0.10
Ti (Ti II)	2.48	0.11	−0.01	0.12	3.21	0.09	+0.35	0.10
V	1.57	0.20	+0.11	0.14	2.42	0.16	+0.58	0.10
Cr	3.26	0.14	+0.08	0.05	3.74	0.14	+0.19	0.07
Mn	2.79	0.12	−0.18	0.05	3.14	0.10	−0.21	0.05
Co	1.85	0.13	−0.68	0.08	2.95	0.11	+0.05	0.07
Ni	3.85	0.09	+0.09	0.13	4.09	0.09	−0.04	0.08
Zn	<2.8	0.16	<+0.7	0.15	–	–	–	–
Sr	<−1.4	0.12	<−1.8	0.14	0.46	0.13	−0.32	0.11
Ba	<−1.6	0.12	<−1.3	0.15	0.01	0.09	−0.09	0.08
[Na/Mg]			−0.56	0.17			−0.14	0.16
[Sc/Ti]			<−0.99	–			−0.60	0.15
[Co/Ni]			−0.77	0.15			+0.09	0.11

[1]National Astronomical Observatory of Japan (NAOJ), 2-21-1 Osawa, Mitaka, Tokyo 181-8588, Japan. [2]Department of Astronomical Science, School of Physical Sciences, The Graduate University for Advanced Studies (SOKENDAI), 2-21-1 Osawa, Mitaka, Tokyo 181-8588, Japan. [3]Department of Physics, Faculty of Science and Engineering, Konan University, 8-9-1 Okamoto, Kobe, Hyogo 658-8501, Japan. [4]Kavli Institute for the Physics and Mathematics of the Universe (WPI), the University of Tokyo, 5-1-5 Kashiwanoha, Kashiwa, Chiba 277-8569, Japan. [5]Department of Physics, University of Notre Dame, 225 Nieuwland Science Hall, Notre Dame, IN 46656, USA. [6]JINA, Joint Institute for Nuclear Astrophysics, University of Notre Dame, Notre Dame, IN 46556, USA. [7]Center for Astronomy, University of Hyogo, 407-2, Nishigaichi, Sayo-cho, Sayo, Hyogo 679-5313, Japan. [8]Department of Astronomy, New Mexico State University, Las Cruces, NM 88003, USA.
*Corresponding author. E-mail: aoki.wako@nao.ac.jp

main sequence. No signature of extra mixing or mass transfer across a binary system, which could change the surface chemical composition of a star, is found for this star. Second, the abundance ratios between adjacent odd- and even-element pairs are very low (Table 1 and Fig. 1, middle panel), which is clear in comparison with the values for G39-36. Third, the upper limits on the abundance of the heavy neutron-capture elements Sr and Ba are anomalously low compared to other stars with similar metallicity (Table 1 and Fig. 1, bottom panel). This feature is sometimes found in more metal-deficient stars ([Fe/H] < −3), for which low contributions of rapid neutron-capture process (or slow neutron-capture process) elements are expected (*14*). It should be noted that many metal-poor stars with low [α-element/Fe] ratios have been identified as members of dwarf galaxies around the Milky Way (*15*). Most of them are, however, not as metal-poor as SDSS J0018-0939 and do not share other properties of this object, suggesting that the origin of the low [α-element/Fe] ratios in these instances is different from that of SDSS J0018-0939.

Although the Fe abundance of SDSS J0018-0939 is not as low as for extremely metal-poor stars ([Fe/H] < −3), the low abundances of C, Mg, and the heavy neutron-capture elements (Sr and Ba) suggest that this star is a very chemically primitive object. It may have recorded the nucleosynthesis from a single progenitor, most likely from a first-generation massive star. If chemical yields from more than one source are mixed, the peculiar abundance pattern produced by a massive progenitor star would have been erased by the nucleosynthesis from other normal core-collapse supernovae and/or heavy-element-producing events.

The chemical-abundance pattern of SDSS J0018-0939, compared with G39-36 and other very metal-poor stars, is not readily accounted for by core-collapse supernovae of stars with several tens of solar masses, even taking into account some of the uncertainties in the explosion mechanism (Fig. 2, top panel). The most constraining sets of abundances are the low [C/Fe], low [α/Fe], and low [Co/Fe] ratios. These signatures impose rather opposing requirements, if they are to be accounted for by normal core-collapse supernovae: the low [C/Fe] and [α/Fe] suggest a higher-energy explosion without fallback, in which iron-peak elements are efficiently synthesized and ejected, whereas the low [Co/Fe] requires a low-entropy environment—that is, a lower explosion energy.

Contributions of type Ia supernovae have been frequently suggested to explain a small fraction of metal-poor stars with low [α-element/Fe] ratios (*12*), because type Ia supernovae are known to yield a substantial amount of iron (Fig. 2, middle panel). The low Co abundance could be explained by the CDD2 model of type Ia supernovae (*16*). On the other hand, all type Ia supernova models predict quite low C, Mg, and Si abundance ratios: [C/Fe] ≲ −3, [Mg/Fe] ≲ −2, and [Si/Fe] ≲ −0.5, independent of the explosion properties (*16*). In order to explain the full abundance pattern of this star, some contribution from a core-collapse supernova is required, but that should not greatly affect the explosively synthesized elements heavier than Si. The contribution from a normal core-collapse supernova ejecting ~0.07 $M_\odot$ of Fe overproduces Si compared to the observed values (Fig. 2, middle). Another difficulty of this scenario is the difference of the time scale of the contributions from core-collapse and type Ia supernovae to chemical enrichment. Contributions of type Ia supernovae are usually presumed to be effective for stars with higher metallicity that formed during later phases of Galactic chemical evolution.

A simpler, and perhaps more likely, interpretation is that the progenitor of SDSS J0018-0939 was a very massive star with a main-sequence mass, M_{ms}, larger than 100 $M_\odot$, a mass range previously suggested to be possible for the first stars (*17*). A star with 140 $M_\odot \lesssim M_{ms} \lesssim 300\ M_\odot$ explodes because of the energy consumption (and subsequent stellar core collapse) arising from an electron-positron pair-production instability during the static O-burning stage (*18*), and is referred to as a pair-instability supernova (PISN). The primary factor influencing the yield of PISN nucleosynthesis is the helium-core mass of the star at the end of its main-sequence evolution, M_{He} ; a PISN associated with a more-massive progenitor produces larger amounts of iron (*18*, *19*). A PISN model with M_{He} = 130 $M_\odot$ is expected to produce low [C/Fe] and [Mg/Fe] ratios and large odd-even effects, which qualitatively explain the observed abundance pattern of SDSS J0018-0939 (Fig. 2, bottom panel). The low Co abundance is naturally explained due to the low entropy of such an explosion. Difficulties are the low Si abundance and an odd-even effect that is still not as large as predicted by the model.

Whereas first generation stars are expected to self-regulate their growth by radiative feedback in the formation process, and to achieve masses typically tens of times that of the Sun (*20*), a fraction of stars might grow to become very-massive objects, with M_{ms} > 300 $M_\odot$ (*4*). Such a star enters the pair-instability region during its evolution but continues to collapse and finally enters an instability region with Fe photodisintegration (*21*, *22*). Such objects are called core-collapse very massive stars. Although it is not clear whether or not such a very massive star can explode, the yield of an explosion with energy of about 6 ×10^{53} ergs can simultaneously explain both the low Si

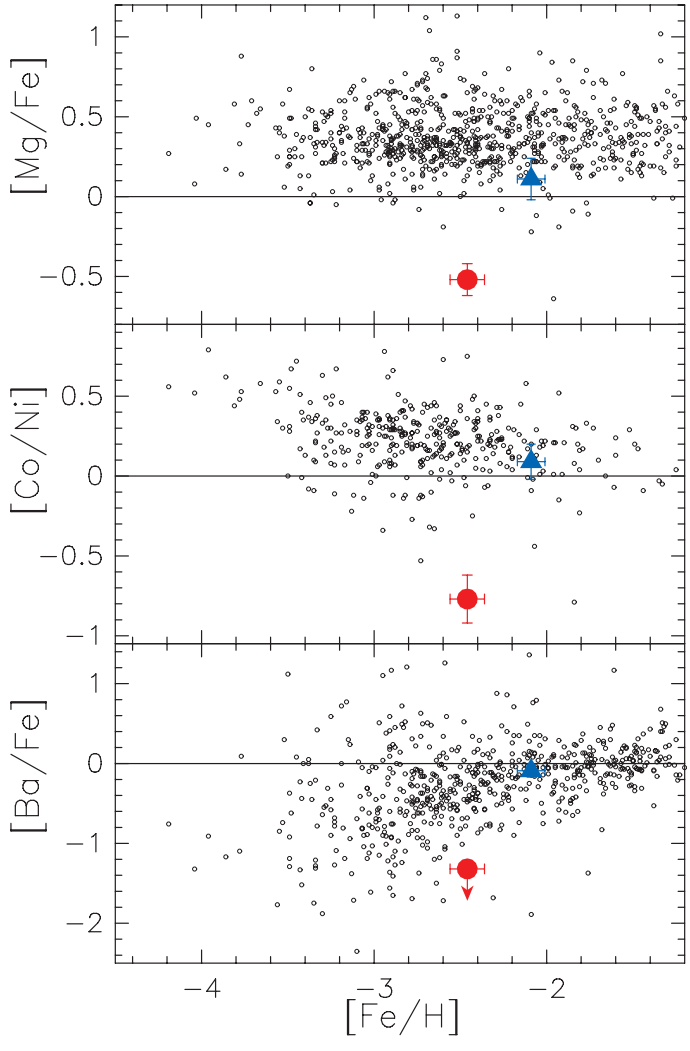

Fig. 1. Observed abundance ratios of [Mg/Fe], [Co/Ni], and [Ba/Fe] in SDSS J0018-0939, as a function of metallicity, compared with those of other metal-poor stars. The large red circles and blue triangles indicate the data for SDSS J0018-0939 and the comparison star G39-36, respectively. The small circles represent data taken from the SAGA database (*25*). The arrow in the bottom panel indicates the upper limit on [Ba/Fe] estimated for SDSS J0018-0939. There is no known star that simultaneously exhibits such low abundances of these three elements other than SDSS J0018-0939. The star having [Mg/Fe] = −0.64 at [Fe/H] = −1.96 is CS 22966-043 (*12*), whereas the object with [Co/Ni] = −0.79 at [Fe/H]= −1.84 is HD 25329 (*26*).

abundance (compared with Mg) and the low C and Mg abundances. Furthermore, the [Co/Fe] in this scenario is as low as the observed ratio of SDSS J0018-0939, even with such a high explosion energy, because a low-entropy environment is achieved due to the high density in the complete Si-burning layer. Hence, if the explosion of such a very massive star actually has occurred, it has the potential to explain the peculiar chemical abundance pattern of SDSS J0018-0939.

Interestingly, theoretical estimates of early chemical enrichment (*23*) predict that the metallicity of polluted primordial gas can reach a level of [Fe/H] = −2.5, due to the large amount of metals produced by the PISN explosions of a first generation of very massive stars, which matches the Fe abundance of SDSS J0018-0939. They also predict that stars formed from gas enriched by PISN are quite rare; only one star among 500 stars with [Fe/H] < −2 is expected, even if a relatively large fraction of very massive stars is assumed among the first stars (7% by number and 40% by mass). This argument also might work for the case of the explosion of core-collapse very massive stars that reproduces the abundance pattern of SDSS J0018-0939, because the yield of metals is comparable to that of a PISN, and the explosion energies could avoid the complete disruption of a cloud with $10^8\ M_\odot$ (*24*). The star SDSS J0018-0939 is unique in its observed abundance pattern; although about 500 stars in the metallicity range −3 < [Fe/H] < −2 have been observed to date with high-resolution spectroscopy, no similar object has been found [see the Stellar Abundances for Galactic Archeology (SAGA) database (*25*)]. Hence, if SDSS J0018-0939 actually records the yields of a PISN or the explosion of a very massive star, the number fraction of very massive stars among primordial stellar populations could be several percent, which is comparable to that predicted by recent theoretical studies on the formation of first-generation stars (*4*). The mass distribution of first-generation stars formed in dark-matter halos is primarily determined by the angular momentum of the gas cloud, which could be related to that of its natal dark-matter halo. The discovery of SDSS J0018-0939 could be the first step toward obtaining a direct comparison between the observations of very metal-poor stars and cosmological 3D radiation-hydrodynamical simulations.

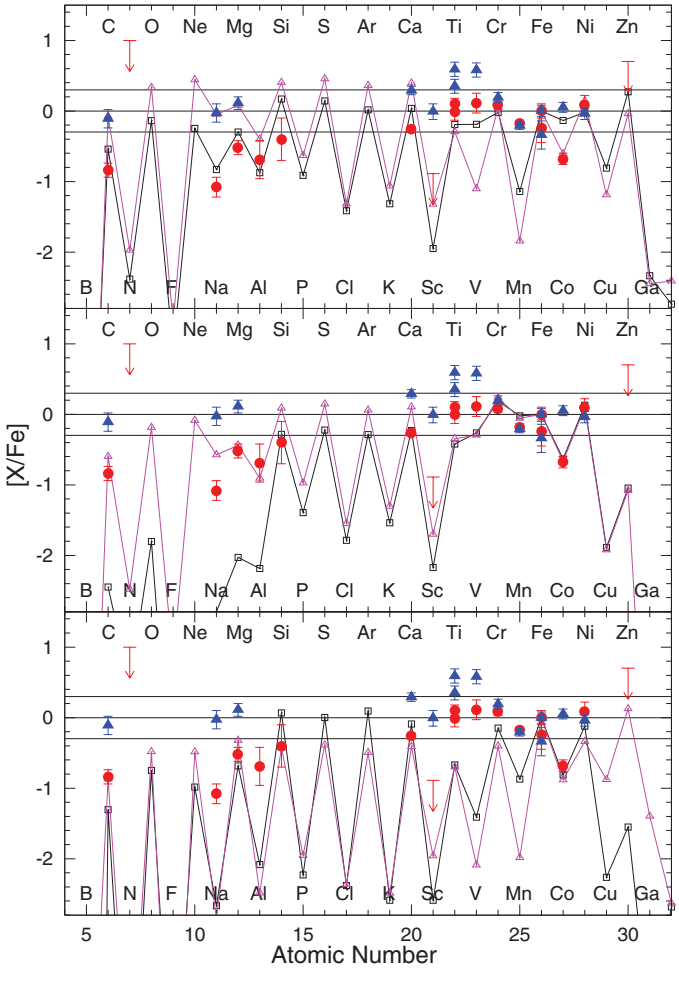

Fig. 2. Comparison of chemical-abundance patterns ([X/Fe] values as a function of atomic number) between our program stars (red circles, SDSS J0018-0939; blue triangles, G39-36) and model predictions. (**Top**) Comparison with core-collapse supernova (SN) models (black line with open squares: 25 $M_\odot$, E_{51} = 10, M(Fe) = 0.68 $M_\odot$; magenta line with open triangles: 25 $M_\odot$, E_{51} = 1, M(Fe) = 0.26 $M_\odot$, where E_{51} and M(Fe) indicate explosion energy in the unit of 10^{51} ergs and mass of Fe ejected, respectively). (**Middle**) Comparison with a type Ia SN (SN Ia) model (*16*) (black line with open squares: CDD2) and a model of SN Ia + core-collapse SN (magenta line with open triangles: CDD2 + normal SN [25 $M_\odot$, E_{51}=1, M(Fe) = 0.07 $M_\odot$]). Here, we adopt the core-collapse SN model ejecting Fe of typical values in the nearby universe (*3*) and assume that a gas cloud from which SDSS J0018-0939 formed has been equally enriched by the SN Ia and the core-collapse SN. The contributions of SN Ia to the total iron mass of the gas cloud is 92.2%. (**Bottom**) Comparison with a PISN model (*18*) (black line with open squares: M_{He} = 130 $M_\odot$, where M_{He} is the helium-core mass) and a model of a core-collapse SN of a very massive star (*21*) [magenta line with open triangles: 1000 $M_\odot$, E_{51} = 667, M(Fe) = 19.16 $M_\odot$, and M_{rem} = 413 $M_\odot$, where M_{rem} is the mass of the central remnant].

REFERENCES AND NOTES

1. V. Bromm, P. S. Coppi, R. B. Larson, *Astrophys. J.* **527**, L5–L8 (1999).
2. D. Yong *et al.*, *Astrophys. J.* **762**, 26 (2013).
3. K. Nomoto, C. Kobayashi, N. Tominaga, *Annu. Rev. Astron. Astrophys.* **51**, 457–509 (2013).
4. S. Hirano *et al.*, *Astrophys. J.* **781**, 60 (2014).
5. SDSS-II SEGUE Collaboration, *Astrophys. J.* **137**, 4377–4399 (2009).
6. K. Noguchi *et al.*, *Publ. Astron. Soc. Jpn.* **54**, 855–864 (2002).
7. W. Aoki *et al.*, *Astron. J.* **145**, 13 (2013).
8. Y. Kim, P. Demarque, S. K. Yi, D. R. Alexander, *Astrophys. J.* **143** (Suppl.), 499–511 (2002).
9. D. Yong, D. L. Lambert, *Publ. Astron. Soc. Pac.* **115**, 22–36 (2003).
10. F. Castelli, R. G. Gratton, R. L. Kurucz, *Astron. Astrophys.* **318**, 841–869 (1997).
11. R. Cayrel *et al.*, *Astron. Astrophys.* **416**, 1117–1138 (2004).
12. I. I. Ivans *et al.*, *Astrophys. J.* **592**, 906–934 (2003).
13. M. Spite *et al.*, *Astron. Astrophys.* **430**, 655–668 (2005).
14. W. Aoki, T. Suda, R. N. Boyd, T. Kajino, M. A. Famiano, *Astrophys. J.* **766**, L13 (2013).
15. E. Tolstoy, V. Hill, M. Tosi, *Annu. Rev. Astron. Astrophys.* **47**, 371–425 (2009).
16. K. Iwamoto *et al.*, *Astrophys. J.* **125** (Supp.), 439–462 (1999).
17. V. Bromm, R. B. Larson, *Annu. Rev. Astron. Astrophys.* **42**, 79–118 (2004).
18. A. Heger, S. E. Woosley, *Astrophys. J.* **567**, 532–543 (2002).
19. H. Umeda, K. Nomoto, *Astrophys. J.* **565**, 385–404 (2002).
20. T. Hosokawa, K. Omukai, N. Yoshida, H. W. Yorke, *Science* **334**, 1250–1253 (2011).
21. T. Ohkubo *et al.*, *Astrophys. J.* **645**, 1352–1372 (2006).
22. T. Ohkubo, K. Nomoto, H. Umeda, N. Yoshida, S. Tsuruta, *Astrophys. J.* **706**, 1184–1193 (2009).
23. T. Karlsson, J. L. Johnson, V. Bromm, *Astrophys. J.* **679**, 6–16 (2008).
24. K. Wada, A. Venkatesan, *Astrophys. J.* **591**, 38–42 (2003).
25. T. Suda *et al.*, *Publ. Astron. Soc. Jpn.* **60**, 1159–1171 (2008).
26. M. Bergemann, J. C. Pickering, T. Gehren, *Mon. Not. R. Astron. Soc.* **401**, 1334–1346 (2010).

ACKNOWLEDGMENTS

This work is based on data collected at the Subaru Telescope, which is operated by the National Astronomical Observatory of Japan. The data obtained with the Subaru/HDS are available on the Subaru Mitaka Okayama Kiso Archive system (SMOKA) (http://smoka.nao.ac.jp). We thank H. Susa for useful discussions about the formation and mass distribution of the first stars. We also appreciate T. Ohkubo for providing us progenitor models of core-collapse very massive stars. W.A. and N.T. were supported by the Japan Society for the Promotion of Science Grants-in-Aid for Scientific Research (23224004). T.C.B. acknowledges partial support from grant PHY 08-22648: Physics Frontiers Center/Joint Institute for Nuclear Astrophysics (JINA), awarded by the U.S. National Science Foundation. Y.S.L. is a Tombaugh Fellow.

SUPPLEMENTARY MATERIALS

www.sciencemag.org/content/345/6199/912/suppl/DC1
Materials and Methods
Supplementary Text
Figs. S1 to S5
Table S1
References (*27*–*55*)

25 February 2014; accepted 8 July 2014
10.1126/science.1252633

NANOPARTICLE GROWTH

Facet development during platinum nanocube growth

Hong-Gang Liao,[1] Danylo Zherebetskyy,[1] Huolin Xin,[1] Cory Czarnik,[2] Peter Ercius,[3] Hans Elmlund,[4] Ming Pan,[2] Lin-Wang Wang,[1] Haimei Zheng[1,5]*

An understanding of how facets of a nanocrystal develop is critical for controlling nanocrystal shape and designing novel functional materials. However, the atomic pathways of nanocrystal facet development are mostly unknown because of the lack of direct observation. We report the imaging of platinum nanocube growth in a liquid cell using transmission electron microscopy with high spatial and temporal resolution. The growth rates of all low index facets are similar until the {100} facets stop growth. The continuous growth of the rest facets leads to a nanocube. Our calculation shows that the much lower ligand mobility on the {100} facets is responsible for the arresting of {100} growing facets. These findings shed light on nanocrystal shape-control mechanisms and future design of nanomaterials.

Important advances have been made in synthesis of nanocrystals with a variety of shapes—including cube, cuboctahedron, octahedron, tetrahedron, decahedron, icosahedron, thin plate, and rod—strongly influencing performance in catalysis, sensing, and many other surface-enhanced applications (*1*–*6*). The Wulff construction has been used to predict the equilibrium shape of nanocrystals (*7*, *8*), where it states that the length of a normal vector drawn from the crystal center to an external surface is proportional to the surface free energy. This model can be traced back to 1873, when Gibbs proposed that the equilibrium shape of a droplet of matter is determined by a surface energy minimization (*9*, *10*). In the growth of nanocrystals, the high-energy facet grows at a higher rate than the low-energy facets; therefore, the fast-growing facets will eventually disappear, resulting in a nanocrystal terminated with low-energy facets (*11*–*13*). It is assumed that the commonly used surfactants modify the energy of specific facets through preferential adsorption, influencing the relative growth rate of different facets and thus the shape of a nanocrystal (*8*, *14*). However, the existing models are based on postreaction characterizations. The evolving facet dynamics during nanocrystal growth is largely unknown.

Microfabricated liquid cells allow for in situ observation of single-nanoparticle growth trajectories using transmission electron microscopy (TEM) (*15*–*18*). A liquid cell encapsulates and maintains a small amount of liquid inside the high-vacuum microscope for an extended period of time. Nanocrystal growth can be initiated by thermal heating or, more commonly, by electron beam irradiation. Nanocrystals that resemble those in flask synthesis have been created in a liquid cell and imaged with TEM (*19*–*21*). However, it is a challenge to image the facet development at the atomic level because of the limited signal-to-noise ratio of the detector, especially when the particle is small and moving dynamically in the field of view. In addition, nanoparticles with well-defined shapes—such as cubes, tetrahedrons, and so on—are hard to achieve when there is frequent coalescence during growth or when the time for reaction in the cell is limited. We studied the growth of platinum nanocubes in a liquid cell under TEM by incorporating an advanced high-resolution fast-detection camera (K2-IS camera from Gatan, Incorporated). The K2-IS camera captures electron images directly on a CMOS (complimentary metal-oxide semiconductor) sensor at 400 fps (frames per second) with 2000 pixel by 2000 pixel resolution. The camera can also be configured to capture images at up to 1600 fps with appropriate scaling of the field of view. The elimination of the traditional scintillation process during image detection results in significant improvement in both sensitivity and image resolution. The thin silicon nitride membrane of the liquid cell window (about 10 nm thick for each membrane) facilitates the high-resolution imaging.

The growth solution was prepared by dissolving $Pt(acetylacetonate)_2$ (20 mg/ml) in a solvent mixture of oleylamine, oleic acid, and pentadecane (4.5:1.5:4). About 50 nl of growth solution were loaded into one of the reservoirs in a liquid cell. The solution was drawn into the cell by capillary force and formed a liquid layer (100 nm) sandwiched between two silicon nitride membranes at the window. We filled the other reservoir with the growth solution. The liquid precursor solution was well sealed inside the cell, allowing an extended period of time for reaction. A FEI Tecnai F20 TEM (200 kV, FEI, Hillsboro, OR) equipped with the K2-IS camera was used, and a beam current density of $4.0 \pm 0.9 \times 10^5$ A/m^2 was maintained during movie acquisition.

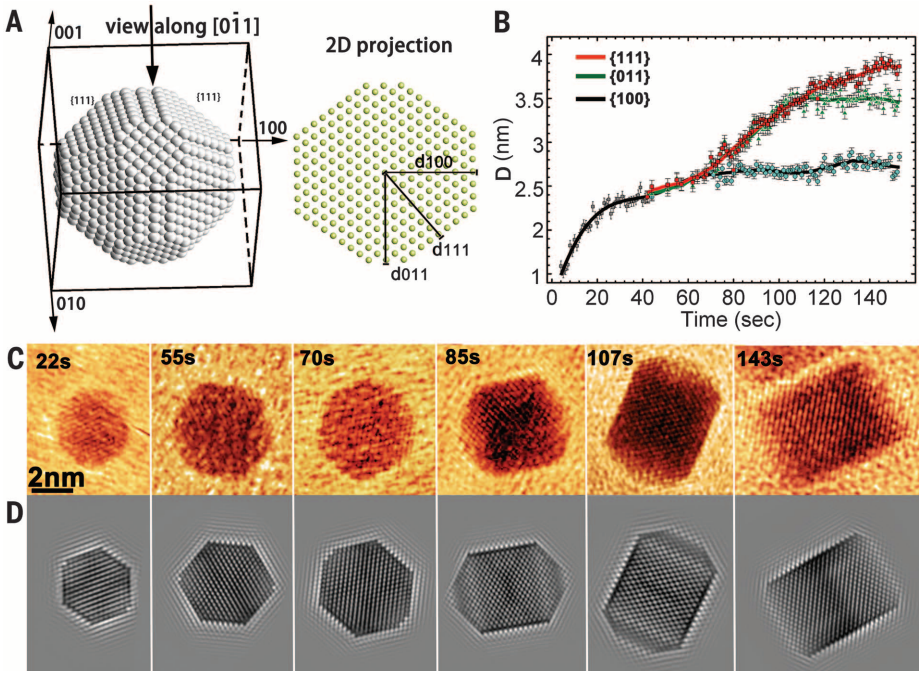

Fig. 1. The facet development of a Pt nanocube viewed along the [0$\bar{1}$1] axis. (**A**) The atomic model of a truncated Pt nanocube and its projection along the [0$\bar{1}$1] view zone axis. The distances from the crystal center to each of the (100), (011), and (111) facets are highlighted. (**B**) The measured average distances from the crystal center to each facet as a function of time. Error bars indicate the standard deviation. (**C**) Sequential images show the growth of the Pt nanocube extracted from movie S2. (**D**) Simulated TEM images of the Pt nanoparticle in (C).

[1]Materials Sciences Division, Lawrence Berkeley National Laboratory, Berkeley, CA 94720, USA. [2]Gatan, Incorporated, 5794 West Las Positas Boulevard, Pleasanton, CA 94588, USA. [3]National Center for Electron Microscopy, Lawrence Berkeley National Laboratory, Berkeley, CA 94720, USA. [4]Department of Structural Biology, Medical School, Stanford University, Stanford, CA 94305, USA. [5]Department of Material Science and Engineering, University of California, Berkeley, CA 94720, USA.
*Corresponding author. E-mail: hmzheng@lbl.gov

The nucleation and growth of platinum nanocrystals is initiated by irradiating the precursor solution with the electron beam. A burst of nucleation is observed at the beginning while the sample is focused for imaging. Subsequently, more nanoparticles appear. Although there are some coalescence events of nanoparticles in the early stage of growth, most nanoparticles eventually develop into nanocubes by the attachment of monomeric species (movie S1). Nanoparticles frequently rotate during the early stage of growth and become more stationary, sitting on a certain facet, during the later development.

We quantified the shape evolution of a Pt nanoparticle by tracking the propagation of different facets. Figure 1 shows a nanoparticle primarily registered along the [110] viewing axis during facet development, which allowed measurements of the distance from the center of crystal to all three facets: {100}, {110}, and {111} (see the three-dimensional model and two-dimensional projection in Fig. 1A). Movie S2 shows the growth trajectory of the nanoparticle: It rotates as a small and round nanoparticle at the early stage, and it sits along the [110] viewing axis while occasionally rocking off-axis as it becomes faceted (see the movie processing in the supplementary materials). Changes in the distance from the center of crystal to each facet as a function of time are plotted in Fig. 1B. Sequential TEM images extracted from movie S2 are displayed in Fig. 1C. At the early stage of growth (0 to 70 s), although the three low-energy facets ({100}, {110}, and {111}) are identifiable, the particle appears to be almost round and rotates frequently. The particle grows while maintaining the truncated octahedron shape; therefore, all three facets have a similar growth rate. When the distance from the center of crystal to the surface of {100} facets reaches about 2.5 nm, growth of these facets stops. During the subsequent period of time (70 to 100 s), both {110} and {111} facets continue to grow with a similar growth rate until the {110} facets reach the limiting point defined by the two neighboring {100} facets. Last, only the {111} facets grow, which is shown as the surface area of each {111} facet becoming smaller and the corners of a cube being filled. Because each {111} facet is confined by three neighboring {100} facets, eventually the {111} facets disappear when the nanoparticle becomes a cube. During these facet developments, the nanoparticle mostly stays along the [110] axis with occasional rocking off-axis. To identify the off-axis angle of the nanoparticle in each image, we simulated collages of images with 5°-by-5° off-axis and selected the best matches from the collage by visual comparison (figs. S10 to S20). As confirmed by the simulated images in Fig. 1D, the nanoparticle is only a few degrees off-axis.

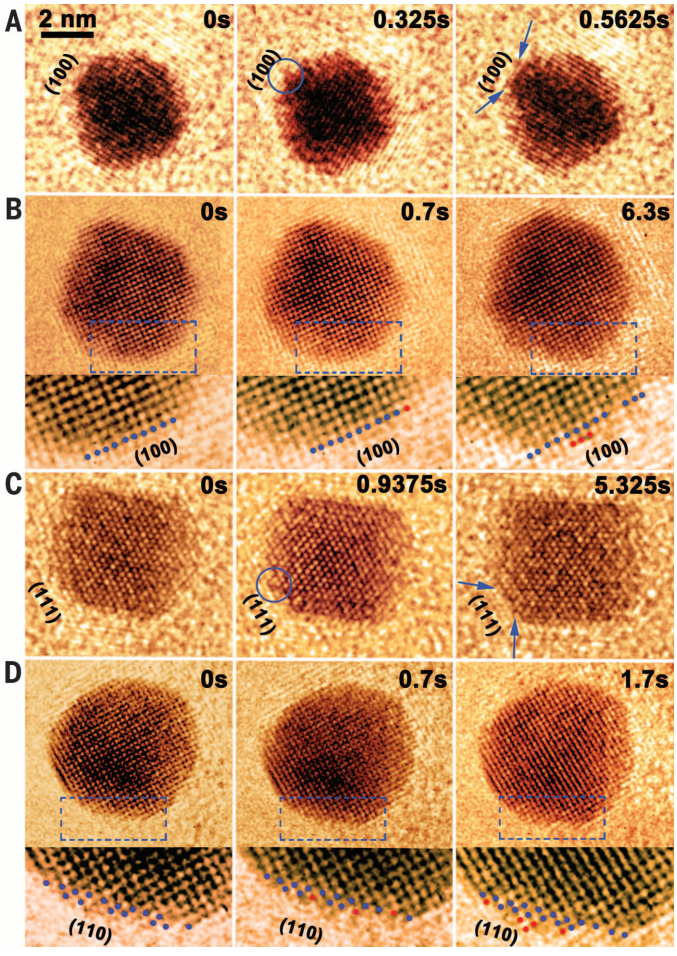

Fig. 2. Snapshots of high-resolution images show the atomic facet development. (**A**) The attachment of a cluster to the (100) facet. (**B**) The atomic layer attachment to the (100) facet and nucleation on flat (100) facet. (**C**) The atomic layer attachment to the (111) facet. (**D**) The atomic growth of the (110) facet shows steps. The circles highlight atoms attaching to the (100) and the (111) facets. Arrows show the atomic layer propagation after nucleation. The red dots show the newly added Pt atoms.

We found that most of the nanoparticles follow the above growth model, where all three low-index facets grow with a similar rate and the shape of the nanoparticle is determined when the {100} facets cease growth. Such a selective facet-arrested shape-control mechanism deviates from what is predicted by the surface energy minimization theories. The similar growth rate of different facets is probably due to the fact that almost all the atoms are near the surface for such small nanocrystals, so atoms can rearrange easily (*21*). The differences in the nucleation barrier on various facets can be very small.

Tracking the nanocrystal growth trajectories reveals the atomic development of different facets. Figure 2 shows the attachment of atoms or clusters to the {100}, {110}, and {111} facets during growth (see image analysis in the supplementary materials and fig. S3). On both the {100} and the {111} facets, it is observed that small clusters of atoms directly attach to the facet. The subsequent addition of atoms leads to the layer-by-layer growth of the facet (Fig. 2, A to C). During the growth of nanoparticles, most of the time we observed the flat propagation of {100} and {111} facets. This implies that, once there is a nucleation event on the flat facet, the lateral growth of the atomic layer can be very fast. Nucleation should be the controlling step of these facets' development. However, the {110} facets grew with steps, and a nonflat surface was observed (Fig. 2D). Apparently, surfactant ligands do not block the attachment of atoms to the nanoparticle surface during the early stage of growth. It has also been observed that some atoms disappeared on certain facets, suggesting that dissociation or rearrangement of atoms may occur. Atoms directly knocked off by electron beam cannot be excluded. Delocalization resulting from spherical aberration produces images with nonsharp edges. However, because we recorded a series of images with high signal-to-noise ratio and with high temporal resolution (2.5 ms per frame), the atomic growth pathways are identified without ambiguity by comparing images frame by frame.

Observations also show that the facet growth rate of nanoparticles fluctuates. As an example, Fig. 3 shows the growth trajectories of a nanoparticle mostly in the [100] viewing direction (movie S3). The growth kinetics of four different {110} facets can be measured (Fig. 3A). The distance from the center of crystal to the edge of each facet—(110), ($\bar{1}\bar{1}$0), (1$\bar{1}$0) and ($\bar{1}$10)—as a function of time is plotted in Fig. 3B. There is a similar growth rate among different facets before the {100} facets' growth halt (fig. S2). However, the subsequent growth of the four (110) facets varies. Figure 3C illustrates that the (110) facet grows slower than the other ($\bar{1}\bar{1}$0), (1$\bar{1}$0), and ($\bar{1}$10) facets. As a result, asymmetric nanoparticles with missing corners were observed in the projected images (also see the simulated images in Fig. 3D). However, the slow-growing (110) facet can catch up eventually, completing a symmetric cubic nanocrystal. These growth fluctuations may arise from the local environmental variations, such as impurity molecules, inhomogeneous

absorption of surfactants, reactant concentration alternation, or the fundamental random nature of atom addition to such small nanoparticles. We have also observed one atomic layer difference of facet-to-facet distances between {100} facets in some nanoparticles, reflecting the growth fluctuations.

A critical question arises: Why do the {100} facets stop growing sooner than the other facets? We calculated the surface energies and binding energies of the ligands on {111} versus {100} facets by using ab initio density functional theory. The amine group of the oleylamine molecule functionalizes the Pt atoms on the surface. Therefore, we simplified the calculations by truncating the long oleyl (-$C_{18}H_{35}$) chain to the ethyl (-C_2H_5) group (see more details in the supplementary materials). We skipped the {110} facets because {110} facets can be considered as an intermediate surface between {111} and {100} surfaces, where a {110} facet can be built with a {111} subfacet and a {001} subfacet or two {100} subfacets. In addition, we have observed that the {110} facets are not flat (Fig. 2), so the surfactant binding to a {110} facet is complex. The unpassivated surface energies for the {100} and {111} facets are 10.33 and 7.68 eV/nm^2 respectively. The maximum surface binding energies are calculated to be –3.19 eV/nm^2 (0.74 eV per molecule) and –2.19 eV/nm^2 (0.58 eV per molecule) for {100} and {111} facets. Thus, after taking into account the ligand binding energy, the surface energy with ligand passivation is 7.14 eV/nm^2 for the {100} facets and 5.49 eV/nm^2 for the {111} facets. These surface energies do not yield a cubic shape according to the Wulff construction. This further confirms that the final shape of the nanocrystal is not determined by thermodynamic equilibrium; rather, it is determined by growth kinetics. Several factors could play an important role to distinguish the {100} from the {111} facets, including the ability to remove one ligand molecule from the surface, the packing density, and the mobility of the ligand molecules on the surface (see more detailed discussions in the supplementary materials). Considering that growth on both {100} and {111} facets starts from the center of the facet (Fig. 2), the surface ligands must make room for platinum to land on the facet. There are different mechanisms to block this process. The calculated ligand packing densities on {100} and {111} facets are about 0.23-nm^2 and 0.26-nm^2 area per ligand molecule, respectively. This small difference in packing density should not differentiate the growth of {100} facets from {111} facets because of the variations in ligand packing resulting from ligand bending, tilting, etc. The calculated energy barriers for a molecule to move from one site to a nearby site are 0.298 and 0.545 eV on the individual {111} and {100} facets, which are smaller than the ligand-surface binding energies of 0.74 and 0.58 eV per molecule on the {100} and {111} facets. (Fig. 4; see details of the calculation in the supplementary materials). Therefore, it is energetically favorable for one ligand molecule to jump from one site to another site on the surface rather than removing from the surface. The hopping time of one ligand from one site to another can be estimated by using

$$t = t_0 e^{E_{\text{barrier}}/k_B T}$$

where t_0 is a phonon vibrational period that is typically 1 ps, E_{barrier} is the calculated hopping energy barrier, k_B is the Boltzmann constant, and T is the room temperature. The resulting hopping time is about 10^{-6} s on the (111) facet

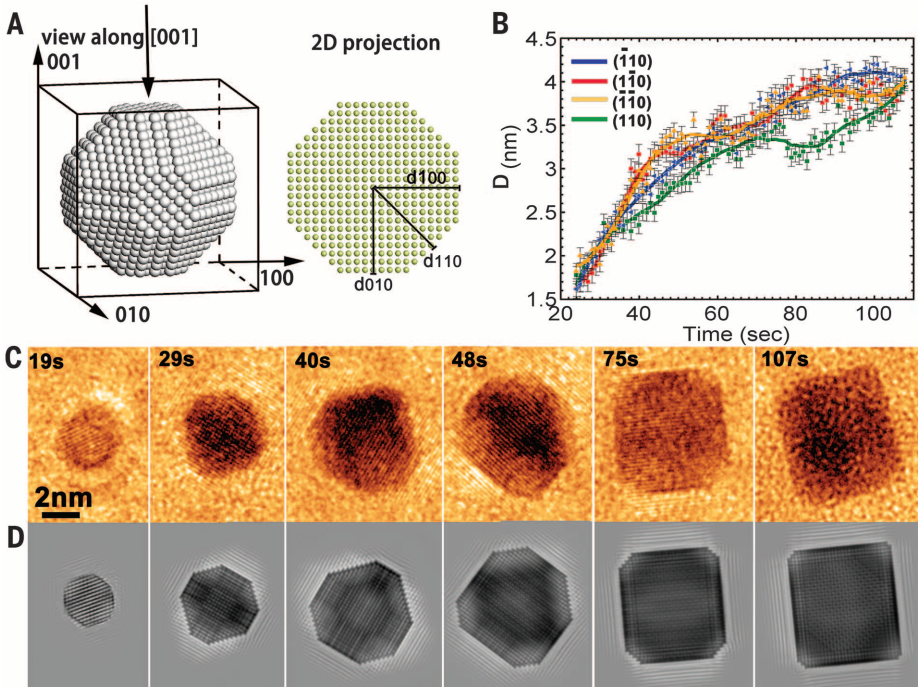

Fig. 3. The facet development of a Pt nanocube viewed along the [001] axis. (**A**) The atomic model of a truncated Pt nanoparticle and its projection along the [001] view zone axis. (**B**) The measured distances from the crystal center to each of the (1̄10), (11̄0), (1̄1̄0), and (110) facets as a function of time. Error bars indicate the standard deviation. (**C**) Sequential images show the growth of the Pt nanocube extracted from movie S3. (**D**) Simulated TEM images of the Pt nanoparticle in (C).

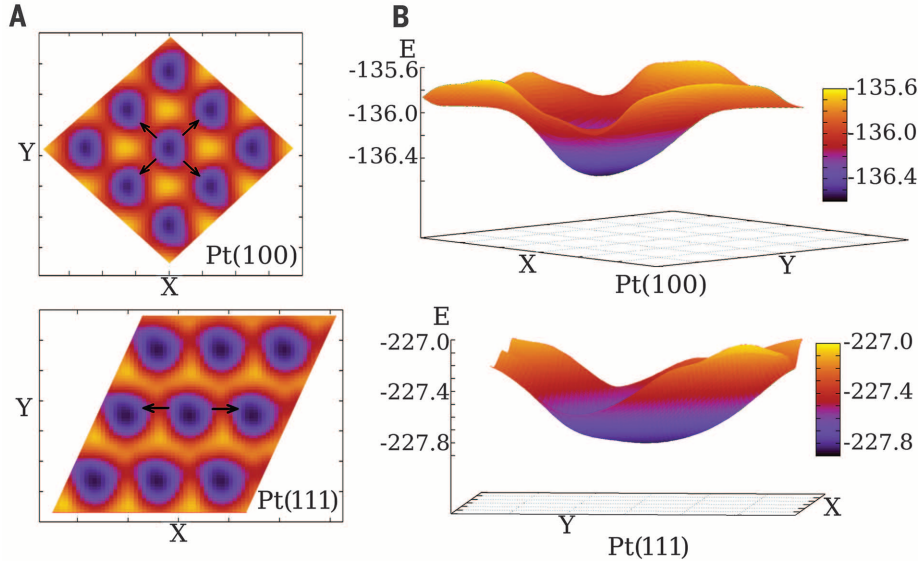

Fig. 4. The calculated potential energy of ethylamine molecule around Pt atoms on the (100) and (111) surfaces. The unit of the energy is eV. (**A**) The potential energy maps of an ethylamine molecule on Pt(100) and (111) surfaces. Arrows show the direction of the lowest energy barriers for the molecule to flip between two neighboring Pt atoms. (**B**) The calculated potential energy maps around one Pt atom on (100) and (111) surfaces. The energy barrier of a molecule to flip between two neighboring Pt atoms is 0.545 eV on the (100) surface and 0.298 eV on the (111) surface.

and 10^{-1} s on the (100) facet. Therefore, the ability of the surfactant ligands to move on the surface allows the (111) facet to grow, whereas the low mobility of the ligands on the (100) facet blocks its growth. However, this mechanism is only for large facets. For small nanocrystals, the ligand molecules can easily fan out to make room for platinum atoms to land (*14*). Therefore, all facets grow when the nanocrystal is small. The critical size of about 5 nm may vary with temperature or the type of ligand. Our proposed ligand mobility–controlled selective facet–arrested shape evolution may apply to other ligands and nanoparticle shapes.

REFERENCES AND NOTES

1. C. J. Murphy *et al.*, *J. Phys. Chem. B* **109**, 13857–13870 (2005).
2. Z. Tang, N. A. Kotov, M. Giersig, *Science* **297**, 237–240 (2002).
3. C. Burda, X. Chen, R. Narayanan, M. A. El-Sayed, *Chem. Rev.* **105**, 1025–1102 (2005).
4. M. Bruchez Jr., M. Moronne, P. Gin, S. Weiss, A. P. Alivisatos, *Science* **281**, 2013–2016 (1998).
5. M. C. Daniel, D. Astruc, *Chem. Rev.* **104**, 293–346 (2004).
6. R. Elghanian, J. J. Storhoff, R. C. Mucic, R. L. Letsinger, C. A. Mirkin, *Science* **277**, 1078–1081 (1997).
7. P. L. Hansen *et al.*, *Science* **295**, 2053–2055 (2002).
8. E. Ringe, R. P. Van Duyne, L. D. Marks, *Nano Lett.* **11**, 3399–3403 (2011).
9. J. W. Gibbs, H. A. Bumstead, R. G. Van Name, W. R. Longley, *The Collected Works of J. Willard Gibbs* (Longmans, Green, City, 1902).
10. G. Wulff, *Z. Kristallogr. Mineral.* **34**, 449–530 (1901).
11. N. Tian, Z.-Y. Zhou, S.-G. Sun, Y. Ding, Z. L. Wang, *Science* **316**, 732–735 (2007).
12. Y. Xia, Y. Xiong, B. Lim, S. E. Skrabalak, *Angew. Chem. Int. Ed.* **48**, 60–103 (2009).
13. A. R. Tao, S. Habas, P. Yang, *Small* **4**, 310–325 (2008).
14. C. R. Bealing, W. J. Baumgardner, J. J. Choi, T. Hanrath, R. G. Hennig, *ACS Nano* **6**, 2118–2127 (2012).
15. M. J. Williamson, R. M. Tromp, P. M. Vereecken, R. Hull, F. M. Ross, *Nat. Mater.* **2**, 532–536 (2003).
16. H. Zheng *et al.*, *Science* **324**, 1309–1312 (2009).
17. J. E. Evans, K. L. Jungjohann, N. D. Browning, I. Arslan, *Nano Lett.* **11**, 2809–2813 (2011).
18. N. de Jonge, F. M. Ross, *Nat. Nanotechnol.* **6**, 695–704 (2011).
19. J. M. Yuk *et al.*, *Science* **336**, 61–64 (2012).
20. Y. Borodko *et al.*, *J. Phys. Chem. C* **117**, 26667–26674 (2013).
21. H.-G. Liao, L. Cui, S. Whitelam, H. Zheng, *Science* **336**, 1011–1014 (2012).

ACKNOWLEDGMENTS

We thank B. Sadtler for useful comments on the manuscript. Part of the in situ experiments was performed at Gatan, Incorporated using a Tecnai equipped with a K2-IS camera. We also used FEI Titan, Tecnai UT20, JOEL3010, and TEAM0.5 microscopes at the National Center for Electron Microscopy of Lawrence Berkeley National Laboratory, which is supported by the U.S. Department of Energy (DOE) Office of Basic Energy Sciences under contract no. DE-AC02-05CH11231. H.Z. was a residency faculty member of SinBeRise program of BEARS at University of California, Berkeley, during July 2013 to January 2014 and thanks the DOE Office of Science Early Career Research Program for support.

SUPPLEMENTARY MATERIALS

www.sciencemag.org/content/345/6199/916/suppl/DC1
Materials and Methods
Supplementary Text
Figs. S1 to S20
References (*22*–*32*)
Movies S1 to S7

10 March 2014; accepted 3 July 2014
10.1126/science.1253149

GLACIERS

Attribution of global glacier mass loss to anthropogenic and natural causes

Ben Marzeion,[1]* J. Graham Cogley,[2] Kristin Richter,[1] David Parkes[1]

The ongoing global glacier retreat is affecting human societies by causing sea-level rise, changing seasonal water availability, and increasing geohazards. Melting glaciers are an icon of anthropogenic climate change. However, glacier response times are typically decades or longer, which implies that the present-day glacier retreat is a mixed response to past and current natural climate variability and current anthropogenic forcing. Here we show that only 25 ± 35% of the global glacier mass loss during the period from 1851 to 2010 is attributable to anthropogenic causes. Nevertheless, the anthropogenic signal is detectable with high confidence in glacier mass balance observations during 1991 to 2010, and the anthropogenic fraction of global glacier mass loss during that period has increased to 69 ± 24%.

Although glaciers store less than 1% of global ice mass (*1*), their mass loss has been a major cause of sea-level rise during the 20th century (*2*). Glaciers are important regulators of the seasonal water cycle, providing meltwater during dry seasons in many regions of the world (*3*, *4*). Glacier retreat often leads to the destabilization of mountain slopes and the formation of unstably dammed meltwater lakes, increasing the risk of rockslides and catastrophic outburst floods (*5*). The worldwide retreat of glaciers over the past decades has therefore had many impacts on human societies, which should increase over the 21st century because of continued mass losses (*6*–*8*).

Even though warming has accelerated over recent decades (*9*), glaciers have contributed to sea-level rise during most of the 20th century with relatively constant mass loss rates (*2*, *6*, *10*). The mass loss during the first decades of the 20th century was presumably governed by the loss of ice at low altitudes, when glaciers retreated from their 19th-century maxima at the end of the Little Ice Age (*11*). Because glacier extent responds to changes in the glacier mass balance (MB) with a lag of decades to centuries (*12*–*14*), glaciers provide an opportunity to directly perceive long-term climate change, unobscured by interannual variability. For this reason, images of retreating glaciers have become widely publicized illustrations of anthropogenic climate change. At the same time, the lagged response of glacier extents to climate changes complicates the attribution of the observed changes to any particular cause, because glacier mass change at any time is in part an ongoing adjustment of the glacier to previous climate change. The global retreat of glaciers observed today started around the middle of the 19th century, coinciding with the end of the Little Ice Age (*10*), when the anthropogenic forcing of the climate system was very weak as compared to today (*15*). Given the response times of glaciers, it is therefore reasonable to hypothesize that glaciers at present are responding both to naturally caused climate change of past centuries and to the anthropogenic warming that has become stronger in recent decades. There is evidence that the recent mass loss of individual glaciers exceeds values expected from internal variability (*16*), and a rough estimate has been made of the influence of anthropogenic warming on global glacier mass loss (*17*), but the explicit attribution of observed changes of individual glaciers is also complicated by the dynamic response of glaciers' geometries to climate forcing, because internal variability alone may cause glacier changes of the magnitude observed since the end of the Little Ice Age (*18*).

Here we quantify the evidence for a causal link between anthropogenic climate forcing and observed glacier surface MBs, not of individual glaciers but of all the world's glaciers outside of Antarctica combined. We then attribute the global glacier retreat since 1851 to natural and anthropogenic causes. We use a model of global glacier evolution that treats the MB of each of the world's glaciers contained in the Randolph Glacier Inventory (RGI) (*19*, *20*) individually, including a simple parametrization of ice dynamics leading to glacier hypsometry change (*6*). Forced by observed climate (*21*, *22*), the glacier model has been independently validated against both annual surface MB observations (fig. S1) and observed, temporally accumulated volume changes of hundreds of glaciers (*23*), and has been used to reconstruct and project the global glacier mass change from 1851 to 2300 (*6*), based on climate reconstructions and projections from the Coupled Model Intercomparison Project phase 5 (CMIP5). See the supplementary materials for a comprehensive description of the model.

For each of 12 reconstructions of the global climate between 1851 and 2010, produced by general circulation models (GCMs) from the CMIP5 ensemble (see table S1 for the list of the experiments used), we reconstructed the area and volume of each glacier in 1851 (*6*). From this

[1]Institute of Meteorology and Geophysics, University of Innsbruck, Austria. [2]Department of Geography, Trent University, Peterborough, Canada.
*Corresponding author. E-mail: ben.marzeion@uibk.ac.at

reconstructed glacier state, we modeled the evolution of each glacier forward in time. This forward model was run twice for each GCM: once subject to all known forcings (i.e., solar variability, volcanic eruptions, land-use change, anthropogenic aerosols, and greenhouse gas emissions; we call these model runs the FULL runs below), and once subject to only natural forcings (i.e., solar variability and volcanic eruptions; we call these model runs the NAT runs below). Figure 1A shows the ensemble mean and standard deviation of the global mean specific MBs for the FULL and NAT runs. Because the global mean specific MB interpolated from observations (*23*) (we call these OBS below) is available as pentadal means only (black lines in Fig. 1A), we determined the pentadal means of the model runs (thick solid lines in Fig. 1A). In order to determine whether the modeled glacier MBs are consistent with observed MBs, we calculated the confidence level of the difference between modeled and observed MBs for each pentad. High confidence in this difference (i.e., red shading in Fig. 1B) thus indicates model results that are inconsistent with observations.

Modeled MBs in both the FULL and NAT runs are negative over essentially the entire period considered. However, a difference emerges over the course of the 20th century: Although the MB of the NAT runs becomes less negative as glaciers retreat to higher altitudes, thus stabilizing their MBs, there is a clear trend toward more negative MBs of glaciers in the FULL runs after 1965. Modeled MBs in the FULL runs are generally consistent with observations during the entire period covered by the latter, whereas the NAT runs are inconsistent with observations for at least the four pentads spanning 1991 to 2010 (Fig. 1B). This means that the anthropogenic signal is detectable in observed MBs over these four pentads with high confidence, unaffected by the result that MBs would have been negative during this period even without anthropogenic climate forcing. The anthropogenic fraction of global specific glacier mass loss rates increased from $-6 \pm 35\%$ during the period 1851 to 1870 to $69 \pm 24\%$ during the period 1991 to 2010 (Fig. 1C, uncertainties correspond to one ensemble standard deviation). Without anthropogenic influence, glaciers would have contributed 99 ± 36 mm to global mean sea-level rise during 1851 to 2010. With anthropogenic influence, this number increases to 133 ± 30 mm (Fig. 1D, uncertainties correspond to one ensemble standard deviation).

When global mean MBs over longer periods than pentads are considered, it becomes evident that the NAT runs are inconsistent with observations for any period spanning 5 to 50 years and ending in 2010 (Fig. 2). The FULL runs are generally consistent with observations (Fig. 1B), but the simulated MBs are more negative than the observations during 2001 to 2010 (Fig. 1A), resulting in a difference between FULL runs and observations above the 85% confidence level for periods spanning 5 to 15 years and ending in 2010 (Fig. 2). This difference is caused by the FULL MBs for Svalbard and the Russian Arctic, which are too negative as compared to the observations.

Glacier mass losses attributable to human activity (shown as a fraction in Fig. 1C) have increased nearly steadily since 1860. In Fig. 3 we plot the year-by-year anthropogenic global mean specific mass balance $MB_{ANTH} = MB_{FULL} - MB_{NAT}$ against the concurrent anthropogenic radiative forcing R (*24*), and find a sensitivity dMB_{ANTH}/dR of -209 ± 33 kg year^{-1} W^{-1} (uncertainty corresponds to the 95% confidence interval). This is about twice as much as a direct calculation based on the latent heat of fusion of ice would give (-94 kg year^{-1} W^{-1}), indicating that feedbacks and the spatial distribution of anthropogenic climate change play an important role.

On the regional scale, the increased signal from internal climate variability, and greater uncertainty of GCM results (*25*), reduce the detectability of the anthropogenic signal. Although there are some regions where the anthropogenic signal is detectable (i.e., FULL runs are consistent with observations, whereas NAT runs are inconsistent), there are also a number of regions where the FULL runs are not consistent with observations (Fig. 2). The anthropogenic signal is detectable with high confidence in Alaska, western Canada and United States, Arctic Canada north and south, Greenland (only peripheral glaciers and not the ice sheet are considered there), north Asia, central Europe, low latitudes, and New Zealand (9 out of 18 regions), and with lesser confidence in Iceland, Scandinavia, and central Asia north (3 out of 18 regions). In Svalbard, the Russian Arctic, the Caucasus and Middle East, and the southern Andes, the FULL runs are inconsistent with observations (4 out of 18 regions), and in central Asia south and west both FULL and NAT runs are consistent with observations (2 out of 18 regions). A closer look at those regions where our method fails reveals that in the Caucasus and Middle East and the southern Andes, both the FULL and NAT runs underestimate the mass losses (in both cases, the FULL runs are closer to observations than the NAT runs).

In Svalbard and the Russian Arctic, the FULL run overestimates the mass loss, whereas the

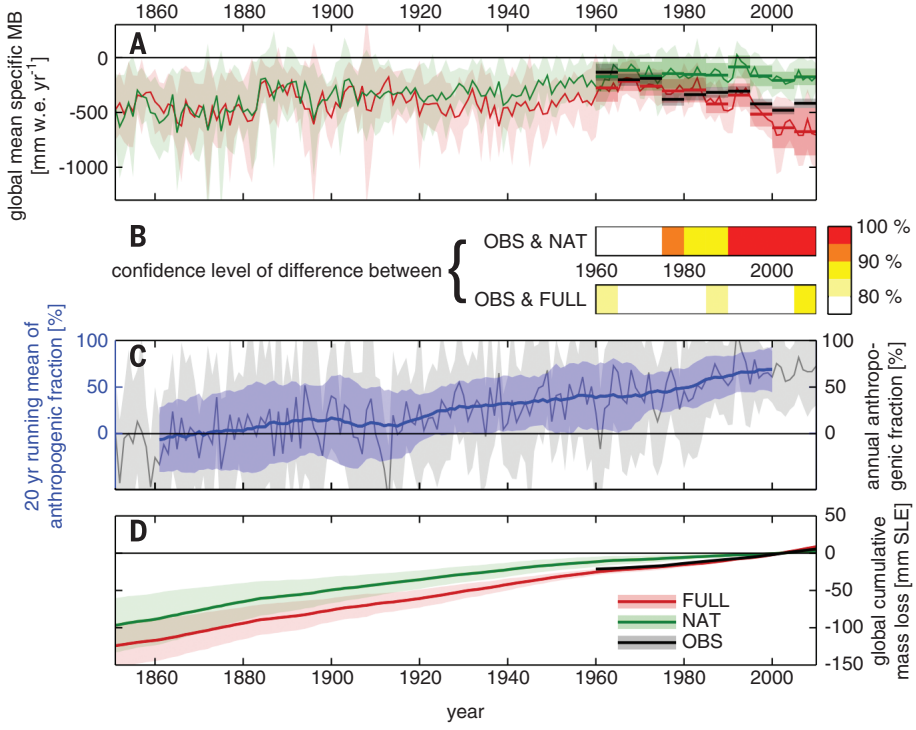

Fig. 1. Attribution of the anthropogenic signal in global mean glacier MBs. (**A**) Global mean specific MB time series (thin lines are the ensemble means, shading indicates one ensemble standard deviation) and pentadal means (thick lines are the ensemble means, shading indicates 1 SE; see the supplementary materials for the derivation of the error) are shown. Green, NAT results; red, FULL results; black, observations. (**B**) Confidence level of the difference between interpolated observations (OBS) updated from Cogley (2009) (*23*) and model results for the NAT and FULL models for each pentad. (**C**) Anthropogenic fraction of total glacier mass loss, annual values (gray), and running mean over 20-year periods (blue); the solid line is the ensemble mean; shading indicates one ensemble standard deviation. (**D**) Glacier contribution to global mean sea-level rise, relative to the mean of 1991 to 2010. Modeled results include modeled glacier area change; observations assume constant glacier area, as in the RGI (*19*) (the solid lines are the ensemble means; shading indicates one ensemble standard deviation).

NAT run is consistent with observations (fig. S2). GCMs tend to have greater errors in this region than on global average (*25*), but they do not generally exhibit a stronger warming during summer months or reduced precipitation as compared to observations (*22*), which could explain too-negative modeled MBs. When we exclude calving glaciers from the observational data set (calving is not accounted for in the glacier model but does affect the observational estimate), the difference is reduced slightly, but not enough to lead to consistent results in these regions. Because validation of the glacier model on individual glaciers, as opposed to the regional mean, does not indicate a general underestimation of the modeled MBs in Svalbard (*6*), the reason for this regional inconsistency has to be related to the sampling of glacier MB observations (*26*), but ultimately remains unclear.

Because the glaciers are considerably out of balance with both modeled FULL and NAT climate at the beginning of the simulation period, it is not possible to distinguish between glacier mass losses caused by internal variability and natural forcing. In order to address this question, it would be necessary to identify the causes that led to the buildup of glacier mass during the Little Ice Age, a period not covered by the CMIP5 experiments. However, our results indicate that a considerable fraction of 20th-century glacier mass loss, and therefore also of observed sea-level rise, was independent of anthropogenic climate forcing. At the same time, we find unambiguous evidence of anthropogenic glacier mass loss in recent decades.

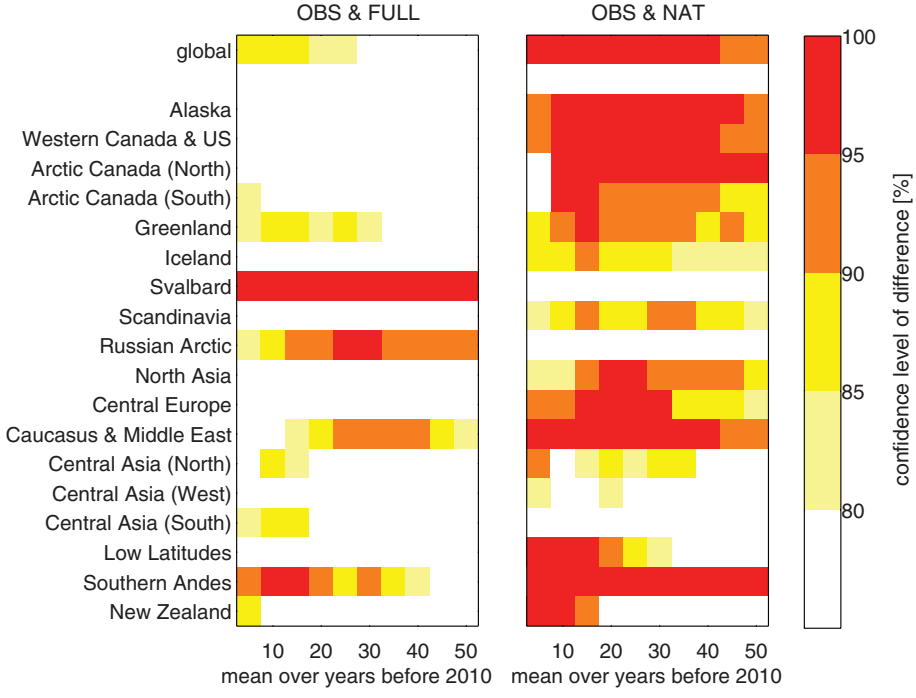

Fig. 2. Detection of the anthropogenic signal in global and regional glacier MBs over longer time intervals. Confidence levels of difference between observations (*23*) and model results for the NAT and FULL models for periods of different length ending in 2010 are shown. Regions are as defined in the RGI (*19*).

Fig. 3. Sensitivity of the instantaneous anthropogenic global mean specific MB to global mean anthropogenic radiative forcing. Annual values of MB_{ANTH} plotted against concurrent anthropogenic radiative forcing *R* (*24*) are shown. The Pearson correlation coefficient between the two is −0.71.

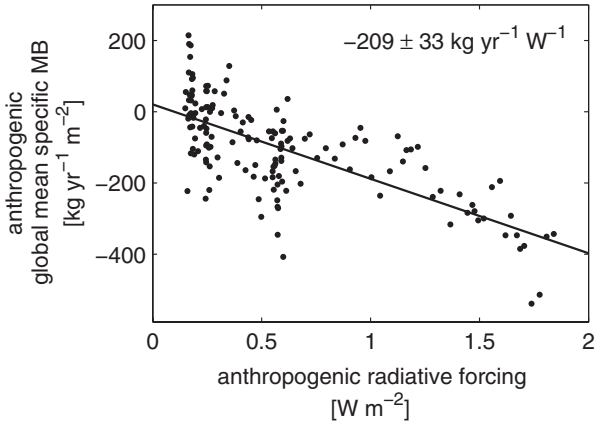

REFERENCES AND NOTES

1. D. G. Vaughan *et al.*, in *Climate Change 2013: The Physical Science Basis. Contribution of Working Group I to the Fifth Assessment Report of the Intergovernmental Panel on Climate Change*, T. F. Stocker, D. Qin, G.-K. Plattner, M. Tignor, S. K. Allen, J. Boschung, A. Nauels, Y. Xia, V. Bex, P. M. Midgley, Eds. (Cambridge Univ. Press, Cambridge, 2013), pp. 317–382.
2. J. M. Gregory *et al.*, *J. Clim.* **26**, 4476–4499 (2013).
3. W. W. Immerzeel, L. P. H. van Beek, M. F. P. Bierkens, *Science* **328**, 1382–1385 (2010).
4. G. Kaser, M. Grosshauser, B. Marzeion, *Proc. Natl. Acad. Sci. U.S.A.* **107**, 20223–20227 (2010).
5. S. D. Richardson, J. M. Reynolds, *Quat. Int.* **65-66**, 31–47 (2000).
6. B. Marzeion, A. H. Jarosch, M. Hofer, *Cryosphere* **6**, 1295–1322 (2012).
7. R. H. Giesen, J. Oerlemans, *Clim. Dyn.* **41**, 3283–3300 (2013).
8. V. Radić *et al.*, *Clim. Dyn.* **42**, 37–58 (2014).
9. D. L. Hartmann *et al.*, in *Climate Change 2013: The Physical Science Basis. Contribution of Working Group I to the Fifth Assessment Report of the Intergovernmental Panel on Climate Change*, T. F. Stocker, D. Qin, G.-K. Plattner, M. Tignor, S. K. Allen, J. Boschung, A. Nauels, Y. Xia, V. Bex, P. M. Midgley, Eds. (Cambridge Univ. Press, Cambridge, 2013), pp. 159–254.
10. P. W. Leclercq, J. Oerlemans, J. G. Cogley, *Surv. Geophys.* **32**, 519–535 (2011).
11. B. Marzeion, A. H. Jarosch, J. M. Gregory, *Cryosphere* **8**, 59–71 (2014).
12. T. Jóhannesson, C. Raymond, E. Waddington, *J. Glaciol.* **35**, 355–369 (1989).
13. W. Harrison, D. Elsberg, K. Echelmeyer, R. Krimmel, *J. Glaciol.* **47**, 659–664 (2001).
14. J. Oerlemans, *Science* **308**, 675–677 (2005).
15. G. Myhre *et al.*, in *Climate Change 2013: The Physical Science Basis. Contribution of Working Group I to the Fifth Assessment Report of the Intergovernmental Panel on Climate Change*, T. F. Stocker, D. Qin, G.-K. Plattner, M. Tignor, S. K. Allen, J. Boschung, A. Nauels, Y. Xia, V. Bex, P. M. Midgley, Eds. (Cambridge Univ. Press, Cambridge, 2013), pp. 659–740.
16. B. K. Reichert, L. Bengtsson, J. Oerlemans, *J. Clim.* **15**, 3069–3081 (2002).
17. J. Oerlemans, *J. Glaciol.* **34**, 333–341 (1988).
18. G. Roe, M. O'Neal, *J. Glaciol.* **55**, 839–854 (2009).
19. A. Arendt *et al.*, *Randolph Glacier Inventory 1.0: A Dataset of Global Glacier Outlines* (Global Land Ice Measurements from Space, Boulder, CO, 2012), digital media.
20. W. T. Pfeffer *et al.*, *J. Glaciol.* **60**, 537–552 (2014).
21. M. New, D. Lister, M. Hulme, I. Makin, *Clim. Res.* **21**, 1–25 (2002).
22. T. D. Mitchell, P. D. Jones, *Int. J. Climatol.* **25**, 693–712 (2005).
23. J. G. Cogley, *Ann. Glaciol.* **50** (50), 96–100 (2009).
24. M. Meinshausen *et al.*, *Clim. Change* **109**, 213–241 (2011).
25. G. Flato *et al.*, in *Climate Change 2013: The Physical Science Basis. Contribution of Working Group I to the Fifth Assessment Report of the Intergovernmental Panel on Climate Change*, T. F. Stocker, D. Qin, G.-K. Plattner, M. Tignor, S. K. Allen, J. Boschung, A. Nauels, Y. Xia, V. Bex, P. M. Midgley, Eds. (Cambridge Univ. Press, Cambridge, 2013), pp. 741–866.
26. A. S. Gardner *et al.*, *Science* **340**, 852–857 (2013).

ACKNOWLEDGMENTS

This work was funded by the Austrian Science Fund (grant PP25362-N26) and supported by the Austrian Ministry of Science Bundesministerium für Wissenschaft und Forschung as part of the UniInfrastrukturprogramm of the Research Platform Scientific Computing at the University of Innsbruck. We acknowledge the World Climate Research Programme's Working Group on Coupled Modelling, which is responsible for CMIP, and we thank the climate modeling groups (listed in the table S1) for producing and making available their model output. For CMIP, the U.S. Department of Energy's Program for Climate Model Diagnosis and Intercomparison provided coordinating support and led the development of software infrastructure in partnership with the Global Organization for Earth System Science Portals.

SUPPLEMENTARY MATERIALS

www.sciencemag.org/content/345/6199/919/suppl/DC1
Methods
Figs. S1 and S2
Table S1
References (*27*–*33*)

11 April 2014; accepted 14 July 2014
10.1126/science.1254702

POLIO ERADICATION

Efficacy of inactivated poliovirus vaccine in India

Hamid Jafari,[1]* Jagadish M. Deshpande,[2] Roland W. Sutter,[3]† Sunil Bahl,[1] Harish Verma,[3] Mohammad Ahmad,[1] Abhishek Kunwar,[1] Rakesh Vishwakarma,[1] Ashutosh Agarwal,[1] Shilpi Jain,[4] Concepcion Estivariz,[5] Raman Sethi,[1] Natalie A. Molodecky,[3] Nicholas C. Grassly,[6] Mark A. Pallansch,[5] Arani Chatterjee,[4]‡ R. Bruce Aylward[3]

Inactivated poliovirus vaccine (IPV) is efficacious against paralytic disease, but its effect on mucosal immunity is debated. We assessed the efficacy of IPV in boosting mucosal immunity. Participants received IPV, bivalent 1 and 3 oral poliovirus vaccine (bOPV), or no vaccine. A bOPV challenge was administered 4 weeks later, and excretion was assessed 3, 7, and 14 days later. Nine hundred and fifty-four participants completed the study. Any fecal shedding of poliovirus type 1 was 8.8, 9.1, and 13.5% in the IPV group and 14.4, 24.1, and 52.4% in the control group by 6- to 11-month, 5-year, and 10-year groups, respectively (IPV versus control: Fisher's exact test $P < 0.001$). IPV reduced excretion for poliovirus types 1 and 3 between 38.9 and 74.2% and 52.8 and 75.7%, respectively. Thus, IPV in OPV-vaccinated individuals boosts intestinal mucosal immunity.

Since the beginning of polio vaccine development in the 1950s, the choice of which vaccine to use, either the Salk inactivated poliovirus (IPV) or the Sabin live-attenuated oral poliovirus vaccine (OPV), has been fiercely contested (*1*, *2*). The debate continued even after the goal of global polio eradication was established in 1988 (*3*). Regardless, the global polio eradication initiative (GPEI) chose OPV to eliminate the final chains of poliovirus transmission (*4*).

Through massive use of OPV, the number of polio-endemic countries decreased from 125 in 1988 to 3 in 2013, and the incidence declined by >99% (*5*). Wild poliovirus type 2 transmission was interrupted globally in 1999 (*6*), and wild poliovirus type 3 was last detected in November 2012 (*7*) (fig. S1). However, parts of three countries (Afghanistan, Nigeria, and Pakistan) continue to report wild poliovirus type 1 (*8*), and exportation of this virus causes outbreaks (*9*, *10*).

Despite the advantages of OPV (superior mucosal immunity, secondary spread to contacts, ease of administration, and lower price), the vaccine has limitations: low immunogenicity in some tropical countries (*11*, *12*); and incomplete intestinal immunity that wanes rapidly (*13*). To interrupt transmission, OPV must be administered to a high proportion of children (*1*, *4*).

The intestinal immunity induced by OPV is incomplete. Even after a full series with OPV, between 10 and 20% of children excrete poliovirus after a challenge with Sabin poliovirus (*1*, *14*). Studies in India demonstrate that a fraction of children excrete Sabin strains after OPV exposure despite having received more than seven doses of OPV (*15*). To address the low OPV immunogenicity, the GPEI developed new formulations of OPV, including monovalent OPVs (mOPVs; mOPV1 and mOPV3) in 2005 and bivalent types 1 + 3 OPV (bOPV) in 2009 (*16*, *17*).

Although IPV administered after OPV effectively closes the humoral immunity gaps (*2*, *18*, *19*), its effect on intestinal mucosal immunity is less-well characterized. Because mucosal immunity appears to wane rapidly (*13*), we initiated a trial in Northern India to assess whether IPV could boost mucosal immunity. We enrolled infants aged 6 to 11 months and children aged 5 and 10 years. On enrollment, the three age groups were randomized to receive IPV, bOPV, or no vaccine (control group). Four weeks later, all participants received a challenge dose of bOPV, and poliovirus excretion was measured on days 3, 7, and 14.

Enrollment was completed within 6 days (i.e., during 11 to 16 October 2011), and follow-up visits were concluded by 11 December 2011. Nine hundred and ninety children were enrolled in the trial (fig. S2). Of these, 36 (3.6%) were excluded or withdrawn (1 due to wrong group assignment, 22 with incomplete stool samples, and 13 with incomplete serology samples), leaving 954 (96.4%) for analysis. Virus titer could not be determined for 18 poliovirus type 1 and 13 type 3 stool samples.

There were no significant differences between the groups with regard to median age,

Table 1. Demographic characteristics and baseline prevalence of poliovirus antibodies (n = 954).

Study group/age group	Median age (years) (IQR)*	Gender [% male (95% CI)]	Father's education [% illiterate (95% CI)]
IPV	5.4 (0.9–10.2)	45.9 (40.3–51.6)	45.1 (39.5–50.8)
bOPV	5.5 (0.9–10.2)	47.7 (42.1–53.3)	44.9 (39.3–50.8)
Control	5.5 (0.9–10.2)	49.2 (43.6–54.9)	43.5 (37.9–49.2)
6–11 months	0.8 (0.7–0.9)	45.8 (40.1–51.5)	44.2 (38.5–49.9)
5 years	5.4 (5.2–5.7)	48.8 (43.2–54.3)	44.3 (38.8–49.9)
10 years	10.4 (10.2–10.6)	48.1 (42.5–53.8)	45.0 (39.4–50.6)

	Seroprevalence		
	Type 1 % (95% CI)	Type 2 % (95% CI)	Type 3 % (95% CI)
Overall	99.6 (98.9–99.9)	91.6 (89.7–93.3)	93.3 (91.5–94.8)
IPV	99.7 (98.2–100)	92.1 (88.5–94.8)	94.6 (91.5–96.8)
bOPV	99.4 (97.9–99.9)	89.1 (85.2–92.3)	91.0 (87.3–93.9)
Control	99.7 (98.3–100)	93.7 (90.4–96.1)	94.3 (91.2–96.6)
6–11 months	99.0 (97.2–99.8)	81.8 (77.0–86.0)†	89.9 (86.0–93.1)‡
5 years	100 (98.9–100)	95.4 (92.5–97.4)	97.5 (95.2–98.9)
10 years	99.7 (98.3–100)	97.2 (94.7–98.7)	92.2 (88.7–94.9)

*IQR, interquartile range. †$P < 0.001$ versus 5-year and 10-year age groups. ‡$P < 0.001$ versus 5-year age group; P value calculated with Fisher's exact (two-sided) test; 95% confidence intervals calculated with Clopper-Pearson method.

[1]World Health Organization, India-National Polio Surveillance Project, R. K. Khanna Stadium, Africa Avenue, Safdarjung Enclave, New Delhi 110029, India. [2]Enterovirus Research Center, Haffkine Institute Compound, Parel, Mumbai, India. [3]World Health Organization, Ave Appia, Geneva, Switzerland. [4]Panacea Biotec Ltd., New Delhi, India. [5]Centers for Disease Control and Prevention, Atlanta, GA, USA. [6]Department of Infectious Disease Epidemiology, Imperial College London, London, UK.
*Present address: Polio Operations and Research Department, World Health Organization, CH-1211 Geneva 19, Switzerland.
†Corresponding author. E-mail: sutterr@who.int ‡Present address: Biological E Ltd., Hyderabad, India.

gender, father's education, or baseline seroprevalence levels, which was high (≥99%) for type 1 and somewhat lower for types 2 and 3, particularly in the youngest age group (Table 1).

The prevalence of poliovirus excretion for type 1 and 3 after challenge with bOPV is shown in table S1. For poliovirus type 1, the highest prevalence was 43.8% [95% confidence interval (CI) 34.1–53.8] in 10-year olds in the control group 3 days after challenge compared with 12.5% (95% CI 6.8–20.4) in the IPV group. For poliovirus type 3, the highest prevalence was 44.8% (95% CI 35.0–54.8) 7 days after challenge in the 10-year-olds of the control group compared to 7.7% (95% CI 3.4–14.6) in the IPV group (Fig. 1). Excluding participants excreting virus on day 0 (n = 17) produced similar results.

The relative reduction in excretion between IPV group and control group was markedly consistent across the poliovirus types. For poliovirus type 1, the decrease in excretion in any stool sample after challenge in the IPV group compared to the control group was 38.9% (8.8% versus 14.4%) in the 6- to 11-month, 62.2% (9.1% versus 24.1%) in the 5-year, and 74.2% (13.5% versus 52.4%) in the 10-year age group; the corresponding decreases for poliovirus type 3 were 71.1% (3.9% versus 13.5%) in the 6- to 11-month, 52.8% (11.8% versus 25.0%) in the 5-year, and 75.7% (12.5% versus 51.4%) in the 10-year age group (table S1).

bOPV significantly decreased excretion of type 1 by 51.9% and type 3 by 40.5% only in the 10-year age group (Fisher's exact test $P < 0.001$ for type 1; $P = 0.002$ for type 3).

For poliovirus type 1, the median duration of excretion was estimated to be 7.6 days (95% CI 6.0–10.1 days) for the IPV group, 8.7 days (95% CI 7.3–10.5) in the control group, and 9.1 days (95% CI 7.4–11.4) in the bOPV group. For poliovirus type 3, the median duration was 10.4 days (95% CI 7.4–15.4) for the IPV group, 13.1 days (95% CI 10.1–17.4) in the control group, and 11.6 days (95% CI 9.0–15.4) in the bOPV group. None of these differences were statistically significant (table S2).

The median virus titers among participants excreting poliovirus type 1 were highest 7 days after challenge, ranging from 4.1 $\log_{10}$ $CCID_{50}$ (50% cell culture infectious dose) per gram of stool (95% CI 3.5–4.7) in the control group to 3.8 log10 $CCID_{50}$ (95% CI 2.1–5.4) in the IPV group, a decrease of 49.9% (Wilcoxon rank-sum test $P = 0.872$). The median titers to poliovirus type 3 were 4.1 $\log_{10}$ $CCID_{50}$ (95% CI 3.6–4.5) in the control group compared to 3.4 $\log_{10}$ $CCID_{50}$ (95% CI 2.6–4.2) in the IPV group, a decrease of 80.0% ($P = 0.143$) (table S3). The relative reduction in the prevalence of excretion in the IPV group compared to the control group was between 38.9 and 75.7%, the absolute decrease in median titer of virus in stool specimens was between 0.3 and 0.7 $\log_{10}$ $CCID_{50}$ (at day 7 after challenge), and the absolute decline in length of excretion was between 1.1 and 2.7 days (Fig. 2).

Four weeks after vaccination, an IPV dose induced a humoral immune response (i.e., seroconversion or fourfold increase in antibody titer) to poliovirus type 1 in 82.9% (95% CI 67.9–92.8), 98.2% (95% CI 90.6–100), and 95.6% (89.1–98.8) of participants in the 6- to 11-month, 5-year, and 10-year age groups, respectively, compared to 2.9% (95% CI 0–15.3), 3.1% (95% CI 0.3–10.8), and 0% (95% CI 0–4.2) in the control group (Fisher's exact test $P < 0.001$ for all age groups). A bOPV dose induced a humoral immune response in 14.3% (95% CI 4.8–30.3), 12.9% (95% CI 5.7–23.9), and 42.4% (32.1–53.1) of participants ($P = 0.198$ for the 6- to 11-month group, $P = 0.052$ for the 5-year group, and $P < 0.001$ for 10-year group, compared to control group; significantly lower than the IPV group, $P < 0.001$ for all age groups). Similar levels in humoral response were noted against poliovirus type 3 (Table 2).

We divided the antibody titers into quartiles and assessed the excretion prevalence in each quartile. Because the antibody titers were high, we collapsed quartiles 3 and 4 (where the median titers were at the final dilution tested, ≥1:1448). The overall excretion of poliovirus type 1 was 0 (n = 1), 18.2, and 9.9% in quartiles 1, 2, and 3-4, respectively, in the IPV group compared to 40.8, 26.5, and 12.9% in the control group and 30.7, 28.4, and 13.0% in the bOPV group, respectively (test for overall trend: Fisher's exact test $P < 0.001$). Similar trends were found for poliovirus type 3.

Our trial provides the following insights: (i) A single dose of IPV boosts intestinal mucosal

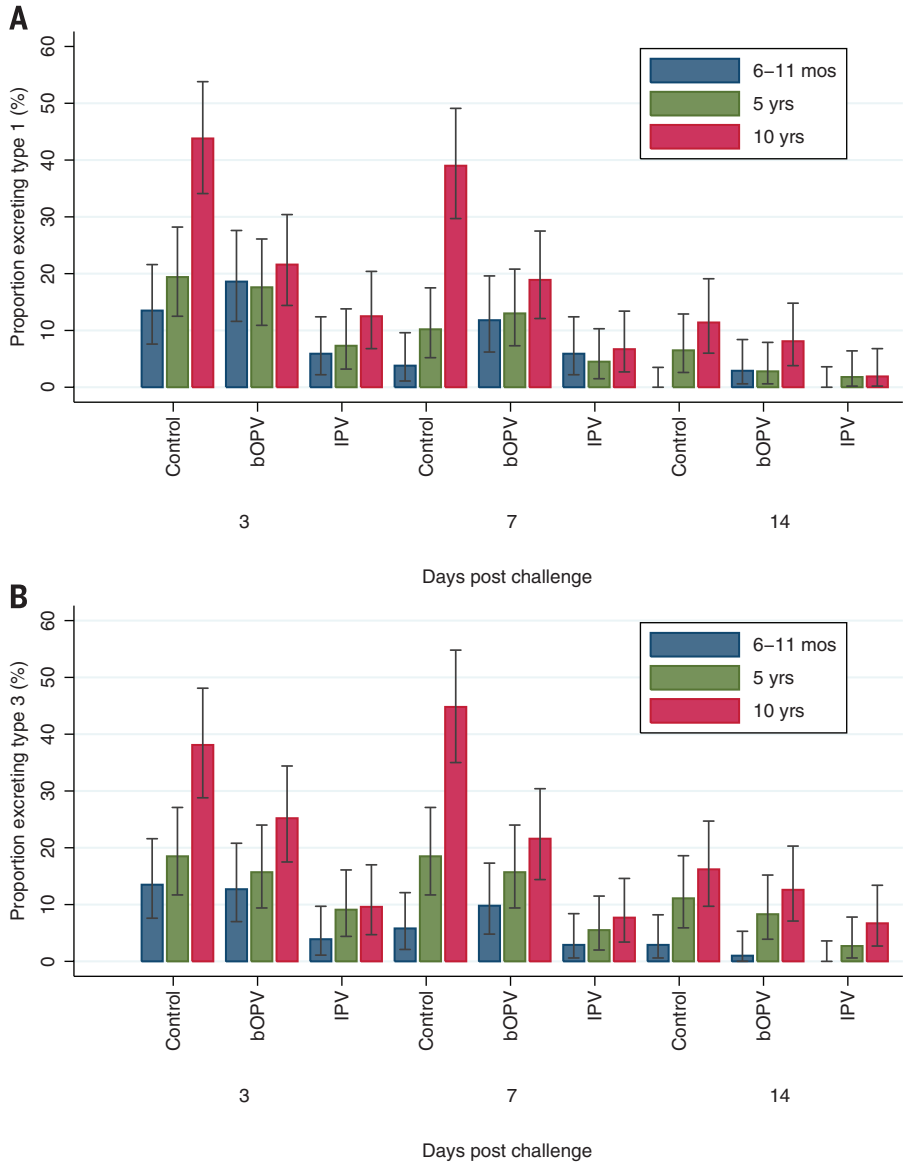

Fig. 1. Excretion of poliovirus type 1 and type 3 after challenge with bOPV. The prevalence of poliovirus type 1 (**A**) and type 3 (**B**) excretions is plotted for each time point after challenge, for each study arm and age group. All subjects (n = 954) are included. Bars represent 95% confidence intervals calculated with the Clopper-Pearson method.

immunity against polioviruses in infants and children with a history of multiple doses of OPV; (ii) the magnitude of this effect is substantially larger after IPV compared to bOPV; and (iii) the oldest age group displayed the highest degree of waning intestinal mucosal immunity manifested by highest prevalence of excretion after challenge.

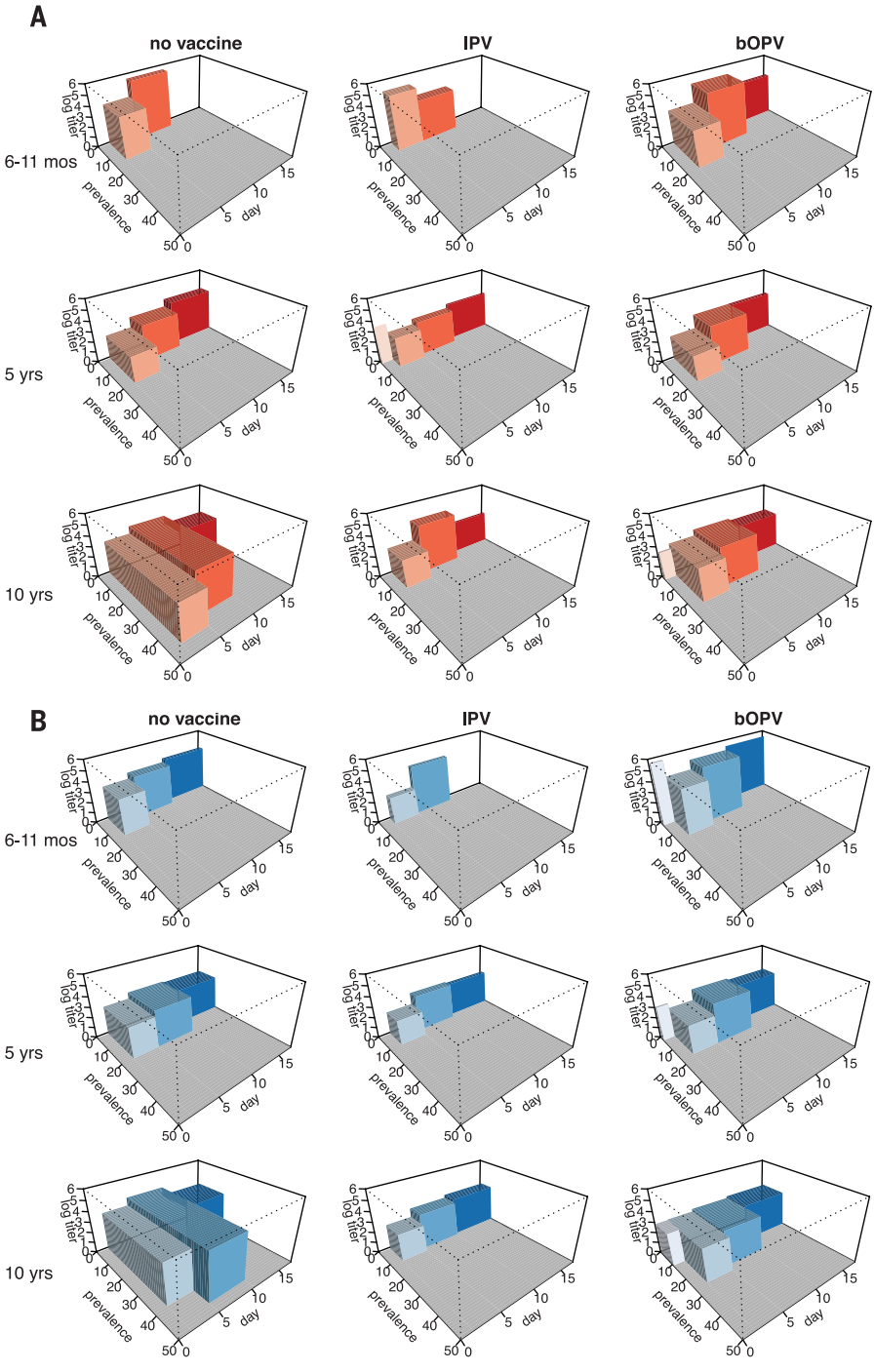

Fig. 2. Magnitude of excretion of poliovirus type 1 and type 3 after bOPV challenge for each study arm and age group. The prevalence of poliovirus type 1 (**A**) and type 3 (**B**) excretion and the mean $\log_{10}$ titer are plotted for each time point after challenge, with the width of the boxes spanning the midpoints between these time points (except for those boxes representing shedding on the day of challenge, where the plot is truncated at day 0). The volume of the boxes therefore roughly represents the total quantity of poliovirus that is excreted (prevalence × quantity × duration). Prevalence measure includes 954 participants. Titer measure includes 303 participants excreting virus after bOPV challenge.

Although IPV reliably induces humoral immunity (*18*–*20*) that is highly efficacious in preventing paralytic poliomyelitis (*21*, *22*), the ability of IPV alone to induce intestinal mucosal immunity is limited (*23*, *24*). Studies in countries that do not use OPV show that >90% of IPV-vaccinated children excrete challenge poliovirus (*25*, *26*). Limited data are available on IPV effectiveness in boosting intestinal mucosal immunity in children with a history of multiple doses of OPV (*19*, *27*, *28*). Live virus contact to mucosal surfaces appears necessary to induce a specific secretory immunoglobulin A response (*29*, *30*).

The most important comparisons are between the IPV and the control group, where a decrease in the prevalence of excretion of 39 to 76% was found in the IPV group compared to the control group. The decrease after a dose of bOPV was considerably lower, not significant in the 6- to 11-month and 5-year age groups, but 41 to 52% among 10-year-olds.

The study also demonstrated that higher humoral antibody titers are associated with decreased challenge virus excretion, as has been shown previously (*4*, *19*, *27*). bOPV increased antibody titers to poliovirus type 2, presumably because of boosting of cross-reacting neutralizing antibodies (*31*), since we did not isolate poliovirus type 2 from any stool samples. The data support the use of IPV (or OPV) to boost intestinal immunity for travelers to and from polio-infected countries.

Our study had a limitation. We conducted the study in Moradabad district in Uttar Pradesh State of India where the immunogenicity of OPV is low (*11*, *12*). Therefore, extrapolation or generalization of these findings to other areas in India or elsewhere must be done with caution.

The Strategic Advisory Group of Experts (SAGE) recommended in 2012 the introduction of ≥1 dose of IPV in all routine immunization programs for risk mitigation before OPV2 withdrawal (*32*). A dose of IPV is expected to induce seroconversion or priming in close to 100% of naïve infants (*33*). Should poliovirus type 2 be reintroduced, a second IPV dose would rapidly boost antibody titers and prevent, or decrease the magnitude of, an outbreak. Furthermore, IPV would be expected to close the remaining type-specific immunity gaps.

Our study provides strong evidence that IPV boosts intestinal immunity among children with a history of multiple OPV doses more effectively than an additional OPV dose. These data provided the scientific foundation for the development of the new polio endgame plan (*34*) and are guiding the development of strategies to hasten the elimination of the final poliovirus reservoirs and to decrease the vulnerability of polio-free areas to epidemic transmission after poliovirus importations.

Thus, more than 25 years after the World Health Assembly resolution to eradicate poliomyelitis, the answer to the vaccine controversy is

Table 2. Seroconversion or fourfold increase in poliovirus antibody titer between days 0 and 28.

	Intervention groups	Type 1			Type 2			Type 3		
		n	% (95% CI)	*P* value	*n*	% (95% CI)	*P* value	*n*	% (95% CI)	*P* value
6–11 months	Control	1/34	2.9 (0.0–15.3)	Ref	3/73	4.1 (0.9–11.5)	Ref	3/69	4.3 (0.9–12.2)	Ref
	IPV	34/41	82.9 (67.9–92.8)	<0.001	55/67	82.1 (70.8–90.4)	<0.001	66/72	91.7 (82.7–96.9)	<0.001
	bOPV	5/35	14.3 (4.8–30.3)	0.198	5/74	6.8 (2.2–15.1)	0.719	10/71	14.1 (7.0–24.4)	0.078
5 years	Control	2/64	3.1 (0.3–10.8)	Ref	1/103	1.0 (0.0–5.3)	Ref	2/81	2.5 (0.3–8.6)	Ref
	IPV	56/57	98.2 (90.6–100)	<0.001	90/95	94.7 (88.1–98.3)	<0.001	80/82	97.6 (91.5–99.7)	<0.001
	bOPV	8/62	12.9 (5.7–23.9)	0.052	7/101	6.9 (2.8–13.8)	0.034	14/88	15.9 (9.0–25.2)	0.003
10 years	Control	0/87	0.0 (0.0–4.2)	Ref	2/101	2.0 (0.2–7.0)	Ref	3/102	2.9 (0.6–8.4)	Ref
	IPV	87/91	95.6 (89.1–98.8)	<0.001	99/103	96.1 (90.4–98.9)	<0.001	98/98	100.0 (96.3–100)	<0.001
	bOPV	39/92	42.4 (32.1–53.1)	<0.001	36/105	34.3 (25.3–44.2)	<0.001	54/101	53.5 (43.3–63.5)	<0.001

P values calculated with Fisher's exact (two-tailed) test; 95% confidence intervals calculated with Clopper-Pearson method.

apparent——both vaccines, IPV and OPV, should be used. As a result, the Word Health Organization (WHO) is no longer recommending an all-OPV schedule; rather, it recommends that all OPV-using countries introduce ≥1 dose of IPV into routine vaccine schedules (*35*).

REFERENCES AND NOTES

1. R. W. Sutter *et al.*, in *Vaccines*, S. A. Plotkin, W. A. Orenstein, Eds. (Saunders, Philadelphia, PA, ed. 6, 2012), vol. 28, p. 598.
2. J. R. Paul, *History of Poliomyelitis* (Yale Univ. Press, Princeton, NJ, 1978.
3. World Health Organization, World Health Assembly (WHA) resolution, 1988 (resolution 41.28).
4. H. F. Hull, N. A. Ward, B. P. Hull, J. B. Milstien, C. de Quadros, *Lancet* **343**, 1331–1337 (1994).
5. World Health Organization, *Wkly. Epidemiol. Rec.* **88**, 153–160 (2013).
6. Centers for Disease Control and Prevention, *Morb. Mortal. Wkly. Rep.* **50**, 222–224 (2001).
7. World Health Organization, *Wkly. Epidemiol. Rec.* **88**, 385–388 (2013).
8. World Health Organization, *Wkly. Epidemiol. Rec.* **87**, 381–388 (2012).
9. World Health Organization, *Wkly. Epidemiol. Rec.* **88**, 349–355 (2013).
10. S. Arie, *BMJ* **347**, f6682 (2013).
11. T. J. John, P. Jayabal, *Am. J. Epidemiol.* **96**, 263–269 (1972).
12. N. C. Grassly *et al.*, *Science* **314**, 1150–1153 (2006).
13. N. C. Grassly *et al.*, *J. Infect. Dis.* **205**, 1554–1561 (2012).
14. World Health Organization Collaborative Study Group on Oral Poliovirus Vaccine, *J. Infect. Dis.* **171**, 1097–1106 (1995).
15. N. C. Grassly *et al.*, *J. Infect. Dis.* **200**, 794–801 (2009).
16. N. El-Sayed *et al.*, *N. Engl. J. Med.* **359**, 1655–1665 (2008).
17. R. W. Sutter *et al.*, *Lancet* **376**, 1682–1688 (2010).
18. B. J. Morinière *et al.*, *Lancet* **341**, 1545–1550 (1993).
19. R. W. Sutter *et al.*, *N. Engl. J. Med.* **343**, 767–773 (2000).
20. C. F. Estívariz *et al.*, *Lancet Infect. Dis.* **12**, 128–135 (2012).
21. S. E. Robertson *et al.*, *Lancet* **331**, 897–899 (1988).
22. T. Francis Jr., *J. Am. Med. Assoc.* **158**, 1266–1270 (1955).
23. T. R. Hird, N. C. Grassly, *PLOS Pathog.* **8**, e1002599 (2012). v
24. E. Anis *et al.*, *Euro Surveill.* **18**, 20586 (2013).
25. The Cuba IPV Study Collaborative Group, *N. Engl. J. Med.* **356**, 1536–1544 (2007).
26. L. Piirainen *et al.*, *Vaccine* **17**, 1084–1090 (1999).
27. WHO Collaborative Study Group on Oral and Inactivated Poliovirus Vaccines, *J. Infect. Dis.* **175** (suppl. 1), S215–S227 (1997).
28. I. Parent. du Châtelet *et al.*, *Vaccine* **21**, 1710–1718 (2003).
29. T. M. Herremans, J. H. Reimerink, A. M. Buisman, T. G. Kimman, M. P. Koopmans, *J. Immunol.* **162**, 5011–5018 (1999).
30. T. Herremans *et al.*, *Clin. Infect. Dis.* **34**, 1067–1075 (2002).
31. R. D. Puligedda *et al.*, *Antiviral Res.* **108**, 36–43 (2014).
32. World Health Organization, *Wkly. Epidemiol. Rec.* **88**, 1–6 (2013).
33. S. Resik *et al.*, *N. Engl. J. Med.* **368**, 416–424 (2013).
34. World Health Organization, WHO, Geneva (WHO/POL/13.02) (2013).
35. World Health Organization, *Wkly. Epidemiol. Rec.* **89**, 73–92 (2014).

ACKNOWLEDGMENTS

Funding was provided by Rotary International Polio Plus Program (through a grant approved by the Polio Research Committee of the World Health Organization). The study was approved by the Drugs Controller General (India), the Indian Council of Medical Research, and the Ethics Review Committees of the WHO. The trial was registered with the Indian Clinical Trials Registry (www.ctri.nic.in) (registration number CTRI/2011/09/002018). We acknowledge the contributions of Uttar Pradesh State Government health staff, social mobilization network of the United Nations Children's Fund and CORE, and the operations team from WHO India-National Polio Surveillance Project who were instrumental in the setup and implementation of the study. We also acknowledge the extensive work performed by the laboratory staff at ERC Mumbai. Finally, we express our sincere thanks to the Government of India Ministry of Health and Family Welfare and the GPEI partners. The data set is available in the supplementary materials. The findings and conclusions of this report are those of the authors and do not necessarily represent the official position of the Centers for Disease Control and Prevention, or other participating organizations.

SUPPLEMENTARY MATERIALS

www.sciencemag.org/content/345/6199/922/suppl/DC1
Materials and Methods
Figs. S1 and S2
Tables S1 to S3
Data set
References (*36*–*40*)

21 April 2014; accepted 15 July 2014
10.1126/science.1255006

CARBON CYCLE

Sunlight controls water column processing of carbon in arctic fresh waters

Rose M. Cory,[1]* Collin P. Ward,[1] Byron C. Crump,[2] George W. Kling[3]

Carbon in thawing permafrost soils may have global impacts on climate change; however, the factors that control its processing and fate are poorly understood. The dominant fate of dissolved organic carbon (DOC) released from soils to inland waters is either complete oxidation to CO_2 or partial oxidation and river export to oceans. Although both processes are most often attributed to bacterial respiration, we found that photochemical oxidation exceeds rates of respiration and accounts for 70 to 95% of total DOC processed in the water column of arctic lakes and rivers. At the basin scale, photochemical processing of DOC is about one-third of the total CO_2 released from surface waters and is thus an important component of the arctic carbon budget.

Carbon dioxide emissions from inland surface waters to the atmosphere are as large as the net carbon transfer from the atmosphere to Earth's surface (~2 Pg C $year^{-1}$; 1 Pg = 10^{15} g) (*1*–*5*). This large flux is affected by the movement of dissolved organic carbon (DOC) from land (*1*, *2*) and its subsequent oxidation to CO_2 in fresh waters (*3*–*5*). The remaining DOC may be unprocessed, flocculated, or partially oxidized and exported in rivers to

oceans, where it has important consequences for coastal ecosystems (*6*). Although the processing and fate of DOC is thus a critical aspect of C cycling, the factors controlling oxidation of DOC in fresh waters are poorly understood (*5*, *6*).

DOC oxidation in inland waters is of special concern for the Arctic because permafrost soils contain twice as much C as there is in the atmosphere (*7*), and they are thawing (*8*) and releasing C to surface waters and the atmosphere. In turn, surface waters mediate C flux to the ocean and atmosphere that could represent up to 40% of the net land-atmosphere carbon exchange (*9*) (maximum freshwater flux of ~0.16 Pg C $year^{-1}$ and a net arctic terrestrial sink of 0.4 ± 0.4 Pg C $year^{-1}$). Because some fraction of newly thawed C is labile to biological and photochemical degradation to CO_2 (*10*, *11*), there is active debate on how and when the arctic C cycle will amplify global climate change (*12*, *13*).

The fate of DOC released to inland waters is controlled by its coupled photochemical and biological oxidation. The current understanding of controls on DOC oxidation is that photochemical mineralization to CO_2 constitutes only about 10% of bacterial respiration (i.e., biological mineralization) in inland or coastal waters (*14*–*19*). However, no study has quantified concurrently all the dominant biological and photodegradation pathways of DOC, which include bacterial respiration to CO_2, photomineralization to CO_2, partial photo-oxidation of DOC (which is likely less labile to bacterial action and has a longer residence time in the DOC pool; DOC_{ox}, Fig. 1), and photostimulated bacterial respiration of partially photo-oxidized DOC that is easily respired by bacteria to CO_2. There is ample evidence that partial photo-oxidation can alter DOC quality and stimulate bacterial respiration (*20*–*22*), and in arctic rivers this photostimulated bacterial respiration can be a substantial portion of dark bacterial respiration of DOC (*11*).

Although no data exist that directly quantify both photochemical and bacterial degradation of DOC in arctic inland waters, these waters are characteristically rich in light-absorbing chromophoric dissolved organic matter (CDOM) labile to photodegradation (*22*), and they tend to be shallow (mean depth <2 m) (*23*, *24*); hence, the entire water column may be exposed to ultraviolet (UV) light (*11*). We quantified the importance of photodegradation in DOC processing by directly measuring dark bacterial respiration and each of the DOC photoproducts listed above. Rates of photomineralization to CO_2 and partial photo-oxidation of DOC were greater than rates of dark respiration by bacteria in the water column of arctic streams and lakes by a factor of 3 to 19, which suggests that sunlight controls the fate of DOC in arctic surface waters.

DOC processing was measured for streams and lakes in and near the Kuparuk River basin on the North Slope of Alaska during the ice-free summers of 2011 to 2013 (*24*) (fig. S1). We quantified dark bacterial respiration (N = 81) and measured the wavelength-specific apparent quantum yields of (i) photomineralization of DOC (N = 97), (ii) partial photo-oxidation of DOC (N = 97), and (iii) photostimulated bacterial respiration (N = 147) as measured by O_2 consumption and CO_2 production (*24*). Areal rates of bacterial respiration and each photochemical process were calculated by integrating apparent quantum yields with incoming UV radiation and light absorption by DOC over mean water column depth (*24*) in 73 different surface waters. Areal rates were then scaled to the entire Kuparuk basin, using optical properties from 135 different lakes and 73 rivers as well as 2153 measures of CDOM from the foothills to the coastal plains in the Alaskan Arctic.

Average areal water column rates of DOC photodegradation exceeded dark bacterial respiration of DOC and accounted for 70 to 95% of total C processed (Table 1). Photomineralization rates alone exceeded dark bacterial respiration rates by a factor of nearly 5 on average; in Imnavait Creek, a representative shallow-headwater stream characterized by high CDOM and low pH, photomineralization exceeded dark bacterial respiration by a factor of more than 10 (table S1). Even in the deepest site measured, Toolik Lake (mean depth 7 m), areal photomineralization was more than half the dark bacterial respiration in the water column (Table 1) and was a similar or greater percentage than comparable measurements made outside the Arctic (*14*–*17*) or in coastal waters (*18*). Areal rates of partial photo-oxidation of DOC also exceeded dark bacterial respiration at every site except for Imnavait Creek, by a factor of 1.7 in Toolik Lake and by a factor of nearly 15 in the low-DOC, glacial-fed Sagavanirktok River (Table 1). Areal rates of photostimulated bacterial respiration were similar to water column rates of dark bacterial respiration in streams but were lower than the dark bacterial respiration rates in the deeper water columns of lakes studied by a factor of 2 to 7 (Table 1) and were similar to or higher than comparable measurements outside the Arctic (*17*).

The dominance of photochemical over biological C processing in the water column of arctic surface waters, relative to that of lower-latitude waters, is likely due to three reasons. First, the measured volumetric rates of dark bacterial respiration tend toward the low end of the range reported for fresh waters (*17*, *25*–*27*), thereby elevating the relative importance of sunlight over bacteria in this study. Second, our apparent quantum yields were on the high end of the range measured in waters outside the Arctic (*16*, *28*, *29*) (fig. S4), which suggests that DOC in arctic surface waters is more labile to photodegradation relative to DOC in other fresh waters; this is consistent with prior evidence for high reactivity of arctic DOC to photodegradation (*11*, *22*, *30*, *31*) (discussed below). Third and perhaps most important, compared to previous, similar measurements in relatively deep lakes of forested regions (*14*–*17*, *29*), the shallow and unshaded surface waters in the Arctic essentially confine photoprocessing of DOC to a thin boundary layer that maximizes DOC exposure to sunlight and facilitates photochemical degradation (table S2 and fig. S3). Given these conditions, it is likely that photochemical DOC degradation is substantial

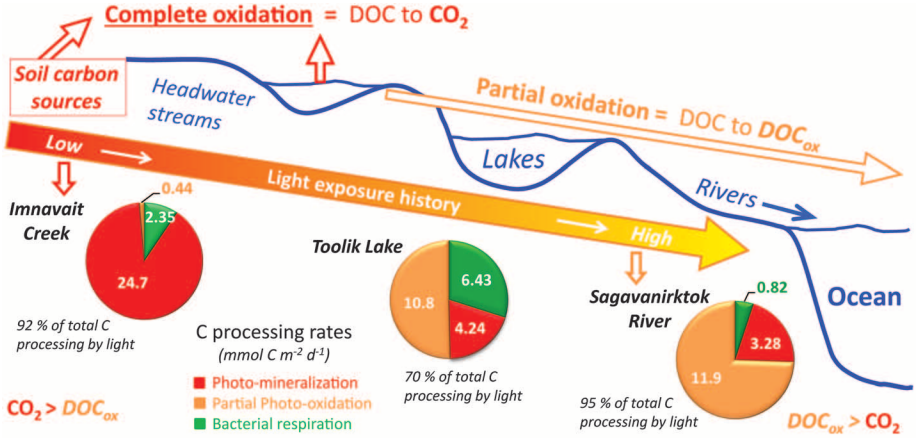

Fig. 1. Conceptual model and pathways of DOC processing and fate. Dissolved organic carbon (DOC) released from soils (left) can be completely oxidized to CO_2 (dark bacterial respiration or photomineralization) or partially oxidized (partial photo-oxidation, DOC_{ox}) and remain in the DOC pool to be transported in rivers to oceans (right). DOC in headwater streams fed directly by soil waters has low prior light exposure and is more labile to photochemical mineralization to CO_2 (e.g., red section of pie for Imnavait Creek) relative to Sagavanirktok River water, where partial photo-oxidation to DOC_{ox} dominates. Mean processing rates of C (mmol C m^{-2} day^{-1}) are shown for three sites representative of the landscape continuum, from low history of light exposure leaving soils (left) to high history of light exposure after a longer time spent in surface waters (right). The C processed by sunlight ranged from 70 to 95% of the total C processed.

[1]Earth and Environmental Sciences, University of Michigan, Ann Arbor, MI 48109, USA. [2]Earth, Ocean, and Atmospheric Sciences, Oregon State University, Corvallis, OR 97331, USA. [3]Department of Ecology and Evolutionary Biology, University of Michigan, Ann Arbor, MI 48109, USA.
*Corresponding author. E-mail: rmcory@umich.edu

in any shallow and unshaded inland surface water and plays an important role in freshwater carbon cycling. For example, a recent study suggested that photomineralization alone provides ~10% of the CO_2 emitted to the atmosphere from inland surface waters globally (*29*), and in our study partial photo-oxidation plus photostimulated bacterial respiration processed twice as much DOC as did photomineralization (Table 2).

We scaled these measures of DOC processing to the open-water period in three water types—small streams, larger rivers, and lakes—using (i) mean biodegradation rates and mean apparent quantum yields for photoreactions (Table 2 and fig. S4), (ii) measured and modeled UV radiation in the atmosphere, and (iii) underwater light absorption (*11*). As expected, measured light attenuation coefficients $K_{d,\lambda}$ were strongly related to underwater light absorption by CDOM ($a_{CDOM,\lambda}$) (R^2 = 0.94, N = 100), and we used our measured $a_{CDOM,\lambda}$ (N = 2153) to predict $K_{d,\lambda}$ when it was not measured directly (fig. S2). Results for the open-water period highlight the day-to-day variability in available UV radiation due to atmospheric conditions and the seasonal decrease in zenith angle after summer solstice (Fig. 2). Although the overall dominance of photochemical

Table 1. Areal rates of water column processing of DOC by sunlight and bacteria in experiments at near-ambient temperature and light conditions. Data are means ± SE averaged over 2011–2013 (*24*). Dark bacterial respiration and photomineralization both oxidize DOC to CO_2. Photo-oxidation includes all photochemical processes (complete or partial oxidation of DOC) that consume O_2. Partial photo-oxidation [calculated as (mol photochemical O_2 consumption) − (mol photochemical CO_2 production) × 0.5, assuming 0.5 mol of O_2 consumed to 1 mol DOC oxidized (*24*, *37*)] represents only the amount of O_2 consumed that does not directly yield CO_2 (i.e., DOC to DOC_{ox} in Fig. 1). Some DOC_{ox} produced by partial photo-oxidation is subsequently oxidized completely by bacteria to CO_2 (i.e., photostimulated bacterial respiration); however, in all but Imnavait Creek, the dominant partial photo-oxidation product was DOC_{ox} remaining in the dissolved C pool. Total C processed is the sum of dark bacterial respiration, photomineralization, and the larger of partial photo-oxidation or photostimulated bacterial respiration. All terms were converted to C basis on the assumption that 1 mol O_2 is consumed per mol CO_2 respired for dark or light bacterial respiration (measured as O_2 consumption relative to killed controls) (*24*). Percentage of C processed by sunlight was calculated as [(photomineralization) + (the larger of partial photo-oxidation or photostimulated bacterial respiration)]/(total C processed). Note that partial photo-oxidation was greater than photostimulated bacterial respiration at all sites except Imnavait Creek. Ratio of photochemical to biological mineralization was calculated as (photomineralization)/(dark bacterial respiration).

	Dark bacterial respiration (mmol O_2 m^{-2} day^{-1})	Photomineralization (mmol CO_2 m^{-2} day^{-1})	Photo-oxidation (mmol O_2 m^{-2} day^{-1})	Photostimulated bacterial respiration (mmol O_2 m^{-2} day^{-1})	Partial photo-oxidation (mmol C m^{-2} day^{-1})	Total C processed (mmol C m^{-2} day^{-1})	Percentage of C processed by light	Ratio of photo- to biomineralization
Imnavait Creek	2.35 ± 0.34	24.7 ± 18.3	22.4 ± 16.7	3.04 ± 1.31	0.44 ± 0.44	30.1 ± 22.4	92.2 ± 1.0	10.5
Kuparuk River	0.92 ± 0.10	4.89 ± 0.69	7.56 ± 0.46	1.01 ± 0.20	5.92 ± 0.75	11.7 ± 1.2	92.2 ± 0.1	5.4
Sagavanirktok River	0.82 ± 0.22	3.28 ± 1.58	11.3 ± 1.2	1.12 ± 0.24	12.0 ± 1.7	16.0 ± 2.2	94.9 ± 0.2	4.0
Toolik Inlet Stream	0.91 ± 0.28	2.98 ± 0.34	4.66 ± 0.41	0.55 ± 0.20	3.60 ± 0.86	7.50 ± 1.03	87.9 ± 0.2	3.3
Toolik Lake	6.43 ± 1.45	4.24 ± 1.15	9.27 ± 2.31	0.92 ± 0.15	10.8 ± 2.8	21.5 ± 3.4	70.1 ± 0.2	0.7
Coastal plain lakes	2.00 ± 0.27	9.15 ± 0.50	7.46 ± 1.55	1.06 ± 0.02	4.84 ± 1.90	16.0 ± 2.0	87.5 ± 0.2	4.6

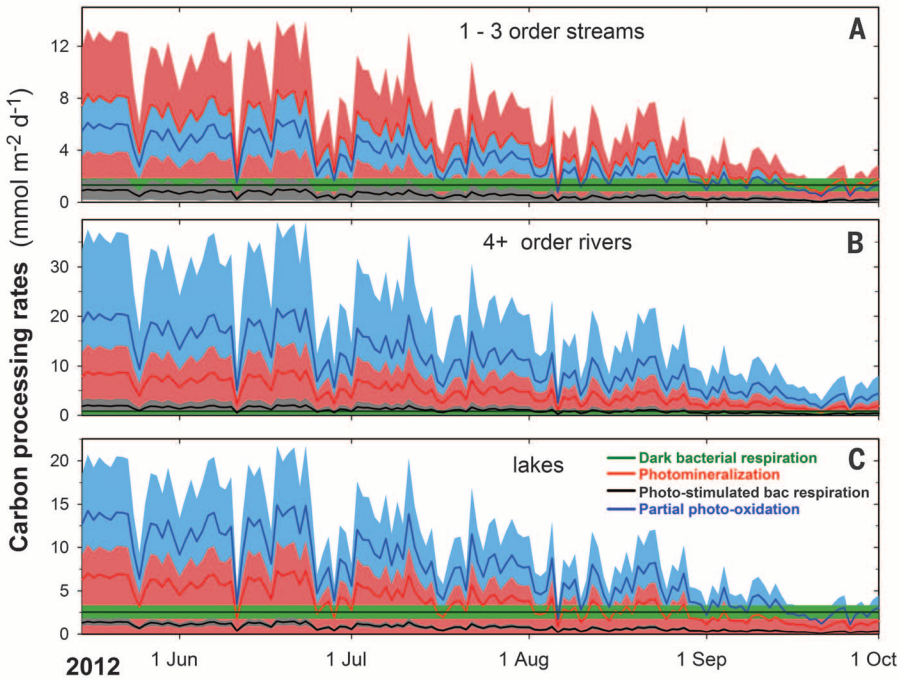

Fig. 2. Seasonal carbon processing in surface waters by bacteria and photochemistry. Daily areal water column rates of dark bacterial respiration, photomineralization, photostimulated bacterial respiration, and partial photo-oxidation of DOC in (**A**) first- to third-order streams, (**B**) fourth-order and larger rivers, and (**C**) lakes in 2012 (2011 and 2013 show similar patterns). Solid lines show the average rate; shaded areas in similar colors denote the upper and lower 95% confidence intervals of the apparent quantum yield and $a_{CDOM,\lambda}$ used to calculate photochemical rates, or the 95% confidence intervals on mean bacterial respiration, for each water type (*24*).

Table 2. Estimates of average annual photochemical and bacterial processing of DOC in the Kuparuk River basin, 2011–2013. Data are means ± SE. Photochemical reaction rates were calculated as defined in Table 1. Estimates are based on 2011–2013 UV and photosynthetically active radiation data at Toolik Field Station, using an ice-out date of 24 May for streams and rivers and 16 June for all lakes; bacterial respiration is calculated for the annual range of temperatures in lakes that do not freeze to the bottom. The surface area of first- to third-order streams, fourth-order and larger rivers, and lakes was 5.937 km^2, 12.26 km^2, and 323.8 km^2, respectively.

	Dark bacterial respiration (Gg C $year^{-1}$)	Photo-mineralization (Gg C $year^{-1}$)	Photostimulated bacterial respiration (Gg C $year^{-1}$)	Partial photo-oxidation (Gg C $year^{-1}$)	Total C processed (Gg C $year^{-1}$)	Percentage of C processed by light	Total CO_2 available to atmosphere (Gg C $year^{-1}$)	Percentage of CO_2 from sunlight
Streams (1st- to 3rd-order)	0.012	0.042 ± 0.002	0.005 ± 0.000	0.031 ± 0.001	0.085 ± 0.003	85.4 ± 0.5	0.059 ± 0.002	79.0 ± 0.7
Rivers (4th order and larger)	0.016	0.092 ± 0.004	0.021 ± 0.001	0.216 ± 0.009	0.323 ± 0.013	95.0 ± 0.2	0.128 ± 0.005	87.5 ± 0.5
Lakes	1.48	1.39 ± 0.06	0.286 ± 0.013	2.83 ± 0.14	5.70 ± 0.20	74.0 ± 0.9	3.16 ± 0.08	53.1 ± 1.2
Sum	1.51	1.53 ± 0.07	0.31 ± 0.01	3.08 ± 0.15	6.11 ± 0.22	75.3 ± 0.9	3.34 ± 0.08	54.9 ± 1.1

processing in streams and lakes remained, the fate of DOC varied consistently by water type. In small streams, DOC was mainly mineralized by sunlight to CO_2, whereas in lakes the main fate of DOC was partial photo-oxidation (Table 1 and Fig. 2). Large rivers were intermediate between these end members, and photomineralization to CO_2 was about equal to or less than partial photo-oxidation (Table 1 and Fig. 2). We suggest that this pattern is a result of light exposure history; DOC leached from soils into headwater streams has little prior light exposure and is labile to complete photo-oxidation, but as light exposure increases in water moving downstream and into lakes with longer residence times, the DOC photolability declines (*11*, *22*, *32*–*34*). Thus, as easily photomineralized moieties are removed, DOC fate shifts toward partial photo-oxidation and downstream export in rivers and lakes.

Carbon processing at the scale of the Kuparuk River basin (~8000 km^2) was estimated by summing areal rates over time (Fig. 2) for the period 2011–2013 and multiplying by the surface area of each water type (Table 2). Year-to-year variation was small because of similar degradation rates and light availability across years (Fig. 2), and photochemical reactions accounted for 75% of the total of 6.11 Gg DOC-C $year^{-1}$ processed in surface waters, of which 3.34 Gg C $year^{-1}$ was released to the atmosphere as CO_2 (~55% from photoreactions; Table 2). Converting to a rate per square meter of land in the Kuparuk Basin, ~0.4 g C m^{-2} $year^{-1}$ was mineralized to CO_2 in the water column, which is 25 to 40% of the estimated CO_2 released to the atmosphere from arctic fresh waters (*4*, *9*). The remaining CO_2 released to the atmosphere is likely generated in soil waters and transferred directly to surface waters (*3*, *4*) or is respired by bacteria and autotrophs in aquatic sediments (*35*, *36*). For example, net benthic respiration of 6.6 mmol CO_2 m^{-2} day^{-1} in a tundra pond (*35*) is about two-thirds of the photomineralization we estimate for coastal ponds (Table 1), and limited data for the Kuparuk River (*36*) show that net benthic respiration could exceed photomineralization (Table 1).

At present, our data show that for the entire Kuparuk basin 55% of the DOC processed in the water column of aquatic ecosystems is completely oxidized to CO_2, and 45% is partially oxidized and transported downstream in the DOC pool (Table 2). This balance of DOC fate may change, as thawing soils will release DOC with little prior light exposure and greater potential for photomineralization to CO_2, while earlier ice-out on lakes could increase UV and photoreactions substantially because solar radiation is highest and clear-sky days are more common in May and June relative to the July–October period (Fig. 2 and fig. S6). Understanding the controls on these pathways of DOC fate, and incorporating photochemical processing into models, will improve predictions of how the arctic C cycle will respond to and perhaps amplify climate change.

REFERENCES AND NOTES

1. T. J. Battin *et al.*, *Nat. Geosci.* **2**, 598–600 (2009).
2. A. K. Aufdenkampe *et al.*, *Front. Ecol. Environ* **9**, 53–60 (2011).
3. J. J. Cole, N. F. Caraco, G. W. Kling, T. K. Kratz, *Science* **265**, 1568–1570 (1994).
4. G. W. Kling, G. W. Kipphut, M. C. Miller, *Science* **251**, 298–301 (1991).
5. P. A. Raymond *et al.*, *Nature* **503**, 355–359 (2013).
6. J. E. Vonk, Ö. Gustafsson, *Nat. Geosci.* **6**, 675–676 (2013).
7. C. Tarnocai *et al.*, *Global Biogeochem. Cycles* **23**, GB2023 (2009).
8. Y. Zhang, W. Chen, D. W. Riseborough, *J. Geophys. Res.* **111**, D22103 (2006).
9. A. D. McGuire *et al.*, *Ecol. Monogr.* **79**, 523–555 (2009).
10. E. A. G. Schuur *et al.*, *Nature* **459**, 556–559 (2009).
11. R. M. Cory, B. C. Crump, J. A. Dobkowski, G. W. Kling, *Proc. Natl. Acad. Sci. U.S.A.* **110**, 3429–3434 (2013).
12. E. A. G. Schuur *et al.*, *Bioscience* **58**, 701–714 (2008).
13. A. H. MacDougall, C. A. Avis, A. J. Weaver, *Nat. Geosci.* **5**, 719–721 (2012).
14. R. M. W. Amon, R. Benner, *Geochim. Cosmochim. Acta* **60**, 1783–1792 (1996).
15. W. Granéli, M. Lindell, L. J. Tranvik, *Limnol. Oceanogr.* **41**, 698–706 (1996).
16. A. V. Vähätalo, M. Salkinoja-Salonen, P. Taalas, K. Salonen, *Limnol. Oceanogr.* **45**, 664–676 (2000).
17. A. V. Vähätalo, K. Salonen, U. Münster, M. Järvinen, R. G. Wetzel, *Arch. Hydrobiol.* **156**, 287–314 (2003).
18. S. Bélanger *et al.*, *Global Biogeochem. Cycles* **20**, GB4005 (2006).
19. L. J. Tranvik *et al.*, *Limnol. Oceanogr.* **54**, 2298–2314 (2009).
20. L. J. Tranvik, S. Bertilsson, *Ecol. Lett.* **4**, 458–463 (2001).
21. K. E. Judd, B. C. Crump, G. W. Kling, *Aquat. Sci.* **69**, 96–107 (2007).
22. R. M. Cory, D. M. McKnight, Y.-P. Chin, P. Miller, C. L. Jaros, *J. Geophys. Res.* **112**, G04S51 (2007).
23. J. E. Hobbie, *Limnology of Tundra Ponds, Barrow, Alaska* (Dowden, Hutchinson and Ross, Stroudsburg, PA, 1980).
24. See supplementary materials on *Science* Online.
25. R. Carignan, D. Planas, C. Vis, *Limnol. Oceanogr.* **45**, 189–199 (2000).
26. M. Pace, Y. Prairie, *Respiration in Lakes* (Oxford Univ. Press, New York, 2005), pp. 103–121.
27. M. Berggren, J.-F. Lapierre, P. A. del Giorgio, *ISME J.* **6**, 984–993 (2012).
28. E. M. White, D. J. Kieber, J. Sherrard, W. L. Miller, K. Mopper, *Mar. Chem.* **118**, 11–21 (2010).
29. B. Koehler, T. Landelius, G. A. Weyhenmeyer, N. Machida, L. J. Tranvik, *Global Biogeochem. Cycles* (2014).
30. R. M. W. Amon, B. Meon, *Mar. Chem.* **92**, 311–330 (2004).
31. P. J. Mann *et al.*, *J. Geophys. Res.* **117**, G01028 (2012).
32. H. E. Reader, W. L. Miller, *Limnol. Oceanogr.* **59**, 182–194 (2014).
33. L. Molot, P. Dillon, *Global Biogeochem. Cycles* **11**, 357–365 (1997).
34. C. Vallières, L. Retamal, P. Ramlal, C. L. Osburn, W. F. Vincent, *J. Mar. Syst.* **74**, 756–773 (2008).
35. P. S. Ramlal *et al.*, *Biogeochemistry* **24**, 145–172 (1994).
36. J. E. Hobbie, G. W. Kling, Eds., *A Changing Arctic: Ecological Consequences for Tundra, Streams, and Lakes* (Oxford Univ. Press, New York, 2014).
37. S. Andrews, S. Caron, O. Zafiriou, *Limnol. Oceanogr.* **45**, 267–277 (2000).

ACKNOWLEDGMENTS

We thank K. Harrold, J. Dobkowski, S. Fortin, S. Michael, J. Olsen, B. Papworth, A. Clinger, A. Rocha, W. Eugster, and researchers and technicians of the Toolik Lake Arctic LTER and Toolik Lake Field Station (GIS, R. Fulweber, J. Stuckey) for assistance. Supported by NSF grants OPP 1023270/1022876, PLR 1107593, and DEB-1147378/1347042. The data set provided by the Arctic Long Term Ecological Research Program (table S1) was supported by NSF grant DEB-1026843. The data set provided by the Toolik Field Station Environmental Data Center (table S1) was supported by NSF grants 455541 and 1048361. Other experimental data are presented in the supplementary materials.

SUPPLEMENTARY MATERIALS

www.sciencemag.org/content/345/6199/925/suppl/DC1
Materials and Methods
Figs. S1 to S9
Tables S1 and S2
References (*38*–*54*)

10 March 2014; accepted 11 July 2014
10.1126/science.1253119

SENSORY BIOLOGY

Evolution of sweet taste perception in hummingbirds by transformation of the ancestral umami receptor

Maude W. Baldwin,[1]*† Yasuka Toda,[2]* Tomoya Nakagita,[2] Mary J. O'Connell,[3] Kirk C. Klasing,[4] Takumi Misaka,[2] Scott V. Edwards,[1] Stephen D. Liberles[5]†

Sensory systems define an animal's capacity for perception and can evolve to promote survival in new environmental niches. We have uncovered a noncanonical mechanism for sweet taste perception that evolved in hummingbirds since their divergence from insectivorous swifts, their closest relatives. We observed the widespread absence in birds of an essential subunit (T1R2) of the only known vertebrate sweet receptor, raising questions about how specialized nectar feeders such as hummingbirds sense sugars. Receptor expression studies revealed that the ancestral umami receptor (the T1R1-T1R3 heterodimer) was repurposed in hummingbirds to function as a carbohydrate receptor. Furthermore, the molecular recognition properties of T1R1-T1R3 guided taste behavior in captive and wild hummingbirds. We propose that changing taste receptor function enabled hummingbirds to perceive and use nectar, facilitating the massive radiation of hummingbird species.

Sensory systems display remarkable flexibility across vertebrates, with some animals losing sensory modalities that are no longer key for survival (*1*, *2*) and others evolving new adaptive sensory capabilities (*3*). The repertoires of sensory receptors for odors, pheromones, and tastes reflect species-specific ecology, with receptor families rapidly expanding and contracting (*4*), and in some lineages, new receptor families evolving (*5*). In the olfactory system, functional expansion of the receptor repertoire predominantly involves a pattern of gene duplication and mutation, leading to novel receptors with altered ligand recognition properties (*6*). This pattern of gene duplication and mutation is also observed in vomeronasal receptors and bitter taste receptors, but not in sweet and savory taste receptors (*4*, *7*). Receptors for these palatable tastes are unique among the chemosensory receptor families in that they are highly conserved in number and amino acid identity. New vertebrate sweet receptors, and the evolutionary mechanisms that underlie their acquisition, have not previously been identified.

In vertebrates, sweet and savory ("umami") tastes are sensed by G protein–coupled receptors (GPCRs) termed T1Rs (*8*). Most vertebrates have three T1Rs, with the T1R1-T1R3 heterodimer mediating umami taste and the T1R2-T1R3 heterodimer mediating sweet taste (*8*, *9*). Human T1R2-T1R3 detects carbohydrates and artificial sweeteners (*10*), and knockout mice lacking T1R2 or T1R3 have defective sweet taste perception (*9*, *11*). In genomes analyzed so far, *T1R* expansions are observed only in some fish species (*12*), whereas losses are observed in other vertebrates, often in accordance with diet. Some obligate carnivores, such as cats, lost T1R2 and appetitive behaviors toward carbohydrates (*1*), whereas the giant panda, which feeds predominantly on bamboo, lost T1R1 (*2*). Chickens, turkeys, and zebra finches also do not have T1R2 (*13*), but the relationship between T1R repertoire and avian ecology is unclear. Birds display tremendous heterogeneity in diet, with different lineages primarily consuming fruits, nectars, animals, and seeds. Hummingbirds are specialized nectar feeders, and their ability to perceive and use sugar-rich resources allowed them to colonize a nectarivorous niche, enabling their extensive diversification (*14*). However, how hummingbirds detect sugars remains unknown, so we characterized the repertoires and functions of bird taste receptors to understand the underlying mechanisms of sugar perception.

We identified T1Rs in whole-genome sequences available for 10 birds with different diets and compared them to T1Rs from other vertebrates (Fig. 1A). Also, we cloned T1Rs from the oral tissue of Anna's hummingbirds (*Calypte anna*); the domestic chicken (*Gallus gallus*), which does not prefer sugars (*7*); and the insectivorous chimney swift (*Chaetura pelagica*), because swifts are the closest living relatives of hummingbirds (Fig. 1B and fig. S2). Expression in oral tissue was verified by reverse transcription polymerase chain reaction (fig. S2). Two *T1R* genes—*T1R1* and *T1R3*—were detected in each available bird genome, and candidate signatures of positive selection were identified in the hummingbird lineage (Fig. 1B and table S2), but not the chicken or swift lineages. We failed to detect *T1R2* in bird genomes, despite the presence of flanking loci. Non-avian reptiles retained *T1R2*, including the Chinese alligator (*Alligator sinensis*), a member of the sister group to birds (fig. S1), suggesting that the loss of *T1R2* occurred within Dinosauria. These findings suggest that an alternative T1R2-independent mechanism for sugar detection arose in avian species that display high behavioral affinity for nectar or sweet fruit.

To identify avian sweet receptors, we analyzed responses of bird taste receptors to sugars and amino acids (Fig. 2). Responses of bird T1Rs were measured in heterologous cells by means of calcium-sensitive photoprotein reporters (*15*). Hummingbird T1R1-T1R3 responded to several carbohydrates, including sucrose, fructose, and glucose. Responses were not observed when T1R1 or T1R3 alone was used, suggesting that hummingbird T1R1-T1R3 functions as an obligate heterodimer. Hummingbird T1R1-T1R3 also detected sucralose and various sugar alcohols, including sorbitol and erythritol, but not cyclamate, acesulfame K, and aspartame, which are sweet to humans (*16*). Low-affinity responses were observed to some amino acids, as with the human sweet receptor, which recognizes carbohydrates as well as proteins, dipeptides, and amino acids (*8*). In contrast, cells expressing chicken or swift T1R1-T1R3 failed to detect carbohydrates at any concentration tested and instead recognized alanine and serine. Thus, T1R1-T1R3 heterodimers from swifts, chickens, primates (humans, squirrel monkeys, baboons, and macaques), rodents (mouse and rat), and teleost fish (zebrafish and medaka) detect palatable amino acids (*8*, *17*, *18*). In contrast, in the hummingbird lineage, this receptor complex acquired a new function in the past 42 to 72 million years (*14*, *19*), evolving the capacity for carbohydrate recognition.

Next, we sought to understand the critical changes in hummingbird T1R1-T1R3 that enabled sugar detection. We designed protein chimeras involving portions of hummingbird T1R1-T1R3, which responds to sugars, and chicken T1R1-T1R3, which does not (Fig. 3 and fig. S3). We focused on the venus flytrap domain, an extracellular region of family C GPCRs that mediates ligand binding (*20*). Introducing the venus flytrap domain of chicken T1R3 into hummingbird T1R3 (chimera 1) rendered the heterodimeric receptor sensitive to amino acids rather than sugars. Reintroducing 109 amino acids (residues 158 to 266) of hummingbird T1R3 into the chicken T1R3 venus flytrap domain restored sucrose responses (chimera 2). Further analysis of this 109–amino acid region identified 19 nonconsecutive amino acids (chimera 3; sites: fig. S3), which were collectively sufficient to impart sucrose and sucralose sensitivity (fig. S4). Subsets of these 19 residues did not similarly support sugar binding (fig. S3). Two identified sites (I206 and S237) displayed

[1]Department of Organismic and Evolutionary Biology, Harvard University, and Museum of Comparative Zoology, Cambridge, MA 02138, USA. [2]Department of Applied Biological Chemistry, Graduate School of Agricultural and Life Sciences, University of Tokyo, 1-1-1 Yayoi, Bunkyo-ku, Tokyo, Japan. [3]Bioinformatics and Molecular Evolution Group, School of Biotechnology, Dublin City University, Glasnevin, Dublin 9, Ireland. [4]Department of Animal Science, University of California, Davis, Davis, CA 95616, USA. [5]Department of Cell Biology, Harvard Medical School, Boston, MA 02115, USA.
*These authors contributed equally to this work. †Corresponding author. E-mail: maudebaldwin@gmail.com (M.W.B.); stephen_liberles@hms.harvard.edu (S.D.L.)

evidence of positive selection (Fig. 1B). Hummingbird T1R1 also contains sites that are under putative positive selection and mutations that contribute to acquired sugar responsiveness, because a mixed receptor pair of chicken T1R1 and hummingbird T1R3 prefers amino acids (fig. S5). Thus, the evolution of carbohydrate detection by hummingbird T1R1-T1R3 involved widespread mutation of both receptor subunits.

We created a homology model of the T1R3 venus flytrap domain based on the x-ray crystal structure of the same region in a related GPCR, metabotropic glutamate receptor 1 (mGluR1) (*20*) (Fig. 3D). This model predicted that the 19 sugar response–conferring substitutions in T1R3 were clustered in three distinct regions of the protein. Three residues (G165, I167, and N211) were in the putative orthosteric ligand-binding site, which in mGluR1 is located at the interface between the two lobes of the venus flytrap domain on the extracellular surface (*20*). G165 and I167 align near S186 and T188 of mGluR1, which form salt bridges to the glutamate ligand (*20*), and all three align near T1R1 residues that are important for ligand responses (*18*, *21*). The remaining residues clustered in two other locations, whose functions in family C GPCRs

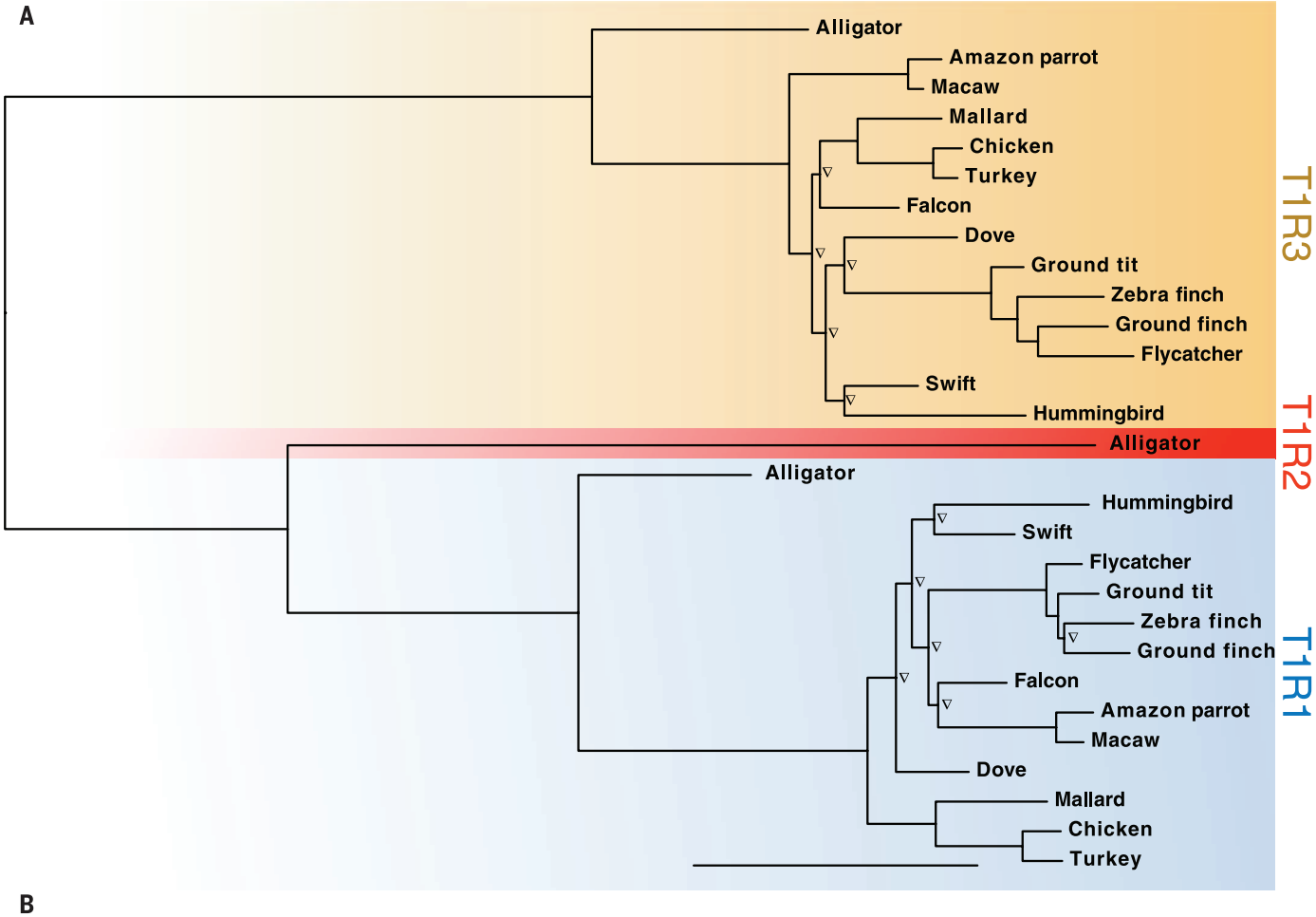

B

```
                1        10        20        30        40        50        60        70        80        90       100       110       120
Chicken         MIPWVLLCMSFGCAAALKPSCLSAQFRRPGDYIIGGLFPFGMDTINLTARSEPTLIVCERLFVDGLIWALGMKFAIDEINNSTSLLPGVELGYDIYDTCFEPLAALQPSLLFVTQNGTTG
Swift           MVPALLLCWSFGYTAALKPTCLSAQFRRPGDYILGGLFPFGMDTVNLTARSEPSLVVCERLFVEGLIWALGMKFAIDQINNSSSLLPGVQLGYEMHDTCFEPLVALQPSLLLLARGGTRA
Hummingbird     MVPTLLLGLSFGYAAAQETVCLSAQFRSPGDYILGGLFPFGMDIVNLTARTEPTSVKCERLFVDGLIWALGMKFAINEINNSSSLLPGVKLGYDMHDTCFEQVVTLQSSLLFLTQKGTTG
                130       140       150       160       170       180       190       200       210       220       230       240
Chicken         IGIACNYTDYQPRVTAVIGPHKSDLCLLTAKLFSFFLIPQVSYGASSEKLSNKELYPSFYRTVPSDKNLVEAVVLLLDEFGWNWIATIGSDDEYGRGAQELFLSTIGNSSICIAYEGLIP
Swift           VAPLCNHSSYQPRVTAVIGPHKSGLCLLTAKLFSSFLIPQVSYAASSEMLSNTNLYPSFYRTVPTDKNLVEAVVLLLKEFGWNWIATIGSDDEYGRGAQGLFLSIAGNHSICIAFEGLIP
Hummingbird     IEVSCNYTNYQPRVTAVIGPYKSDLCLLTAKLFSFFLLPQISYGGSIEKLSNTDSYPSFYRTVPGDNNLVEAVAQLLNKFGWNWIITIGSNDEYGRGAQGHFVSIAENRNICIAFEGLIP
                250       260       270       280       290       300       310       320       330       340       350       360
Chicken         SDLTDPRAEKQLEETIQYINKTNVNIIVLFAFRQPAQALLEQSIKMRLSKKVWIGTEAWLLSDIAASIPNIQNIGTVLGFIMKASTVPGFQKYVANLLSSVQQDEFCQKSREFYRHVSSD
Swift           TDLADPKAKKQLEDTIKSINRTKVNVIVLFAFSHPAQALLEHSIRMGLSKKVWIGTEAWILSDIIASIPNIQSIGTVLGFIIKTGTVPGFQQYVANLFTSIQQDKFCQESREFNQLMNSE
Hummingbird     TDLADPKTTNQLENIIKAINKTDANVIVLFAFSQTALALLEHSIRMGLSKRVWIGTETWTLSHKAASISNIQSIGTVLGFVMKAGTVPGFHKYVTDLFSSAQHDEFCQQSRKSNHLMSSD
                370       380       390       400       410       420       430       440       450       460       470       480
Chicken         TLGTQCQQCDHISLNDISSTLSHSQIQPVYIAVYSVAYALHRALGCTHQGCPRASIRSWQLLHFMNTVPFTVNGQSFRFDESHGTNSGYNLIFWHWENGSLTHLPVGDYQESLYLNKSLI
Swift           VLDTPCEQCDHISLHQVLSTLSHSQVQPVHIAVHSVATALHRALGCTHQACPKAPVRPWQLLHFMNTLPFQVNGQSFRFDQSHGTNTGYQLMFWSWKNSTLTYLPVGDYEESLYINKSQI
Hummingbird     VLSTPCEQCDYATLPQILPTLNHLKIIPVYLAVYSVANALHRALGCTHQACPKAPLKSWQLLHFMNTFPFTVNGQSFRFDKFHGTNPGYQLIFWLWRNGTLEYLPVGEYKESLAINVSQI
                490       500       510       520       530       540       550       560       570       580       590       600
Chicken         QFHTTDQKEPTSECFRCEPGQIRQIKGFHLCCYDCTDCPENTFCSSKDSSTCTPCLEHQWSPARSTQCYDRSERYLRWNEPLTAGLLISMSIIISLICLTAVLFVKNLNTPLVQAAGGN
Swift           QFHTADQKEPTSECFRDCSPGQFRQIKGFHLCCYDCTDCPENTFWSSKDSSSCSPCPQQHWAPARSTRCHLRSDRFLFWSEPLSIALLTLMSITLSLTCLTALLFFKSLETPLVQASGGK
Hummingbird     QFHTPNQERPSSQCFAQCLPGQIRQIKGLHMCCYDCRDCPENTFSSAKDQSRCTSCQKQQWAPTSSIQCYDRSERYLFWNEPLTIALLLGMSLTLSLTCATALIFLKNLETPLVQASGGK
                610       620       630       640       650       660       670       680       690       700       710       720
Chicken         LNLFALFALTLMCLSSCLFIGKPTNNLCMMQQIVCALCLNACFSTFFIKSLEIVLLTEFPRCARTALRWVTPSRSWLLVALCLLTECLFCFCYLHLGPDYVLPDYSSLPTEVLLMCSTAS
Swift           LSLFALFALVLLCLSCCLYIGKPSHHLCMTQQMVHALCLNGCFSTFFIKSLEITLVTEFPRCAPTFLPWLTQRRAWLLVALCLLTQALLCLCYLHVGPDYLLSDYKSLPTEVLLVCDTRS
Hummingbird     LNLFGLFMLTLQSLSCCLYVGKPSDNLCTIQQIVYALCLNGSFSTFFIKSLEIILVTEFPRCAPTFLPWLTQRRAWLLVALCLLIQSFLSFCYVQLGPDYLQADYESLRSEVLLVCDTKS
                730       740       750       760       770       780       790       800       810       820       830       836
Chicken         WPAFALMHGYNGCLAFVCFLCTFMVQSSGKKYNMARGITFTILIYFIIWIFFITVFATLRTVLMSVIQISTILMVSLGIVGTYYIPKCYILLLKPDLNREDYFQYSTKEEPEGD
Swift           WFAFTLLHGYNSCLAFVSFLGTFMVQTSSRKYNIARGITFAILIYFIIWIFFIAIFVTLKTVLRSVTQIGTILTTTLGIIGTYYIPKCYILLLKPDLNTVDYFQNSIKEEPGEDSQ
Hummingbird     WFAFTLLQGYNCCLAFVCFLCTFMVQTSGKQYNIARGITFAILTYFIIWIFFVAIFTTLKTVLRPATQMGTILATSLGIIGTYYIPKCYLILLKPELNKVDYFQHSIKEEPDEDSQ
```

Fig. 1. Analysis of T1R sequences in birds. (**A**) A maximum-likelihood tree was constructed using *T1R* sequences from 13 birds and the Chinese alligator (∇ = nodal bootstrap <80%; scale bar, 0.4 substitutions per site). (**B**) Amino acid sequences of T1R3 cloned from birds. Gray, transmembrane domains; red, putatively selected sites (table S3).

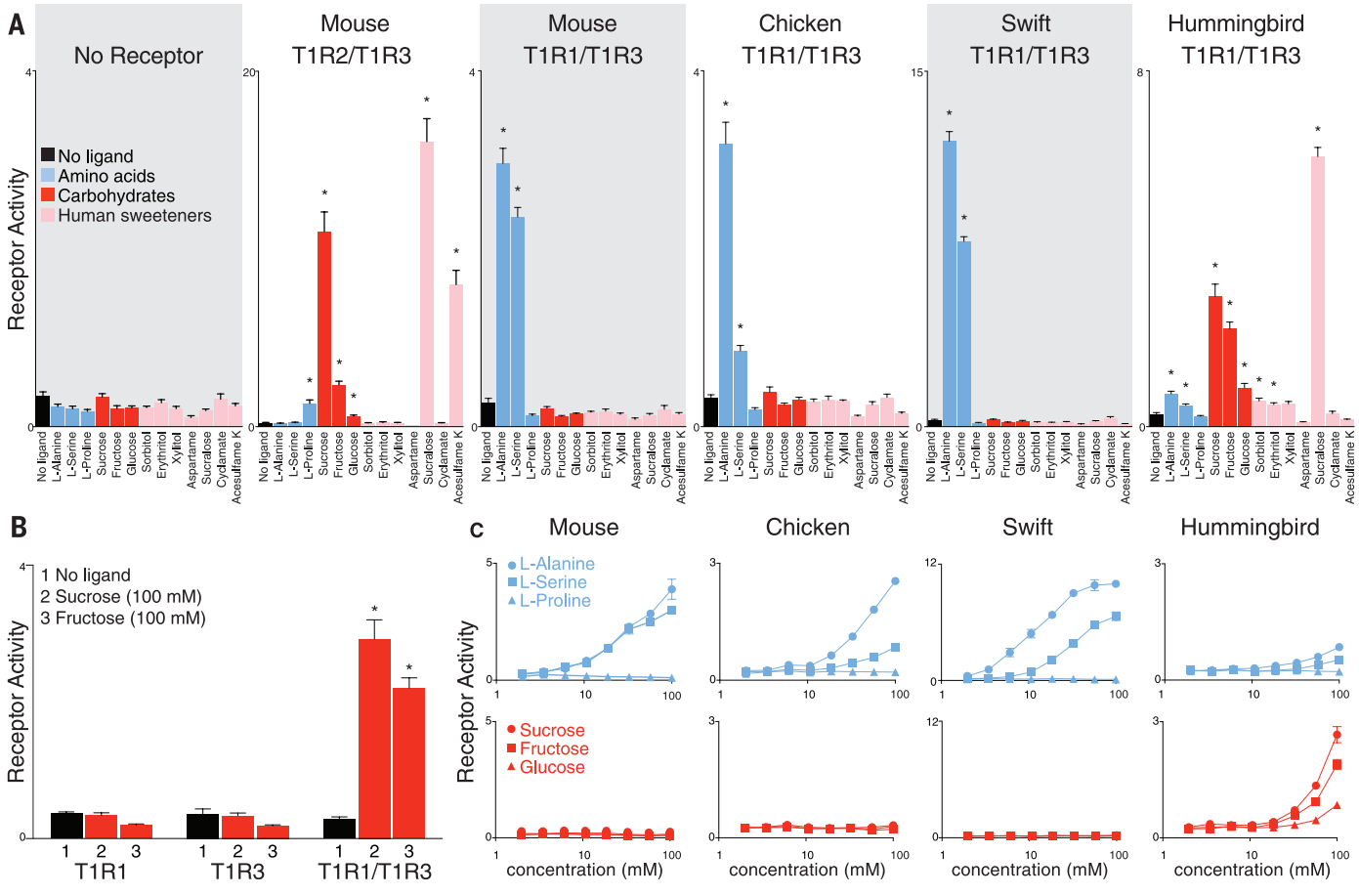

Fig. 2. Evolution of a sugar receptor in hummingbirds. (**A**) Functional expression of avian and rodent taste receptors to stimuli [100 mM, except aspartame (15 mM); n = 6 independent experiments, mean ± SE, *$P \leq 0.05$]. (**B**) Sugar responses of hummingbird T1Rs alone or in combination (n = 6 independent experiments, mean ± SE, *$P \leq 0.05$). (**C**) Dose-dependent responses of T1R1-T1R3 from species indicated to amino acids (blue) and sugars (red).

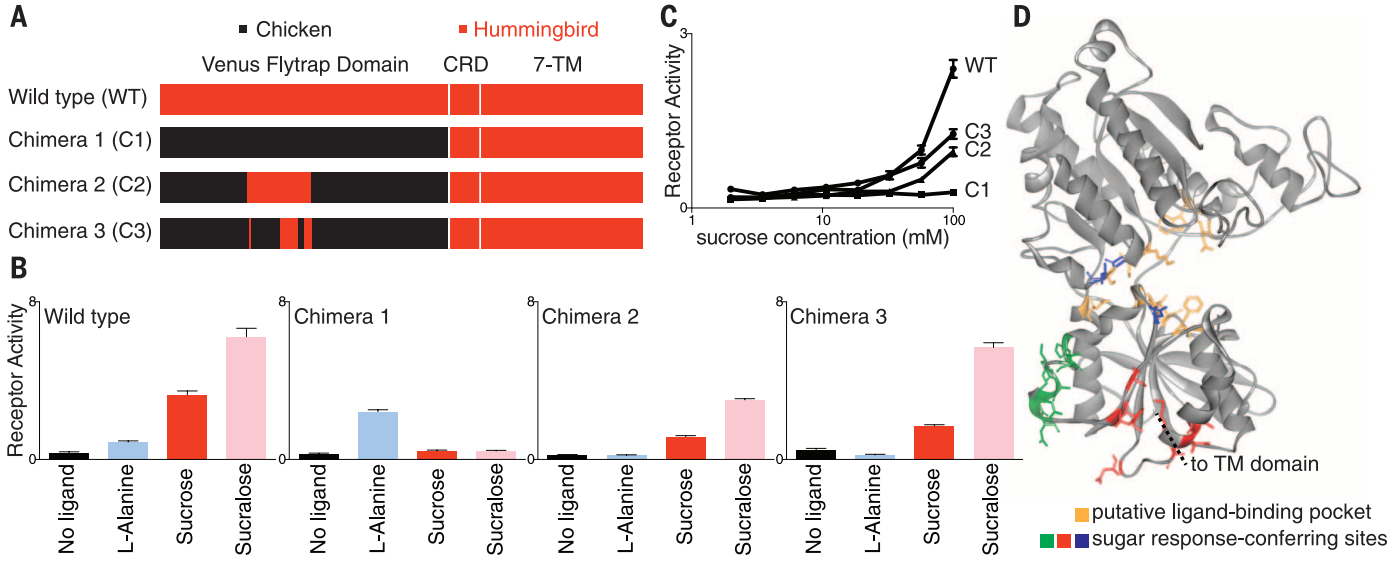

Fig. 3. Molecular basis for the acquisition of sugar binding in hummingbird T1R1-T1R3. (**A**) T1R3 chimeras containing chicken (black) and hummingbird (red) amino acids were designed (CRD, cysteine-rich domain; TM, transmembrane domains). (**B**) Responses of T1R3 chimeras and hummingbird T1R1 to L-alanine, sucralose, and sucrose (100 mM). (**C**) Dose-dependent responses of T1R3 chimeras and hummingbird T1R1 to sucrose. (**D**) A homology model of the venus flytrap domain of T1R3 shows the putative ligand binding site (yellow), predicted by alignment with ligand-contacting sites of rat mGluR1 (*20*), and mutations that confer sugar binding, which cluster in three distinct locations (red, green, and blue).

are unknown but may be important for folding topology, interdomain or intersubunit interactions, or G protein activation. The dramatic redecoration of the T1R1-T1R3 protein surface that occurred in hummingbirds to allow for sugar binding makes sense, given that carbohydrates and amino acids adopt completely different structures.

We next asked whether T1R1-T1R3 function would dictate hummingbird taste behavior. We reasoned that nonnutritive agonists of T1R1-T1R3 without caloric value would be palatable to hummingbirds, like artificial sweeteners are to humans. Hummingbirds prefer sugars (*22*), but behavioral responses to many other human sweeteners are unknown. We developed a brief-access, two-choice gustatory preference paradigm in captive ruby-throated hummingbirds (*Archilochus colubris*) to measure taste responses to T1R1-T1R3 ligands (Fig. 4A). As expected, hummingbirds displayed strong behavioral affinity for sucrose over water, as measured by an increase in mean drinking bout length, number of long bouts (>1 s of uninterrupted drinking), and overall time spent drinking. High-speed video recordings (movie S1) indicated extremely rapid choice decisions; water trials terminated within three or four tongue licks (~250 ms), suggesting that sugar preference involves rapid processing of taste information rather than post-ingestive effects. Ruby-throated hummingbirds equally consumed solutions of sucrose and erythritol, a nonnutritive agonist of hummingbird T1R1-T1R3, but displayed a strong preference for sucrose over aspartame, a sweetener to humans that failed to activate hummingbird T1R1-T1R3.

We also developed a behavioral assay involving Anna's hummingbirds because we cloned T1R1 and T1R3 from this species (Fig. 4B and movie

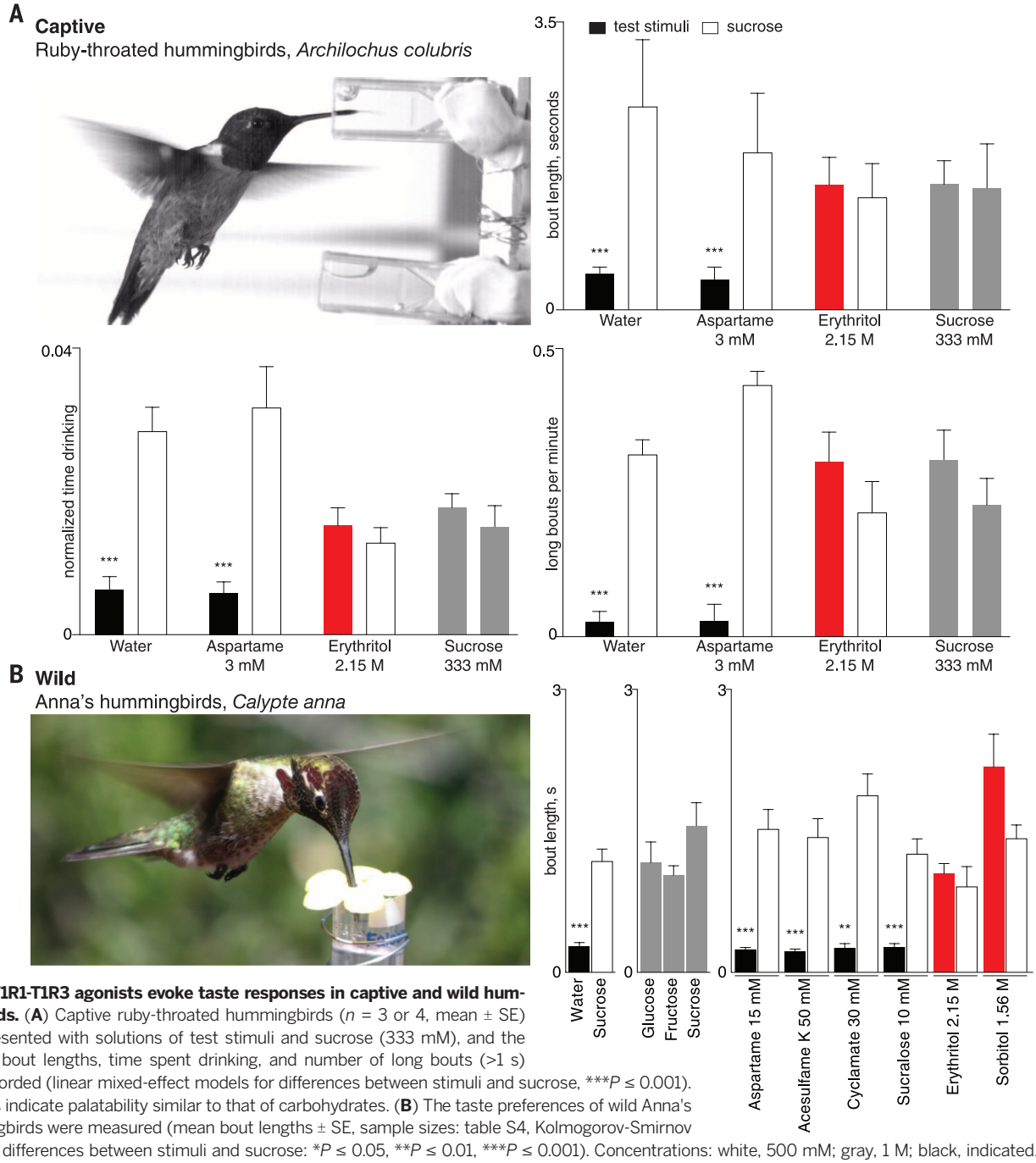

Fig. 4. T1R1-T1R3 agonists evoke taste responses in captive and wild hummingbirds. (**A**) Captive ruby-throated hummingbirds (n = 3 or 4, mean ± SE) were presented with solutions of test stimuli and sucrose (333 mM), and the drinking bout lengths, time spent drinking, and number of long bouts (>1 s) were recorded (linear mixed-effect models for differences between stimuli and sucrose, $^{***}P \leq 0.001$). Red bars indicate palatability similar to that of carbohydrates. (**B**) The taste preferences of wild Anna's hummingbirds were measured (mean bout lengths ± SE, sample sizes: table S4, Kolmogorov-Smirnov tests for differences between stimuli and sucrose: $^{*}P \leq 0.05$, $^{**}P \leq 0.01$, $^{***}P \leq 0.001$). Concentrations: white, 500 mM; gray, 1 M; black, indicated. Red bars indicate equal preference. [Photo credits: (A) M.W.B. and F. Peaudecerf, (B) M.W.B.]

S2). Experiments were performed in the Santa Monica Mountains at a field site frequented by wild hummingbirds. We recorded the behavior of birds presented for 15 min with test stimuli, and in control experiments, hummingbirds displayed strong preference for sucrose over water and high behavioral affinity for several sugars abundant in nectar, including sucrose, glucose, and fructose. Next, we presented solutions of sucrose and test stimuli, and measured the mean drinking bout length. Anna's hummingbirds displayed a strong behavioral attraction to the T1R1-T1R3 agonists erythritol and sorbitol, with responses similar to those to sucrose. In contrast, Anna's hummingbirds displayed a strong preference for sucrose over other structurally diverse human sweeteners that failed to activate hummingbird T1R1-T1R3, including aspartame, cyclamate, and acesulfame K. Furthermore, these synthetic human sweeteners were aversive at high concentrations, because birds rejected mixed solutions containing these chemicals and sucrose (fig. S6 and movie S2) and often displayed a characteristic behavioral pattern involving beak withdrawal, head shaking, and/or spitting that was previously observed in response to the ingestion of bitter plant metabolites (*23*). This reaction was also observed toward sucralose solutions, and mixtures of sucrose and sucralose were not consumed (fig. S6), indicating that sucralose is also actively rejected. Other species of hummingbirds (black-chinned and Allen's hummingbirds) visited and displayed similar taste preferences (fig. S6). Together, these behavioral experiments show that several agonists of hummingbird T1R1-T1R3, including simple sugars and sugar alcohols, evoke fast, appetitive gustatory responses in hummingbirds. Other synthetic human sweeteners that do not activate hummingbird T1R1-T1R3 are not similarly attractive and are often actively rejected. We conclude that the molecular recognition properties of hummingbird T1R1-T1R3, together with those of other gustatory receptors, instruct taste behavior in both captive and wild hummingbirds.

We studied the repertoire and function of taste receptors to provide a molecular basis for variations in animal ecology and the evolutionary events that cause them. We identified a transformation of taste receptor function that occurred in hummingbirds after their divergence from an insectivorous ancestor. We propose this to be a key evolutionary adaptation that contributed to the acquisition of nectar-feeding behavior and enabled the extensive radiation of hummingbird species. The molecular basis for this change in taste behavior is an altered ligand-binding preference of T1R1-T1R3 from amino acids to carbohydrates, a complex feat that involved dramatic structural changes in the receptor surface. It has been proposed that the ancestral T1R heterodimer, as well as the ancestral family C GPCR, were amino acid receptors (*17*, *24*). The mammalian sweet receptor probably derived from a similar transformation that occurred earlier in vertebrates. Birds descended from carnivorous theropod dinosaurs (*25*), and like mammalian carnivores, it appears that an ancestor of birds lost T1R2, perhaps another example of the close relationship between diet and taste receptor repertoire. Based on evidence presented here, hummingbirds recently evolved a new sugar receptor and consequently regained sweet taste perception.

REFERENCES AND NOTES

1. P. Jiang *et al.*, *Proc. Natl. Acad. Sci. U.S.A.* **109**, 4956–4961 (2012).
2. H. Zhao, J. R. Yang, H. Xu, J. Zhang, *Mol. Biol. Evol.* **27**, 2669–2673 (2010).
3. E. O. Gracheva *et al.*, *Nature* **464**, 1006–1011 (2010).
4. M. Nei, Y. Niimura, M. Nozawa, *Nat. Rev. Genet.* **9**, 951–963 (2008).
5. S. D. Liberles *et al.*, *Proc. Natl. Acad. Sci. U.S.A.* **106**, 9842–9847 (2009).
6. D. M. Ferrero *et al.*, *ACS Chem. Biol.* **7**, 1184–1189 (2012).
7. P. Shi, J. Zhang, *Mol. Biol. Evol.* **23**, 292–300 (2006).
8. D. A. Yarmolinsky, C. S. Zuker, N. J. Ryba, *Cell* **139**, 234–244 (2009).
9. G. Q. Zhao *et al.*, *Cell* **115**, 255–266 (2003).
10. G. Nelson *et al.*, *Cell* **106**, 381–390 (2001).
11. S. Damak *et al.*, *Science* **301**, 850–853 (2003).
12. Y. Ishimaru *et al.*, *Mech. Dev.* **122**, 1310–1321 (2005).
13. P. Feng, H. Zhao, *Chin. Sci. Bull.* **58**, 2198–2204 (2013).
14. J. A. McGuire *et al.*, *Curr. Biol.* **24**, 910–916 (2014).
15. Y. Toda, S. Okada, T. Misaka, *J. Agric. Food Chem.* **59**, 12131–12138 (2011).
16. D. Glaser, *Pure Appl. Chem.* **74**, 1153–1158 (2002).
17. H. Oike *et al.*, *J. Neurosci.* **27**, 5584–5592 (2007).
18. Y. Toda *et al.*, *J. Biol. Chem.* **288**, 36863–36877 (2013).
19. J. W. Brown, D. P. Mindell, in *The Timetree of Life*, S. Hedges, S. Kumar, Eds. (Oxford Univ. Press, Oxford, 2009), pp. 454–456.
20. N. Kunishima *et al.*, *Nature* **407**, 971–977 (2000).
21. F. Zhang *et al.*, *Proc. Natl. Acad. Sci. U.S.A.* **105**, 20930–20934 (2008).
22. N. Medina-Tapia, J. Ayala-Berdon, L. Morales-Pérez, L. M. Melo, J. E. Schondube, *Comp. Biochem. Physiol. A Mol. Integr. Physiol.* **161**, 307–314 (2012).
23. D. Kessler, I. T. Baldwin, *Plant J.* **49**, 840–854 (2007).
24. D. Kuang *et al.*, *Proc. Natl. Acad. Sci. U.S.A.* **103**, 14050–14055 (2006).
25. G. Dyke, G. Kaiser, *Living Dinosaurs: The Evolutionary History of Modern Birds* (Wiley-Blackwell, Chichester, UK, 2011).

ACKNOWLEDGMENTS

We thank those who supported these experiments (see the supplementary materials for the full list). Grants to M.W.B. (NSF grant DDIG 1110487, Society for Integrative and Comparative Biology, and Sigma Xi); M.J.O'C. (Fulbright Commission and Science Foundation Ireland Research Frontiers Program, grant EOB2673); S.D.L. (NIH, grant R01DC013289); S.V.E. (NSF); and T.M. (Japan Society for the Promotion of Science, grant LS037) are acknowledged. T1R sequences and alignments are available at GenBank and Dryad.

SUPPLEMENTARY MATERIALS

www.sciencemag.org/content/345/6199/929/suppl/DC1
Materials and Methods
Supplementary Text
Figs. S1 to S6
Tables S1 to S4
References (*26*–*44*)
Movies S1 and S2

22 April 2014; accepted 1 July 2014
10.1126/science.1255097

PLANT DEVELOPMENT

Arabidopsis NAC45/86 direct sieve element morphogenesis culminating in enucleation

Kaori Miyashima Furuta,[1]*† Shri Ram Yadav,[1]*‡ Satu Lehesranta,[1]* Ilya Belevich,[1] Shunsuke Miyashima,[1]† Jung-ok Heo,[1] Anne Vatén,[1]§ Ove Lindgren,[1] Bert De Rybel,[2,3]‖ Gert Van Isterdael,[2,3] Panu Somervuo,[1] Raffael Lichtenberger,[1] Raquel Rocha,[1] Siripong Thitamadee,[1]¶ Sari Tähtiharju,[1] Petri Auvinen,[1] Tom Beeckman,[2,3] Eija Jokitalo,[1]# Ykä Helariutta[1,4,5]#

Photoassimilates such as sugars are transported through phloem sieve element cells in plants. Adapted for effective transport, sieve elements develop as enucleated living cells. We used electron microscope imaging and three-dimensional reconstruction to follow sieve element morphogenesis in *Arabidopsis*. We show that sieve element differentiation involves enucleation, in which the nuclear contents are released and degraded in the cytoplasm at the same time as other organelles are rearranged and the cytosol is degraded. These cellular reorganizations are orchestrated by the genetically redundant NAC domain–containing transcription factors, NAC45 and NAC86 (NAC45/86). Among the NAC45/86 targets, we identified a family of genes required for enucleation that encode proteins with nuclease domains. Thus, sieve elements differentiate through a specialized autolysis mechanism.

Long-distant transport sustains life in multicellular organisms. In plants, phloem sieve element cells form a transport network specialized for long-distance allocation of photoassimilates and signaling molecules (*1*). Unlike in the animal circulatory system, contents are transported through cells rather than between cells. Differentiation of sieve elements elaborates specialized structures (such as sieve plates with pores) and eliminates others (vacuoles,

Golgi stacks, the nucleus, and some other organelles) (*2*). At the same time, the cytosol becomes degraded (*3*–*6*). Nuclear elimination in animal erythrocytes and lens fiber cells, and in some unicellular eukaryotes, occurs by extrusion from the cell body (*7*), programmed cell death–like process (*8*), or nucleophagy (*9*). Here, we analyze the mechanisms by which the nucleus is removed from developing sieve element cells in the plant *Arabidopsis*.

The two files of protophloem sieve elements in the *Arabidopsis* root display a longitudinal time series through development, from apparently undifferentiated cells to mature enucleated cells (*10*–*12*) (Fig. 1, E and F). We reconstructed a three-dimensional (3D) representation from a series of ultrathin (40-nm) sections (n = 3) generated through serial block-face scanning electron microscopy (SEM) (*13*) (Fig. 1A, fig. S1, and movie S1) in parallel with live cell imaging (see supplementary materials and methods). We identified three stages of development: (i) stage one, in which the nuclear structure is modified, cell wall thickening occurs, and typical sieve element structures are formed; (ii) stage two, in which the nucleus and other organelles become distorted; and (iii) stage three, during which enucleation is completed and cytosol density decreases (Fig. 1, A and C, and figs. S2 to S4). During stage one, the nucleus deforms from a smooth sphere to crimpled, irregular, and nucleolus fragments (Fig. 1, A and C, and fig. S3), as previously noted (*6*, *14*, *15*). At the end of stage two, the nucleus shrinks, together with the signal of NUCLEAR PORE PROTEIN 1 marker (NUP1-YFP, where YFP is yellow fluorescent protein) (table S1, fig. S5, and movie S2). The spread of the NUP1 signal suggests disorganization of the nuclear envelope (fig. S5). Histone 2B (H2B)–YFP, typically confined to the nucleus, also spreads throughout the cytoplasm and becomes diluted in ~10 min (Fig. 1G and movie S3). During stage three, remnants of the disorganized nuclear envelope persist (Fig. 1C and fig. S3). Consistent with this, NUP1-YFP was retained after enucleation (fig. S5). While the nucleus is disintegrating, many organelles, including mitochondria and vacuoles, form two perinuclear clusters at opposite sides of the nucleus (Fig. 1A and fig. S4), and the mitochondria gradually change their shape (figs. S2 and S4). The dilution of the H2B-YFP signal coincides with the completion of cytosol degradation, as shown by the abrupt disappearance of electron-dense matter (Fig. 1A), and the disappearance of a cytoplasm-localized protein At3g14780-YFP (fig. S5); this suggests a type of enucleation wherein the nuclear contents are released and subsequently degraded in the cytosol, leaving behind a disorganized nuclear envelope. This differs from previously described enucleation processes in various organisms (*7*–*9*). Sieve elements lack the large central vacuole characteristic of programmed cell death (fig. S5); the lytic vacuoles are rather small and persist through cytoplasmic reorganization (figs. S2 and S5) (*16*). There is also no evidence for autophagy, based on the ATG8a marker, a homolog of which surrounds the degrading nucleus in *Tetrahymena* (*17*) (fig. S5).

To unravel the molecular mechanisms regulating cellular remodeling of sieve elements, we analyzed gene expression downstream of a key transcription factor [ALTERED PHLOEM DEVELOPMENT (APL)] (*11*) that controls phloem development in sorted phloem cells and identified a pair of NAC-type transcription factors [*NAC045* (*NAC45*) and *NAC086* (*NAC86*)] (Fig. 2I, fig. S6, and table S2). We observed specific expression of these two genes in a few sieve element cells before enucleation, as well as in phloem-pole

[1]Institute of Biotechnology, Department of Biological and Environmental Sciences, University of Helsinki, FIN-00014, Finland. [2]Department of Plant Biotechnology and Bioinformatics, Ghent University, Technologiepark 927, B-9052 Gent, Belgium. [3]Department of Plant System Biology, VIB, Technologiepark 927, B-9052 Gent, Belgium. [4]Cardiff University Cardiff School of Biosciences, The Sir Martin Evans Building, Museum Avenue, Cardiff, CF10 3AX, UK. [5]The Sainsbury Laboratory, University of Cambridge, Bateman Street, Cambridge CB2 1LR, UK.
*These authors contributed equally to this work. †Present address: Graduate School of Biological Sciences, Nara Institute of Science and Technology, Takayama 8916-5, Ikoma, Nara 630-0192, Japan. ‡Present address: Department of Biotechnology, Indian Institute of Technology, Roorkee-247667, India. §Present address: Department of Biology, Stanford University, Stanford, CA 94305–5020, USA. ||Present address: Laboratory of Biochemistry, Wageningen University, Dreijenlaan 3, 6703HA Wageningen, Netherlands. ¶Present address: Department of Biotechnology, Faculty of Science, Mahidol University Rama VI Road, Bangkok 10400, Thailand. **#Corresponding author. E-mail: yrjo.helariutta@slcu.cam.ac.uk (Y.H.); eija.jokitalo@helsinki.fi (E.J.)**

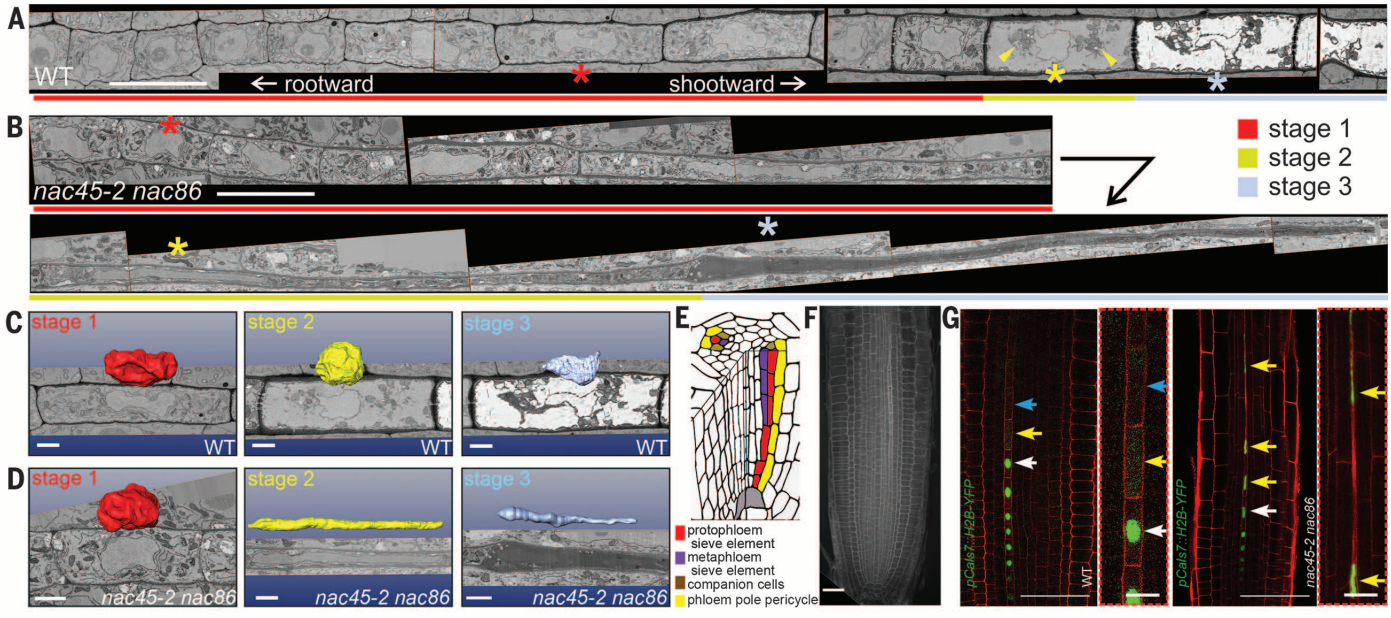

Fig. 1. Dynamic enucleation and other subcellular rearrangements during sieve element differentiation. (**A** and **B**) Overview of sieve element differentiation in the wild type (A) and *nac45-2 nac86* (B). Asterisks and color coded lines indicate various stages (stages one to three). (**C** and **D**) 3D models of nuclei in the wild type (C) and *nac45-2 nac86* (D) during various stages of sieve element differentiation. (**E**) Pattern of *Arabidopsis* primary root vasculature, establishing the two phloem poles with protophloem sieve elements located between two companion cells and two phloem pole pericycles. Metaphloem sieve elements develop later. (**F**) Modified pseudo-Schiff–propidium iodide (mPS-PI) staining (*19*) shows sieve element cell files by their thickened cell walls. (**G**) *pCALS7::H2B-YFP* demonstrates sieve element enucleation with diffusion (yellow arrows) and dilution (blue arrows) in the wild type, but nuclear retention in *nac45-2 nac86* (yellow arrows). White arrows indicate the nuclei before nuclear degradation. Panels surrounded by dashed red boxes show magnified views of the panels at left. Scale bars represent 10 μm in (A) and (B), 2 μm in (C) and (D), 25 μm in (F), 50 μm in (G, main panels), and 10 μm in (G, dashed boxes).

pericycle cells (Fig. 2, A to F). This expression pattern overlaps with that of *APL* (*11*) (fig. S6), and expression was reduced in *apl* (Fig. 2, G and H, and fig. S6), indicating dependence of these genes on *APL*. *NAC45* expression was up-regulated in DEX-treated p*APL*::*APL-GR/apl* plants in the presence of the protein synthesis inhibitor cycloheximide, suggesting that *NAC45* may be a direct transcriptional target of APL (fig. S6).

Next, we characterized loss-of-function mutants of *NAC45* and *NAC86* (*NAC45/86*). The

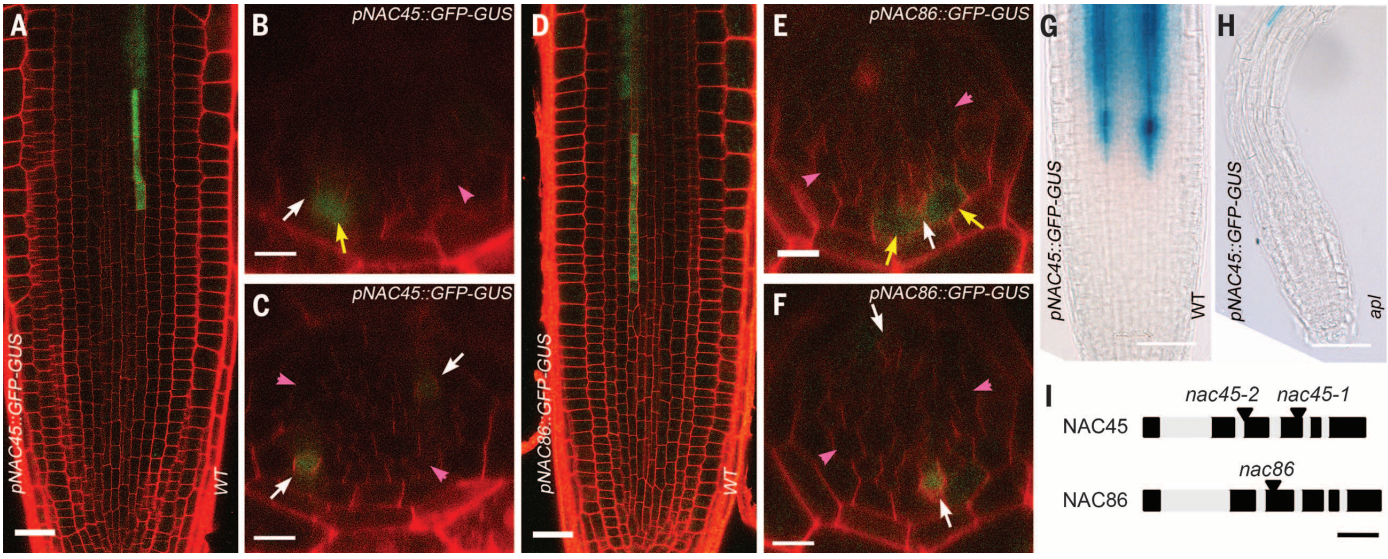

Fig. 2. Molecular characterization of NAC45/86. (**A** to **F**) The expression of *pNAC45::GFP-GUS* and *pNAC86::GFP-GUS* is first detected in the developing protophloem sieve elements (white arrows) and at later stages in the phloem pole pericycles (yellow arrows) in the root. Pink arrowheads indicate the xylem axis. (**G** and **H**) Expression of *pNAC45::GFP-GUS* in the wild type (G) and the *apl* mutant (H). (**I**) Schematic of gene organization of *NAC45* and *NAC86*. Transferred DNA insertion sites are marked with black arrowheads. Scale bars represent 25 μm in (A) and (D); 20 μm in (B), (C), (E), and (F); 50 μm in (G) and (H); and 100 base pairs in (I).

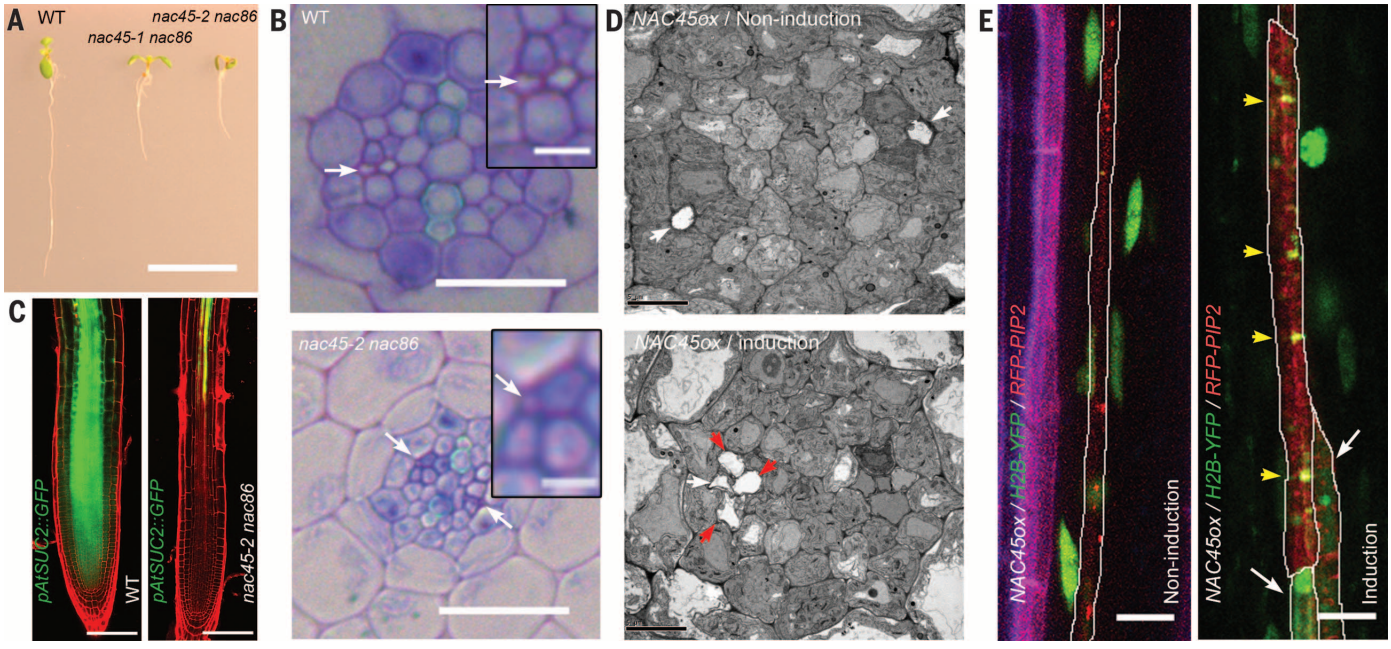

Fig. 3. NAC45 is necessary and sufficient for sieve element nuclear and cytosol degradation. (**A**) WT, *nac45-1 nac86*, and *nac45-2 nac86* seedlings, showing root-growth phenotypes. (**B**) Toluidine blue–stained root cross sections of the wild type and *nac45-2 nac86*. Protophloem sieve elements are indicated by white arrows and are magnified in inset boxes. (**C**) *AtSUC2::GFP* in the wild type and *nac45-2 nac86* shows defective transport of free GFP in the mutants. (**D**) Transmission electron microscopy imaging of the p*G1090*-XVE::*NAC45* line with or without induction. White arrows highlight protophloem sieve cells; red arrows mark ectopic white cells at the phloem pole. (**E**) Plants harboring p*G1090*-XVE::*NAC45*, p*At5g48060*::*H2B-YFP*, and *At5g48060*::*RFP-PIP2* with or without induction. Red cells with dotted or diffused H2B-YFP signals are occasionally seen in ectopic positions after induction. Red cells without YFP signals are shown in normal sieve element position with and without induction. The magenta signal in the left panel indicates PI staining. Scale bars represent 1 cm in (A), 20 μm in (B, main panels), 5 μm (top) and 2.5 μm (bottom) in (B, insets), 100 μm in (C), 5 μm in (D), and 10 μm in (E).

single mutants appeared normal (fig. S7), but the *nac45-1 nac86* double mutant exhibited delayed growth (Fig. 3A), and the *nac45-2 nac86* double mutant displayed determinate growth and seedling lethality, like *apl* (Fig. 3A). The *nac45-2 nac86* phenotype was rescued by expressing YFP-fused NAC86, specifically in the sieve element (fig. S7), suggesting that NAC86 functions cell-autonomously. Histological analysis revealed no mature protophloem sieve elements in either of the double mutants, whereas differentiation of other tissues appeared normal (Fig. 3B and fig. S7). Defective sieve element formation in *nac45-2 nac86* impairs phloem transport, as demonstrated by the loss of phloem-mediated transport of free green fluorescent protein (GFP) from the companion cells into the root tip region of p*AtSUC2*::*GFP* (*18*) (Fig. 3C). p*AtSUC2*::*GFP* is expressed in the companion cells of *nac45-2nac86*, indicating normal companion cell development. Imaging of sieve element differentiation in *nac45-2 nac86* by serial block-face SEM revealed that the cells in the sieve element position exhibit normal cell wall architecture, including a sieve plate with developed sieve pores (Fig. 1B and fig S2). Some organelle morphogenesis, such as gradual mitochondrial shape changes (figs. S2 and S4) and sieve element plastid development (fig. S2), also seem to occur properly; however, the perinuclear organelle clusters were not formed in *nac45-2 nac86* (fig. S4). Neither enucleation nor a decrease of cytosol density were completed in *nac45-2 nac86* (Fig. 1, B and D). Consistent with this, both H2B-YFP and the cytoplasmic At3g14780-YFP protein were retained in fully elongated sieve element cells in *nac45 nac86* mutants (Fig. 1G and figs. S3 and S5). By contrast, NAC45/86 are not required for formation of lytic vacuoles or the expression and localization of ATG8a in sieve elements (fig. S2 and S5).

We overexpressed NAC45 in transgenic plants under an estradiol-inducible promoter (*pG1090-XVE::NAC45*). After 4 days of induction, the cells neighboring sieve elements in *pG1090-XVE::NAC45* took on characteristics of differentiated sieve elements (Fig. 3D and fig. S7), indicating that ectopically expressed NAC45 is sufficient to promote cytosol degradation at the phloem pole. To examine the function of NAC45 in enucleation, two additional nuclear- and plasma-membrane markers (H2B-YFP and RFP-PIP2, respectively, where RFP, is red fluorescent protein) were introduced into p*G1090-XVE*::*NAC45* under the NAC45-inducible *At5g48060* promoter. After NAC45 induction, we observed that RFP-positive cells in ectopic positions occasionally exhibited several small dots of diffused YFP signals in their cytoplasm, rather than the large round signal typically observed in nuclear-localized H2B-YFP, indicating ongoing nuclear degradation (Fig. 3E and fig S7). This suggests that NAC45 is sufficient to promote enucleation in non–sieve element cells at the phloem pole. We conclude that NAC45/86 regulate sieve element differentiation, culminating in enucleation and cytosol degradation.

To understand the downstream targets of NAC45/86, we analyzed RNA expression of wild-type (WT), *nac45-2 nac86*, and NAC45-overexpression roots (fig. S8). We validated six genes as NAC45/86 downstream targets in plants and studied their subcellular localization (fig. S8). In addition, we identified a family of DEDDh exonuclease-like domain-containing proteins and designated them *NAC45/86-DEPENDENT EXONUCLEASE-DOMAIN PROTEIN 1 to 4* (*NEN1 to NEN4*) (Fig. 4C and figs. S10 and S11). The expression of *NEN1* and *NEN2* begins in stage one and increases toward enucleation, whereas *NEN4* is expressed from late stage one or stage two (fig. S9). The expression level of these genes was reduced in *nac45-2nac86*, indicating their dependence on NAC45/86 (fig. S9). We also confirmed that *NEN2* expression is ectopically induced by NAC45 overexpression (fig. S9). The NEN4-YFP fusion protein accumulates in the nuclei of one or a few sieve element cells before enucleation, whereas both NEN1-YFP and NEN2-YFP change subcellular localization from the cytoplasm to the nucleus during enucleation (Fig. 4A). This shift of NEN2 localization does not occur in *nac45 nac86* (fig. S9), suggesting that NEN2 is regulated by NAC45/86 both transcriptionally and posttranslationally.

Next, we examined the role of NEN1 to NEN4 via gene silencing and mutant analysis (fig. S10). The *nen4-1* and *nen4-2* mutants, which exhibited ~28 and ~21% reduction of root length compared with the *Wassilewskija* (*Ws*) wild type (Fig. 4D and fig. S10), retained amorphous H2B-YFP signals (Fig. 4B and fig. S10). Serial block-face SEM revealed that sieve element differentiation events, including cytoplasmic degradation, nuclear envelope disorganization, and organelle clustering,

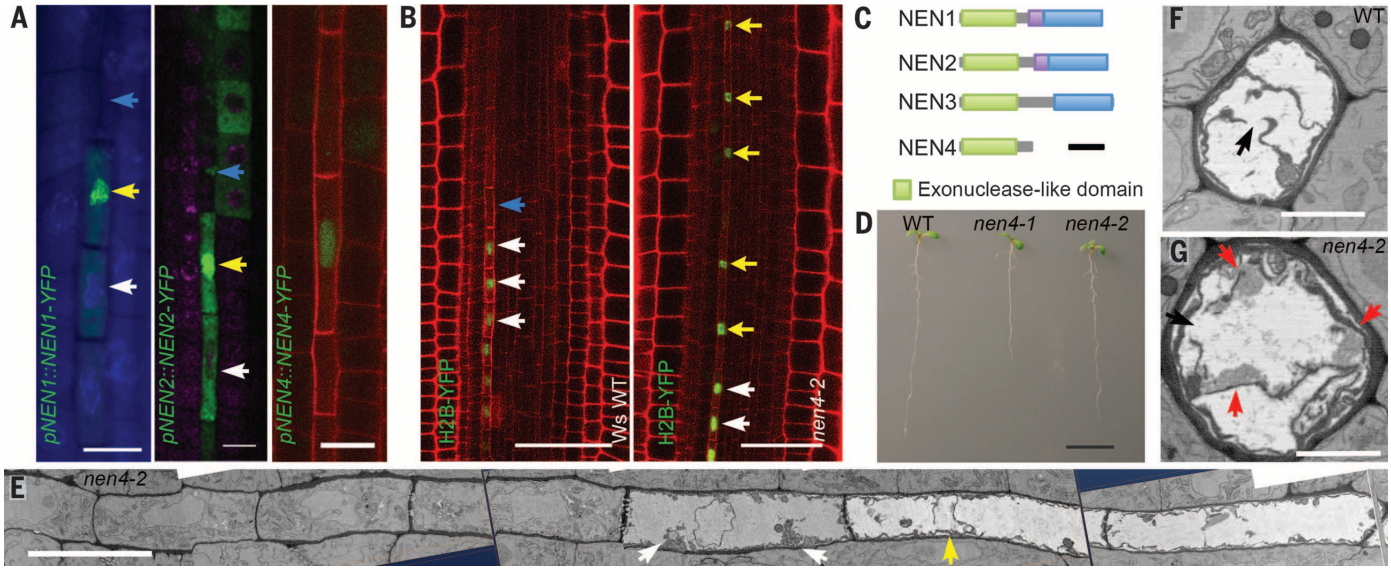

Fig. 4. NEN4 is a downstream effector of *NAC45/86*-dependent enucleation. (**A**) Subcellular localization of NEN1-YFP and NEN2-YFP are shifted from the cytoplasm (white arrows) to the nucleus (yellow arrows; blue and magenta signal indicate staining with 4′,6-diamidino-2-phenylindole); the signal then disappears (blue arrows). Nuclear-localized NEN4-YFP is transiently expressed before sieve element enucleation. (**B**) The *pCALS7*::*H2B-YFP* signal is degraded in the *Ws* wild type (blue arrow) but is retained in *nen4-2* (yellow arrows). White arrows indicate the nuclei before nuclear degradation. (**C**) Protein domains of the NEN family. (**D**) *Ws* WT, *nen4-1*, and *nen4-2* seedlings. (**E**) Overview of sieve element differentiation of *nen4-2* by serial block-face SEM. Perinuclear clustering (white arrows) and cytosol degradation occur normally. A yellow arrow highlights the retained nucleus. (**F** and **G**) Serial block-face scanning electron microscope image of *Ws* wild type (F) and *nen4-2* (G). The *nen4-2* protophloem sieve elements show agglomerated nuclear contents associated with the nuclear envelope (red arrows). Black arrows indicate nuclear envelope disorganization. Scale bars represent 10 μm in (A), 50 μm in (B), 1 cm in (D), 10 μm in (E), and 2 μm in (F) and (G).

occurred normally in *nen4-1* (n = 4 sieve element files) and *nen4-2* (n = 2) (Fig. 4E and figs. S1 and S10). However, agglomerated structures abutting on the inner side of the nuclear envelope were observed after stage three (Fig. 4G and fig. S10), which was not observed in either *Ws* (n = 2) (Fig. 4F) or the *Columbia* (*Col*) wild type (n = 3) (Fig. 1A and fig. S3). The amorphous H2B-YFP remnants were located in the peripheral region of the nucleus in *nen4-1* and *nen4-2* (Fig. 4G and fig. S10). Furthermore, the defective enucleation in *nen4-1* was transgenically complemented (fig. S10). Taken together, this indicates that NEN4 is required for completing the NAC45/86-regulated enucleation process.

We have outlined the process by which sieve element cells in *Arabidopsis* differentiate and divest themselves of a nucleus. NAC45/86 orchestrate the enucleation, perinuclear organelle clustering, shift in NEN1 and NEN2 localization, and cytosol degradation by regulating the expression of a set of target genes, including NEN1, NEN2, and NEN4. The interdependence of these various NAC45/86-mediated subcellular processes remains to be investigated. We also observed a set of NAC45/86 independent processes, such as the formation of cell wall architecture and callose accumulation, the latter of which appears to be dependent on the upstream transcription factor APL. Our results add to the diversity of autolytic processes by which eukaryotic cells restructure their contents.

REFERENCES AND NOTES

1. W. J. Lucas *et al.*, *J. Integr. Plant Biol.* **55**, 294–388 (2013).
2. K. Esau, *Bot. Rev.* **16**, 67–114 (1950).
3. J. Cronshaw, K. Esau, *J. Cell Biol.* **38**, 292–303 (1968).
4. E. P. Eleftheriou, I. Tsekos, *Protoplasma* **113**, 221–233 (1982).
5. R. D. Sjolund, *Plant Cell* **9**, 1137–1146 (1997).
6. H. Wu, X. F. Zheng, *Acta Bot. Sin.* **45**, 322–330 (2003).
7. M. Bessis, M. Bricka, *Rev. Hematol.* **7**, 407–435 (1952).
8. M. A. Wride, *Philos. Trans. R. Soc. London Ser. B* **366**, 1219–1233 (2011).
9. D. Mijaljica, R. J. Devenish, *J. Cell Sci.* **126**, 4325–4330 (2013).
10. J. S. Busse, R. F. Evert, *Int. J. Plant Sci.* **160**, 241–251 (1999).
11. M. Bonke, S. Thitamadee, A. P. Mähönen, M. T. Hauser, Y. Helariutta, *Nature* **426**, 181–186 (2003).
12. A. P. Mähönen *et al.*, *Genes Dev.* **14**, 2938–2943 (2000).
13. W. Denk, H. Horstmann, *PLOS Biol.* **2**, e329 (2004).
14. K. Esau, *Ann. Bot. (London)* **36**, 703–710 (1972).
15. L. Wang *et al.*, *Protoplasma* **234**, 87–96 (2008).
16. W. G. van Doorn *et al.*, *Cell Death Differ.* **18**, 1241–1246 (2011).
17. M. L. Liu, M. C. Yao, *Eukaryot. Cell* **11**, 494–506 (2012).
18. A. Imlau, E. Truernit, N. Sauer, *Plant Cell* **11**, 309–322 (1999).
19. E. Truernit *et al.*, *Plant Cell* **20**, 1494–1503 (2008).

ACKNOWLEDGMENTS

We thank K. Kainulainen, M. Herpola, M. Lindman, A. Salminen, and I. Sevilem for technical assistance; R. Siligato, A. Mähönen, the University of Ghent, the Arabidopsis Biological Resource Center, and the Nottingham Arabidopsis Stock Centre for published materials; A. Mähönen, E.-L. Eskelinen, A. Suomalainen-Wartiovaara, and P. Runeberg-Roos for discussions; and P. Benfey, K. Nakajima, and S. El-Showk for their critical comments. The serial block-face electron microscopy was supported by Biocenter Finland. S.M. was financially supported by the Japanese Society for the Promotion of Science. Work in the lab of T.B. was partly financed by grants of the Research Foundation-Flanders (project FWO – GO20011N) and the Interuniversity Attraction Poles Programme from the Belgian Federal Science Policy Office. Work in the E.J. laboratory is funded by the Academy of Finland, Biocenter Finland, and the University of Helsinki. Financial support for the lab of Y.H. was provided by the Academy of Finland Centre of Excellence programme, the University of Helsinki, the European Research Council Advanced Investigator Grant Symdev, Tekes (the Finnish Funding Agency for Technology and Innovation), and the Gatsby Foundation. The supplementary materials contain additional data.

SUPPLEMENTARY MATERIALS

www.sciencemag.org/content/345/6199/933/suppl/DC1
Materials and Methods
Supplementary Text
Figs. S1 to S11
Tables S1 to S6
References (*20*–*33*)
Movies S1 to S3

21 March 2014; accepted 3 July 2014
Published online 31 July 2014;
10.1126/science.1253736

RIBOSWITCHES

A riboswitch-containing sRNA controls gene expression by sequestration of a response regulator

Sruti DebRoy,[1]* Margo Gebbie,[2]* Arati Ramesh,[3] Jonathan R. Goodson,[2] Melissa R. Cruz,[1] Ambro van Hoof,[1] Wade C. Winkler,[2]† Danielle A. Garsin[1]†

The ethanolamine utilization (*eut*) locus of *Enterococcus faecalis*, containing at least 19 genes distributed over four polycistronic messenger RNAs, appears to be regulated by a single adenosyl cobalamine (AdoCbl)–responsive riboswitch. We report that the AdoCbl-binding riboswitch is part of a small, trans-acting RNA, EutX, which additionally contains a dual-hairpin substrate for the RNA binding–response regulator, EutV. In the absence of AdoCbl, EutX uses this structure to sequester EutV. EutV is known to regulate the *eut* messenger RNAs by binding dual-hairpin structures that overlap terminators and thus prevent transcription termination. In the presence of AdoCbl, EutV cannot bind to EutX and, instead, causes transcriptional read through of multiple *eut* genes. This work introduces riboswitch-mediated control of protein sequestration as a posttranscriptional mechanism to coordinately regulate gene expression.

Riboswitches are an important class of regulatory RNA; they typically regulate expression in cis of downstream open reading frames in response to binding of metabolic ligands, usually by affecting the transcription or translation (*1*–*3*). Small regulatory RNAs (sRNAs) are another class, and they commonly regulate gene expression by interacting with target mRNAs to affect translation or stability (*3*). Herein, we report the discovery of an sRNA, EutX, that contains a riboswitch aptamer and a EutV-binding site named P3/P4 (fig. S1A). The presence of ethanolamine (EA) causes the sensor histidine kinase EutW to phosphorylate the response regulator, EutV, which thereby converts it into an active RNA binding protein (*4*, *5*). Thus, in the absence of EA, EutV is unphosphorylated and inactive. Adenosyl cobalamine (AdoCbl) is a cofactor required in the first enzymatic step of EA catabolism (*6*). Under conditions in which EA is present, but AdoCbl is not, our model states that EutX uses P3/P4 to bind and sequester active EutV~P, which prevents its antitermination activity (fig. S1A). When AdoCbl is also present, it binds to the AdoCbl riboswitch and induces termination before generating the P3/P4 loops, which prevents sequestration. Unhindered, EutV is then able to promote antitermination at the four *eut* polycistronic RNAs to drive gene expression. By this mechanism, the Eut system demands the presence of both the catabolic substrate (EA) and the key cofactor (AdoCbl) (fig. S1A).

To gain a more complete understanding of the effect of AdoCbl and EA on *eut* gene expression, *Enterococcus faecalis* cells were cultured to exponential growth phase in modified minimal medium in the presence or absence of EA and AdoCbl. Total RNA was then extracted and subjected to RNA-sequencing (RNA-seq) analysis (Fig. 1 and table S1). This revealed increased expression across the *eut* locus for cells that had been cultured with EA and AdoCbl compared with those cultured only in minimal medium. Metabolism of EA is believed to occur within a protein-bound organelle called a microcompartment [reviewed by (*7*)]. Electron microscopy revealed microcompartments only for cells cultured in EA and AdoCbl (fig. S1B). These aggregate data demonstrate that *eut* gene

[1]Department of Microbiology and Molecular Genetics, The University of Texas Health Science Center at Houston, TX 77030, USA. [2]Department of Cell Biology and Molecular Genetics, University of Maryland, College Park, MD 20742, USA. [3]Department of Biochemistry, The University of Texas Southwestern Medical Center, Dallas, TX 75390, USA.
*These authors contributed equally to this work. **†Corresponding author. E-mail: danielle.a.garsin@uth.tmc.edu (D.A.G.), Wade C. Winkler wwinkler@umd.edu (W.C.W.)**

expression and microcompartment formation can indeed be induced in the presence of both EA and AdoCbl.

Of the four constitutive promoters in the *eut* locus, three are followed by a EutV RNA binding site (P1/P2, P5/P6, and P7/P8). The distal hairpin in each case overlaps the 5′ sequence of an adjacent, intrinsic terminator. Phosphorylated EutV dimerizes, which increases the affinity for the dual hairpin, which prevents the formation of the terminator structure and thereby induces gene expression (fig. S1A) (*4*, *5*, *8*, *9*). A fourth promoter was detected just upstream of the AdoCbl riboswitch (*8*). Moreover, we discovered that another two-hairpin motif (P3/P4) is located downstream of the AdoCbl riboswitch (fig. S1A). To more closely examine the transcripts in this region, we analyzed total RNA by Northern blotting. An antisense RNA probe that spanned 301 nucleotides (nt) of the *eutT-eutG* intergenic region (Fig. 2A) revealed an RNA species of ~300 nt in length that was not present in medium containing AdoCbl, detectable in minimal medium, and notably enhanced (about fivefold) upon addition of EA without AdoCbl (Fig. 2B). A second RNA of ~150 nt was produced upon addition of AdoCbl. To resolve which parts of the *eutT-eutG* intergenic region corresponded to these different RNA species, the membranes were hybridized with antisense probes corresponding to the left and right halves of the 301-nt antisense probe (Fig. 2A). This analysis revealed that the ~300-nucleotide and ~150-nucleotide RNAs both included the AdoCbl riboswitch. Quantitative reverse transcription polymerase chain reaction (qRT-PCR), using primers within and outside

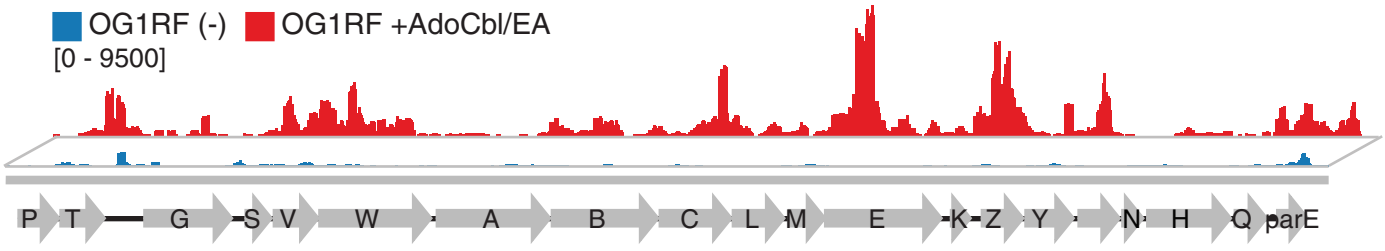

Fig. 1. EA and AdoCbl induce *eut* gene expression. By RNA-seq, all the *eut* genes were expressed in the presence of EA and AdoCbl, whereas little or no expression was observed in minimal medium.

Fig. 2. AdoCbl binding to the riboswitch causes premature termination within a sRNA, preventing generation of the P3/P4 hairpins that bind EutV. (**A**) Location of ^{32}P-radiolabeled RNA antisense probes used to analyze the *eutT-eutG* intergenic region. (**B**) Total RNA was isolated from cells grown in the indicated medium conditions, resolved by denaturing polyacrylamide gel electrophoresis, transferred to a membrane, and hybridized with different antisense probes (1, 2 and 3). (**C**) The mapped 5′ and 3′ termini and the M3 mutation are indicated on a secondary structure depiction of EutX. A putative intrinsic terminator is highlighted by a gray-shaded box. (**D**) In vitro transcription termination assays with wild-type EutX template display a premature termination product only in the presence of AdoCbl. Termination is lost in the M3 mutant template. (**E**) EMSA of binding of EutV to EutX. A 117-nt fragment of EutX (117EutX) and EutVD54E protein [constitutively active for RNA binding (*5*)] were used. Controls included addition of 30 μM of an unlabeled competitor P1/P2 RNA and an unrelated RNA. (**F**) DRaCALA to assess EutV binding to the 117EutX RNA by using the same reaction conditions and control RNAs as in (**E**). (**G**) EMSA to investigate whether EutX could compete for EutV binding to P1/P2.

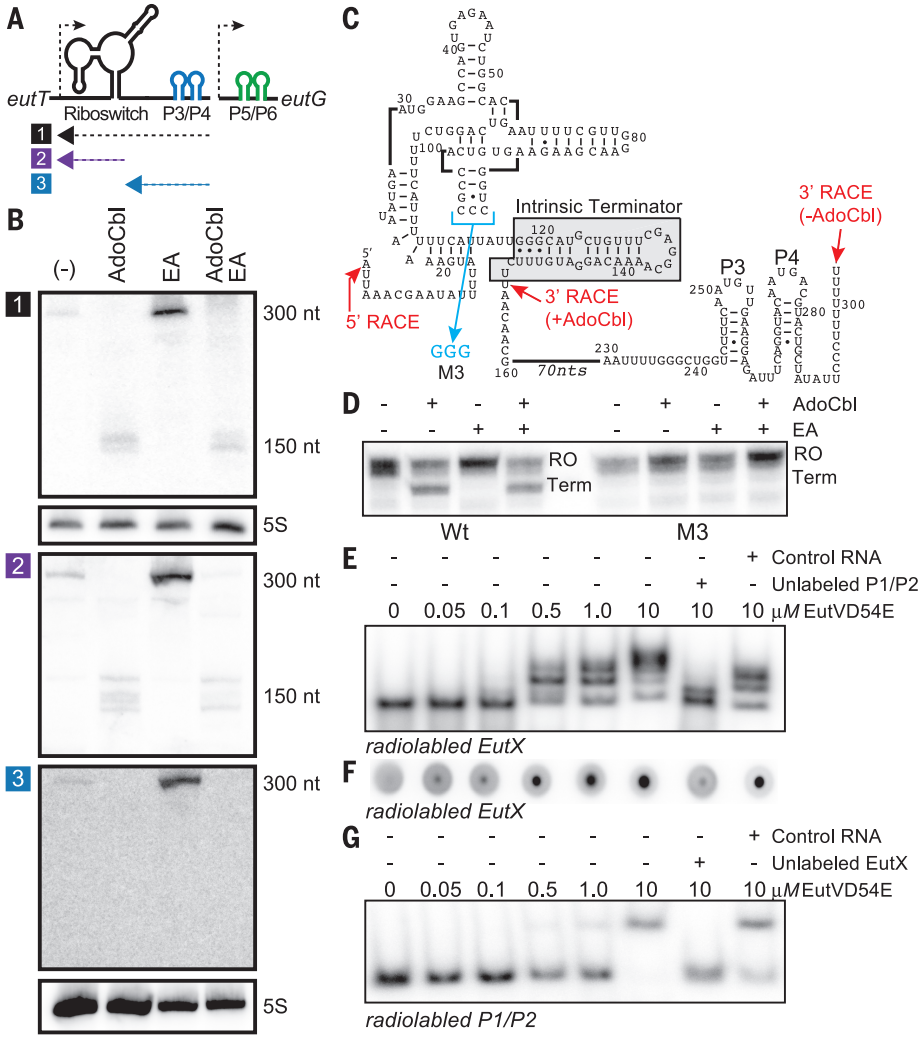

of EutX, detected full-length EutX primarily in medium containing only EA (fig. S2). Together, these data demonstrate that an sRNA, coined EutX, is produced from the *eutT-eutG* intergenic region.

To map the difference between the 300-nucleotide and 150-nucleotide RNAs, we used 3′ rapid amplification of cDNA ends (3′ RACE). By using cells grown in EA without AdoCbl, 3′ RACE located the 3′ terminus within an oligouridylate tract that occurs downstream of P3/P4 and just before the promoter of *eutG*, a length consistent with the Northern blot analysis (301 nts) (Fig. 2C). Using RNA from cells grown with just AdoCbl revealed a 3′ terminus at the end of the riboswitch aptamer where another stretch of U's exists. The latter sequence appears to be part of an intrinsic terminator hairpin, which is formed from sequences at the 3′ end of the AdoCbl riboswitch aptamer (Fig. 2C), consistent with previous in vitro studies (*8*). Indeed, addition of low-micromolar AdoCbl promoted transcription termination at this site in vitro (Fig. 2D and fig. S3). AdoCbl riboswitches have a small loop containing three cytosines that forms a pseudoknot with downstream guanosines and is necessary for ligand binding (*10*, *11*). The *eut* AdoCbl riboswitch is predicted to contain this characteristic L5 loop (Fig. 2C) (*4*). Consistent with a role in sensing AdoCbl, when we mutated these residues, it disrupted termination in response to AdoCbl (Fig. 2D). Also, structural probing revealed that AdoCbl-induced changes were limited to the riboswitch portion of EutX (fig. S4). In addition, a construct in which *lacZ* is fused downstream of the terminator resulted in moderately decreased expression upon addition of AdoCbl (fig. S5).

To further characterize the function of EutX, the ability to bind EutV was confirmed by electrophoretic mobility assays (EMSAs) and differential radial capillary action of ligand assays (DRaCALA) (*12*). Upon addition of micromolar concentrations, purified EutV bound to a portion of EutX that included P3/P4, as shown in Fig. 2, E and F. On the basis of comparative data of EutV binding to the P1/P2 hairpins, we speculate that the binding affinity to EutX may be moderately better (Fig. 2G) (*5*). Unlabeled 30 μM competitor RNA (EutX or P1/P2) could fully compete for binding to EutV in the context of radiolabeled EutX or P1/P2 (Fig. 2, E to G). However, an unrelated RNA of similar length was unable to compete for EutV, which demonstrated that binding of EutV to EutX is specific.

On the basis of the observation that the riboswitch exerts transcription attenuation–mediated control over a EutV binding site, we hypothesized that the EutX sRNA affects *eut* expression in trans. We therefore generated a *eutG-lacZ* fusion that contained the entire intergenic region between *eutT* and *eutG* (Fig. 3, A and B, blue construct), as well as fusions that either deleted P3/P4 (green), the riboswitch (red), or both (orange). These plasmids were transformed into a strain lacking the endogenous *eutX* or a wild-type strain. Expression of wild-type *eutG-lacZ* (blue) was induced by the presence of EA and AdoCbl when cells were grown in a modified minimal medium (Fig. 3B). No expression was observed for this construct in minimal medium, medium containing only AdoCbl, or in a background lacking EutV and EutW (fig. S6). The following data indicate that EutX acts in trans. First, the constructs that lacked P3/P4 were normally regulated in a wild-type strain that still contains P3/P4 in the chromosome (Fig. 3B), which suggested that P3/P4 is not needed in cis. Second, in the strain that lacked endogenous EutX, these same constructs were induced both in +EA and +EA+AdoCbl conditions (Fig. 3B), which suggested that the endogenous EutX prevents *eut* mRNA expression by sequestering EutV. Third, the construct that lacked the riboswitch aptamer, but still contained P3/P4, remained uninduced even in the presence of EA and AdoCbl, consistent with constitutive sequestration of EutV by P3/P4 (Fig. 3B). Because the regulation of the *lacZ* constructs could be altered by the presence or absence of EutX in the chromosome, these data demonstrate that the sRNA can regulate in trans and are consistent with the sequestration model (fig. S1A). Remarkably, in addition to inducing *eutG-lacZ* expression with only EA, the *eutX* strain has the additional property of supporting the formation of visually normal microcompartments in this medium, unlike the wild-type strain (fig. S7). Together, these data show that, in the absence of EutX, EA is sufficient to induce functional expression of the entire *eut* locus.

To further test the sequestration model, we introduced point mutations into the *eutG-lacZ* construct instead of deletions. An adenosine (A) at the first position and a guanine (G) at the fourth position of the six-nucleotide loops were

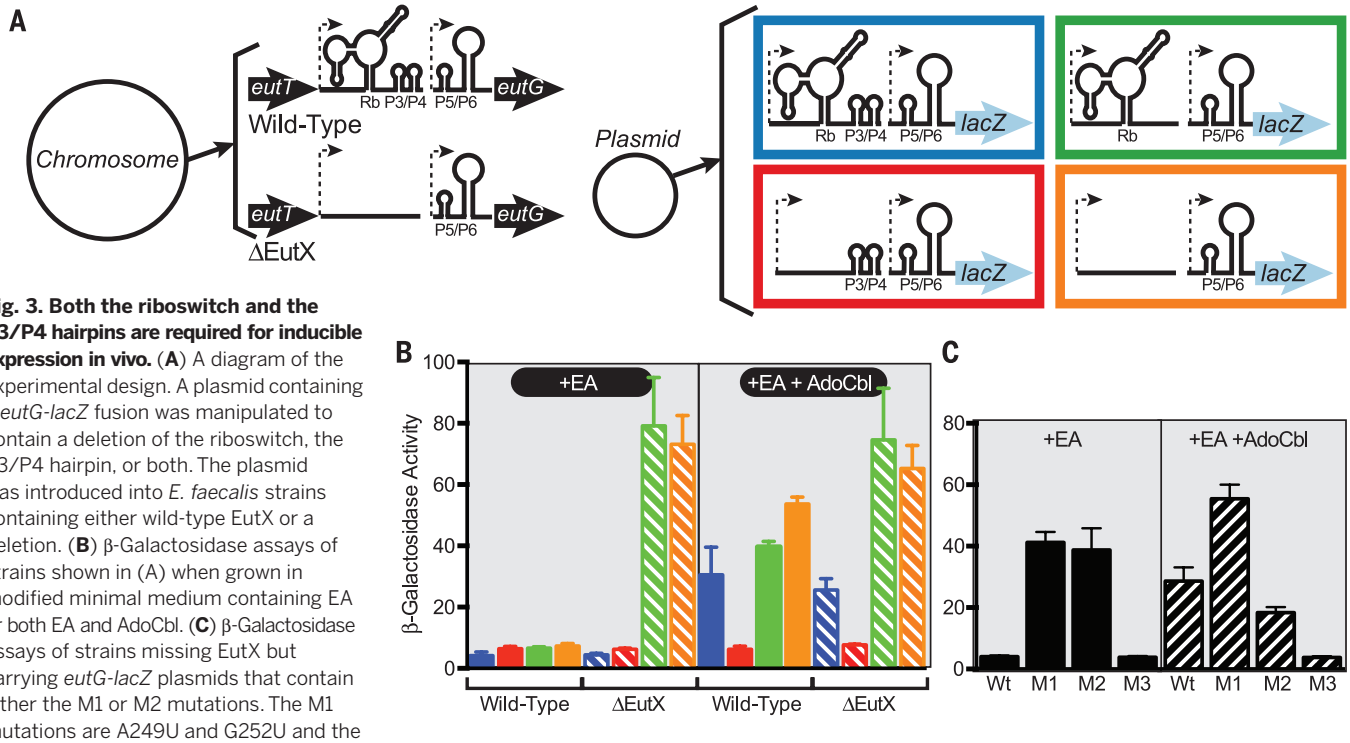

Fig. 3. Both the riboswitch and the P3/P4 hairpins are required for inducible expression in vivo. (**A**) A diagram of the experimental design. A plasmid containing a *eutG-lacZ* fusion was manipulated to contain a deletion of the riboswitch, the P3/P4 hairpin, or both. The plasmid was introduced into *E. faecalis* strains containing either wild-type EutX or a deletion. (**B**) β-Galactosidase assays of strains shown in (A) when grown in modified minimal medium containing EA or both EA and AdoCbl. (**C**) β-Galactosidase assays of strains missing EutX but carrying *eutG-lacZ* plasmids that contain either the M1 or M2 mutations. The M1 mutations are A249U and G252U and the M2 mutations are A273U and G276U site-directed changes. The data are presented as the average of three or more independent experiments, and the error bars represent the standard deviation.

previously shown to be required for EutV binding of dual-hairpin substrates (*5*). We tested one mutant, in which these critical residues of the P3 loop were mutated (M1) and a second, in which the same changes were made to the P4 loop (M2). Similar to deletion of P3/P4, these mutant constructs were both induced by EA alone in the *eutX* strain, in contrast to wild-type *eutG-lacZ* (Fig. 3D). Therefore, these data confirm that P3/P4 mutations that prevent EutV binding affect regulation. We also examined the M3 mutation predicted to abrogate AdoCbl binding and cause constitutive inclusion of P3/P4 in EutX (Fig. 2, C and D). As expected, this resulted in uninducible expression (Fig. 3C).

In conclusion, we present evidence of a riboswitch acting in trans, the second described (*13*). In the prior example, a classical sRNA that acts by base-pairing to a target mRNA can be prematurely terminated by a riboswitch. However, EutX acts in a signal transduction pathway that is subject to riboswitch-mediated control within the confines of an sRNA. A few other sRNAs, like EutX, have been shown to affect gene expression by sequestering RNA-binding proteins. The best-studied examples are CsrB and CsrC, which titrate CsrA, a translational inhibitor protein, away from its mRNA targets [reviewed by (*14*)]. EutX demonstrates a mechanism for how protein sequestration can be placed under signal-responsive regulatory control by a riboswitch.

REFERENCES AND NOTES

1. A. Roth, R. R. Breaker, *Annu. Rev. Biochem.* **78**, 305–334 (2009).
2. A. Serganov, E. Nudler, *Cell* **152**, 17–24 (2013).
3. L. S. Waters, G. Storz, *Cell* **136**, 615–628 (2009).
4. K. A. Fox *et al.*, *Proc. Natl. Acad. Sci. U.S.A.* **106**, 4435–4440 (2009).
5. A. Ramesh *et al.*, *PLOS Genet.* **8**, e1002666 (2012).
6. F. A. Scarlett, J. M. Turner, *J. Gen. Microbiol.* **95**, 173–176 (1976).
7. D. A. Garsin, *Nat. Rev. Microbiol.* **8**, 290–295 (2010).
8. K. A. Baker, M. Perego, *J. Bacteriol.* **193**, 2575–2586 (2011).
9. M. F. Del Papa, M. Perego, *J. Bacteriol.* **190**, 7147–7156 (2008).
10. J. E. Johnson Jr., F. E. Reyes, J. T. Polaski, R. T. Batey, *Nature* **492**, 133–137 (2012).
11. A. Peselis, A. Serganov, *Nat. Struct. Mol. Biol.* **19**, 1182–1184 (2012).
12. K. G. Roelofs, J. Wang, H. O. Sintim, V. T. Lee, *Proc. Natl. Acad. Sci. U.S.A.* **108**, 15528–15533 (2011).
13. E. Loh *et al.*, *Cell* **139**, 770–779 (2009).
14. P. Babitzke, T. Romeo, *Curr. Opin. Microbiol.* **10**, 156–163 (2007).

ACKNOWLEDGMENTS

The data reported are presented in the main paper and the supplementary materials. This work was supported by the NIH grants R01AI076406 (D.A.G.), R56AI110432 (D.A.G. and W.C.W.) and R01GM099790 (A.V.H.), a NSF grant MCB-1051440 (W.C.W.) and a Welch Foundation grant AU-1773 (A.V.H.). For transmission electron microscopy imaging, we thank S. Kolodziej and P. Navarro; J. R. Mellin and P. Cossart are acknowledged for valuable discussions.

SUPPLEMENTARY MATERIALS

www.sciencemag.org/content/345/6199/937/suppl/DC1
Materials and Methods
Figs. S1 to S7
Tables S1 and S2
References (*15*–*17*)

21 April 2014; accepted 26 June 2014
10.1126/science.1255091

RIBOSWITCHES

Sequestration of a two-component response regulator by a riboswitch-regulated noncoding RNA

J. R. Mellin,[1,2,3] Mikael Koutero,[1,2,3] Daniel Dar,[4] Marie-Anne Nahori,[1,2,3] Rotem Sorek,[4] Pascale Cossart[1,2,3]*

Riboswitches are ligand-binding elements contained within the 5′ untranslated regions of bacterial transcripts, which generally regulate expression of downstream open reading frames. Here, we show that in *Listeria monocytogenes*, a riboswitch that binds vitamin B_{12} controls expression of a noncoding regulatory RNA, Rli55. Rli55, in turn, controls expression of the *eut* genes, whose products enable ethanolamine utilization and require B_{12} as a cofactor. Defects in ethanolamine utilization, or in its regulation by Rli55, significantly attenuate *Listeria* virulence in mice. Rli55 functions by sequestering the two-component response regulator EutV by means of a EutV-binding site contained within the RNA. Thus, Rli55 is a riboswitch-regulated member of the small group of regulatory RNAs that function by sequestering a protein and reveals a distinctive mechanism of signal integration in bacterial gene regulation.

Ethanolamine is an abundant molecule in the vertebrate intestine (*1*, *2*), and genes of the ethanolamine utilization pathway (*eut*) are widely conserved in pathogenic bacteria (*3*–*5*). This includes the Gram-positive intracellular human pathogen *Listeria monocytogenes,* in which *eut* expression has been shown to be up-regulated in the intestine during infection of mice (*6*), which suggests that ethanolamine is important for *Listeria* pathogenesis. In *Enterococcus faecalis*, *eut* expression is activated in response to ethanolamine by a two-component response regulator, EutVW (*7*, *8*). In *Salmonella enterica*, ethanolamine utilization requires vitamin B_{12} as a cofactor (*9*), and we noted the presence of a B_{12}-binding riboswitch located upstream of the first gene in the *eut* locus of *L. monocytogenes* (Fig. 1A) (*10*), which suggested that *eut* expression might also be regulated in response to B_{12} availability.

To investigate a role for B_{12}, we examined expression of the *eut* locus in response to B_{12} and ethanolamine by RNA sequencing (RNA-seq) (Fig. 1B) and quantitative reverse transcription polymerase chain reaction (qRT-PCR) (fig. S1). We observed expression of the *eutVW* genes under all conditions, albeit at low levels, which suggested that the cell maintains a pool of EutVW to sense and respond to ethanolamine. In contrast, higher-level expression of *eutVW* and expression of other *eut* genes require both B_{12} and ethanolamine (Fig. 1B). These data indicated B_{12} is required to activate *eut* expression and suggested that the B_{12} riboswitch does not prevent transcription of the *eut* locus in the presence of B_{12}, as might be expected for a classical riboswitch (*11*).

To clarify whether the riboswitch has a role in the B_{12}-dependent regulation of *eut* expression, we examined transcription of the riboswitch locus (Fig. 1C) in response to B_{12} and ethanolamine. We were unable to detect any long transcript, which might extend into the downstream *eut* locus. However, we did detect a ~450-nucleotide (nt) transcript, Rli*55* (*10*, *12*), in the absence of B_{12} (Fig. 1D), and a smaller (~200-nt) transcript that accumulated in the presence of B_{12} (Fig. 1D). This result suggested that the riboswitch mediates transcription termination of the ~450-nt Rli*55* transcript in response to B_{12}, and any remaining long transcript is rapidly degraded (fig. S2A). A strain with a deletion in the B_{12} riboswitch (Δribo) constitutively expressed the long Rli*55* transcript under all conditions (Fig. 1E and fig. S2B), which confirmed B_{12}-dependent regulation by the riboswitch. Conversely, neither the long or short Rli*55* transcripts were detected in a strain (Δ*rli55*) in which the entire *rli55* locus was deleted (Fig. 1E and fig. S2B). Thus, the B_{12} riboswitch determines whether Rli55 is expressed as a long or short transcript in response to B_{12}.

We reasoned that Rli*55* might act as a regulatory RNA controlling expression of the *eut* locus. To test this hypothesis, we examined expression of *eut* genes by qRT-PCR in the wild-type, Δribo, and Δ*rli55* strains. In the wild-type strain, *eut* expression was elevated only when both ethanolamine and B_{12} were present in the media (Fig. 1F and fig. S3, A and B), whereas in the Δribo strain, which constitutively expresses the long Rli*55*, *eut* genes were never expressed under any conditions. In contrast, in the Δ*rli55* strain, expression of the *eut* genes was high in the presence of ethanolamine alone in addition

[1]Unité des Interactions Bactéries-Cellules, Institut Pasteur, F-75015 Paris, France. [2]INSERM, U604, Paris, F-75015 France. [3]INRA, USC2020, F-75015 Paris, France. [4]Department of Molecular Genetics, Weizmann Institute of Science, Rehovot, Israel.
***Corresponding author. E-mail: pcossart@pasteur.fr**

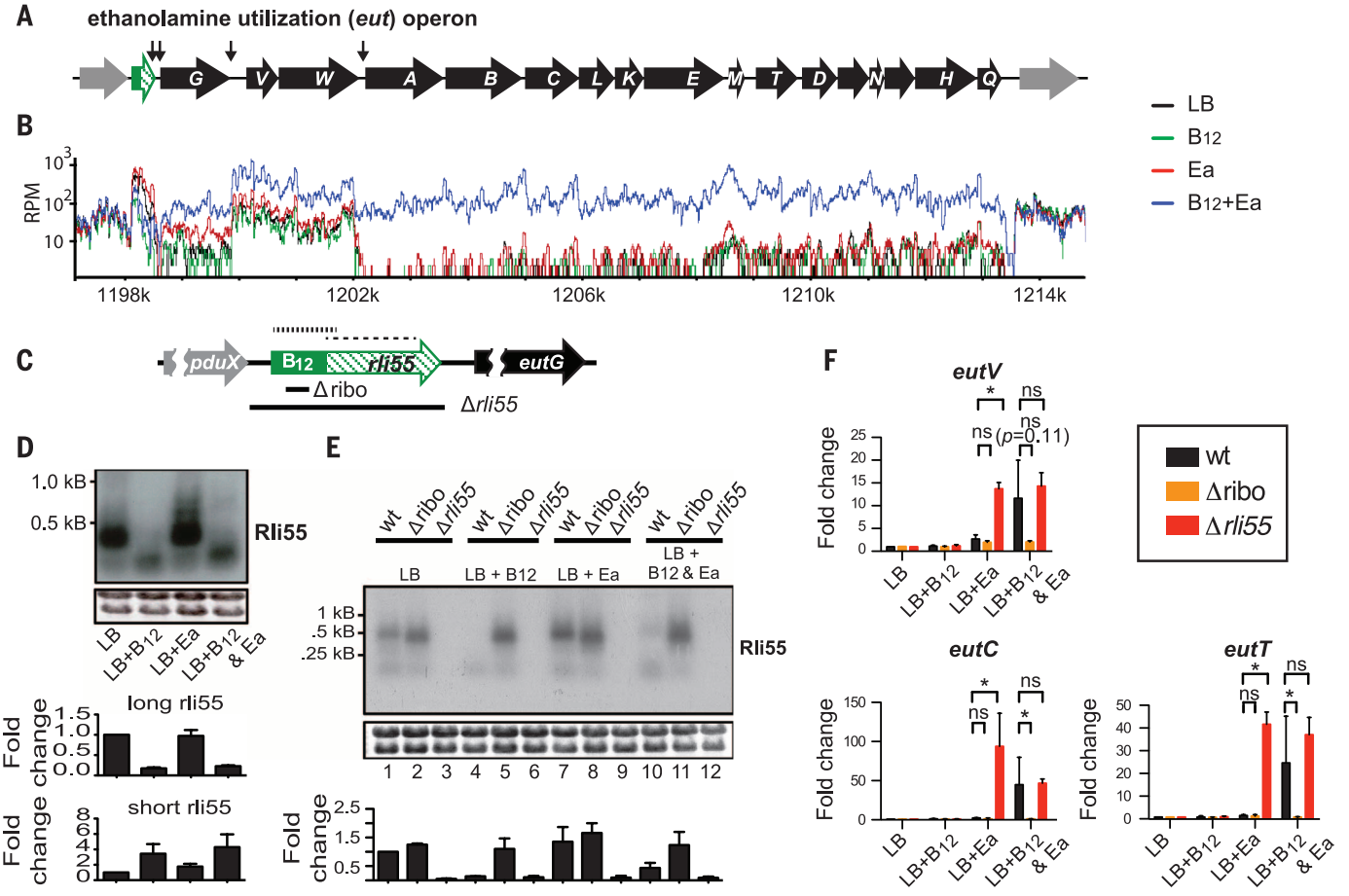

Fig. 1. Control of ethanolamine utilization (*eut*) genes by a B_{12} riboswitch–regulated ncRNA. (**A**) The *eut* locus. Green arrow denotes B_{12} riboswitch. Vertical arrows denote positions of ANTAR elements (*13*) (**B**) RNA-seq coverage of *eut* operon. (**C**) Regions deleted in the Δ*rli55* and Δribo strains are indicated by solid black lines. Northern blot of the *rli55* transcript in the (**D**) wild-type strain with probe indicated by thick dashed line in schematic or (**E**) wild-type (wt), Δribo, or Δ*rli55* strains with probe indicated by thin dashed line in schematic. Ethidium bromide staining of ribosomal RNA is shown as a loading control. Quantification of bands from three experiments is shown below each blot. Expression of the (**F**) *eutV*, *eutC*, and *eutT* genes was evaluated by qRT-PCR in the indicated strains. LB, Luria broth. Values represent means ± SEM, $n = 3$; $^*P < 0.05$; ns, not significant.

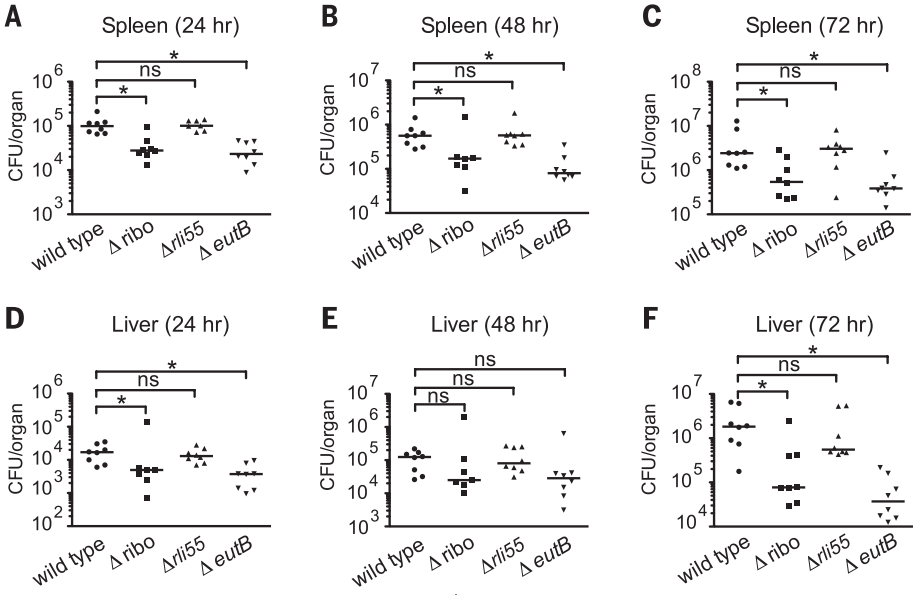

Fig. 2. Ethanolamine utilization and pathogenesis. BALB/c mice were injected intravenously with ~4500 colony-forming units (CFU) of the indicated strain. Mice were killed at (**A**) and (**D**) 24 hours, (**B**) and (**E**) 48 hours, or (**C**) and (**F**) 72 hours, and spleens and livers were removed to assess bacterial load per organ. Results represent two independent experiments with three or four mice per group in each experiment. $^*P < 0.05$, ns, not significant.

to ethanolamine and B_{12} together. Together, these data support a model in which Rli55 prevents the expression of the *eut* locus in the absence of B_{12}, ensuring that the *eut* genes are expressed only in the presence of both ethanolamine (substrate) and B_{12} (cofactor) (fig. S3C).

We tested whether defects in ethanolamine utilization, or its regulation, impacted *L. monocytogenes* virulence by examining the wild-type, Δribo, and Δ*rli55* strains in a mouse intravenous infection model. We also tested a mutant lacking the *eutB* gene encoding an ethanolamine lyase subunit, which is unable to catabolize ethanolamine. The Δribo and Δ*eutB* strains both had significantly reduced bacterial loads at 24 hours after infection compared with the wild-type strain, and these differences increased at 48 hours and 72 hours postinfection (~10- to 50-fold) (Fig. 2, A to F). In contrast, the Δ*rli55* strain, in which *eut* expression is not inhibited, was present in amounts comparable to those in the wild-type strain in the spleen and liver. Thus, defects in ethanolamine utilization or activation of *eut* expression significantly attenuate *L. monocytogenes* virulence.

In *E. faecalis*, ethanolamine is sensed by the sensor-kinase EutW, which subsequently phosphorylates the response regulator EutV (*7*). Phosphorylated EutV in turn binds ANTAR elements (AmiR and NasR transcriptional antiterminator regulator) in the 5′ untranslated regions of actively transcribed *eut* mRNAs, which prevents the formation of a transcription terminator and consequently activates *eut* expression (*13*). In *L. monocytogenes*, ANTAR sites were identified upstream of the *eutA* and *eutV* genes, and a third site was identified in the *rli55* locus upstream of the *eutG* gene and downstream of the B_{12} riboswitch (*13*). We also identified a second ANTAR site in the *rli55* locus (Fig. 3A), which suggested that one or both of these ANTAR elements could be transcribed as part of the 3′ end of Rli55 RNA. Indeed, our RNA-seq data showed that, in the absence of B_{12}, high levels of Rli55 are transcribed as a long transcript encompassing the first ANTAR element (Fig. 3A). In contrast, *rli55* transcription terminates abruptly after the riboswitch in the presence of B_{12}, which indicates that the riboswitch determines whether Rli55 is transcribed with or without an ANTAR element. This notion was supported by the detection of putative Rli55 orthologs in *E. faecalis* and *Streptococcus sanguinis* (fig. S4). In the latter, the riboswitch, in conjunction with a single ANTAR element, has undergone an inversion relative to the adjacent *eutG* gene, which suggests that the riboswitch and the first ANTAR element are functionally linked (fig. S4B) and that this is also the case in *L. monocytogenes*.

To test if the ANTAR elements are involved in Rli55-mediated regulation, we complemented the Δ*rli55* strain with chromosomally integrated *rli55* alleles carrying mutations in the ANTAR elements and examined which ones restored Rli55-mediated regulation of *eut* expression (Fig. 3, B and C, and fig. S5). A strain with an empty

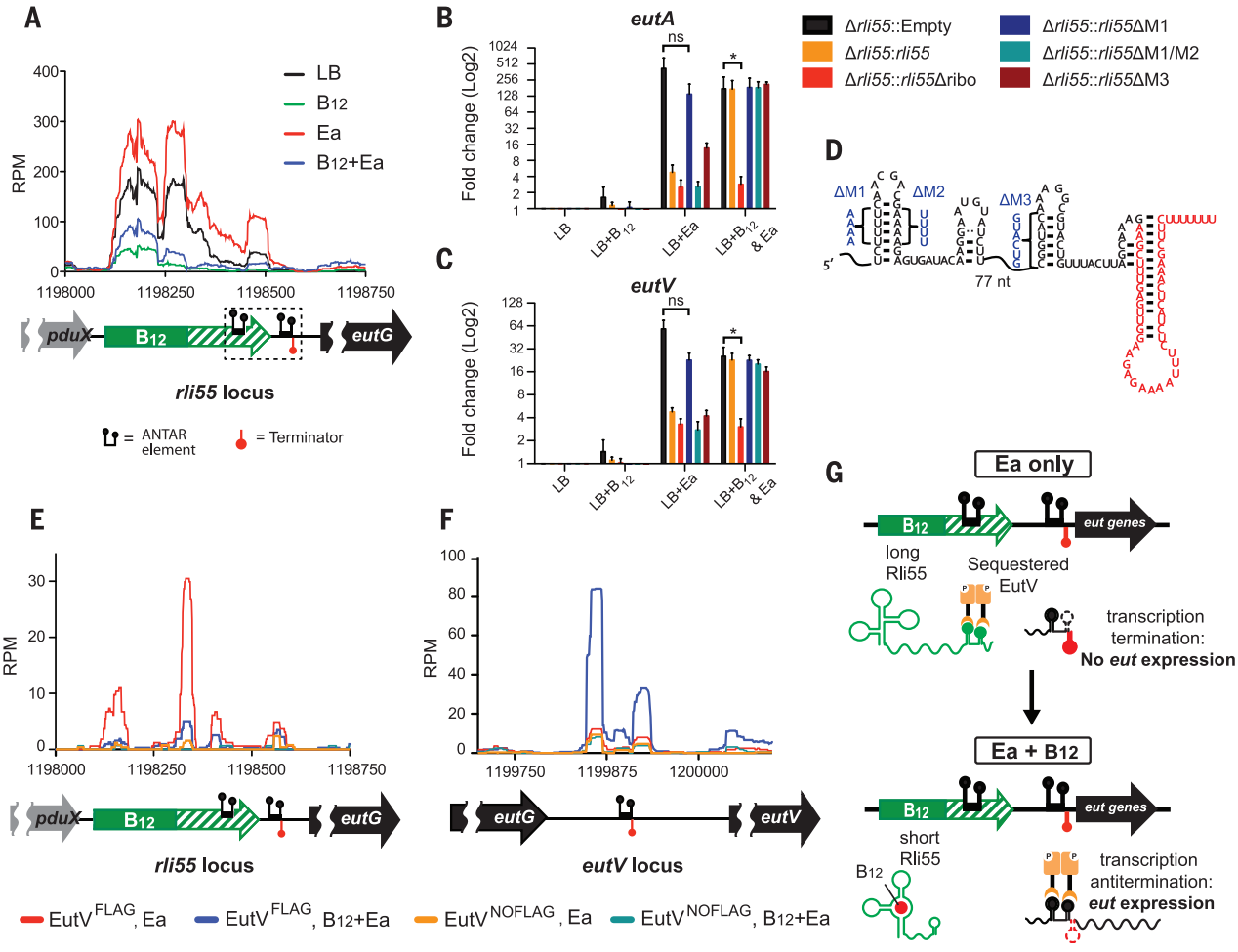

Fig. 3. Rli55 sequesters the two-component response regulator EutV. (**A**) RNA-seq coverage in reads per million (RPM) of the *rli55* locus from bacteria grown as indicated. (**B** and **C**) qRT-PCR of *eutV* and *eutA* genes. Vitamin B_{12} (B_{12}), ethanolamine (Ea). Values represent means ± SEM, $n = 3$. All differences were significantly different (*$P < 0.05$) from the Δ*rli55*::Empty strain in the Ea condition, except where indicated (ns). All differences were not significantly different from the Δ*rli55*::Empty strain in the B_{12} + Ea condition, except where indicated. (**D**) Secondary structure of the ANTAR elements encoded in the boxed region of Fig. 3A. Mutations are shown in blue. (**E** and **F**) RNA-seq coverage in RPM of the *rli55* and *eutV* loci with RNA isolated by coimmunoprecipitation of cell lysates from either $EutV^{FLAG}$ or $EutV^{NOFLAG}$ cultures grown in the presence of ethanolamine (Ea) or ethanolamine and B_{12} together. (**G**) Proposed model of Rli55-mediated regulation of *eut* expression in the presence of ethanolamine (Ea) alone or ethanolamine + B_{12} (Ea + B_{12}).

construct (Δ*rli55*::Empty) could not prevent expression of the *eut* genes in ethanolamine alone (as in the parental Δ*rli55* strain), whereas a strain with a wild-type copy of *rli55* (Δ*rli55*::*rli55*) fully restored Rli55-mediated inhibition. However, a strain with a deletion in the riboswitch (Δ*rli55*::Δribo) inhibited *eut* expression in all conditions, as the riboswitch can no longer terminate *rli55* transcription in response to B_{12}. In strain Δ*rli55*::*rli55*ΔM1, wherein four uridine residues in the first ANTAR site were mutated to adenines (Fig. 3D, ΔM1), inhibition of *eut* expression by Rli55 was abolished in the presence of ethanolamine alone. In contrast, in strain Δ*rli55*::*rli55*ΔM1/M2, where compensatory mutations were made to the opposite side of the ANTAR stem-loop (Fig. 3D, ΔM2), wild-type regulation of *eut* expression was restored. Mutation of the six nucleotides in the stem-loop of the second ANTAR element (Fig. 3D, ΔM3, Δ*rli55*::*rli55*ΔM3) had no significant effect on Rli55-mediated regulation. Thus, the first ANTAR element is necessary and sufficient for Rli55-mediated regulation.

The long form of Rli55 containing an ANTAR element might bind and sequester EutV and so prevent it from activating expression of the *eut* genes in the presence of ethanolamine but absence of B_{12}. When sufficient levels of B_{12} accumulate, B_{12} would bind the riboswitch, producing truncated Rli55 transcripts, which would lack an ANTAR element and be unable to sequester EutV. To examine this hypothesis, we constructed a strain with an additional copy of the *eutV* gene carrying a 2XFLAG-tag ($EutV^{FLAG}$) and first showed that expression of $EutV^{FLAG}$ protein is regulated identically to the native *eutV* gene in response to ethanolamine and B_{12} (fig. S6A). We also constructed a strain with an additional *eutV* gene lacking a FLAG tag ($EutV^{NOFLAG}$). Anti-FLAG immunoprecipitations of cell lysates from these two strains (fig. S6, B and C), followed by RNA-seq analysis (Fig. 3, E and F), showed that Rli55 is enriched by co-immunoprecipitation with $EutV^{FLAG}$ primarily when bacteria are grown in the presence of ethanolamine alone, although we saw no enrichment in a parallel immunoprecipitation with the $EutV^{NOFLAG}$ strain (Fig. 3E). In contrast, the ANTAR element upstream of the *eutV* gene (Fig. 3F) is enriched by coimmunoprecipitation of lysates from $EutV^{FLAG}$ bacteria, but not $EutV^{NOFLAG}$ bacteria, grown in the presence of ethanolamine and B_{12} together but not from lysates of bacteria grown in ethanolamine alone. To a lesser extent, the ANTAR-containing region upstream of *eutA* and the entire *eutA-Q* locus are enriched under the latter condition (fig. S7). These data support a model in which the majority of EutV is bound and sequestered by Rli55 in the presence of ethanolamine alone. Conversely, in the presence of ethanolamine and B_{12}, the riboswitch produces short truncated Rli55 transcripts, which cannot bind EutV, and so allows EutV to bind *eut* mRNAs and to activate *eut* expression (Fig. 3G).

This riboregulatory mechanism coordinates expression of the ethanolamine utilization (*eut*) locus with the availability of B_{12}, the essential cofactor for ethanolamine catabolism. Previously, ethanolamine utilization has been shown to be important after oral infection by *Salmonella enterica* serovar Typhimurium and enterohemorrhagic *Escherichia coli* (*3*, *4*, *14*); however, the contribution of ethanolamine utilization to *L. monocytogenes* pathogenesis in an intravenous mouse infection model suggests that ethanolamine utilization is important outside of the intestine and possibly in the intracellular environment. This study also extends the role of riboswitches in the regulation of noncoding RNAs (*15*, *16*). Finally, our data show that Rli55 represents a new member of the small family of regulatory RNAs that function by sequestering a protein, which also includes the *6S* and CsrB/C RNAs (*17*), and highlights a distinctive means of signal integration in bacterial gene regulation.

REFERENCES AND NOTES

1. D. A. Garsin, *Nat. Rev. Microbiol.* **8**, 290–295 (2010).
2. K. Koichi, F. Michiya, N. Makoto, *Biochim. Biophys. Acta* **369**, 222–233 (1974).
3. P. Thiennimitr *et al.*, *Proc. Natl. Acad. Sci. U.S.A.* **108**, 17480–17485 (2011).
4. Y. Bertin *et al.*, *Environ. Microbiol.* **13**, 365–377 (2011).
5. O. Tsoy, D. Ravcheev, A. Mushegian, *J. Bacteriol.* **191**, 7157–7164 (2009).
6. C. Archambaud *et al.*, *Proc. Natl. Acad. Sci. U.S.A.* **109**, 16684–16689 (2012).
7. M. F. Del Papa, M. Perego, *J. Bacteriol.* **190**, 7147–7156 (2008).
8. K. A. Fox *et al.*, *Proc. Natl. Acad. Sci. U.S.A.* **106**, 4435–4440 (2009).
9. J. R. Roth, J. G. Lawrence, T. A. Bobik, *Annu. Rev. Microbiol.* **50**, 137–181 (1996).
10. A. Toledo-Arana *et al.*, *Nature* **459**, 950–956 (2009).
11. W. C. Winkler, R. R. Breaker, *Annu. Rev. Microbiol.* **59**, 487–517 (2005).
12. O. Wurtzel *et al.*, *Mol. Syst. Biol.* **8**, 583 (2012).
13. A. Ramesh *et al.*, *PLOS Genet.* **8**, e1002666 (2012).
14. S. E. Winter, A. J. Bäumler, *Gut Microbes* **2**, 58–60 (2011).
15. J. R. Mellin *et al.*, *Proc. Natl. Acad. Sci. U.S.A.* **110**, 13132–13137 (2013).
16. G. André *et al.*, *Nucleic Acids Res.* **36**, 5955–5969 (2008).
17. S. Gottesman, G. Storz, *Cold Spring Harb. Perspect. Biol.* **3**, a003798 (2011).

ACKNOWLEDGMENTS

We are grateful to D. Garsin and W. Winkler for their exchange of ideas and discussion of unpublished data. We also thank, N. King and J. Pederson for helpful and insightful discussions and Y. Chao and J. Vogel for assistance with the CLIP-seq protocol. This work was supported by grants to P.C., European Research Council advanced grant (233348), ANR (BACNET 09-BLAN-0024-02), ANR Investissement d'Avenir Programme (10-LABX-62), Fondation Le Roch, and Fondation Jeantet. P.C. is an International Senior Research Scholar of the Howard Hughes Medical Institute.

SUPPLEMENTARY MATERIALS

www.sciencemag.org/content/345/6199/940/suppl/DC1
Materials and Methods
Figs. S1 to S7
Tables S1 and S2
References

21 April 2014; accepted 24 June 2014
10.1126/science.1255083

IMMUNOGENETICS

Chromatin state dynamics during blood formation

David Lara-Astiaso,[1]* Assaf Weiner,[2,3]* Erika Lorenzo-Vivas,[1] Irina Zaretsky,[1] Diego Adhemar Jaitin,[1] Eyal David,[1] Hadas Keren-Shaul,[1] Alexander Mildner,[1] Deborah Winter,[1] Steffen Jung,[1] Nir Friedman,[2,3]† Ido Amit[1]†

Chromatin modifications are crucial for development, yet little is known about their dynamics during differentiation. Hematopoiesis provides a well-defined model to study chromatin state dynamics; however, technical limitations impede profiling of homogeneous differentiation intermediates. We developed a high-sensitivity indexing-first chromatin immunoprecipitation approach to profile the dynamics of four chromatin modifications across 16 stages of hematopoietic differentiation. We identify 48,415 enhancer regions and characterize their dynamics. We find that lineage commitment involves de novo establishment of 17,035 lineage-specific enhancers. These enhancer repertoire expansions foreshadow transcriptional programs in differentiated cells. Combining our enhancer catalog with gene expression profiles, we elucidate the transcription factor network controlling chromatin dynamics and lineage specification in hematopoiesis. Together, our results provide a comprehensive model of chromatin dynamics during development.

Chromatin plays a major regulatory role in cell-type–specific functions and response (*1*, *2*). The current dogma of cellular differentiation suggests that there is a progressive closing of the regulatory potential of the genome. According to this model, differentiation is a gradual transition from an open chromatin state in multipotent stem cells to a compacted chromatin state in differentiated cells. However, genome-wide histone modification profiling of embryonic stem cells and terminally differentiated cells is not fully compatible with this model

(*3*–*7*). Resolving this discrepancy requires observation of chromatin dynamics during intermediate stages of differentiation.

An important model system for differentiation is hematopoiesis, in which a single hematopoietic stem cell gives rise to a large number of cell types (comprising the blood) through a series of characterized intermediate progenitor cells (*8*, *9*). Chromatin regulation has a central role in hematopoiesis: Mutations or loss of chromatin factors lead to hematopoiesis defects and diseases (*10*). Moreover, genome-wide chromatin profiling studies have revealed large-scale differences in the histone modifications and transcription factor binding maps between mature immune cell types (*3*–*6*, *11*). Thus, dramatic chromatin reorganizations during hematopoiesis are critical for early hematopoietic decisions (*12*).

Comprehensive study of the chromatin events during hematopoiesis has been hampered by the low sensitivity and reproducibility for small cell numbers with current chromatin immunoprecipitation (ChIP) protocols. These protocols require several enzymatic steps with limited performance when the input DNA is below the nanogram range. Whereas an average diploid mammalian cell has roughly 4 to 8 pg of DNA, losses after ChIP reduce the available DNA for analysis by 2 to 3 orders of magnitude, setting the lower limit for genome-wide chromatin analysis at 50,000 cells (*13*). Amplification of ChIP material partially alleviates this problem at the cost of introducing amplification biases (*14*, *15*).

To profile chromatin dynamics of scarce in vivo cell populations, we developed an indexing-first chromatin IP approach (iChIP). In this protocol, barcoding is performed directly on the total cellular chromatin (Fig. 1A), thereby avoiding the low-input enzymatic reactions occurring in conventional ChIP. Importantly, this enables multiple chromatin-barcoded samples to be pooled for ChIP in the same well, further reducing initial input requirements and increasing cross-sample reproducibility. To minimize centrifugation steps, cells are fixed before sorting and sonication. Then, the sheared chromatin is immobilized on magnetic beads coated with antibody to H3 and then indexed. The indexed chromatin is released from the H3 beads and pooled with chromatin from other samples. Finally, ChIP is performed with the desired antibody, and a single chromatin-barcoded pool can be divided among multiple ChIPs for profiling various chromatin modifications.

The iChIP protocol is highly reproducible for low cell numbers (a few hundred cells) while increasing the sensitivity and throughput (Fig. 1). To benchmark iChIP, we barcoded decreasing amounts (10,000 to 500 cells) of chromatin isolated from bone-marrow–derived dendritic cells (BMDCs), in triplicate, and performed ChIP on the barcoded chromatin with an antibody to mono- and trimethylated histone H3 lysine 4 (H3K4me1 and H3K4me3) (Fig. 1, B to D, and fig. S1). We confirmed reproducibility of H3K4me3 peaks between replicates of 10,000 cells (r = 0.95) down to 500 cells (r = 0.85). iChIP profiles correlated with conventional ChIP-seq on 10 million BMDCs (r = 0.92) (*16*). iChIP is applicable to profile other histone modifications and transcription factors for low cell numbers (Fig. 1, C and D, and fig. S1). The reproducibility and sensitivity for small cell numbers of iChIP open the way for in vivo characterization of chromatin dynamics during hematopoiesis.

We profiled four histone modifications (H3K4me1, H3K4me2, H3K4me3, and H3K27ac) (*17*) in three in vivo replicates at 16 developmental stages of hematopoietic commitment using 5000 cells per mark. The cell populations chosen comprise all multipotent progenitor stages and the common lineage oligopotent progenitors from each of the major blood lineages (myeloid, lymphoid, and erythroid), as well as several terminally differentiated cell types from each of the lineages (https://www.immgen.org) (*16*) (Fig. 2A). Replicates of histone modifications ChIP and RNA-seq displayed high reproducibility [average r = 0.95 (*16*)] (fig. S2 and tables S1 and 2). We used histone marks to define promoter (high H3K4me3) and enhancer (high H3K4me1/2 and low H3K4me3) regions, resulting in analysis of 48,415 enhancers and 17,923 promoters (*16*). Enhancer activity was defined from H3K27ac levels and RNA expression values of the nearest gene (*16*–*18*). Genome-wide analysis of RNA expression and promoter activity (H3K4me3 signal) identified four major patterns for progenitor, lymphoid, myeloid, and erythroid cells (Fig. 2B and figs. S2 and S3). In contrast, H3K4me1 signal revealed that lineage progenitors were more similar to the differentiated cells within their lineage than to progenitors from other cell lineages (Fig. 2B and figs. S2 and S3). This distinction suggests that enhancer establishment is initiated in early lineage commitment and can reveal the differentiation potential of progeny before the execution of the RNA expression program.

Changes in chromatin marks during hematopoiesis (particularly H3K4me1 and H3K4me2) suggest lineage-specific activity of regulatory elements. Of the 48,415 hematopoietic enhancers, 90% (43,428) changed state during hematopoiesis (*16*). We found that 60% (26,393) of these dynamic enhancers show the stereotypical behavior in which they are initially marked in hematopoietic stem cells (HSCs) but are maintained only in the relevant lineage [Fig. 2C (Gata2) and fig. S4A (Meis1 and CD34)]. Surprisingly, we discovered that a large proportion of dynamic enhancers (40%, 17,035) are established de novo during the differentiation process (*16*). For example, enhancers present in myeloid gene loci IL-1b, CD14, S100a8, and F7 (coagulation factor VII) are either established de novo or become more prominent in the myeloid lineage (Fig. 2C and fig. S4A). Similarly, Ebf1 and Cr2 enhancers are established in B cells; Bcl11b and CD3g enhancers in T cells; Granzyme A and Ncr1 enhancers in natural killer cells (NK) cells; and Gata1, Gypa (glycophorin A), and Cpox (coproporphyrinogen oxidase) enhancers in the erythroid lineage (Fig. 2 and figs. S3B and S4A).

The establishment of de novo lineage-specific enhancers occurs mainly at the root of the commitment point in the first progenitor of the lineage, whereas closing of enhancers occurs more gradually (Fig. 2). For example, S100a8, F7 and F10 loci display H3K4me1 signal specifically in the myeloid lineage, with de novo establishment of the enhancers at the root of the myeloid commitment point in common myeloid progenitor (CMP) (Fig. 2C and figs. S3B and S4A). Similarly, the Cpox and Gypa loci display H3K4me1 signal specifically in the erythrocyte lineage, with de novo establishment of the enhancers at the root of the erythrocyte commitment point in the megakaryocyte erythroid progenitor (MEP) (Fig. 2C). Importantly, we observe a stepwise acquisition of the different chromatin modifications in the lineage-specific enhancers during hematopoiesis (Fig. 2D and figs. S4B and S5). For example, in both S100a8 (myeloid lineage) and Gypa (erythroid lineage) loci, H3K4me1/2 appear first in the root lineage progenitor (CMP and MEP, respectively), whereas H3K27ac (locus activation) is acquired together with active RNA transcription only once the cells (granulocytes and erythrocyte B) are terminally differentiated (Fig. 2D and fig. S4B). Globally, 32% of the activated (H3K27ac) enhancers in terminally differentiated cells are initially poised (H3Kme1 only) in the lineage progenitors (*16*).

Clustering of all 48,415 H3K4me1 peaks by their dynamic profiles during hematopoiesis revealed nine major clusters, consistent with the underlying biology of the system (Fig. 3A and fig. S6, A and B) (*16*). H3K4me2 signal shows similar patterns in all nine clusters (fig. S6A). Cluster I comprises enhancers shared throughout hematopoiesis. Clusters II to IV group lineage-specific enhancers already marked in HSCs and shared with hematopoietic progenitors. Finally, clusters VI (Fig. 3B, middle), VII, VIII, and IX (Fig. 3B, bottom) group de novo enhancers that are specific to a particular lineage and were not marked in HSCs with 6382 myeloid, 5834 lymphoid, and 4819 erythroid enhancers. We also found a group of 6612 enhancers (cluster V) shared exclusively among progenitors (Fig. 3B, top). Interestingly, the erythrocyte and progenitor enhancer clusters exhibit relatively high sequence conservation (*16*) in the mammalian clade, with the myeloid and lymphoid enhancers displaying lower conservation. These data suggest differential rates of evolutionary dynamics in these cis-regulatory regions (*16*) (Fig. 3A).

Newly formed enhancers could either be established at a specific branching point or established gradually during the development process. To further examine these dynamics, we generated a catalog of enhancers that are dynamic (gained or lost) during the process of differentiation from

[1]Department of Immunology, Weizmann Institute of Science, Rehovot, Israel. [2]Institute of Life Sciences, The Hebrew University, Jerusalem, Israel. [3]School of Computer Science and Engineering, The Hebrew University, Jerusalem, Israel. *These authors contributed equally to this work. †**Corresponding author. E-mail: nir@cs.huji.ac.il (N.F.); ido.amit@weizmann.ac.il (I.A.)**

the long-term hematopoietic stem cells (LT-HSCs) to mature, terminally differentiated cells (Fig. 3C). We determined, for each enhancer, the stage of gain or loss along the differentiation path. In erythroid differentiation, 65% of the de novo enhancer repertoire are gained in the MEP stage (Fig. 3D). Similarly, 40 to 50% of the de novo myeloid enhancers are gained in the first step of myeloid commitment, during the multipotent progenitor (MPP) to CMP transition, whereas the CMP to GMP transition involves fewer gains (15 to 30%). Together, the CMP and GMP stages are responsible for 63 to 80% of gained enhancers in terminally differentiated myeloid cells (Fig. 3D), consistent with the global

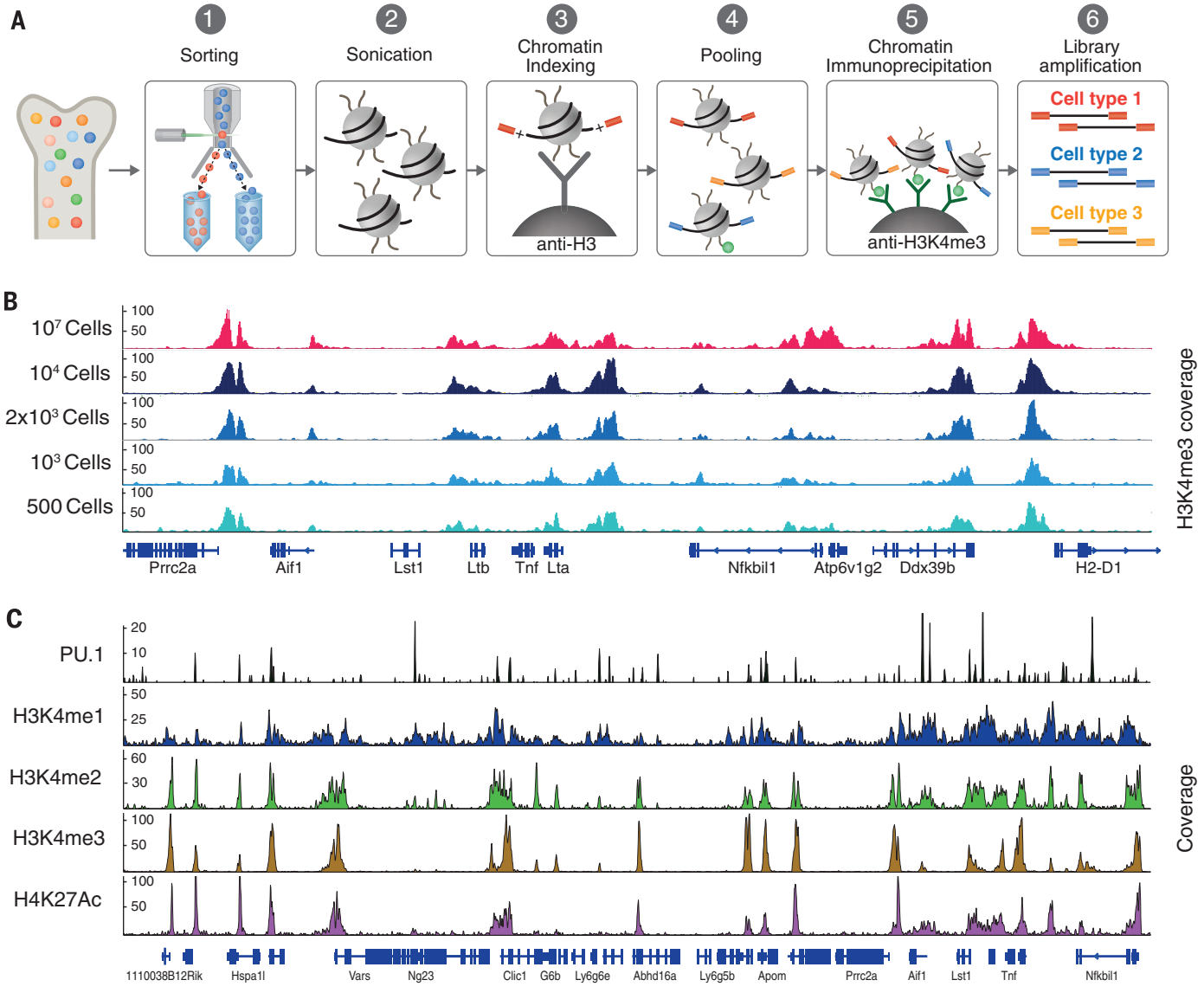

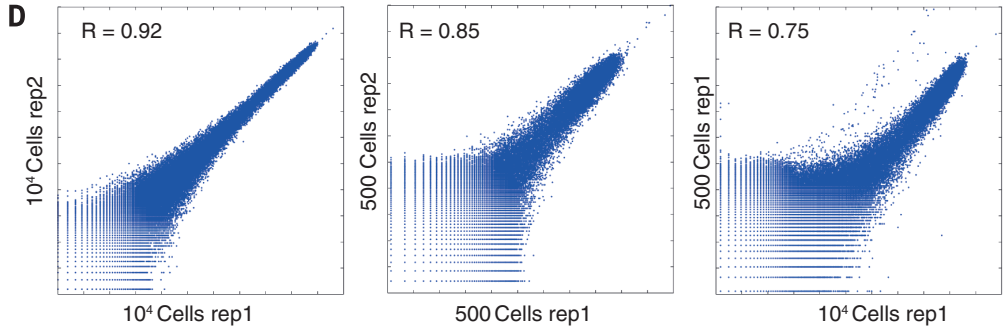

Fig. 1. iChIP for profiling histone modifications and transcription factor binding. (**A**) Schematic diagram of the iChIP approach to chromatin immunoprecipitation involving an initial chromatin barcoding step before ChIP with the desired antibody. (**B**) Normalized H3K4me3 profiles of peaks found in a 100-kb region in the tumor necrosis factor (TNF) locus (genes are indicated below) obtained with iChIP of decreasing amounts of BMDCs. (Top) In red, H3K4me3 profile obtained using conventional ChIP with 20 million cells (*15*). Below, in shades of blue, H3K4me3 profiles obtained with iChIP. (**C**) Normalized profiles of PU.1, H3K4me1, H3K4me2, H3K4me3, and H3K27ac found in a 250-kb region in the TNF locus obtained with iChIP with 10^4 BMDCs. (**D**) Scatter plots showing correlation between representative HK4me3 iChIP replicates. From left to right: correlation between 10^4 cell replicates, 500 cell replicates, and 500 cells compared with 10^4 cells.

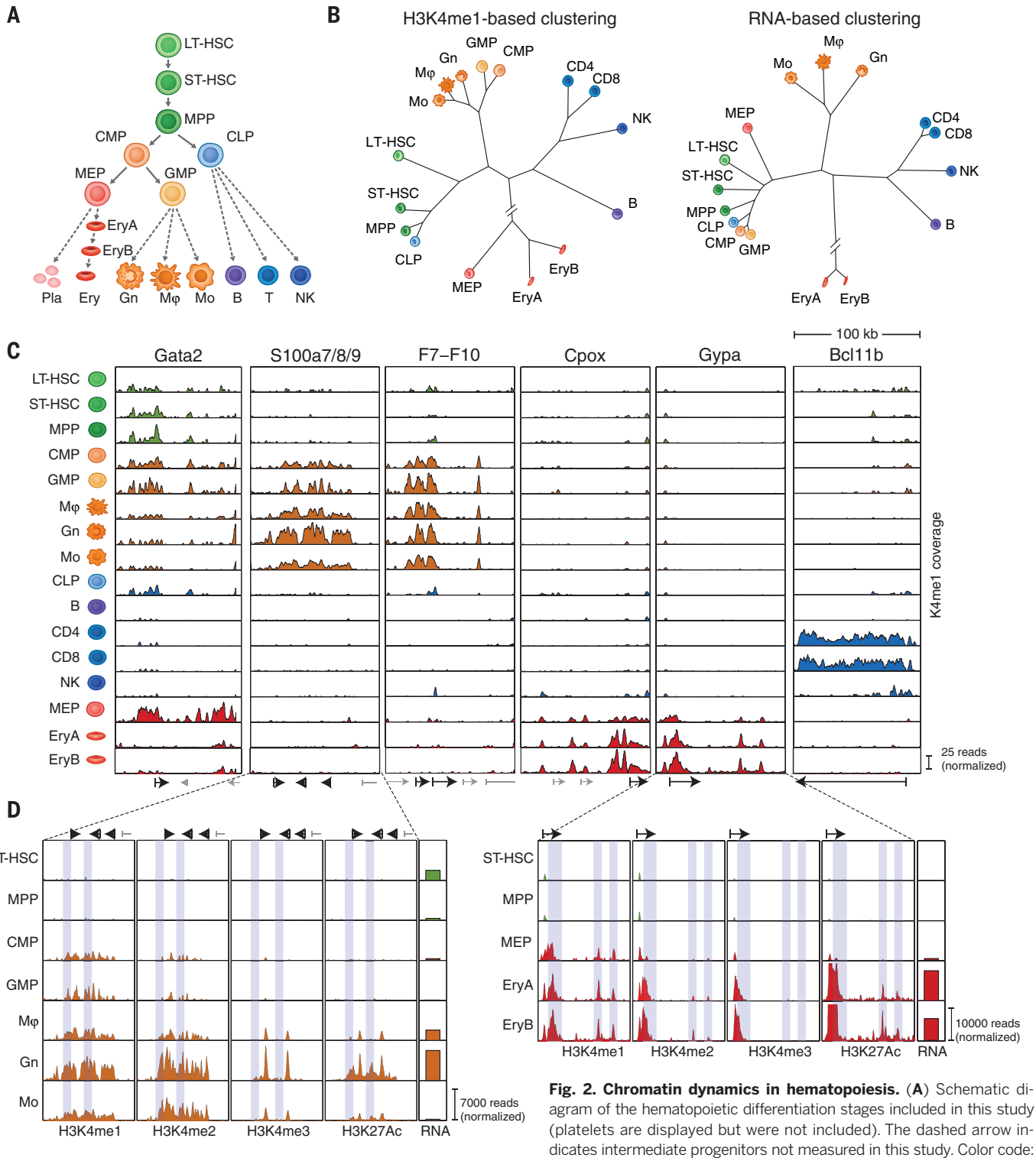

Fig. 2. Chromatin dynamics in hematopoiesis. (**A**) Schematic diagram of the hematopoietic differentiation stages included in this study (platelets are displayed but were not included). The dashed arrow indicates intermediate progenitors not measured in this study. Color code: green for multipotent progenitors, orange for myeloid lineage (including the oligopotent progenitors CMP and GMP), blue for lymphoid lineage, and red for erythroid lineage. (**B**) Clustering dendrogram of cell types based on H3K4me1 profiles (left) and RNA-seq levels (right) showing the differential association of lineage progenitors (CMP, GMP, and MEP). (**C**) Representative examples of H3K4me1 signal (cell types labeled at left) in several loci (from left to right): Gata 2 for progenitors, F7-F10 and S100a8 for myeloid lineage, Gypa and Cpox for erythroid lineage, and Bcl11b for T cells. Displayed are normalized reads coverage in a 100-kb region around the gene body. (**D**) Profiles of H3K4me1, H3K4me2, H3K4me3, and H3K27ac modifications and RNA expression levels in two lineage-specific gene loci: S100a8 (myeloid) and Gypa (erythroid). Displayed are profiles for the lineage-specific cell types and multipotent progenitor cells over a 100-kb region around the gene body. Putative lineage-specific enhancers are shadowed in blue. Lineage-specific genes are indicated below (black), as well as other genes in the loci (light gray).

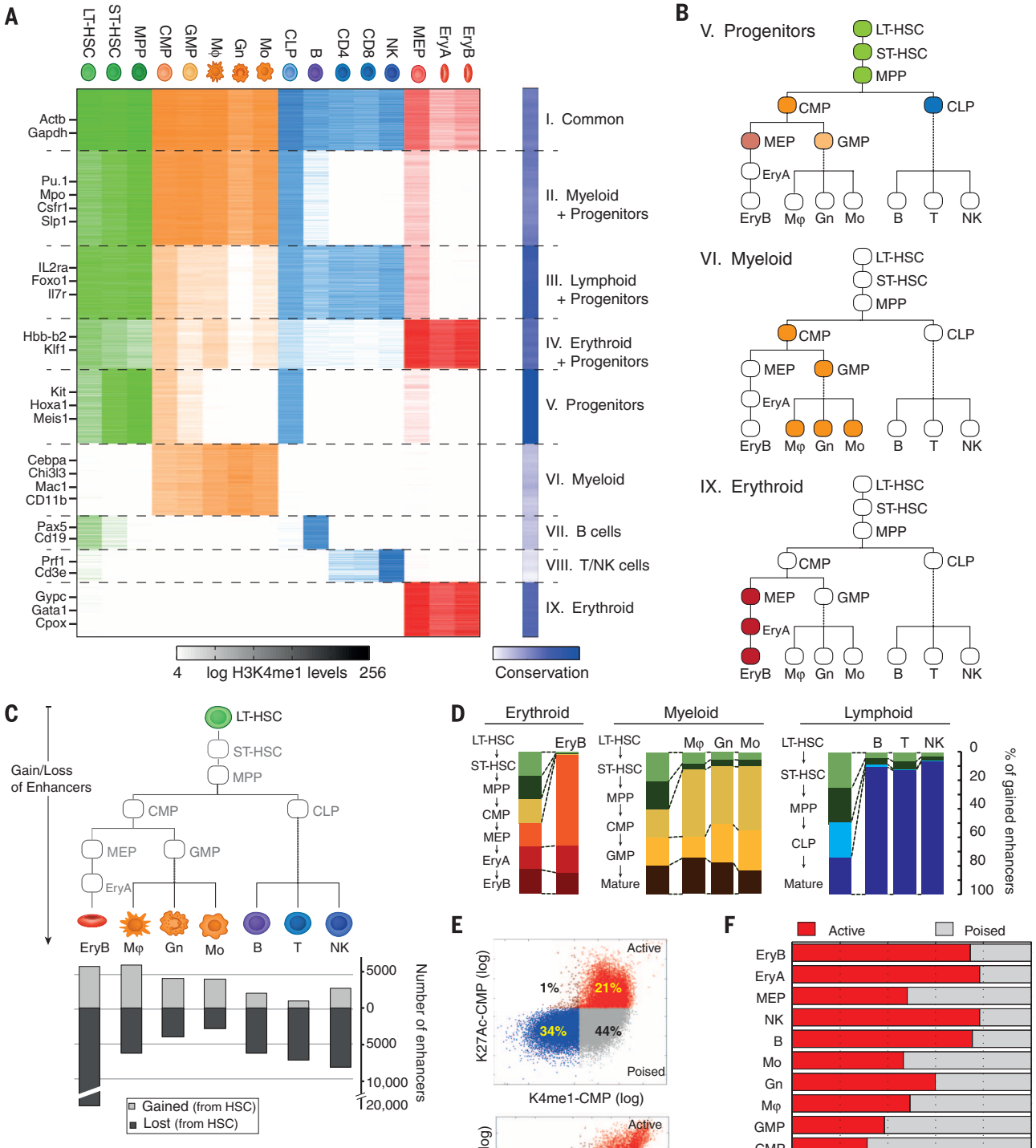

Fig. 3. Hematopoiesis progresses through gain and loss of lineage-specific enhancers. (**A**) Heat map showing 48,415 hematopoiesis enhancers clustered with K-means (K = 9) of average reads count within H3K4me1 regions (*16*) annotated with the genomic sequence conservation of the enhancers, right (blue scale) (*16*). Annotations for important lineage-specific gene loci are shown on the left. (**B**) Schematic tree view of three representative enhancer clusters; progenitors (V), myeloid (VI), and erythroid (IX). Color fill represents stages with H3K4me1 mark at the enhancer. (**C**) Bar plot showing the number of enhancers gained (top, light gray) and lost (bottom, dark gray) during the development from HSC to mature hematopoietic cells along each lineage. (**D**) Bar plot showing the percent of de novo enhancers [from (C)] established at each developmental stage from HSC to mature hematopoietic cells. (**E**) Scatter plots showing H3K27ac signal versus H3K4me1 signal in both CMPs and EryA cells. Active enhancers (H3K4me1 positive and H3K27ac positive) are colored in red, poised enhancers (H3K4me1 positive and H3K27ac negative) in light gray, and inactive enhancers (H3K4me1 negative and H3K27Ac negative) in blue. (**F**) Proportions of active (red) and poised (light gray) enhancers in each of the cell types studied.

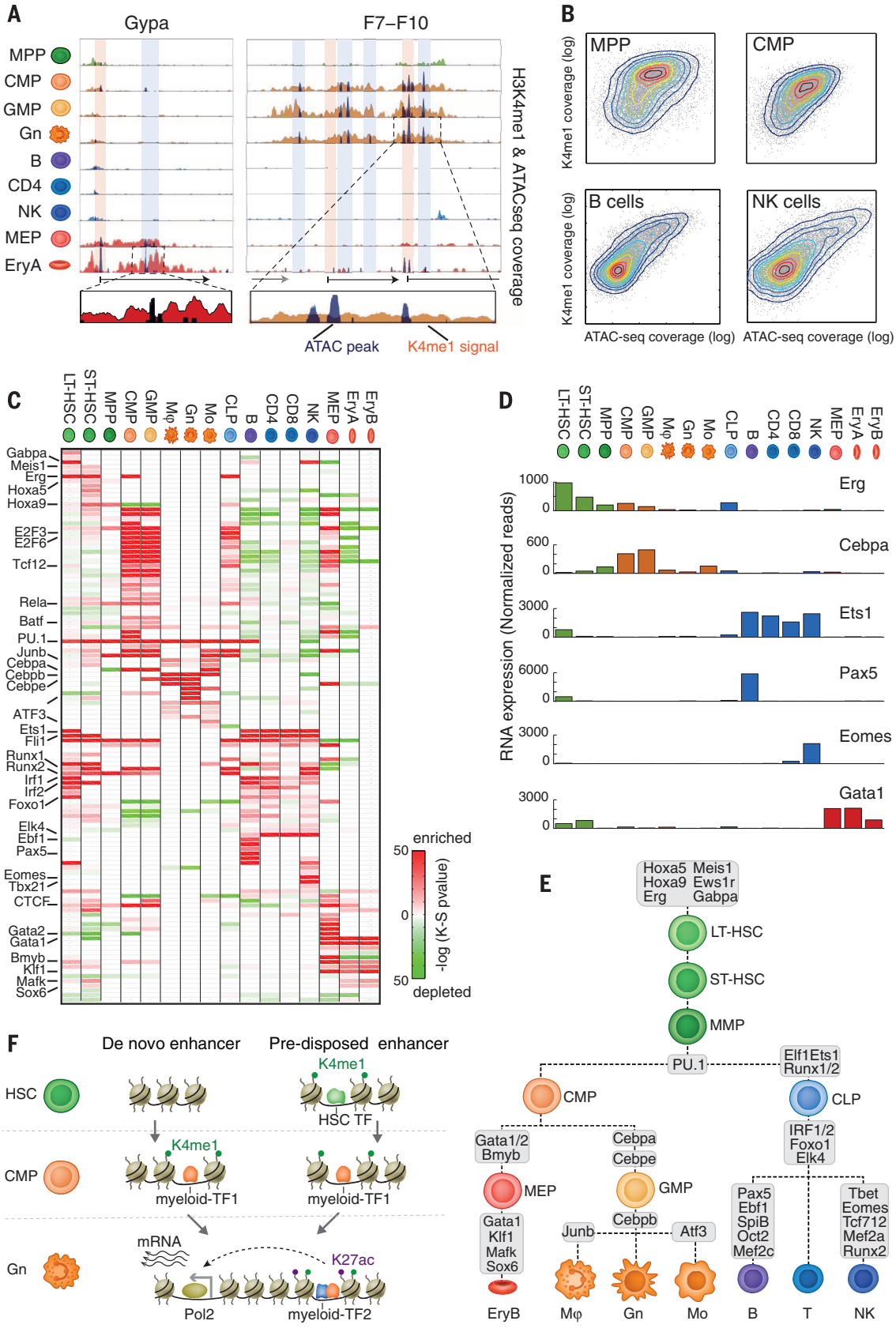

Fig. 4. Lineage-specific enhancers are associated with transcription factor cohorts. (**A**) ATAC-seq signal co-occurs temporally with H3K4me1 in lineage-specific enhancers. Shown are normalized profiles in nine hematopoietic cells for ATAC-seq (black) and H3K4me1 in erythroid-specific Gypa (red) and myeloid-specific F7-10 loci (orange). Displayed are peaks found in a 100-kb region around the gene body. Putative enhancers (K4me1) shadowed in blue; transcriptional start site shadowed in red. Enlargement of ATAC-seq peak is shown below. (**B**) Scatter plot showing correlation between H3K4me1 signal and enhancer-restricted ATAC-seq signal in four cell types: B cells, NK cells, MPPs, and CMPs (colors represent density or points). (**C**) Heat map showing the *P* values of transcription factor motif (Kolmagorov-Smirnov test) for the indicated cell-type–specific enhancers (*16*). Red indicates significant enrichment ($P < 1 \times 10^{-5}$) of motif associated to the labeled transcription factor; green indicates motif depletion ($P < 1 \times 10^{-5}$). White indicates either no significant enrichment or no RNA expression. (**D**) Bar plots showing gene expression profiles across the hematopoietic cell types for representative transcription factors [from (C)]. (**E**) Schematic of the hematopoietic tree showing the representative transcription factors regulating the lineage enhancers at each cell type as predicated by the logistic model. (**F**) Schematic of establishment of lineage-specific enhancers in the myeloid lineage by a conventional mechanism (right) as well as through transcription factor–mediated establishment of de novo enhancers (left).

enhancer similarity of CMP and GMP with the myeloid lineage (Fig. 2B). In contrast, enhancer loss is a more gradual process that initiates in the CMP or MEP stage (for myeloid and erythrocyte development, respectively) with a large proportion (40 to 50%) of enhancers lost in the last and definitive differentiation step to mature cells (fig. S6C).

Genome-wide studies show that, whereas H3K4me1 marks both poised and active enhancers, H3K27ac marks only active enhancers (*19*, *20*). Because poised enhancers represent potential gene expression programs, the ratio of these enhancers in a given cell type approximates the current regulatory potential of the cell (*20*). Analysis of the regulatory potential in hematopoiesis shows that progenitor cells are more plastic than differentiated cell types, with erythrocytes using most (78%) of their enhancers, whereas CMPs use only 33% of their enhancer potential (Fig. 3, E and F, and fig. S6D) (*16*). Within the progenitor group, CMP and GMP are more plastic than the multipotent stem cells (33 to 37% versus 62 to 65% of enhancer use), likely due to the de novo expansion of myeloid enhancers (Fig. 2B and Fig. 3, A and F). Notably, there is a wide spectrum of plasticity across the terminally differentiated cells, with the myeloid lineage (macrophages, monocytes, and granulocytes) showing higher degrees of plasticity than erythrocytes, B cells, and NK cells; this is consistent with the higher functional versatility of myeloid cells in comparison with other hematopoietic cell types (*21*).

De novo H3K4me1 establishment in hematopoiesis is concomitant to an increase in chromatin accessibility (Fig. 4, A and B). We measured chromatin accessibility, "open chromatin" (*22*), during the developmental process in 10 hematopoietic cell types using the assay for transposase-accessible chromatin followed by sequencing (ATAC-seq) (*23*). In erythroid (Gypa) and myeloid (F7 and F10) gene loci, chromatin accessibility follows the temporal pattern observed for H3K4me1 (Fig. 4A). As expected, the ATAC signal is enriched both in active promoters and H3K4me1-positive enhancers, as well as in insulators and other regulatory regions (*23*). To evaluate the proportion of de novo enhancers that also display de novo establishment of open chromatin, we plotted the ATAC-seq signal in the regions from the H3K4me1 enhancer catalog (fig. S7A). We compared the ATAC-seq signal to H3K4me1 and H3K27ac intensities. We observed a similar pattern between ATAC and H3K4me1 signal (r = 0.75) and a weakened agreement with H3K27ac (r = 0.62) (Fig. 4B and fig. S7B), suggesting that the process of gain or loss of H3K4me1 mark on enhancers occurs concomitantly with formation of open chromatin sites.

Establishment of lineage-specific enhancers is regulated by the activity of lineage-specific transcription factors (*24*) (Fig. 4, C to E). Using the ATAC peaks (*16*) and our enhancer catalog, we searched for enriched transcription factor binding motifs in each cell type (Fig. 4C and fig. S8) (*16*) to identify lineage-determining factors. We found that, in line with their identified functions, PU.1, Gata1, and Foxo1 can be classified as potential regulators of myeloid, erythroid, and lymphoid enhancers, respectively (*3*, *11*, *25*, *26*).

To systematically identify potential regulators, we generated a logistic regression model to predict enhancer activity at each stage from the DNA binding motif scores and transcription factor expression (Fig. 4, D and E, and figs. S8 to S11) (*16*). Our logistic model accurately predicts enhancer cell-type–specific activity with 75% accuracy (with 70% sensitivity and 80% specificity) (fig. S10B). Importantly, the model allowed us to elucidate the transcription factors controlling chromatin dynamics and lineage specification in hematopoiesis (*25*, *26*). Our model identified the known myeloid lineage determining factors PU.1, Cebpb, and Cebpa as regulators of myeloid enhancers; additionally, our model suggests a hierarchy between the Cebp factors, with Cebpa active in the progenitors (CMP/GMP) and Cebpb replacing Cebpa in the differentiated cell types (Fig. 4E and fig. S11C). Similarly, we identify Meis1, Hoxa9, and Erg as potential regulators of stem cell enhancers; Pax5 in B cells; Klf1 in erythroid cells; and Ets1 in lymphoid cells (Fig. 4, C to E, and fig. S11). We identify many transcription factors that have been implicated in lineage development but have not previously been associated with chromatin regulation of lineage determination, such as Irf1 and Irf2 in B cells and Cebpe in granulocytes (*27*, *28*). We also highlight new potential regulators of hematopoietic lineages: ATF3 in monocytes and Tcf7l2, Mef2a, and Runx2 in NK cells (Fig. 4E). All together, our findings show that chromatin is highly dynamic during hematopoiesis, orchestrated by a defined set of transcription factors.

In conclusion, iChIP enables the execution of reproducible and sensitive ChIP on only a few hundred cells in a manner broadly applicable across organisms and tissues. We show that poised enhancers are established in lineage progenitors before their activation and precede RNA expression in subsequent lineage differentiation. These enhancers are established concomitantly with the formation of open chromatin sites. We then show that most of the enhancer dynamics can be accounted for by the activity of known lineage-specific factors as well as new candidate regulators. These results suggest a new model for chromatin dynamics during differentiation (Fig. 4F) and show that development involves massive dynamic reorganization of the chromatin landscape. Whereas some enhancers are preset in hematopoietic stem cells, as suggested by the conventional development model, a comparable number of enhancers appear to be established de novo during hematopoiesis. We believe that the establishment of newly poised enhancers in the early lineage commitment steps initiates regulatory programs that are subsequently applied in differentiated cells, whereas the closing of enhancers occurs during later differentiation stages. This suggests that cellular enhancer potential reaches its maximum not at the HSC stage but during the oligopotent progenitor stages. Taken together, these observations reshape our understanding of the role of chromatin and pioneer factors during differentiation.

REFERENCES AND NOTES

1. L. Ho, G. R. Crabtree, *Nature* **463**, 474–484 (2010).
2. V. W. Zhou, A. Goren, B. E. Bernstein, *Nat. Rev. Genet.* **12**, 7–18 (2011).
3. S. Ghisletti *et al.*, *Immunity* **32**, 317–328 (2010).
4. E. M. Mercer *et al.*, *Immunity* **35**, 413–425 (2011).
5. G. Wei *et al.*, *Immunity* **30**, 155–167 (2009).
6. R. Revilla-i-Domingo *et al.*, *EMBO J.* **31**, 3130–3146 (2012).
7. T. S. Mikkelsen *et al.*, *Nature* **448**, 553–560 (2007).
8. J. Seita, I. L. Weissman, *Wiley Interdiscip. Rev. Syst. Biol. Med.* **2**, 640–653 (2010).
9. S. Doulatov, F. Notta, E. Laurenti, J. E. Dick, *Cell Stem Cell* **10**, 120–136 (2012).
10. A. H. Shih, O. Abdel-Wahab, J. P. Patel, R. L. Levine, *Nat. Rev. Cancer* **12**, 599–612 (2012).
11. S. Heinz *et al.*, *Mol. Cell* **38**, 576–589 (2010).
12. H. Ji *et al.*, *Nature* **467**, 338–342 (2010).
13. T. S. Furey, *Nat. Rev. Genet.* **13**, 840–852 (2012).
14. P. Shankaranarayanan *et al.*, *Nat. Methods* **8**, 565–567 (2011).
15. M. Garber *et al.*, *Mol. Cell* **47**, 810–822 (2012).
16. Materials and methods are available as supplementary materials on *Science* Online.
17. C. M. Rivera, B. Ren, *Cell* **155**, 39–55 (2013).
18. M. U. Kaikkonen *et al.*, *Mol. Cell* **51**, 310–325 (2013).
19. A. Rada-Iglesias *et al.*, *Nature* **470**, 279–283 (2011).
20. M. P. Creyghton *et al.*, *Proc. Natl. Acad. Sci. U.S.A.* **107**, 21931–21936 (2010).
21. T. A. Wynn, A. Chawla, J. W. Pollard, *Nature* **496**, 445–455 (2013).
22. R. E. Thurman *et al.*, *Nature* **489**, 75–82 (2012).
23. J. D. Buenrostro, P. G. Giresi, L. C. Zaba, H. Y. Chang, W. J. Greenleaf, *Nat. Methods* **10**, 1213–1218 (2013).
24. L. A. Cirillo *et al.*, *Mol. Cell* **9**, 279–289 (2002).
25. A. B. Cantor, S. H. Orkin, *Oncogene* **21**, 3368–3376 (2002).
26. W. Ouyang, M. O. Li, *Trends Immunol.* **32**, 26–33 (2011).
27. T. Matsuyama *et al.*, *Cell* **75**, 83–97 (1993).
28. R. Yamanaka *et al.*, *Proc. Natl. Acad. Sci. U.S.A.* **94**, 13187–13192 (1997).

ACKNOWLEDGMENTS

We thank members of the Amit and Friedman laboratories for critical discussions. We thank G. Brodsky for artwork. This work was supported by grants from the European Research Council (nos. 309788 and 340712), the Israeli Science Foundation (1782/11), the Human Frontier Science Program, Career Development Award (CDA00028/2011-c) (I.A.), a European Molecular Biology Organization Young Investigator Award (I.A.), the National Human Genome Research Institute Center for Excellence in Genome Science (1P50HG006193), and the Israeli Centers of Research Excellence (I-CORE). RNA-seq, ChIP-seq, and ATAC-seq data are deposited in the Gene Expression Omnibus under accession number GSE60103. The data can be viewed from the following Web site: http://compbio.cs.huji.ac.il/blood-chromatin/index.html. A patent application for iChIP has been filed by Yeda, Weizmann Institute of Science, Israel.

SUPPLEMENTARY MATERIALS

www.sciencemag.org/content/345/6199/943/suppl/DC1
Materials and Methods
Figs. S1 to S13
Tables S1 to S4
Reference (*29*, *30*)

19 May 2014; accepted 28 July 2014
Published online 7 August 2014;
10.1126/science.1256271

PLANT GENETICS

Early allopolyploid evolution in the post-Neolithic *Brassica napus* oilseed genome

Boulos Chalhoub,[1]*† France Denoeud,[2,3,4]* Shengyi Liu,[5]* Isobel A. P. Parkin,[6]† Haibao Tang,[7,8] Xiyin Wang,[9,10] Julien Chiquet,[11] Harry Belcram,[1] Chaobo Tong,[5] Birgit Samans,[12] Margot Corréa,[2] Corinne Da Silva,[2] Jérémy Just,[1] Cyril Falentin,[13] Chu Shin Koh,[14] Isabelle Le Clainche,[1] Maria Bernard,[2] Pascal Bento,[2] Benjamin Noel,[2] Karine Labadie,[2] Adriana Alberti,[2] Mathieu Charles,[15] Dominique Arnaud,[1] Hui Guo,[9] Christian Daviaud,[16] Salman Alamery,[17] Kamel Jabbari,[1,18] Meixia Zhao,[19] Patrick P. Edger,[20] Houda Chelaifa,[1] David Tack,[21] Gilles Lassalle,[13] Imen Mestiri,[1] Nicolas Schnel,[13] Marie-Christine Le Paslier,[15] Guangyi Fan,[22] Victor Renault,[23] Philippe E. Bayer,[17] Agnieszka A. Golicz,[17] Sahana Manoli,[17] Tae-Ho Lee,[9] Vinh Ha Dinh Thi,[1] Smahane Chalabi,[1] Qiong Hu,[5] Chuchuan Fan,[24] Reece Tollenaere,[17] Yunhai Lu,[1] Christophe Battail,[2] Jinxiong Shen,[24] Christine H. D. Sidebottom,[14] Xinfa Wang,[5] Aurélie Canaguier,[1] Aurélie Chauveau,[15] Aurélie Bérard,[15] Gwenaëlle Deniot,[13] Mei Guan,[25] Zhongsong Liu,[25] Fengming Sun,[22] Yong Pyo Lim,[26] Eric Lyons,[27] Christopher D. Town,[7] Ian Bancroft,[28] Xiaowu Wang,[29] Jinling Meng,[24] Jianxin Ma,[19] J. Chris Pires,[30] Graham J. King,[31] Dominique Brunel,[15] Régine Delourme,[13] Michel Renard,[13] Jean-Marc Aury,[2] Keith L. Adams,[21] Jacqueline Batley,[17,32] Rod J. Snowdon,[12] Jorg Tost,[16] David Edwards,[17,32]† Yongming Zhou,[24]† Wei Hua,[5]† Andrew G. Sharpe,[14]† Andrew H. Paterson,[9]† Chunyun Guan,[25]† Patrick Wincker[2,3,4]†

Oilseed rape (*Brassica napus* L.) was formed ~7500 years ago by hybridization between *B. rapa* and *B. oleracea*, followed by chromosome doubling, a process known as allopolyploidy. Together with more ancient polyploidizations, this conferred an aggregate 72× genome multiplication since the origin of angiosperms and high gene content. We examined the *B. napus* genome and the consequences of its recent duplication. The constituent A_n and C_n subgenomes are engaged in subtle structural, functional, and epigenetic cross-talk, with abundant homeologous exchanges. Incipient gene loss and expression divergence have begun. Selection in *B. napus* oilseed types has accelerated the loss of glucosinolate genes, while preserving expansion of oil biosynthesis genes. These processes provide insights into allopolyploid evolution and its relationship with crop domestication and improvement.

The Brassicaceae are a large eudicot family (*1*) and include the model plant *Arabidopsis thaliana*. Brassicas have a propensity for genome duplications (Fig. 1) and genome mergers (*2*). They are major contributors to the human diet and were among the earliest cultigens (*3*).

B. napus (genome $A_nA_nC_nC_n$) was formed by recent allopolyploidy between ancestors of *B. oleracea* (Mediterranean cabbage, genome C_oC_o) and *B. rapa* (Asian cabbage or turnip, genome A_rA_r) and is polyphyletic (*2*, *4*), with spontaneous formation regarded by Darwin as an example of unconscious selection (*5*). Cultivation began in Europe during the Middle Ages and spread worldwide. Diversifying selection gave rise to oilseed rape (canola), rutabaga, fodder rape, and kale morphotypes grown for oil, fodder, and food (*4*, *6*).

The homozygous *B. napus* genome of European winter oilseed cultivar 'Darmor-*bzh*' was assembled with long-read [>700 base pairs (bp)] 454 GS-FLX+ Titanium (Roche, Basel, Switzerland) and Sanger sequence (tables S1 to S5 and figs. S1 to S3) (*7*). Correction and gap filling used 79 Gb of Illumina (San Diego, CA) HiSeq sequence. A final assembly of 849.7 Mb was obtained with SOAP (*8*) and Newbler (Roche), with 89% nongapped sequence (tables S2 and S3). Unique mapping of ~5× nonassembled 454 sequences from *B. rapa* ('Chiifu') or *B. oleracea* ('TO1000') assigned most of the 20,702 *B. napus* scaffolds to either the A_n (8294) or the C_n (9984) subgenomes (tables S4 and S5 and fig. S3). The assembly covers ~79% of the 1130-Mb genome and includes 95.6% of *Brassica* expressed sequence tags (ESTs) (*7*). A single-nucleotide polymorphism (SNP) map (tables S6 to S9 and figs. S4 to S8) genetically anchored 712.3 Mb (84%) of the genome assembly, yielding pseudomolecules for the 19 chromosomes (table S10).

The assembled C_n subgenome (525.8 Mb) is larger than the A_n subgenome (314.2 Mb), consistent with the relative sizes of the assembled C_o genome of *B. oleracea* (540 Mb, 85% of the ~630-Mb genome) and the A_r genome of *B. rapa* (312 Mb, 59% of the ~530-Mb genome) (*9*–*11*). The *B. napus* assembly contains 34.8% transposable elements (TEs), less than the 40% estimated from raw reads (tables S11 to S14) (*7*), with asymmetric distribution in the A_n and C_n subgenomes (table S12) as in the progenitor genomes (*9*–*11*). A small TE fraction has proliferated since *B. napus* separated from its progenitors (*7*), at lower rates in the *B. napus* subgenomes than the corresponding progenitor genomes (table S14 and figs. S9 and S10).

The *B. napus* genome contains 101,040 gene models estimated from 35.5 Gb of RNA sequencing (RNA-seq) data (tables S15 and S16) in combination with ab initio gene prediction, protein and EST alignments, and transposon masking (*7*). Of these, 91,167 were confirmed by matches with *B. rapa* and/or *B. oleracea* predicted proteomes. Genes are abundant in distal euchromatin but sparse near centromeric heterochromatin (Fig. 2). RNA-seq data revealed alternative splicing in 48% of genes, with frequent intron retention (62%) and rare exon skipping (3%) (tables S17 and S18 and fig. S11).

The *B. napus* A_n and C_n subgenomes are largely colinear to the corresponding diploid A_r and C_o

[1]Institut National de Recherche Agronomique (INRA)/Université d'Evry Val d'Essone, Unité de Recherche en Génomique Végétale, UMR1165, Organization and Evolution of Plant Genomes, 2 rue Gaston Crémieux, 91057 Evry, France. [2]Commissariat à l'Energie Atomique (CEA), Institut de Génomique (IG), Genoscope, BP5706, 91057 Evry, France. [3]Université d'Evry Val d'Essone, UMR 8030, CP5706, Evry, France. [4]Centre National de Recherche Scientifique (CNRS), UMR 8030, CP5706, Evry, France. [5]Key Laboratory of Biology and Genetic Improvement of Oil Crops, Ministry of Agriculture of People's Republic of China, Oil Crops Research Institute, Chinese Academy of Agricultural Sciences, Wuhan 430062, China. [6]Agriculture and Agri-Food Canada, 107 Science Place, Saskatoon, SK S7N 0X2, Canada. [7]J. Craig Venter Institute, Rockville, MD 20850, USA. [8]Center for Genomics and Biotechnology, Fujian Agriculture and Forestry, University, Fuzhou 350002, Fujian Province, China. [9]Plant Genome Mapping Laboratory, University of Georgia, Athens, GA 30602, USA. [10]Center of Genomics and Computational Biology, School of Life Sciences, Hebei United University, Tangshan, Hebei 063000, China. [11]Laboratoire de Mathématiques et Modélisation d'Evry–UMR 8071 CNRS/Université d'Evry val d'Essonne–USC INRA, Evry, France. [12]Department of Plant Breeding, Research Center for Biosystems, Land Use and Nutrition, Justus Liebig University, Heinrich-Buff-Ring 26-32, 35392 Giessen, Germany. [13]INRA, Institut de Génétique, Environnement et Protection des Plantes (IGEPP) UMR1349, BP35327, 35653 Le Rheu Cedex, France. [14]National Research Council Canada, 110 Gymnasium Place, Saskatoon, SK S7N 0W9, Canada. [15]INRA, Etude du Polymorphisme des Génomes Végétaux, US1279, Centre National de Génotypage, CEA–IG, 2 rue Gaston Crémieux, 91057 Evry, France. [16]Laboratory for Epigenetics and Environment, Centre National de Génotypage, CEA–IG, 2 rue Gaston Crémieux, 91000 Evry, France. [17]Australian Centre for Plant Functional Genomics, School of Agriculture and Food Sciences, University of Queensland, St. Lucia, QLD 4072, Australia. [18]Cologne Center for Genomics, University of Cologne, Weyertal 115b, 50931 Köln, Germany. [19]Department of Agronomy, Purdue University, WSLR Building B018, West Lafayette, IN 47907, USA. [20]Department of Plant and Microbial Biology, University of California, Berkeley, CA 94720, USA. [21]Department of Botany, University of British Columbia, Vancouver, BC, Canada. [22]Beijing Genome Institute–Shenzhen, Shenzhen 518083, China. [23]Fondation Jean Dausset–Centre d'Étude du Polymorphisme Humain, 27 rue Juliette Dodu, 75010 Paris, France. [24]National Key Laboratory of Crop Genetic Improvement, Huazhong Agricultural University, Wuhan 430070, China. [25]College of Agronomy, Hunan Agricultural University, Changsha 410128, China. [26]Molecular Genetics and Genomics Laboratory, Department of Horticulture, Chungnam National University, Daejeon-305764, South Korea. [27]School of Plant Sciences, iPlant Collaborative, University of Arizona, Tucson, AZ, USA. [28]Department of Biology, University of York, Wentworth Way, Heslington, York YO10 5DD, UK. [29]Institute of Vegetables and Flowers, Chinese Academy of Agricultural Sciences, Beijing, China. [30]Division of Biological Sciences, University of Missouri, Columbia, MO 65211, USA. [31]Southern Cross Plant Science, Southern Cross University, Lismore, NSW 2480, Australia. [32]School of Plant Biology, University of Western Australia, WA 6009, Australia.

*These authors contributed equally to this work. **†Corresponding author. E-mail: chalhoub@evry.inra.fr (B.C.); other e-mail addressees are given in the supplementary materials.**

genomes, with asymmetric gene distribution (42,320 and 48,847, respectively) and 93% of the diploid gene space in orthologous blocks (fig. S12) (*7*). We identified 34,255 and 38,661 orthologous gene pairs between the A_n and C_n subgenomes and their respective progenitor genomes (fig. S13). Comparison of A_n-A_r and C_n-C_o orthologous gene pairs suggested a divergence 7500 to 12,500 years ago (fig. S14), indicating formation of *B. napus* after this date. Synteny with *Arabidopsis* (table S19) confirmed the triplicated mesoploid structure (*9*–*11*) of the A_n and C_n subgenomes, with the recent allopolyploidy conferring on *B. napus* an aggregate 72× genome multiplication since the origin of angiosperms (Fig. 1) (*7*).

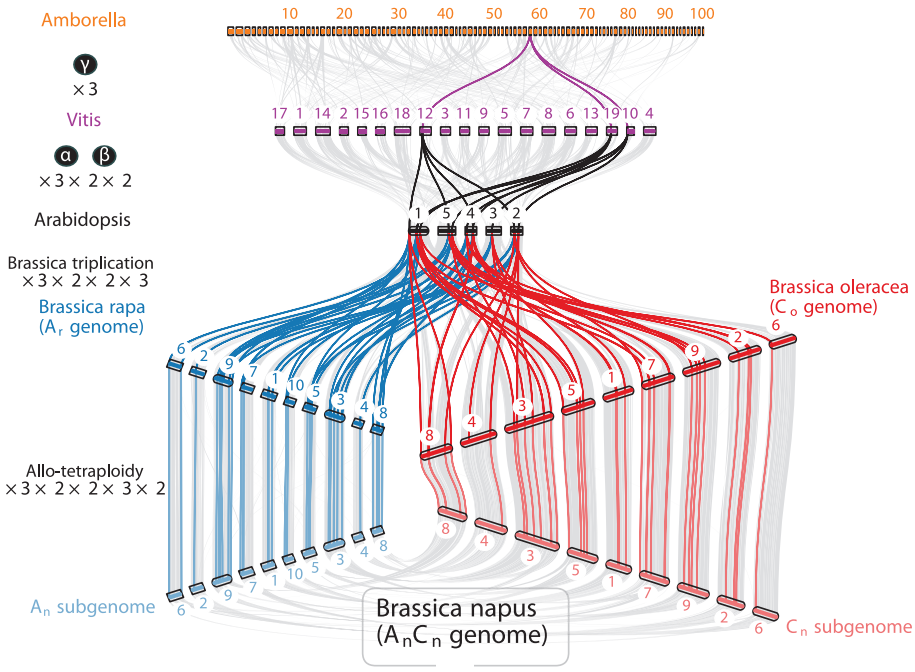

Fig. 1. Recurrent genome duplications in *B. napus*. Genomic alignments between the basal angiosperm *Amborella trichopoda* (*24*), the basal eudicot *Vitis vinifera* (*25*), and the model crucifer *A. thaliana*, as well as *B. rapa* (*9*), *B. oleracea* (*10*, *11*), and *B. napus*, are shown. A typical ancestral region in *Amborella* is expected to match up to 72 regions in *B. napus* (69 were detected for this specific region). Gray wedges in the background highlight conserved synteny blocks with more than 10 gene pairs.

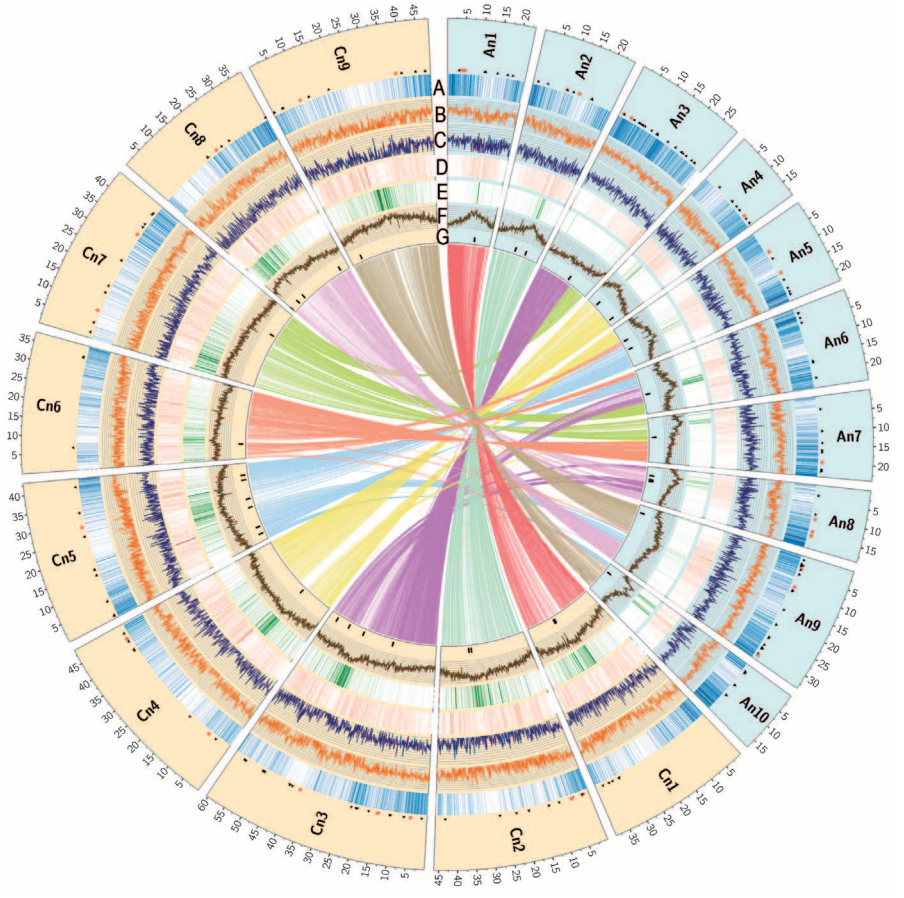

Fig. 2. The genome of the *B. napus* oilseed cultivar 'Darmor-*bzh*'. The genome comprises 9 chromosomes belonging to the C_n subgenome and 10 to the A_n subgenome, scaled on the basis of their assembled lengths. Tracks displayed are (**A**) gene density (nonoverlapping, window size = 100 kb for all tracks). Positions showing loss of one or more consecutive genes are displayed (triangles) along with homeologous exchanges, detected as missing genomic segments that have been replaced by duplicates of corresponding homeologous segments (red rectangles). (**B** and **C**) Transcription states estimated by RNA-seq in leaves (B) and roots (C) (in nonoverlapping 100-kb windows). (**D**) DNA transposon density. (**E**) Retrotransposon density. (**F**) CpG methylation in leaves (green) and roots (brown); both curves are overlapping. (**G**) Centromeric repeats (densities exaggerated for visual clarity). Homeologous relationships between A_n and C_n chromosomes are displayed with connecting lines colored according to the C_n chromosomes.

Most orthologous gene pairs in *B. rapa* and *B. oleracea* remain as homeologous pairs in *B. napus* (tables S19 to S25 and figs. S12 to S17) (*7*). DNA sequence analysis (*7*) confirmed the loss of 112 A_n and 91 C_n genes in *B. napus* 'Darmor-*bzh*' (tables S21 to S26), ~2.6 times higher than the 41 and 37 genes lost in *B. rapa* 'Chiifu' and *B. oleracea* 'TO1000' respectively (tables S26 and S27; χ^2 test $P = 5.3 \times 10^{-14}$). Further analyses of a *Brassica* diversity set showed that ~47% of Darmor-*bzh* A_n and 31% of C_n deleted genes were also deleted in at least one additional progenitor genotype (tables S28 and S29), indicating that their deletion probably predated allopolyploidization of *B. napus* (*7*). A high proportion (27% to 54%) of the remaining Darmor-*bzh* deleted genes were also deleted from diverse *B. napus* genotypes (tables S28 and S29).

Homeologous exchanges (HEs), including crossovers and noncrossovers, are frequent between *B. napus* subgenomes and range in size from large segments to single SNPs (*7*) (Fig. 3, figs. S17 to S24, and tables S30 to S39).

At the chromosome segment level, HEs are characterized by replacement of a chromosomal region with a duplicated copy from the corresponding homeologous subgenome (*7*). We identified 17 HEs, 14 C_n to A_n and 3 A_n to C_n (Fig. 3, fig. S19, and tables S30 and S31). Sequences from seven diverse *B. napus* genotypes revealed both shared and specific segmental HEs. These are of varying sizes and are most frequent between chromosomes A_n1-C_n1, A_n2-C_n2, and A_n9-C_n9 (table S32, Fig. 3, and fig. S19). Larger HEs found in the synthetic *B. napus* H165 affect, for example, most of chromosomes A_n1-C_n1 and A_n2-C_n2 (Fig. 3 and fig. S19). Functional annotation of genes within HEs suggests some have experienced selection, contributing to the

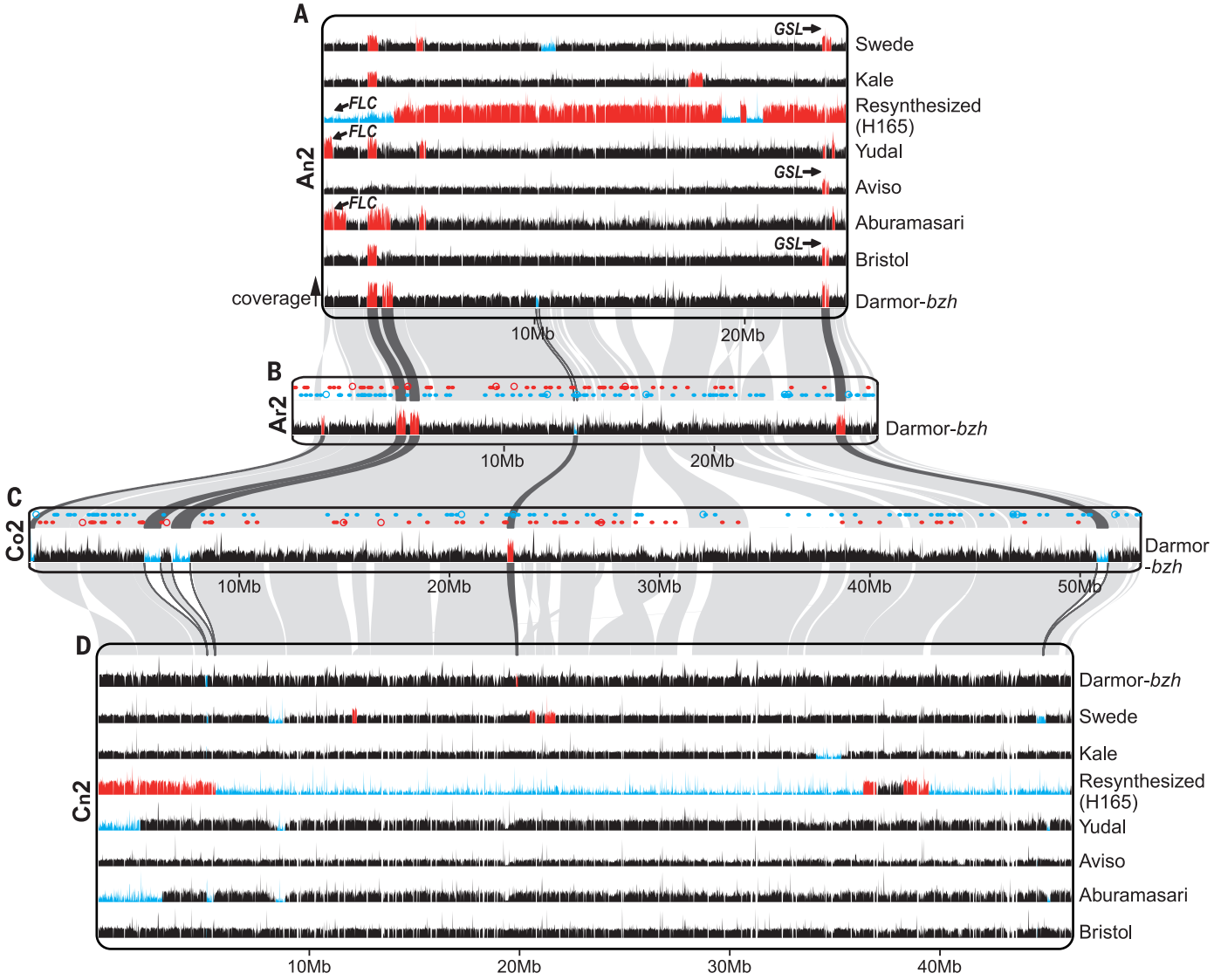

Fig. 3. HEs between *B. napus* chromosomes A_n2 and C_n2. (**A**) Coverage depth obtained along the A_n2 chromosome after mapping Illumina sequence reads from seven natural and one resynthesized *B. napus* genotypes (named on the right) to the reference genome of *B. napus* 'Darmor-*bzh*.' (**B** and **C**) Coverage depth obtained for A_r2 and C_o2 chromosomes, respectively, after mapping >21 genome-equivalents of Illumina sequence reads from *B. napus* Darmor-*bzh* on the *B. rapa* and *B. oleracea* genome assemblies concatenated together. (**D**) Similar to (A), where the C_n2 chromosome of Darmor-*bzh* is displayed. Segmental HEs are revealed based on sequence read coverage analysis, where a duplication (red) is revealed by significantly greater coverage for a given segment than the rest of the genome (black) and a deletion (blue) by little or no coverage for the corresponding homeologous segment. Sizes of chromosomes are indicated in Mb. A_n-to-C_n converted genes (at 60% or more conversion sites) are plotted as blue dots on A_r2 (B) and red dots on C_o2 (C). C_n-to-A_n converted genes are plotted as blue dots on C_o2 (C) and red dots on A_r2 (B). Open circles denote entirely converted genes using the same color code. Light gray lines connecting (A), (B), (C), and (D) indicate orthology relationships, and dark gray lines highlight segmental HEs in Darmor-*bzh* (names and descriptions detailed in table S31). Further HEs occurring between other homeologous chromosomes are shown in fig. S19. Black arrows in (A) indicate HEs involving *GSL* and *FLC* genes.

diversification of winter, spring, and Asian types of oilseed rape, rutabaga, and kale vegetables (Fig. 3B, fig. S19, and table S33).

We also identified 37 C_n to A_n and 56 A_n to C_n whole-gene conversions (*12*) (table S34).

At the single-nucleotide scale, exchanges between homeologous subgenomes account for ~86% of allelic differences between *B. napus* and its progenitors, with nearly ~1.3 times more conversions from the A_n to the C_n subgenome than the reverse (χ^2, $P < 1.6 \times 10^{-16}$) (tables S35 and S36). A total of 16,938 A_n and 13,429 C_n genes (with 10,258 from homeologous pairs) had at least two conversion sites (table S37); 842 A_n and 579 C_n genes were highly converted with 60 to 90% conversion sites (table S37).

Transcript abundance indicated that 96% of genes are expressed in leaves, roots, or both (*7*) (figs. S25 to S29 and tables S40 to S42). Subgenome and tissue effects and tissue-by-subgenome interactions were statistically significant (χ^2, $P < 0.01$), with 45 expression patterns (fig. S26) grouping into nine clusters (table S41).

A_n and C_n homeologs contributed similarly to gene expression for 17,326 (58.3%) gene pairs (χ^2, $P < 0.01$) (fig. S27 and table S41). Both tissues showed higher expression for 4665 (15.7%) A_n homeologs and 5437 (17.3%) C_n homeologs (fig. S28 and table S41). There were 1062 gene pairs (3.7%) with higher expression of the A_n homeolog over the C_n homeolog in leaves, whereas the reverse was true in roots (fig. S28 and table S41). Conversly, for 966 gene pairs (3.3%), A_n homeologs had lower expression than C_n homeologs in leaves, with the pattern inverted in roots (fig. S28 and table S41).

Gene expression is generally inversely related to CpG, CHG, and CHH cytosine DNA methylation levels (p is phosphate, implying a C is directly followed by a G, and H is A, C, or T) (*7*). Methyl bisulfite sequencing in Darmor-*bzh* (figs. S30 to S32 and tables S43 to S45) showed 4 to 8% higher methylation in C_n genes than in their homoelogous A_n genes (table S44), possibly because of greater transposon density in the C_n subgenome (Fig. 2F). Of the ~3100 gene pairs with differential gene body and/or untranslated region methylation between A_n and C_n homeologs in both roots and leaves, 51% were equally expressed. Only ~34% showed higher expression for the less-methylated homeologs, and the remaining ~15% showed the opposite pattern (table S45).

It is interesting that partitioning of homeolog gene expression is largely established in *B. napus* with patterns of both genome dominance and genome equivalence. The absence of significant bias toward either subgenome of the recent *B. napus* allopolyploid contrasts with many old and recent polyploids (*13*–*17*) but concurs with other old polyploids (*18*).

Oilseed *B. napus* has undergone intensive breeding to optimize seed oil content and lipid composition, decrease nutritionally undesirable erucic acid and glucosinolates (GSLs), optimize flowering behavior, and improve pathogen resistance.

The expansion of *B. napus* lipid biosynthesis genes exceeds that known in other oilseed plants, with 1097 and 1132 genes annotated in the A_n and C_n subgenomes, respectively (*7*) (tables S46 to S48). Most lipid biosynthesis genes identified in the progenitor genomes are conserved in *B. napus*. For 18 acyl lipid orthologs, 3 and 2 genes appeared to be deleted from A_n and C_n subgenomes, respectively. Another 13 have been converted by HEs, nine from A_n to C_n and four from C_n to A_n (tables S47 and S48) (*7*).

Genetic variation for reduced seed GSLs also appears to be under breeding-directed selection. GSLs are sulfur-rich secondary metabolites important for plant defense and human health (*19*); however, high levels in seeds form toxic breakdown products in animal feeds (*20*). All 22 GSL catabolism genes identified in *B. rapa* and *B. oleracea* (*10*) are conserved in *B. napus* (*7*), and orthologs of only three C_o and one A_r GSL biosynthesis genes are missing (table S49). One deleted homeologous pair, corresponding to orthologs of *B. oleracea Bo2g161590* and *B. rapa Bra02931*, colocates with two quantitative trait loci (QTLs) for total aliphatic GSL content (*21*) and corresponds to a HE in which a segment of A_n2, with a missing GSL gene, has replaced the C_n2 homeolog (Fig. 3). Two additional QTLs for aliphatic GSL content (*21*) colocalize with a deletion of the *B. rapa Bra035929* ortholog on A_n9 and its nondeleted homeolog on C_n9 (*BnaC09g05300D*, fig. S17).

We identified 425 nucleotide binding site leucine-rich repeat (NBS-LRR) sequences encoding resistance gene homologs (245 on C_n and 180 on A_n). Of these, 75% (153 A_n and 224 C_n) are syntenic to A_r and C_o progenitors (*7*) (table S50 and figs. S33 and S34). We confirmed the absence of five NBS-LRR genes from the A_n subgenome, three from the C_n subgenome, and three from *B. rapa* (A_r), with none absent from *B. oleracea* C_o. This variation may reflect differential selection for resistance to diseases.

B. napus morphotypes show broad adaptation to different climatic zones and latitudes. A key adaptive gene controlling vernalization and photoperiod responses, *FLOWERING LOCUS C* (*FLC*) is expanded from one copy in *A. thaliana* to four in *B. rapa* and *B. oleracea* and nine or more in *B. napus* (*7*) (table S51). Different *FLC* homologs lie within HEs, from C_n2 to A_n2 in the Asian semiwinter oilseed forms Yudal and Aburamasari (Fig. 3) and C_n9 to A_n10 in late-flowering swedes (fig. S19 and table S51). These loci correspond to important QTLs for vernalization requirement and flowering time (*22*).

Human cultivation and breeding of *B. napus* morphotypes may have selected favorable HEs, causing subgenome restructuring of regions containing genes controlling valuable agronomic traits such as those shown here for oil biosynthesis, seed GSL content, disease resistance, and flowering. Because *B. napus* is a young allopolyploid beginning gene loss and genome reorganization, further partitioning of expression may become a key determinant for the long-term preservation of its duplicated genes (*23*). The integrative genomic resources that we report provide unique perspectives on the early evolution of a domesticated polyploid and will facilitate the manipulation of useful variation, contributing to sustainable increases in oilseed crop production to meet growing demands for both edible and biofuel oils.

REFERENCES AND NOTES

1. I. Al-Shehbaz, *Taxon* **61**, 931 (2012).
2. U. Nagaharu, *Jpn. J. Bot.* **7**, 389 (1935).
3. S. Prakash, in Brassica *Crops and Wild Allies: Biology and Breeding*, S. Tsunoda, K. Hinata, C. Gomez-Campo, Eds. (Japan Scientific Society Press, Tokyo, 1980), pp. 151–163.
4. C. J. Allender, G. J. King, *BMC Plant Biol.* **10**, 54 (2010).
5. C. Darwin, *The Variation of Animals and Plants Under Domestication* (Murray, London, 1905), vol. 2, pp. 398–403.
6. H. L. Liu, *Rapeseed Genetics and Breeding* (China Agricultural University, Beijing, 2000), pp. 1–81.
7. Supplementary materials for this article are available on *Science* Online.
8. R. Li, Y. Li, K. Kristiansen, J. Wang, *Bioinformatics* **24**, 713–714 (2008).
9. X. Wang *et al*., *Nat. Genet.* **43**, 1035–1039 (2011).
10. S. Liu *et al*., *Nat. Commun.* **5**, 3930 (2014).
11. I. A. Parkin *et al*., *Genome Biol.* **15**, R77 (2014).
12. A. H. Paterson *et al*., *Nature* **492**, 423–427 (2012).
13. J. C. Schnable, N. M. Springer, M. Freeling, *Proc. Natl. Acad. Sci. U.S.A.* **108**, 4069–4074 (2011).
14. H. Tang *et al*., *Genetics* **190**, 1563–1574 (2012).
15. M. J. Yoo, E. Szadkowski, J. F. Wendel, *Heredity* **110**, 171–180 (2013).
16. D. C. Ilut *et al*., *Am. J. Bot.* **99**, 383–396 (2012).
17. R. J. Buggs *et al*., *Curr. Biol.* **21**, 551–556 (2011).
18. O. Garsmeur *et al*., *Mol. Biol. Evol.* **31**, 448–454 (2014).
19. I. E. Sønderby, F. Geu-Flores, B. A. Halkier, *Trends Plant Sci.* **15**, 283–290 (2010).
20. B. Wittkop, R. J. Snowdon, W. Friedt, *Euphytica* **170**, 131–140 (2009).
21. R. Delourme *et al*., *BMC Genomics* **14**, 120 (2013).
22. X. Zou *et al*., *PLOS ONE* **7**, e45751 (2012).
23. M. Lynch, A. Force, *Genetics* **154**, 459–473 (2000).
24. A. G. Sharpe, D. J. Lydiate, *Genome* **46**, 461–468 (2003).
25. N. Foisset, R. Delourme, P. Barret, M. Renard, *Theor. Appl. Genet.* **91**, 756–761 (1995).

ACKNOWLEDGMENTS

Sequence Read Archive accession numbers of *B. napus* sequencing data are ERP005275 and PRJEB6069, and those of *B. rapa* and *B. oleracea* data are PRJNA248388 and PRJNA158027. The *B. napus* assembly is available at ENA (European Nucleotide Archive), in the WGS section for contigs (accession numbers CCCW010000001 to CCCW010044187) and the CON section for scaffolds, chromosomes, and annotation (accession numbers LK031787 to LK052685). The *B. napus* genome is also available at CoGe (https://genomevolution.org/CoGe/) and at (www.genoscope.cns.fr/brassicanapus) the Genoscope Genome Database, with additional tools for comparative genomic analysis. The *B. napus* segregating populations Darmor-*bzh* × Yudal and Darmor × Bristol are available at INRA-IGEPP, Rennes, France, under a material transfer agreement. This project was funded by the French ANR (Agence Nationale de la Recherche, www.agence-nationale-recherche.fr) 2009 (ANR-09-GENM-021) to B.C., P.W., D.B., and R.D., with additional funding from Sofi-Proteol for bioinformatic personnnel (J.J.); the National Basic Research Program of China (2011CB109300) for S.L., Y.Z., C.G., and W.H.; and the Canadian Canola Genome Sequencing Initiative (http://aafc-aac.usask.ca/canseq/, Genome Alberta, and industry partners) for I.A.P.P., A.G.S., C.K., and C.S. Research leaders are B.C., S.L., I.A.P.P., X.W., I.B., R.D., J.B., D.E., Y.Z., W.H., A.G.S., A.H.P., C.G., and P.W. Additional acknowledgements and author contributions are included in the supplementary materials.

SUPPLEMENTARY MATERIALS

www.sciencemag.org/content/345/6199/950/suppl/DC1
Materials and Methods
Supplementary Text
Figs. S1 to S34
Tables S1 to S51
References (*26*–*145*)

17 March 2014; accepted 29 July 2014
10.1126/science.1253435

Ultralow Adhesion Plates

Lipidure-Coat low adhesion plates and dishes are shown in cited research to be one of the most effective tools for state-of-the-art 3-D spheroid cell culture. These new plates and dishes are available in 384-well format optimized for drug screening or other high throughput applications. Spheroid cell culture is based on the spontaneous formation of an aggregation of cells in an environment where the interactions between cells are superior to the interactions between cells and substrate. This can be achieved by using low-adhesion cell culture conditions. Lipidure-Coat surfaces use MPC (2-methacryloyloxtethyl phosphorylcholine), a biocompatible synthetic polymer with the same structure as the phosphorylcholine polar bases that form cell membranes. As a consequence of the high biocompatibility of this coating, cells will not adhere to the surface of Lipidure-Coat plates or dishes. Different well shapes available for 96-well plates (U, V, and flat-bottom) can be used to control size, position, and density of spheroids.

AMS Biotechnology
For info: +44-(0)-1235-828200
www.amsbio.com/lipidure-coat.aspx

Sample Automation System

The new sample automation system for the minispec mq and mq-one series is a new, easy to use, and cost-effective system that brings sample automation to routine time-domain nuclear magnatic resonance (TD-NMR) applications. Its fast sample exchange of 10 mm OD sample tubes delivers new levels of maximum throughput and thanks to automated and precise tempering times measurement reliability is improved, significantly boosting productivity of the minispec series. Complex solid fat content (SFC) analysis, one of the major minispec applications, now benefits from highly accurate sample temperatures, delivering results in strictest accordance with SFC International Standard Methods. The minispec sample automation system is available as a standalone accessory to existing minispec systems from the mq and mq-one Series, or as a packaged system with a new minispec spectrometer. The sample automation setup includes an x-y-z sample changer mounted on a robust platform that holds the minispec system, racks, tempering devices, and balance securely in one place.

Bruker Corporation
For info: +49-721-5161-6500
www.bruker.com/minispec-automation

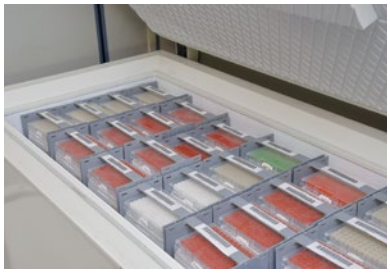

Modular Chest Freezer Rack

The Modular Freezer Rack provides a flexible and low cost solution for organizing sample storage in a chest freezer. The lightweight modular storage system fits into all chest freezers and is fully compatible with all ANSI/SLAS standard footprint storage racks. To set up the easy-to-use modular system simply click individual rack holders (height: 68 mm) together to construct a tower of up to 15 holders. Each rack holder has the capacity to house a single storage rack (Roborack-96, Comorack-96, Comorack-24, and Arctic Rack-24). When using the Micronic Loborack-96 with a low profile cover, one rack holder accommodates two Loboracks, providing a space saving storage solution. Manufactured from a special durable high grade plastic, Micronic Modular Vertical Freezer Racks are ideally constructed for long-term storage at ultralow temperatures. In addition to offering lower ongoing energy consumption, chest freezers typically tend to have longer life cycles than upright models.

Micronic
For info: +31-320-277070
www.micronic.com

Spectrometer

The new Ultima Expert ICP-OES Spectrometer combines ease of use, a unique plasma torch design, comprehensive tools, highest resolution, lowest detection limits, and full wavelength coverage optics for the most challenging applications. Ultima Expert is designed with a unique plasma torch that offers a radial viewing mode far superior to competitive systems, thanks to the measurement of the entire normal analytical zone. The vertical torch, the original sheath gas device and the wide injector make the Ultima Expert more tolerant to difficult matrices, and offer the benefits of robust operation with minimal maintenance. High resolution and excellent sensitivity allow elements with high, low, and trace concentrations to be measured accurately. Ultima Expert delivers the highest resolution with less than 5 pm for the ultraviolet range and less than 10 pm for the visible range, all due to its unique optical design which integrates a high density holographic grating and one meter focal length optics.

Horiba Scientific
For info: 732-623-8142
www.horiba.com/scientific

DMSO Solutions

Two new reagent solutions expand the volume range measurable with the line of DMSO (dimethyl sulfoxide) products. For use with the MVS Multichannel Verification System and Liquid Handler Performance Verification Service, these reagents enable users to accurately calibrate and verify their liquid handlers when dispensing DMSO-based solutions. DMSO is a solvent widely used for storage and transfer of small-molecule compounds during high-throughput screening campaigns in drug discovery. Because of its unique physical properties DMSO behaves differently than water when handled by air-displacement pipettors and acoustic droplet ejectors. The Artel reagents now cover all volumes less than 10 µL, enabling DMSO solvent-specific volume verification in a real-world setting. The MVS is an easy-to-use, universal system that verifies the volume-transfer performance of automated liquid handling systems and multichannel handheld pipettes. The MVS consists of equipment, software, sample solutions, and highly characterized microtiter plates.

Artel
For info: 888-406-3463
www.artel-usa.com

Electronically submit your new product description or product literature information! Go to www.sciencemag.org/products/newproducts.dtl for more information.

Newly offered instrumentation, apparatus, and laboratory materials of interest to researchers in all disciplines in academic, industrial, and governmental organizations are featured in this space. Emphasis is given to purpose, chief characteristics, and availability of products and materials. Endorsement by *Science* or AAAS of any products or materials mentioned is not implied. Additional information may be obtained from the manufacturer or supplier.

Downloaded from www.sciencemag.org on August 24, 2014

Science Careers Advertising

For full advertising details, go to ScienceCareers.org and click For Employers, or call one of our representatives.

Tracy Holmes
Worldwide Associate Director
Science Careers
Phone: +44 (0) 1223 326525

THE AMERICAS
E-mail: advertise@sciencecareers.org
Fax: 202-289-6742

Tina Burks
Phone: 202-326-6577

Nancy Toema
Phone: 202-326-6578

Marci Gallun
Sales Administrator
Phone: 202-326-6582

Online Job Posting Questions
Phone: 202-312-6375

EUROPE / JAPAN / INDIA / AUSTRALIA / NEW ZEALAND / REST OF WORLD
E-mail: ads@science-int.co.uk
Fax: +44 (0) 1223 326532

Axel Gesatzki
Phone: +44 (0)1223 326529

Sarah Lelarge
Phone: +44 (0) 1223 326527

Kelly Grace
Phone: +44 (0) 1223 326528

CHINA / KOREA / SINGAPORE / TAIWAN / THAILAND
Ruolei Wu
Phone: +86-186-0082-9345
E-mail: rwu@aaas.org

All ads submitted for publication must comply with applicable U.S. and non-U.S. laws. *Science* reserves the right to refuse any advertisement at its sole discretion for any reason, including without limitation for offensive language or inappropriate content, and all advertising is subject to publisher approval. *Science* encourages our readers to alert us to any ads that they feel may be discriminatory or offensive.

Science Careers
From the Journal Science AAAS

ScienceCareers.org

POSITIONS OPEN

ASU Arizona State University

POSTDOCTORAL SCHOLARS and Early Career Tenure Track Program Arizona State University Bisgrove

Arizona State University Graduate Education is now accepting applications for the Bisgrove Postdoctoral and Early Career Tenure Track Program. The award (sponsored by Science Foundation Arizona) is designed to attract the nation's best early career scientists and engineers who exhibit the potential for outstanding competence and creativity in their research areas, strong communication skills, a passion for communicating the importance of their research to society, and a keen interest in educational outreach to the community. *Individuals eligible to apply are U.S. citizens or permanent residents of the U.S.* Applicants should demonstrate research training and potential to transform ideas into value for society and the interest to work at the convergence of several disciplines. For application and submission procedures, go to website: http://graduate.asu.edu/bisgrove.

Alexander von Humboldt Stiftung/Foundation

CONDUCT YOUR RESEARCH IN GERMANY!

The Alexander von Humboldt Foundation funds **POSTDOCTORAL** and experienced researchers to spend 6–24 months in Germany on a research project of their creation. Funding for junior research group leaders available as well.

Apply for the Humboldt Research Fellowship or the Sofja Kovalevskaja Award!

Website: http://www.humboldt-foundation.de/web/home.html.

POSTDOCTORAL POSITION
Bacterial Gene Regulation and Lyme Disease Pathogenesis

A postdoctoral position is available to study virulence gene regulation in *Borrelia burgdorferi*, the Lyme disease spirochete. Studies will focus on the RpoN (Sigma54)-RpoS alternative sigma factor regulatory cascade and, in particular, the role of BosR as an accessory molecule for pathway activation (see: Z. Ouyang *et al.*, "BosR [BB0647] controls the RpoN-RpoS regulatory pathway and virulence expression in Borrelia burgdorferi by a novel DNA-binding mechanism" *PLOS Pathogens* 7:e1001272 [2010]). The position offers the opportunity to conduct research in an attractive, dynamic research environment with outstanding resources. Candidates should have a Ph.D. with a background in bacterial genetics, gene regulation, bacterial pathogenesis, and molecular biology. Experience in spirochetology, animal models, and/or tick biology is a plus. Please send curriculum vitae and three letters of recommendation to: **Dr. Michael V. Norgard, Chair, Department of Microbiology, University of Texas Southwestern Medical Center, 6000 Harry Hines Boulevard, Dallas, TX 75390-9048** (**e-mail: michael.norgard@utsouthwestern.edu**). *University of Texas Southwestern Medical Center is an Equal Opportunity Institution.*

POSITIONS OPEN

Harvard Medical School

OPPORTUNITIES FOR INFORMATICS RESEARCH at Harvard Medical School

The Biomedical Informatics Research Training (BIRT) Program is a consortium of leading informatics laboratories at Harvard. It is supported by a grant from the National Library of Medicine, National Institutes of Health. For United States citizens and permanent residents, this **POSTDOCTORAL FELLOWSHIP** provides stipend, tuition, and travel funds. Selected fellows are provided with many opportunities for training, research, interaction, and collaboration. All fellows also pursue the two-year Harvard Medical School Biomedical Informatics MMSc.

The MMSc is a postdoctoral degree program that consists of course work and mentored research. Fellows in our program choose from one of four possible tracks: Bioinformatics, Clinical Informatics, Imaging Informatics, and Population Health Informatics.

To learn more, visit **website: http://informaticstraining.hms.harvard.edu/.**

In addition to the BIRT program, the Center for Biomedical Informatics (CBMI) offers a number of other training and research opportunities.

For more information about our programs, contact **Aimee Doe,** Program Coordinator, at **e-mail: aimee_doe@hms.harvard.edu.**

Your career is our cause.

Get help from the experts.

www.sciencecareers.org

- Job Postings
- Job Alerts
- Resume/CV Database
- Career Advice
- Career Forum

Science Careers
From the journal *Science* AAAS

Get your questions answered.
Careers Forum
www.ScienceCareers.org

The Transferrable Postdoc

Now more than ever, experts say, postdoctoral fellows need to cultivate a broad base of beyond-the-bench skills and capitalize on transferring them to the next stage of their career to be as competitive as possible. In today's competitive job market, it is vitally important for postdocs to accumulate skill sets on their CVs right alongside their publications—whether their next career move is research-based or not. Postdocs who repurpose their lab leadership and project management skills into star candidate qualities have an advantage when looking to step into their next position. By Kendall Powell

When an infectious disease fellowship at the Centers for Disease Control and Prevention in Atlanta turned out to be a poor fit for **Melissa Ramirez,** she moved on to other postdoctoral opportunities where she picked up skills in grant writing, student mentoring, and teaching. Her last stop was as a postdoctoral teaching scholar at North Carolina State University in Raleigh, where she was immersed in teaching and curriculum development for the campus's undergraduate microbiology students.

At each stage of postdoctoral development, Ramirez gained valuable skills that have now successfully translated into a new career as a teaching assistant professor at NC State.

Her success was not a given, but came after several years of gathering broad expertise across areas and matching those skills to her interests. Ramirez' approach should make her postdoctoral colleagues sit up and take note—no matter which direction they take next, it's a tough job market out there. Almost every sector of the science and technical labor market has tightened since the Great Recession began in 2008.

"It's very hard to find research positions, in general," says **Paula Stephan,** professor of economics at Georgia State University in Atlanta and a research associate at the National Bureau of Economic Research. "Postdocs, for the last couple of years, have had particular difficulty because of a soft economy."

Universities in both the United States and Europe are hiring more contract-based faculty or faculty in tenure-track positions that have no salary guarantee and require outside grant funding. Stephan notes that a combination of factors have hit biomedical job candidates especially hard, including the flattening of the U.S. National Institutes of Health budget and the consolidation, downsizing, and off-shoring of jobs among pharmaceutical firms. Some of the largest chemistry labs in the United States, such as DuPont, are also downsizing. "Once we get updated data from the Survey of Earned Doctorates and Survey of Doctorate Recipients, I think we'll see that industry is hiring fewer Ph.D.s for research positions as well."

Compounding the problem is the expectation gap that exists among the roughly 56% of postdocs who believe they will continue on to tenure-track academic positions and the 21% who actually did in 2012 (scim.ag/XWZwhv). In addition, the definition of a successful academic job candidate has also shifted in the last decade. Beyond stellar research and publication records, faculty candidates must also collaborate across disciplines and the globe, and have a sharp talent for fundraising.

Although this might all seem bleak, Doctorate-holding scientists are highly employable in many arenas. While postdocs tend to put their heads down and toil to collect data, Stephan and others urge them to periodically step away from their research to make sure they collect transferrable skills, too.

"Actually many of the skills we need for academic careers are the same for non-academic careers," says **David Bogle,** chemical engineer and pro-provost of the Doctoral School at University College London. Strengths in analytical thinking, problem solving, written and oral communication, and collaboration make postdocs universally attractive. "No employer wants somebody that is narrow-minded" or too narrowly focused, say Bogle.

Got skills?

A variety of self-assessment resources can help postdocs track their progress. "Young scientists need to periodically sit back and think, what skills do I have? What skills do I need for my project? And what am I lacking?" says Bogle.

He recommends the Researcher Development Framework created by Vitae (scim.ag/1IVhLtb), a career development organization based in Cambridge, United Kingdom. continued>

PHOTOS (FROM TOP): BPLANET/SHUTTERSTOCK.COM; MEG BUSCEMA

Paula Stephan urges postdocs to periodically step away from their research to make sure they collect transferrable skills, too.

Upcoming Features

Faculty: Professionalism 1—Sept. 12 ■ *Faculty: Professionalism 2—Oct. 3* ■ *Top Employers Survey—October 17th*

Postdoc and research **opportunities** in Brazil

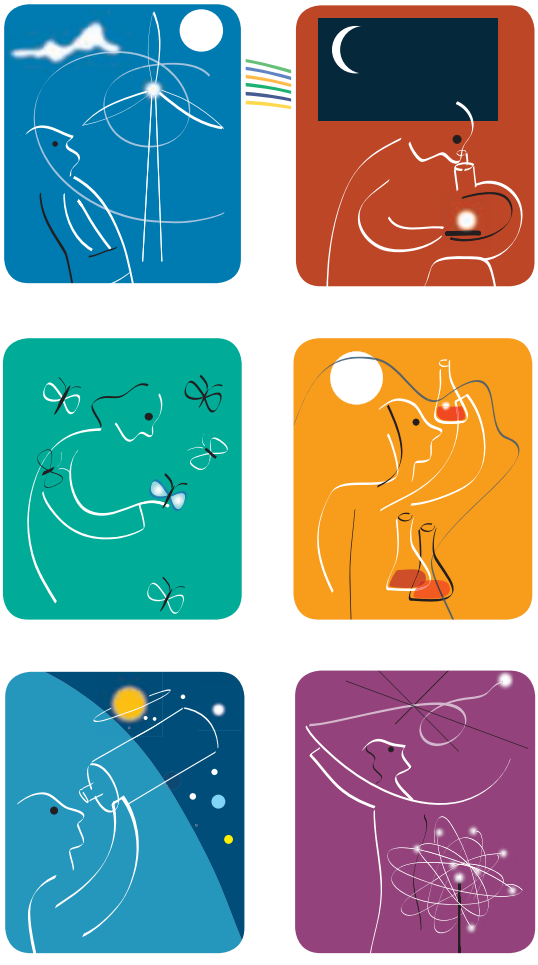

About us

Fifty percent of all science created in Brazil is produced in the State of São Paulo. The state hosts three of the most important Latin American universities: USP, UNICAMP and UNESP. Other universities and 19 research institutes are also located in São Paulo, among them the renowned Instituto Tecnológico de Aeronáutica (ITA), Instituto Nacional de Pesquisas Espaciais (INPE) and Laboratório Nacional de Luz Síncrotron, besides most of Brazilian Industrial P&D.

The São Paulo Research Foundation (FAPESP), one of the leading Brazilian agencies dedicated to the support of research, has ongoing programs and support mechanisms to bring researchers from abroad to excellence centers in São Paulo.

The **Young Investigators Awards** is part of FAPESP's strategy to strengthen the State research institutions, favoring the creation of new research groups. See more about it at www.fapesp.br/yia.

FAPESP **Post-Doctoral Fellowship** is aimed at distinguished researchers with a recent doctorate degree and a successful research track record. The fellowship enables the development of research within higher education and research institutions in São Paulo. Postdoc fellowships are available when calls for applications are issued internationally, or as individual fellowships requested on demand.

In the first case, positions are advertised at www.fapesp.br/oportunidades/ and candidates are selected through international competition. In the second, the proposal must represent an addition to a pre-existent research group and should be developed in association with faculty in higher education and research institutions in São Paulo. More information at www.fapesp.br/en/postdoc.

Location: São Paulo, SP, Brazil

Primary Contact Details:
Rua Pio XI, 1500 – Alto da Lapa
05468-901
São Paulo, SP – Brazil
Phone: +55-11-3838-4224
URL: www.fapesp.br

FAPESP 50 YEARS

FAPESP
SÃO PAULO RESEARCH FOUNDATION

Science Careers online @sciencecareers.org
POSTDOCTORAL OPPORTUNITIES

The framework covers four domains scientists need to be effective: intellectual knowledge, personal effectiveness, professional standards, and working with others.

Similarly, the myIDP website (myIDP.sciencecareers.org) is particularly well-suited to helping biomedical scientists explore careers and set goals for career development. **Sibby Anderson Thompkins,** director of postdoctoral affairs at University of North Carolina (UNC), Chapel Hill, advises using the National Postdoctoral Association's Core Competencies document and the checklist at the end of it (scim.ag/1pmZp9l) as a concrete way to discuss professional development and specific skills goals with postdoctoral advisors.

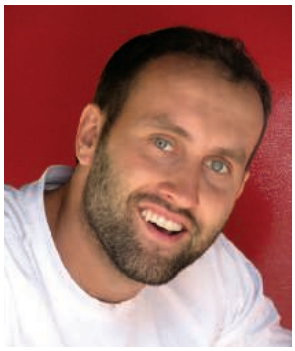

Grzegorz Wicher attends "business pub" meetings every couple of weeks to chat with others starting companies.

A skills frame-shift

The core skills that every postdoc needs to transition to a successful academic career are well known. Professorships go to those who exhibit clever experimental design and efficient research project management, who can deliver persuasive scientific arguments, and who are able to write clear, concise, and winning publications and grant proposals. But many postdocs may overlook that those same skills—with a slight tweak in frame-of-mind—make them highly marketable for other positions as well.

Anderson Thompkins says postdocs have to shift their own thinking about their acquired skills and how best to present them to potential future employers. "Postdocs are, in fact, mini project managers," she says, and should describe themselves as such. "Think more broadly—can you manage people, manage time, meet deadlines, and organize? All those skills are really useful in any job. Any job."

Bogle points to another skill that is highly valued in the workplace, but often undervalued by scientists: "The communication of complex ideas in a clear, transparent way. It's difficult to deliver complex messages quickly."

Joe Hardy adds that problem solving, analytical thinking, and understanding how to run proper experiments translate beautifully in today's companies operating within Internet-based commerce. "Right now, the way companies think about developing and marketing products is essentially an experimental model," says Hardy, the vice-president for research and development at Lumosity, a cognitive-training software company based in San Francisco.

Web-based and technology firms often take the approach of an A-B test, he says, with different customers exposed to different experiences. Then, companies measure behaviors like clicking links or purchasing in response. Postdocs understand the importance of random assignment of conditions, good experimental controls, and how to process the data coming back. "In this world of the Internet, millions of experiments are happening simultaneously. Experimental design and analysis are big players now," Hardy notes.

Another invaluable skill postdocs must possess to succeed in almost any later venture is writing clearly and concisely. Doing three paleontology postdocs in France, Berlin, and New York—and writing multiple fellowship applications to fund them—prepared **Faysal Bibi** for pursuing the large grant he needs to secure a permanent faculty position. Now in a five-year "habilitation" post as an assistant professor of paleontology at the Museum für Naturkunde in Berlin, Bibi says he has the confidence to write a proposal for the €1–2 million grants necessary to sustain a research program.

When it dawned on **Christine Gould** that she actually enjoyed the process of writing up her thesis and postdoctoral work, she investigated scientific writing careers. As a medical writer for Health Interactions in San Francisco she prepares manuscripts, slide presentations, and abstracts for biotechnology clients. Careers that employ scientific writing skills include science communications and journalism, medical writing, regulatory affairs, and continuing medical education (or CME).

Jeff Sfakianos even found that his manuscript-writing skills were extremely handy when filing patent applications for his therapeutics startup company. Sfakianos, who did a postdoc at Genentech, found that the back-and-forth with patent examiners mirrored the process of peer review. "Writing my own papers was more important than I imagined," he says.

Even though writing clearly, presenting complex ideas, and successful completion of projects comes with the postdoc territory, job seekers might need to spell these abilities out for employers. Hardy of Lumosity stresses that if postdocs are transferring outside of their immediate research field, then they must describe in detail (and perhaps in a profession-matched vocabulary) their accomplishments and what useful, relevant skills they have attained.

Gould did this by flipping her curriculum vitae on its head. She listed all of her writing experience at the top—including contract editing work, blogging, and courses in science writing—and de-emphasized her research. "I described myself as a medical writer who happens to have eight years of experience in cancer biology." Later, she was told her resume stood out to the human resources department.

Missing from the toolkit

Most postdocs make good project managers, shepherding multiple lines of research into a coherent final publication, but they often lack other types of management training. Fiscal, personnel, and time management are critical for careers both inside and outside academia. These skills, along with teaching and business know-how, should top the list of anyone heading out on the job market, but obtaining them requires extra effort.

As a senior postdoctoral researcher at Uppsala University in Sweden, **Grzegorz Wicher** has acquired an impressive list of technical skills from specialized mass spectrometry to microdissection and primary cell culture. But when it came to starting up his own cell culture company, PrimeCell, he took advantage of the Uppsala Innovation Centre, which helps researchers commercialize their ideas.

Through the center, he took the three-month Business Lab program to gain some business, marketing, and legal knowledge and to get connected to experts in those areas. He also attends "business pub" meetings every couple of weeks to chat with others starting companies and "exchange knowledge with a beer in your hands."

Chris Blagden, director of CME development and strategy for HealthmattersCME in New York notices continued>

PHOTO: COURTESY OF GRZEGORZ WICHE

Roche Postdoc Fellowship (RPF) Program

The RPF Program has built up a worldwide reputation and become a continuous source of innovation. This is reflected not only in high quality publications in peer-reviewed journals, but is also evident from the influence of the RPF findings on pharmaceutical research and early development at Roche.

"The RPF program provides an excellent way for academics to transition into industrial research. The topics offer a good balance between exploratory science and application moving towards development. As well as affording access to state-of-the-art facilities and expertise, the fellowship allows participants to gain an insight into the entire drug value chain. The most exciting part for me is shifting perspectives to accommodate industry requirements into my research in the area of cardiotoxicity testing and assessing how I can add value to it."

Mamta (34) from India

"Being a postdoctoral fellow at Roche offered me the possibility to work on a scientific question that is destined for application in the near future. Even though postdoc projects are designed as stand-alone projects, they may complement drug discovery efforts conducted at Roche. This allowed me to gain first-hand experience in industrial research."

Sebastian (33) from Germany

"The program gives me the opportunity to work on a hands-on early stage drug discovery project with a talented team of biologist, chemists and biochemists within Roche and academia. The collaboration with an interdisciplinary team challenges me with unique scientific questions every day. It also sharpens my soft skill set, as working in teams is all about effective communication. It is a truly unique program in this respect that advances my personal and professional career."

Daniel (28) from Switzerland

Key facts

Currently we have close to 100 ongoing RPF collaborations covering an exciting range of innovative and intellectually stimulating research programs which both encompass and focus on cutting-edge scientific endeavors on a worldwide stage. Each Postdoc has two mentors, one from Roche and one at the partnering university. The annual Postdoc Symposium, held for all Postdocs at one of the Roche locations worldwide, as well as Postdoc lunches and journal clubs provide additional networking opportunities for our Postdocs.

Duration: Initially for 2 years, with the option of extension for another 1-2 years.

Location: RPFs can be located at Roche in Basel, Zurich, Penzberg, Shanghai, or at the partnering universities.

Main areas: Oncology, Neuroscience, Infectious Diseases, Ophthalmology, Pharmaceutical Sciences (DMPK, Non-Clinical-Safety, Modelling & Simulation, Translational Technologies, Bioinformatics), Therapeutic Modalities (Small & Large Molecules Research, Discovery Technologies).

How to apply? All positions are posted on our Roche Careers Website. Please apply online. New positions may be expected to be online from October 2014 onwards.

To apply online for positions visit www.careers.roche.ch

Faysal Bibi

Problem solving, analytical thinking, and understanding how to run proper experiments translate beautifully in today's companies operating within Internet-based commerce.

— Joe Hardy

Featured Participants

Georgia State University
www.gsu.edu

Health Interactions
www.healthinteractions.com

HealthmattersCME
healthmatterscme.com

Lumosity
www.lumosity.com

Museum für Naturkunde
www.naturkundemuseum-berlin.de/en

National Bureau of Economic Research
www.nber.org

North Carolina State University
www.ncsu.edu

PrimeCell
www.primecell.se

University College London
www.ucl.ac.uk

University of North Carolina, Chapel Hill, Office of Postdoctoral Affairs
research.unc.edu/offices/postdoctoral-affairs

Uppsala University
www.uu.se/en

Additional Resources

American Society for Microbiology's Teaching Fellows Program
www.asmgap.org/index.php/asm-science-teaching-fellows-program

National Postdoctoral Association's Core Competencies
www.nationalpostdoc.org/competencies

Preparing for Academic Practice Program, Oxford University
www.apprise.ox.ac.uk

Uppsala Innovation Centre
www.uic.se

Vitae
www.vitae.ac.uk

another skills gap: while postdocs get loads of practice at bringing projects to an endpoint, they get "very little training in the way of doing it cost-effectively and time-effectively." These are key for CME projects—and for many other client- or product-based projects—that must come in on time and under budget. Postdocs who have managed their own research budget or met tight deadlines may have a leg up.

Considerable skills gaps can exist even for postdocs remaining in academia. The leap from postdoc to lab head comes with considerable shifts in focus and responsibilities—teaching, lab management, dealing with interpersonal conflicts, and a penchant for fundraising (scim.ag/1mCSOTf)—which don't necessarily come naturally. Academic career development programs, like the popular Preparing for Academic Practice at Oxford University in the United Kingdom, can pave the way for postdocs moving toward tenure-track posts.

Ramirez' teaching scholars program at North Carolina State University provides a foundation for transitioning to teaching faculty positions. With other fellows, she helped teach, organize, and administer the courses and answered student questions. Postdocs can also explore teaching careers through programs such as the American Society for Microbiology's Teaching Fellows Program, a five-month online development course.

Ramirez says her past research career greatly influences her teaching. She was already skilled at distilling down her research to a few sentences to grab the attention of scientists outside her field. "It's the same thing with students—you have a few minutes to capture their attention in a lecture or you've lost them for 50 minutes."

Running a successful marketing campaign

Regardless of whether postdocs transfer skills to a permanent professorship or to another field entirely, they must think broadly about how to market themselves when the time comes. Much like a presidential bid, running a successful self-marketing campaign requires starting years ahead.

Anderson Thompkins says that postdocs who come to the UNC office early realize they must have a clear sense of their end goal to maximize their postdoctoral time. The most successful postdocs, she says, consider different options, having multiple "plan Bs" and do not bank on one particular career path.

Bogle suggests that trainees ponder career choices at two special times: research highs and research lows. "Take a break and look around. Go to the pub with friends and talk about it. Explore, get out there and find out what's on offer. Make all the connections you can and make use of all the external contacts you can."

Young scientists have things backwards if they research intensely for 10–12 hours per day and then only spend 15 minutes on a job search, says Hardy. "You should spend significant amounts of time investigating, networking, and understanding what people like you have gone on to do."

Although self-promotion doesn't always come naturally to scientists, postdocs need to think strategically about how best to position themselves in the research enterprise. In his various postdoc posts, Bibi soaked up cutting-edge techniques, such as evolutionary meta-analysis and genomics, and made valuable personal connections.

"What paid off is that I liked to be a bit of the odd one out, surrounded by people who worked on different things or in different [geologic] time periods." This way, he gained both innovative technical skills and expanded his network well beyond his subfield. As an academic job candidate, he says, "this is something I think I can sell much better than simply saying that I study fossil antelopes."

Bibi has landed on the exact right word: "sell." Job searching in today's market is fundamentally about selling yourself, your ideas, and your skills and convincing a potential employer of your value. Luckily, that's one skill many postdocs have already unwittingly mastered. After all, how many times have you given a seminar and successfully persuaded the crowd to believe you and your data?

Kendall Powell is a freelance science writer based in Lafayette, Colorado.

DOI: 10.1126/science.opms.r1400144

PHOTO: BY BRIAN KRAATZ

HHMI janelia farm research campus

LAB HEADS AT JANELIA

Janelia Research Campus is looking for independent, hands-on scientists to direct small teams on high-impact research.

Our pioneering biomedical research complex near Washington, DC provides opportunities for researchers from diverse disciplines to pursue science that could have a transformative impact on society.

Highlights
- Internally funded, requiring no extramural grants
- No formal teaching duties
- Minimal administrative responsibilities
- Highly interactive and collaborative environment

Application Deadline
December 2, 2014, 2 p.m. ET

Learn More
Janelia.org/sci/lh

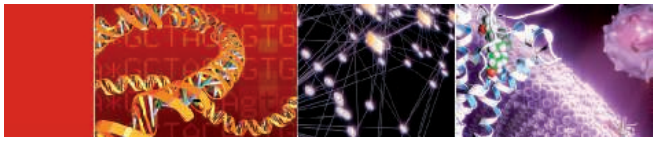

Novartis Institutes for BioMedical Research Postdoctoral Program

Would you like to contribute to innovative research with the goal of improving human health? Novartis Institutes for BioMedical Research is the pharmaceutical research arm of Novartis, a global healthcare company. We host a postdoctoral program that provides excellent research training in a drug discovery environment. Postdoctoral scholars have a unique opportunity to conduct interdisciplinary research and publish their results in leading journals.

We are currently seeking candidates for postdoctoral positions in multiple research areas and locations and encourage applications from candidates interested in academic or industry careers.

- Cancer Biology
- Chemistry
- Computational Sciences
- Immunology
- Infectious Diseases
- Musculoskeletal
- Neurobiology
- Pathways Biology
- Regenerative Medicine
- Structural Biology

Qualifications: PhD degree holders, and PhD students within one year of completing of their degrees are eligible to apply.

For more information, and to download the cover letter template and apply, please visit http://postdoc.nibr.com/

Novartis is an equal opportunity employer committed to embracing and leveraging diverse backgrounds. M/F/D/V.

NOVARTIS INSTITUTES FOR BIOMEDICAL RESEARCH

SESYNC National Socio-Environmental Synthesis Center

POSTDOCTORAL FELLOWSHIPS

Food Systems Resilience to Climate Change
SESYNC invites applications for a 2-year postdoctoral fellowship as part of a new SESYNC–USDA collaboration to catalyze data-driven research on food systems resilience to climate change. We seek applications from PhD-level researchers with an interest in and/or prior research experience with data-driven analytical and/or modeling approaches to synthesize existing climate, socio-economic, demographic, and environmental data to address pressing questions related to food/agro-ecological systems resilience to climate change. The Fellow will also lead the planning, organization, and management of the new SESYNC–USDA "Data to Motivate Synthesis" Program.

Visit http://sesync.us/foodsystems for details. For best consideration, apply by October 1, 2014.

Ecological Systems, Social Systems & Environmental Change
SESYNC invites applications for 2-year postdoctoral fellowships for our new Postdoctoral Socio-Environmental Immersion Program, in which early career scholars will be immersed in a formal program, cohort, and setting dedicated to understanding socio-environmental systems and solving the challenges they face. Working with Research Collaborators and supported by in-house computational resources, Fellows will co-develop postdoctoral projects focused on ecological systems and/or social systems and environmental change. Framing this experience is a series of collaborative workshops, led by eminent scholars, on foundational theories relevant to environmental insight.

Visit http://sesync.us/immerse for details. Pre-screening applications due September 22, 2014; final applications due November 3, 2014.

CHARITÉ
UNIVERSITÄTSMEDIZIN BERLIN

The **Pediatric Infectious Disease & Vaccines Workgroup at the Department of Pediatrics, Charité University Medical Center,** are recruiting a

Bioinformatician/ Epidemiologist/ Biostatistician (Postdoc)

(Reference Number: DM.78.13)

Charité – University Medical Center Berlin is a top-level European institution for biomedical research and patient care. Our multi-disciplinary clinical research team is actively involved in several national and international research networks, including EU- funded consortia. Scientifically, we are seeking an individualized approach to the management and treatment of acute infections in infants and children, based on an improved understanding of immunologic and genetic factors. Innovative mathematical, epidemiological and biostatistical models and methodologies will be key to advancing our knowledge in this important subject area.

Your Tasks

- Independent analysis and management of large and complex clinical datasets
- Development of advanced statistical/ mathematical models, pattern recognition, feature analysis and machine learning.
- Analysis of virus load kinetics, interactions between "omics" biomarkers and clinical parameters
- Writing scientific manuscripts, supervision of doctoral students, acquisition of funding.

Formal Requirements

- PhD or equivalent degree in bioinformatics, biostatistics, or advanced epidemiology.
- Well-established scientific track record with outstanding results
- High-impact publications and track record of successful international research activities
- Excellent command of English language (written, oral). German language skills are not required
- Excellent methodological competencies including advanced statistical and analytical skills
- Hands-on experience with the dry-lab analysis of complex 'omics and clinical datasets, quality/plausibility checks and data protection/security
- Target-oriented and effective work style, achieving milestones within deadlines
- Ability to work independently and to supervise junior scientists
- Reliability, team competency, effectiveness, flexibility

Desirable Additional Qualifications

- Research experience in infectious diseases and/or public health/ regulatory
- Experience in the acquisition of funding
- Experience with multidisciplinary research consortia
- Experience with m-health tools
- A genuine interest in innovation and interdisciplinary work, translational/ bench-to bedside research.

Applications, including (1) curriculum vitae, (2) list of publications and (3) three letters of reference, should be sent by e-mail to the attention of: **kinderinfekte@charite.de**

With your application, please include the following **reference number DM.78.13**

Department of Health and Human Services
National Institutes of Health
National Institute on Deafness and Other Communication Disorders

NIH

Robert Wenthold Postdoctoral Research Fellowship

The Robert Wenthold Fellowship supports NIDCD intramural research training of the most highly promising postdoctoral research fellows seeking to become independent investigators and leaders within the mission areas of NIDCD. A Wenthold Fellow is encouraged to design a research training and career development plan that takes advantage of the multi-disciplinary training, dedicated core facilities, and the breadth and depth of communication sciences expertise within the NIDCD intramural research program (**http://www.nidcd.nih.gov/research/**). NIDCD intramural research includes basic and clinical studies of normal and disordered processes of hearing, balance, taste, voice, speech and language.

The Fellowship is designed to maximize the probability of success for a long-term independent research career in the multi-disciplinary field of communication sciences. Acquisition of new scientific approaches and methodologies is encouraged, with the opportunity for multi-disciplinary training and structured co-mentoring. The Fellowship includes an initial two-year commitment of salary, benefits, travel and annual supplies, with the potential for performance-based salary increases and extension of the appointment beyond two years.

Eligible individuals will have an MD and/or PhD, or an equivalent doctoral degree, and 0-2 years of prior postdoctoral research experience at the time of initial appointment. Prior postdoctoral experience may be in an NIH intramural or extramural laboratory.

Please submit: (1) a curriculum vitae with bibliography, (2) up to three publication reprints written as first or co-first author, and (3) a one page research statement including summary of previous research training and accomplishments, research interests, training and career goals, and a proposal for multi-disciplinary mentorship and training to **Ms. Linda de Iberri, Office of the Scientific Director, NIDCD, 35A Convent Drive, Bldg. 35A, Room GF102, Bethesda, MD 20892 (deiberril @nidcd.nih.gov**). Also arrange for three letters of reference to be sent directly to Ms. Linda de Iberri. Applications are due by **October 1, 2014**.

DHHS and NIH are Equal Opportunity Employers and encourage applications from women and minorities.

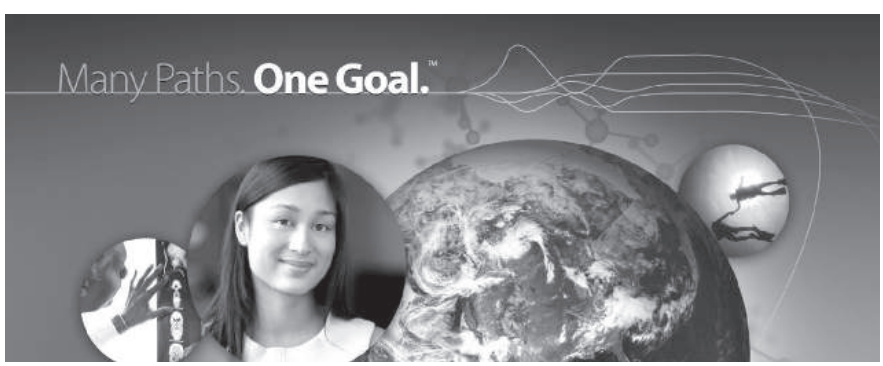

Pfizer R&D Postdoctoral Program

In 2010, the Pfizer Research and Development organization launched an ambitious postdoctoral training program that encompasses its Research, Biotech, and Technology Units. We recruit highly motivated Ph.D. recipients with a demonstrable track record of scientific productivity during their graduate training and a strong interest in performing an academic-style postdoc in an industrial setting. Successful candidates for entry into the program express a passion for creative research that facilitates the translation of novel biological or technological advances into innovative therapies for human diseases.

Our postdoctoral program is designed to provide the research foundation that will lead to future improvements in disease therapy, while at the same time offering our trainees an exceptional career-building experience in the biomedical sciences. Our trainees perform cutting-edge research leading to publications in top-tier journals, attend high-profile scientific meetings, and interact with well-known academic labs worldwide.

To explore and apply for specific opportunities, visit us online at: www.pfizercareers.com.

Pfizer Working together for a healthier world®

www.pfizercareers.com

NATIONAL RESEARCH COUNCIL
OF THE NATIONAL ACADEMIES

Research Associateship Programs

Graduate, Postdoctoral and Senior Research Awards
offered for research at
US Government Laboratories and affiliated institutions

Opportunities for graduate, postdoctoral and senior research in all areas of science and engineering

- Awards for independent research at over 100 participating laboratory locations
- 12-month awards renewable for up to 3 years
- Annual stipend $45,000 to $80,000 - higher for senior researchers; graduate entry level stipend is $30,00 and higher for additional experience
- Relocation, professional travel, health insurance
- Annual deadlines are February 1, May 1, August 1, November 1
- Open to US and non-US citizens

Detailed program information, including instructions on how to apply online, is available on the NRC website at :
www.nationalacademies.org/rap

Applicants must contact Adviser(s) at the lab(s) prior to application deadline. Questions should be directed to the: **National Research Council** TEL: (202) 334-2760
E-MAIL: rap@nas.edu

Qualified applicants will be reviewed without regard to race, religion, color, age, sex or national origin.

THE NATIONAL ACADEMIES
Advisers to the Nation on Science, Engineering, and Medicine

UAB THE UNIVERSITY OF ALABAMA AT BIRMINGHAM

Postdoctoral Positions

The University of Alabama at Birmingham (UAB) is one of the premier research universities in the US with internationally recognized programs in AIDS & bacterial pathogenesis, bone biology & disease, cancer, diabetes & digestive & kidney diseases, free radical biology, immunology, lung disease, neuroscience, trauma & inflammation, and basic & clinical vision science among others. UAB is committed to the development of outstanding postdoctoral scientists and has been consistently ranked in recent years as one of the top locations among US universities for training postdoctoral scholars.

UAB is recruiting candidates for postdoctoral positions in a variety of research areas. UAB faculty are well funded (top 25 in NIH funding), utilize multidisciplinary approaches, and provide excellent research training environments that can lead exceptional candidates to entry level positions in academia, government or the private sector. Full medical coverage (single or family), competitive salaries/stipends, sick leave, vacation, and maternity/ paternity leave are offered with every position as well as AD& D, disability and life insurance. Depending on the source of funding, retirement benefits may also be available. Birmingham is a mid-size city centrally located in the southeast near beaches and mountains and enjoys a moderate climate for year round outdoor activities and a cost of living rate lower than most metropolitan areas.

Visit our website at **www.uab.edu/postdocs**, Openings, to view positions. See info also on MERIT Program, an NIH IRACDA program. Send your CV to the contact name for the positions that you are interested. **University of Alabama at Birmingham, Office of Postdoctoral Education, 205-975-7020**.

UAB is an Equal Employment Opportunity Employer.

EGL
Charitable Foundation

The EGL Charitable Foundation invites you to apply to the

Gruss Lipper Post-Doctoral Fellowship Program

Eligibility

- Israeli citizenship
- Candidates must have completed PhD and/or MD/PhD degrees in the Biomedical Sciences at an accredited Israeli University/Medical School or be in their final year of study
- Candidates must have been awarded a postdoctoral position in the U.S. host research institution.

Details regarding the fellowship are available at www.eglcf.org

NW210508R

Post-doctoral opportunities in Systems Medicine and Bioinformatics at Stanford University

The laboratory of Dr. Atul Butte at Stanford Medical School is seeking highly motivated investigators to develop and study novel approaches in data-driven biomedical research to discover new biomarkers, therapeutics, and to revolutionize health and health-care. Post-doctoral fellowships are fully funded for at least 2 years.

Ideal candidates will have an M.D. and/or Ph.D. with a strong background in bioinformatics, computational biology, biostatistics, and genomics, excellent communication and programming skills, and a great publication record.

Strong problem-solving skills, creative thinking, and the ability to build new software tools as needed are required. A dual background in both computation and molecular biology or medicine or pharmacology will be a strong plus. Prior experience with genetic, microarray, drug, or clinical databases, text-mining, knowledge representation, or parallel computing platforms is a plus. Applicants must possess good communication skills and be fluent in both spoken and written English.

This exciting work will be guided by multidisciplinary collaborations with top scientists in stem-cell, immunology, diabetes, and cancer biology research at Stanford.

To apply, please send your CV, a brief statement of research interests, and contact information for three references. **E-mail: butte-lab-jobs@lists.stanford.edu**

Argonne NATIONAL LABORATORY

The Argonne Named Fellowship Program

Argonne National Laboratory is accepting applications for the 2015 Named Fellowship. Argonne awards these special fellowships internationally on an annual basis to outstanding doctoral-level scientists and engineers who are at early points in promising careers. The fellowships are named after scientific and technical luminaries who have been associated with Argonne and its predecessors, and the University of Chicago, since the 1940's.

Candidates for these fellowships must display superb ability in scientific or engineering research, and must show definite promise of becoming outstanding leaders in their fields. Fellowships are awarded annually and may be renewed up to three years. The 2015 fellowship carries a highly competitive salary with an additional allocation research support and travel. The deadline for submission of application materials is October 7, 2014.

Applicants should identify an Argonne staff member to sponsor the nomination. The sponsor could be someone who is already familiar with your research work and accomplishments through previous collaborations or professional societies. If you have not yet identified an Argonne sponsor, visit the detailed websites of the various research efforts at www.anl.gov/science .

Applications must be submitted online through: **http://www.anl.gov/careers/apply-job**. Correspondence and supporting letters of recommendation should be submitted to **Named-Postdoc@anl.gov**.

For more information visit the Argonne Postdoc Blog at https://blogs.anl.gov/postdoc/ or by contacting the Postdoctoral Program Coordinator, **Kristene Henne** at **khenne@anl.gov**.

Argonne is an equal opportunity employer and we value diversity in our workforce. Argonne is a U.S. Department of Energy laboratory managed by UChicago Argonne, LLC

AAAS Award for Science Diplomacy

Many scientists and engineers contribute valuable time away from the established career paths of research, teaching, and publishing to foster activities and develop programs that both address key science questions and build important societal links. AAAS seeks to recognize an individual or a limited number of individuals working together in the scientific or engineering community for making an outstanding contribution to furthering science diplomacy.

The recipient receives US $5,000 award, a commemorative plaque, complimentary registration, and reimbursement for reasonable travel and hotel expenses.

The award is open to all regardless of nationality or citizenship. Nominees must be living at the time of their nomination. **Please visit http://www.aaas.org/aboutaaas/awards/int/ for more information and nomination instructions.**

All materials must be received by September 1.

AAAS ADVANCING SCIENCE, SERVING SOCIETY

Two Faculty Career Features

September 12, 2014
Reserve ads by August 26 to guarantee space *

October 3, 2014
Reserve ads by September 16 to guarantee space**

There's only one **Science**

Hiring Faculty? The Sept. 12 feature offers advice for faculty who are working with professionals in different industries/government/academic cultures. **The Oct. 3 feature** explores how faculty can best collaborate with professionals in different cultures and countries.

Why you should advertise in these issues of *Science*:

Reach: Your job ad is seen by 570,400 readers around the globe

- The Sept. 12 issue includes a special bonus distribution to 100,000 scientists beyond our regular circulation

To book your ad:
advertise@sciencecareers.org
THE AMERICAS
202 326 6582
EUROPE/ROW
+44 (0) 1223 326500
JAPAN
+81 3 3219 5777
CHINA/KOREA/SINGAPORE/TAIWAN
+86 186 0082 9345

Science Careers
From the journal *Science* AAAS
ScienceCareers.org

*Ads accepted until September 5 if space is still available.
**Ads accepted until September 26 if space is still available.
Produced by the *Science*/AAAS Custom Publishing Office.

Science Careers

CER

"《科学》职业" 已经与赛尔互联(CER)开展合作。中国大陆的高校可以直接联系CER进行国际人才招聘。

请访问
Sciencecareers.org/CER
点得联系信息。

Science

AAAS SCIENCE & TECHNOLOGY POLICY FELLOWSHIPS®

"My fellowship transformed my scientific training into a vehicle for public service."

I HAD A MONUMENTAL EXPERIENCE. YOU CAN TOO.

— Kevin Haninger, PhD, Psychology,
2009-11 Executive Branch Fellow

MAKE A DIFFERENCE. TRANSFORM YOUR CAREER.

Apply your scientific analysis and technical knowledge to inform policy through assignments in the Legislative, Executive and Judicial Branches.

Stipends from $75,000 to $100,000. Applications due **November 1.**

Details at:
aaas.org/policy-fellowships/science1

Enhancing Policy, Transforming Careers

SCIENCE & TECHNOLOGY **POLICY FELLOWSHIPS**
AAAS

POSTDOCTORAL OPPORTUNITIES
Science Careers online @sciencecareers.org

UCONN HEALTH CENTER

The Jackson Laboratory
Leading the search for tomorrow's cures

Tenure Track Faculty Position in Single Cell Genomics

The University of Connecticut School of Medicine (UConnSoM) and the Jackson Laboratory (JAX) are jointly seeking to recruit an outstanding individual with expertise in genomics and/or computational genomics for a tenure-track faculty positions at the Assistant, Associate or Full Professor level. We are seeking an individual with a strong background in single cell profiling and genomic analyses and applying such technology to research in areas such as stem cells, immunology, neuroscience or reproductive biology.

UConnSoM has exceptionally strong translational and clinical research programs in many areas including genetics, computational cell biology, quantitative medicine and human pluripotent stem cells. JAX is a world-leader in the genetic analysis of mouse models of human disease and has recently established The Jackson Laboratory for Genomic Medicine (JAX-GM; **www.jax.org/ct**) in Farmington, Connecticut. The successful candidate will hold a tenure track appointment in the appropriate academic Department in the UConnSoM and a faculty appointment at JAX-GM. S/he will also be cross appointed with the University of Connecticut Institute for Systems Genomics. This unique rich combination of research capabilities in a very dynamic and emerging environment provides the new faculty recruit with an opportunity to create a truly transformative research program. The candidate should be a consummate team player in a highly interdisciplinary and dynamic environment that brings together clinicians, biologists, molecular geneticists, and quantitative scientists.

JAX-GM represents an expansion of JAX and draws on the Laboratory's eight decades of research in mammalian genetics. JAX will continue to grow its basic research campus in Bar Harbor, Maine, while the new facility in Farmington, Connecticut focuses on medical applications of genomics with academic and clinical research partners from Connecticut and around the world. The 183,500-square-foot JAX-GM facility will open in October 2014 and will house 300 biomedical researchers, technicians and support staff in state-of-the-art computing facilities and laboratories.

UConnSoM is engaged in a major expansion of its research programs in computational biology, bioinformatics, and systems biology/genomics, as part of several transformative state initiatives. The Bioscience Connecticut initiative, totaling approx. $1 billion, will expand UConnSoM research capabilities. Other initiatives, totaling over $2 billion, include the Next Generation Connecticut initiative at the main campus in Storrs, expanding the overall research efforts of the University. The Institute for Systems Genomics has also been formed to integrate the genomics activities across the University of Connecticut and JAX including the establishment of the new joint Center for Single Cell Genomics.

Minimum qualifications include a doctoral degree in an appropriate field, postdoctoral experience, and an outstanding record of research accomplishments. Equivalent foreign degrees are acceptable. A demonstrated ability to secure external research funding and publication in top peer-reviewed journals is expected. Preferred qualifications include the ability to contribute through research, teaching, outreach and public genomic literacy engagement to the diversity and excellence of the learning experience, and to perform research in an area that develops and complements ongoing efforts in the Institute and the University.

Applicants should apply at **https://jobs.uchc.edu**, search (2014-1059) with a CV, cover letter and concise statements of research and teaching interests. In addition, applicants should arrange to have at least three letters of reference sent to Dr. Marc Lalande at **statgenuconn@uchc.edu** as a PDF document on letterhead with signature. To ensure full consideration, applications should be received by **October 1, 2014**.

Affirmative Action/Equal Opportunity Employer (M/F/M/PwD/PV)

UCONN HEALTH CENTER

The Jackson Laboratory
Leading the search for tomorrow's cures

Tenure Track Faculty Position in Computational/Systems Genomics

The University of Connecticut School of Medicine and the Jackson Laboratory (JAX) are jointly seeking to recruit an outstanding individual with expertise in computational and systems genomics for a tenure-track faculty position at the Assistant, Associate or Full Professor level. Areas of interest include, but are not limited to, computational and systems genomics, network biology, cutting-edge analyses of large, population-scale exome data sets, whole genome analyses or human evolutionary genomics.

UConn Health has exceptionally strong translational and clinical research programs in many areas including genetics, computational cell biology, quantitative medicine and human pluripotent stem cells. The Jackson Laboratory is a world-leader in the genetic analysis of mouse models of human disease and has recently established The Jackson Laboratory for Genomic Medicine (JAX-GM; **www.jax.org/ct**) in Farmington, Connecticut. The successful candidate will hold a tenure track appointment in the appropriate academic Department at UCH and a faculty appointment at JAX-GM. S/he will also be cross appointed with the University of Connecticut Institute for Systems Genomics. The unique combination of rich research capabilities and a very dynamic and emerging environment provides an opportunity to create a truly transformative research program. The candidate should be a consummate team player in a highly interdisciplinary environment that brings together clinicians, biologists, molecular geneticists, and quantitative scientists.

The JAX-GM represents an expansion of JAX and draws on the Laboratory's eight decades of research in mammalian genetics. JAX will continue to grow its basic research campus in Bar Harbor, Maine, while the new facility in Farmington, Connecticut focuses on medical applications of genomics with academic and clinical research partners from Connecticut and around the world. The 183,500-square-foot JAX-GM facility will open in October 2014 and will house 300 biomedical researchers, technicians and support staff in state-of-the-art computing facilities and laboratories.

UCH is engaged in a major expansion of its research programs in computational biology, bioinformatics, and systems biology/genomics, as part of several transformative state initiatives. The Bioscience Connecticut initiative, totaling approx. $1 billion, will expand UCH health care offerings and research capabilities. Other initiatives, totaling over $2 billion, include the Next Generation Connecticut initiative at the main campus in Storrs, expanding the overall research efforts of the University. The Institute for Systems Genomics has also been formed to integrate the genomics activities across the University of Connecticut and The Jackson Laboratory including the establishment of the new joint Center for Single Cell Genomics.

Minimum qualifications include a doctoral degree in an appropriate field, postdoctoral experience, and an outstanding record of research accomplishments. Equivalent foreign degrees are acceptable. A demonstrated ability to secure external research funding and publication in top peer-reviewed journals is expected. Preferred qualifications include the ability to contribute through research, teaching, outreach and public genomic literacy engagement to the diversity and excellence of the learning experience, and to perform research in an area that develops and complements ongoing efforts in the Institute and the University.

Applicants should apply at **https://jobs.uchc.edu**, search (2014-1057) with a CV, cover letter and concise statements of research and teaching interests. In addition, applicants should arrange to have at least three letters of reference sent to Dr. Brenton Graveley at **Statgenuconn@uchc.edu** as a PDF document on letterhead with signature. To ensure full consideration, applications should be received by **October 1, 2014**.

Affirmative Action/Equal Opportunity Employer (M/F/M/PwD/PV)

TRINITY COLLEGE DUBLIN
COLÁISTE NA TRÍONÓIDE, BAILE ÁTHA CLIATH
THE UNIVERSITY OF DUBLIN

TRINITY IS EMBARKING ON AN AMBITIOUS CAMPAIGN TO ATTRACT

WORLD LEADERS IN RESEARCH

Are you a world leader in any of the following fields of research?

- Bioengineering
- Cognitive Neuroscience
- Creative Technologies
- Immunotherapeutics
- Low Energy Computing
- Personal Health Informatics
- Pharmaceutical Chemistry
- Smart Cities
- Structural Biology
- Sustainable Energy Systems

Join us at **www.tcd.ie/worldleaders**

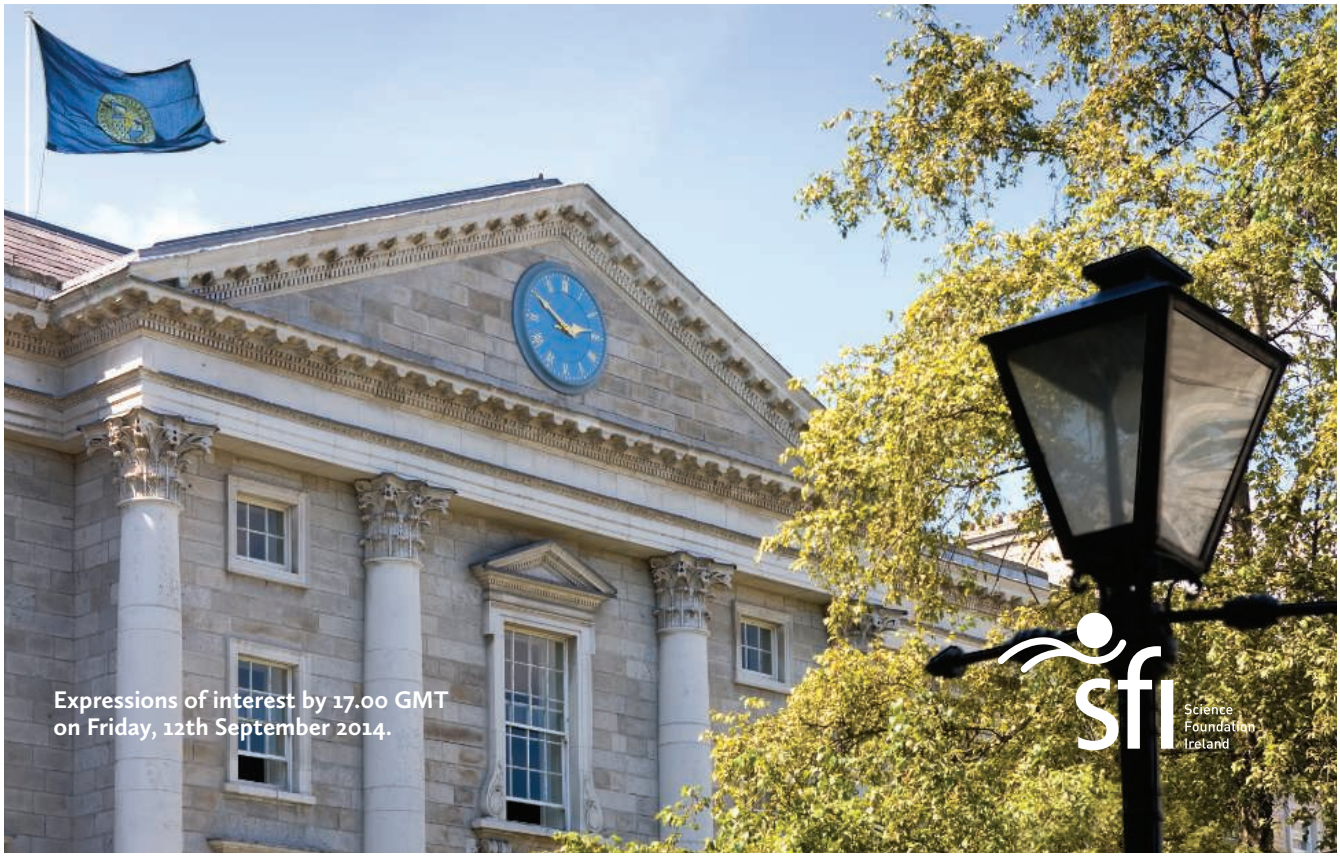

CityU 30
香港城市大學
City University of Hong Kong
30th Anniversary

Worldwide Search for Talent

City University of Hong Kong is a dynamic, fast-growing university that is pursuing excellence in research and professional education. As a publicly-funded institution, the University is committed to nurturing and developing students' talents and creating applicable knowledge to support social and economic advancement. The University has seven Colleges/Schools. As part of its pursuit of excellence, the University aims to recruit **outstanding scholars** from all over the world in various disciplines, including **business**, **creative media**, **energy**, **engineering**, **environment**, **humanities**, **law**, **science**, **social sciences**, **veterinary sciences** and other strategic growth areas.

Applications and nominations are invited for:

Dean *[Ref. A/125/29]*
College of Science and Engineering

The Position
Reporting to the Provost, the Dean will provide visionary, strategic leadership for the College, in alignment with the vision, mission and Strategic Plan of the University. In collaboration with the College's faculty and other academic units, the Dean will advance the College's academic excellence in research and professional education, and further its international standing.

The Person
The individual shall possess a doctorate degree with strong academic and professional qualifications, a distinguished record of teaching, research and scholarship, and substantial relevant experience in academic leadership roles; the vision and capability to build on and expand the College's strengths; outstanding management effectiveness; commitment to interdisciplinary collaboration and teamwork; and strong communication and networking skills to build and nurture internal and external contacts to the benefit of the College.

Salary and Conditions of Service
The appointee will be offered appointment to an academic rank commensurate with qualifications and experience. The deanship appointment will be on a concurrent basis for an initial period of three years. Remuneration package will be attractive and driven by market competitiveness and individual performance. Excellent fringe benefits include gratuity, leave, medical and dental schemes, and relocation assistance (where applicable).

Information and Application
Further information on the post and the University is available at http://www.cityu.edu.hk.

City University of Hong Kong is being represented in this search by the Perrett Laver Ltd. Please send the nomination or application with a current curriculum vitae to Ms. Ilona MOTYER, Perrett Laver Ltd., 8-10 Great George Street, London SW1P 3AE or email to "ILONA.MOTYER@PERRETTLAVER.COM" or upload at www.perrettlaver.com/candidates, quoting reference number 1502. **Applications and nominations received before 19 September 2014 will receive full consideration.** The University's privacy policy is available on the homepage.

The University also offers a number of visiting positions for current graduate students, postdoctoral scholars, and for early-stage and established scholars, as described at http://www.cityu.edu.hk/provost/CityU_Visiting_Positions.htm.

City University of Hong Kong is an equal opportunity employer and we are committed to the principle of diversity. We encourage applications from all qualified candidates, especially those who will enhance the diversity of our staff.

City University of Hong Kong was ranked 4th among the world's top 50 universities under the age of 50 in the *Quacquarelli Symonds* 2014 survey, and 1st in Engineering/Technology and Computer Sciences in greater China in the Shanghai Jiao Tung University 2013 survey
http://www.cityu.edu.hk

FRANKLIN & MARSHALL COLLEGE

PUBLIC HEALTH/EPIDEMIOLOGY

The Biology Department of Franklin & Marshall College invites applications for a tenure-track ASSISTANT PROFESSOR position in epidemiology and public health, beginning July 2015. Candidates should have the Ph.D. or terminal degree, demonstrated strengths in teaching and research, and broad interests in epidemiology and public health. The teaching load is 3/2, and responsibilities will include epidemiology, introduction to public health, and upper-level courses in the candidate's area of specialization, with opportunities to contribute to our Biology curriculum. Individuals with the ability to teach introductory biostatistics are encouraged to apply. The successful candidate will be expected to engage undergraduates in research, and start-up support is available. Franklin & Marshall is a small (enrollment 2400), highly selective coeducational liberal arts college with a tradition of excellence in science and student research.

Applicants should arrange to have letters from three referees, a letter of application, *curriculum vitae*, copies of graduate transcripts, teaching evaluations, a statement of teaching philosophy, and a research statement that includes plans for actively engaging undergraduates in research submitted electronically to **Dr. Janine Everett**, Search Committee Chair, via **http://apply.interfolio.com/25595**. Priority will be given to complete applications received by **September 26, 2014**. **Ph: 717-291-4118; e-mail: janice.kaufman@fandm.edu**; websites: **www.fandm.edu/biology** and **www.fandm.edu/public-health.**

Franklin & Marshall College is committed to having an inclusive campus community where all members are treated with dignity and respect. As an Equal Opportunity Employer, the College does not discriminate in its hiring or employment practices on the basis of gender, race or ethnicity, color, national origin, religion, age, disability, family or marital status, or sexual orientation.

FACULTY POSITION IN CHEMISTRY
Department of Chemistry
MOLECULAR DESIGN INSTITUTE
ARTS AND SCIENCE

The Department of Chemistry at New York University (NYU) invites applications for a faculty position in experimental materials chemistry as part of its Molecular Design Institute. While we expect to hire at the junior level, exceptional senior level candidates will be considered. Candidates with a background and interest in polymer chemistry are encouraged to apply. The anticipated start date is September 1, 2015, pending budgetary and administrative approval. The Department of Chemistry at NYU is implementing a significant growth plan, including the creation of the Biomedical Chemistry Institute, the Molecular Design Institute, the Laboratory for Molecular Nanoscience, and the addition of numerous senior and junior faculty members

In addition to establishing a vigorous research program, duties will include undergraduate and graduate teaching. Applicants should have an outstanding record of research and a commitment to teaching. Applications must include a curriculum vitae, a list of publications, and statements of future research and teaching plans. These materials, as well as three reference letters, must be submitted to our web-based application system using the following link: **http://chemistry.fas.nyu.edu/object/chem.nyufacultypositions**.

Application review will begin ***October 15, 2014***. Questions about this position can be sent by Email to **chemistry.search@nyu.edu.**

NEW YORK UNIVERSITY

NYU is an Equal Opportunity/Affirmative Action Employer.

SciLifeLab

Can you lead Sweden's largest center for life sciences?

SciLifeLab seeks an ambitious Director who can lead the scientific, technological and structural development of the center. We are looking for someone with extensive experience in both large-scale molecular biosciences and hypothesis-driven research; a person highly motivated to create a scientific, multidisciplinary and cutting-edge national center.

The position begins July 1st 2015 and is a six-year appointment as Director of SciLifeLab, which can be combined with a professorship at any of the four host universities. The appointment includes a significant research grant and start-up package.

Learn more about the position at www.scilifelab.se/director

SciLifeLab (Science for Life Laboratory) is a national resource for large-scale bioscience research with a focus on health and environment. The center is run collaboratively between Karolinska Institutet, KTH Royal Institute of Technology, Stockholm University and Uppsala University. Today, approximately 1,500 people work at the center's two sites in Stockholm and Uppsala.

Karolinska Institutet

KTH VETENSKAP OCH KONST

Stockholms universitet

UPPSALA UNIVERSITET

Science Careers online @sciencecareers.org

WASHINGTON STATE UNIVERSITY

Assistant/Associate/Full Professor
School of Molecular Biosciences

The School of Molecular Biosciences (http://www.smb.wsu.edu/) and Center for Reproductive Biology (http://crb.vetmed.wsu.edu/) in the College of Veterinary Medicine at Washington State University in Pullman, WA seek an outstanding individual for a permanent, full-time tenure-track position at the rank of Assistant, Associate, or Full Professor depending on qualifications. Successful candidates will have research space in a state-of-the-art building specifically designed and equipped for biological research. The research interests of applicants should complement the existing focus areas of the School and Center. These include germ cell biology, uterine biology, toxicology, and developmental biology. **Duties will include** maintaining a strong, externally funded research program, teaching in undergraduate and graduate courses on topics of reproductive and developmental biology, and participating in service at the school, college, and/or university level. **Job requirements include** a PhD degree in biosciences or closely related field with a minimum of two years of post-doctoral training in basic science, veterinary medicine, medicine, or a related discipline. Candidates for an Assistant Professor position must demonstrate potential to establish and maintain an externally funded research program. Applicants for Associate and Full Professor must have an active extramurally-funded research program with a record of peer-reviewed publications and national/international recognition. The successful candidate must demonstrate a commitment and relevant ability to successfully advocate diversity and values of diversity.

Applications, including a cover letter, curriculum vitae, and a statements of research interests and teaching philosophy, should be submitted electronically via: **https://www.wsujobs.com/postings/13076**. The candidate should also solicit three letters of recommendation that will be requested from the reference provider by email. The screening of applications will begin **October 1, 2014**. Start date is negotiable and salary will be commensurate with experience. Direct questions to the search committee chair, Dr. Jon Oatley (**joatley@vetmed.wsu.edu**).

Washington State University is an Affirmative Action/Equal Opportunity Employer. Women and minorities are encouraged to apply.

WASHINGTON STATE UNIVERSITY

Faculty Position in Cellular Microbiology
Assistant/Associate/Full Professor
School of Molecular Biosciences

The School of Molecular Biosciences in the College of Veterinary Medicine at Washington State University in Pullman, WA and its Director, Dr. Jonathan Jones, seek to hire outstanding individuals for permanent, full-time tenure-track positions at the rank of Assistant, Associate, or Full Professor (http://www.smb.wsu.edu/) depending on qualifications. Successful candidates will have the opportunity to establish their research programs in a state-of-the-art building specifically designed and equipped for biological research. The research interest of the applicant should be in the area of microbiology with a focus on microbe-cell interactions and their cellular trafficking. **Duties will include** maintaining a strong, externally funded research program, teaching undergraduate and graduate courses on topics of cellular and molecular biology, and participating in service at the school, college, and/or university level. **Job requirements include** a PhD degree in biosciences or a closely related field with a minimum of two years of post-doctoral training in basic science, veterinary medicine, medicine, or a related discipline. Candidates for an assistant professor position must demonstrate the potential to establish and maintain an externally funded research program. Applicants for the position of associate or full professor must have an extramurally-funded research program with a record of peer-reviewed publications and national/international recognition. The successful candidate must demonstrate a commitment and ability to successfully advocate for diversity and values of diversity.

Applications, including a cover letter, curriculum vitae, and a statement of research interests and teaching philosophy, should be submitted electronically via: **https://www.wsujobs.com/postings/13077**. The candidate should also solicit three letters of recommendation that will be requested from the reference provider by email. Screening of applications will begin **October 1, 2014**. Start date is open, and salary will be commensurate with experience. Direct questions to **pinter@vetmed.wsu.edu**.

Washington State University is an Affirmative Action/Equal Opportunity Employer. Women and minorities are encouraged to apply.

HEAD AND PROFESSOR
Department of Mechanical Science and Engineering
University of Illinois at Urbana-Champaign

The University of Illinois at Urbana-Champaign invites applications and nominations for the position of Head of the Department of Mechanical Science and Engineering (MechSE). The MechSE Department at Illinois is a leader in mechanical engineering and theoretical & applied mechanics education and research, with programs consistently ranked in the top five nationally, and approximately $24 million of externally funded research per year. The Department Head is a tenured full Professor and serves as the chief executive officer, responsible for all administrative, budgetary, hiring, and promotion decisions. The search committee seeks candidates with a distinguished record of achievement and internationally recognized for their research excellence, leadership, and scholarship. Further details about the MechSE Department and the position can be found at **mechse.illinois.edu/about-us/department-head-search.**

The desired start date is January 16, 2015, or as soon as possible thereafter. Applications should be received by **October 1, 2014**, for full consideration, but applications will be accepted until the position is filled. **Please apply at jobs.illinois.edu**.

Nominations for this position are also encouraged. Nominations should be in the form of a brief letter detailing the accomplishments of the nominee. Nominations and questions regarding the position of Department Head should be addressed to the chair of the search committee: **Prof. David Cahill, Email: d-cahill@illinois.edu**

ILLINOIS
UNIVERSITY OF ILLINOIS AT URBANA-CHAMPAIGN

Illinois is an EEO Employer/Vet/Disabled – www.inclusiveillinois.illinois.edu

The University of Tennessee
College of Pharmacy
Medicinal Chemistry Faculty Position

The Department of Pharmaceutical Sciences in the College of Pharmacy at the University of Tennessee Health Science Center in Memphis, TN, is seeking applications for a twelve-month full-time, tenure-track faculty position at the full, associate, or assistant professor level that is state supported. The successful candidate is expected to devote a major effort to research. The applicant should have core expertise in medicinal chemistry, or related discipline such as structural biology focused on drug discovery and development. Candidates with a well-funded program in cancer, diabetes, antibiotics, drug delivery, nano-medicine, nano-technology, bio-imaging, or lipid research are highly encouraged to apply. The successful candidate is expected to have a Ph.D. or equivalent degree, the ability to acquire sustained external, investigator-initiated funding, including National Institutes of Health principal investigator funding, a commitment to excellence in teaching, and excellent oral and written communication skills.

Applications will be processed until the position is filled. Please submit curriculum vitae, summary of research interests, and contact information of three references to: **Duane D. Miller, Ph.D. Professor and Chair Department of Pharmaceutical Sciences, Chair of Medicinal Faculty Search Committee, Department of Pharmaceutical Sciences, 881 Madison Avenue, Room 435, Memphis, TN 38163**.

The University of Tennessee Health Science Center is located in Memphis, TN, an economically vibrant center, with a metropolitan population of more than 1.3 million, reflecting the richness along the bluffs of the mighty Mississippi River. The College of Pharmacy is located in a new, 187,000 square-foot building on the Health Science Center complex.

The University of Tennessee Health Science Center is an Equal Opportunity/Affirmative Action Employer.

Creation?
Innovation?
Ambition?

KU Leuven Biomedical Sciences invites applicants for several senior academic staff positions (m/f)

- Health economics
- Proton therapy and pre-clinical high precision image-guided radiotherapy
- Fundamental/Translational research in oncology
- Synthetic biology
- Morphology and molecular pathology
- Cardiovascular rehabilitation
- Musculoskeletal rehabilitation
- Cristallography and modelling of multi-enzyme complexes in virology
- Pharmacometrics
- Microbiological bioinformatics
- Pre-clinical multimodal imaging
- Insurance medicine
- Development of innovative radiotracers for molecular imaging and/or radionuclide therapy (research senior academic staff Bijzonder Onderzoeksfonds)
- Systems biology in cellular and molecular medicine (research senior academic staff Bijzonder Onderzoeksfonds)

For more information about these vacancies:
https://gbiomed.kuleuven.be/english/career-opportunities-1/career-opportunities

top employer België Belgique 2014

Discover yourself, start with your job.

KU LEUVEN

The University of Leuven pursues a policy of equal opportunity and diversity.

www.kuleuven.be/jobsite

FACULTY POSITION IN CHEMISTRY

Department of Chemistry
BIOMEDICAL CHEMISTRY INSTITUTE
ARTS AND SCIENCE

The Department of Chemistry at New York University (NYU) invites applications for a tenure-stream faculty position in synthetic organic chemistry as part of its Biomedical Chemistry Institute. While we expect to hire at the junior level, exceptional senior level candidates will be considered. The anticipated start date is September 1, 2015, pending budgetary and administrative approval. The Department of Chemistry at NYU is implementing a significant growth plan, including the creation of the Biomedical Chemistry Institute, the Molecular Design Institute, the Laboratory for Molecular Nanoscience, and the addition of numerous senior and junior faculty members.

In addition to establishing a vigorous research program, duties will include undergraduate and graduate teaching. Applicants should have an outstanding record of research and a commitment to teaching. Applications must include a curriculum vitae, a list of publications, and statements of future research and teaching plans. These materials, as well as three reference letters, must be submitted to our web-based application system using the following link: **http://chemistry.fas.nyu.edu/object/chem.nyufacultypositions**.

Application review will begin **October 15, 2014**. Questions about this position can be sent by Email to **chemistry.search@nyu.edu.**

NEW YORK UNIVERSITY

NYU is an Equal Opportunity/Affirmative Action Employer.

FACULTY POSITION IN CHEMISTRY

Department of Chemistry
LABORATORY FOR
MOLECULAR NANOSCIENCE
ARTS AND SCIENCE

The Department of Chemistry at New York University (NYU) invites applications for a tenure-stream faculty position in experimental physical, biophysical, or inorganic chemistry as part of its Laboratory for Molecular Nanoscience. While we expect to hire at the junior level, exceptional senior level candidates will be considered. The anticipated start date is September 1, 2015, pending budgetary and administrative approval. The Department of Chemistry at NYU is implementing a significant growth plan, including the creation of the Biomedical Chemistry Institute, the Molecular Design Institute, and the addition of numerous senior and junior faculty members.

In addition to establishing a vigorous research program, duties will include undergraduate and graduate teaching. Applicants should have an outstanding record of research and a commitment to teaching. Applications must include a curriculum vitae, a list of publications, and statements of future research and teaching plans. These materials, as well as three reference letters, must be submitted to our web-based application system using the following link: **http://chemistry.fas.nyu.edu/object/chem.nyufacultypositions**.

Application review will begin ***October 15, 2014***. Questions about this position can be sent by Email to **chemistry.search@nyu.edu.**

NEW YORK UNIVERSITY

NYU is an Equal Opportunity/Affirmative Action Employer.

POSITIONS OPEN

FACULTY POSITION in Molecular Physiology and Metabolic Disease

The Duke Molecular Physiology Institute (DMPI) at Duke University Medical Center is partnering with the Department of Medicine, Division of Endocrinology, Nutrition, and Metabolism to recruit outstanding basic scientists to develop a nationally competitive research program relevant to nutrition, fuel homeostasis, and regulation of metabolism. Applications will be considered at the **ASSISTANT PROFESSOR** or **ASSOCIATE PROFESSOR** levels. The ideal candidate will have strong training in basic sciences and a demonstrated interest in molecular mechanisms of chronic metabolic disorders or conditions such as obesity, diabetes, cardiovascular disease, and aging. Although candidates with expertise in all areas of metabolic research will be considered, preference will be given to those with experience in neuroendocrine circuitry and Central Nervous System control of metabolism, or application of mass spectrometry combined with 13C tracer methodologies for assessment of metabolic flux. This position offers a vibrant and highly interactive academic setting, competitive startup funds, space in a new state-of-the-art research facility, access to outstanding technology platforms, and strong, collaborative faculty colleagues in both the clinical and basic sciences. Minimal qualifications for the position are the M.D. or Ph.D. degree and three years of postdoctoral research experience. Interested candidates should submit application materials including cover letter, curriculum vitae, statement of accomplishments and future research goals (three-page limit), electronic reprints of up to three recent articles, and arrange to have three letters of reference provided. Materials should be addressed to **Dr. Deborah Muoio**, Faculty Search Committee, and submitted electronically to **e-mail: kristy.thompson@duke.edu.**

To ensure full consideration, the application materials must be received by October 15, 2014, but the committee will continue to accept applications until the position is filled.

ASSISTANT PROFESSOR in Population Genetics

The Department of Ecology and Evolutionary Biology at the University of Colorado, Boulder invites applications for an Assistant Professor in Population Genetics. We are especially interested in individuals using genomic data for investigating microevolution. The successful candidate will contribute to research, mentoring, and teaching at graduate and undergraduate levels and will be expected to develop an externally funded research program. To apply, please collate the following into a single PDF file: cover letter, curriculum vitae, a list of at least three references and their contact information, and no more than four pages total on research, mentoring, and teaching. Submit application materials electronically at **website: https://www.jobsatcu.com (#F01649)** by October 15, 2014. *The University of Colorado is Equal Opportunity/Affirmative Action Employer committed to building a diverse workforce. We encourage applications from women, racial and ethnic minorities, individuals with disabilities and veterans. Alternative formats of this ad can be provided upon request for individuals with disabilities by contacting the ADA Coordinator at* **website: http://hr-ada@colorado.edu.**

Stop searching for a job; start your career.

Science Careers
From the journal *Science* AAAS

www.ScienceCareers.org

POSITIONS OPEN

COMPUTATIONAL BIOLOGIST Assistant/Associate/Full Professor Biochemistry and Molecular Biology

The Biochemistry and Molecular Biology (BCMB) program seeks to fill a tenure-track position, starting in August 2015. Primary responsibilities will be to develop a computational biology course, contribute to introductory and intermediate courses in the Biology and BCMB majors, participate in the College's First Year Seminar program, and mentor undergraduates in our nationally recognized senior research program. Ph.D. and postdoctoral research required; some teaching experience preferred.

Send cover letter, curriculum vitae, undergraduate and graduate transcripts, a two-page summary of research plans, and a one-page statement describing approach in teaching and supervising student research in an undergraduate liberal arts setting to **e-mail: biology@wooster.edu.** Three letters of recommendation should also be provided under separate cover. Address questions regarding the position to **Dean Fraga** (**e-mail: biology@wooster.edu**), Chair of BCMB. Review of applications will begin October 1, 2014 and continue until the position is filled.

Wooster seeks to ensure diversity by its policy of employing persons without regard to age, sex, color, race, creed, religion, national origin, disability, veteran status, sexual orientation, or political affiliation. The College of Wooster is an Equal Opportunity/Affirmative Action Employer.

Your career is our cause.

Get help from the experts.

www.sciencecareers.org

- Job Postings
- Job Alerts
- Resume/CV Database
- Career Advice
- Career Forum

Science Careers
From the journal *Science* AAAS

☑ More scientists agree —we are the most useful website.

www.ScienceCareers.org

Nontraditional Careers: Opportunities Away From the Bench Webinar

Want to learn more about exciting and rewarding careers outside of academic/industrial research? View a roundtable discussion that looks at the various career options open to scientists and strategies you can use to pursue a nonresearch career.

Now Available On Demand
www.sciencecareers.org/webinar

Produced by the *Science*/AAAS Business Office.

Science Careers
From the journal *Science* AAAS

UTHealth
The University of Texas
Health Science Center at Houston

FACULTY POSITION
NEUROBIOLOGY

The Department of Neurobiology and Anatomy at The University of Texas Medical School at Houston invites applications for a tenure-track appointment in the broad area of circuit neuroscience. We particularly encourage applications from candidates who employ novel computational or experimental techniques including electrophysiology, imaging, and viral approaches to record, manipulate, and analyze in vivo neuronal activity with single-cell resolution. Applications at both junior and senior levels will be considered, with rank dependent on experience and qualifications. We are located within the Texas Medical Center and its very rich and collaborative neuroscience community including Baylor College of Medicine, Rice University and the University of Houston.

Individuals will be expected to develop a strong, independent research program and contribute to our departmental teaching mission. Interested applicants should submit electronically their curriculum vitae, a statement of their research and teaching interests, and the names of four references through our online application system at **https://jobs.uth.tmc.edu**. The position will remain open until a suitable candidate is identified.

UTHealth is an EEO/AA Employer. UTHealth does not discriminate on the basis of race, color, religion, gender, sexual orientation, national origin, genetics, disability, age, or any other basis prohibited by law. EOE/M//F/Disabled/Vet.

Williams

IMMUNOLOGIST
Tenure-Track Faculty Position
Biology Department

The Biology Department at Williams College, a premier liberal arts college with a long-standing tradition of excellence in the sciences, invites applications for a tenure-track position at the rank of Assistant Professor to begin July 2015. We seek a broadly trained immunologist who will teach upper level courses in his or her area of specialty and contribute to our introductory course in cellular and molecular biology. The individual will advise undergraduates in research and participate in interdisciplinary programs in biochemistry & molecular biology, and/or bioinformatics, genomics and proteomics. Normally, faculty members teach one course and two associated laboratory sections (or the equivalent) each semester. A vibrant research program that is attractive to extramural funding agencies and involves talented undergraduates is expected. Start-up funds and internal funding for research are available. A Ph.D., postdoctoral experience, and a strong research record are required. We anticipate the appointment at the beginning assistant professor level, although more senior appointments are possible under special circumstances.

All applications should be submitted through Interfolio **http://apply.interfolio.com/25516**. Email and paper applications will not be accepted. Through Interfolio submit: a letter of application addressed to Professor Steve Swoap (department chair), a curriculum vitae, statements of teaching and research plans, and three current letters of recommendation. All offers of employment are contingent upon completion of a background check **http://faculty.williams.edu/prospective-faculty/background-check-policy/**. Application deadline is **October 10, 2014**.

Williams College is a coeducational liberal arts institution located in the culturally rich Berkshire Hills area of western Massachusetts with easy access to the cities of Albany, Boston, and New York City. The College is committed to building and supporting a diverse population of approximately 2,000 students, and to fostering an inclusive faculty, staff and curriculum. Williams has built its reputation on outstanding teaching and scholarship and on the academic excellence of its students. Please visit the Williams College website (**http://www.williams.edu**) and the Williams Biology website (**http://biology.williams.edu**). Beyond meeting fully its legal obligations for non-discrimination, Williams College is committed to building a diverse and inclusive community where members from all backgrounds can live, learn, and thrive.

AAAS is here –
helping scientists achieve career sucess.

Every month, over 400,000 students and scientists visit ScienceCareers.org in search of the information, advice, and opportunities they need to take the next step in their careers.

A complete career resource, free to the public, *Science* Careers offers hundreds of career development articles, webinars and downloadable booklets filled with practical advice, a community forum providing answers to career questions, and thousands of job listings in academia, government, and industry. As a AAAS member, your dues help AAAS make this service available to the scientific community. If you're not a member, join us. Together we can make a difference.

To learn more, visit
aaas.org/plusyou/sciencecareers

AAAS + U = Δ

WASHINGTON STATE UNIVERSITY

DIRECTOR
INSTITUTE OF BIOLOGICAL CHEMISTRY, #80329
WASHINGTON STATE UNIVERSITY PULLMAN, WA

The College of Agricultural, Human and Natural Resource Sciences (CAHNRS) at Washington State University seeks an internationally distinguished researcher and academic leader to be Director of the Institute of Biological Chemistry (IBC) (**http://cahnrs-cms.wsu.edu/ibc**). CAHNRS is home to nearly 300 tenure track faculty distributed among 15 academic units. The faculty are recognized for excellence in their contributions to mission-oriented and fundamental areas of the plant sciences.

Applications are invited for a full-time, 12 month position at the rank of Associate Professor or Professor eligible for tenure to begin July 1, 2015, or as negotiated, at the Pullman, Washington campus. The position offers an exciting opportunity for leadership in developing new strategic initiatives and in further advancing established areas of departmental excellence in modern plant science. Members of the Institute employ biochemical, biophysical, genetic and systems biology approaches to investigate and understand fundamental processes in plants. There will be opportunities to hire new faculty over the next 3 - 5 years, and the Institute is scheduled to move into a new world class building on the Pullman campus which is currently in the design phase.

QUALIFICATIONS: Required: Earned Ph.D. in a fundamental area of modern plant science or a related discipline at date of hire; and demonstrated record of success in unit leadership, fiscal and personnel management in a department, program or highly diverse scientific or academic unit. **Preferred:** Demonstrated experience in graduate education and a commitment to professional education at all levels; internationally recognized, extramurally funded research activity with disciplinary leadership complementary to existing department and college strengths; demonstrated effectiveness in developing and delivering graduate level courses in an area of modern plant biology; demonstrated record of success in fiscal and personnel management in an academic environment; excellent interpersonal communication skills including ability to articulate and implement a strategic vision and assess the impacts of generated outcomes; and demonstrated successful engagement in and commitment to the recruitment, retention, development, and enrichment of a diverse faculty, staff and student community.

Screening of applications will begin **October 1, 2014**, and will continue until position is filled. To apply or obtain more detailed information go to **www.wsujobs.com**. For questions or about this position candidates may email or telephone **Dr. Mark Lange, Search Committee Chair**, at **lange-m@wsu.edu** or **509-335-3794**.

WSU is an EO/AA Educator Employer.

By **Jim Austin**

Playing a new tune

Russian-born pianist Igor Lovchinsky attended the Juilliard School in New York City and the New England Conservatory of Music in Boston. He has won several competitions and performed at the John F. Kennedy Center for the Performing Arts and Carnegie Hall. *Time Out* voted his debut album one of the top five classical recordings of 2008, making comparisons to Walter Gieseking and Martha Argerich. But now he is changing course: Lovchinsky is enrolled in the Ph.D. program in physics at Harvard University. We caught up with him after a performance at the Franco-American Heritage Center in Lewiston, Maine. This interview has been edited.

Q: Which came first, piano or physics?
A: I started off as a pianist; in fact, I didn't even like physics until I was in my mid-20s! I grew up in a musical bubble, where everyone I knew was a musician, and the thought of doing anything else really never even entered my head. I spent all my time practicing: preparing for performances, competitions, etc. But several years ago, I got interested in science and started reading some books on my own. One thing led to another, and now I'm a graduate student at Harvard, working with Professor Mikhail Lukin.

Q: What are you working on?
A: I'm working on using solid-state defects in diamonds as magnetic field sensors, with the goal of using them as little nanoscale MRI machines that can study the structure and dynamics of single biological molecules (e.g., proteins).

Q: Do you think of your move into physics as a career transition?
A: I never planned to give up the piano, and I hope to keep playing, at least until they stop paying me! A truly successful career as a musician takes a full-time effort, and that's simply not realistic when I spend most of my time in the laboratory, but I've learned to be much more efficient in my practicing and have adopted a more scientific approach to problem-solving in the practice room.

Q: Do you have any insights to offer readers making their own career transitions?
A: This transition certainly wasn't easy. There were obvious difficulties in learning a new field and having to catch up to people who have been doing it all their lives. But the harder part was the social pressure from people who said I was crazy for giving up a promising career in music to start from scratch in science. I didn't care, since I was determined to do it no matter what anyone said. I found it helpful to set realistic expectations and to realize that it will not be easy, and that I will fail many times along the way. It's also important to find people in your new field who are supportive but also not afraid to be honest with you.

"I hope to keep playing, at least until they stop paying me!"

Q: Does your experience performing music help your science?
A: Public speaking is a type of performance, and the quality of the delivery (or lack thereof) is almost as important as the content. It's also true that performing on stage is a great way to get used to being under pressure. But there are important differences. If you have a memory slip in the middle of a performance, you can usually just put down the pedal and improvise your way out of it before most people realize anything happened. Unfortunately, there isn't an equivalent to "pedaling-through" for a physics talk. Every professional musician frequently finds himself in a situation in which he has to learn a new piece or prepare for a performance on short notice and has to practice 10-plus hours per day. Concentrating for that long, with no recourse to Facebook or YouTube, does not come naturally to people, but doing this for many years taught me to shut off all distractions and focus on my work. In addition to work ethic, learning to play an instrument on a serious level trains your memory, coordination, and abstract reasoning—all useful skills that can be applied elsewhere. ■

Jim Austin is the editor of Science *Careers. Got an unusual career story? Send it to SciCareerEditor@aaas.org. For more on life and careers, see www.sciencecareers.org.*

ILLUSTRATION: ROBERT NEUBECKER

Downloaded from www.sciencemag.org on August 24, 2014

Published by AAAS